Proceedings of the 16th International Workshop on Laser Ranging

SLR – the Next Generation

Volume 2

October 13-17, 2008
Poznań, Poland

Book Title
Proceedings of the 16th International Workshop on Laser Ranging
October 2008, Poznań, Poland
Volume 2

Publisher
Space Research Centre, Polish Academy of Sciences
ul. Bartycka 18A
00-716 Warszawa
Poland
Tel: +48 22 840 3766
Fax: +48 22 840 3131

Published
December 2009

Printer
Drukarnia Oświatowa
ul. Głogowska 149
60-313 Poznań
drukoswiat@neostrada.pl

Edited by
Stanisław Schillak

TABLE OF CONTENTS

Scientific Achievements, Applications and Future Requirements (second session)

The role of Satellite Laser Ranging in the Global Geodetic Observing System

Network and Station Performance

Lunar and Interplanetary Laser Ranging

High repetition-rate systems

Lasers, Detectors, and Timers

Software and Automation

New and Upgraded Stations, Extended Facilities

Operational Issues and New Missions

Targets, Signatures and Biases

Advanced Systems and Techniques: Transponders, Altimeters, and Time Transfer

Lasers, Detectors and Timers

Chairs: Ivan Prochazka and Yurij Artyukh

Session Summary

Totaly 8 orals and 2 posters were presented in this session.
Related to the lasers and optics Huber Heinz et al presented a review on commercially available kHz diode pumped lasers, Josef Koelbl et al described the new high voltage Pockels cell driver for kHz SLR lasers, T. Oldham et al described the application of the new saturable absorber in the SLR laser transmitter and V.L.Moshkov presented a novel and promissing narrow-band holographic filters for SLR.

Related to detectors the Prague group presented new photon counting detectors for future space missions. The Riga group represented the new version of the Riga event timer with improved resolution and the high-speed event timer design based on common-used TDC chips. Basic results of the integration of Riga event timers into Chinese SLR network was reported by the Chinese group. The potentialities of commonly used TDC chips for high-speed event timer design was displayed by E. Boole et al. The design and construction of the compact event timing and laser fire control device for one way laser ranging and the new timing principle and device for sub-picosecond performance were presented by Prague group.

Advances of High-precision Riga Event Timers

Yu. Artyukh, V.Bespalko, E.Boole, V.Vedin
Institute of Electronics and Computer Science, Riga, Latvia
artyukh@edi.lv

Abstract

Two main directions to advancement of high-precision Riga event timers are considered. The first direction is related to updating of the well-known event timer A032-ET. Retaining the basic operating characteristics of the A032-ET, RMS resolution of the updated model (A033-ET) has been increased from previous 7-8 ps to 3-4 ps. The second direction concerns development an event timer module (ETM) fitted to including into various customized timing systems. The ETM is similar to the A033-ET in precision but differs by an extended functional flexibility and hardware compactness.

Introduction

The Riga Event Timer A032-ET is one of a few high-performance event timer systems commercially available for SLR applications (Bespal'ko et al., 2008). Generally it still well conforms to the current demands of these applications in terms of price/performance ratio. However, to make such event timer commercially available in the future, some obsolete electronic components of its hardware (which became unavailable) should be replaced by the latter-day ones. This is the main practical reason to update the A032-ET, replacing it by next model A033-ET. At the same time we wished to increase the timer precision, optimise its design, extend applicability, etc., retaining the familiar basic features of the previous model.

Additionally we have taken into account actual demands for high-performance event timer modules that can be used as a basis for creating different customised event timing systems. We suppose that the basic concept of Riga event timer development is well suited for such module design, combining high performance characteristics with compact hardware implementation.

Basics of the Riga event timer designs

Usually the high precision of event timers is provided by an interpolation measurement that is used in addition to the basic measurement performed in a digital way. There are a few well-known methods for interpolation measurements (such as time interval stretching, time-to-amplitude conversion, vernier method, etc). However, mostly the interpolation measurements performed on the basis of these methods are characterised by a high hardware complexity, requiring considerable engineering know-how for designing, manufacturing and adjusting of the hardware. Mainly for this reason the most of top-quality event timers are distinguished by rather high manufacturing costs.

To solve this problem, a specific DSP-based method for event timing is used in the latest designs of Riga Event Timers (Artyukh, 2001). According to this method, each input event is converted to an analog signal with some predefined shape. Actually this is simply a generating of such signal at the time instant determined by the respective input pulse. Then this signal is digitised using typical A/D converter and digitally processed to estimate its

position relative to the periodic sampling pulse sequence (Fig.1). If the ordinal numbers of the processed signal samples are known, the signal processing made in the proper way will result in an estimate of the time of event occurring.

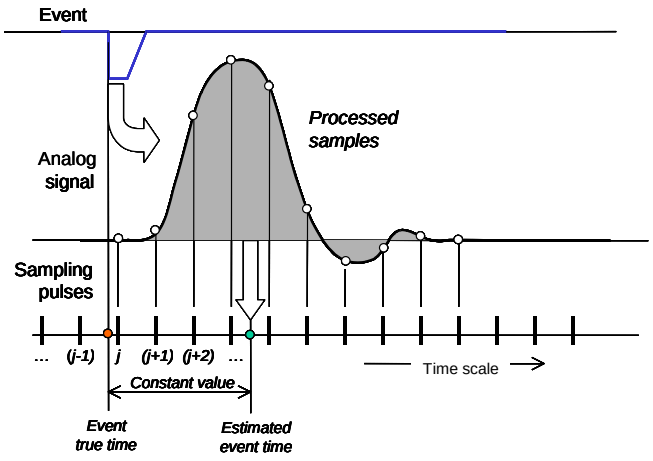

Figure 1. Principle of DSP-based method for event timing

Thus, in comparison with the traditional methods, this method provides considerable reducing of highly specialized hardware components by using instead of them typical DSP facilities. This results in hardware simplifying and increasing its reliability.

As for achievable performance characteristics, there are many essential realisation details to provide good final result. First and foremost, it is important to correctly choose the best practice of analog signal generation and matched algorithm for signal processing. Specifically, we generate the analog signal in the shape of near-triangular pulse. To provide sufficiently high measurement rate, we use not more than four samples of each such signal for further processing. Algorithm for such processing is based on a specific selection of two most informative samples of the signal and non-linear conversion of the difference between them to the target time-tag.

Updating the event timer A032-ET

Background for precision increasing

To avoid confusion, let us note that we define the timer's precision as the standard deviation of measured time for single event, unlike the timer's resolution, which traditionally is defined as the standard deviation of measured difference (time interval) between two events. The precision can be simply translated into the resolution and contrariwise if desired.

Three basic error components can be marked out as the main reasons for precision limitation of the Riga event timers:

- quantizing errors which directly depends on the resolution of A/D converter;
- integral non-linearity errors which mainly are caused by an imperfectness of the timer calibration;
- internal noise caused by trigger errors, sampling jitter, induced interferences, etc.

Note that the integral non-linearity errors are considered as systematic ones only in the case of synchronous measurements; otherwise they are like internal noises (Artyukh et al., 2008).

Correspondingly all these three kinds of errors in the most cases can be specified in statistical terms (by RMS values). In particular, the A032-ET precision is typically characterized by the following RMS values of error components:

- Quantizing errors: 3.5 ps approx.
- Integral non-linearity errors: 2.6 ps approx.
- Internal noises: 2.0 ps approx.

Considering these error components as statistically independent, the precision and resolution of the A032-ET can be estimated as follows:

- Precision: 4.8 ps
- Resolution: 6.8 ps

These estimates well conform to the RMS resolution (6-8 ps) experimentally evaluated for a number of the A032-ET event timers.

As can be seen, the quantizing errors dominate in the total error of the A032-ET. Correspondingly, the use of the A/D converter with higher resolution should noticeably increase the timer's precision. In addition, more careful hardware design and advancing of calibration procedure have to reduce other error components.

Hardware redesign

First and foremost, in the process of redesign the previous 10-bit A/D converter has been replaced by more advanced 12-bit converter AD9432 from "Analog Devices Inc." and obsolete high-speed logical NECL chips - by the modern LVPECL chips. Additionally, some special means for stabilization of temperature-depended parameters of the analog signal have been added, RF lines between the most sensitive hardware components have been revised and more careful PCB design has been carried out. All these modifications resulted in a fully new main board of the timer's hardware (Fig.2).

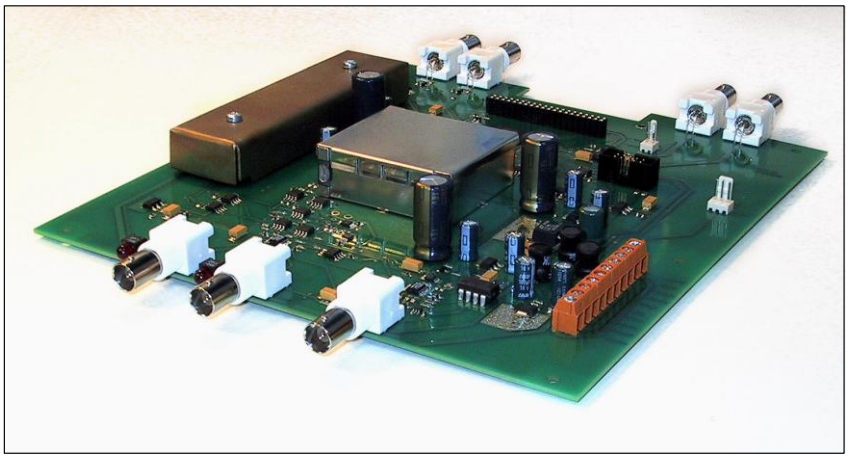

Figure 2. Main board of the A033-ET hardware

All blocks of the A033-ET hardware (the main board, clock frequency synthesizer and power supply) are assembled in a standard enclosure (EUROCASE; dimension: 367x250x76 mm). To provide compatibility of the A033-ET with the previous model, most interfacing connectors and their arrangement are preserved.

Software modifications

Functional features of the A033-ET are almost identical to those of the previous model. There are some software modifications caused by the changing of data formats and minor

distinctions in control commands. In addition, more complicated calibration procedure is used to minimize the integral non-linearity. But this procedure is defined as a library function and its using does not require any special skill from the user.

Preliminary A033-ET tests

Preliminary tests of the A033-ET pilot version showed, that, as a result of the mentioned modifications, the A033-ET error components are characterized by the RMS values as follows:

- Quantizing errors: 1.1 ps approx.
- Integral non-linearity errors: 1.7 ps approx.
- Internal noises: 1.1 ps approx.

In this case the dominating integral non-linearity errors have been experimentally evaluated directly after device calibration (Fig.3).

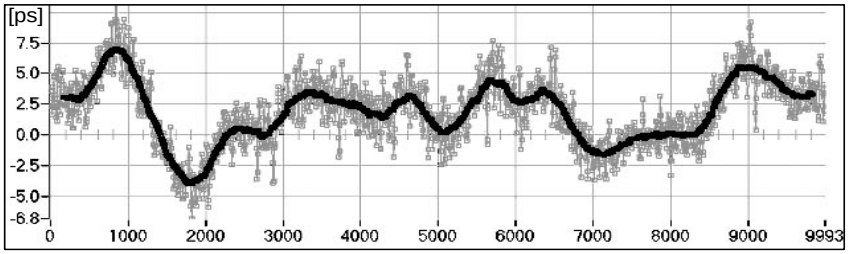

Figure 3. A033-ET integral non-linearity errors over interpolation interval

The above estimates conform to the calculated RMS precision of about 2.3 ps and RMS resolution of about 3.3 ps. Broadly speaking, the precision of the A033-ET has to be twice as better than that for the A032-ET. Such assumption was confirmed by the resolution test under temperature-varying operating conditions (Fig.4).

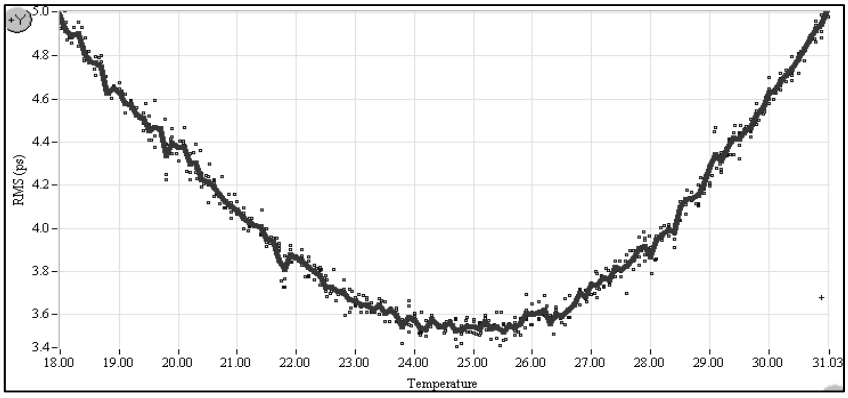

Figure 4. A033-ET RMS resolution vs. ambient temperature variation

As can be seen, the best RMS resolution (about 3.5 ps) is supported if the ambient temperature is close to the ambient temperature 25 ^{0}C when the device has been calibrated. Note that in this case an acceptable level of RMS resolution is supported without re-calibration in a sufficiently wide range of ambient temperature variation.

We also have tested long-term instability of the internal time-base through repetitive measurement of pulses strictly synchronised to the external 10 MHz frequency standard. It

was established that such instability basically depends on the ambient temperature variation. In the case of temperature variation up-and-down in the range 10 to 40 ^{0}C, the results of synchronous measurements vary in the range of 35 ps approx. (Fig.5). In other words, the evaluated long-term instability of the internal time-base surely does not exceed 2 ps /1^{0}C.

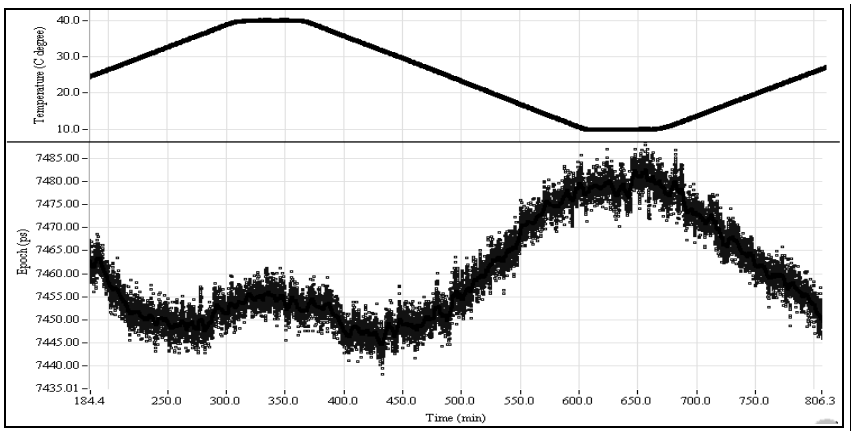

Figure 5. Internal time-base instability vs. ambient temperature variation

Event Timer Module

We consider the A033-ET as a completed product (like the A032-ET). As for the Event Timer Module (ETM), it is developed as a semi-customized product fitted to including into various customized timing systems after final ETM rework with due regard to the specific requirements. For example, the ETM can be configured so that its features will be close to those of the A033-ET.

Principles of the ETM operation are almost the same as that of the A033-ET but emphasis in its realisation is made on achievement of hardware compactness. For these purposes there are some modifications in the analog signal shaper (bulky cable delay line is removed), PLL-based clock signal synthesizer is incorporated in a module card. Re-programmable large-scale integration chip (Cyclone II) is used to provide customized modifications in ETM operation according to the specific requirements of application. Due to all these modifications a relatively small size of the ETM card (130x210 mm) and power consumption less than 6W have been achieved (Fig.6).

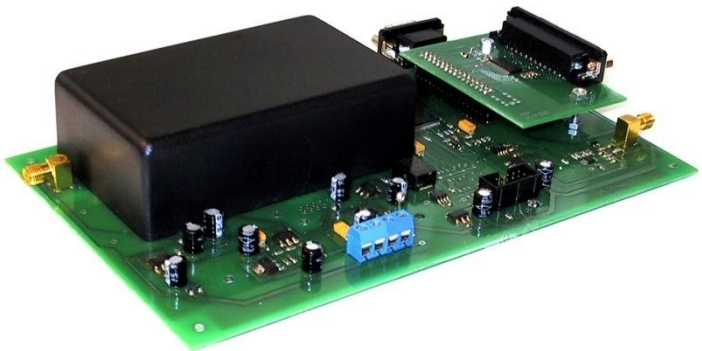

Figure 6. ETM design

As for the ETM precision, we expect that it will be not worse than that for the A033-ET, at least the preliminary tests confirm that. We also expect that operation speed for the ETM can be higher than that for the A033-ET. Specifically, the ETM pilot version already provide 25 MHz maximum burst rate and up to a few MHz of maximum average rate when high-speed USB 2.0 interface is used. Forasmuch as the ETM development is not completed in some details, its further improvement is possible.

Summary

The A033-ET continues the line of Riga Event Timers commercially available on multiple requests. Forasmuch as the A033-ET performance characteristics (especially precision) seem much better than that for the previous model, we hope that it can successfully replace the last one. But the final conclusion about ensured performance of the A033-ET will be made after additional checking of its performance repeatability in a small-scale production.

Unlike the A033-ET, conceptually the ETM is considered as an important component of more complicated application-specific event timer systems designed in the framework of various R&D projects. In addition, currently the ETM is used as a flexible platform for further development of DSP-based event timing technology.

Acknowledgements

The considered event timers represent the results of collective efforts made not only by the authors of this paper. Many thanks to our colleagues from ILRS community, which already use the Riga event timers and help us to advance them in right directions.

References

Artyukh, Yu.: Method of continuous extreme-precision time-interval measurement // Automatic Control and Computer Sciences, Vol.35, No.5, pp.11-18, 2001.

Artyukh, Yu., Bespal'ko V., Boole, E.: Non-linearity errors of high-precision event timing // Automatic Control and Computer Sciences, Vol. 42, No. 4, pp. 191-196, 2008.

Bespal'ko, V., Boole, E., Vedin, V.: The Model A032-ET of Riga Event Timers. Proceedings of the 15th International Workshop on Laser Ranging, Canberra, Australia, Vol.2, pp. 321-326, 2008.

Advances of multi kHz repetition rate picosecond laser system for satellite laser ranging

Heinz Huber, Michael Schmidt, Sandra Zoppel
High Q Laser Production GmbH, Austria
heinz.huber@highqlaser.at

Abstract

Saturable absorber mode locked and diode pumped picosecond laser systems at a repetition rate of 2 kHz have been successfully introduced for SLR (by the Graz station) nn previous years. These system were based on the laser material Nd:Vanadate. A better candidate to reach higher pulse energies is the laser material due to its higher laser state life time.
Here we present a new Nd:YLF laser system delivering 1.2mJ at 1 kHz and 0.6mJ at 2 kHz. The system exhibits a simpler set-up and can run up to higher repetition rates.

Compact Event Timing and Laser Fire Control Device for One Way Laser Ranging

Jan Kodet, Ivan Prochazka
Czech Technical University in Prague, Czech Republic
kodet@fjfi.cvut.cz

Abstract

We are presenting the design, construction and performance of the compact control circuit, which can be used as an event timing unit and time laser fire control unit in one way ranging experiments. The main design goals were to construct compact device, which can measure time epochs with resolution of hundreds picoseconds and which can control the time of laser fire with resolution of 100 nanoseconds. The unit is controlled by 10 MHz and 1 pps signals from local time base.
The electronic board is designed using SMD technology; the precise voltage stabilizer is included. The external power of 4.5 to 9 Volts 0.5 A DC is required. The input signals receivers accept TTL (1 pps) and NIM (Event) signal levels via SMA connectors. The epochs are determined using coarse counter and time interpolator. The coarse counter determines both the epoch of laser fire and received pulses with resolution of 100 nanoseconds, it is based on programmable gate array. The time interpolator by Acam provides the epoch of received pulses resolution of hundreds of picoseconds. The unit is controlled by microcontroller made by Microchip, it communicates through standard serial line - RS232 using ASCII characters. The user friendly controlling application for the device was developed. Maximum measurement rate exceeds 100 Hz.
The device was tested in our lab and complete set of measurement were produced. The timing unit was compared to Pico Event Timer (P-PET2k) and the epoch timing resolution of the device is 130 picoseconds rms, the warm up characteristics does not exceed ~160 ps/K, the warm up time is one hour. The long term stability is as low as 10 ps/hour and the non linearity is below +/- 125 ps.
The device may be simply integrated to any SLR (or similar) system, it is compact, easy to control and friendly to use hence it satisfies the requirements variety range of experiments. The device was mainly designed for one way laser ranging of the Lunar Reconnaissance Orbiter and similar experiments.

Introduction

The main design goals were to construct event timing module with timing resolution of 100 ps and dead time less than 100 μs. The device can be calibrated witch 1pps signal. The timing unit must be able to generate programmable laser fire control signal, which enable to control the epochs of laser fire with resolution of 100 nanosecond. These properties allow using the timing unit in one way laser ranging experiments and applications.
The device can be included in Satellite Laser Ranging stations, which will be participated in Lunar Reconnaissance Orbiter (LRO) project. The LRO will orbit the Moon and the timing unit can trigger the laser in advance known epochs and the real laser fire will be measured to provide one way range measurements between the Earth based station and LRO to better than 10 cm precision [1].

Block diagram

The timing unit is based on Time-to-Digital converter (TDC-GP1), which was developed by Acam company [2]. This chip can measure only time intervals. To keep the generous purpose of the timing unit it is possible to run the unit in two different modes. The first is measuring of epochs (event timing mode) and second is measuring of time intervals start - stop. The block diagram of timing unit is shown in Figure 1. The input signals receivers of Event respectively Start, Stop and reference clock signal are based on fast comparators. The input signal of the comparators are NIM for event, TTL for stop (calibration of the timing unit) and 1 volt Vpp for reference clock of 10 MHz.

The coarse counter is implemented in programmable logic device form Lattice company with name ispLSI1032 for more information see [3]. It provides 10 MHz counter and gives the resolution of the generated laser fire and epochs of 100 ns.

The Time-to-Digital converter (TDC-GP1) from Acam company makes the resolution of the entire timing unit. As it was said this chip only time intervals start - stop measure. From this reason the last bits of epochs are derived from time intervals from received event and a first rising edge of the reference clock.

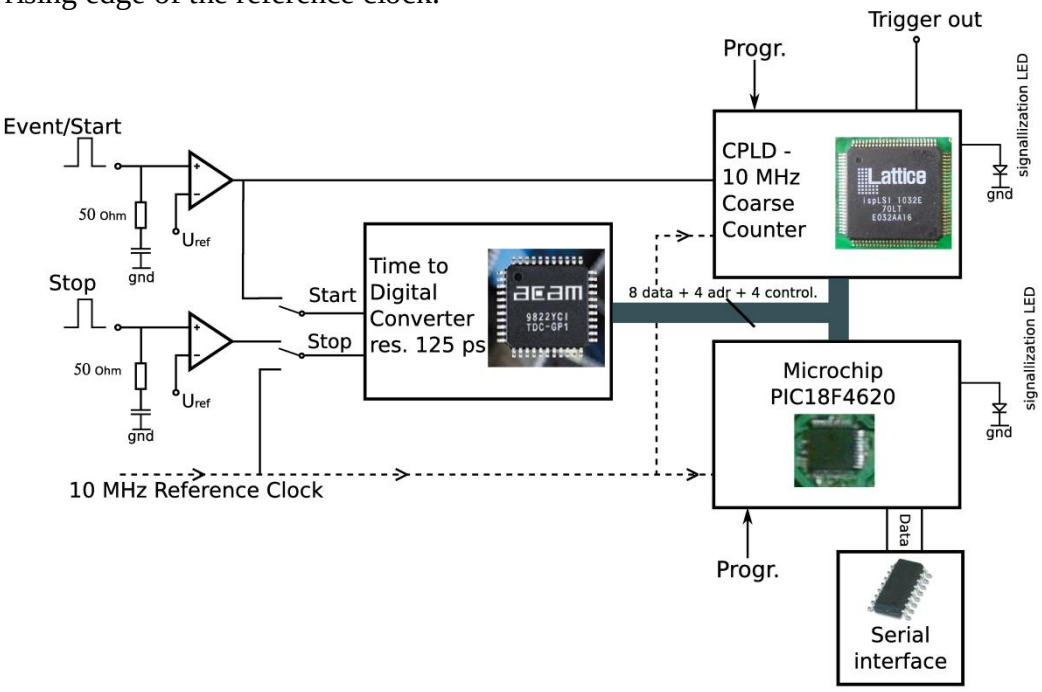

Figure 1. The block diagram of the timing unit

As a control heart of the timing unit a microcontrollers PIC18F4620 was chosen , which is produced by Microchip company [4]. It is 8 bit powerful RISC controller with 64 kb program memory and 3986 bytes of RAM memory. The advantages of all PIC18 microcontrollers are namely, high computational performance at an economical price and low power. Those devices incorporate a range of features that can significantly reduce power consumption during operation and big advantage is also In Circuit Serial Programming (ICSP) via two pins. The device can be set and driven by computer through standard serial line of 19200b and 8N1 configuration.

Prototype of the device

Very important was to develop the device from cheap and ordinary components. The entire board is designed using SMD technology and power consumption is about 200 mA at 5 volts. The board includes DC/DC converter, which enables to power the device with voltage from 5 to 9 dc volts. The signals 10 MHz reference clock, event and TTL (calibration – 1pps) can be connected via SMA connectors, see Figure 2, which are located on the front panel of the timing unit. There are also signalization diodes, which give the visual information of power on, connected reference clock, receiving of events and generating of trigger signal for fire of the laser.

Figure 2. The front panel of the timing unit.

On the back side of the device are power supply connector and serial line communication connector, see Figure 3. The back panel of the timing unit.Figure 3. The entire device is pretty small 16x9 centimeters in size and 3.5 centimeters of height.

Figure 3. The back panel of the timing unit.

To control the timing unit the demo software can be used. It includes all feature of the device. That mean the timing unit can be programmed with in advance known epochs, which can be uploaded in ascii file to the device. In consequence the device can measure epochs of events and the program can read the epochs and save them in file. The timing unit can be also calibrated using this demo software and the calibration 1pps signal. The window of the demo software can be seen in

Figure **4**.

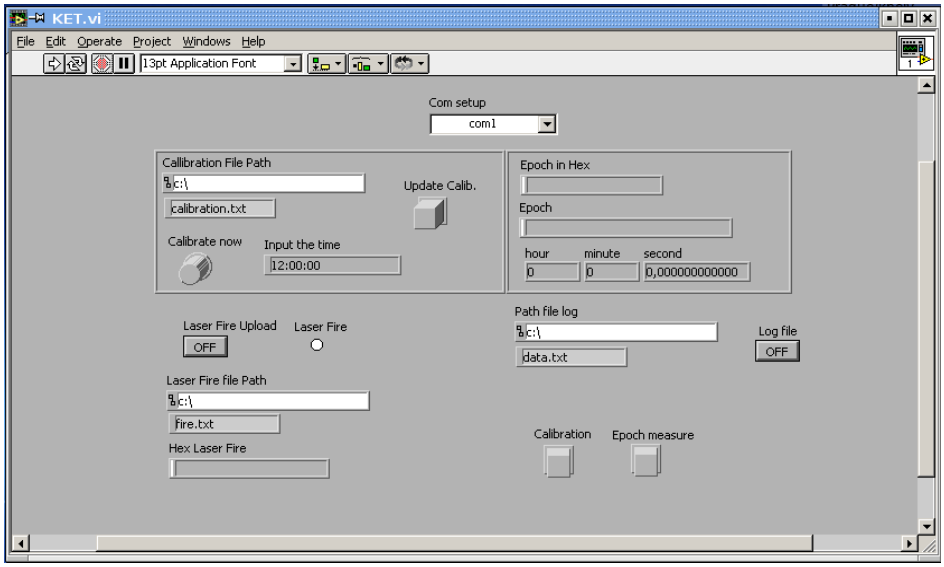

Figure 4. The demo software for work with the timing unit.

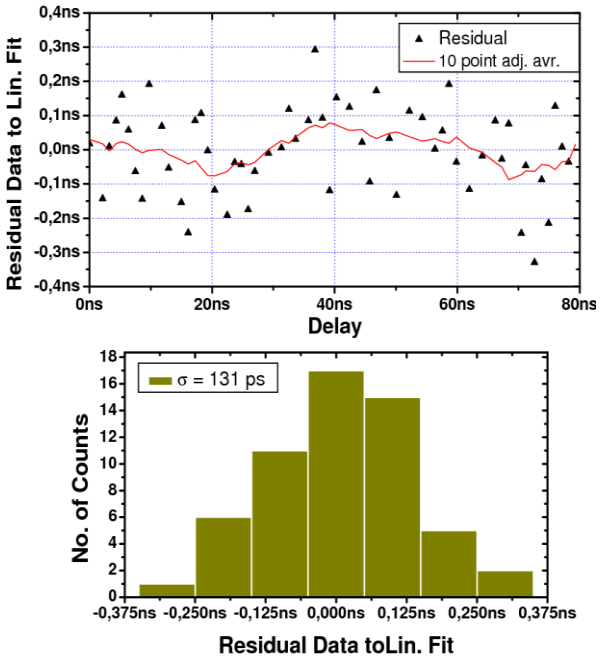

Figure 5. The first graph shows the residual data to linear fit, the adjacent averaging over 10 points was applied. The second graph illustrates the histogram of residual data, with standard deviation of 131 picoseconds.

Tests of the timing unit

At first the timing linearity of the device was investigated. The timing unit was driven from 10MHz reference clock, which was derived from GPS receiver. From the reference clock the epochs were generated and preciously delayed with Stanford delay line. The results were fitted with linear function and the residual data to linear fit were computed, the graph is in Figure 5. The results are uniformly spread with peak to peak of ±100 picoseconds of adjacent averaging. The histogram of residual data has been plotted with 131 picoseconds of rms.

Next important characteristic of the device is warm up characteristics. The warm up characteristics were measured in both regimes, event timing and time intervals measurement. The entire timing unit was closed in box and the temperature sensor was glued to the TDC-GP1 chip. First the devices (power supply, GPS receiver, Stanford pulse generator) were more then one hour switched on to warm up. Then the timing unit was connected to a power supply and the epochs/time intervals were measured. As a source of events the programmable output from GPS receiver was used and the repetition rate of 100 Hz was set. Graph in Figure 6 illustrates the warm up characteristic of the timing unit in event timing regime. Each point represents average over 255 samples. The start temperature was 23.4 °C and it increased up to 38.4 °C, which gives the temperature change of 15 °C. The time has changed about 2.5 ns during 1500 s. It gives the change of 167 ps/°C.

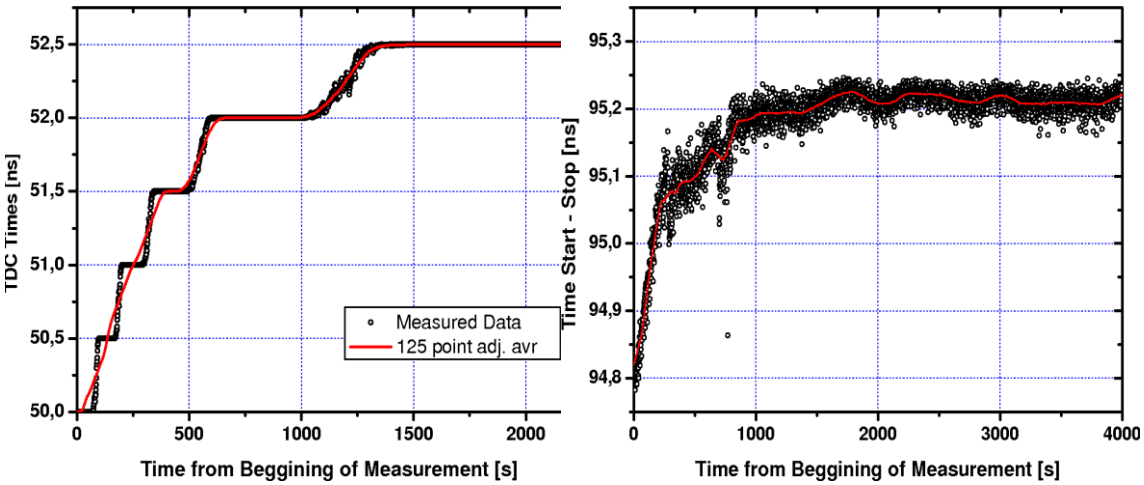

Figure 6. The first graph shows the warm up characteristics of the timing unit in event timing regime. Each point represents average of 255 samples. The second graph shows the warm up characteristics of timing unit in start - stop regime. Each point represents average of 255 samples.

Completely different results have been obtained in start - stop regime. The start temperature was 26.6 °C and in the end of the measurement it was 37.0 °C, which gives the temperature change of 10.4 °C. As a source of time intervals the Stanford digital pulse generator was used. The measured time intervals were averaged through 255 samples and a graph was plotted (see Figure 6). The average value of measurement has changed by 400 ps over 2000 seconds. It gives the change of 38 ps/°C.

The both regimes has been measured over 2000 sec in event timing regime and over 4000 sec in time intervals measurement to investigate the long term stability. The repetition rate was

set to 100 Hz and averaging over 255 samples was applied. The results are shown in Figure 7, y-axis represents time, which was obtained from epochs or time intervals.

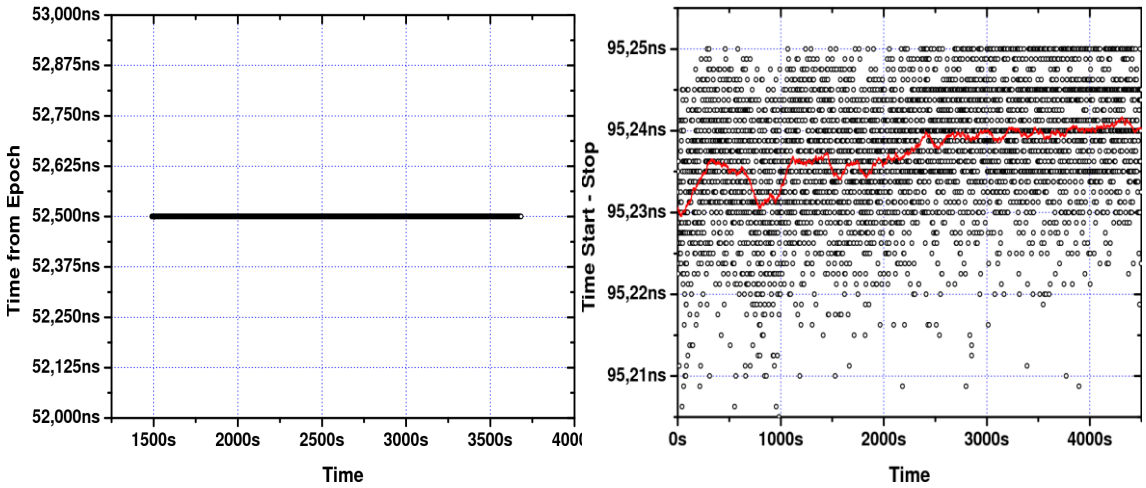

Figure 7. The first graph shows the long term stability of event timing. Each point represents average over 255 points. The second graph shows the long term stability of time intervals measurement. Each point represents average over 255 points and adjacent averaging over 100 points was applied.

Conclusion

By here the development of the event timing and time of laser fire device was presented. The timing unit is based on three chips, time interpolator - time to digital converter TDC-GP1, Complex programmable logic device (CPLD) ispLSI1032 and microcontroller PIC18F4620 which controls the entire timing unit. The timing unit can operate in two modes. The default mode is the event timing, which is realized by a counter which overflows every 30.5 hours. The second is the time intervals measurement of maximum 7.6 μs. The input signal pulses of TTL, NIM can be used. The whole signals can be connected using SMA connectors. The complete set of programs were presented and discussed. This work provides the set of measurement - linearity measurements, warm up characteristics and long term stability. The foreseen application of the timing unit is Lunar Reconnaissance Orbiter project and the unit can be used in one way ranging experiments.

References

[1.] Acam Messelectronic gmbh, WWW: http://acam.de/

[2.] Jan McGarry, Lunar Reconnaissance Orbiter, WWW: http://www.oca.eu/gemini/ecoles_colloq/colloques/ilrs2007/PresentationsPdf/4_Session.pdf/$.1_McGarry_LRO.pdf

[3.] ispLSI 1000EA Family Architectural Description. http://www.latticesemi.com/, Oct. 2001.

[4.] Microchip, PIC18F2525/2620/4525/4620, Data Sheet, Enhanced Flash Microcontrollers. http://microchip.com/, 2004.

Photon counting detectors for future laser time transfer missions

Ivan Prochazka, Josef Blazej
Czech Technical University in Prague, Czech Republic
prochazk@fjfi.cvut.cz /Fax +420 224 922 822,

Abstract

We are reporting on research, development and indoor tests of the photon counting detectors that are being developed in our lab for future space missions related to precise time transfer by laser pulses. The detectors are optimized for an on-board detection and precision time tagging of an incoming laser pulse. The key parameters of the detectors are: detection delay stability, broad operation temperature range, capability to operate under high background photon flux, radiation tolerance, mass and power consumption and overall ruggedness. The timing resolution, detection quantum efficiency and the dark count rate are of lower importance. The most challenging requirements are the detection delay stability of the order of units to tens of picoseconds within the temperature range of -30 to +50 C and the detection delay stability under the conditions of extremely high background photon flux well exceeding 10^8 photons per second hitting the detector active area. The detectors are based on the K14 SPAD chips. The new active quenching and gating electronics has been developed, it enables the operation in both gated and non gated modes. In a gated mode the detector is capable to operate – detect individual photons – under the condition of background photon flux exceeding 10^9 (!) photons per second.

Detector space application

One of the many attractive applications for solid state photon counters [1-3] in space is the technique of the time transfer by means of laser pulses. Two projects of time transfer by the laser pulses are in preparation. The Time Transfer by the Laser Light (T2L2) project has been completed by the French group [4]. The Laser Time Transfer (LTT) project was prepared by the Academy of Sciences of China [6]. The project is a spin-off of the existing projects of laser ranging of artificial Earth satellites [9]. The range is determined on the basis of the measured picosecond laser pulse propagation time toward the target satellite and back again. The epoch of transmission of laser pulse is monitored with respect to the local clock for each range measurement. For the time transfer by the laser light the existing satellite laser ranging ground stations will be employed, and new satellites have to be constructed and launched. The satellites are be equipped with retro reflectors and with an optical detector of laser pulses. The satellite range is measured by laser ranging to the on board retroreflectors. In addition the arrival time of the laser pulse to the satellite is recorded by stable on board clock and the recorded time tags will be transmitted to ground via satellite telemetry channel. Once the range and time tagging measurements have been received from several ground stations, combining the laser pulse emission times, propagation delays and satellite arrival time differences, the local clocks at the stations may be compared. The satellite laser ranging (SLR) technique has been well developed in recent years, ranging and epoch timing precision of the order of 1×10^{-11} seconds may be achieved. The range is related to time interval via the speed of light, one millimeter range corresponds to 6.7 picoseconds of two way propagation time. The accuracy of the range measurements is limited mainly by the atmospheric propagation delay model. Its accuracy is high, the absolute error expected to be well below

4×10^{-11} seconds. This accuracy is at least one order of magnitude better in the optical region than in the radio frequency wavelength region [9]. This is the main reason time transfer by laser light technique has been selected for the accurate comparison of time scales [4].

The average optical signal intensity on the LTT satellite is 1 photo-electron per event. The photon counting approach to the optical detection greatly simplifies the optical detector design – the analogue components of the detection chain are completely avoided. The incoming optical signal is selected in wavelength using blocking grass only. The effective optical band pass filter width is 10 nm. This setup results in both detector simplicity and its long term stability. Omitting the collecting optics simplifies the device design and its optical alignment, reduces the device mass and radiation damage problems associated with the optical components in space. The background photon flux conditions vary by several orders of magnitude. The relatively broad field of view of 28 degrees and the optical band pass filter required represent a challenge for signal to noise ratio of the entire experiment. In the very rare situations, when the satellite is moving in the Earth's shadow and when in the detector field of view is the non illuminated Earth's surface only, the background photon flux is well below $1*10^5$ photons per second. For the situation, when the detector is pointing toward illuminated Earth's surface, the background photon flux may reach $3*10^8$ photons per second. In the case when the Sun is within the detector field of view, what is quite common situation, the background photon flux exceeds $5*10^{10}$ photons per second. That is why the photon counting detector is required to operate under extremely high background photon flux conditions.

Detector concept

For the joint project with the Shanghai Observatory, Academy of Sciences of China, we developed the detector package dedicated to the project of synchronizing the hydrogen masers based time scales by laser pulses [12]. The detector key parameters were defined by the Laser Time Transfer project requirements as follows: active quenching, active area 25 μm in diameter, resolution 200 picoseconds FWHM, quantum efficiency 10 % at 532 nm, temperature range –20 … +65 ^oC. In comparison to other application of SPADs, the requirements on the detector dark count rate, detection efficiency and timing resolution are modest. Rather high dark count rates of the order of ~ 10^4 counts per second may be tolerated in the real operation, the background photon flux will be anyway substantially higher than the detector dark count rate. A detection efficiency of 10 % is acceptable thanks to the energy balance of the entire experiment and the signal to background noise ratio. The modest timing resolution requirement is a consequence of the existing ground segment parameters. However, the detection delay stability is a key parameter of the detector; the stability must be within +/– 25 picoseconds over the entire operating temperature range. The Single Photon Avalanche Detection (SPAD) chip manufactured using the K14 technology on silicon has been selected [11]. Our experience of previous space applications influenced this selection. The Active Quenching and Gating Circuit (AQGC) based on ECL logic is used. It allows the operation of the detection diode within the range of 0.2 to 1.1 Volts above its break down voltage. For operation in space a bias of 0.7 Volts above the breakdown voltage was used. This voltage above the break down voltage provides the desired timing resolution of 200 picoseconds Full Width Half Maximum (FWHM) and a detection efficiency of 10 % at 532 nanometres. The detector dead time was set in the quenching circuit to 160 nanoseconds.

The detector is successfully operating on-board the Compass M1 – Beidou satellite since its launch April 14, 2007 [13]. However, high background photon flux is strictly limiting data

yield, timing resolution and timing biases, as well. That's why, the new concept of the detector and its AQGC was developed. The detector is capable of both gated and not gated operation, switching between both modes does not cause any detection delay change. The block scheme is in Figure 1.

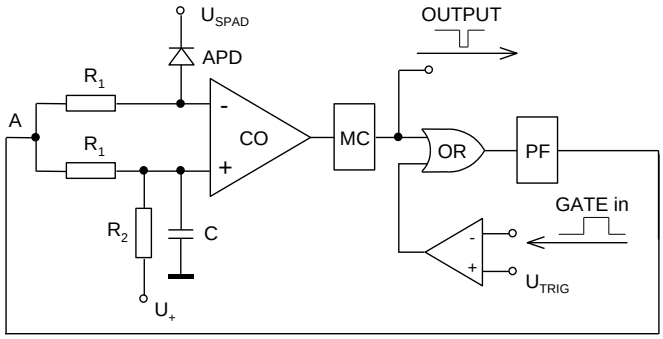

Figure 1. The active quenching and gating circuit block scheme**.**

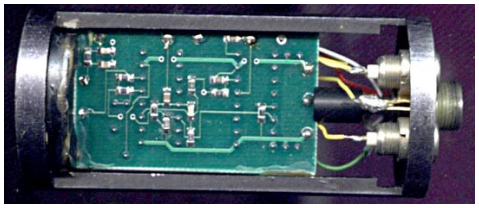

Figure 2. Laboratory sample of the detector package, board is installed in the coaxial holder. The SPAD detection chip is on the left, the SPAD chip is located in the left cylindrical holder.

All the logical components are formed using available space qualified fast ECL comparators. The laboratory sample of the detector with the AQGC is in Figure 2.

Detector basic characteristics tests

The detector has been tested in a conventional scheme of Time Correlated Photon Counting (TCPC). The picosecond laser diode Hamamatsu C4725 providing 42 ps wide pulses at 778 nm has been used as a signal source. The timing chain consisted of an ORTEC Time to Amplitude Converter 566, feeding data to a multi-channel analyser card in a personal computer. The timing resolution of the entire chain is 50 picoseconds Full Width at Half Maximum (FWHM). The timing resolution of the detector is typically < 100 ps FWHM for both operation modes.

The dark count rate of the detector in the not gated mode as a function of SPAD detector temperature is in Figure 3.

The operation of the detector under the conditions of extremely hight background photon flux was tested in the TCSPC set-up, see Figure 4. Note the bulb brightness and the fact, that the detection chip is located in the white cylinder in the right without any spatial or frequency filtering and optical attenuation. The laser diode signal was attenuated using a neutral density filters stack (silver rings, left from the bulb) down to the average signal level of single photons on the detection chip aperture.

The set of TCSPC experiments was carried out for various background photon flux level. The resulting main parameters- the data yield, timing resolution and detection delay stability are plotted in Figures 5 and 6 for gated and not gated operation respectively. The measurements in a gated operation mode were arranged in such a way, that the detector was gated ON 30-35 nanoseconds prior to arrival of photon of interest. The data yield was normalized to unity corresponding to the situation of low background photon flux. This situation simulates the best possible gating strategy for the foreseen application – synchronization of the clock in space using laser pulses. The experiment was carried out at rather low repetition rate of 1kHz to simulate low repetition rates of the proposed experiment. The timing resolution in the form

of r.m.s. (root mean square) jitter of the detection delay for the gated operation and in the form of Full Width Half Maximum (FWHM) for the not gated one. For normal data distribution, the FWHM value is 2.3 times the r.m.s. value. The detection delay is referred to different origin in the gated and not gated measurement series.

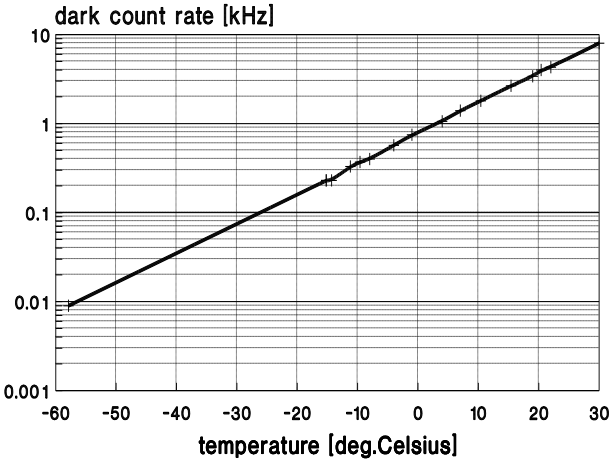

Figure 3. The detector dark count rate as a function of chip temperature, SPAD 25 um in diameter biased 0.7 V above, the slope corresponds to a drop of dark count rate of one decade per 30 K.

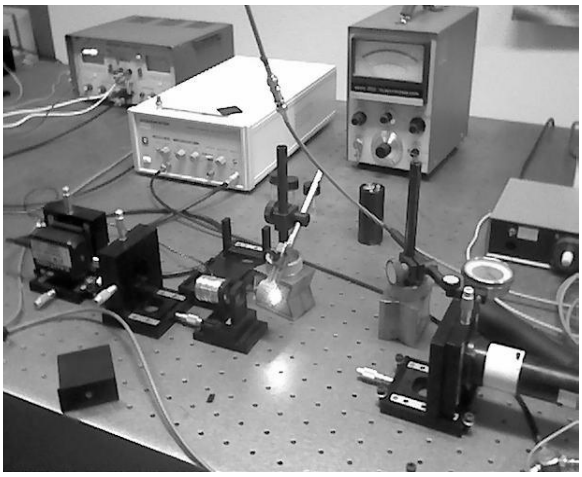

Figure 4. The TCSPC experimental setup. Left to right: laser diode, collimating optics, neutral density filters stack, tungsten bulb, SPAD detector holder on X-Y-Z stage. The tungsten bulb (bright in the middle) is used to generate

Several serious conclusions may be made on the basis of experiments mentioned above:

- the detector is operational in both gated and not gated modes in the presence of a background photon flux exceeding $2 * 10^9$ photons per second hitting the active area

- the data yield is dropping down with background photon flux intensity due to photon counting statistics (as expected) and due to after-pulsing effects in the case of not gated operation mode.

- in the gated operation mode, the detection delay and timing resolution are stable independent on background photon flux within measurement errors.

- from all the studied parameters point of view, the use of gated operation mode is favourable in comparison to the non gated one

To demonstrate the detector capability in the gated mode, the analogical TCSPC experiment was carried out with even stronger background illumination reaching $5 * 10^9$ photons per second. Gating the detector 5-6 nanoseconds before the photon of interest arrival the relative data yield of 0.02 was obtained, while the timing resolution and detection delay remained unchanged even for this extremely high background photon flux.

Conclusion

The optimized detector is able to detect single photon events in both gated and not gated operation modes. The timing resolution is 200 psec FWHM, dark count rate is below 10 kHz and the timing stability is of the order of 10 psec. The detector is capable of operation under the conditions of extreme background photon flux conditions reaching $2 * 10^9$ photons per

second hitting the detector active area in both operating regimes. For background photon flux exceeding 10 millions photons per second, the gated operation mode is preferable. The gated operation mode enables us to operate the detector at the background photon flux exceeding 5 * 10^9 without scarifying the detector timing performance. The detector design and construction is a promising candidate for the next phase of the space project of Laser Time Transfer recently under preparation in China.

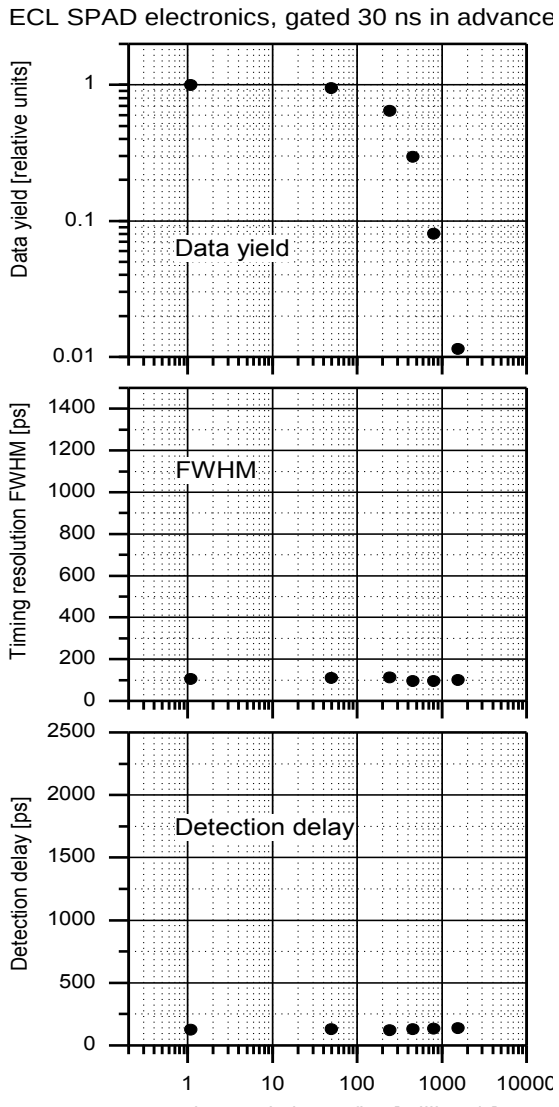

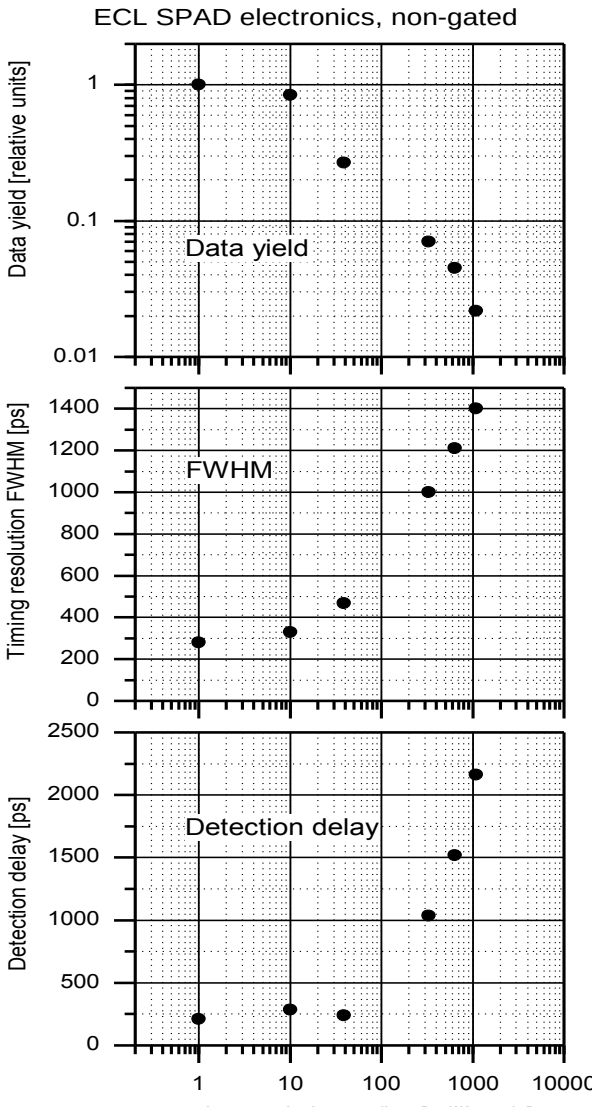

Figure 5 (left). The results summary of TCSPC experiments, SPAD gated 30 ns before arrival of photon of interest, data yield (up), timing resolution r.m.s. and detection delay (bottom) versus background photon flux intensity in millions per second hitting the detector active area.

Figure 6 (right). The results summary of TCSPC experiments, SPAD not gated, data yield (up), timing resolution FWHM and detection delay (bottom) versus background photon flux intensity in millions per second hitting the detector active area.

Acknowledgement

This work has been carried out at the Czech Technical University in Prague. Numerous grants were provided by the Czech Grant Agency, Czech Technical University in Prague, the Czech Ministry of Education, and by international agencies. Recently, the research and development of solid state photon counting detectors and their applications is supported MSM6840770015. The contribution of Lukas Kral is acknowledged.

References

[1] S. Cova, IEEE J. Quantum Electron. **19**, pp. 1211–1218 (1983).
[2] I. Prochazka, K. Hamal, B. Sopko, J. Mod. Opt. **51** 9–10, pp. 1289–1313 (2004).
[3] I. Prochazka, K. Hamal, S. Pershin, Proc. SPIE **4546**, pp. 64–65 (2002).
[4] M. Ravet, *et al.*, online at: http://www.roa.es/14workshop-laser/#Presentations (accessed 10th Nov 2005).
[5] E. Samain, Available online ahttp://cddisa.gsfc.nasa.gov/lw13/docs/papers/detect_samain_1m.pdf Y. Fumin, private communication, Shanghai, China (2005).
[6] T. Y. Huang (editor), *Proceedings of the First International ASTROD Symposium on Laser Astrodynamics,* published in Int. J. Mod. Phys. D **11** 7, pp. 1035-1048 (2002).
[7] J.J. Degnan, paper presented at the 12th International Workshop on Laser ranging, Matera, Italy, November 2000; available online at: http://geodaf.mt.asi.it/html/news/iwlr/ J.J. Degnan, in Contribution of Space Geodesy to Geodynamics – Geodynamics Series **25** (American Geophysical Union, Washington, 1993), edited by D.E. Smith and L.Turcotte, pp. 133–162.
[8] X. Sun, *et al*., J. Mod. Opt. **51** 9–10, pp. 1333–1350 (2004).
[9] I. Prochazka, *et al.*, Inst. of Physics, Series No. 126, Bristol and Philadelphia, pp. 147–149 (1991).
[10] [?? A Prochazka, I., Hamal, K., Kral, L **Journal of Modern Optics,** Vol. 54, No.2-3, p.151-162, 2007
[11] Yang Fumin, et al, http://www.oca.eu/gemini/ecoles_colloq/colloques/ilrs2007 /PresentationsPdf/8_Session.pdf/8.2_Fumin_LTTExperiment.pdf [accessed May 20,2008]

Potentialities of Common-used TDC Chips for High-Speed Event Timer Design

E.Boole, V.Vedin.
Institute of Electronics and Computer Science, Riga, Latvia
buls@edi.lv

Abstract

Potentialities and drawbacks of the off-the-shelf Time-to-Digital Converter (TDC) chips for building high-speed event timers are considered. To overcome the main shortcoming of TDCs, which is their limited measured interval range, a new technique to obtain the continuous and unlimited time scale is proposed and realized in a pilot version of a TDC-based high-speed event timer. The performance parameters of the pilot device such as RMS resolution vs. aggregate input event rate, non-linearity of time interval measurement between adjacent events, and non-linearity of event instance measurement have been evaluated. It is noted that, although the results show applicability of TDC chips for Laser Ranging related applications, the performance of the TDCs is still not up to the mark and might be improved.

Introduction

During last years the chips called Time-to-Digital Converters (TDC) became available on the market. Such chips provide time interval measurements with high event rate and multiple input channels with independent control. The independent channels allow measuring very short time intervals between Start and Stop events, including small negative time intervals. The chips employ digital interpolation circuitry, which allows achieving a very short dead time for each input channel. As a rule the dead time is limited by maximum write rate of internal buffer memory. Some TDC chips have arithmetic logic unit that are used for interpolation data preprocessing, including the averaging of results to increase the precision.

One of the best TDC products is the chip TDC-GPX from ACAM Mess-electronic Gmbh. It offers several modes with different resolution and available number of channels. The mode with 8 LVTTL channels for Stop events offers typical RMS resolution of 81 ps and up to 182 MHz burst event rate for each channel (up to 32 events in one burst). Continuous average aggregate (for all channels) event rate in this mode is up to 40 MHz. Such rate can be supported by employing fast PC buses or new generation interfaces, for example USB 3.0. For lower average aggregate rates up to 15 MHz could be used existing interfaces: USB 2.0, FireWire. In the most accurate measurement mode only two LVPECL differential inputs for Stop events are available. In this mode 10 ps RMS resolution can be obtained - although, at relatively low event rate (up to 500 KHz).

The main drawback of TDC chips is that they are implemented according to the traditional time interval measurement technique and have a limited time interval measurement range. It means that they cannot be used directly to build true Event Timers. The goal of this work was to solve that problem and develop a high-speed TDC-GPX-based Event Timer with unlimited time range. The other goal was to evaluate potentialities and actual performance of such Event Timers.

Constructing of Unlimited Single-valued Time Scale

To solve the problem of the limited measurement range the manufacturer of TDC-GPX offered the possibility of an internal Start generation with controlled periodicity for a time counter re-triggering. Additional Restart counter allows to extend the measurement range up to 1.28 ms. The simplified block diagram of this mechanism is shown in Fig. 1.

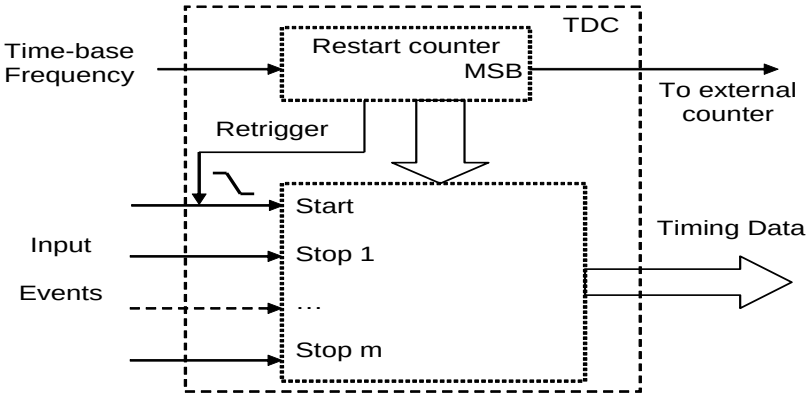

Figure 1. A TDC with Additional Restarting Circuitry

The manufacturer suggested to count the most significal bit (MSB, Fig.1) changes in the external counter to get the unlimitted measurement range. Such simple way to extend the range can not be easily realized due to the problems with correct data reading, especially at high event rates. Indeed, if the user just directly employs an external counter, the state of the counter should be read at the moments when the input events arrive. It may lead to errors of association between codes that are written into the internal FIFO and those read from the external counter (so-called timing uncertainty) into some external FIFO. Even if such design is done correctly, with the use of a proper circuitry of timing uncertainty ellimination, it nevertheless is bulky and may degrade the accuracy performance of a timer. Besides, the amount of data to be transferred increases according to the required time scale extension length. And finally, the timeless measurement range cannot be obtained at all.

To solve this problem we have come to a different solution (Artyukh[1], 2008). One measurement input of the TDC was assigned as a specific marker input (see Fig. 2). The MSB signal of the restart counter is delayed (to avoid any timing uncertainty (Беспалько, 1985)) and then is fed into this input. The marker input is configured for accepting both positive and negative edges. In this way we insert specific marker events, corresponding to transitions of the MSB of the restart counter, into the output digital data stream that is transmitted further (into some controller block based on μC, CPLD or FPGA).

The constructing of single-valued time scale could be done either by the controller block firmware or by PC software where the data finally come in most of applications. The firmware or software detects the marker measurement data blocks and constructs the extension time scale simply as a variable to use for composing resultant time stamps. When it is done on a PC, this solution not only allows constructing practically limitless single-valued time scale by means of software but also substantially reduces the amount of transferred data for high rate event streams.

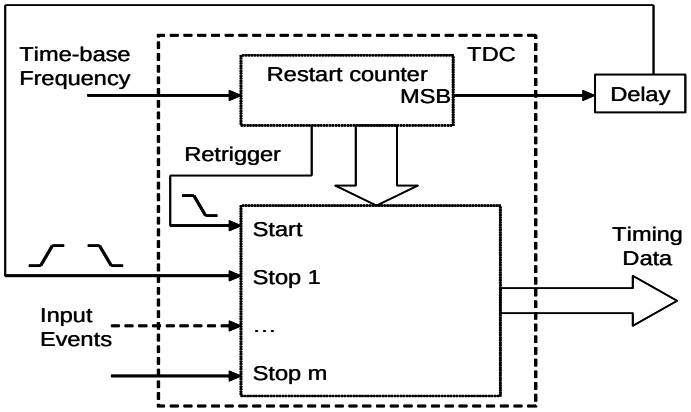

Figure 2. A TDC with Restarting and Marker Event Insertion Circuitry

Event Timer Implementation

The described method was realized in a pilot model of 6-channel High Speed Event Timer (HSET) with unlimited range of time measurements. The HSET Block diagram is shown in the Fig.3. HSET employs the TDC-GPX as its main measurement core. All settings and data exchange in accordance with the TDC-GPX functionality and controls functions, issued from the PC, are implemented by a control block, which is written in VHDL and realized on a Cyclone II FPGA from Altera Corp. USB chip (CY7C68013A from Cypress Semiconductor Corp.) memory is used as a buffer memory for control data transfer into TDC-GPX and for measurement data accumulation. The HSET is a PC based instrument and communicating with the PC is done via USB port (USB 2.0 High Speed).

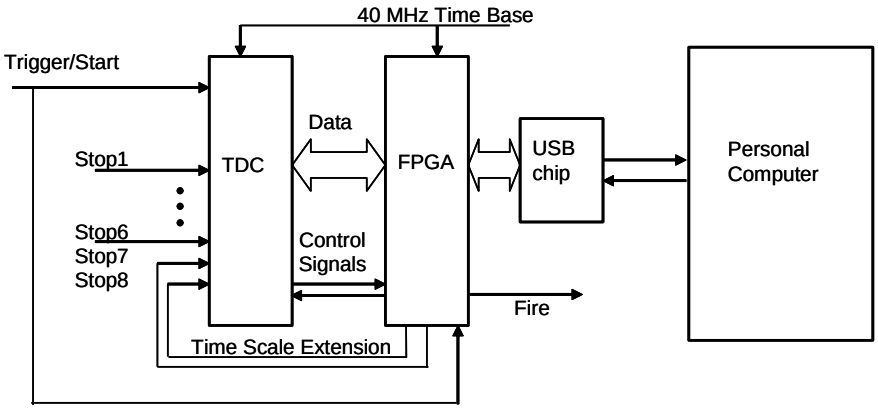

Figure 3. HSET Block Diagram

PC software for interacting with the HSET is written in C under National Instruments LabWindows/CVI. The latter includes means for USB interface configuring, programming, and interacting according to the Virtual Instrument Software Architecture. Specialized HSET software comprises program functions that support control and data read operations for HSET. These functions can be incorporated into application-specific timing system. They were included into the programs for evaluating the HSET performance characteristics. The methods and techniques for performance evaluation were presented in (Artyukh[2], 2008; Boole, 2007).

Photography of the HSET front view is shown in Fig. 4. There are 4 input channels and Trigger/Start input on the front panel. Two more channels, time-base input and some additional connectors are placed on the rear panel.

Figure 4. A Photo of HSET

Evaluation of HSET Characteristics

To evaluate the RMS resolution of HSET a direct repetitive measurement of test signal with low jitter was performed. The generator (ROHDE&SCHWARZ SML 02) was used to generate a stable signal with RMS jitter less than 10 ps. This signal was connected to one channel, then it was split into two and four channels for increasing the burts aggregate event rate up to 600 millions events per second.

In the process of HSET evaluation it was noticed that its RMS resolution considerably varies from 60 ps to 310 ps depending on the amount of employed channels and the aggregate event rate (see Fig. 5). The main reason of the resolution degradation is the on-chip PLL performance degradation caused by internally induced noises, especially at high-intensity bursts.

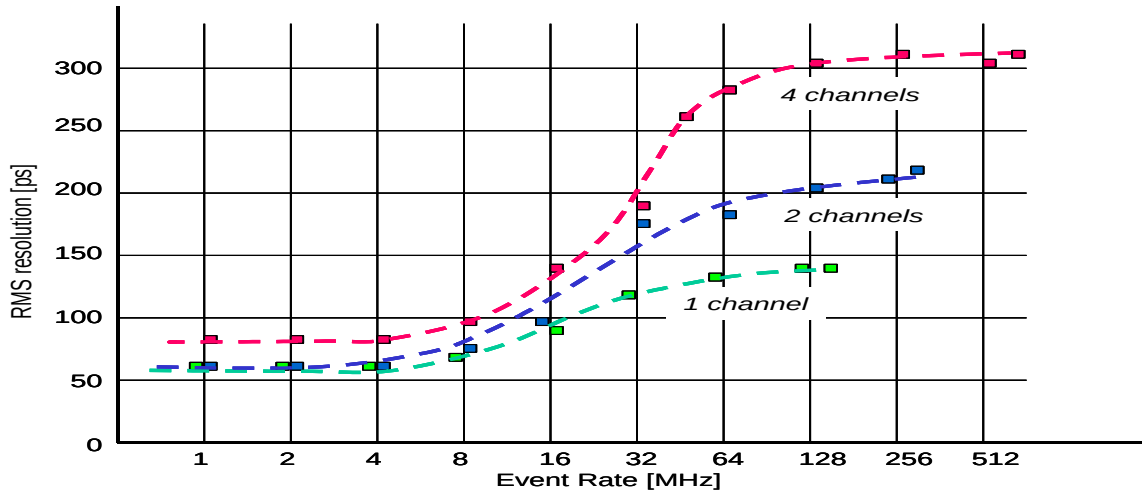

Figure 5. RMS Resolution vs. Aggregate Input Event Rate

It was anticipated that there should be cross correlation between events coming in different channels in the case of short time intervals between them. The statistical testing approach [3] shows that such correlation exists and causes noticeable non-linearity of time interval measurement between adjacent events (see Fig. 6).

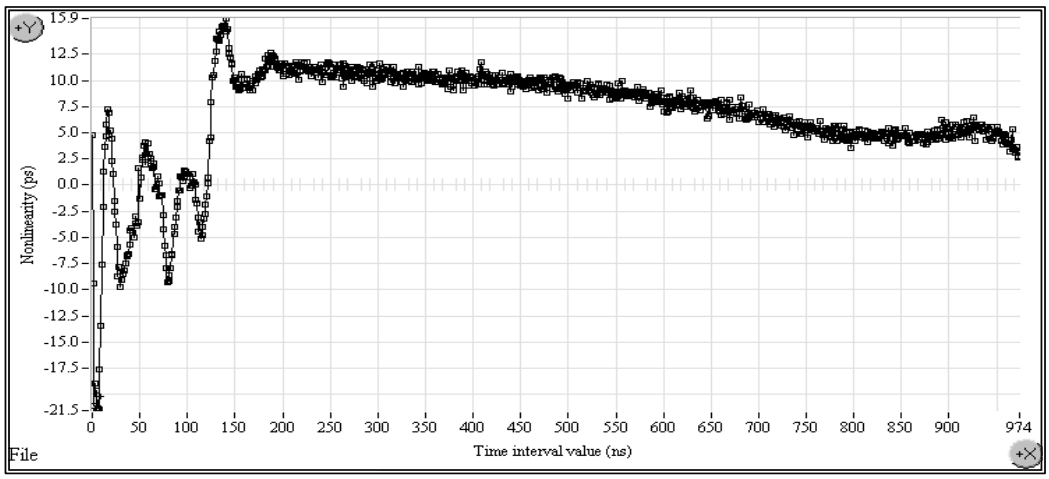

Figure 6. Non-linearity of Time Interval Measurement

Taking into account, that the RMS resolution of the timer is about 60-90 ps at low and medium aggregate input event rate (up to 6…8 MHz), the non-linearity error is regarded as settled and non-essential for intervals more than 150-200 ns.

One of the components of RMS resolution is the integral nonlinearity of the timer [4]. Noticable dependence of the event instant measurement error on the instant relative position within the interpolation interval was detected in the process of integral nonlinerity evaluation of HSET.

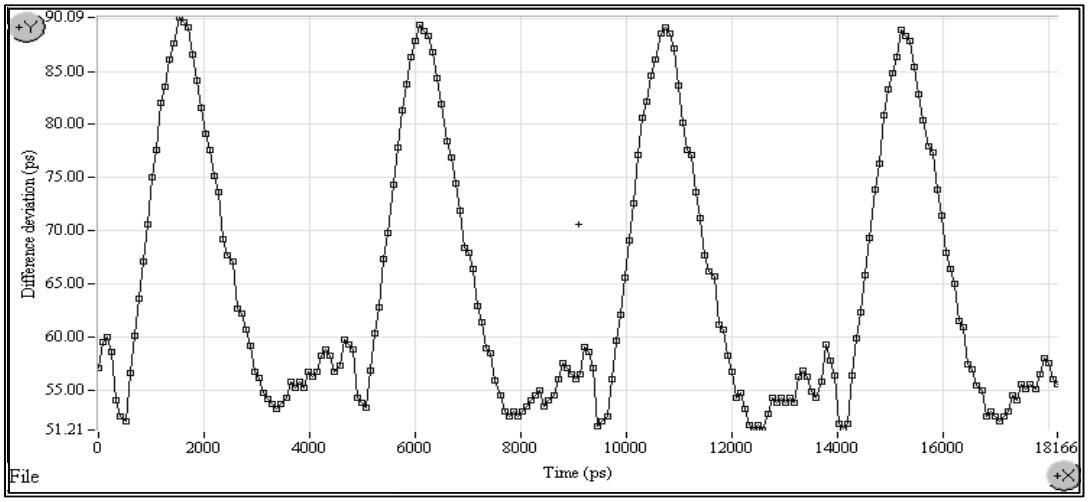

Figure 7. Non-linearity of Time Measurement

The graph in Fig.7 reflects the non-linearity of the TDC-GPX discrete interpolator over 4 periods of its operation. The peak-to-peak non-linearity error is about 40 ps and it is one of the error components of the evaluated RMS resolution.

Conclusions

Generally it can be concluded that some of currently available commercial TDC chips (such as TDC-GPX) are applicable for event timer designs that target the applications where compact implementation and high rate of multi-channel event timing are mostly needed.

As for the achievable resolution, it is not up to the mark (especially at very high event rates); the existing limitations are caused by imperfectness of TDC-chip realization. It seems that a custom design of a TDC chip, specificlly tailored for building the true event timers (in cooperation with a manufacturer), may lead to much better results.

The High-Speed Event Timer designed in the framework of the presented research offers a good price/performance ratio as compared to the commercially available devices of such kind. We hope that this can make it (or its options) attractive for the applications related to Laser Ranging.

References

Artyukh[1] Yu., Vedin V. Constructing of Unlimited Single-valued Time Scale for TDC-based Event Timers// Electronics and Electrical Engineering, ISSN 1392-1215, 2008, No.4(84), pp. 17-20.

Artyukh[2] Yu., Bespal'ko V., Boole E.. Non-linearity errors of high-precision event timing // Automatic Control and Computer Sciences, 2008, Vol. 42, No. 4, pp. 191-196.

Беспалько В. А., Ведин В. Ю. Устранение неоднозначности в комбинированных время-цифровых преобразователях. // Метрология. - 1985.- № 9. - С. 9-15.

Boole. E. The characterization of the Riga Event Timer A032-ET. - ILRS Fall 2007 Workshop, 25-27 September, Grasse, France.

Progress in sub-picosecond timing system development

Ivan Prochazka, Petr Panek
Czech Technical University in Prague
prochazk@fjfi.cvut.cz / Fax +420 224 922 822,

Abstract

We are reporting on research, development and indoor tests of the novel principle event timing system based on Surface Acoustic Wave (SAW) filter excitation as a time interpolator. Its operating principle is based on the fact that a transversal SAW filter excited by a short pulse can generate a finite signal with highly suppressed spectra outside a narrow frequency band. If the responses to two excitations are sampled at clock ticks, they can be precisely reconstructed from a finite number of samples and then compared so as to determine the time interval between the two excitations. We have designed and constructed a two-channel device which allows independent timing of two events. The device has been constructed using commercially available components, it is built in a standard 19'' rack of 2 unit height. The inputs are two NIM signals for epoch channels A and B and the 100MHz or 200MHz clock signal. The device is interfaced using USB type 1 interface to a host personal computer for data acquisition and processing. We have assessed the single-shot event time measurement precision of 0.9 ps r.m.s. per channel. The device exhibits extremely high timing linearity; the non-linearity is well below +/- 0.2 ps over an entire interpolator range. The temperature drift of the measured time interval is lower than 0.5 ps / K, the long term stability is typically better than +/- 0.03 ps per hour. These are to our knowledge the best values ever reported. These values were measured on the first prototype constructed without any additional temperature compensation or stabilization. The theoretical measurement dead time is 10 microseconds, the maximum continuous measurement rate is 300Hz. The limiting factor is the data transfer and computing power of the connected PC.

Introduction

The "time interval" (TI) or "time of arrival" (TOA) measurements are commonly used in a number of experimental techniques. We do report on construction of a time interval measurement device dedicated for application in extreme accuracy satellite laser ranging system. This application requires the picosecond timing resolution and precision as well as sub-picosecond timing device stability with respect to aging, temperature and other external influences [1].

All the high-resolution time interval meters are based on time interpolation. Traditional time interpolation methods can be found in comprehensive overviews [2], [3]. These methods usually utilize interval to voltage increment conversion, different variants of vernier principle or on pulse propagation through tapped delay lines. At the present time, the last of these methods is frequently used [3]-[5]. A novel time interval measurement method that makes use of a transversal SAW filter as a time interpolator has been introduced in [6]. The method is based on the fact that a transversal SAW filter excited by a short pulse can generate a finite signal with highly suppressed spectra outside a narrow frequency band. It results from the sampling theorem that if the responses to two excitations are sampled at clock ticks, they can be precisely reconstructed from a finite number of samples and then compared so as to determine the interval between the two excitations. An analysis of the deterministic

measurement error – nonlinearity - of this method has been given in [7]. It results from the analysis that the method excels in time interpolation efficiency since the time-interpolation error relative to clock period is very small. In other words, an accurate measurement can be achieved even with relatively low clock frequency. A detailed analysis of all random errors is the subject of the paper [8]. It implies from the analysis that even in a single-shot measurement all the random errors can be partially suppressed. It is possible thanks to averaging effect as the interpolation process is not based on the only one but many observations.

The ultimate goal of our project was the time interval measurement device providing the picosecond timing performance, simple and rugged design, low mass and low power and last but not least, not requiring any adjustment and recalibration in the field operation. According to the theoretical analysis as well as numerical simulations the SAW filter technique should provide all the performance required.

Measurement device

The interval measurement device has been designed in a two-channel configuration [9]. This enables to determine the TOAs of two independent pulses in a local time scale. The time interval between these two pulses may be computed as a difference of the two TOAs. This set up enables to measure both positive and negative time intervals without any dead time. The block scheme of one channel of the device is shown in Fig. 1.

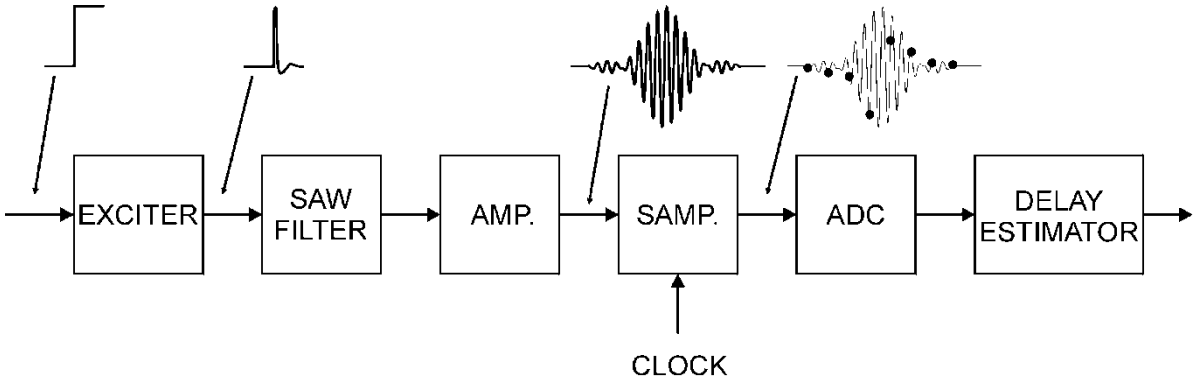

Figure 1. Architecture of the time interpolator based on SAW filter excitation

The external input pulses excite a transversal SAW band-pass filter whose output is sampled at clock ticks, see Fig. 2.

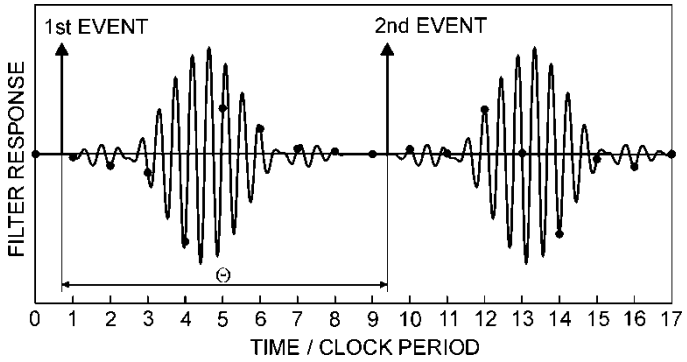

Figure 2. Sampled responses of the SAW transversal filter.

The samples are then converted by an analog to digital converter (ADC) and buffered. Once the external input pulse has been processed, the internally generated time mark is applied to the same circuit. This internal time mark is generated synchronously with the time base reference. After both responses have died out, they are reconstructed from the samples and then compared by means of cross correlation to estimate the time interval between the two events. All the processing steps can be integrated into a simple algorithm based on fast Fourier transformation (FFT). In Fig. 3 there is a photo of the prototype.

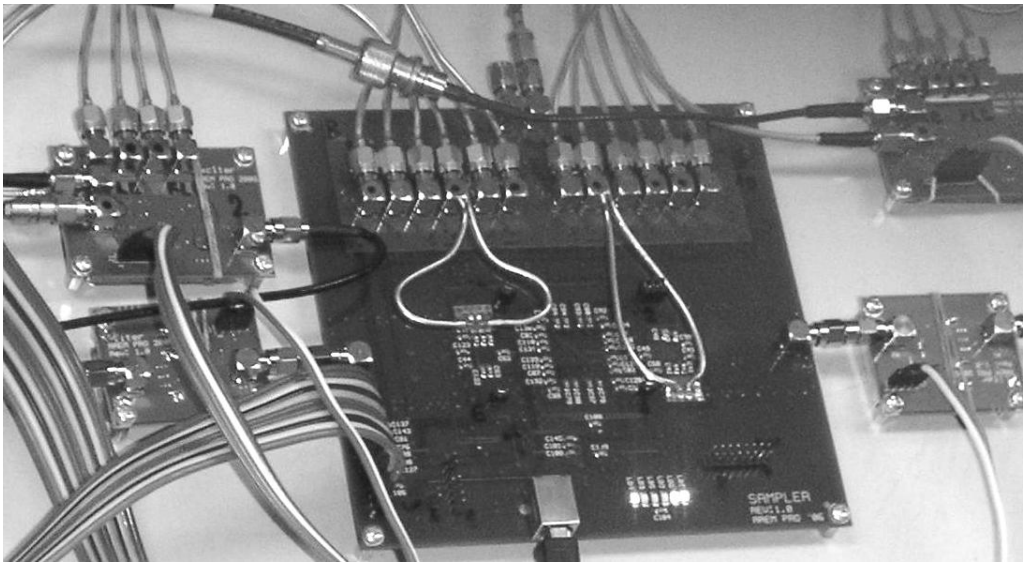

Figure 3. Photograph of the time interval measurement device prototype, the two timing channel version, the control, sampling, and communication module in a centre, the exciter modules in upper corners, the filter modules in lower corners.

The device consists of two exciter modules, two SAW filter modules and one control, sampling, and communication module, which is common for both channels. The device has been constructed strictly using commercially available components. The input and clock distribution circuits use the fast SiGe components to ensure low jitter and good delay stability. The other logical circuits use common CMOS components. Most of the device control, data collection, and communication functions are concentrated into a field programmable gate array (FPGA). The raw data from the device are collected via USB interface to a host computer where the TOAs and the length of time interval are computed. As the reference clock source we have used a frequency module built at the University of Applied Sciences, Deggendorf, Germany. This module provides 200 MHz LVECL clock signal with jitter below 1 ps rms. The filter response to the input time mark recorded by an oscilloscope is shown in the Fig. 4.

The upper trace shows the signal itself, the frequency spectrum of this pulse has been computed by the oscilloscope and plotted in a lower trace. The response is not longer than 500 ns and can be fully covered by 64 samples.

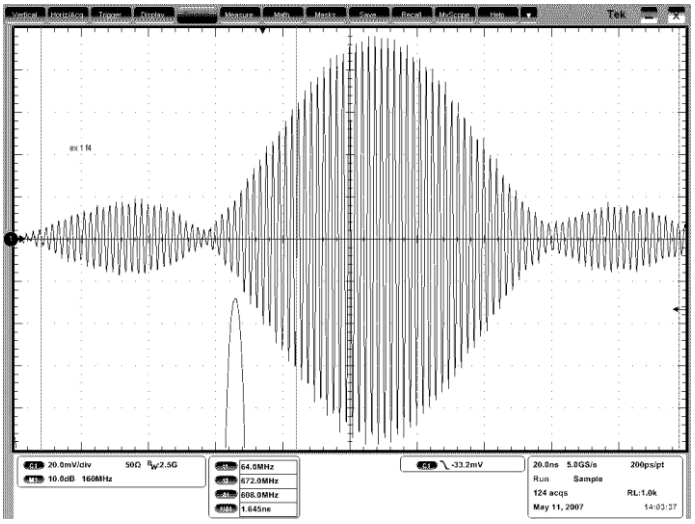

Figure 4. The shape of the output of the SAW filter (upper trace) and its frequency spectrum (lower trace), 2.5 GHz bandwidth oscilloscope, 10 ns/div, 156 MHz/div horizontal scale, 0.02 V/ div and 10 dB vertical scale.

Experimental results

The operational performance of the time interval measurements device has been proved by several tests. All the tests have been carried out in common laboratory environment. In the first test the both channels were triggered by the same time mark generated from an external fully asynchronous pulse generator. The repetition frequency of the time mark was set to ~10 Hz. The length of the trigger pulse active edge was to 100 ps. Due to different cable delays the channel B was triggered approximately 4.2 ns later than the channel A. We have taken sequence of 400 measurements. The measured TOAs and time intervals have been recorded and analysed. The resulting standard deviation of the time interval measurements is 1.3 ps. The histogram of the measured intervals is in Fig. 5. The error distribution is obviously close to normal.

The aim of the third test was verification of the long therm stability and the temperature dependence of the device. We have taken sequences of 400 measurements and evaluated the mean value from every sequence. We have completed series of measurements over the time interval of 4 hours after the device power on. Simultaneously we measured the temperature of the most critical component – the Exciter module. The results are plotted in Figure 6.

The device temperature raised for $+6^{o}$ Celsius within 30 minutes after power on and remained stable until the end of measurement. The drift of the mean value of the time interval is plotted as a function of time after power on. It can be noticed, that after the complete warm up, which takes several hours, the timing stability is excellent – the measured drift is better than +/- 0.03 picosecond / hour.

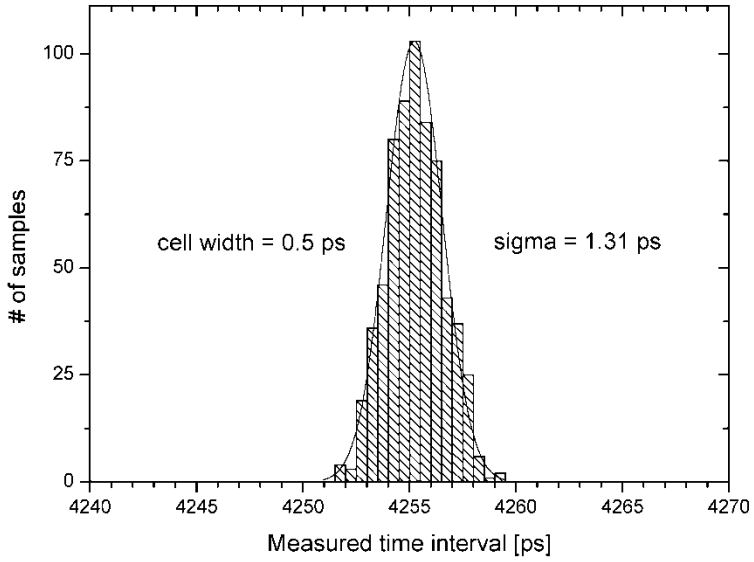

Figure 5. Histogram of time interval measurements. Times of arrival of pulses from the pulse generator have been measured on two channels. The time interval was evaluated as their difference. The generator output was passively divided into two equal pulses, these two pulses were fed to the channels A and B of the timing device using non-equally long cables. Horizontal scale is 0.5 ps per histogram cell, time units are picoseconds. The data distribution is very close to normal.

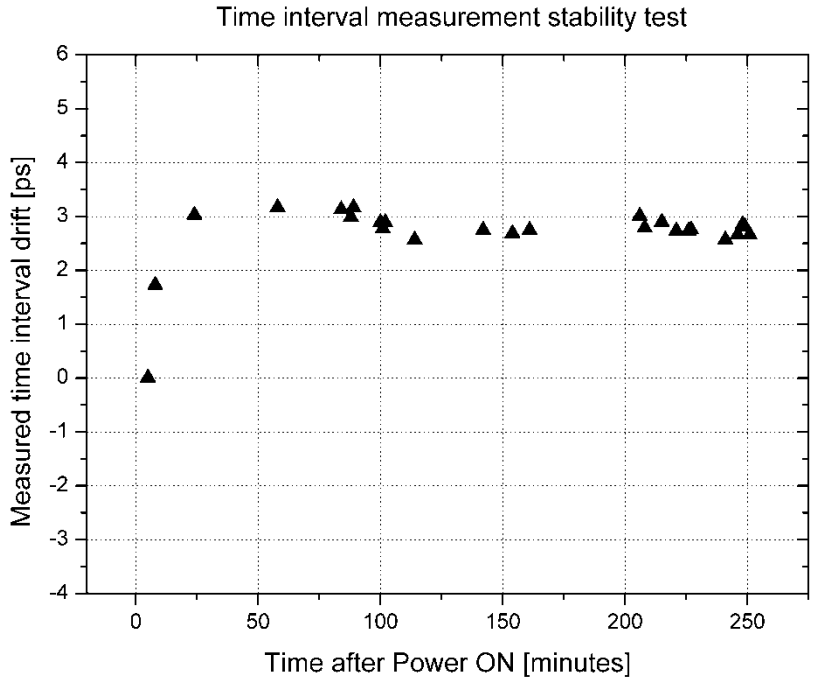

Figure 6. Temperature dependence and temporal stability of the time interval measurements. The device temperature raised for +6 K within 30 minutes after power on and remained stable until the end of measurement. The mean value of the series of 400 time interval measurements is plotted.

Summary and discussion

The goal of this work was to demonstrate the concept and capabilities of the new time interval measurement principle for picosecond precision timing. We have developed and constructed the time interval measurement device, which is based on a SAW filter as a time interpolator. The first results proved the concept. We have assessed the single-shot interval measurement precision of 1.3 ps rms which corresponds to the time of arrival precision of 0.9 ps rms in each channel. The error distribution is close to normal. The results are in good agreement with the error budget based on the theoretical analysis. We have identified the noise of the excitation as the source of the dominant contribution in the overall error budget. We suppose that after redesign of the excitation circuits the level of this noise can be reduced and the precision further improved. The temperature drift of the measured time interval on temperature is lower than 0.5 ps/K, the long term stability is better than +/- 0.03 ps per hour.

The entire device requires no calibration and parameter adjustment and hence it might be attractive also for applications, where long term stability, high reproducibility and low maintenance are obligatory. The time interval measurement system will be applied in the satellite laser ranging station with millimeter ranging precision.

Acknowledgements

This work has been carried out at the Czech Technical University in Prague. Recently, the research and development of high accuracy timing systems and their applications is supported by the Grant MSM6840770015. The authors are grateful to Josef Kolbl and Peter Sperber from Deggendorf for providing the 200 MHz clock source, Martin Kropik and Pavel Jirousek from the Czech Technical University in Prague for printed circuit boards design and device assembly, and Jiri Plasil for design of the measurement software.

References

[1] Král L., Procházka I., Hamal K. **Optics Letters**. 2005, vol. 30, no. 14, s. 1767-1769.
[2] D.I. Porat, *IEEE Trans. Nucl. Sci.*, vol. NS-20, pp.36-5I, Oct. 1973.
[3] J. Kalisz, *Metrologia.,* vol.4, pp. 17-32, Feb. 2004.
[4] M. Mota, J. Christiansen, *IEEE J. Solid-State Circuits,* vol.34, pp. 1360-1366, Oct. 1999.
[5] E. Raisanen-Ruosalainen, T.E. Rahkonen, J.T. Kostamovaara, *IEEE J. Solid-state Circuits, V*ol. 35, pp. 1507-1510, Oct. 2000.
[6] P.Pánek, U.S. Patent 7,057,978 B2, Jun. 2006.
[7] P. Pánek, *IEEE Trans. Instrum. Meas,* , vol. 57, no. 11, pp. 2582-2588, Nov 2008
[8] P.Pánek, *IEEE Trans. Instrum. Meas.*, vol. 57, no. 6, pp. 1244-1250, Jun 2008
[9] P.Panek, I.Prochazka, Review of Scientific Instruments, Vol. 78, No1, pp 78-81, 2007

Fast Switching Pockels Cell Driver for SLR Laser System

J. Kölbl[a], M. Fröschl[a], A. Seedsman[a], Y. Gao[b], M. Dawson[b]

[a]EOS Optronics GmbH, Ulrichsberger Str. 17, D-94469 Deggendorf, Germany
[b]EOS Space Systems, 111 Canberra Avenue, Griffith ACT 2603, Australia

Abstract

The presented research concentrates on the development of an ultrafast Pockels cell driver for use as part of an ultrafast, high repetition rate and high energy Laser system. Pockels cells can be used for regenerative amplifiers, pulse slicers (pulse picker), and other fast optical switching systems in SLR Lasers and other types of Laser systems.

The devised driver electronics for the actual Pockels cell is specifically characterized such that two Pockels cells can be connected and simultaneously driven with a fast slope of 9.5 kV in less than 11 ns, even at high Laser repetition rates of up to 2 kHz. By using a push-pull switching arrangement, a variable and low-jitter impulse width from 80 ns to 2.3 μs is achieved. Due to the drive capability of the circuit, more than one Pockels cell can be cascaded whilst maintaining very fast switching performance.

1. Pockels Cell

Pockels cells for ultrafast, high repetition rate, and high energy Laser systems require the electro-optic crystal material to exhibit virtually no piezo-electric effect with electrical signals between DC and 100 kHz. There should be no ringing superimposed on the transmitted optical beam passing through the crystal so that the Pockels cell can be utilized with high energy Lasers operating at high repetition rates, and therefore having a useful optical wavelength range from 350 nm to 4300 nm. For these reasons Rubidium Titanyl Phosphate - $RbTiOPO_4$ (RTP) is normally selected as the electro-optic crystal material for the Pockels cell. Unfortunately only a few companies in the world can grow good quality RTP crystals, and at the present time 7.5 mm diameter RTP based Pockels cell is the largest diameter that can be sourced commercially. Pockels cells with this size are not large enough for many of our high repetition rate and high energy Lasers.

New Beta Barium Borate (b-BaB_2O_4, or BBO) crystal based Pockels cells have been developed by EOS. BBO crystals can be grown at a much larger size than RTP. Furthermore, BBO crystals have a higher transmittance and lower insertion loss at visible and infrared wavelength regions, and a higher damage threshold than RTP. Pockels cells of diameter 8 mm, 12 mm, and 14 mm diameter Pockels cells have been designed, and developed. So far 8 mm and 12 mm Pockels cells have been assembled, tested, and used in our Laser systems successfully. All the design specifications have been achieved. These Pockels cells exhibit negligible piezo-electric ringing effect at repetition rate up to 10 kHz. These are some of the world's largest Pockels cells for ultrafast, high repetition rate and high-energy laser applications.

Testing of 14 mm BBO based Pockels cell is still in progress. The driver electronics for the Pockels cell is specifically characterized that two Pockels cells can be connected and simultaneously driven with a fast slope of 9.5 kV in less than 11 ns, even at high Laser repetition rates of up to 2 kHz.

Pockels cells are high-voltage controlled wave plates. As the speed of state change of the cell is quite important from a Laser system point of view, the terminal capacitance together with the quarter wave voltage are the key specifications. As the actual Pockels cell is an expensive device, an emulation device (high voltage capacitor) is used for development process of the driver electronics. It was found that the classical plate's capacitor formula can be used to estimate the Pockels cell's capacitance. An electromagnetic simulation is performed to verify that the capacitor's formula can be applied. As shown in Figure 1**,** the Pockels cell simulated capacitance yields 2.2 pF, whereas the popular capacitor's formula yields 1.8 pF.

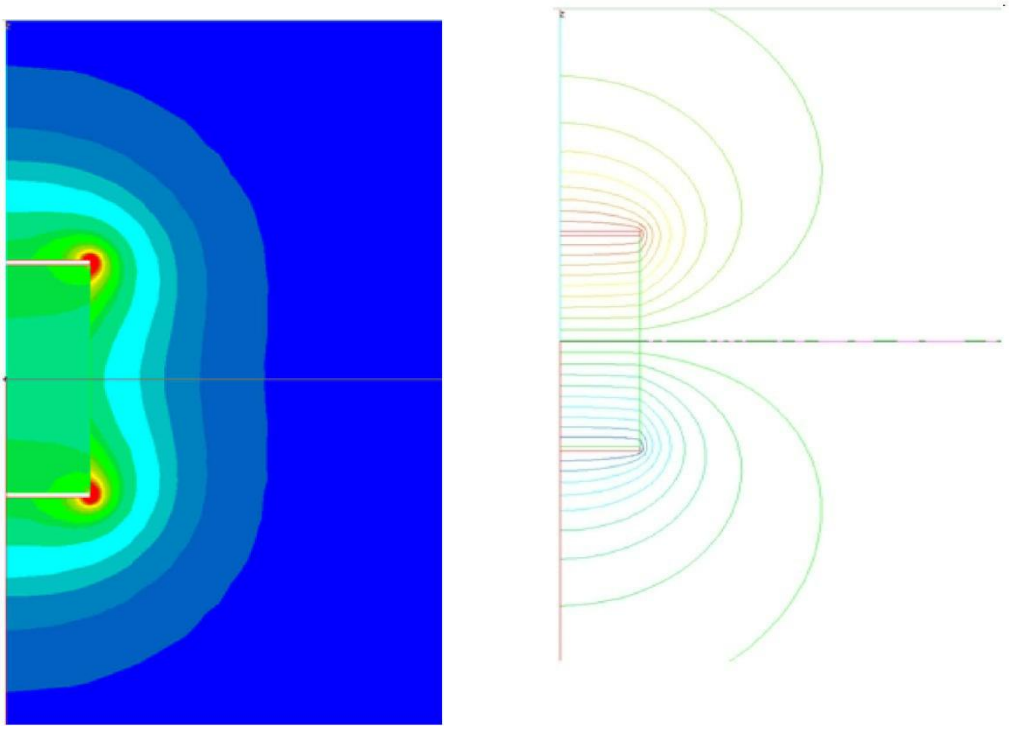

$E := 1.1144610^{-4}\,J$

(energy content computed by program)

$U := 10000\,V$

(Pockels cell terminal voltage)

$C := \frac{2 \cdot E}{U^2}$

$C = 2.2 \cdot pF$

Figure 1. Field simulation using finite element computation to find equivalent Pockels cell's capacitance and compare to classical capacitor formula

The field simulation requires the circular equivalent (radius of 10.55 mm) of the rectangular plates (14 mm x 25 mm) in order to model the electrical field. Finally, the energy content of the system is calculated. A voltage difference of 10 kV is used to compute the capacitance.

2. Pockels Cell Driver Electronics

As shown in Figure 2, the basic switch consists of two very fast switches. Switch SW1 closes first, whereas switch SW2 closes after a variable delay (250 ns as example in Figure 2), which is forming a push-pull arrangement. The delay generator is implemented in a separately shielded analogue electronics assembly to prevent electromagnetic interference.

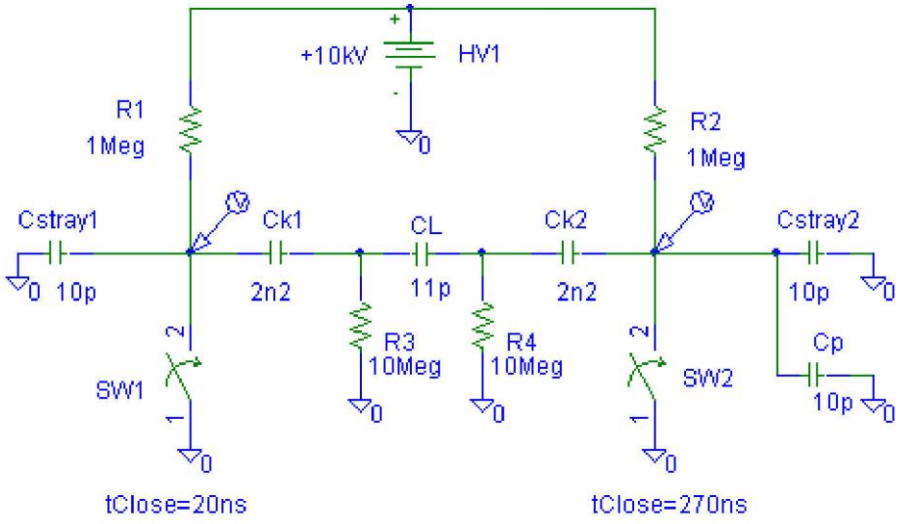

Figure 2. Basic topology of Pockels cell push-pull switching arrangement (CL is actual Pockels cell crystal, delay setting is 250 ns)

The delayed switch in Figure 2 is variable by means of a potentiometer. The delayed switching is required to provide a differential impulse seen by the Pockels cell load. The circuit theory shows that the capacitances (labelled Cstray1 and Cstray2) are critical in combination with the load capacitance. It is found that an additional capacitor (Cp) needs to be placed in parallel to Cstray2 in order to adjust the plateau signal voltage, as shown in Figure 3, as it acts as capacitive voltage divider. The simulation and measurement results are compared against each other as shown in Figure 3.

By using a standard measurement probe (model type TT-HVP l5HF from company Testec) with 50 MHz bandwidth (7 ns rise time), 1 pF capacitance and 100 MΩ impedance, the transition of the final Pockels cell driver device was measured as shown in Figures 4 and Figure 5.

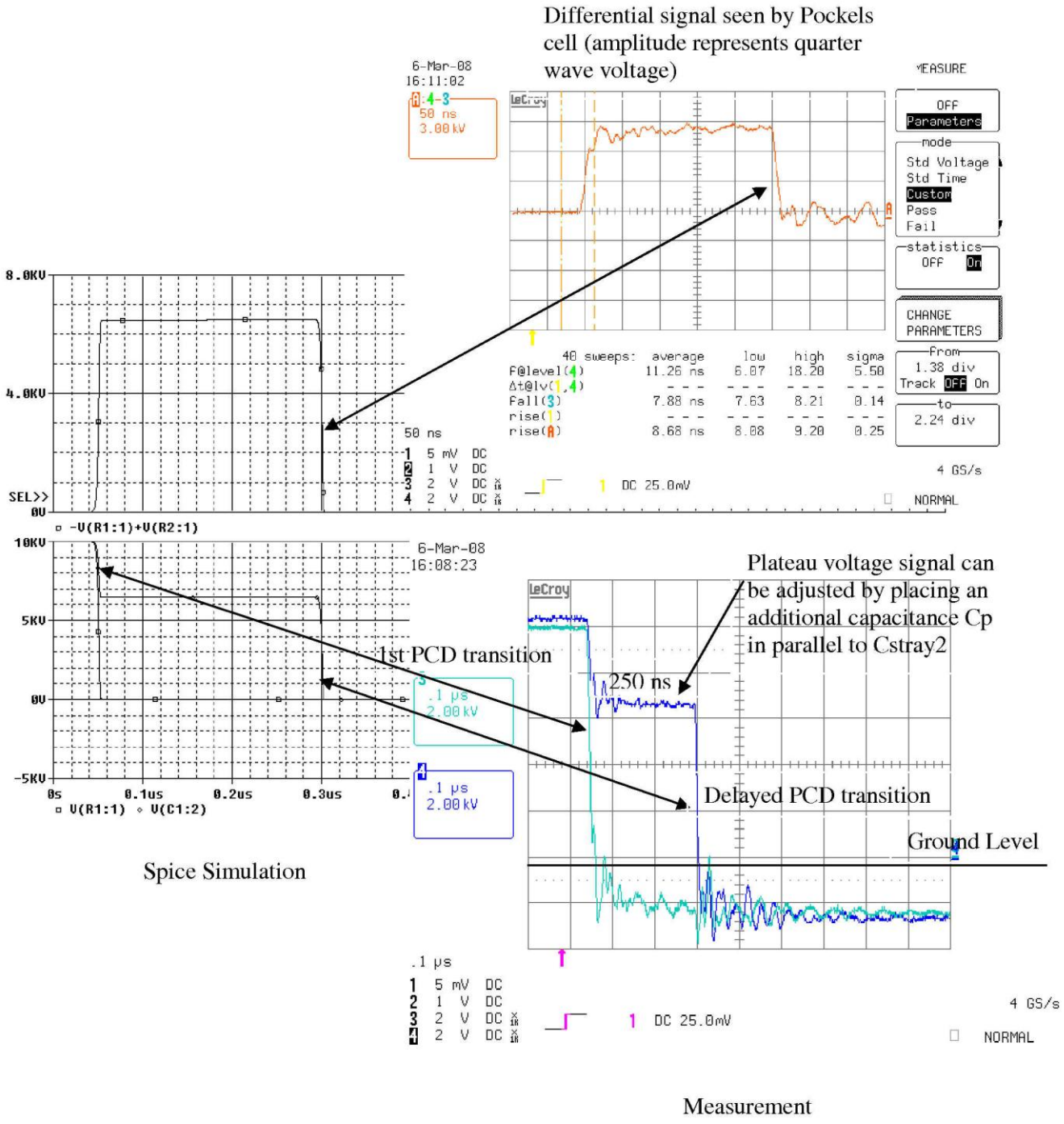

Figure 3. Comparison of Simulation and Measurement

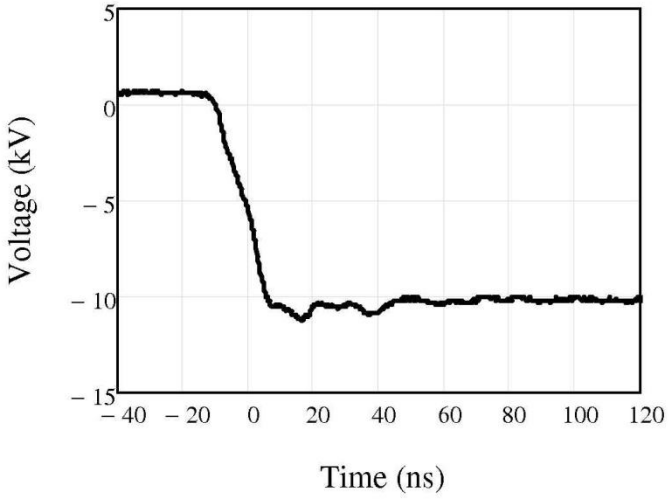

Figure 4. Typical fall time with a load capacitance of 11 pF, probe's capacitance not included (< 11 ns for 20 % - 80 % criteria)

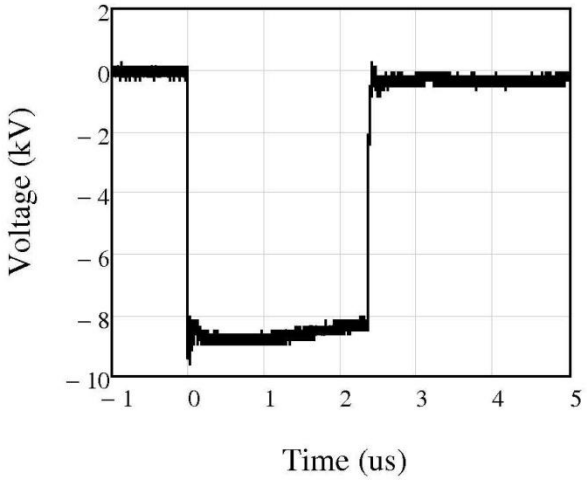

Figure 5. Differential probe measurement with 2 probes of maximum pulse width of 2.3 µs as seen by load capacitance of 11 pF,
(2 probe capacitances not included)

3. Summary

The 10 kV Pocke1s cell driver is EOSO's latest development in high voltage, high frequency and fast switching power supplies. The module as shown in Figure 6, has been developed to safely and reliably provide the high voltage switching required to drive the latest Pocke1s cells in high power Laser applications.

Figure 6. 10 kV Pocke1s cell driver in a compact aluminium box that can be placed directly adjacent to Pocke1s cell to ensure best performance
(leads run from the back of the box)

Table 1. Technical Specifications

Max. input power requirements	+24 V/3 A
Typical output quarter wave voltage range	< 9000 V (see Fig. 5)
Rise and fall time (20 % - 80 %)	< 11 ns (see Fig. 4)
RMS jitter	< 500 ps
Pulse width	80 ns – 2.3 µs
Maximum repetition rate	< 2.4 kHz
Load capacitance	≤ 12 pF
Size (length x height x depth) cm	35 x 12 x 25
Monitor output	Pulse width TTL @ 50 Ω
Trigger input	TTL

2.

Production of narrowband holographic selectors for SLR

V.D. Shargorodsky, A.P. Popov, Yu.L.Korzinin, A.V. Veniaminov, V.L. Moshkov
Federal scientific center, Federal state unitary enterprise
"Scientific Research Institute for Precise Instruments Engineering"
Moscow, Russia
www.niipp-moskva.ru /phone: +7-495-707 1348

Abstract

The article reports about organization of full serial production cycle for the narrowband holographic selectors for laser remote sensing purposes particularly for SLR. The main stages of production cycle are discussed, the photos of main facilities are represented, characteristics of first serial samples are given and ways for further development are analyzed.

Introduction

Achievement of high efficiency of the laser locator is always trade off between a spectral selectivity of the receiving channel and its energetic transmittance. Therefore a narrowband spectral selector becomes an integral part of any device. Intensive use of the SLR systems during last decade has laid down the requirements to them:

- ✓ Narrow transmittance band (about 100 pm)
- ✓ High energetic efficiency (85-90%)
- ✓ High time stability
- ✓ Low temperature drift
- ✓ Reasonable cost

Today the following optical elements meet most the requirements:

- ✓ Interference filter
- ✓ Atomic filter
- ✓ Faraday's filter
- ✓ Holographic selector

The latter, in our opinion, not only possesses excellent selective properties but also suitable for serial production.

Basic relations

The great technical potential of 3D holography has been attracting attention since its very early days; the unique spectral selectivity of thick holograms has given an impetus for many potential applications.

Optical layout of the recording and reconstruction (use) of the narrowband holographic selector is shown in Fig.1. The reflection geometry makes it possible to avoid undesirable narrow angular selectivity of a spectrally selective hologram.

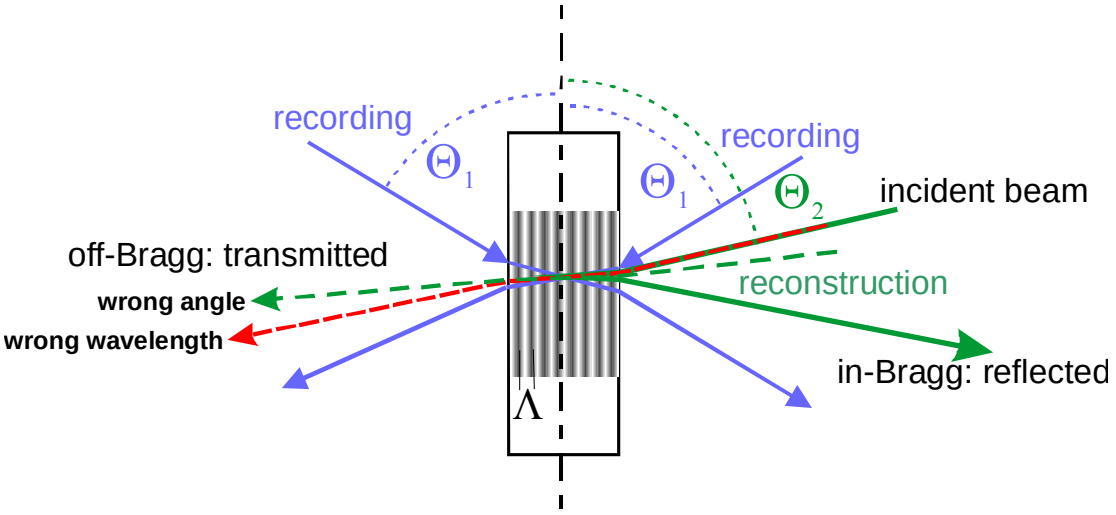

Figure 1. Optical layout of the recording and reconstruction of the holographic selector

The relation between a holographic grating period, beam-path geometry and the half-width of the spectral selectivity contour may be expressed as follows:

$$\Delta\lambda \approx \frac{6n \cdot \Lambda^2 \cdot \sin\Theta_2}{\pi \cdot d}.$$

where Λ is the grating period, Θ_2– incidence angle of the reconstructing beam in the material, n and d – refractive index and thickness of the photo-sensitive medium, respectively. Obviously that appropriate choose of the parameters may give theoretically any value of the spectral selectivity. For instance, to obtain 100 pm bandwidth at λ= 532 nm and Θ_2= 2.5^0 the grating should be 1 mm thick.

The univocal relation between spectral selectivity and angular one for the holographic selector:

$$\delta\lambda(\Theta) \approx \frac{\lambda}{n^2}\left(\left(\frac{\pi}{2} - \Theta_2\right) \cdot \Theta + \frac{\Theta^2}{4}\right)$$

provides a convenient opportunity to substitute the measurements of spectral selectivity by angular measurements.

Manufacturing stages and their implementation

The main stages of manufacturing of holographic selector are shown in Fig. 2:

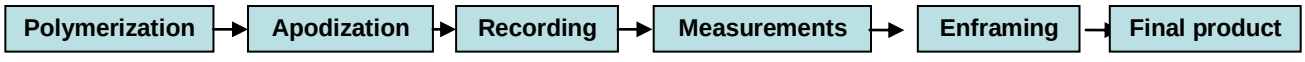

Figure 2. Main stages of manufacturing holographic selector

Phenanthrenequinone (PQ)-doped Poly(methyl methacrylate) remains at present the most realistic candidate as the material for thick holographic selective optics possessing necessary time and thermal stability characteristics, due to ability of PQ to bind to polymer chains under exposure and the effect of elimination of complementary gratings. Since their invention (Veniaminov, 1991), the PQ-based materials have served in many examples of selective holographic elements (e.g. Ludman, 1997, Mahilny, 2006, Russo, 2007), including the spectral selectors for laser detection and ranging (Popov, 2000); now we report the establishment of systematic production.

The material is manufactured by radical bulk polymerization of methyl methacrylate with PQ and radical initiator in inert atmosphere under elevated pressure and temperature following the schedule optimized for optical quality, maximal conversion to polymer and minimal mechanical stresses. The view of the bulk polymerization facility is shown in Fig. 3:

Figure 3. The facility for production of photosensitive material by polymerization method

It is known (Kogelnik, 1969) that the selectivity contours of 3D holograms recorded uniform in the material depth demonstrate multiple side-maxima whose relative intensity grows with diffraction efficiency, thus broadening the apparent selectivity. However, using a bell-shaped, e.g. Gaussian, distribution of the grating strength leads to dramatic suppression of the side-maxima (apodization). Such a distribution can be achieved by recording a hologram in the material with spatially non-uniform concentration that in turn can be created by bleaching the light-sensitive centers predominantly in the superficial layers in the course of pre-exposure incoherent illumination (Fig. 4) whose spectrum and duration controls the parameters of the resulting distribution, hence the selective properties (Popov, 1994).

Recording of the hologram is a principal stage of the narrowband holographic selector manufacturing. Optical layout of the process based on Zender-Mach interferometer is represented in Fig. 5. Argon-ion CW laser Spectra Physics® model 2060 is used as a light source. Special care has to be taken to provide high mechanical and thermal stability.

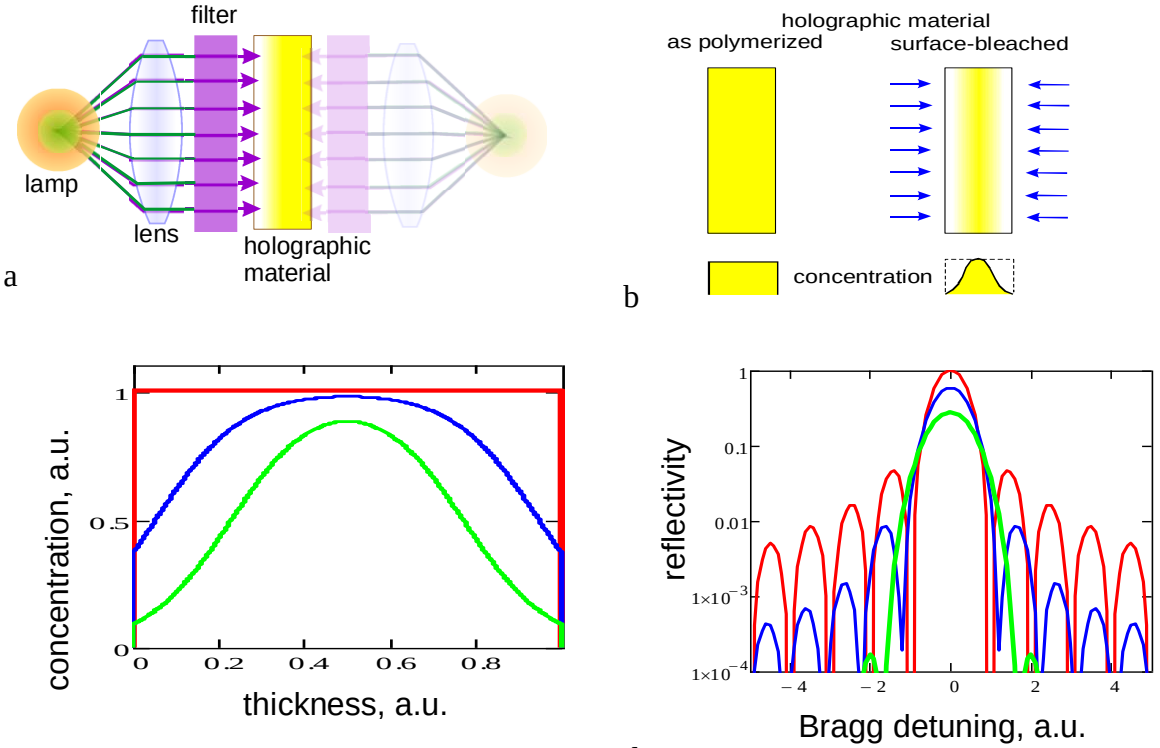

Figure 4. Photoapodization: schematic representation of pre-exposure treatment (a, b), light-sensitive centers distribution at different depths of apodizing treatment (c) and corresponding selective response functions of holographic gratings recorded in thus "apodized" material (d)

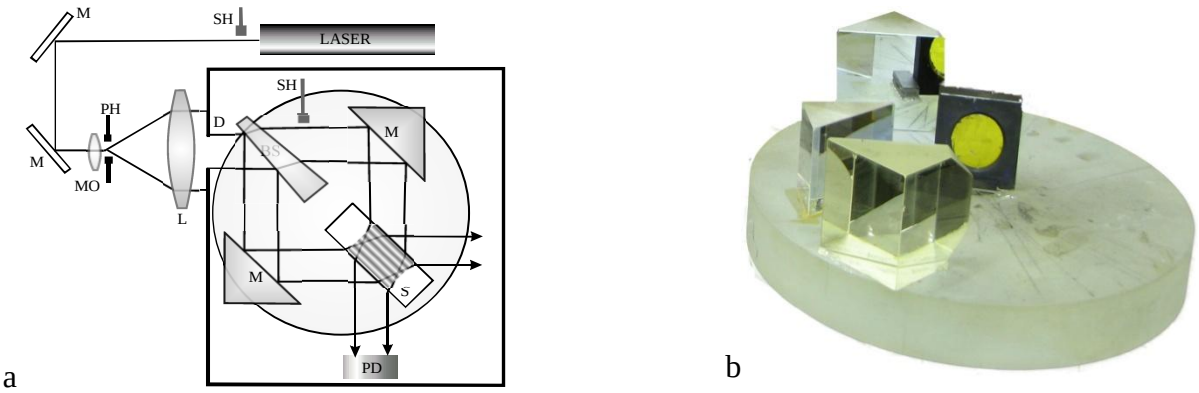

Figure 5. Optical layout (a) and general view (b) of the interferometer used for the hologram recording

The duration of the recording process is about 1 hour. Fig. 6 illustrates a general view at the recording facility during its final pre-exposure adjustment. After the exposure, the hologram should be kept at moderately elevated temperature during a few hours for self-development, and then fixed by uniform incoherent illumination.

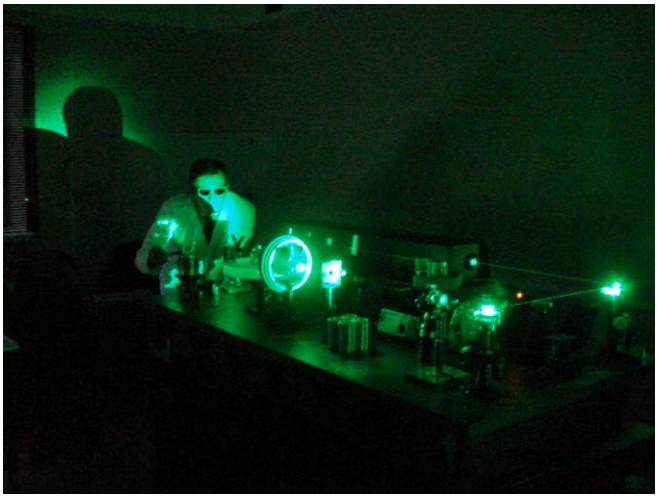

Figure 6. General view of the recording facility

Measurements of characteristics of the holographic selector take place in the next stage. Optical arrangement of the angular selectivity measurement is shown in Fig. 7. The light emitted by stabilized CW DPSS YAG:Nd^{+3} laser (532 nm) collimated by the lenses L and MO (micro objective) with the pinhole PH hits the sample S with a holographic grating in it installed on the top of the precise rotary table RT. The light beams diffracted back from the grating and passing through it are projected by two objective lenses OL to the photodetectors PD. The electronic unit controls the stepping motor of RT and transfers the signals from PD to the computer. The angular resolution of RT is 3.5×10^{-5} radians that corresponds to 0.35 pm spectral resolution.

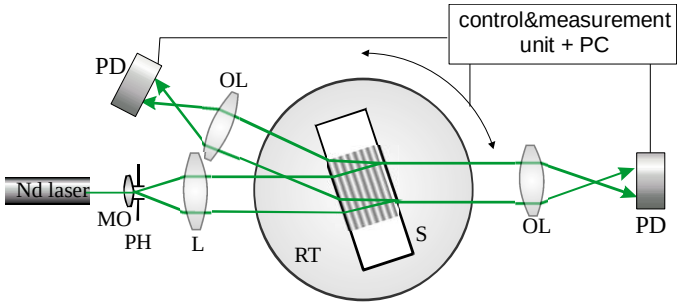

Figure 7. Optical arrangement of the angular selectivity measurement: Nd laser, collimator consisting of lenses, rotary table RT , objective lenses OL collecting transmitted and diffracted light on the two photodetectors PD, and the electronic unit responsible for controlling the stepping motor, signal acquisition and its transfer to the computer.

At the final stage of the production cycle holographic selector is placed into sealed-off container between two AR-coated windows in order to prevent the material from contacts with a humid atmosphere and thus keep constant characteristics at different application conditions. A ready-to-use narrowband holographic selector and its typical spectral curve i.e. a dependence of the reflectance coefficient upon wavelength are shown in Figs. 8 a and b, respectively:

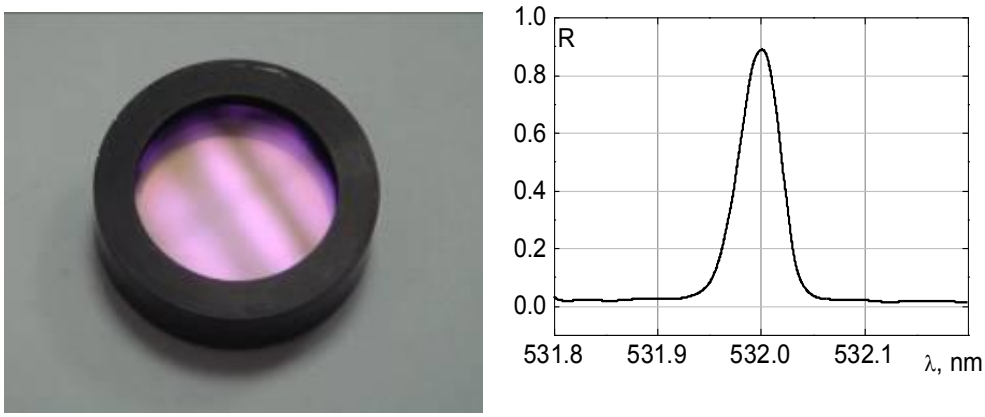

Figure 8. Narrowband holographic selector (a) and its typical spectral curve (b)

As a result the narrowband holographic selector possesses the following characteristics:

- ✓ spectral selectivity $\Delta\lambda$ ~ 100 pm
- ✓ maximal selective reflectivity ~ 90%
- ✓ spectral range: visible and NIR regions (typically λ = 532 nm)
- ✓ thermal wavelength shift ~5 pm/K
- ✓ lifetime: years (at moderate temperatures < 60^0C)
- ✓ selective reflection angle $5 \div 7^0$
- ✓ angular selectivity $\Delta\theta = 0.5^0$

Current status and prospects of the work

Lifetime of the selector i.e. stability of the characteristics in time is one of its most important features. The first prototypes produced in 1980s (Sukhanov, 1984) based on reoxan proved useful but revealed relatively low values of both diffraction efficiency and lifetime. (see Fig. 9).

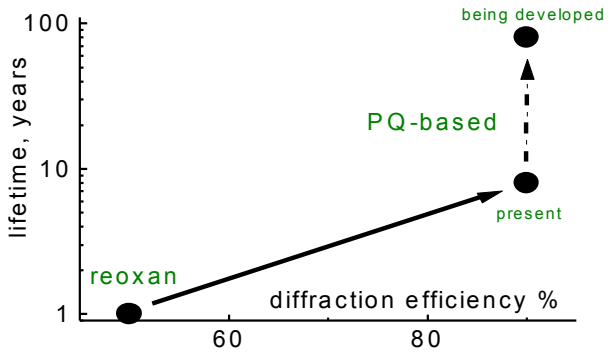

Figure 9. The diagram illustrates a current status of the development of the narrowband holographic selectors

Using phenanthrenequinone doped polymethyl methacrylate has substantially improved these figures. The holographic elements produced today keep their properties for several years and their diffraction efficiency reaches a practical limit. The major remaining problem consists in slow tiny diffraction angle drift that is often considered negligible but may nevertheless lead to some deviation of grating parameters from their initial values. Further progress may go different ways. For instance, fine mechanical or thermal adjustment of the incidence angle can be provided with the help of diffracted light intensity feedback. Alternatively, the material can be enforced with a microporous network or microscopic inert particles. Our main efforts are concentrated in finding stable material compositions least sensitive to changes rather than compensating the effects of such changes.

References

Kogelnik, H. Bell Syst. Tech. J. V.48, p. 2909-2947, 1969.
Ludman, J. E. et al. Optical Engineering, V.36, p.1700-1705, 1997.
Mahilny, U. V. et al. Appl. Phys. B: Lasers and Optics V.82, p.299 – 302, 2006.
Russo, J. M. & Kostuk, R.K. Appl. Optics V.46, p.7494-7499, 2007.
Popov, A. et al. J. Optics A: Pure Appl. Opt. V.2, p.494-499, 2000.
Popov, A. P. et al. Opt. Comm. V.110, p.18-22, 1994
Sukhanov, V. I. et al. Sov. Tech. Phys. Lett. V.10, p.387-388, 1984.
Veniaminov, A. V., Goncharov, V. F., Popov, A. P. Opt. and Spectr. V.70, p.505-508, 1991.

Dye Cell used in Active-Passive Laser Oscillator replaced with a Cr^{4+}:YAG crystal Saturable Absorber for NASA SLR Stations

T. Oldham (1)**, H. Donovan** (1)**, M. Blount** (1)**, J. Horvath** (1)**, O. Brogdon** (1)**, D. McCollums** (1)**, D. Carter** (2)**, C. Emerson** (2)

(1) Honeywell Technology Solutions Incorporated (HTSI)
(2) National Aeronautics and Space Administration (NASA)

Howard.Donovan@Honeywell.com /Fax 301-805-3974

Abstract

Since 1983, the current network of NASA Satellite Laser Ranging (SLR) stations used an Nd:YAG oscillator cavity in an active-passive configuration to generate 150-200 psec (2mj) 1064nm pulses for satellite ranging. This cavity (active-passive) used a liquid (chlorobenzene) dye cell as the passive saturable absorber. The dye consisted of Exciton (Kodak-9740) Q-Switch I dye and monochlorobenzene as a solvent. The dye mixture would degrade during use and would require daily maintenance. Chlorobenzene is a hazardous substance that requires special handling equipment and procedures.
The dye cell was replaced with a Cr^{4+}:YAG crystal used as a saturable absorber in an active-passive mode-locked Nd:YAG laser. The new absorber requires little or no daily maintenance and the improved stability and laser performance is equal to or better than the dye cell. Pulse widths of 150psec were easily obtained and output energy variations of less than 10% shot to shot.

Introduction

Since 1983, the current network of NASA Satellite Laser Ranging (SLR) stations [3] used an oscillator cavity in an active-passive configuration to generate 150-200 psec (200mj) 1064nm pulses for satellite ranging. This flashlamp pumped cavity used a liquid (chlorobenzene) dye cell as the passive saturable absorber. The dye consisted of Exciton (Kodak-9740) Q-Switch I dye and monochlorobenzene as a solvent. The dye mixture would degrade during use and would require daily maintenance. Chlorobenzene is a hazardous substance that requires special handling equipment and procedures.

Two types of saturable absorber were investigated: SAM and then Cr^{4+}:YAG. Testing of a SAM in the cavity produced only marginal results and unstable pulses at the nanojoule level. Flashlamp pumping of the modelocked cavity needs to produce pulses at the 2 mj level to make it useful in the single amplifier laser.

Research into an alternative saturable absorber led to a manufacturer of Cr^{4+}:YAG material for use as a Q-switch for generating giant pulses [1, 2] and in active-passive mode locked lasers.

A Cr^{4+}:YAG crystal with the dimensions of 7.5x7.5x4.0 mm with anti-reflective coatings for 1064nm on both surfaces was installed into the oscillator cavity as shown in Figure 1.

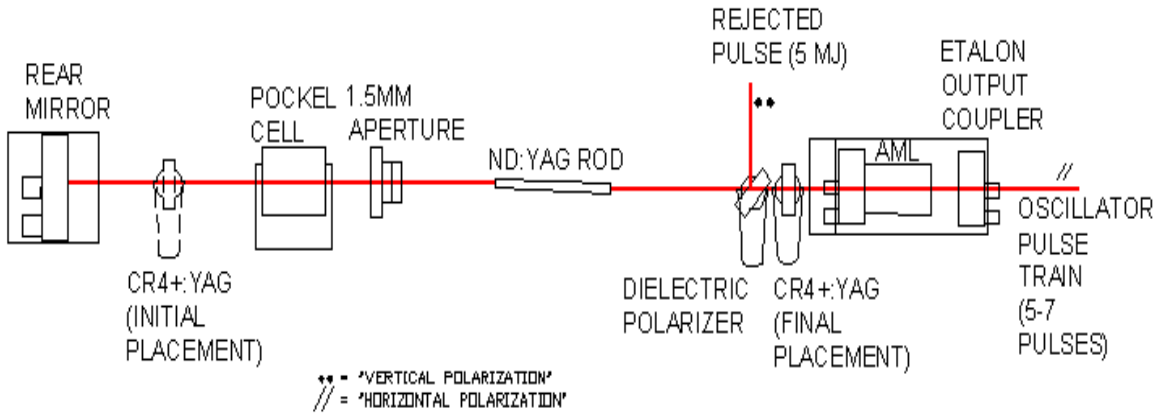

Figure 1. Laser Oscillator Cavity

Modification

The dye cell was part of the rear mirror assembly so the initial placement of the Cr^{4+}:YAG crystal was installed between the rear mirror and Pockels cell as shown in Fig. 1. During initial testing, approximately 1% of pulse leakage was being rejected from the cavity. Because of polarization effects caused by the anti-reflective coatings on the Cr^{4+}:YAG absorber, the placement (final placement) of the Cr^{4+}:YAG crystal was moved to the other side of the polarizer. In this case, any leakage cause by the anti-reflective coating was reflected off of the polarizer in the opposite direction of the rejected pulse.

The cavity mirrors consist of a 99% reflective rear cavity mirror and a solid etalon for the front cavity. Output pulse width can be controlled by changing the feedback into the cavity from the front reflector. By changing the etalon feedback reflector, the spectral line width narrows, effectively decreasing cavity feedback and narrowing the output pulse (See Table 1).

Table 1. Oscillator (Cr^{4+}:YAG) Pulse Width versus Etalon Thickness

Etalon Thickness (mm)	PulseWidth-1064nm (psec)	PulseWidth-532nm (psec)
5	348	238
3	289	218
2	260	160
1	230	140
0.5	179	115
0.25	153	105

The oscillator using the dye cell produced a pulse width shown below in Table 2.

Table 2. Oscillator (Dye) Pulse Width versus Etalon Thickness

Etalon Thickness (mm)	PulseWidth-1064nm (psec)	PulseWidth-532nm (psec)
5	225	90-138

For use with the Cr^{4+}:YAG crystal, the etalon that produced the pulse width closest to the original width using the dye cell was chosen. A 1mm etalon was selected. The Pockels cell is used in the cavity to reject a single pulse from the cavity. The output pulse train is fed into a detector that is used to fire a chain of avalanche transistors. The output high voltage pulse (1/4 wave voltage) is applied to the single crystal Pockels cell to rotate the polarization by 90 degrees and then reflect out of the cavity from the polarizer.

The original polarizer was a thin film dielectric polarizer mounted at 56 degrees with an isolation of 200:1. This was replaced with a CVI Melles Griot thin film dielectric polarizer mounted at 45 degrees with an isolation of 500:1. The coating also seems more robust and not as susceptible to damage.

The original cavity used two 1.5mm mode limiting apertures. During testing, it was difficult to align two apertures and the 2nd aperture was removed. The addition of a 2nd aperture seems to distort the output beam profile and appears to lose its Gaussian energy distribution.

The Nd:YAG rod remained the same for this modification. The rod is 7mm round, 115mm long with both ends cut at 2 degrees and AR coated on both surfaces.

The Cr^{4+}:YAG saturable absorber is cut to 7x7 mm square and 4mm thick. Both surfaces have anti-reflective coating optimized for 1064nm. Before the rod is pumped using 2 flashlamps (18J), the energy population of the saturable absorber is at the ground state and the transmission through the Cr^{4+}:YAG crystal is low. When the rod is pumped, energy in the cavity builds until all ions in the absorber are stimulated quickly to the first and second energy states. This causes the absorber transmission to increase allowing for unity gain and lasing to begin. Following lasing, the ions return to the ground state.

The acousto-optic modulator (70MHz) mode locks the cavity to produce a stable train of 5 – 7 pulses. The cavity length is optimized to generate the most stable narrow (150psec) and stable pulse.

Experimental Results and Analysis

The Cr^{4+}:YAG saturable absorber was installed into the NASA SLR Moblas-7 laser on September 11, 2007 and initial ranging began 2 days later. Initial data results had indicated that the number of rejected data points was higher than using the dye cell. It also appeared that the laser was outputting pre-pulses with a ratio of 100:1 of the main selected pulse. This caused the receive discriminator to trigger early on the pre-pulses with strong receive signal strength from the target. This can be seen in Figure 2 showing multiple line residuals for each laser pre-pulse.

On October 24, 2007 the position of the saturable absorber was changed (Fig. 1) to the opposite side of the 45 degree polarizer. Apparently the anti-reflective coating on the saturable absorber was affecting the polarization of the cavity beam causing the polarizer to reflect a small portion of the beam out of the cavity during each pass through the cavity. By moving the saturable absorber to the opposite side of the polarizer, the non linear component of the beam is reflected in the opposite direction of the amplifier and dumped. Figure 3 shows

a time line of the number of rejected data points per pass. It indicates that after the relocation of the saturable absorber, the number of rejected data point decreased to acceptable levels.

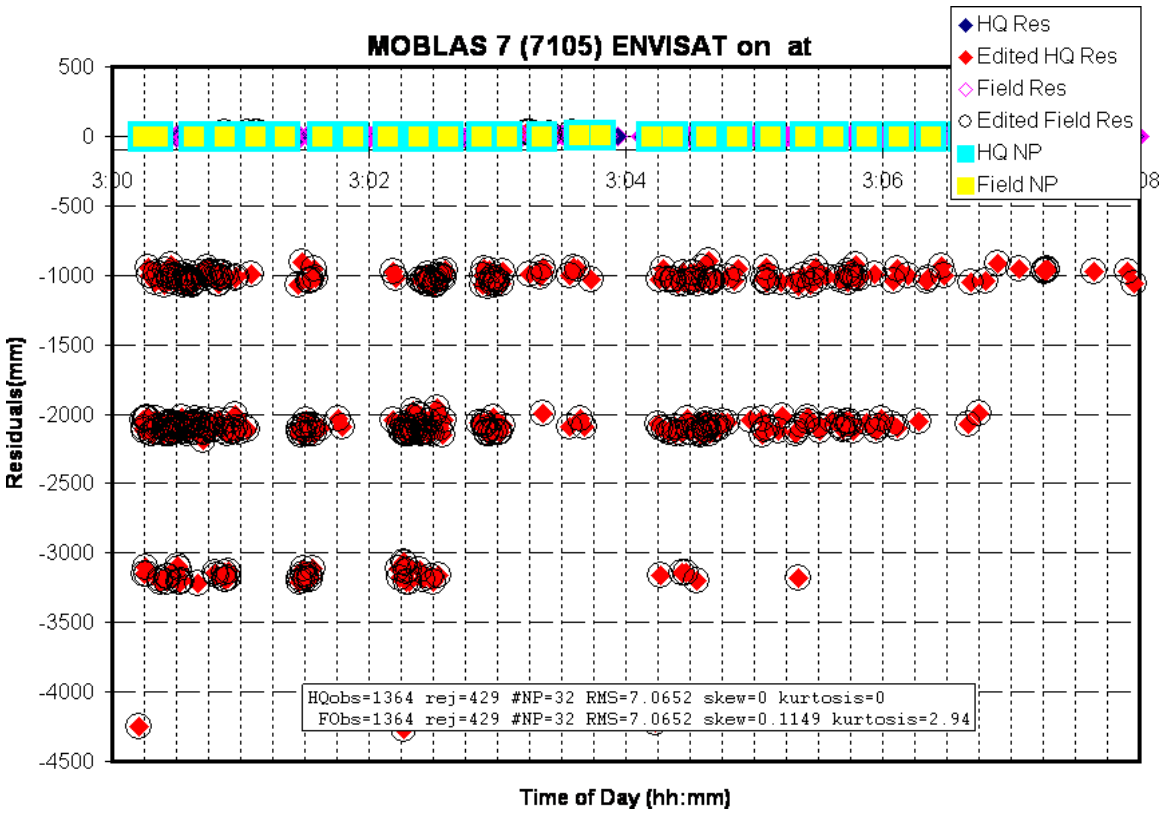

Figure 2. Initial Pass Results Showing Oscillator Cavity Leakage.

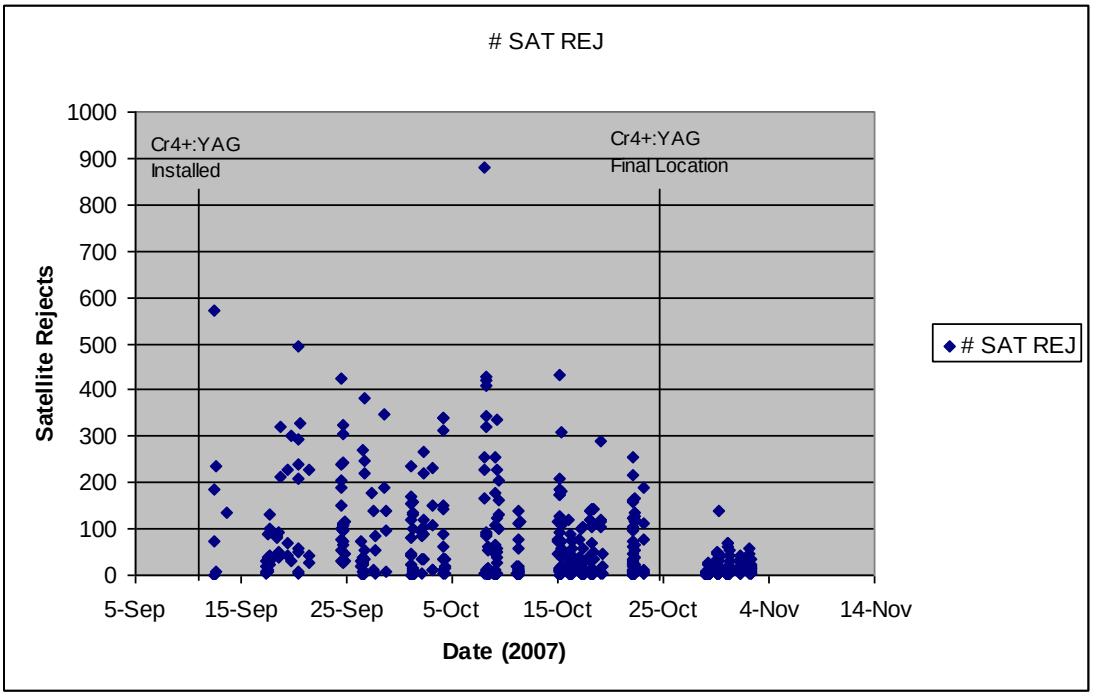

Figure 3. Time Line Showing the Number of Rejected Pulses per Pass.

Conclusion

The modification has been performed at three of the five Moblas SLR stations. The original intention of this modification was to be transparent to system performance; however, between the upgrade of the laser and improved alignments procedures, the system performance has actually improved. The number of data points per pass, data quality and system delay stability have all improved.

In addition, it has been reported that the usual daily laser maintenance has decreased from hourly/daily optimization alignments to weekly, monthly or in some cases 3 or 4 months. After a 15 minute warm-up, laser power and stability becomes optimal without alignments.

Because of the additional pulse width stability, this should also minimize the likelihood of exceeding the damage threshold of several optics on the laser table. This should reduce annual operational costs of the laser systems and reduce the likelihood of a laser failure and lost data opportunities.

Special thanks to the Moblas crews, data analysis and engineering group for making this successful improvement in safety and performance for all the NASA SLR stations.

References

1. Leng Yuxin, Lu Haihe, Lin Lihuang, Xu Zhizhan; Active-passive mode-locking using Cr^{4+}:YAG crystal as saturable absorber; Optics & Laser Technology 33 (2001) 403-407
2. R. Feldman, Y. Shimony, Z. Burshtein; Passive Q-switching in Nd:YAG/ Cr^{4+}:YAG monolithic microchip laser; Optical Materials 24 (2003) 393-399
3. Pearlman, M.R., Degnan, J.J., and Bosworth, J.M., "The International Laser Ranging Service", Advances in Space Research, Vol. 30, No. 2, pp. 135-143, July 2002, DOI:10.1016/S0273-1177(02)00277-6.

Applications of Riga Event Timer at Shanghai SLR Station

Zhang Zhongping (1)**, Zhang Haifeng** (1)**, Yang Fumin** (1)**, Wu Zhibo** (1)**, Chen Juping** (1)**, Yu. Artyukh** (2)

(1) Shanghai Astronomical Observatory, Chinese Academy of Sciences, China
(2) Institute of Electronics and Computer Science, Riga, Latvia

zzp@shao.ac.cn /Fax:+86-21-64696290

Abstract

The Shanghai SLR station is the first one in China which has chosen Riga Event Timer A032-ET in view of its advanced performance and reasonable price. Thereupon several LSR stations in China also began using this event timer. The paper presents the applications of A032-ET to routine SLR, high repetition rate SLR and Laser Time Transfer experiment. The advanced performance of A032-ET is also described.

Introduction

Since 2006, Shanghai SLR station commenced researching the kHz SLR. As known, the event timer is an indispensable timing device for kHz SLR. Since Riga event timers have the advanced performance and reasonable price, we have chosen one of them (the model A032-ET) for developing kHz SLR. That is for the first time used in China.

A032-ET can be easily utilized by users. Specifically, we successfully applied this Event Timer for the Routine SLR, 1KHz repetition rate SLR and Laser Time Transfer (LTT) at Shanghai SLR station. According to the applications of A032-ET at Shanghai SLR station, several SLR stations in China, such as Changchun, Beijing and so on, use the same Event Timer for kHz SLR and as advanced test equipment.

Performance of Riga Event Timer A032-ET

There are some A032-ET performance characteristics, like precision temperature stability and non-linearity, that are important for the applications at Shanghai SLR station and were not specially noted early.

RMS resolution vs. ambient-temperature

One of important parameters of Event Timer is stability of RMS resolution vs. ambient temperature. The matter is that A032-ET supports the best RMS resolution about 7-8 ps after calibration under condition that the operating temperature does not noticeably vary during following measurements. There are some test results (Bespal'ko et al., 2006) that the RMS resilution temperature stability is about 0.1 ps/^{o}C. This parameters defines ability of the A032-ET to support acceptable resolution without recalibration under time-varying operating conditions.

Effect of non-linearity

There are two basic kinds of A032-ET non-lineary: a systematic error for time-interval measurement between two adjacent events (so called interval non-linearity) and a systematic error in single event measurement over epoch time (so called integral non-linearity). Figure 1

shows the A032-ET integral non-linearity error. As can be seen, such non-linearity does not exceed 1.0 ps for greater than 100 ns time intervals.

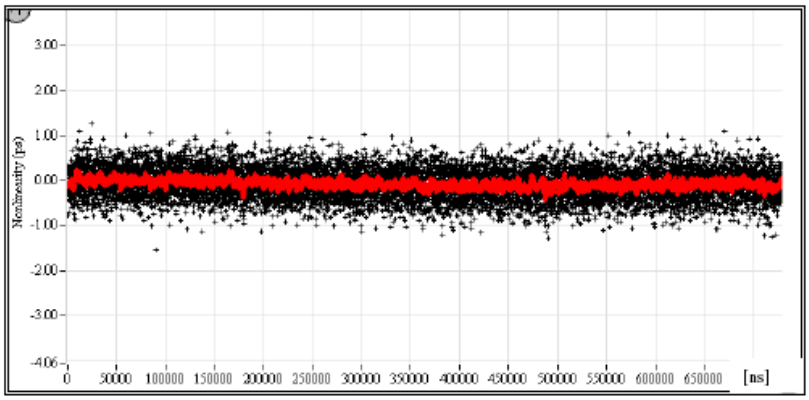

Figure 1. Interval non-linearity vs. time interval

Figure 2 and Figure 3 show the integral non-linearity over the input frequency period 100 ns (10MHz) and the internal clock period 10 ns (100MHz) respectively.

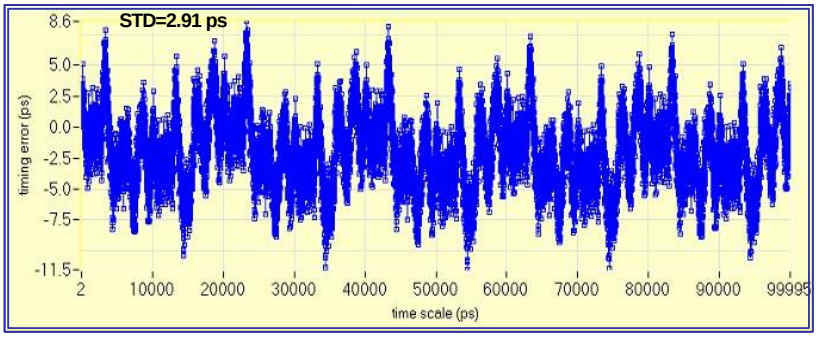

Figure 2. Integral non-linearity over input frequency period 100 ns

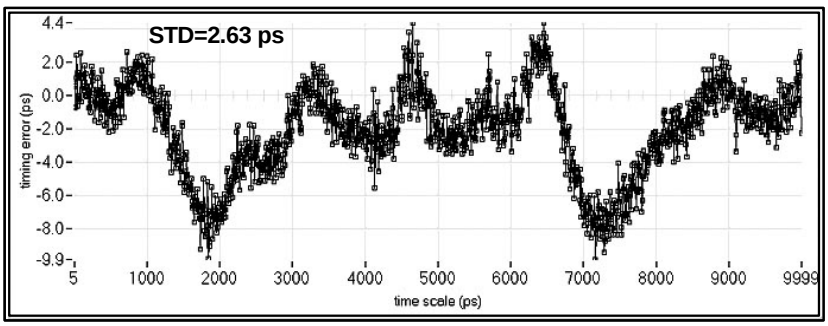

Figure 3. Integral non-linearity over internal clock period 10 ns

As can be seen in Figure 2, the maximum integral non-linearity error (peak-to-peak) does not exceed 20 ps. The non-linearity error over internal clock period is only a little less. This confirms the fact that the internal frequency multiplier (10 MHz to 100 MHz) does not add noticeable error into common integral non-linearity.

Applications at Shanghai SLR station

Routine SLR

A032-ET performs its measurement functions partly by hardware means and partly by software means. Figure 4 shows the schematic control diagram for A032-ET comprehended by us according to the principle of operating this event timer.

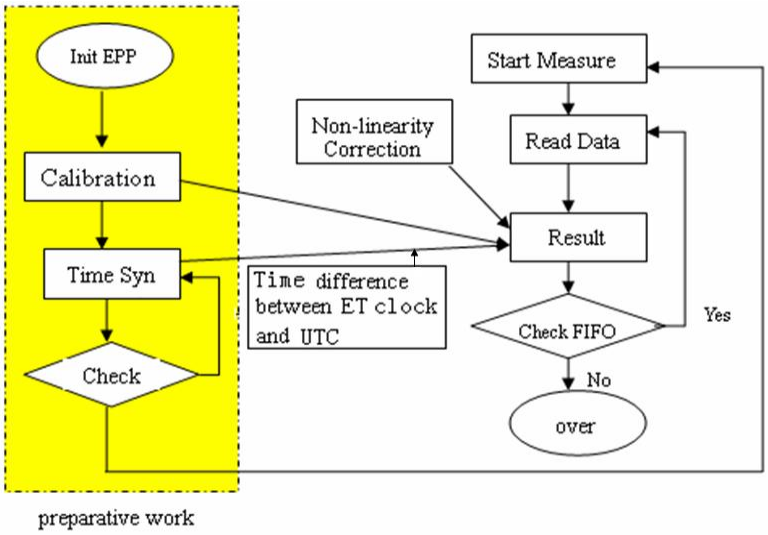

Figure 4. The schematic control diagram of A032-ET

There are two interfacing modes of measurement for users developing program.

- **TCP/IP mode.** Based on the well-known "Client/Server" network, Client (application software) connects to the A032-ET Server via TCP/IP network to receive measurement data for further processing and system control. What the users need to do is to develop own Client applications. This mode is convenient for users needing remote interaction with A032-ET. But due to the uncertain delays of network, this mode is basically fitted to low-rate data acquisition.
- **EPP mode.** In this mode the measurement data is obtained directly from the A032-ET hardware by user-made software via EPP. It is easy for users to create own timing measurement system based on library functions which defines device-specific functions to interact with A032-ET hardware. EPP mode is a way to high-rate data acquisition and avoids the uncertain delays caused by network.

In Shanghai routine SLR (10 Hz), we use TCP/IP mode to get measurement data from A032-ET. Figure 5 shows the interface of main and client applications of Shanghai routine SLR.

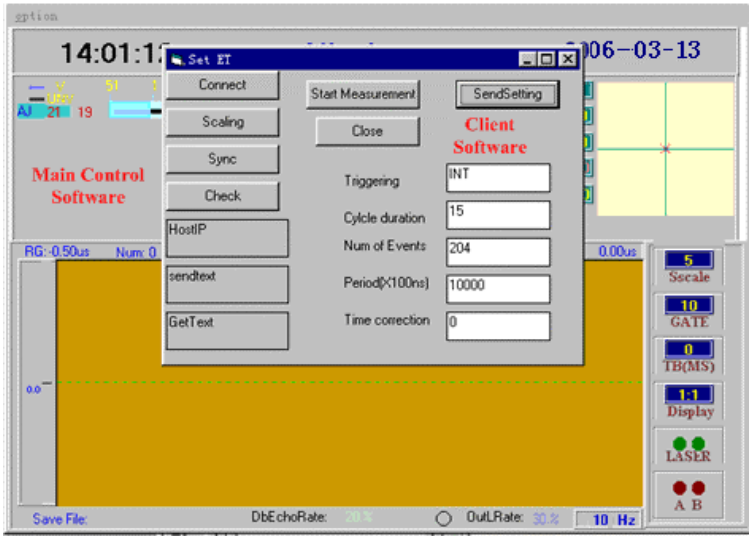

Figure 5. The interface of main and client applications

After adopting A032-ET and developing the corresponding software, Shanghai SLR station can range kinds of satellites with 10 Hz repetition rate (limitation to laser of 10Hz output rate). With the increase of ranging repetition rate, more returns and passes are got.

1 kHz repetition rate SLR

Shanghai SLR station gets the support from National Natural Science Foundation of China to research and develop the key technology of kHz SLR in 2006. Event Timer is one of the key technologies and it is a necessary timing device in kHz SLR.

Due to the huge amounts of measurement data for kHz SLR, it requires high speed of data reading (Kirchner et al, 2004). For kHz SLR, the EPP mode for A032-ET was chosen in order to make the maximum available reading speed. A032-ET has a 12000 time-tags buffer (FIFO). This is very good for data reading and allows avoiding any measurement data lost. Figure 6 is the interface of main control application at EPP mode.

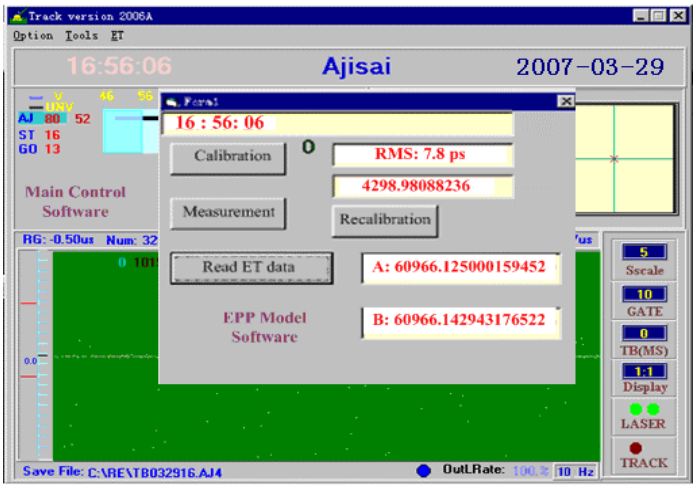

Figure 6. EPP mode for A032-ET

For Shanghai 1kHz SLR, two computers are used. One of them is to get measurement data from Event Timer, identifying start event and stop event, showing range, saving data and so on. Figure 7 is the interface of application executing the above mentioned functions.

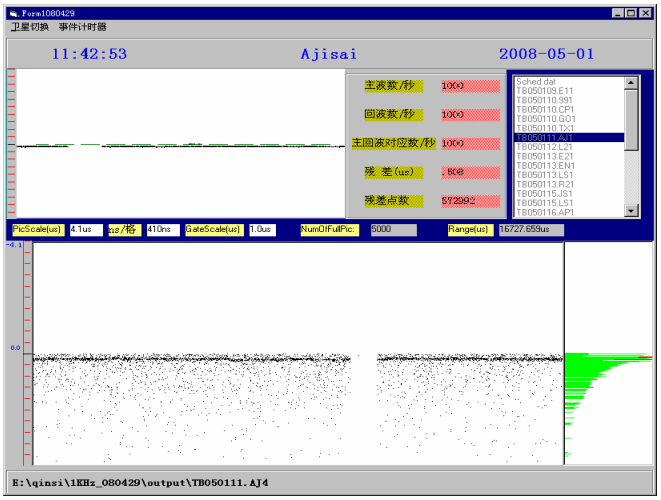

Figure 7. The real-time interface of 1 kHz SLR

Shanghai 1kHz SLR shows that EPP mode of A032-ET operation meets the demand for high speed of measurement data reading.

Laser Time Transfer (LTT)

Shanghai Astronomy Observatory carried out Laser Time Transfer in July, 2007 - March, 2008 at Changchun SLR station. The LTT payload is onboard the Chinese experimental navigation satellite, MEO orbit, altitude 21500km. The ground laser output rate is 20 Hz.

Laser Time Transfer is a high precision time measuring technology (Fumin et al., 2006). The timing precision and stability of timing device play an important role in LTT. Figure 8 is the principle of Laser Time Transfer.

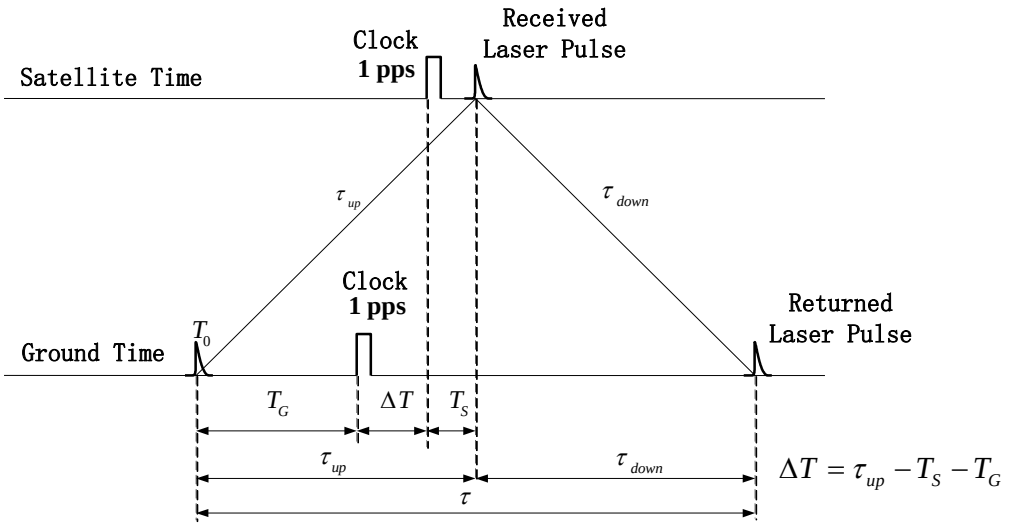

Figure 8. The principle of Laser Time Transfer, where:

ΔT - clock difference between satellite and ground clocks

T_G - time interval between the transmitting laser pulse and 1PPS of the ground clock

T_S - time interval between the received laser pulse and 1PPS of the satellite clock
τ - laser pulse flight time for ground-satellite-ground
τ_{up} - laser pulse flight time for ground-satellite
τ_{down} - laser pulse flight time for satellite-ground

For LTT experiment, two Event Timers must be used on the ground. Figure 9 shows the application of two Event Timers: Event Timer 1 and Event Timer 2. Event Timer 1 is applied to measure start and stop events for high precision SLR. Through identifying corresponding Start-and-Stop events, the laser pulse flight time for ground-satellite-ground τ is obtained. After considering the correction of the Earth rotation (Sagnac effect), the laser pulse flight time for ground-satellite τ_{up} is to be calculated. Event Timer 2 measures the time interval T_G between start event and 1PPS on the ground clock. According to the principle of LTT, the precision of measured τ_{up} and T_G directly affects that of clock difference between satellite and ground.

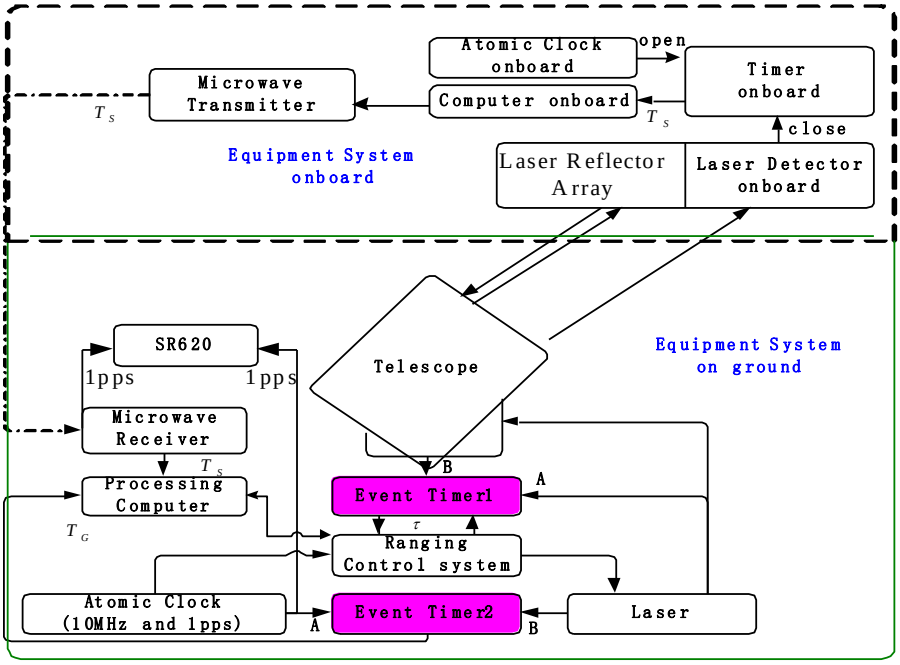

Figure 9. Diagram of LTT

From the results of LTT experiment, it can be concluded that A032-ET provides necessary performance characteristics to achieve the anticipated measurement level. Thus, A032-ET could act as high-precision timing device in LTT experiments.

Summary

Shanghai SLR station is the first one from the China SLR stations which, in collaboration with Riga Institute of Electronics and Computer Science, began using of Riga Event Timer A032-ET for SLR and the related applications. After integration of A032-ET into specific event timer systems, it has been successfully applied to SLR and LTT experiment. The analysis of the obtained measurement data showed that the performance characteristics of Riga Event Timer (such as RMS resolution, stability, non-linearity, etc.) satisfy the

requirements of high precision SLR and LTT. Following to the A032-ET applications at Shanghai SLR station, it is also adopted by several SLR stations in China for developing kHz SLR and as advanced test equipment.

References

G. Kirchner, F. Koid, *Graz KHz SLR System: Design, Experiences and Results*, 14th International Workshop on Laser Ranging, San Fernando, Spain, 7-11 June, 2004.

V. Bespal'ko, E. Boole, V. Vedin, *The Model A032-ET of Riga Event Timers*, 15th International Workshop on Laser Ranging, Canberra, Australia, 15-20 October, 2006.

Yang Fumin, Huang Peicheng, Chen Wanzhen, Zhang Zhongping, Chen Juping etc, *Progress on Laser Time Transfer Project*, 15th International Workshop on Laser Ranging, Canberra, Australia, 15-20 October, 2006.

Software and Automation

Chair: Randall Ricklefs

Session Summary

Several themes ran through the 6 papers and 1 poster that comprised this session. Modularity, robustness, and automation of geodetic systems were of major concern in 3 papers. Another dealt with a novel approach to telescope mount modeling. One paper dealt with automated preprocessing of SLR data and predictions. The topic of XML, which has gained importance in the software industry, was discussed as the basis of intermediate data formats in 2 of the papers. The new ILRS CRD format was discussed in several papers, either in terms of creation or validation of data files.

The paper by Neidhardt describes a project at Wettzell to create a modular software system to control SLR stations. The distributed client-server modules are implemented with open rpc (remote procedure calls) over tcp networks on Linux-based computer systems. The modularity allows for simple but robust systems in which each computer handles a specific SLR station function, such as the telescope or event timer control. The approach also allows autonomy and remote operations, as the user interface is yet another distributed module.

Salminsh discusses upgrades at Riga which also use a client-server architecture, running on Windows-based computers. Ranging, predictions, and related data are saved in a data base system (Firebird). Then, as part of processing, internal XML data files are converted to the CRD format using XLST (extensible style sheets).

The use of XML to create the new CRD format was also discussed in a paper by Moore. In redeveloping Mt. Stromlo software to generate various formats of SLR full rate and normal point data, a system was created using XML intermediate files and XLST (style sheets). The XML technique can be used to create any number of file formats and reports and incorporate new data types without much additional work. Another presentation by Moore dealt with automation upgrades at Mt. Stromlo.

Medvedsky and Pap describe a method of determining a telescope mount model from observations of azimuth and elevation position errors recorded during every second of satellite laser ranging. This technique removes the need to perform a separate mount modeling procedure with stars. The results after 40 passes and 18,000 measurements was the discovery of unexpected mount error terms which were then used to improve the mount model.

Ding discusses experiments aimed at providing automated SLR data filtering for the Beijing station. The suitability of CPF files to provide the basis for filtering was evaluated. Satisfied with the CPFs' accuracy, the the raw ranging data was flattened by subtracting the interpolated predictions. The data was further processed by minimizing the residual and time span to isolate data from noise.

Validation of laser station data in the new CRD format was the subject of the paper by Kuzmicz-Cieslak and Pavlis. In this pilot project, the JCET team compared MLRS normal points in the old ILRS QLNP and new CRD formats. This required converting the CRD data into the expanded Merit format required by GEODYN and taking into account differences due to the greater precision of the new format.

Automation - Recent Progress at Mt Stromlo SLR Station

Christopher Moore
EOS Space Systems, Australia
cmoore@eos-aus.com

Abstract

A short report on the progress made at Mt Stromlo SLR station on the development of new automation facilities is presented. Auto-tracking has been in routine operation for over a year and new software applications to support auto-processing have recently been completed.

New concepts in control systems for SLR with remotely accessible, autonomous process cells

Alexander Neidhardt[1], Martin Ettl[1], Pierre Lauber[1], Andreas Leidig[1], Reiner Dassing[2], Matthias Mühlbauer[2], Christian Plötz[2]

[1]Forschungseinrichtung Satellitengeodäsie, Technische Universität München, Geodätisches Observatorium Wettzell
[2]Bundesamt für Kartographie und Geodäsie, Geodätisches Observatorium Wettzell

Abstract

The demands for data acquisition systems in space geodesy like satellite laser ranging systems increase continuously. Shared observations of future transponder targets, the distribution of the resulting data in real-time and the increasing number of possible targets with fast switching between passages will offer new possibilities but will also require new solutions for the controlling software. In response to these demands (semi-) automated, remote control systems will become more and more reality. Such complex systems require reliable, transparent and modular structures from upper controlling layers down to the basic single components in combination with sophisticated safety mechanisms in automation. A new idea with remote assessable, autonomous process cells, which can solve component specific requirements encapsulated and autonomously, can generally help to split up the complex system into maintainable, modular units. These units are remote controllable and highly automated. In the design of the new Satellite Observing System Wettzell these ideas have been implemented. A similar approach has been proposed for the remote control of the radio telescope at the German Antarctic Receiving Station O'Higgins for geodetic VLBI experiments, where the first tests are successfully done.

Satellite laser ranging systems as distributed computer systems

Modern laser ranging systems, like the newly designed Satellite Observing System Wettzell (SOSW) at the Fundamentalstation Wettzell, consist of numerous, separate components for single, specific tasks. In most cases each part runs as an independent, autonomous hardware like a processing unit or memory and with an independent timing. Only for realtime dependent aspects the internal clocks of the specific components are synchronized to the time standard of the site. All of the components are connected together via local networks or other communication links, like serial lines, to allow a synchronous performance of the entire laser ranging process.

Because of this given situation modern laser ranging systems can be described as distributed systems in terms of computer science, where a distributed system consists of several independent computers (processors), which are connected together to solve a collective task in a cooperative way. During the processing time they don't share memory, clocks or other hardware and just communicate information while transferring messages via a computer network [SING94]/[PUD01].

Within a laser ranging system the following independent components can be identified:

- the telescope
- the dome

- the laser
- the transmit and receive unit
- the timing system and eventtimer
- different cameras
- a database which interacts with the outer world, like data centers
- the control system

and

- an additional, independent system monitoring for security and safety reasons

The human operator interacts with all of these components (mainly in a hierarchical structure via the control system but in some specific cases, e.g. development tests, also directly). The complete system itself is then a direct representation of the identified, independent, but interacting components. Therefore each hardware device is represented as a software component connected together via a client-server-model on the basis of a communication with Transmission Control Protocol over Internet Protocol (TCP/IP) or User Datagram Protocol over Internet Protocol (UDP/IP). In such a client-server-model a service requesting client starts the communication and sends an order request via message communication to a service offering server. At server side the order is processed and an answer message is returned to the client [SING94].

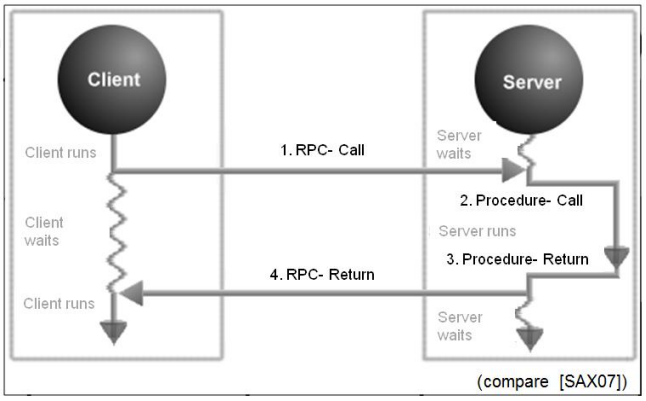

Figure 1. Remote procedure call

In classical communication networks each client server interaction is individually programmed during the software development process. Another attempt reduces the efforts of communication programming by defining a standardized way for the transmission of remote procedure calls (RPC). RPCs are comparable to local calls of procedures in a structured program but realized as control and data flows over a communication network to allow a standardized interaction between a requesting client and a service offering server [SING94]. Then the client just calls a procedure or function without the knowledge of the processing location and an additional RPC communication layer realizes the transfer between the remote processing server and the client. The response follows the same way vice versa to the client, so that the procedure call appears to be local (see figure 1). To reduce the programming effort the complete communication layer within this model is created by a special RPC generator which reads an interface definition file and produces all of the necessary modules. These can directly be used in the application code. There are several realizations available because this communication method is also the basis for the distribution platforms of modern web services.

But for the challenges of simplifying the communication within distributed systems for laser ranging, low-level realizations are more flexible and reliable than huge, sophisticated, additional communication packages. Here the Open Network Computing Remote Procedure Call (ONC RPC) is the preferred communication technique, because it is available in each Linux operating system as a standard and well developed since the year 1988. To generate the actual communication code units of RPC in the programming language C, the generator „rpcgen“ is used, which is also part of the operating system Linux. The generated code also includes the platform independent conversion of procedure parameter data using the External Data Representation (XDR) [STEV92]. So there is only the necessity to update the interface paradigms for modern object oriented implementations as an additional C++ layer over the C coded communication. This is done with a self-made additional generator.

The RPC-generator "idl2rpc.pl" and the usage of autonomous process cells

The new generator "idl2rpc.pl" is based on a script written in Perl language containing C++/C code templates, which uses a specific Interface Definition Language (IDL) as a high level description of an interface. So it converts the IDL description into RPC equivalent code using also the RPC environment already integrated in the operating system Linux . Several C++ adaptor classes to the C written RPC communication are created as well as the needed modules for threads creating parallel tasks or semaphores to protect critical sections (see figure 2). But for the application programmer only the following files are important where he has to include his specific code while the rest is just internally used for the communication:

On client side:
- "<INTERFACEFILENAME>[1*]_client.hpp" contains the class with the interface methods for remote procedures
- The client main program (e.g. a graphical user interface) which must be written completely by the application programmer

On server side:
- „<INTERFACEFILENAME>[2*]_server.cpp“ contains the skeleton methods where the application programmer has to include his own code into the method body

In this way the application programmer doesn't have to worry about communication matters but can concentrate on the actual application tasks. However he should use the provisions on the server side like threaded periodic loop activities etc. to realize independent servers. These should always keep stable states e.g. for the hardware devices connected to them . The servers can be located wherever they are needed so that they set up a distributed system. For stabilization each server contains something like a watchdog process which always restarts it after an unexpected crash. And it is planed also to include something like a "dead man's handle" comparable to trains. There it is used to check if the driver is still able to control the train. So he has to push a dedicated button periodically. In the distributed application a similar concept is used to check at server side if an active client exists. Therefore each client has to activate remote server functions periodically. These automatic safety devices can be activated optionally and starts a specific server routine which can lead to a stable and safe state again after a case of interaction failure [NEID08].

1 [1]*,[2]* <INTERFACEFILENAME> is replaced by the actual filename of the interface definition file

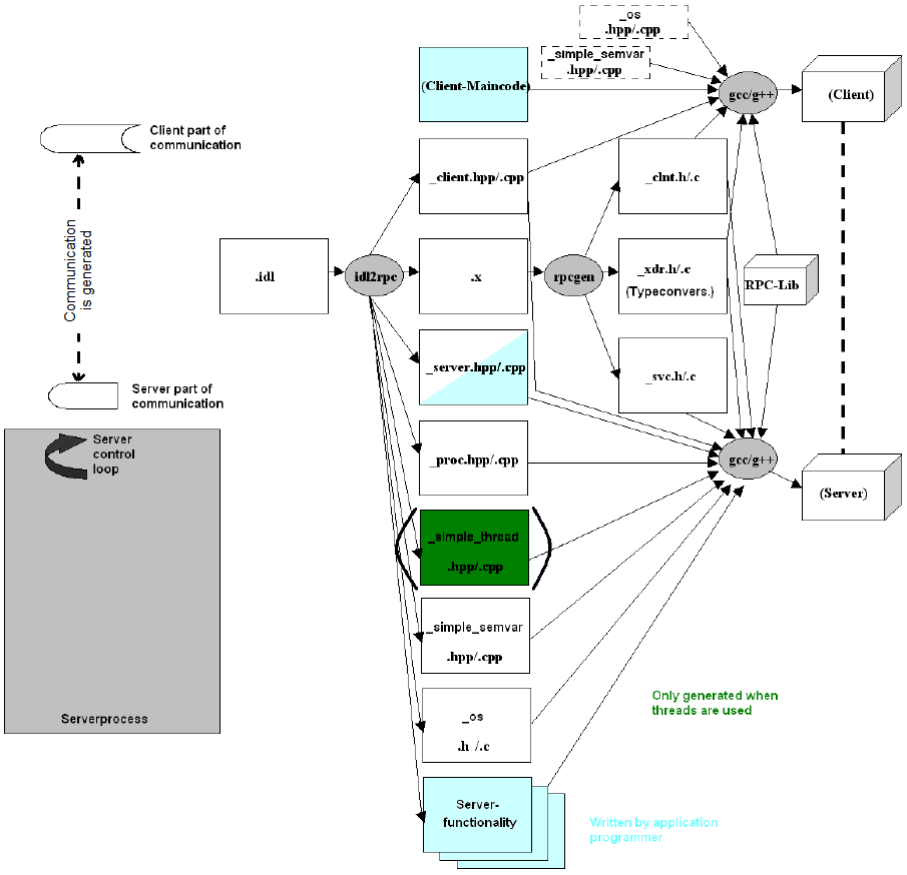

Figure 2. The generation process of "idl2rpc.pl" and the created files

All in all such method allows the creation of a distributed system consisting of several independent servers which act completely autonomous, so that these units are called autonomous process cells. These splits up a complex system like a laser ranging system into several manageable units interacting together with a general, standardized but also flexible communication. And in this communication all user or operator interactions can be included as additional clients realized as more or less complex user interfaces.

User interaction

The generated systems allow the integration of several different and parallel available user interface clients with different styles. This is because of the consequent separation between control and presentation logic. So it is possible to implement command line clients as well as high sophisticated web applications or graphical user interfaces. All of these possibilities are realized at SOSW so that for example the dome controller can be managed via browser window, command line and/or graphical user interface. And because of the automatically generated communication layer all of the user interfaces can directly be used to control the applications remotely.

For a first general realization all servers provide a command line control and a graphical user interface on the basis of wxWidgets. It is a C++ based open source framework for platform independent developments of graphical user interfaces [SMAR05]. Although the current RPC generator only supports Linux systems (32 and 64 Bit) the graphical user interface is modular enough to support different platforms like Windows, Linux, OSX and others. So a remote

operator can run the applications with highly sophisticated graphical interfaces. Because of the physical separation between the operator and the system it must be realized such that it protects human beings and the system itself from dangerous and error-prone situations.

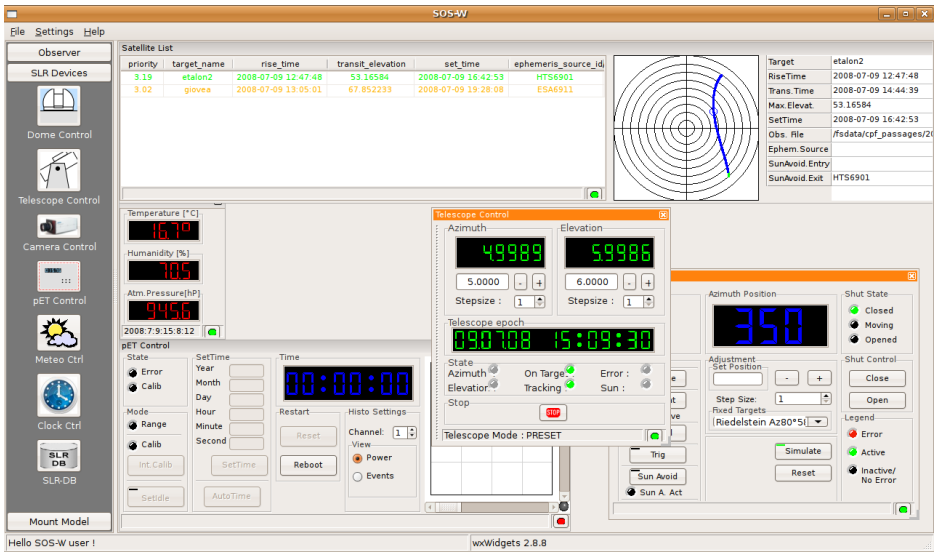

Figure 3. The graphical user interface on the basis of wxWidgets

Safety and security with the system

To realize such a protection safety and security concepts are in development. Safety hereby means the local protection given by local error states or local situations, like automatically moving hardware. One way to realize this is to write stable and autonomous software as given in the distributed process cells. In addition to that it is an advantage when the programmers follow some design rules as defined at Wettzell. They describe in general how code must be structured, documented, commented and so on. But no software is safe enough to have no bugs. So an additional, modular and multi-layered system monitoring hardware is in production which checks all of the important system states, like temperatures, weather conditions, safety switches and so on. This hardware is realized with standard equipment on a robust, well known architecture and supports several individual, vendor independent sensor devices. It is based on open source products in combination with the Linux operating systems (also with a minimal installation) and implements internally also the "idl2rpc.pl" created communication system. So it is an additional parallel monitoring system to ensure safety, also dealing with emergency issues.

Security in this case means the protection of the system from not allowed activities by unauthorized attackers or users without sufficient access right. Because all of the communication activities are based upon simple socket communications with TCP/IP or UDP/IP with fixable ports on which the additional RPC layer is established, Secure Shell (SSH) based tunneling methods can be used to build up efficient access protections. SSH hereby allows several authentication options like passwords, passphrases and key files or a combination of them. For the internal access right control for operator actions it is planned to realize an authentication (registration of a user with username and password) and authorization (personification of a user for a specific remote procedure with dedicated rights) as already implemented for other projects at Wettzell [NEID06]. This allows a safe and secure remote control from almost any place.

Remote control

To proof the functionality of the remote control and the general character of the implementations as well, several tests were initiated to run radiotelescopes for geodetic Very Long Baseline Interferometry (VLBI) also with the described software. Therefore adapted servers and clients were programmed to monitor the VLBI fieldsystem, which controls the VLBI experiments. Test sites were the radiotelescopes of the German Antarctic Receiving Station (GARS) O'Higgins in Antarctica, the Transportable Integrated Geodetic Observatory (TIGO) at Concepción/Chile and Wettzell. Several 24 hour and 1 hour intensive experiments were successfully run by remote control. These tests will be extended and will lead into a routinely operation for VLBI experiments at Wettzell. Co-operations with other institutes like the Max Planck Institute for Radioastronomy Bonn and the developers of the fieldsystem for VLBI are the first steps to establish this concept in the VLBI community.

Summary

The newly created software concept is a product of a long development done by several developers at Wettzell. The result is an option for upcoming Fundamentalstations with several different measuring systems like SLR systems and radiotelescopes to realize remotely controllable, autonomous subsystems on a basis of a stable, flexible and general communication platform. It can be used to reduce development time for highly available systems especially along the goals of the Global Geodetic Observing System (GGOS). But nevertheless there are always some situations which cannot be controlled and handled by such an automated system (like power failures where the dome is not closed automatically), so that responsible, well educated engineers at the sites should always be the final instance of automation.

References

[NEID06] Neidhardt, Alexander: Verbesserung des Datenmanagements in inhomogenen Rechnernetzen geodätischer Messeinrichtungen auf der Basis von Middleware und Dateisystemen am Beispiel der Fundamentalstation Wettzell. Dissertation, Mitteilungen des Bundesamtes für Kartographie und Geodäsie, Nr. 37, Bonifatius GmbH 2006

[NEID08] Neidhardt, Alexander: Manual for the remote procedure call generator "idl2rpc.pl". Geodetic Observatory Wettzell 2008 (latest version)

[SAX07] Saxonia Systems: Remote Procedure Call, http://www.linuxfibel.de/rpc.htm, Download 2007-04-23

[SING94] Singhal, Mukesh; Shivaratri, Niranjan G.: Advanced Concepts in Operating Systems. McGraw-Hill, Inc. 1994

[SMAR05] Smart, Julian; Hock, Kevin; Csomor, Stefan: Cross-Platform GUI Programming with wxWidgets. Prentice Hall International 2005

[STEV92] Stevens, W. Richard: Programmieren von UNIX-Netzen. Grundlagen, Programmierung, Anwendung. Prentice-Hall International, Inc. London 1992

[PUD01] Puder, Arno; Römer, Kay: Middleware für verteilte Systeme. 1. Auflage. dpunkt-Verlag GmbH Heidelberg 2001

A Method of SLR Data Automatic Preprocessing

DING Jian, QU Feng, WEI Zhibin
BeiJing SLR Station, Chinese Academy of Surveying and Mapping

Abstract

To get the range from observation station to satellite is the object of SLR. Data and its processing play an important role in SLR engineering. Data processing includes ephemeris prediction, producing tracking file, incepting initial data, preprocessing and producing result data, converting the format, and so on. And preprocessing is the most complex step in SLR data processing. The meaning of preprocessing is that noise is eliminated. How to realize automatic processing is the goal of this paper and it is also the object of next SLR generation. Reliability and efficiency are two necessary factors taken into account in automatic processing method.
Based on the reality of SLR engineering, a method of SLR data automatic preprocessing is introduced in this paper.

Introduction

Satellite Laser Ranging (SLR) observation data is used to satisfy the objectives of a wide range of scientific, engineering, and operational applications and experimentation. The basic observable is the precise time-of-flight of an ultrashort laser pulse to and from a satellite, corrected for atmospheric delays. These data sets are used by the ILRS to generate a number of fundamental data products, including:

- Centimeter accuracy satellite ephemerides
- Earth orientation parameters (polar motion and length of day)
- Three-dimensional coordinates and velocities of the ILRS tracking stations
- Time-varying geocenter coordinates
- Static and time-varying coefficients of the Earth's gravity field
- Fundamental physical constants (From http://ilrs.gsfc.nasa.gov)

But all these are based on SLR observation data sets of sufficient accuracy.
How to get high accuracy observation data is the first problem for SLR engineering and its application. In SLR engineering, the data flow includes satellite prediction, producing tracking file, incepting initial data, data preprocessing and building normal point (NP) observation data. Sites in the United States and Europe have been relatively stable over the past several years, with efforts continuing to improve overall performance or reducing the cost of SLR operations. The goal is to realize an automated SLR station. And the paper thinks that preprocessing is the most complex step in realizing automated SLR. To improve the ability of SLR station in preprocessing, we make great efforts that include SLR satellite ephemeris analysis, initial data distraction analysis, the indicator of standard built and automatic processing method proposed.

SLR data processing introduction

In this paper, the SLR data processing means that the work is done in SLR tracking station from satellite prediction to NP data built, and doesn't indicate that work done in ILRS data

centers, where they receive ranging data and create all kinds of scientific data products. So, the SLR data processing only includes satellite prediction (tracking file built), preprocessing (noise of initial observation data eliminated) and NP data built.
Satellite prediction is the foundation of SLR. Consolidated Prediction Format (CPF) is a new laser ranging prediction format.

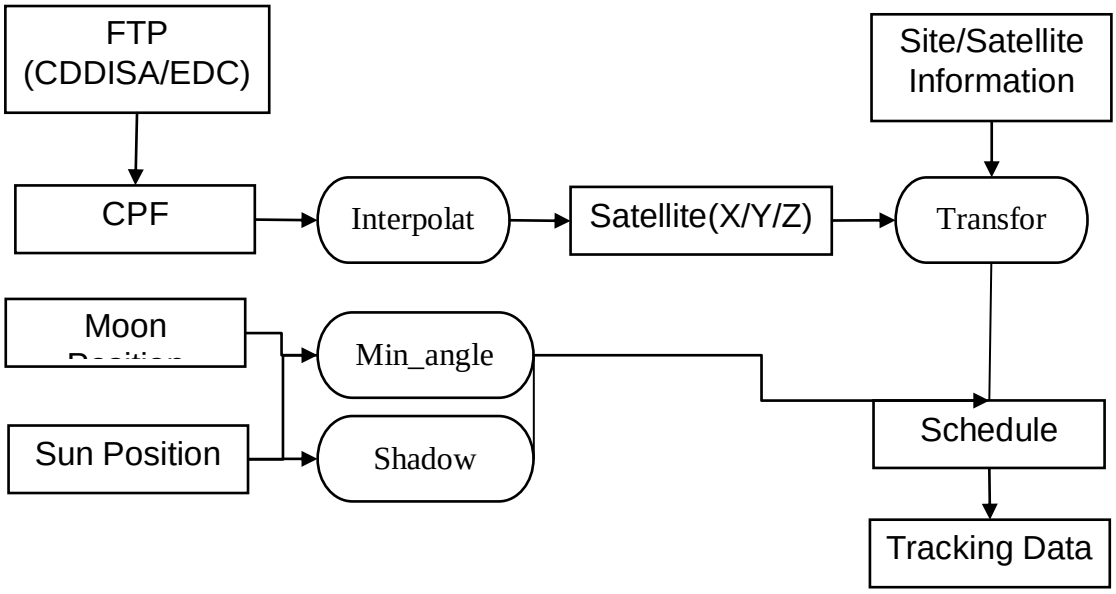

Figure 1. The data processing flow of before tracking

The data processing before tracking is the first step of data processing and is also the foundation in SLR engineering, which includes satellite prediction interpolation, Moon and Sun position computation, coordinate transforming and so on (see Fig.1). This object is to get tracking data to prepare the telescope to carry out ranging. Automation has been realized for this step, for every computation is well known. The second step is to eliminate noise from raw data and to form NP data. How to realize this step as automatic processing is the main goal of this paper.

Automatic preprocessing method

1. Main idea
SLR work is based on satellite predictions in either IRV or CPF format, so the quality of CPF is one determining factor in data preprocessing. And precision of the satellite prediction orbit should be in determinate range, so we can eliminate big noise from raw data if we know the precision range of satellite prediction orbit. For example, we compare the CPF to IGS(SP3) of GPS satellite prediction orbit to evaluate the precision of CPF satellite orbit based on IGS accuracy satellite ephemeris(to see Fig.2). The standard deviation seen in table 1.

Table 1. The compare of CPT to IGS of GPS satellite

Period	dX(CM)	dY(CM)	dZ(CM)
Pro-two days	±2.36	±6.30	±5.58
All five days	±14.21	±12.37	±8.09

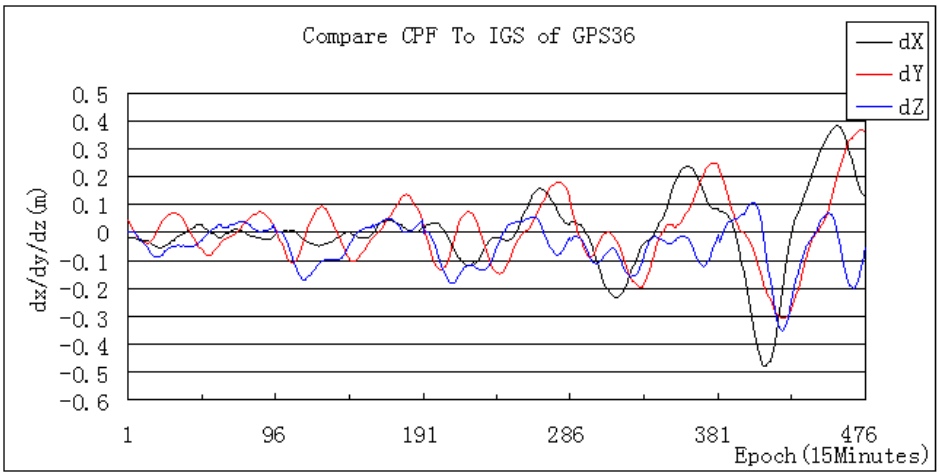

Figure 2 The compare of CPT to IGS of GPS satellite

In theory, satellite orbit is sequential, so the range of SLR observation and its change should be continuous. This is first very important information. The other important fact is that noise and true data is mutually exclusive, so a point is either noise or data. The true data must be in a line, and the noise is not. So we propose a spatial distribution comparison method to eliminate noise. First, setting the raw data based on prediction and its precision range, we can draw remaining data of O-C on time series. Second, cutting the O-C in scale, as formula (2-1).

$$\begin{aligned} &\frac{Max(o-c)-Min(o-c)}{100}=\Delta R \\ &Num(i)\geq All/100, i=1,2,\ldots,k_1 \\ &Num(j)\leq All/100, j=100,99,\ldots,k_2 \end{aligned} \qquad (2\text{-}1)$$

Then we obtain the new remaining range of O-C on $R_{\max New}$ and $R_{\max New}$.

$$\begin{aligned} R_{\max New} &= Max(0-c)-k_1\times\Delta R \\ R_{\min New} &= Min(0-c)+(100-k_2)\times\Delta R \end{aligned} \qquad (2\text{-}2)$$

The same method is used to cut on time series in scale. We can obtain the new time range. $T_{\max New}$ and $T_{\max New}$. At last, we obtain the new data range. In this range, the rate of signal to noise is very high, which is the prime indicator to realize automatic processing.

2. Application

In this part, we use the method in real data processing based on Beijing SLR station. Given a pass of BeaconC satellite as example.

(1) Using CPF precision scope to eliminate large noise

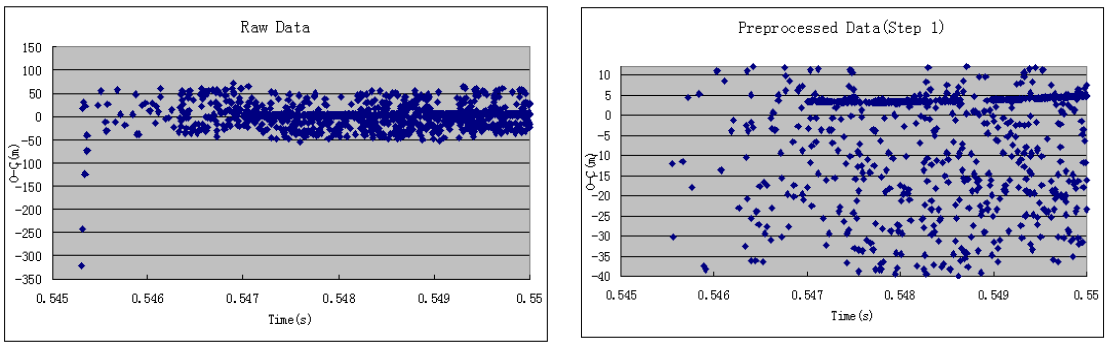

(a) Raw data (b) After first step processing

Figure 3. First step processing based on ephemeris precision scope

(2) Filtering on O-C range and Time serial

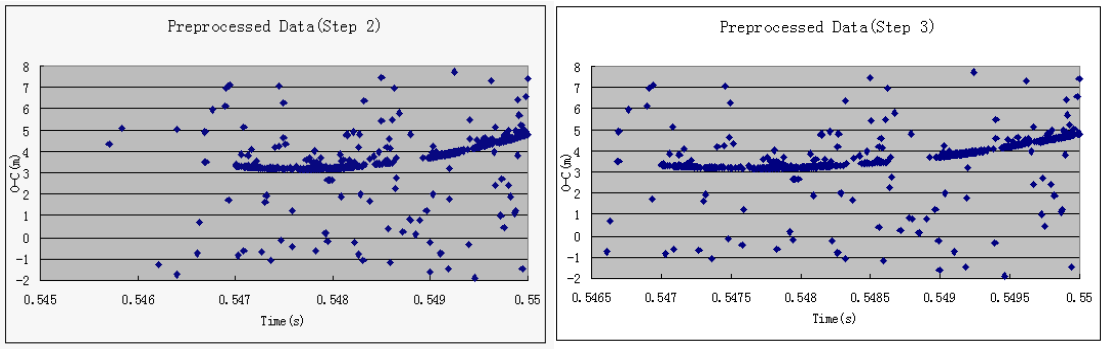

(a) After filtering on Range (b) After filtering on Time

Figure 4. After second and third processing step

Conclusion

To improve the automation in SLR tracking work and data processing is the aim in the future. Data preprocessing is a necessary part in SLR station. How to realize its automation is a quite complex problem, for there are lots of differences in every pass of observation data. So it is difficult to find a simple and unified method for all data. We make lots of experiments on this problem and draw a conclusion that rate of signal-to-noise is the prime indicator during data preprocessing. And the method mentioned in this paper purposes an approach in data automatic preprocessing and can perform the function to a certain extent. In fact, we only process observation data if the rate of signal-to-noise is very low. So we must make deep scientific researchers on this problem and wish to find reliable and effective method.

SLR Station Riga Software Upgrade.

K.Salminsh
Institute of Astronomy University of Latvia
kalvis@lanet.lv /Fax: +371-67034582

Abstract

The SLR station Riga is currently being upgraded with the new windows based data management, prediction and on-site data processing software. The new software is designed as client-server applications for use at the station and as a 3-tier application to access part of the system functionality via WWW. Comparing to the previous version the prediction generation and on-site data processing workflow is improved. Upcoming implementation of CRD format and kHz ranging support is discussed as well.

Introduction

Organization of the currently used software of the SLR station Riga can be represented as a number of independent subsystems:

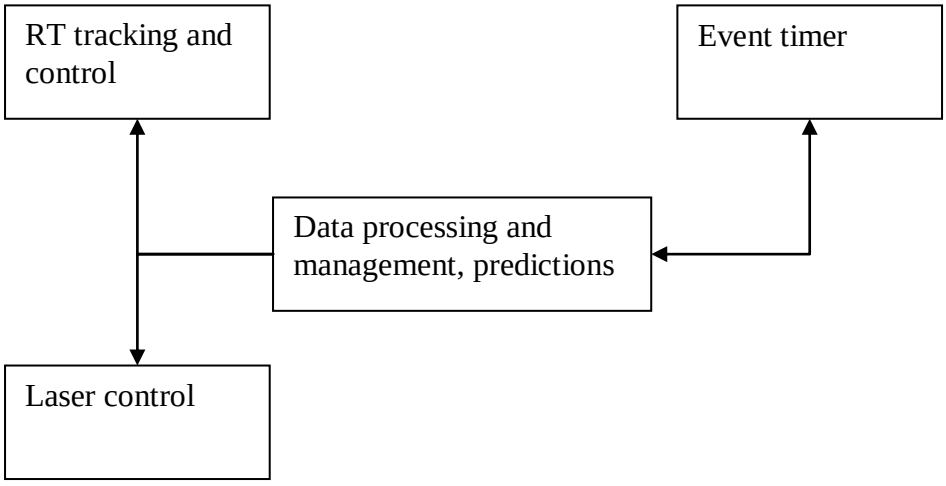

Figure 1. Software organization at SLR station Riga

1.Real time tracking and telescope control
2.Event timer software – handles RT-2006 event timer
3.Predictions, data post processing and management
4.Laser control

Data exchange between subsystems is implemented mostly on the file level e.g. prediction files are transferred to the telescope control and event timer and satellite ranging data are passed back later for the processing. The data management and processing subsystem is largely based on the developments dated back to the 1993 [Zarins, 1993] and it's starting to show its limitations. With the arrival of the new laser ranging data formats – CPF and CRD, the upgrading and maintaining the old, DOS based system, was not feasible anymore and it was decided to replace data management and post processing part with completely new,

Windows based system while maintaining compatibility with the other software and even keeping some parts of the previous subsystem like tracking scheduling, which may be upgraded later if necessary.

Functionality and design

The components of the new software are designed as a client-server and multitier applications and some of the solutions used are already previously tested in SLR operations. The software architecture overview is presented in the Figure 2.

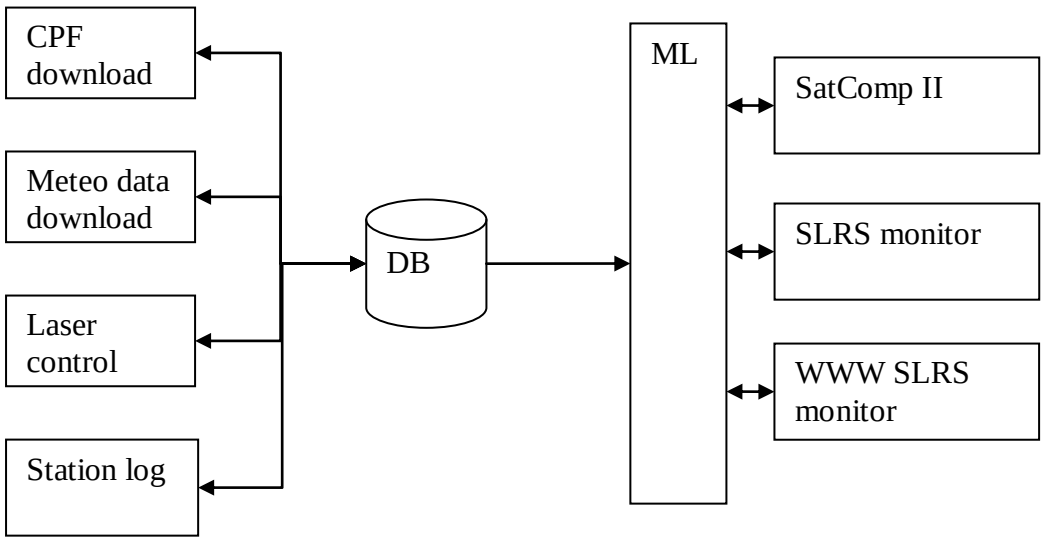

Figure 2. Data processing and management

The brief description of the components:

- DB – Firebird 2.1 [3] database where all SLR station relevant data is stored. All non-atomic data entities like satellite orbital data e.g. CPF, ranging data and produced reports are stored within the database in the compressed form using open source bzip2/libzip2 [4] compression library to save database disk space and reduce network traffic. For the ranging data is used XML based internal format [Salminsh, 2003].
- CPF Download – downloads latest CPF via FTP and stores in the database. Runs under scheduler each hour
- Meteo data download – each 10min reads Vaisala WXT-512 weather station and stores recorded data in the database. More than one sensor is supported so it's possible to record data from additional temperature sensors
- Laser control – implements restricted satellite tracking, can turn laser on/off according to the predefined pass segments and "Go/Nogo" flag settings.
- Station log – maintains history of the station activities like calibration history, satellite tracking statistics and additional parameters
- ML – software components, factoring out common data access functionality and providing services to other applications

- SatComp II – main application for data processing, predictions and data management. Calibration procedure now includes Engineering Data files (EDF) generation
- SLRS monitor – view station data like recorded meteorological data, EUROLAS station status etc.
- WWW SLRS monitor – similar to SLRS monitor but works in web browser.

All system components can run on the Windows 2000/XP based systems and most of them can be either operated remotely or can be installed on the remote computer and used from remote location. This flexibility allows setting up different configurations; easily replace computers in case of hardware failure and to work with the data from station and outside locations simultaneously. While it is possible to run all necessary software on a single computer for data safety and performance reasons the database and some of the service utilities are running around the clock on the separate Windows XP system. The Firebird database is a cross platform and can be also be run on any of the supported platforms like Linux. Additional feature is a capability to process the data from other stations. The only requirement is to convert ranging data to the defined XML format and enter station coordinates in the database.

Predictions and data processing

One of the important goals was to improve station workflow and to simplify routine operations: making predictions, calibration and ranging data post processing. After implementing automatic CPF download the prediction calculation is basically reduced to a few keystrokes and easily can be updated to the completely automatic mode. The prediction screenshot is shown in Figure 3.

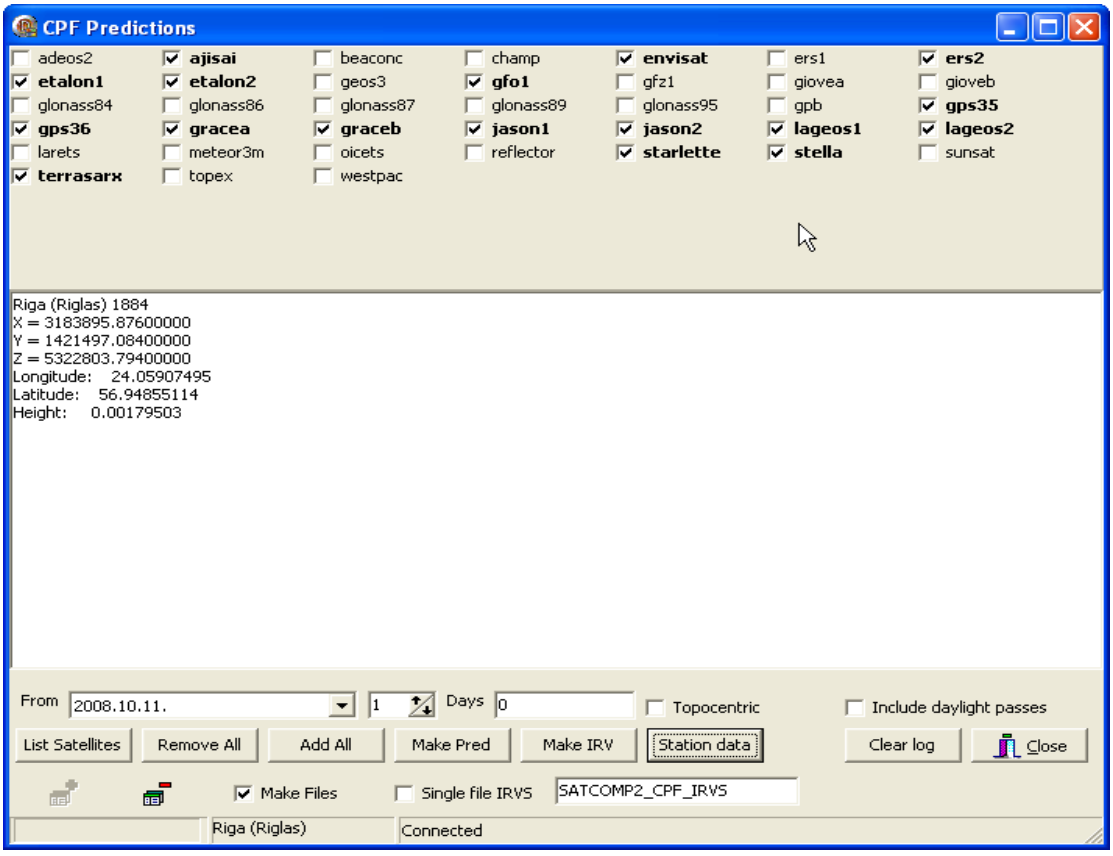

Figure 3. CPF predictions

For testing purposes generation of IRV's from CPF is also supported. Data processing organization (Figure 4) is also changed by adding generation of EDF and support for the new CRD format. CRD creation is based on using XSLT transformation from the internal XML format. Processed data can be sent directly to the analysis centre without using external mail client software.

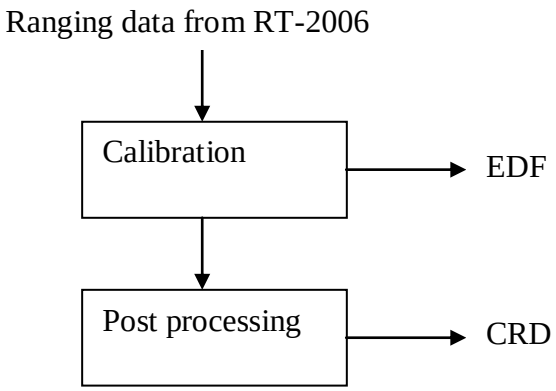

Figure 4. Data processing

Other improvements are mostly intended for testing and diagnostic purposes like error reporting in case of errors.

KHz ranging data handling

One of the requirements for the new software is to be able to work with the KHz ranging data, and this feature is currently under development. The tests were made to verify that the database and client software is able to handle large amount of the measurements in the KHz ranging data taking into the account that the XML size overhead which is negligible with the common ranging frequency 10Hz could be a performance problem in case of 2 KHz. Example of one of the preliminary test results: unprocessed Giove-A pass from Graz SLR station containing 248174 range measurements:

- Original size 9.8 Mb
- Size in XML format 18 Mb
- Compressed XML 2290 Kb
- Compressed original 2219 Kb
- Average time to parse XML 1-3 sec

Tests were done in virtual machine (Windows XP running under Window XP host system) approximately equivalent to 1.6GHz Intel Pentium dual core PC with 1Gb RAM. It should be noted that the size difference between compressed XML and compressed original plain text data is around 4-6 % while uncompressed XML file is about twice of the original size. Even in case of using full pass data when we can expect ~1,000,000 returns from Lageos [Kirchner and Koidl, 2004] the single pass dataset size and expected processing speed is still within estimated acceptable limits imposed by the local network speed (100 MBit), XML parser and typical client PC performance. While the latest versions of Firebird database

engine on NTFS file system used in Windows XP can handle database sizes in terabyte ranges [3] for practical reasons like performance and limitations of the typical computer used in SLR station it would be necessary to periodically offload the KHz ranging and associated data to the external storage to keep the database size within reasonable limits e.g. 4-10 Gb size.

References

[1.] Zarins, A. Satellite Observation Support Package for IBM PC", University of Latvia, Scientific papers, vol. 586, p 38-45, Riga, 1993
[2.] Salminsh, K. XML applications in SLR, Proceedings of the 13th International Workshop on Laser Ranging. Washington, USA, October 7-11, 2003.
[3.] http://www.ibphoenix.com
[4.] http://www.bzip.org
[5.] Kirchner, G., Koidl, F. Graz Khz SLR System: Design, Experiences and Results, 14th International Workshop on Laser Ranging, San-Fernando, Spain, June 7-11, 2004

On the Generation of SLR Output Files at Mt Stromlo

C.J. Moore, P. Wilson
EOS Space Systems Pty. Canberra, Australia.
cmoore@eos-aus.com / Fax +61 2 6287 2951

Abstract

As part of the re-establishment and improvement of the Mt Stromlo SLR station, much of the software systems have been redeveloped, including new post-processing software. With the advent of the new CRD format this has provided an opportunity to consider new approaches to the generation of data products. This paper provides a description of the approach adopted, using XML and XSLT technologies.

Introduction

When considering the redevelopment of the software modules responsible for the generation of output data files resulting from the processing of satellite laser ranging (SLR) data, the following design requirements were established;

- Raw ranging data should be processed only once.
- All useful data should be extracted and stored in a single data repository/file.
- Output data should be accessible to different users regardless of processing platforms and location.
- Data subsets can be easily extracted for the generation of various reports including current normal point, full rate and new CRD formats.
- Software architecture should easily allow for future functional extensions (eg new data types) with minimal impact on the current software base.

One technology that has recently evolved to meet these types of requirements uses files structured with extensible mark-up language (XML). It was considered that the use of XML files provides a much more flexible solution than alternatives based on, for example, relational databases, unstructured files or proprietary binary files. In fact XML query language provides powerful database-like search and extraction facilities eliminating the need for a conventional database.
There is increasing popularity in the use of XML as a means for data exchange (e.g see Salminsh, 2003) and it is of note that the new ILRS CRD format (Ricklefs and Moore, 2008) has a structure and "mark-up" elements that give some resemblance to an XML document. The CRD format was in fact designed to support an evolutionary path to the adoption of XML and in practice we have found it convenient to create an XML file having a CRD-like format as an intermediary stage in the generation of CRD format reports.

SLR Post Processing

Figure 1 shows an overview of the typical data flow associated with the processing of data obtained during laser ranging sessions. A "raw" file of ranging data collected during a satellite pass is processed to identify and extract true signal data, from which full rate, normal point and other useful data are determined and stored as an XML file in a "local" format. Similar files are generated while ranging to calibration targets. Such

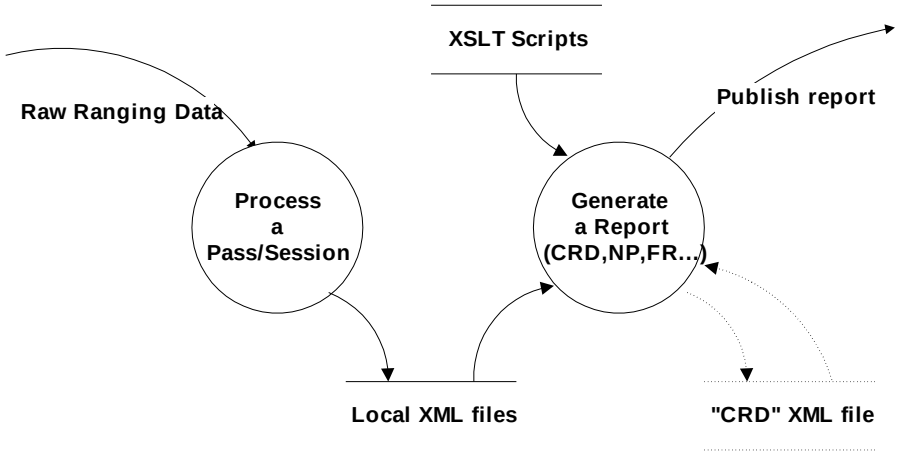

Figure 1. SLR Data Flow Diagram

files contain many other data that are considered to be useful for the station and other users of the data.

It is expected that new data items will be identified for inclusion over time, but using XML, such data can be easily added without impacting existing users and software applications. As far as this "local" data format is concerned, it is important that the requirements of the station are not inhibited by externally defined formats or restrictions (which may change over time), but this provides a responsibility for the station to capture all necessary and available data to meet both station and external or client requirements. A sample XML file in "local" format is shown in Listing 1. Note that Listings 1 to 3 refer to sample files whose format is expected to change in response to on-going development and user requirements.

Software Design

The key point with the use of XML files is that additional data fields can be added without impacting on the existing data sets. Also with object oriented software architecture, the addition of new data types can be made at any appropriate node in the XML tree structure, by simply adding additional software classes or modules. The software responsible for generation and formatting of the existing data sets should not require modification. Figure 2 shows a schematic of the software architecture used at Mt Stromlo where independent groups of data sets are identified and associated with their own software classes for processing and storage. If a new set of closely coupled data is identified, then it is simply a matter of writing a new class for these data that will *inter alia* have the responsibility for updating the output XML file.

In this way software design and development can be minimized while maximizing the robustness of the existing code base. Existing and stable third-party XML/XSLT libraries such as the MSXML or Xerxes/Xalan libraries have been adopted to further minimise software development and maintenance.

Report Generation

Once generated, the "local" XML files is used as the data source for the generation of required report files i.e. data files suitable for publication to external bodies or clients using agreed formatting rules. Even quite complex transformations from the local XML structure to such reports can be accomplished using extensible stylesheet language

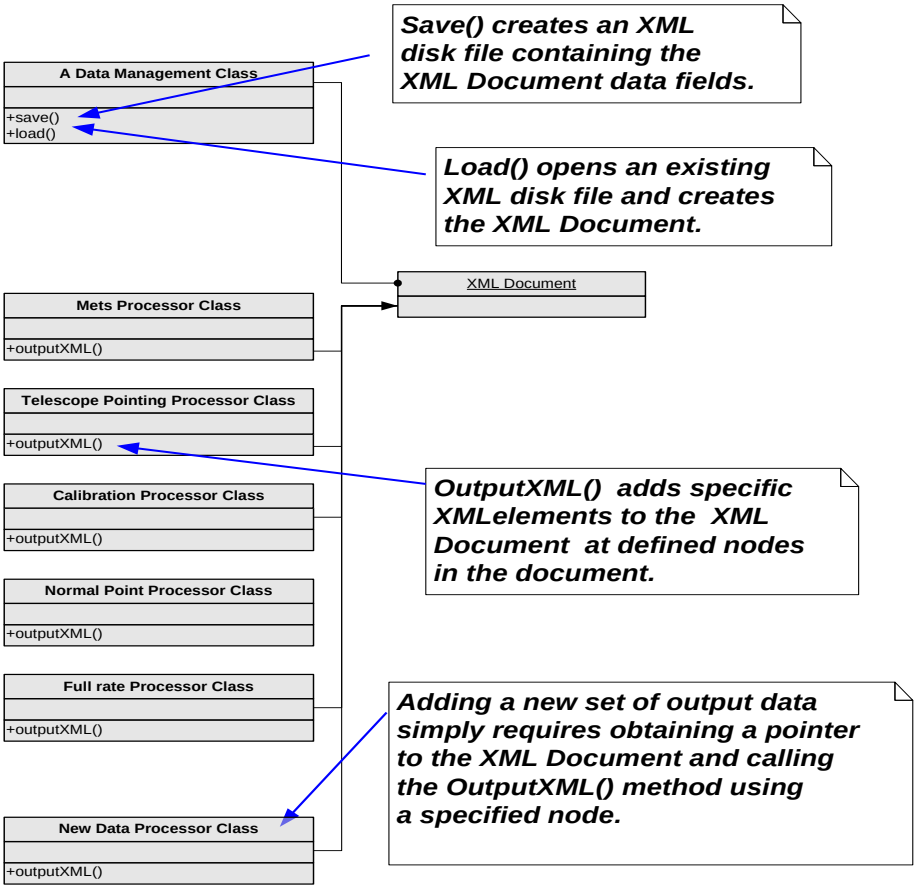

Figure 2. Typical software classes to append/insert records in an XML document.

transformation (XSLT) transforms. Generation of new reports or modifications to existing reports can therefore be managed without any modification to software binaries.

This approach has been used successfully to create all of the station generated ILRS reports including files in the new CRD format (Ricklefs and Moore, 2007), as well as files in the currently required ILRS normal point and full rate formats. As mentioned, to simplify the transformation process we also generate a temporary CRD-like XML file, currently having a format similar to that shown in Listing 2. This file is then used for subsequent transformation to actual CRD format reports, and to current ILRS normal point and full rate reports. An example of an XSLT transform to complete the generation of an ILRS normal point format file is shown in Listing 3.

File Sizes

One criticism of XML files, given they are in ASCII and contain mark up tags, is that they can be quite verbose. For example a “local” format XML file containing full rate and other data from a Lageos pass at 60Hz fire rate, has a size of about 100 Kbytes and an intermediary CRD-like XML file has a size of about 150 Kbytes. The corresponding combined full rate and normal point CRD File has a volume of about 60 Kbytes. Compression reduces all of these files to about 10% of their original size.

Conclusions

Redevelopment of processing software at Mt Stromlo is well advanced and now incorporates XML technology in the generation of output files. This approach is particularly well suited for the generation of data files in the new CRD format. It is hoped that these developments show that the use of XML files is a suitable and appropriate technology for storage and publication of SLR data.

References

Ricklefs, R.L and C. J. Moore, 2007. Consolidated Laser Ranging Data Format (CRD). http://ilrs.gsfc.nasa.gov/products_formats_procedures/crd.html

Salminsh, K., 2003. XML Applications in SLR, cddis.nasa.gov/lw13/docs/papers/upg_salminsh_1m.pdf

Listing 1: Sample of a "Local" XML File

```
<?xml version="1.0" encoding="UTF-8" standalone="no"?>
<eos:root xmlns:eos="schemas.eos-aus.com/BrdDataAnalysis/1">
    <MetaData FileCreated="25/02/2009 01:12" RangeUnits="nanoseconds" SchemaName="BrdDataAnalysis" SchemaVersion="1">
        <SourceFiles>
            <BrdFile Filename="ERS2_20060731_232154.brd"/>
        </SourceFiles>
        <Software>
            <Application Built="Thu Feb 19 04:07:24 2009 UTC" Platform="Win32" Name="Profits.exe" Version="5-2-1"/>
            <Library Built="Thu Feb 19 01:13:10 2009 UTC" Platform="Win32" Name="BrdAnalysis.lib" Version="1-0-10"/>
…etc…
        </Software>
    </MetaData>
    <System CdpOcc="01" CdpPadId="7825" CdpSys="90" Height="805.027300" Latitude="-35.316144" Location="Stromlo"
Longitude="149.009880" Name="" Network="Stromlo" TimeScale="GPS">
        <Target CoM="0.000000" Cospar="9502101" NPIndex="3" Name="ERS2" Sic="6178" Signature="0.200" Type="1">
            <Session StartDay="31/07/2006" StartDoY="212" StartMjd="53947.975880" StartSeconds="84329.0" StartYear="2006"
        StopDay="31/07/2006" StopMjd="53947.980995" StopSeconds="84758.0">
                <ProcessOptions AmpCorrApplied="FALSE" CoMApplied="FALSE" EpochEventType="Station Laser Fire"
            Quality="Good" RangeDataType="2-way" RefractionApplied="FALSE" Release="0" SDApplied="TRUE"/>
                <SystemConfig>
                    <Laser Divergence="30.0" FireRate="60.0" PulseEnergy="20.800" PulseWidth="12.0" SemiTrain="1" Type="Nd-
                YAG" Wavelength="532.00"/>
                    <Detector DarkCount="0.0" Polarizer="Linear" PulseType="ECL" PulseWidth="0.0" QE="0.2" SpatialFilter="15.0"
                SpectralFilter="1.0" Transmission="100.0" Type="CSPAD" Voltage="0.0" Wavelength="532.0"/>
                    <Timer EpochDelay="232.200" FreqSource="TrueTime_OCXO" TimeSource="TrueTime_XLi" TimerSN="NA"
                Type="MRCS"/>
                    <Enclosure AirWindowDiameter="1.362" DomeDiameter="4.5070" GlassWindowDiameter="1.362"
                GlassWindowRI="1.474" GlassWindowThickness="0.0190" NormalWindowDelay="0.063" Type="Typhoon"/>
                <FullRateData>
                    <Segment StartDay="31/07/2006" StartSeconds="84329.0" StopSeconds="84758.0">
                        <EnclosureWindow WindowUsed="GLASS"/>
                        <SystemCal Kurtosis="2.7" MeanDelay="168.306" Method="Post Cal" NumData="26488"
                    NumDataUsed="14901" PeakOffset="0.000" Rms="0.024" Seconds="29412068.5" Shift="0.117" ShiftType="Peak
                    To Peak" Skew="0.2" TargetDistance="632.575"/>
                        <Shot Range="8257253.3031" Refraction="25.4315" Residual="25.4510" Seconds="84514.211781815495"/>
…etc…
                    </Segment>
                </FullRateData>
                <NormalPoints IntervalSecs="15.00">
                    <NormalPoint Bin="5634" Humidity="69.6" Kurtosis="-0.76" NumTotal="282" NumUsed="19" Peak="0.0000"
                Prediction="8224488.6565" Pressure="926.8" Range="8224412.2734" Rate="6.88" Refraction="25.2938"
                Residual="0.0016" Rms="0.0113" Seconds="84518.645115210" Skew="-0.03" Temperature="5.30"/>
…etc…
                </NormalPoints>
                <SummaryStatistics Bin="637" Humidity="68.4" Kurtosis="-0.73" NumTotal="3678" NumUsed="92" Peak="0.0155"
            Prediction="8156254.8181" Pressure="926.9" Quality="0" Range="8156254.8171" Rate="3.88" Refraction="29.6284"
            Residual="-0.0009" Rms="0.0138" Seconds="84554.592019940" Skew="-0.01" Temperature="5.26"/>
                </SystemConfig>
                <Mets Origin="Measured">
                    <MetData Humidity="69" Pressure="926.9" Seconds="84469.645115211169" Temperature="5.2"/>
…etc…
                </Mets>
                <Pointing Origin="Measured">
                    <Tel Azim="166.482633" Elev="17.945640" Seconds="84328.899965"/>
…etc…
                </Pointing>
            </Session>
        </Target>
    </System>
</eos:root>
```

Listing 2: Sample of a "CRD" XML File

```
<?xml version="1.0" encoding="iso-8859-1"?>
<crd xmlns:eos="schemas.eos-aus.com/BrdDataAnalysis/1">
    <format record_type="H1" version=" 0" year="2009" month="02" day="25" hour="01" minute="12">
        <!--Station Header-->
        <station record_type="H2" station_name="Stromlo" cdppad_id="7825" cdp_sys="90" cdp_occ="01" timescale="GPS">
            <!--Target Header (H3)-->
            <target record_type="H3" name="ERS2" cospar_id="9502101" sic="6178" norad_id="000000"
        SpacecraftEpochTimeScale="0" TargetType="1" />
            <!--Unique Laser Records-->
            <Laser record_type="C1" unique_id="IDASCXFB" Divergence="30.0" FireRate="60.0" PulseEnergy="20.800"
        PulseWidth="12.0" SemiTrain="1" Type="Nd-YAG" Wavelength="532.00" />
            <!--Unique Detector Records-->
```

```
        <Detector record_type="C2" unique_id="IDA0CXFB" DarkCount="0.0" Polarizer="Linear" PulseType="ECL"
        PulseWidth="0.0" QE="0.2" SpatialFilter="15.0" SpectralFilter="1.0" Transmission="100.0" Type="CSPAD" Voltage="0.0"
        Wavelength="532.0" Processing="Profits_5-2-1" />
        <!--Unique Timer Records-->
        <Timer record_type="C3" unique_id="IDAGDXFB" EpochDelay="232.200" FreqSource="TrueTime_OCXO"
    TimeSource="TrueTime_XLi" TimerSN="NA" Type="MRCS"/>
        <!--Unique Enclosure Records-->
        <Enclosure unique_id="IDAMDXFB" AirWindowDiameter="1.362" DomeDiameter="4.5070"
        GlassWindowDiameter="1.362" GlassWindowRI="1.474" GlassWindowThickness="0.0190" NormalWindowDelay="0.063"
        Type="Typhoon" />
        <!--Unique Transponder (Clock) Records (not used at Mt. Stromlo)-->
        <!--Unique Configuration Records-->
        <system_configuration_record unique_id="IDARCXFB" record_type="C0" wavelength="532.0">
            <component laser_id="IDASCXFB" detector_id="IDA0CXFB" timer_id="IDAGDXFB" />
        </system_configuration_record>
        <!--Session Header (Full Rate)-->
        <session record_type="H4" data_type="0" start_year="2006" start_month="07" start_day="31" start_hour="23"
        start_minute="25" start_second="29" end_year="2006" end_month="07" end_day="31" end_hour="23" end_minute="32"
        end_second="38" >
            <StartDoY>212</StartDoY>
            <ProcessOptions AmpCorrApplied="FALSE" CoMApplied="FALSE" EpochEventType="Station Laser Fire"
            Quality="Good" RangeDataType="2-way" RefractionApplied="FALSE" Release="0" SDApplied="TRUE" />
            <!--Summary Statistics-->
            <SummaryStatistics record_type="50" unique_config_id="IDARCXFB" Bin="637" Day="31/07/2006" Humidity="68.4"
            Kurtosis="-0.73" NumTotal="3678" NumUsed="92" Peak="0.0000000000155" Prediction="0.008156254818100001"
            Pressure="926.9" Quality="0" Range="0.0081562548171" Rate="3.88" Refraction="0.0000000296284" Residual="-
            0.0000000000009" Rms="0.0000000000138" Seconds="84554.592019940" Skew="-0.01" Temperature="5.26" />
            <Mets record_type="20" Origin="Measured">
            <MetData Humidity="69" Pressure="926.9" Seconds="84469.64511521" Temperature="5.2" /><MetData Humidity="68"
        Pressure="926.8" Seconds="84579.578448514367" Temperature="5.3" />
...etc...
            <segment starting_year="2006" starting_month="07" starting_day="31" start_hour="23" start_minute="25"
        start_second="29" end_hour="23" end_minute="32" end_second="38">
                <!--Calibration Record-->
                <calibration record_type="40" seconds_of_day="29412068.5" type_of_data="0" unique_config_id="IDARCXFB"
                data_points_recorded="26488" data_points_used="14901" one_way_target_distance="632.575"
                cal_sys_delay="0.00000016830" cal_delay_shift="0.000000000117" Rms="0.000000000024" Skew="0.2"
                Kurtosis="2.7" sys_delay_peak="0" cal_type="2" cal_shift_type="3" detector_channel="0" />
                <EnclosureWindow WindowUsed="GLASS" />
                <data record_type="10" seconds="84514.211781815495" epoch_event="2" unique_config_id="IDARCXFB"
            Range="0.0082572533031" />
...etc...
            </segment>
            <!--Pointing Angles Records-->
            <Pointing record_type="30" Origin="Measured">
                <Telescope seconds_of_day="84331.94495" Azimuth="165.059559" Elevation="16.809546" TxRxDirection="0"
            RefractionCorrected="0" />
...etc...
            </Pointing>
        </session>
        <!--Session Header (normal points)-->
        <session record_type="H4" data_type="1" start_year="2006" start_month="07" start_day="31" start_hour="23"
        start_minute="25" start_second="29" end_year="2006" end_month="07" end_day="31" end_hour="23" end_minute="32"
        end_second="38" >
            <StartDoY>212</StartDoY>
            <ProcessOptions AmpCorrApplied="FALSE" CoMApplied="FALSE" EpochEventType="Station Laser Fire"
            Quality="Good" RangeDataType="2-way" RefractionApplied="FALSE" Release="0" SDApplied="TRUE" />
            <!--Summary Statistics-->
            <SummaryStatistics record_type="50" unique_config_id="IDARCXFB" Bin="637" Day="31/07/2006" Humidity="68.4"
            Kurtosis="-0.73" NumTotal="3678" NumUsed="92" Peak="0.0000000000155" Prediction="0.008156254818"
            Pressure="926.9" Quality="0" Range="0.0081562548171" Rate="3.88" Refraction="0.0000000296284" Residual="-
            0.0000000000009" Rms="0.0000000000138" Seconds="84554.592019940" Skew="-0.01" Temperature="5.26" />
            <Mets record_type="20" Origin="Measured">
                <MetData Humidity="69" Pressure="926.9" Seconds="84469.645115211169" Temperature="5.2" />
...etc...
            </Mets>
            <!--Calibration Record-->
            <calibration record_type="40" seconds_of_day="29412068.5" type_of_data="0" unique_config_id="IDARCXFB"
            data_points_recorded="26488" data_points_used="14901" one_way_target_distance="632.575"
            cal_sys_delay="0.0000001683" cal_delay_shift="0.000000000117" Rms="0.000000000024" Skew="0.2" Kurtosis="2.7"
            sys_delay_peak="0" cal_type="2" cal_shift_type="3" detector_channel="0" />
            <!--NormalPoints-->
            <NormalPoints DoY="212" Year="2006">
                <normal_point record_type="11" seconds="84518.645115210" Range="0.008224412273400001"
                Prediction="8224488.6565" Residual="0.0016" unique_config_id="IDARCXFB" epoch_event="2"
```

```
                    WindowLength="15.00" Day="31/07/2006" RawRanges="19" BinRMS="0.0000000000113" BinSkew="-0.03"
                    BinKurtosis="-0.76" ReturnRate="6.88" Peak="0" Humidity="69.6" Pressure="926.8" TemperatureC="5.30"
                    Refraction="25.2938" />
...etc...
                </NormalPoints>
            </session>
        </station>
    </format>
</crd>
```

Listing 3 – Example of an XSLT transform to convert a CRD-XML file to ILRS NP format.

```
<?xml version="1.0" encoding="UTF-8" ?>
<xsl:stylesheet version="1.0" xmlns:xsl="http://www.w3.org/1999/XSL/Transform" xmlns:eos="www.eos-aus.com">
        <xsl:output method="text" version="1.0" indent="no" encoding="ISO-8859-1" />
        <xsl:template match="/">
                <xsl:apply-templates select="//NormalPoints" />
        </xsl:template>
        <xsl:template match="NormalPoints">99999
<xsl:value-of select="format-number(../../target/@cospar_id, '0000000')" />
<xsl:value-of select="substring(@Year, 3, 2)" />
<xsl:value-of select="format-number(@DoY, '000')" />
<xsl:value-of select="../../@cdppad_id" />
<xsl:value-of select="format-number(../../@cdp_sys, '00')" />
<xsl:value-of select="format-number(../../@cdp_occ, '00')" />
<xsl:value-of select="format-number((../../Laser/@Wavelength * 10), '0000')" />
<xsl:value-of select="format-number((../../session/segment/calibration/@cal_sys_delay * 1000000000000.0), '00000000')" />
<xsl:choose>
        <xsl:when test="(../../session/segment/calibration/@cal_delay_shift &lt; 0)">
                <!-- force the negative number, positive -->
                <xsl:value-of select="format-number((../../session/segment/calibration/@cal_delay_shift * 1000000000000.0) * -1.0,
'000000')" />
        </xsl:when>
        <xsl:otherwise>
                <xsl:value-of select="format-number((../../session/segment/calibration/@cal_delay_shift * 1000000000000.0),
'000000')" />
        </xsl:otherwise>
</xsl:choose>
<xsl:value-of select="format-number((../../session/segment/calibration/@Rms * 1000000000000.0), '0000')" />
<xsl:choose>
                        <xsl:when test="normal_point[1]/@WindowLength='5.00'">1</xsl:when>
                        <xsl:when test="normal_point[1]/@WindowLength='15.00'">3</xsl:when>
…etc…
                        <xsl:when test="normal_point[1]/@WindowLength='300.00'">9</xsl:when>
                        <xsl:otherwise>0</xsl:otherwise>
                </xsl:choose>
<xsl:choose>
        <xsl:when test="//crd/format/station/@timescale = 'GPS'">4</xsl:when>
</xsl:choose>
<xsl:text>0</xsl:text>
<xsl:text>4</xsl:text>
<xsl:choose>
        <xsl:when test="../../session/segment/EnclosureWindow/@WindowUsed='AIR'">1</xsl:when>
        <xsl:when test="../../session/segment/EnclosureWindow/@WindowUsed='GLASS'">2</xsl:when>
</xsl:choose>
<xsl:value-of select="format-number((../SummaryStatistics/@Rms * 1000000000000.0), '0000')" />
<xsl:text>0</xsl:text>
<xsl:text>00</xsl:text>2
<xsl:apply-templates />
        </xsl:template>
        <xsl:template match="normal_point">
<xsl:value-of select="format-number((@seconds * 10000000.0), '000000000000')" />
                <xsl:value-of select="format-number((@Range * 1000000000000.0),'000000000000')" />
                <xsl:value-of select="format-number((@BinRMS * 1000000000000.0),'0000000')" />
                <xsl:value-of select="format-number((@Pressure * 10.0), '00000')" />
                <xsl:value-of select="format-number(((@TemperatureC + 273.15) * 10.0), '0000')" />
                <xsl:value-of select="format-number(@Humidity, '000')" />
                <xsl:value-of select="format-number(@RawRanges,'0000')" />
                <xsl:text>0</xsl:text>
                <xsl:text>0</xsl:text>
                <xsl:text>0</xsl:text>
                <xsl:text>00</xsl:text>00
</xsl:template>
</xsl:stylesheet>
```

Implementing the New ILRS CRD Data Format

M. Kuźmicz-Cieślak, E. C. Pavlis
JCET/UMBC and NASA Goddard, Maryland, USA
epavlis@umbc.edu/Fax: +1-410-455-5832

Abstract

The new CRD format is now set to replace the current formats used to disseminate the ILRS data. Stations are expected to pass compliance tests and then submit their data in CRD by sometime in 2010. We have used data provided in the new format to generate test results, and put in place the process by which we will be "digesting" such data into the current analysis scheme at the JCET AC (using NASA's GEODYN). We will show results obtained using a small sample data set of NP from MLRS. These will be compared to the nominal results obtained from the exact same data set provided in the current ILRS format. Our intention is that following the Poznan workshop, the JCET AC will be ready to accept CRD data from the ILRS network in order to validate stations that wish to convert to this format.

Introduction

In anticipation of ILRS' transition to a new data format, the Consolidated Laser Ranging Data Format (CRD) [Ricklefs and Moore, 2008], we have developed a mechanism to ingest the current SLR data in CRD format in Goddard's GEODYN data analysis environment. We use this mechanism to compare results obtained from the original data in the ILRS Quick Look Normal Point (QLNP) format to those obtained with the data transmitted in the new format. The ILRS Analysis Working Group (AWG) has been tasked to validate the CRD-formatted data from each ILRS site, before that site can switch its delivery format to the new one. This contribution documents one approach for this validation task and results for the first site to successfully complete this process.

Importing CRD data into GEODYN

As most data analysis software packages, GEODYN has its own format options for the various data that it is capable to analyze. This is the result of a preprocessing software called the Tracking Data Formatter or TDF, which accepts the data in several formats, binary or ascii, and generates a binary output file that is the format recognized by GEODYN. In the case of ILRS SLR data, up to this date the data could be delivered either in the ILRS QLNP format or the Full Rate (FR) format, both of which are formatted text files. The process of importing them in GEODYN involves two steps:

- For the QLNP data:
  a. Reformatting the QLNP to the (binary) TDF input format
  b. Converting the above file to a GEODYN data (binary) input file
- For FR data:
  a. Use TDF's option to ingest data in the FR format directly, and convert the file to a GEODYN data (binary) input file in one step

The new CRD format has an entirely different structure from either QLNP or FR, with groups of records of different types, some mandatory, some optional, the content of these

records being variable and free-formatted, etc. Above all, the freedom in the way that each quantity enters each record allows a much greater precision for these quantities than the previously fixed formats allowed. The CRD format allows also for a multitude of additional parameters from the engineering qualification of the data to be passed on to the analyst, which however are by and large not necessary for the reduction of the data. This meant that instead of modifying TDF to read the CRD files directly, we could use an interim format to achieve the same effect, as long as that format could accommodate the higher precision in the CRD data records.

We chose to modify the FR format to what we internally call an "extended FR" format (x-FR), which allows for practically any precision in the most important quantities, e.g. the time, the range and the meteorological data. We then modified TDF adding an option that can handle this x-FR formatted data. This allows the data to be readily used in GEODYN with minimal changes in the code and the processing mechanics. This extension can now be used operationally to process ILRS CRD data with GEODYN while at the same time we can also handle data in any of the previously used formats. This flexibility is extremely useful, as it will become apparent in the next section.

Validation of CRD data releases

The first site to release CRD data is the McDonald Laser Ranging Station (MLRS – 7080). In order to be able in the future to validate stations efficiently when a large number of sites will be submitting CRD data simultaneously, we developed an automated procedure that compares the results on a weekly basis. The process is run in parallel to our operational weekly solution for the official Pos+EOP product. Once the data of the week have been reduced and the final fitted orbits are available, we generate a new data set for input to GEODYN: this one contains all the data from the standard (current) format, QLNP, and in addition, all the CRD data from all stations that submitted data during that week, except that in this case the tracking station number for those stations is modified: the leading digit is replaced by a "9". This way, the GEODYN input data set contains both types of data from the same station, yet we can differentiate how each group will be treated during the reduction process.

Within the GEODYN environment, we have the option to weigh data differently for different stations. We thus choose to use the QLNP data full weight, so that the orbital fit is based on that data, and assign a zero weight to the CRD data (from the "9xyz" sites), so that while they do not affect the orbital fits and they are not considered in the computation of the statistics, we can still obtain residuals to the fitted model. The premise is that if the two groups describe the collected data correctly, then they should produce comparable residuals when compared to the same orbit.

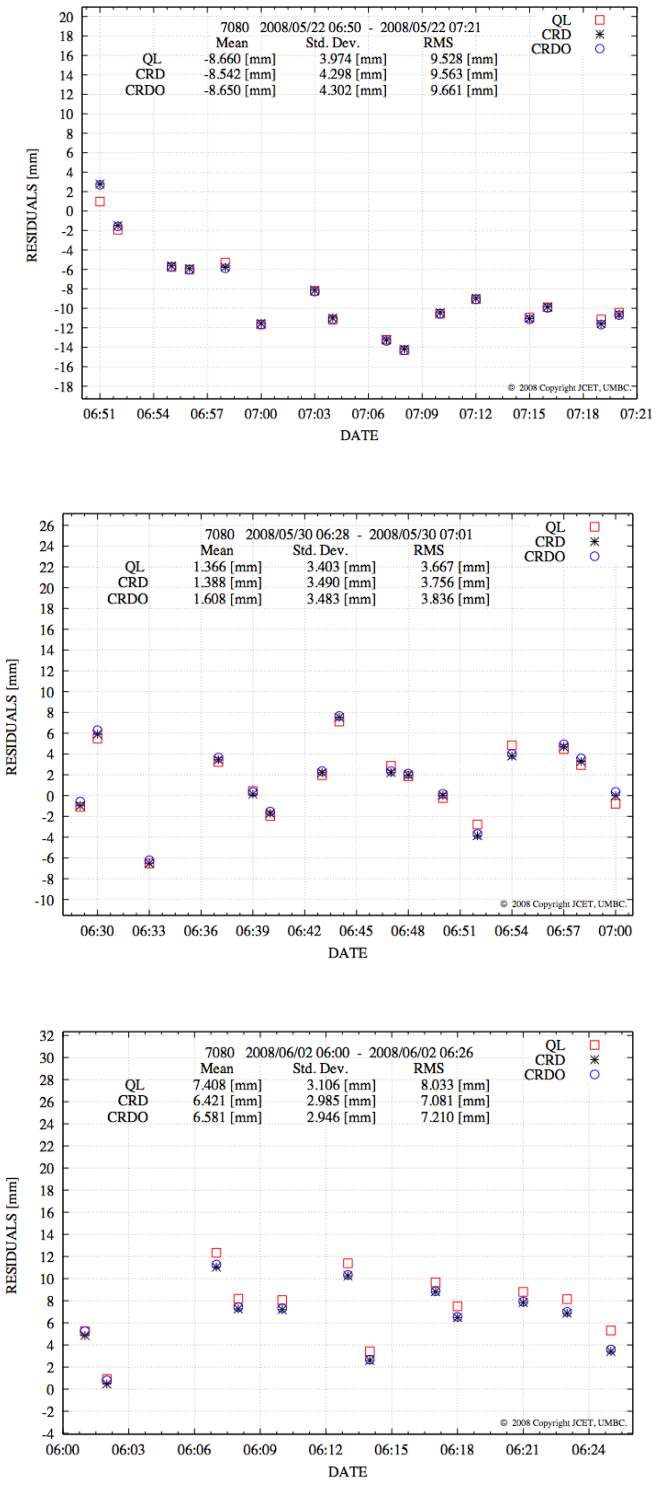

Figure 1. Visualization of residual differences from variously-formatted data. QL denotes the old ILRS format, CRD denotes data obtained from the new CRD format using an in-house developed s/w, and CRDO are those converted the ILRS-supplied s/w.

The residuals cannot be identical because as it was already mentioned, the new format affords higher precision in many of the recorded quantities, so small differences are expected and justified. A quick way to verify the consistency between these two sets of residuals is to form their statistics for each pass and to visualize them on a pass-by-pass basis (Fig. 1). Note that depending on the case, there is more or less agreement between the various formats. We have discovered that this is mostly due to the way the meteorological data are applied, i.e. whether interpolated to the observation time (as in QLNP files) or used as supplied in the CRD format. Table 1 shows the statistics for a number of MLRS LAGEOS passes collected in July and August of 2008. These results indicate that the agreement is at the 0.5 mm level, which is consistent with the fact that we do expect a small difference between the two sets due to the increased precision in some of the key recorded quantities.

Table 1. Residual statistics from the same orbital fit for QLNP and CRD data.

STATION	YY/MM/DD	HH:MM	Std. Dev.	Mean	RMS	Pass No.	Min	Max
70802419	2008/7/11	9:31	0.992	16.257	16.287	1	15.040	17.470
90802419	2008/7/11	9:31	2.152	15.557	15.705	1	12.590	17.630
70802419	2008/7/12	4:42	6.916	15.933	17.369	2	3.795	24.730
90802419	2008/7/12	4:42	7.035	15.701	17.205	2	3.543	24.720
70802419	2008/8/4	8:32	6.164	1.918	6.456	1	-7.832	11.080
90802419	2008/8/4	8:32	6.096	1.750	6.342	1	-7.824	10.780
70802419	2008/8/5	7:16	3.482	8.968	9.620	2	4.309	14.520
90802419	2008/8/5	7:16	3.500	8.812	9.482	2	4.158	14.410
70802419	2008/9/6	2:26	16.616	1.115	16.654	1	-24.400	24.930
90802419	2008/9/6	2:26	16.428	1.056	16.462	1	-25.310	24.500
70802419	2008/9/18	17:08	2.432	-22.455	22.586	1	-26.540	-20.400
90802419	2008/9/18	17:08	3.056	-22.693	22.897	1	-27.900	-20.090
70802419	2008/10/3	0:43	10.689	-12.649	16.561	1	-30.610	-2.797
90802419	2008/10/3	0:43	10.659	-12.643	16.536	1	-30.610	-2.827
70802419	2008/10/6	10:12	6.468	-8.319	10.538	1	-16.550	0.754
90802419	2008/10/6	10:12	6.463	-8.381	10.584	1	-16.630	0.670
70802419	2008/10/7	2:34	22.476	-1.146	22.505	2	-32.640	32.370
90802419	2008/10/7	2:34	22.326	-1.427	22.372	2	-32.970	31.670
70802419	2008/10/7	5:56	4.498	-3.343	5.604	3	-8.887	4.358
90802419	2008/10/7	5:56	4.486	-3.382	5.618	3	-8.965	4.300
70802419	2008/10/8	11:01	4.663	-4.055	6.179	5	-10.520	2.924
90802419	2008/10/8	11:01	4.682	-3.879	6.080	5	-10.420	3.078
70802419	2008/10/8	4:40	16.561	7.350	18.119	4	-29.230	30.660
90802419	2008/10/8	4:43	16.340	5.128	17.126	4	-29.030	30.690

The initial tests indicated that although the observed differences are acceptable and can be explained by the increased precision, there are also cases where the two files differ drastically. In several instances, the number of normal points in the two files differed because of the way that they were formed and the difference in the precision of the epoch time or the range values. We also encountered cases when a pass was present in one file but not in the other, although infrequently, because of modified editing criteria, again primarily as a result of the different precision. All these were communicated back to the station, so that it could be investigated if there was any s/w issue in generating the new, CRD-formatted files or a

legitimate difference as explained above. As a result of these encounters with these test cases, we formed a "benchmark" test that was delivered to all AWG AC, where all special differences between the provided QLNP and CRD files were documented. A successful replication of these results provides some assurance that all AC involved in validating CRD submissions are "seeing" the same differences, so candidate stations need only be validated by a single AC, something that will help distribute the load the AWG will face in the next months and accelerate the station validation process across the entire network.

Conclusions

We have developed a procedure to use CRD-formatted ILRS normal points in Goddard's GEODYN package and to compare them to results obtained from ILRS QLNP-formatted data for the same observed ranges. We used this procedure to process several months of MLRS data and to validate the stations CRD formation process. The performed tests revealed some differences between the two versions of formatted data, which were easily explained by the difference in precision of key recorded quantities. We used a two-week period of data from MLRS to form a "benchmark" that we have shared with the other ILRS AC that will participate in the validation of the CRD data delivered by the network in the next year.

References

Pavlis, D. E. et al., *GEODYN II, Systems Description Vol. 3 (NASA GSFC, Greenbelt, MD*, 2008.

Ricklefs, R. L., and C. J. Moore, Consolidated Laser Ranging Data Format (CRD) Version 1.01, http://ilrs.gsfc.nasa.gov/docs/crd_v1.01.pdf, 2008.

The new pointing model of telescope based on tracking data

Medvedsky M., Pap V.
Main Astronomical Observatory National Academy of Sciences of Ukraine
medved@mao.kiev.ua, vic@mao.kiev.ua

Abstract

There is a new error model for pointing the telescope to the satellite for satellite laser ranging. It is based only upon data which is obtained during SLR observations. The observations from about 40 satellites passes have been taken from beginning of September of the year 2008 for the construction of the model. The parameters of the model, and the mode of constructing the model are included in this article. We analyze advantages and disadvantages of the model. This model is currently used at SLR station "Kyiv-Golosiiv 1824".

Introduction

The trend of the SLR technique has been directed to creation of automatized systems which can do observations of satellites in semiautomatic and automatic modes, thereby making the jobs of station personnel easier. Thus it is necessary to have as exact a model of errors of the telescope as possible for successful satellite tracking. These errors always have the characteristics caused by telescope type, quality of adjustments of the optical system, workmanship of mechanical systems, etc. It is possible to provide automatic supervision, if we have high-precision model of errors of the telescope and the possibility of operator control or specification of this model. Besides, using a system with exact prompting and object support essentially raises the overall performance of a laser station even if it works under active management of the observer. This is especially true when operating on a daylight schedule when the majority of satellites are invisible to the observer.

Such a model of telescope errors can be constructed by using laboratory methods of characterizing discrepancies in manufacturing of an azimuthal platform, and the encoders errors (if there are encoders). It is also possible to construct a model of errors by observing stars as, for example, the system which has been developed in MAO of NAS of Ukraine [1]. This system can be realized only with photodetectors of PMT type as it is necessary to count the photons from a star. PMT works in a counting mode and has no "dead time", as contrasted with semi-conductor avalanche photodetectors (APD, SPAD). Avalanche photodetectors can register separate photons, but after each pulse they have some interval of time when their sensitivity is very low. As some photons will arrive from a star during these intervals of time, the system cannot register them. It will lead to decrease sensitivity on the one hand and errors of measurement of intensity of a star on the other hand. It all leads to an increase in errors of measurements.

We offer a way to construct an error model of a telescope which is based on the data received during satellite ranging. The principles of constructing a model in such a way are described in [5]. In summary, this method is based on encoder data which are captured at the beginning of every second during ranging. Further the difference between observed positions of the target (at the moment of time when the return from satellites has been received) and calculated position (ephemeris) is analyzed.

Zenith distance, degrees

The given method has some advantages: time for supervision, a considerable quantity of points over the sky, the possibility of the operator control of the correction model, independence from the photodetector, and freedom from spending time on separate mount model data gathering.

It is sufficient to use 10 – 40 passes for construction of the model; it is dependent on how these passes cover the hemisphere of the sky. For this discussion, 40 passes were used. This data totals 18 thousand points. The width of a laser beam during ranging was 15´´. The sky covering is shown in fig. 1. Initial O-C residuals are presented in fig. 2-5.

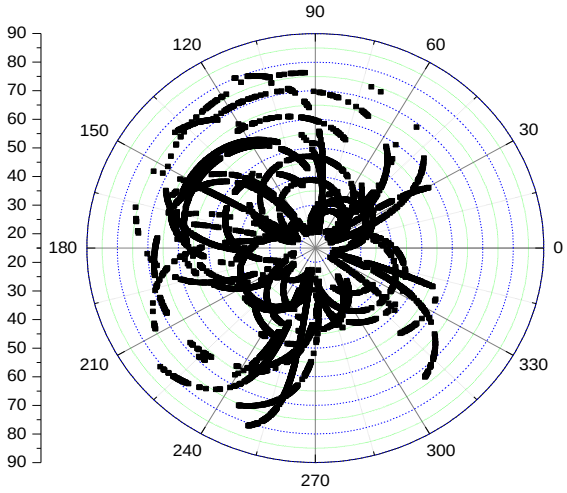

Azimuth,

Figure 1. Sky

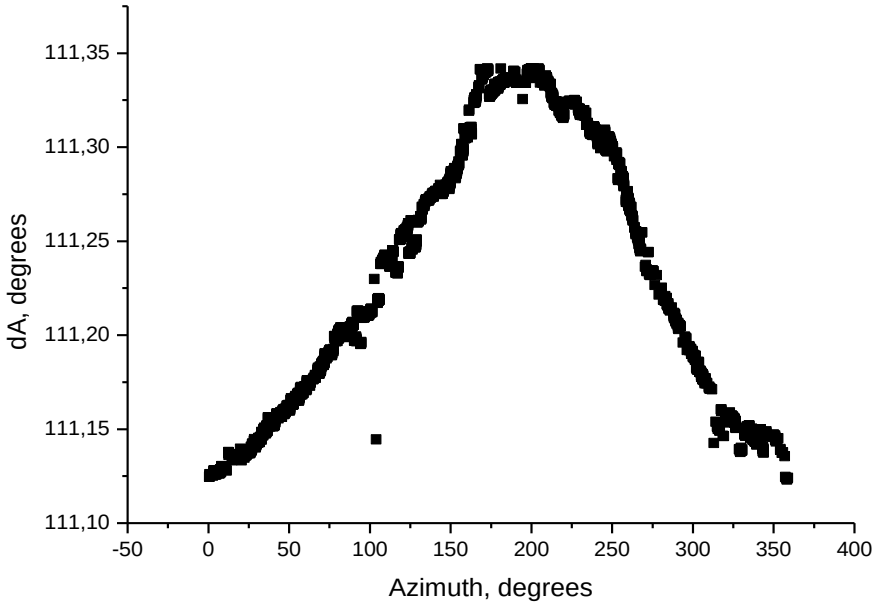

Figure 2. Dependence of azimuth differences O-C on azimuth

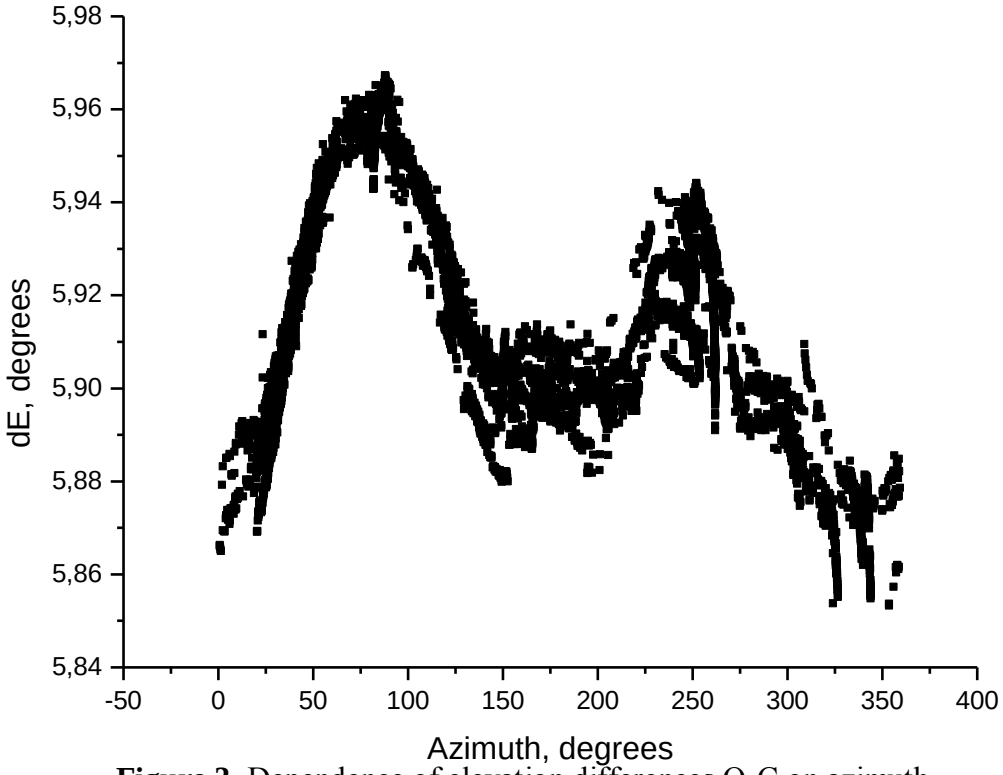

Figure 3. Dependence of elevation differences O-C on azimuth

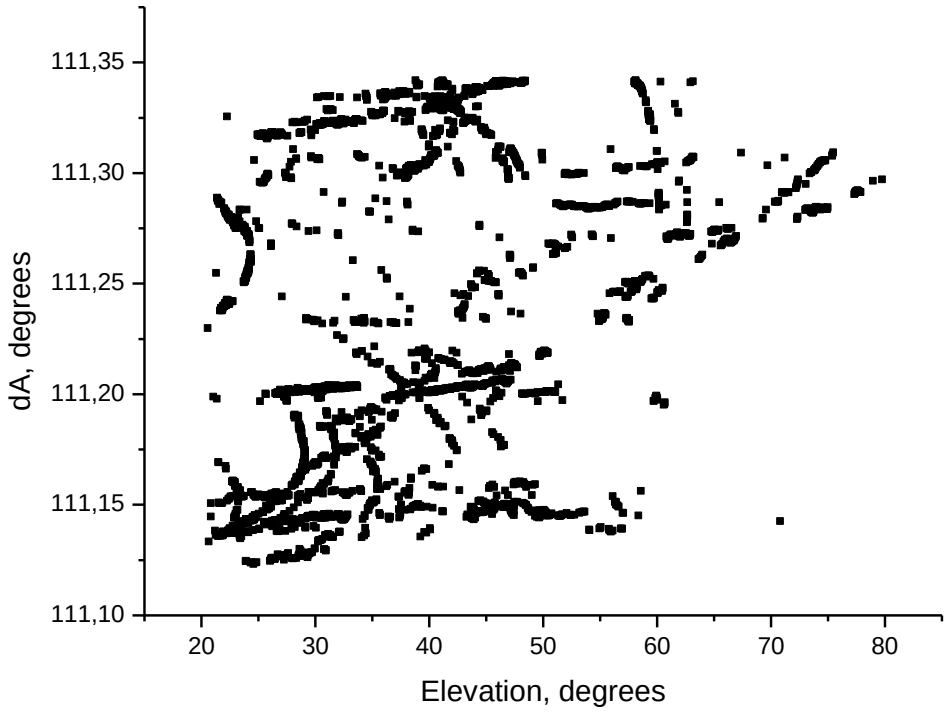

Figure 4. Dependence of azimuth differences O-C on elevation

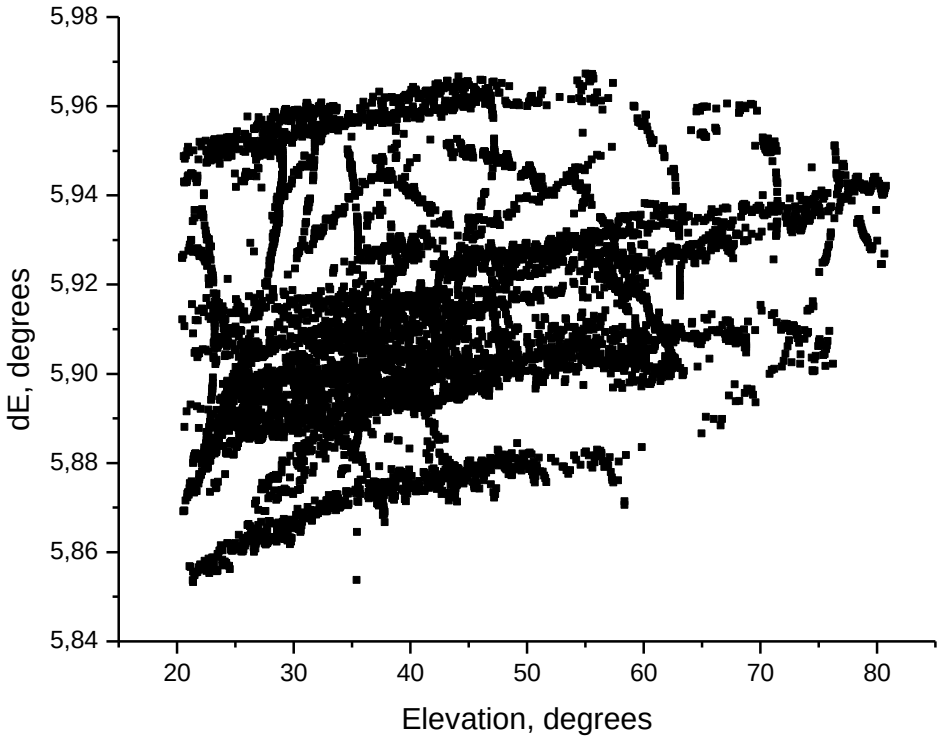

Figure 5. Dependence of elevation differences O-C on elevation

It was not obvious that there would be a dependence of the azimuth O-C residuals on elevation; only azimuth O-C dependences on azimuth were defined. It is apparent from fig. 3 that elevation O-C residuals depend on azimuth. When both curves (fig.2 and 3) are divided into 10 parts; in each it is possible to describe the O-C residuals as polynomial of 1 or 2 degrees. Resulting coefficients and intervals are presented in table 1.

The azimuthal model looks like: $\mathbf{dA=A+B1*az+B2*az^2}$

The elevation model accordingly: $\mathbf{dE= A+B1*az+B2*az^2}$,

Where the coefficients A, B1, B2 for each intervals are different, one set for azimuth, and one set for elevation, and

az – azimuth.

Table 1. The parameters of model

№	Interval, degrees	Azimuth, arcsec			Elevation, arcsec		
		A	$B1*10^{-4}$	$B2*10^{-5}$	A	$B1*10^{-4}$	$B2*10^{-5}$
1	0-20	111.12346	7.18078	0	5.86998	9.93361	0
2	20-50	111.11447	9.63814	0	5.84123	19.0	0
3	50-113	111.10540	11.4	0	5.80338	38.4	-2.40053
4	113-132	111.11167	11.1	0	6.08559	-13.5	0
5	132-164	112.20648	-139.1	5.17286	5.93494	-2.32794	0
6	164-224	110.43937	94.2	-2.46413	6.00440	-11.4	3.08847
7	224-250	112.93676	-125.8	2.41212	5.86798	2.28252	0
8	250-270	112.09860	-31.8	0	6.10770	-7.34310	0
9	270-346	112.83370	-94.0	1.30325	6.03878	-4.96045	0
10	346-360	112.13579	-28.4	0	5.96367	-2.48787	0

After subtraction of the new model terms we have received the following residuals dA and dE, figures 6,7:

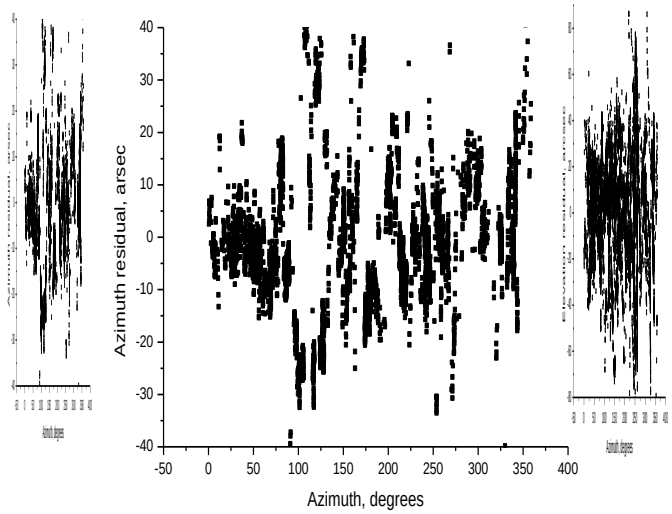

Figure 6. Dependence of azimuth residual on azimuth

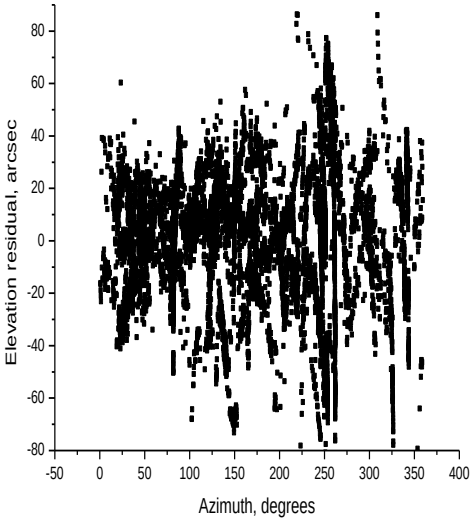

Figure 7. Dependence of elevation residual on azimuth

In figures 8 – 9 it is shown, how azimuth residuals depend on elevation and the elevation residuals depend on elevation.

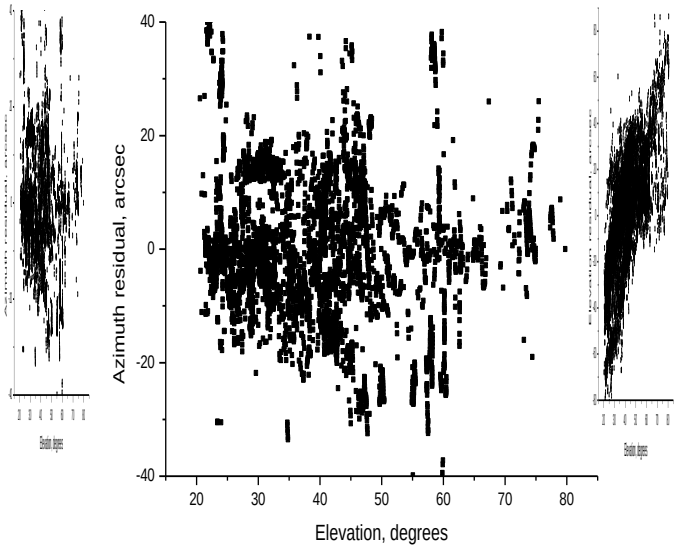

Figure 8. Dependence of azimuth residual on elevation

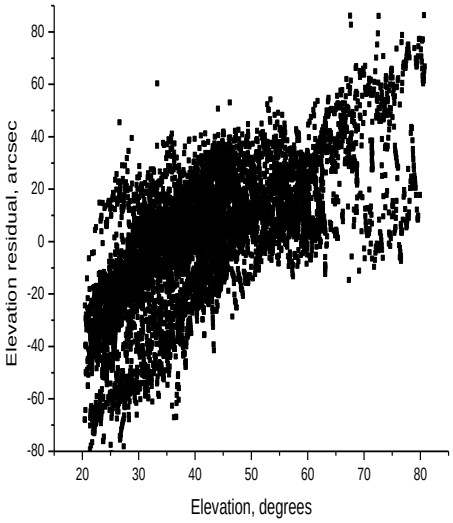

Figure 9. Dependence of elevation residual on elevation

The obvious dependence of the residual in azimuth on elevation had not been previously noticed. There is considerable dependence of the residuals of elevation on elevation in figure 9. This dependence is approximated by a parabola:

$$dE = -0.02972 + el*9.70274*10^{-4} - el^2*5.79624*10^{-6},$$

where el – elevation, dE – residuals on elevation. This parabola has been removed, with the following result (figure 10).

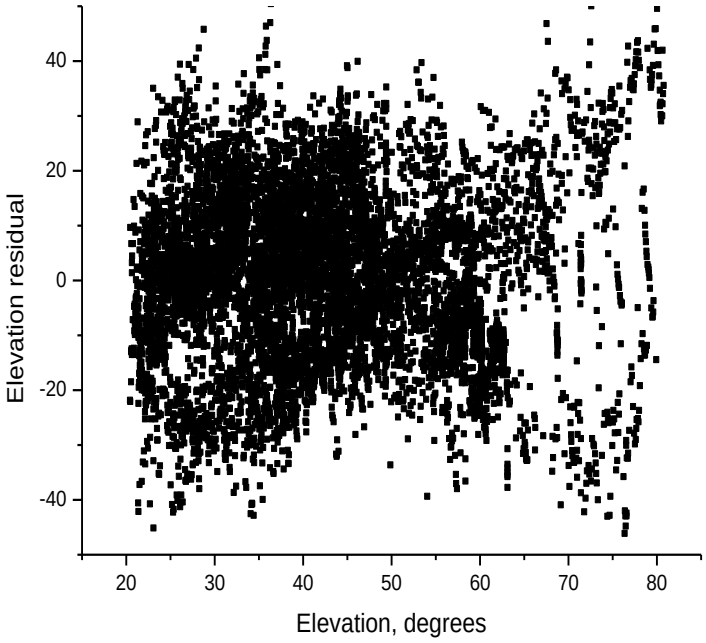

Figure 10. The elevation residual

Conclusion

The model which has an accuracy of 20´´ is constructed using about 40 passes which have been taken over 6 nights. The present model has allowed us to observe invisible satellites. This model is used at station Kyiv-Golosyiv 1824 at present time.

References

1. Medvedsky M.M., Suberlyak V.R. Mount errors model for the Kyiv SLR station, *Artifical Satellites, vol 37, p. 3-16,* 2002
2. Michelson N.N. Some questions of alt-azimuth theory of telescope assembling, *News of Main Astronomical Observatory in Pulkovo, v.185.- p. 279-305* .- 1970
3. Nesterov N.S. Systematical mistakes of telescope pointing by 22th, *News of Crimean Astrophysics Observatory, vol. 73.- p.189-198,*1985
4. Schillak S., Butkiewicz E., Latka J.K. Mount error model of BOROWIEC-2 SLR system, *Artificial Sattelites, vol.29, no 3, p.119 – 128,* 1994
5. Medvedsky M.M., Pap V.O.(2007) Construction of telescope inaccuracy model according to data of satellites laser ranging, *Artificial Satellites,. 41, no 3, p. 105 – 114*, 2006

New and Upgraded Stations, Extended Facilities

Chairs: Francis Pierron and Stanisław Schillak

Session Summary

In the Chinese network, modernization of all stations(6) with new technology: kHz, Event Timers, Cspad, Gravimeters..
In Korea transportable system TROS operational and ARGO project for promising developments (fixed and mobile SLR stations in 2013).
In France New Meo station operating again on Moon and satellites, mobile system Ftlrs upgraded with Dassaults ET for T2L2 project.
Herstmonceux station toward kHz Ranging and multitechnique operations.
Major upgrade achieved with the Borowiec station.
Ukrainian Kiev and Simeiz/Katzively stations still in progress and operations.
In South America San Juan SLR system in efficient operations today and TIGO ranging again after delicate optical replacements.
In Russia Komsomolsk, Baikonur and new Altay station are operational, the next few stations will be operational in the near future.
New Chinese stations in Urumchi and mobile TROS-2 are expected in 2010 and 2011.

Upgrading Plan of the Chinese SLR Network

Yang Fumin (1)**, Wu Bin** (1)**, Zhang Zhongping** (1)**, Guo Tangyong** (2),
Zhao You (3)**, Qu Feng** (4)**, Xiong Yaoheng** (5)

(1) Shanghai Astronomical Observatory, Chinese Academy of Sciences, China
(2) Institute of Seismology, China Earthquake Administration, Wuhan, China
(3) Changchun Observatory, Chinese Academy of Sciences, Changchun
(4) Chinese Academy of Surveying and Mapping, Beijing
(5) Yunnan Observatory, Chinese Academy of Sciences, Kunming

yangfm@shao.ac.cn /Fax: +86-21-64696290

Abstract

Under the support of the second stage of the state key project "Crustal Movement Observation Network of China", the Chinese SLR stations will be upgraded to better performance in two years. The main improvements will be kHz ranging and routine daylight tracking. The upgrading proposal for the San Juan SLR station is also under consideration.

Introduction

There was a state key project "the crustal Movement Observation Network of China (CMONOC)" during the years of 1997-2000. The main technique adopted for the project was to set up a national GPS network for monitoring the crustal deformation in the main land of China. The other techniques, such as SLR, VLBI, gravity and leveling measurement, were also used in the project. Therefore, the Chinese SLR network obtained some supports from the project and the performance of the stations had been obviously upgraded with the installation of the new detectors (C-SPAD), GPS time and frequency receiver, etc. Since 2008, the second stage of the CMONOC project has been initiated, and the same techniques will be supported, and more core GPS stations (260 sets) will be set up. Fortunately, the SLR stations are also obtained quite strong supports from the second stage of the project. The goals, main technical measures and the status are introduced in the paper.

Goals and main technical measures of the upgrading

The fixed stations to be upgraded are: Changchun, Shanghai, Beijing, Kunming and Wuhan. The mobile system TROS-1 will not be included in the upgrading plan, but a new powerful mobile system TROS-2 will be supported by the project and be developed by the Institute of Seismology in Wuhan during 2008-2011.The goals of the upgrading for both the fixed stations and the new TROS-2 system are shown in Table 1.

Table 1. Goals of the upgrading

Precision	for starlette-like single shot rms < 8 mm for LAGEOS single shot rms < 12 mm normal point rms < 1-3 mm
Stability	10-15 mm
Ranging capability	up to GNSS satellites > 26000 km
Operation mode	routine daylight tracking to LAGEOS by all stations

The major technical measures for the upgrading are as follows:

1) kHz lasers
   5 sets of the kHz picoseconds lasers from the Photonics Industrial International Inc. of USA have been ordered and will arrive at the stations by June 2009. One set of the kHz laser from the High Q laser of Austria for the Beijing station will arrive at the same time. The main parameters of the Photonics Industries laser are:
   3 mJ in 532 nm per pulse, 1 kHz repetition, < 25 ps pulse width, 0.6 mrad divergence, <2 mm output beam diameter, TEM00 mode, M^2<1.3, 15-30℃ operating temperature.
2) Event timers with timing jitter of 10 ps from Riga for all stations.
3) kHz ranging controllers for all stations will be made by ourselves.
4) Daylight tracking packages for all stations will be also made by ourselves.

Having built and completed the kHz ranging controller, some stations will start the kHz ranging to satellites by the summer of 2009.

The TROS-2 mobile system will have 1 meter aperture telescope and kHz laser, and will be operational by 2011.

The proposal of construction of a new SLR station in the Urumqi Observatory, Chinese Academy of Sciences was approved in 2008, but the plan has been postponed. The proposed station will have 1 meter telescope and kHz laser, and will be in collocation with VLBI and IGS/GPS station.

The upgrading proposal for the productive San Juan Station is under serious consideration and is expected to be approved soon by the Ministry of Science and Technology of China.

Summary

Under the support of the state key project “CMONOC”, the Chinese SLR network will be great upgraded in two years. One new mobile system will be added into the Chinese network by 2011. The San Juan station will get the funding for upgrading soon. All the systems will go to kHz ranging and routine daylight tracking.

Status and Progress of ARGO

J. Park, H. Lim, Y. Seo, J. Park, Y. Kim (1)**, Y. Son** (2)**, Y. Kim** (3)

(1) Korea Astronomy and Space Science Institute
(2) Korea Institute of Machinary and Materials
(3) Kongju National University

jupark@kasi.re.kr /Fax: +82-42-861-5610

Abstract

Over the last few years, Korea Astronomy and Space Science Institute had prepared for introducing the SLR system in Korea. Even though we spent a lot of time to overcome the many barriers just same as other projects, we could finally start the ARGO project to make the series of SLR from this year. ARGO, new SLR systems of Korea, stands for the Accurate Ranging system for Geodetic Observation and this was the name of ship on which Jason and Argonauts voyaged to retrieve the Golden Fleece in Greek mythology. The goal of ARGO project is to make two SLR systems, one is a 40 centimeter mobile SLR system and another one is an 1 meter fixed SLR system, and to start the operation from the year 2011 and 2013 respectively. The participants of ARGO project are involved in five working groups related with the components of SLR system, for example Electro-Optics, to work more specifically. Due to their efforts including the visiting to several SLR sites in abroad, we could determined the more detailed requirements and scheduling for ARGO system. In this paper, we will give the current status and future plan of ARGO project with the context of requirements and scheduling of ARGO.

Introduction

ARGO means Korean SLR system and stands for 'Accurate Ranging system for Geodetic Observation', which comes from the ship on which a great group of heroes boarded to find the Golden Fleece in the ancient Greek mythology. The final goal of ARGO program is to develop two SLR systems for 7 years from 2008 to 2014, one 40cm mobile system(ARGO-M) and one 1m fixed system(ARGO-F). The objectives of ARGO program can be categrorized into three items; i) space geodesy research and GEOSS/GGOS contribution by laser ranging for satellites with LRA, ii) precise obit determination(POD) through laser ranging measurement with mm level accuracy, iii) contribution to international SLR societies and ILRS network participation. ARGO will be developed with the cooperation of foreign institutes and under supports of international advisory committee and domestic advisory committee which consist of ten experts, respectively. As shown in Figure 1, ARGO-M will be completed by 2011 and then ARGO-F by 2014. Two Korean satellites with LRA, STSAT-2 and KOMPSAT-5 will be launched in 2009 and 2010, respectively. So, ARGO-M and ARGO-F will be used for laser tracking of these two Korean satellites.

System requirements of ARGO-M was generated by five working groups in September 2008, optics subsystem, opto-electronics subsystem, laser subsystem, tracking mount subsystem and ARGO operation system. Until now, system configuration and conceptual design of ARGO-M were made and its detailed specifications were also generated. Major characteristics of ARGO-M are following:

- **Tracking Capability**
  - Possible to track satellites between 300km and 25,000km altitude
    - STSAT-2(300x1,500km), KOMPSAT-5, GPS, Galileo
  - KHz laser ranging
  - Daylight and night tracking
- **Ranging Accuracy**
  - Lageos : 10mm(SS), 5mm(NP)
  - Ground Target : 3mm(SS), 1mm(NP)
- **Operational Functions**
  - All subsystems can be controlled from the remote site
  - Automated scheduling, planning and orbit prediction capability
  - Automatic ranging according to the schedule and aircraft detection
  - Automated diagnostic warning to monitoring system

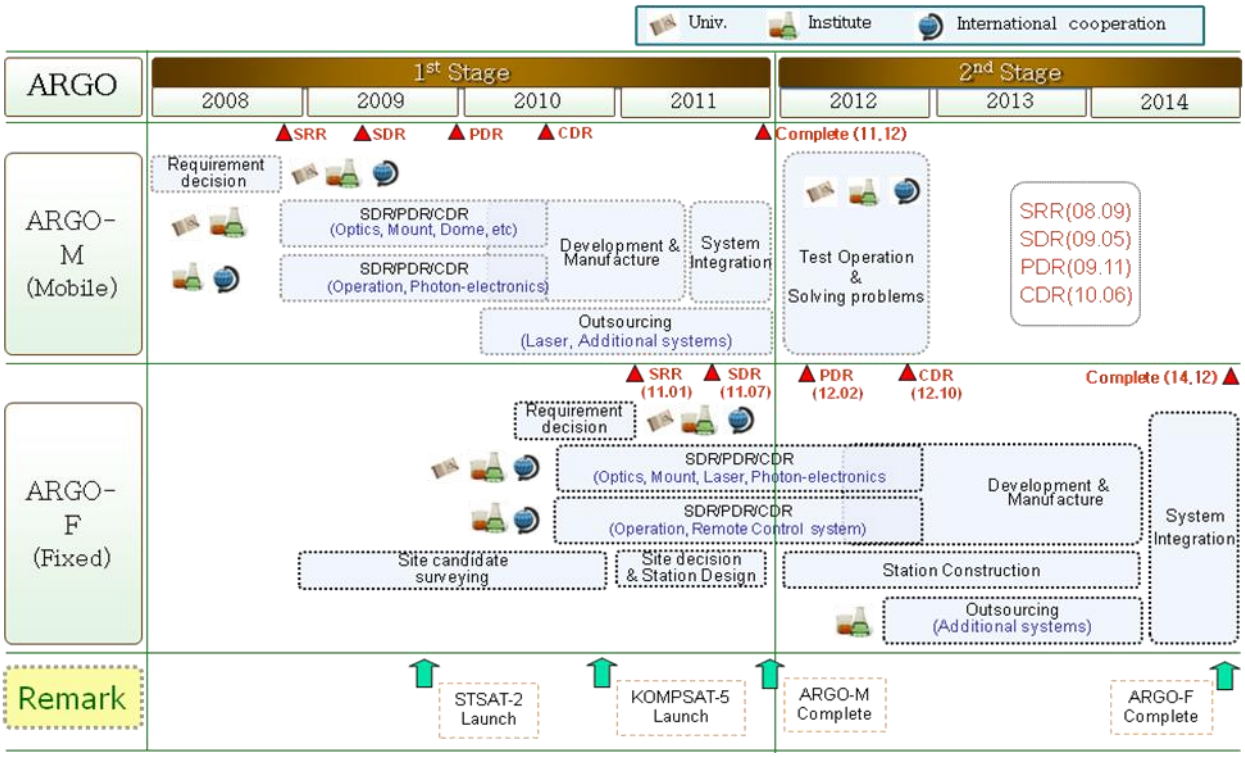

Figure 1. Milestone of ARGO program

Overview of ARGO system

The optical path of ARGO-M is separate type but ARGO-F is common type for both optical tracking and laser tracking of space debris. In addition ARGO-F has larger laser energy than ARGO-M because it is not capable of KHz laser ranging. Some important characteristics of ARGO system is summarized in Table 1.

As for ARGO-M, many requirements and specifications are determined. It has satellite tracking camera to get an image of laser scattering from satellites and aircraft detection camera to detect aircrafts besides radar system. It has also the beam divergence optics and the

tilt mirror for both satellite acquisition and tracking. For low earth orbiting satyellites, fast event timer will be intalled within FPGA board and digital RGG will be also used intead of programmable delay chip. FPGA board will perform the function of laser pulse shift to prevent the overlap of transmitting and receiving beam. Laser system will be introduced from foreign company because it is required to be very stable for KHz laser ranging, whose status will be monitored from a remote site. The tracking mount is designed such that it can support the maximum payload of 300kg, whose maximum slew rates are 20deg/sec for azimuth and 10 deg/sec for elevation. Pointing and tracking accuracy are required to be under 5arcsec. The requirements and specification of operation system are following:

- Ground calibration for the computation of system delay
  - Calibration type : external within dome
- Available for both local and remote operation
- Control subsystems through the monitoring of subsystems
- Generation of tracking schedule considering sunlight direction, satellite priority and satellite elevation angle(>20deg)
- Generation of FR(full rate) date and NP(normal point) data
- System safety from monitoring of the sun, aircraft and weather
  - Surveillance range of radar < 40km for airplanes, hang gliders and paragliders
  - Weather sensor : temperature, pressure, humidity, rain, wind speed and direction
  - All sky monitoring system with Infrared camera(TBD)
- Station surveillance system to monitor SLR station and its surroundings

Table 1. Configuration of ARGO-M and ARGO-F

Item	ARGO-M	ARGO-F
Tx/Rx Path	Separate	Common
Aperture of Receiving Telescope	40cm	100cm
Aperture of Transmitter	10cm(TBD)	100cm
Mount and Pointing Accuracy	Al/Az, 5arcsec	Al/Az, <5arcsec
Pulse Energy (532 nm)	0.4mJ	20mJ
Pulse Width	10ps	<100ps
Repetition Rate	2KHz	20Hz
Receiver Type	C-SPAD	C-SPAD
Time Interval Unit	Event Timer	Event Timer
Ranging Accuracy	5mm (NP), 10mm (SS)	3mm (NP), 10mm(SS)

Summary

ARGO is the name of forthcoming Korean SLR Systems, officially started from Jan. 1st, 2008 to build a 40 cm mobile SLR system and 1 meter fixed SLR system. The lightweight telescopes, remote control and fully automation concept are introduced for the development

of ARGO-M and ARGO-F. ARGO will be the member of ILRS sites in 2012 and 2014, respectively. Additionally, Korea has a plan to build the fundamental station because Korea has operated about 80 GPS stations and 3 VLBI systems.

The Requirements of ARGO Operation System

Yoon-Kyung Seo, Hyung-Chul Lim, In-Kwan Park, Hong-Suh Yim, Jong-Uk Park
Korea Astronomy and Space Science Institute, Korea
ykseo@kasi.re.kr /Fax: +82-42-8615610

Abstract

Korea Astronomy and Space Science Institute (KASI) has developed one mobile and one fixed SLR system since last year named as ARGO-M and ARGO-F, respectively. KASI is in the step of making the system requirements. The requirements describe the definition and scope of the various software and hardware subsystem, which are necessary for developing the ARGO operation system. It also defines function, performance and interface requirements. The operation system consisting of ARGO-M site, ARGO-F site and Remote Operation Center (ROC) inside KASI is designed for un-manned remote access and the automatic tracking and control system which are the main operation concept of ARGO system. To accomplish the un-manned remote operation, we are considering the remote access to ARGO-F and ARGO-M from ROC. The mobile-phone service allows us to access the ARGO-F remotely and to control the system in an emergency. To implement the fully automatic tracking and control function in ARGO-F, we has investigated and described the requirements about the automatic aircraft detection system and the various meteorological sensors.

Introduction

KASI had a meeting for ARGO System Requirements Review (SRR) on fifth Sep., 2008. After having a SRR meeting, ARGO Operation System working group submitted the SRR documents which describe the sub-system definition, functional & performance requirements and interface requirements to Project Management part. As for H/W, we derived the general requirements and some specifications. This paper addresses the requirements of ARGO Operation System.

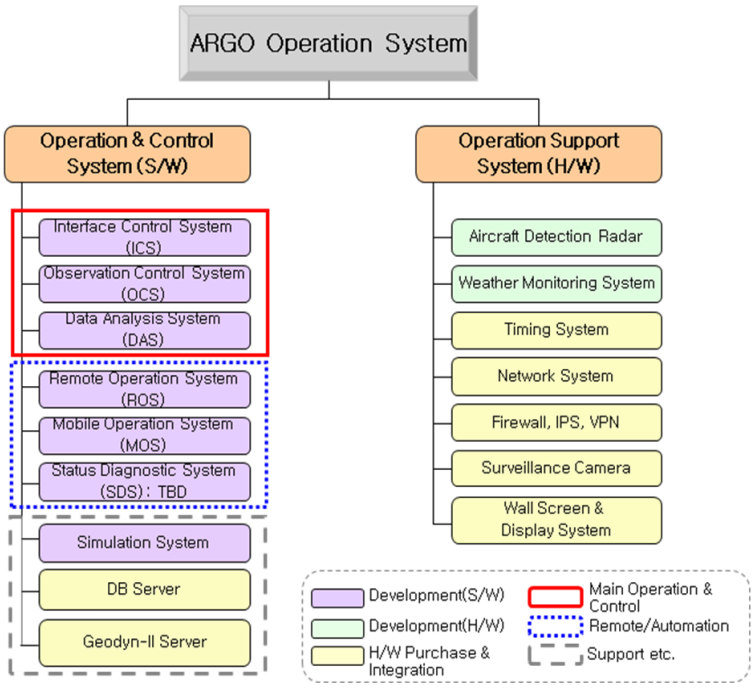

Figure 1. The configuration of ARGO Operation System

ARGO Operation System is classified into two categories, as this is illustrated in Figure 1: i) Operation & Control System (S/W part), ii) Operation Support System (H/W part).

ICS, OCS and DAS in the solid box, are main systems for satellite tracking and the acquired data processing in fixed-ARGO or mobile-ARGO sites. And another three systems in the dotted box are necessary for automatic and remote control function from Remote Operation Center (ROC). We are going to set up ROC inside KASI headquater. ARGO-F and ARGO-M will be controlled remotely from this center. Operation Support System is composed of several H/W systems necessary for an automatic SLR system. Radar system and a part of weather monitoring sensors will be manufactured by order.

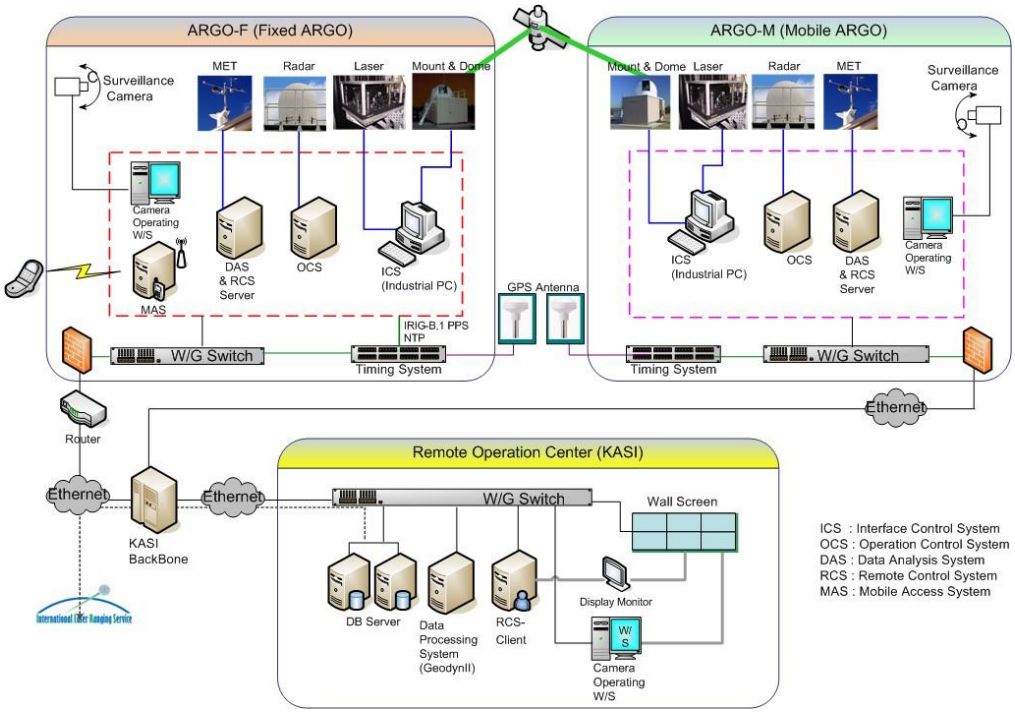

Figure 2. The Block diagram of ARGO Operation System

The block diagram in Figure 2 shows what system shall be installed to ARGO-F, ARGO-M and ROC. ARGO-M will have a same configuration as ARGO-F except for mobile server which is expected to be applied to ARGO-F firstly. This means that ARGO-F can be controlled from ROC by using the mobile phone. Wall-Screen will be installed in ROC for displaying the progress status of observation and image transferred from ARGO-F or ARGO-M. And ROC will also have "Remote Operation System" for connection to ARGO-F or ARGO-M.

Requirements – Operation & Control System(S/W)

(1) Interface Control System (ICS)

ICS has several interface cards of ISA or PCI type for delivering the commands or calculated values to several systems (Laser, Tracking Mount, FPGA card and Star Camera). All delivering data on ICS shall be passed to and from OCS. The software runs under RTOS. The main functions are Mount

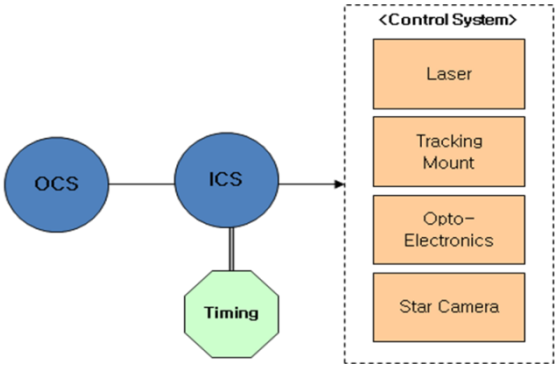

Figure 3. Interface diagram of ICS

control, Star Camera control, Laser control, Timing synchronization, and collection of system status check value from related systems.

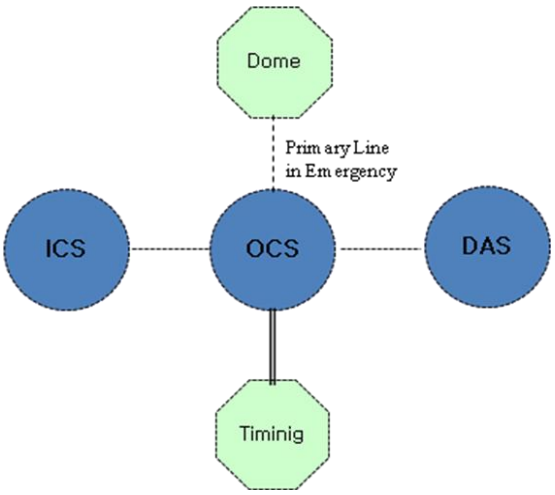

Figure 4. Interface diagram of OCS

(2) Operation Control System (OCS)

OCS is the main system which reflects operator's decision and makes the real-time prediction and scheduling. OCS shall perform star & ground calibration, and command Dome to be closed in emergency. The software runs under non-RTOS. But, because OCS is supplied the time code signal from timing system, it shall be synchronized to other system (ICS) and maintain the exact time. For ARGO system, OCS will be free of processing burden because Opto-Electronics part will perform the measurement of the laser round trip time and many computation logics required the tracking in real-time.

(3) Data Analysis System (DAS)

DAS shall generate "Full-rate" data and the final data product ("Normal Points") after observing one pass of satellite, and send Normal Points data to ILRS periodically. DAS shall collect the meteorological data from Weather Monitoring System and system status data from several systems. DAS shall undertake a role of "Server" for remote access from ROC or anywhere available for internet.

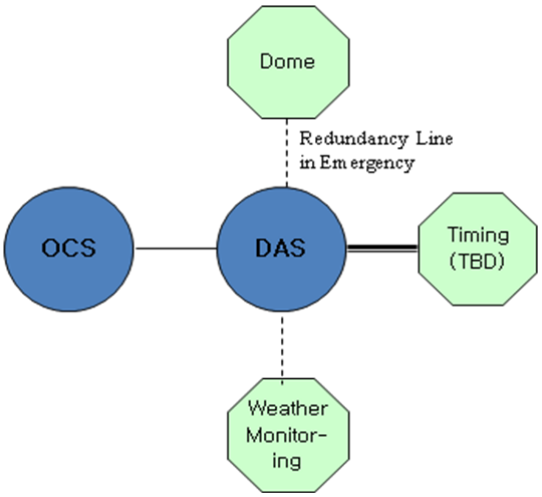

Figure 5. Interface diagram of DAS

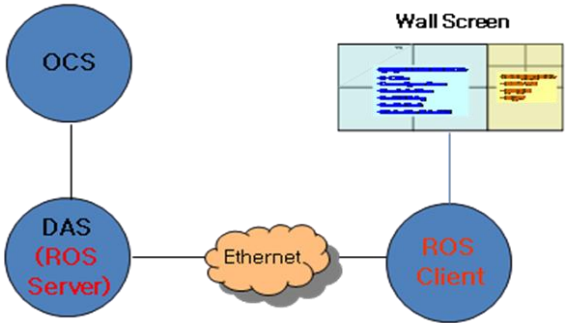

Figure 6. Interface diagram of ROS

(4) Remote Operation System (ROS)

ROS shall be able to monitor or control the observation process in real-time. ROS has a Server-Client structure. The received observation data through ROS client shall be displayed on Wall Screen in ROC located in KASI headquarter.

(5) Mobile Access System (MAS)

MAS shall be able to control "ARGO-F" remotely by using mobile-phone. MAS shall consist of "Server" in ARGO-F and "mobile-phone" for user, which needs cooperation with Telecommunication Service Company in order to use the mobile network.

Figure 7. Interface diagram of MAS

Requirements – Operation Support System (H/W)

(1) Aircraft Detection Radar

Because we use the Nd: VAN Laser, not eye-safe, it is necessary to establish the RF radar and other device for detecting the aircraft to prevent an accident. (Beam does harm to the pilot's eyes.) Radar shall be able to detect the military & civilian aircraft (including helicopter) and a hang-glider for prevent an accident. The available data shall be position (including height) and speed of aircraft. And the period of transmitting output shall be controlled manually by an operator. Let us suppose that the maximum altitude which the aircraft can cruse is 15km. Thus radar shall be able to cover airspace above 20 deg elevation and the maximum length of target detection shall be about 40km (Figure 8).

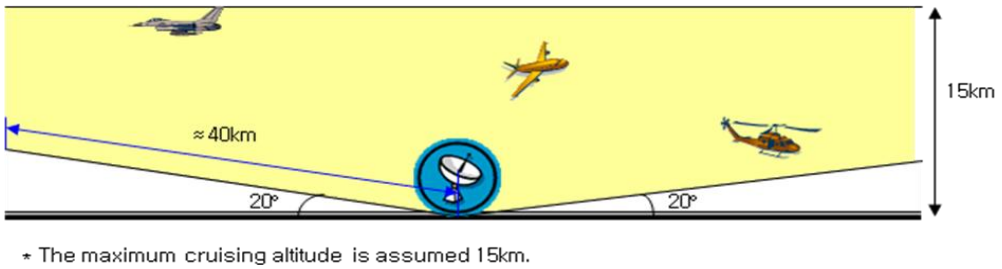

Figure 8. Coverage range requirements of Aircraft Detection Radar

Radar shall be able to receive the pointing data from OCS and synchronize two directions, the laser beam and radar pointing. And radar shall be able to recognize the Start/Stop signal from OCS. But radar shall not be pointed below the horizontal level.

Before radar is installed, it shall be needed for RF analysis to prevent damage about Opto-Electronics detector and other electronic equipments. Radar shall be installed at place which is not harmful to telescope and mount system.

(2) Weather Monitoring System (WMS)

For autonomous system, we are going to install the several kinds of sensors for acquiring the meteorological data. Pressure, Temperature and Humidity data is used to correct range measurements of refraction. Precipitation, Fog and Wind data is needed for system health

and safety (ex. Dome Closing). Visibility and All sky cloud sensors are also needed for a fully autonomous system.

The output from each sensor shall be processed and displayed to an operator all at once by using the Total Integrated Solution. The operator shall control the sampling rate of data collected from several meteorological sensors.

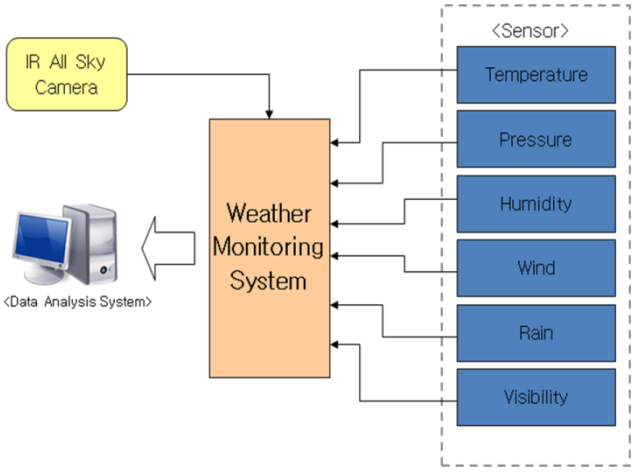

Figure 9. Weather Monitoring System

(3) Network & Fire-wall

If ARGO-M can connect to a network of the closest facility equipped with internet conditions, ARGO-M shall be allocated minimum 3 static IP from facility nearby. ARGO-F shall be built up the new network with the considering the minimum construction cost for connecting the dedicated line when ARGO-F site is selected. ROC shall be located in KASI and have to follow the disciplines of KASI networking and communication security.

(4) Timing System

Timing system is needed for synchronizing the system time to reference time from GPS. And timing system is composed of several equipments, GPS antenna & receiver, Oscillator, NTP Server & Client and interface card for receiving the distributed time signal in computer system (Table 1).

Table 1. General requirements for Timing System

GPS Antenna & Receiver	- GPS Antenna with over-voltage protector. - GPS Antenna Operating Temp. : –50°C ~ +80°C - Better than RG-59/U connecting cable - 12 channel GPS receiver - Acquisition time: Cold Start < 20 min. - 1PSS Output Accuracy : UTC(USNO): ±30ns RMS 100ns peak - Freq. Output Accuracy : 1 x 10^{-12}@ 1 day
Oscillator	- Maintain the accuracy over 5 days without GPS signal
Output & Distribution	- UTC(IRIG-B) - 1PPS - Selectable Frequencies (1, 5, 10MHz)
NTP	- Client time Accuracy ≤ 10ms
Interface Card	- Support to RTOS system

(5) Surveillance Camera

Table 2. General requirements for Surveillance Camera

Functional Requirements	- Available in night time - Automatic Zooming & Focusing Control - Pan : ±170°, Max Speed 100°/sec - Tilt : -30°~ 90°, Max Speed 90°/sec - Remote control from ROC(KASI)
Installation & Housing Requirements	- Operating Temperature: -20℃~50℃ - Including Fan & Heater & Waterproof - Exposed wire shall be covered with Shielding Tube.
Operating W/S & S/W Requirements	- The imaging data shall be transmitted by wire/wireless network (Wireless is optional) - Monitor & store the minimum 4 cameras simultaneously. - Image storage capacity: within 1TB in a week (4 Cameras). - Image replay using MPEG-4 media player. - Image capture according to preset time interval - Auto-Scheduling function which is changeable by surveillance object, purpose and method

(6) Wall Screen & Display System

Wall Screen & Display System will display the status of the observation which is processing in ARGO-F or ARGO-M in real-time. And the image transferred from surveillance camera is also displayed on Wall Screen.

Table 3. General requirements for Wall Screen & Display System

Wall Screen	- Resolution per cell : more than 1,400 × 1,050 - Luminance Accuracy : more than 95% - Screen Gap : within 1 mm
Wall Controller	- Maximize, Minimize and PIP control - Hybrid duplex composition with RGB Matrix Swircher - Quadrant Viewer
RGB Matrix Switcher	- Video input/output signal is controlled by LAN or RS-232
PC Interface	- Branch off the video signal to RGB Matrix Switcher without a loss.
Integrated Control System	- Supplys Touch Panel for operator's console - Changes the display layout easily

Future Work

According to development schedule of ARGO program, "System Design Review (SDR)" meeting for ARGO-M will be held on end of April 2009. For this SDR, in S/W part, we are going to review the system configuration and main algorithm needed for automatic tracking more specifically. For analysis of the established requirements, we will draw "Usecase

Diagram" and then feed back to the requirements again. In H/W part, we are going to review and determine the specification for selecting the proper equipments. For the interface requirements, we are going to survey and discuss the interface between the related subsystems.

References

Anthony Mallama, Jan McGarry, John Degnan, John Cheek, *The Weather Sensors for SLR2000*, 12th International Workshop on Laser Ranging, Matera, Italy, 2000.

Jan McGarry, Brion Conklin, Anthony Mann, Mahtab Sadeghighassami, Mike Perry, Jack Cheek, Tony Mallama, Nick Ton, Randy Ricklefs, *SLR2000 Software Design Document*, Nov. 13, 1998

W. Gurtner, E. Pop, J. Utzinger, *Automation and Remote Control of the Zimmerwald SLR Station*, 12th International Workshop on Laser Ranging, Deggendorf, Germany, 1998.

MeO: The new French lunar laser station

Etienne Samain[1], Abdel Abchiche[2], Dominique Albanese[1], Nicolas Geyskens[2] ,Gilles Buchholtz[2], Aurelien Drean[1], Julien Dufour[1], Jerome Eysseric[3], Pierre Exertier[1], Francis Pierron[1], Monique Pierron[1], Gregoire Martinet-Lagarde[1], Jocelyn Paris[1], Jean-Marie Torre[1], Herve Vioe[1]

[1]OCA, 2130 route de l'observatoire, 06460 Caussols, France
[2]OHP, France
[3]INSU DT, France

etienne.samain@obs-azur.fr

Abstract

Since the beginning of the year 2004 a new organization focused on the Lunar Laser Ranging (LLR) and the mobile laser stations has been set up at OCA. In 2005 the LLR station was stopped in order to make some important modifications. The LLR station is now renamed MeO for "Metrology and Optics". Data acquisitions on low Earth altitude satellites, that were performed until now by the SLR station, will be done by MeO.
Since 2005, many developments was done:

Telescope: high speed motorisation, high accuracy pointing Dome: new guiding device
Building: offices, focus laboratory
Optics: optical benches for experimental research, optical path
Operational telemetry: lasers, high speed laser commutation, photo-detection
Software.

First echoes in the new configuration scheme on both low and high altitude satellite has been obtained in July 2008.

1. Introduction

In the past, the activities around the French Lunar laser ranging station [1] was primarily based on the observations of the moon and high altitude satellites. Since 2004, we have renovated the instrument in order to enlarge the program of the station:
- New facilities to make some instrumental research (new optical links, time transfer, astronomy)
- New performances to track some low altitude satellites or very distant targets
The instrument is now called MeO.

We have at OCA 4 instrumental projects based on the laser thematic:
- MeO station
  - Lunar laser ranging
  - Low and high altitude satellites laser ranging
  - Time transfer
  - Research

- FTLRS « French Transportable Laser Ranging System» [2]
    - Low altitude satellites laser ranging (up to lageos)
    - Altimetry calibration
    - Time transfer
- Time and frequency laboratory
    - Time Scale
    - Local time and frequency distribution
    - Time Transfer comparison: T2L2, TWSTFT, GPS
- Time transfer by laser link [3] [4],
    - Very high resolution Time transfer
    - One way laser ranging demonstration
    - Optical and microwave link Time transfer comparison

2. MeO Project overview

The station is based on a 1.5 meter Cassegrain telescope installed on an Alt-Az mount. The total weight of the mobile elements of the instrument is roughly 20 tons. The diameter of the dome is 9 meters with a total weight of 14 tons. The station use a Nd:YAG laser @ 10 Hz and a common optic (the main telescope) for both the laser emission and reception.

The renovation is divided in 4 themes:
- Motorization - Dome
    - Increase the maximum speed of the telescope at 5°/s with an acceleration of 1°/s-^{2}
    - Increase the pointing accuracy below 1 arcsec.
- Coudé, focal laboratories
    - Operational laser ranging observation with a dedicated laboratory for that purpose.
    - Instrumental research with some dedicated optical benches directly connected to the optical flux of the telescope.
- Software
    - Upgrade the software for both laser ranging observation and research activities.
- Renovation of the monument
    - Renovation of the existing surface.
    - Construction of new surface.

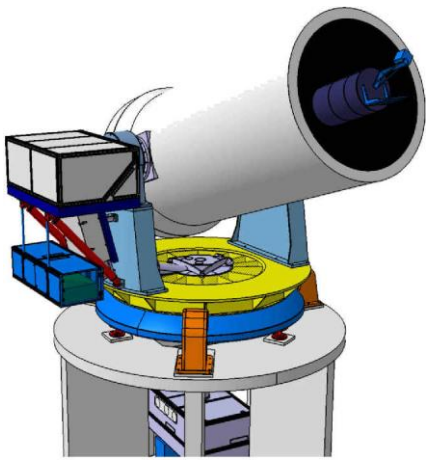

Figure 1. Overview of the MeO station. Telescope diameter: 1.5 m.
In the real configuration, there is a floor in the plan of the Yellow disk

3. Focal Laboratories

There are 2 laboratories (Fig. 2): one for research and development, the other for operational laser ranging.

The first one is based on a 60 m^2 circular room located under the telescope and centred on the azimuth axis of the telescope. There are in this lab 4 optical benches for the projects. A fifth one, in the middle of the room is devoted for the flux distribution. This bench is equipped with a fold mirror on a rotation stage that permits to send the light form the telescope to one of the other optical benches.

The second one is 6 m apart from the azimuth axis. It has a surface of 45 m^2. All the instrumentation for laser ranging is located in this lab. It is built around a single large optical bench for both laser and reception unit. This architecture permits to have the same optical path in the Coudé for both emission and reception. The laser has 2 cavities, one for the Moon (200 ps 300 mJ), the other one for the satellites (20 ps, 50 mJ). Currently, the detection unit is located on the Nasmyth bench. It will be installed in the final operational lab by the end of the year 2009.

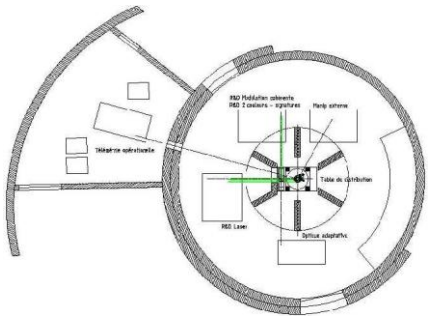

Figure 2. Focal laboratories. The circular shape is the wall supporting the dome.

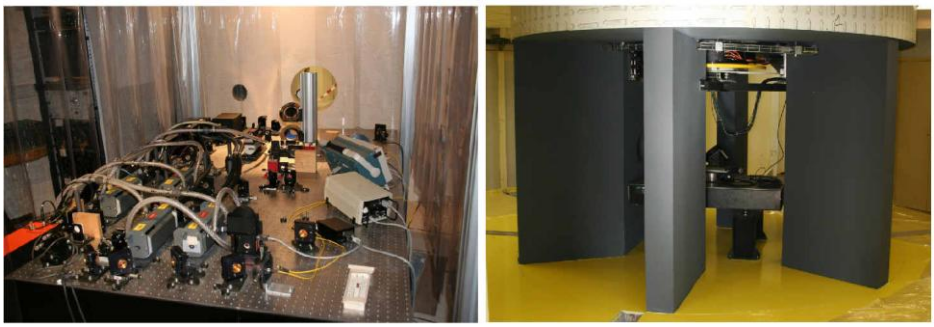

Figure 3. On the left, photography of the laser ranging optical bench.
On the right, the pillar of the telescope in the focal laboratory

4. Coudé

The coudé permits to manipulate the optical beacon coming either from the laser or the telescope. It is made with some large 200 mm flat fold mirror. These mirrors are made in Zerodur with some dielectric layers. The layers are organized in order to obtain a very large

bandwidth between 350 to 1200 nm. In the band 400-1100 nm, the reflection factor is higher than 98 % for both s and p polarizations. The damage threshold is greater than 10 J/cm^2 for ns pulses. The diameter of the mirrors was chosen to obtain a field of view of 5 arcmin on the distribution bench and 2 arcmin on the laser ranging bench.

Figure 4. 200 mm high energy Fold mirrors; distribution bench on the left.

5. Motorization

As compared to the previous design (based on a worm wheel), the objective was to increase both the speed and the acceleration by one order of magnitude to get: 5^o/S for the speed and 1^o/s^{-2} for the acceleration. It has been achieved with some direct drive motors and some direct encoders (Fig. 5).

The motors are made by Etel. The main characteristics are:
- Torque: 1000 kg.m
- Diameter 800 mm and 1000 mm
- Drive by a DSPC2 drive made by Etel

The encoders are made by Heidenhain. The main characteristics are:
- Absolute for the elevation axis ; incremental for Azimuth
- Linearity < 1 arcsec
- Precision: 0.01 arcsec

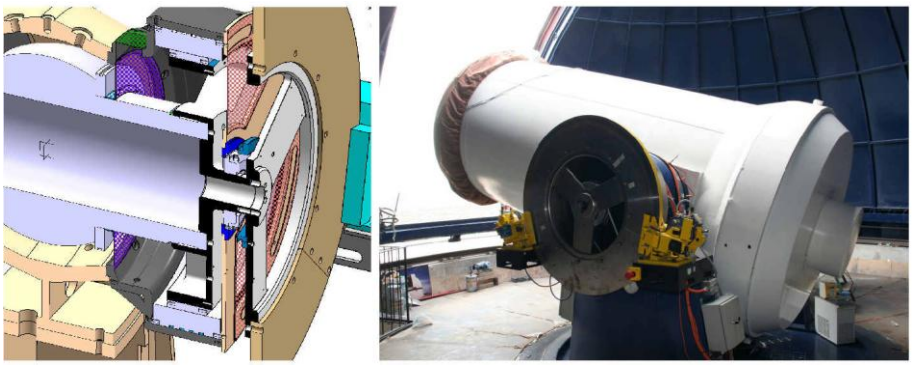

Figure 5. Motorization of the Elevation axis. The disk on the first plane is the brake. On the left view, the rotor and stator can be seen just after the disk. The absolute encoder is at the end of the axis.

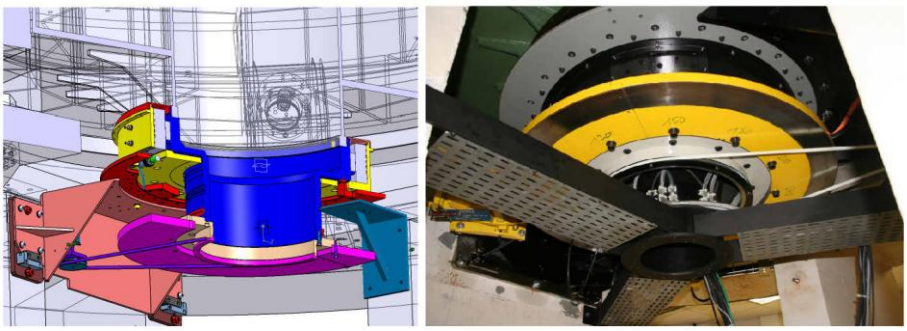

Figure 6. Motorization of the azimuth axis.

The pointing precision for both axis are 0.015 arcsec rms. The accuracy is corrected through a calibration process using position of stars. This calibration is based on a 6 order harmonic decomposition model. With a table built through 48 starts, one obtains an absolute accuracy better than +/- 2 arcsec. Two inclinometers have been attached to the pillar of the telescope to improve (in the next future) this absolute accuracy. They will permit to correct in real time the pillar tilt which is currently the main inaccuracy source.

6. Dome

The dome was redesigned for the same reasons: increase the speed and the acceleration of the dome in order to get the same performances: 5°/s. It has been achieved with a circular rail attached on the wall, and 10 guiding modules maintained by some springs for both the vertical axis and the radial axis (Fig. 7). The motorization is made with an asynchronous motor drives in frequency.

Figure 7. Guiding module of the dome. The rotation is obtained with a 30 meters chain and an asynchronous motor located downstairs

7. Software

The new software is based on an architecture with several PC machines.

- Telescope:
    - Generation of tables giving the prediction positions of the targets as a function of time.
    - Coudé steering
    - Communication with Etel's drives through a dedicated machine

- Security of the telescope
- Smart interface

- Laser ranging
  - Rotating mirror, neutral density, filters,
  - Computation of the real time residuals
  - Event timers interface

In the future, another PC machine will control the whole instrumentation through an unique interface.

8. Results

The first light of the telescope in the new configuration was obtained in May 2008, the first echoes (Etalon) in July 2008 and the continuous observation by the end of October. The observations on the Moon restarted in April 2009, but up to now, one doesn't get any echoes (some fine adjustment are still necessary in the laser).

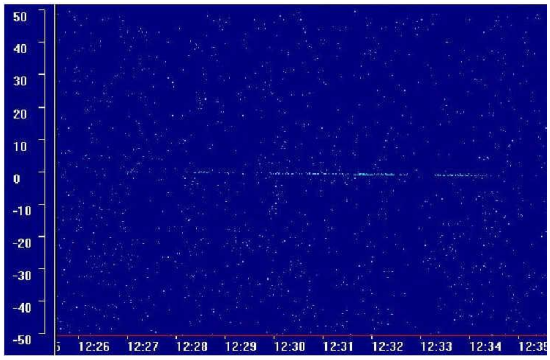

Figure 8. Echoes on Lageos

9. Conclusions

The capability of the station is now extended from low altitude satellite to the moon. The Moon will continue to be a major objective for the station together with Time transfer and high altitude satellite. The new configuration of the station will permit to perform both laser ranging and experimental research.

Reference

[1] E. Samain et al, Astron/ Astrophys. Suppl. Ser. 130,235-244 (1998)
[2] J. Nicolas et al, Surveys in GeoPhysics 22 : 449-464, 2001
[3] E. Samain et al, International journal of modern Physics D, Vol. 117, No.7, 1043-1054, 2008
[4] E. Samain et al, Proceedings of the 23th EFTF / 63th IEEE-IFCS Joint Meeting, 2009

The upgrading of the Borowiec SLR station

S. Schillak, J. Bartoszak, P. Michałek
Space Research Centre, Polish Academy of Sciences, Astrogeodynamic Observatory, Borowiec, Poland
sch@cbk.poznan.pl

Abstract

The paper reports on the modernisation of the Borowiec SLR station (7811) carried out in 2007 and 2008. The modernisation was necessary for improvement of the quality and efficiency of measurements and for extension of the range of observations. In 2007 the measures included renovation of the laser pavilion, especially the operator room and the laser room with a new air-conditioning, and installation of the new optical elements of the telescope. The most important change in 2008 was installation of the microchannel plate photomultiplier tube with 30% QE. Preliminary results of calibration with the new MCP-PMT are presented. The results indicate improved stability of the calibration system but a little worse single shot RMS. The main changes in the electronics include installation of a new gating system of the accuracy of 1 ns for the time interval counter and the photomultiplier photocathode. Significant changes were introduced in the real time programs. The plans for 2009 include installation of the Event Timer and the indoor calibration system.

1. Introduction

The Borowiec SLR station has carried out observations since 1993 with no significant breaks. New objectives of the station such as an increase in the number of observations (daytime observations), improvement in the accuracy of measurements up to a few mm, observations of high satellites, one-way measurements (time transfer, lunar satellite) induced the necessity of significant changes in the laser system. At the first stage the laser pavilion was renovated (Fig. 1) to ensure better conditions of work for the apparatuses (precise air-conditioning). The work was realised from November 2006 to March 2007. At the second stage the transmitting – receiving optical system of the telescope was modernised, the main and the secondary mirrors of the telescope were covered with new coating, a new transmitting telescope was installed, the prisms in the Coude system were replaced by dielectric mirrors, a new receiving package with new filters and a CCD camera was installed. At the third stage the software of the system was upgraded, new controlling computers and a new gating system were introduced. All these tasks were realised in 2007 and 2008 and their realisation significantly restricted or even sometimes prevented regular observations. The partial results of the modernisation were presented at the ILRS Fall Workshop at Grasse 25-28.09.2007 (Schillak, 2008).

2. The aim of modernisation

The main aim of modernisation is to ensure the possibility of continuation of SLR station observations at a level of the requirements (quantity and quality) of ILRS. The Borowiec SLR system was outdated and needed essential changes. The main objectives were:
- improvement of single shot RMS and the accuracy of observations,
- increase in the effectiveness of observations,

- regular observations of high satellites including Galileo,
- participation in the project Time Transfer by Laser Link (T2L2) and participation in the one-way measurements to the lunar satellite in the LRO project.

Figure 1. SLR pavilion in Borowiec.

3. Changes in the system in the years 2007-2008

3.1 Modernisation of the optical elements of the telescope

The earlier used optical elements were considerably worn out and needed to be replaced. The most important change was coating of the main mirror (65 cm in diameter) and secondary mirror (20 cm in diameter) of the receiving telescope. Another important improvement was the replacement of the five prisms of the Coude path by dielectric mirrors and the replacement of their regulation systems by new ones permitting more precise regulation of the mirrors positions (Fig. 2). After these measures, a new model of errors of the telescope was determined and the Coude path was precisely adjusted. As a result the effectiveness and the range of observations were improved (Schillak, 2008). A new transmitting telescope was made of the 10 cm in diameter with regulation of the laser beam divergence. Unfortunately, the hitherto tests of this telescope have not brought satisfactory results. The earlier used transmitting telescope of the 20 cm diameter is also tested. The exchange of the receiving package has not been completed yet. The package contains a new interference filter of the spectral width of 0.3 nm or 1.0 nm, a regulated space filter, a CCD camera for control of the position of the laser beam on the day.

3.2 New MCP-PMT detector

To extend the range, to improve the effectiveness and precision of observations a microchannel plate photomultiplier tube Hamamatsu R5916U-64-3MCP with quantum efficiency 30% (Fig. 3) was installed. The parameters of the photomultiplier are given in Table 1.

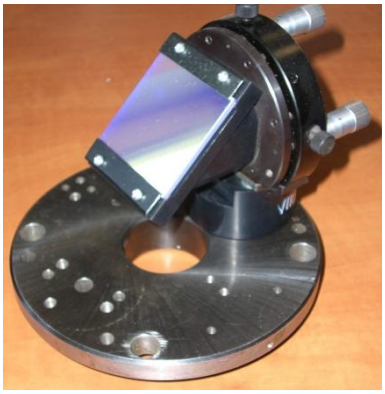

Figure 2. The dielectric mirror with the regulation system in the Coude path.

Table 1. Parameters MCP-PMT HAMAMATSU R5916U–64–3MCP.

Average Current Gain at -3600V	1.5×10^6
Average Dark Current	0.33 nA
Quantum Efficiency at 532 nm	30%
Rise Time	182 ps
Transit Time Spread	110 ps
Gate Rise Time	687 ps
Max. voltage supply	-4200V
Ambient Temperature in Operation	-50+50 C deg.

High efficiency of the photomultiplier (QE=30%, gain 1.5×10^6 at 532 nm) and small Transit Time Spread (TTS) should guarantee satisfaction of the above-mentioned objectives. The first observations with the new photomultiplier were performed on May 29th, 2008. However, a too small number of the hitherto observations related to realisation of the other tasks did not permit a comprehensive evaluation of the new detector. Preliminary data indicated a too great dependence of single shot RMS on the signal strength, both for calibration and satellite observation. For weak signals RMS exceeds 20 mm, which is a considerable deterioration in comparison to the 15 mm reached with the earlier used photomultiplier (Hamamatsu H5023). For strong signals the results are somewhat better (Fig. 5c). In Fig. 5a particular colours correspond to the neutral filters from the strongest 616 adjusted to the number of photons expected from high satellites to the weakest 602 adjusted to low satellites. The strength of the signal is determined by the percent of good calibration results and the number of the neutral filter. The signal strength versus the power supply of the photomultiplier is shown in Fig. 5a. A calibration stability determined by the dependence of delay on the signal strength is within 50 ps (Fig. 5b), which is much better than for the earlier used photomultiplier. Further works require tests at different levels of the constant fraction discriminator and increased power supply of the photomultiplier up to 4200V.

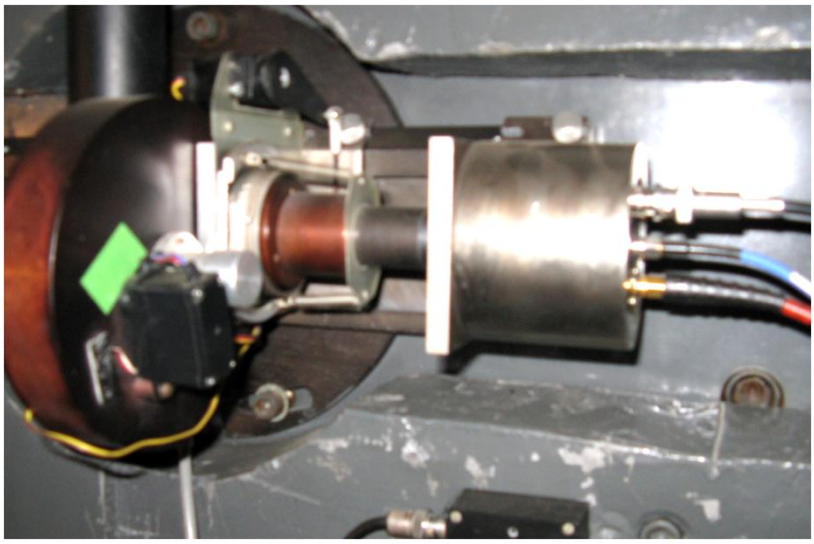

Figure 3. MCP-PMT (right) and neutral filters wheel (left).

Figure 4. Generator of the gate window (above) and the power supply of MCP-PMT (below).

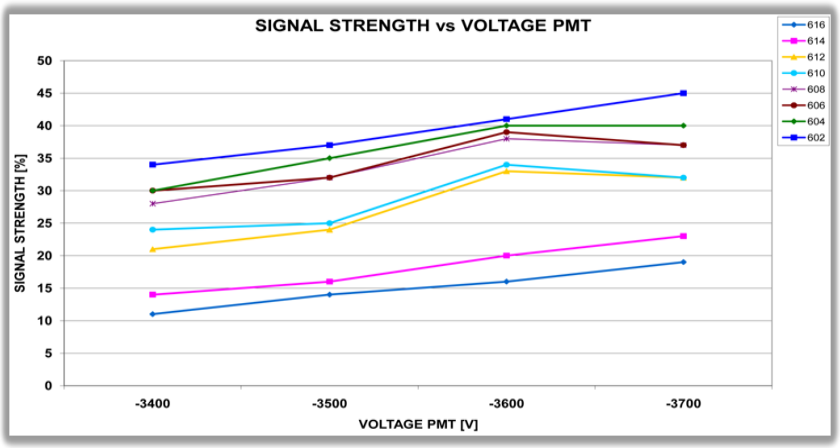

Figure 5a. Signal strength versus the photomultiplier voltage.

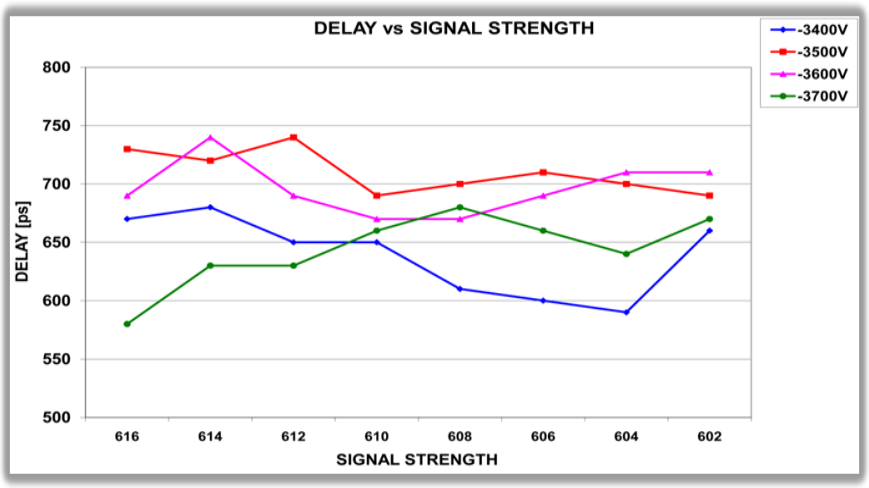

Figure 5b. Delay versus signal strength.

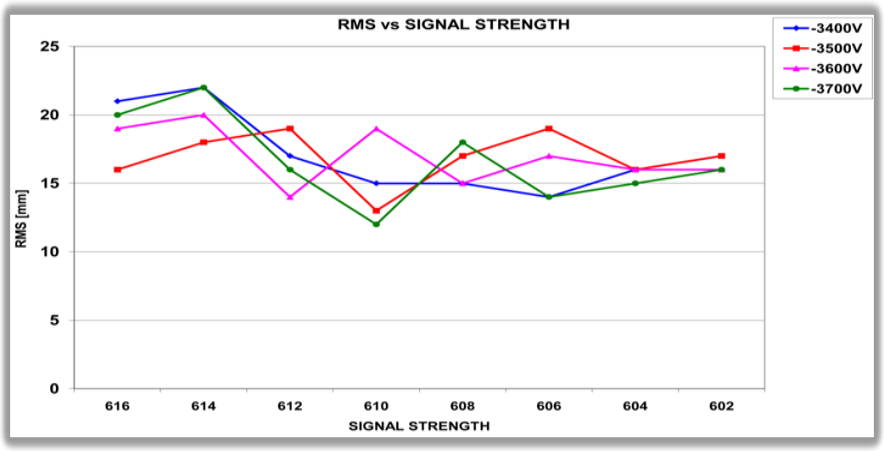

Figure 5c. Single shot RMS versus signal strength.

3.3 Software upgrading

The earlier used real time software in the DOS operational system installed at two linked computers; MASTER (real-time control program) and SLAVE (input/output programs) did not ensure correct work of the system. Two new and faster computers were introduced but they worked with the same basic software but with the possibility of gradual change into the Linux operational system. Additional loading influencing the speed of the programs realisation was introduction of a gate generator Stanford DG-535, necessary for gating the time interval counter and the photocathode of the photomultiplier. For the photocathode gating a regulated gate window was introduced in the range from 10 mcs to 10 ns (Fig. 4). The changes in the software did not increase the speed of the programs, while the delay introduced by the new gating system and the transmission between the computers led to essential problems and mistakes in their execution. At present efforts are made to eliminate these problems. An additional task is to adapt the software to work with the Event Timer.

4. Conclusions and future work

The schedule of Borowiec SLR modernisation has been much delayed because of the engagement of the SLR staff in organisation of the 16th Workshop, staff reduction and too many changes introduced simultaneously. The wintertime 2008/2009 is not suitable for testing because of the weather. The work concentrated on the measures ensuring the station full activity, in particular on more effective use of MCP-PMT, on testing the two transmitting telescopes in reaching the high satellites and on adaptation of the software to the changes in the system. An important task is the implementation of the Event Timer A032-ET and a new CRD format needed to participate in the project of laser time scale comparison T2L2.

Further work will concentrate on exchange of the outdated system of telescope control, including the engines and angle encoders, which is expected to permit more accurate tracking and realisation of daytime observations. Installation of the indoor calibration system is underway.

Unfortunately, the modernisation efforts have led to reduced activity of the station. It is expected that the effects of the modernisation will already in 2009 bring about a significant improvement in the quality of results of the Borowiec SLR. The far-ranging plans aimed at ensuring high quality of the station work are the installation of a new telescope, a kHz laser and new driving software in the Linux system working on the FPGA processor.

Acknowledgement

The authors wish to thank all the personnel engaged in modernisation of the Borowiec SLR, in particular Danuta Schillak and Stanisław Zapaśnik from the Observatory in Borowiec and Roman Baranowski and Przemysław Bartczak from the Astronomical Observatory of AMU in Poznan. This work has been partially supported by financial resources for science in 2006-2009 as a research project No. 4T12E 007 30.

Reference

Schillak S., 2008, Upgrading of the Borowiec SLR station in 2006/2007, Proceedings ILRS Fall 2007 Workshop, Grasse, 25– 28 September 2007, 9.1, CD.

Herstmonceux: towards kHz ranging and multi-technique status

Graham Appleby, David Benham, Philip Gibbs, Christopher Potter, Robert Sherwood, Toby Shoobridge, Vicki Smith, Matthew Wilkinson
NERC Space Geodesy Facility Herstmonceux, UK

Abstract

The NERC Space Geodesy Facility (NSGF) at Herstmonceux, UK has developed a kHz satellite ranging system alongside the traditional 10 Hz ranging ability without any disruption to continuous observation. This report highlights some of the important steps along the way and reports on 2 years of kHz ranging experience. The NSGF also manages two IGS systems, an absolute gravimeter and an emerging LIDAR programme to run simultaneously with laser ranging.

1.Upgrades to the Herstmonceux SLR system

The newly installed event timer and high repetition rate solid state laser are the two major upgrades to the SLR system. The event timer came online at the beginning of 2007 and improved the accuracy and precision of all observations. The new laser fires a 10ps, 0.42mJ pulse at 2kHz. First test observations were made in October 2006 and data was first submitted in the spring of 2007. Both upgrades have given clear improvement to the calibration RMS as seen in the Lageos calibration RMS plot for Herstmonceux available from the ILRS website and shown left. There is a clear drop in RMS at the beginning of 2007 on the installation of the event timer. A further drop in RMS is present for later passes, indicating kHz observations. The later higher RMS passes are due to the temporary use of an older SPAD detector.

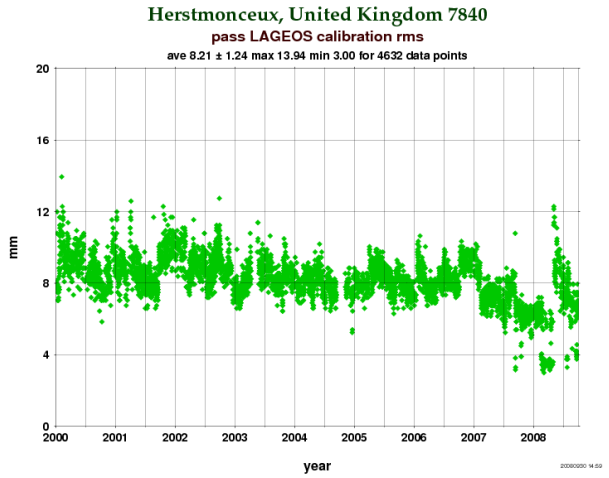

The NSGF now operates a dual laser system. A movable mirror installed in the laser bed allows easy selection of either laser. Alignment between the two lasers must be closely matched as once beyond this mirror both lasers share the same optical path. In the near future, switching from kHz to Hz and back again will be controlled by software. This will involve automatically switching the start diode, laser fire and directing the safety systems, including the radar, telescope switches and observer control, to the appropriate laser.

To date the 2kHz laser has not met expectations with regard to a high enough return rate and ease of satellite acquisition. We are therefore investigating potential loses to the outgoing laser energy using a set of energy monitors which can take measurements of the laser energy at any point in the optical path. We aim to identify any losses due to any individual optic or orientation of the telescope. Initial results were presented in Grasse in 2007 and showed an 8% variation in a 360° azimuth rotation.

A further difficulty experienced in kHz ranging is that a lot of daylight noise can appear in the range gate window. Any noise that triggers the C-SPAD detector before the satellite return pulse arrives prevents an observation being made. This effectively reduces the firing rate of the SLR system. A faster gating system is being investigated which involves either introducing a very fast shutter in the form of a Pockels Cell or switching detectors to and MCP-PMT.

The telescope detector box was recently upgraded and now has 3 working ports for the light to either go to the C-SPAD detector, the daytime camera or a LIDAR photometer. Switching between these ports will eventually be automatically driven. The LIDAR photometer was originally situated to detect reflections from the dichroic, but this was determined to be too weak a signal.

The Linux secondary observing PCs were upgraded to SUSE 11.0. The new package provides gfortran, which gives more decimal places to a real number variable (REAL*12). This was enough to give the necessary precision for the new CRD format, 1 picosecond for epoch.

2.Problems overcome and remaining from switching to kHz SLR

The kHz system was in operation less than 50% of the time in 2008. Different reasons for this include the loss of energy due to the burnout of optics, problems with the frequency doubler crystal, damage to the C-SPAD detector, failure of the daytime intensifier and general work needed on the laser. To avoid critical damage of the ND filters from the laser intensity incident at the eyesafe filter the beam path was increased by about 2m to allow the beam to naturally diverge and better disperse the energy.

A new TCP-IP communication ability was incorporated into the system in anticipation of a large increase in data volume. Data epochs from the event timer are matched by the primary observing PC and this data is sent to two secondary PCs by TCP-IP communication for the displaying and recording of data. Occasionally this flow has been fallen behind the continuous sending of data and PCs have crashed. A congested data display port is now 'flushed' for continuous operation should it get behind.

Once data has been collected for a pass, the satellite data needs to be extracted and formed into normal points. The NSGF reduction system now uses a single software program for both Hz and kHz data. The main difference between the two data set types is the signal to noise ratio, which is significantly less for the kHz data. Satellite track is identified in real time by software and this serves as a starting point for the reduction. It is important that enough satellite observations are present in any part of the data set used. This is particularly a problem for Etalon satellites which have large array sizes. A comparison between the satellite track of an Etalon pass and that of a GPS satellite shows a much greater spread of range measurements for the Etalon satellite. Consequently the range data from the Etalon satellite it is much more difficult extract from the background noise.

Etalon 1. The plot shows 6 minutes of an Etalon 1 pass. The satelli
clearly visible in a large range gate but difficult to see clearly close up.

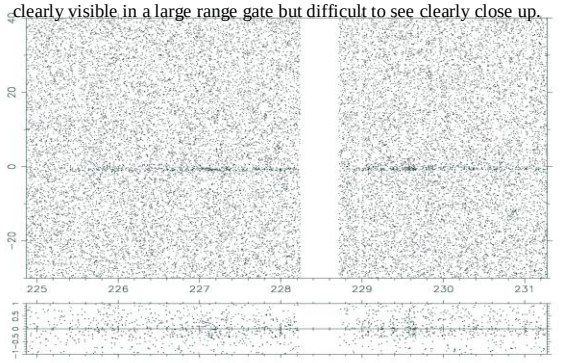

GPS 36. The plot shows 6 minutes of an GPS 36. The satellite is
clearly visible in a large range gate and closer up.

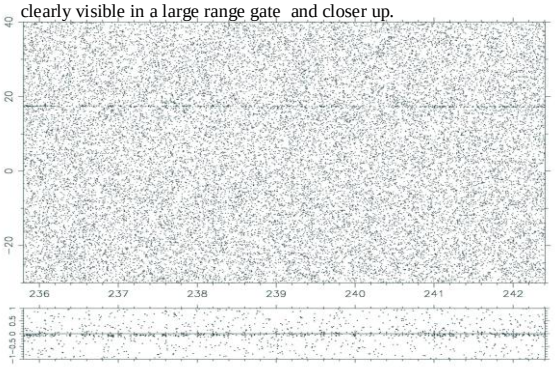

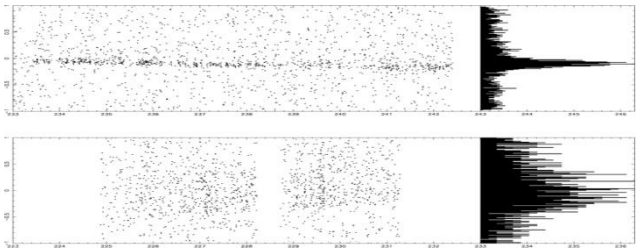

3.Other Techniques at Herstmonceux

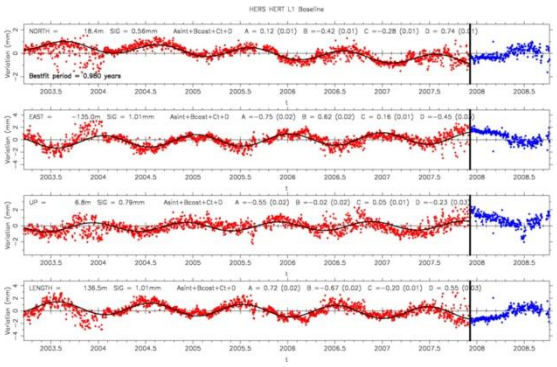

The NSGF has two IGS GPS receivers, HERS and HERT, and recently installed a third on a nearby solar pillar situated between the two. HERS and HERT are approximately 136.5m apart. Their close proximity allows single frequency (L1 or L2) baselines to be calculated because they share the same atmospheric delays. Using the freely available GAMIT GPS analysis software, a daily baseline is calculated between the HERS and HERT sites. The resulting baseline plots show a close to annual variation with an amplitude of about 3 mm.

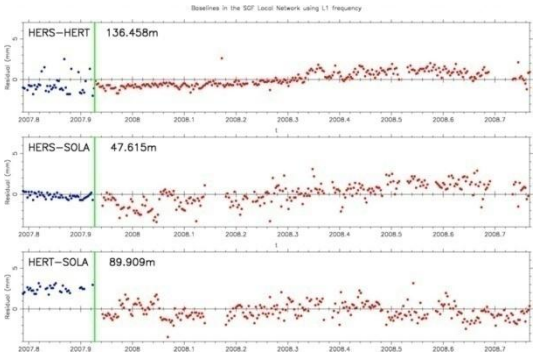

The new site between HERS and HERT, locally called SOLA, identified the poor data quality from the HERT Z-18 receiver. A new Lecia receiver was initially sited on the SOLA pillar and then later switched with the HERT Z-18 receiver bringing the observed signal noise to the SOLA site. Hopefully in time this additional site will also explain the annual variation in the baseline.

The NSGF permanently installed an absolute gravimeter in the facility basement and it has been operational since October 2006. The gravimeter is routinely run mid week for 24 hours and gives a gravity reading to ±2µGal, with 1µGal being equivalent to ~3mm. This produces an ongoing time series of local gravity shown right.

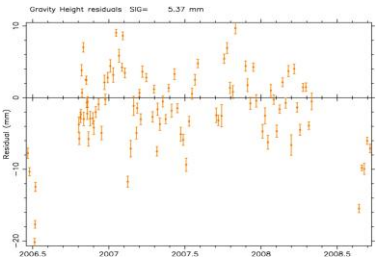

In November 2007, the gravimeter was taken to the intercomparison in Walferdange, Luxembourg and was found to agree within specification with other gravimeters. At the GGEO conference in Crete this year, the very close proximity of the NSGF gravimeter to the SLR telescope and GPS receivers was highlighted as important for future GGOS developments.

4.Conclusions

The NSGF is Herstmonceux is now a more accurate laser station with better precision thanks to an event timer and a kHz laser. Not only does a dual system allow SLR to continue during development periods but retaining the original 10Hz system means that the station is suitable to take part in the LRO satellite and T2L2 missions. At present the kHz system still needs to prove itself as a fully capable SLR system.

Ftlrs : Past and currents missions, upgrade for future

M.Pierron[1], F.Pierron[1], M.Furia[1], JM.Torre[1], P.Bonnefond[1], P.Exertier[1], E.Samain[1] , Laser Staff[1], R.Coleman[2], C.Watson[2] , P.Tregoning[3], J.Zhang[3]

[1]Observatoire de la Côte d'Azur, Grasse, France
[2]University of Tasmania, Hobart, Australia
[3]The Australian National University, Canberra, Australia

monique.pierron@obs-azur.fr

Abstract

This paper describes recent campaigns as well technological upgrades for future projects.
- Tasmania campaign (November 2007-April 2008) in collaboration with Australian colleagues
- Corsica campaign for Jason1/Jason2 Calval activities to inter-calibrate radar altimeters on the spacecrafts
- Recent installation of Dassaut Event Timers on mobile system to add the capability of accurate time stamp at the picosecond level.

FTLRS recent missions:

1. **Calibration/validation project on Jason1 satellite in Tasmania, a collaboration between University of Tasmania at Hobart and Observatoire de la Côte d'Azur in France**

Burnie is the only calibration site in the southern hemisphere for Jason1

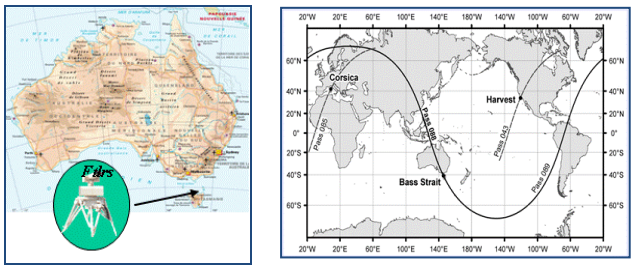

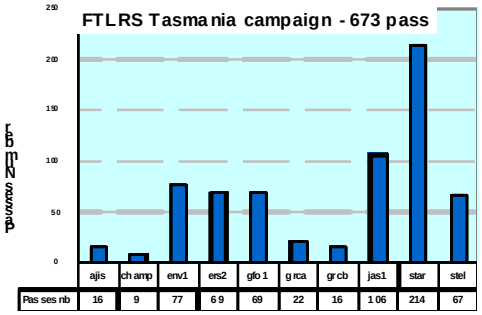

Figure 1. Burnie (Tasmania) , calibration site for Jason1 in south hemisphere

As shown on
, Burnie is very close under the trace of Jason1 (like Ajaccio in Corsica). This cooperation was 5 months (2007/2008) in Burnie for permanent observations on site;

Sciences, research project were established by both institutes.
- *OCA contribution: Technological issue for Ftlrs and engineers*
- *Australian contribution: Site installation and missions funding*

Results: about 10.000 NPs, more than 650 passes, including 106 for Jason1

2. Corsica campaigns for Topex, Jason1/Jason2 calibration/validation

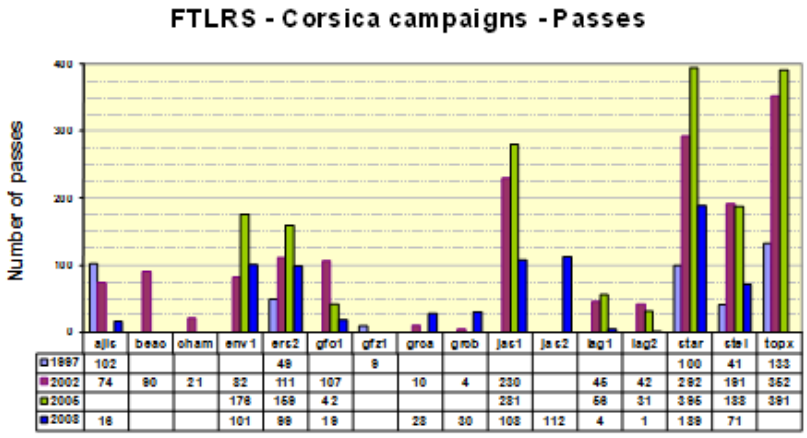

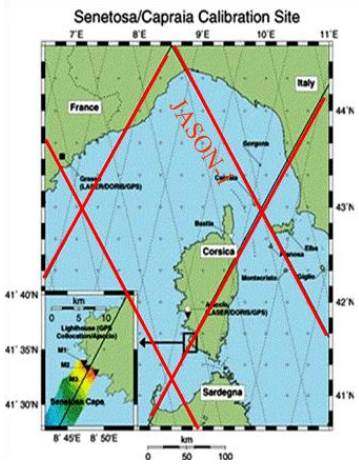

Installation of Dassaut Event Timers:

Dassaut Event Timers were installed in spring 2008 on mobile system, to add the capability of accurate time stamp at the picosecond level. This very important upgrade has been achieved to imply Ftlrs in Time Transfer experiment on T2L2/Jason2 with a very quick identification of triplets by the Grasse Center in July 2008, some days after the launch of Jason2.

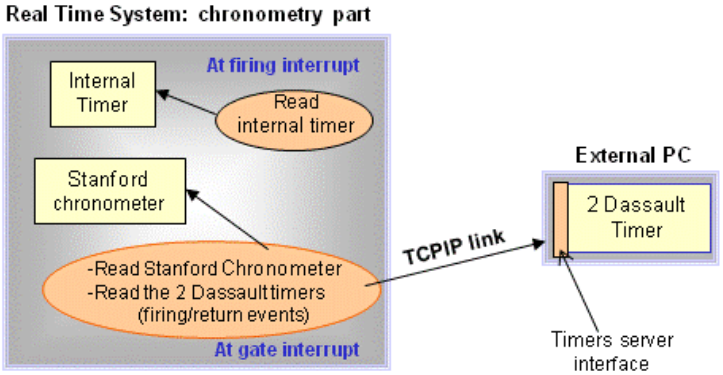

Our choice has been to conserve the 2 timing systems very useful for engineering and failure:

- internal timer and Stanford chronometer
- Two Dassault timers (start and stop channels)

.

Now we have no more linearity problems, ground target is at 20 ps Rms; the resolution and chronometry noise are at some ps level; ftlrs has now a better accuracy on every targets.

First T2L2 results:

These data on Jason2 are from Ftlrs at Grasse and at Ajaccio, and from MEO at Grasse in July 2008, just some days after launch

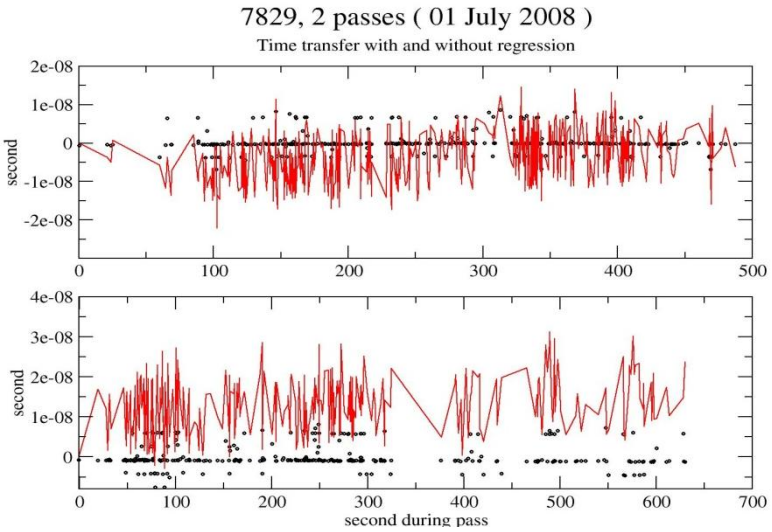

Ukrainian SLR network

O. Bolotina, M. Medvedsky, V. Pap
Main astronomical observatory of NAS of Ukraine.
olga@mao.kiev.ua /Fax: +380-44-5262147

Abstract

The structure of Ukrainian SLR network is described in the article. Technical description and current activities for each of the station are presented. Perspectives and plans for future of the Ukrainian SLR network are outlined.

Current Status

The Ukrainian SLR network was created by several organizations and includes four permanent SLR stations: Golosiiv-Kiev, Simeiz, Katzively, and Lviv (Bolotina, 2007). The permanent SLR stations Uzhgorod, Dunaivtsi, Alchevsk, and Evpatoria operate in an experimental mode.

The satellite laser ranging station Golosiiv-Kiev of the Main Astronomical Observatory of the National Academy of Sciences of Ukraine (MAO NASU) was founded in 1985. The third-generation equipment of the station was mounted in 1985. Due to some reasons the station was not in operation up to 1996. The experimental ranging of satellites started on 1 April 1997. The routine ranging of night passes has been carried out since January 2000, and its results have been sent to the Eurolas Data Center (EDC) at DGFI/ILRS Global Data Center. The SLR station Golosiiv-Kiev was included in the International Laser Ranging Service (ILRS) in 2000. The satellite laser ranging station Golosiiv-Kiev was added to the list of the National objects of Ukraine.

The satellite laser ranging station Lviv of the Astronomical Observatory of the Ivan Franko National University of Lviv was founded in 1987. The third-generation equipment of the station was mounted during 1997-1998. The experimental ranging of satellites were started on 23 December 1998. The routine ranging of night passes are being carried out since 1 January 1999, and since 2002 the results are being sent to the Eurolas Data Center (EDC) at DGFI/ILRS Global Data Center. The SLR station Lviv was included in the International Laser Ranging Service (ILRS) in 2002.

The satellite laser ranging station Simeiz was founded in 1988 by the Crimean Astrophysical Observatory, Crimea, Ukraine. In 1991 the station was certificated by European Space Agency using mobil SLR station from Munich. The third-generation equipment of the station was mounted. Experimental night passes started in 1988. The routine ranging of night passes of satellites (all low at the station. The SLR station Simeiz was included in the International Laser Ranging Service (ILRS).

The satellite laser ranging station Katzively was founded in 1984 on the basis of the Crimean Scientific Station of the FIAN. The second-generation equipment of the station was mounted in 1984. The third-generation equipment of the station was mounted in 1990. The experimental ranging of the satellites LAGEOS started in 1984. The routine ranging of night passes has been carried out since 1988, and the results have been sent to the Eurolas Data

Center (EDC) at DGFI/ILRS Global Data Center. Since 1992 the SLR station Katzively becomes a laboratory of the Crimean Laser Observatory (CLO) of the FIAN. Since 2000 the satellite laser ranging station Katzively, as well as the CLO, becomea department of the Main Astronomical Observatory of the National Academy of Sciences of Ukraine (MAO NASU). The SLR station Katzively was included in the International Laser Ranging Service (ILRS) in 2000.

Ukrainian stations Simeiz and Katzively are observed regullary. Since 2007 discontinues in data sets of these stations do not exceed 14 days. Several exceptions took place during 2007-2008 when upgrade of equipment on stations were made. SLR stations Golosiiv-Kiev and Lviv are operating
unregulary.

Seasonal and monthly variations of a number of observations take place in data sets of all ukrainian SLR stations. Since 2005 number of observations are increase for ukrainian SLR station Golosiiv-Kiev, Simeiz and Katzively.

Ukrainian SLR stations Golosiiv-Kiev, Lviv, Simeiz do not correspond to the ILRS station qualification criteria (data quantity) for Low Earth Satellite Passes. Since 2007 SLR station Katzively fulfills qualification criteria for Low Earth Satellite Passes. Ukrainian SLR stations do not fulfill qualification criteria for LAGEOS 1 & LAGEOS 2 Passes. After modernization two ukrainian SLR stations, Simeiz and Katzively, can locate of High Satellites. Since 2008 ukrainian SLR station Katzively corresponds to the ILRS station qualification criteria for High Satellite Passes.

Plans for Future

Ukrainian SLR stations Simeiz and Katzively will fulfill qualification criteria (data quantity) for Low Earth Satellite, LAGEOS 1 & LAGEOS 2, High Satellite Passes already in 2009-2010.

Ukrainian SLR stations Golosiiv-Kiev and Lviv will correspond to qualification criteria (data quantity) for Low Earth Satellite, LAGEOS 1 & LAGEOS 2 to 2011-2012.
All ukrainian SLR stations will fulfill qualification criteria (data quality) to 2010.
Daily location of Low Earth Satellite will be realised by all ukrainian SLR station to 2010.

References

Bolotina O., Medvedskij M., *Some results of investigation of the stability of the Ukrainian SLR stations*, Kinematics and Physics of Celestial Bodies, 2007, Vol. 23, No 1, p.11-17.

About Current Status of Katzively SLR Station

A. Makeyev
Crimean Laser Observatory, Katzively, Yalta, Crimea, Ukraine
clogao@rambler.ru

Abstract

Upgrades and achievements that took place over the last few years on the SLR station Katzively-1893 along with its current capabilities are listed in this paper.

In the late 2005 our station received a new Russian YAG:Nd laser made in "Poljus" Research Institute (pulse width about 250 ps, repetition rate 2–10 Hz, output energy approximately 50–100 mJ, output wavelength 532 nm). Introduction of user-friendly interactive time-table in 2006 allowed observers to schedule passes for the whole night in the evening and quickly switch from one satellite to another in the case of necessity. In the beginning of 2008 old photomultiplier Hamamatsu H6279 was replaced with more sensitive H6780. Due to these upgrades our station significantly increased satellite ranging data quantity and crossed ILRS quantity baseline for LEO and HEO satellite passes. During first nine months of 2008 in spite of station building renovation that spoiled about 40 cloudless summer nights we managed to observe 1311 passes of 27 satellites from CHAMP (350 km) up to GIOVE (24500 km).

In spring 2008 we have installed simplified program packages for ephemeris preparation and for processing of ranging results, so nowadays most of our observers can send normal points to data centers as soon as there would be a little break between passes. It has essentially reduced the data delivery latency.

After installation of CCD camera onto the main guide of the telescope in 2007, our system became more eyesafe for operators, though there left optical paths with open laser radiation yet.

At present our observers work in couples in three shifts, 7 nights per week. Because of the absence of angular encoders our station can range satellites only in nighttime when they are not eclipsed.

Although most of our measuring equipment was made more than 20 years ago (except for SR-620 which is 10 years old), personnel of our station makes efforts to improve the SLR data quality performing maintenance repairs and adjustments of our devices in order to meet international guidelines.

Progress in Changchun SLR

Y. Zhao, C. B. Fan, X. W. Han, G. Zhao, Z. Zhang, X. Dong, H. T. Zhang, J. Y. Shi
Changchun Observatory/NAOC, CAS, China
youzhao@cho.ac.cn, fancb@cho.ac.cn, hanxw@cho.ac.cn

Abstract

The paper presents the summary and progress of Changchun SLR during the past years. It includes some special satellites observation, such as ETS-8, GIOVE-A, B, and Compass (Beidou) ; the laser time transfer and comparison experiment cooperated with shanghai observatory; aintenance and improvement of the system; the design and development of any frequency fire rate control system; the basic process and application of SLR data.

1. System upgrading for LTT project

The LTT (Laser Time Transfer) experiment has been carried out at Changchun SLR station since August 2007. Changchun SLR was upgraded for the LTT project:

- New laser: (loan from the NCRIEO in Beijing)
  Active-active mode-locked Nd:YAG laser
  100-150mJ in 532nm, 250ps, 20Hz
- New Coude mirrors
- 210mm diameter transmitting telescope with 10 aresec laser beam divergency
- 2 sets of ET-A320 event timer (Riga Univ.)
- 1 set of hydrogen maser (Shanghai Obs.)
- LTT software: laser firing control, LTT data analysis

Figure 1. Active-active mode-locked Nd:YAG laser with 100-150mJ (532nm), 250ps,20Hz

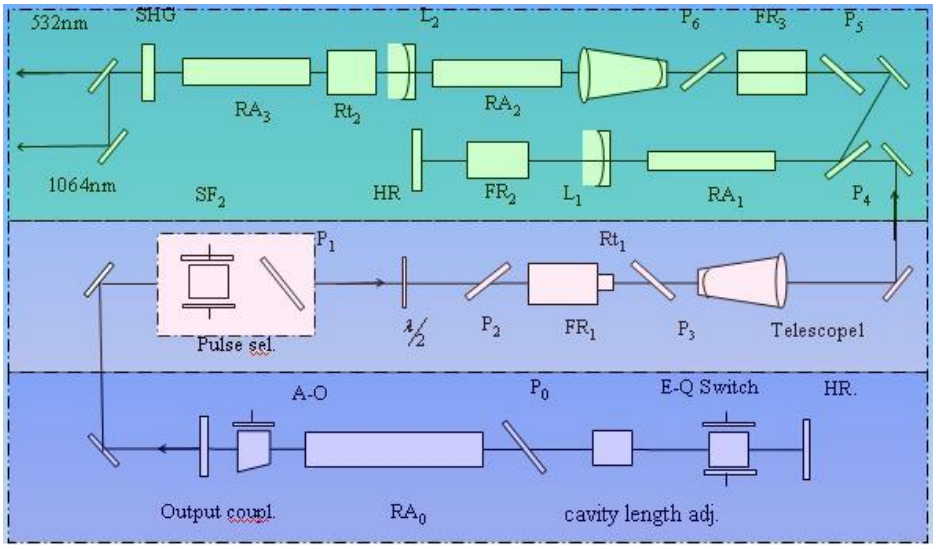

Figure 2. Diagram of Active-active mode-locked laser for LTT

Figure 3. Changchun SLR & LTT Control Room

Preliminary results of the LTT experiment has been obtained. The clock differences between the space rubidium clocks and ground hydrogen maser have been measured with a precision of 300ps (single measurement). The LTT experiment at Changchun SLR station was successful.

2. Special satellites observation in Changchun SLR station

Some special satellites observation, such as ETS-8, GIOVE-A, GIOVE-B, and Compass-M1 (Beidou) is fine (shown in Table. 1). Especially Changchun station is interested in ETS-VIII observation. For this one is a geosynchronous satellite. Changchun SLR station obtains 32

passes successfully**.** The elevation angle is 36°. When SLR station observes ETS-VIII, the range is more then 38000 km. A night time pass of Compass (BD-MEO) with 29k returns was also got (shown in figure 4).

Table 1. High Satellites SLR Data (Passes) tracked

Satellites	Pass		
	2007	2008	Total
Compass（BD -MEO）	34	47	81
GIOVE-A	72	33	105
ETS-8	28	4	32
GIOVE-B		24	24

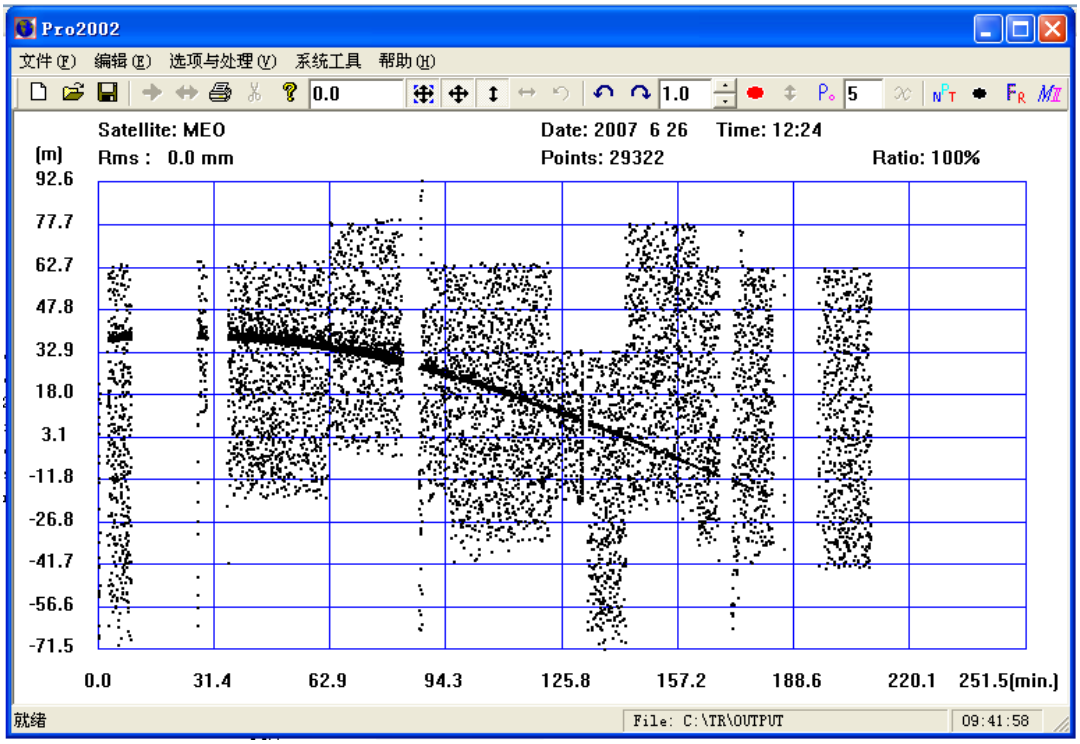

Figure 4. Plot of data from a night time pass of Compass with 29k returns

3. KHz SLR Experiments

The high repetition-rate control system has been developed and used in Changchun SLR station. The system can make the SLR system work at from 1 Hz to more than 2 KHz. The real-time control hardware and software run under Windows XP environment. The hardware control circuit includes three parts: accurate timing part, range gate control part and laser firing control part. A 2KHz laser which borrowed from Wuhan SLR Group was used to work together with the controlling system to test the performance. The experimental results show that the any frequency fire rate control system can work very well at or less than 2 KHz.

Figure 5. Real time control interface

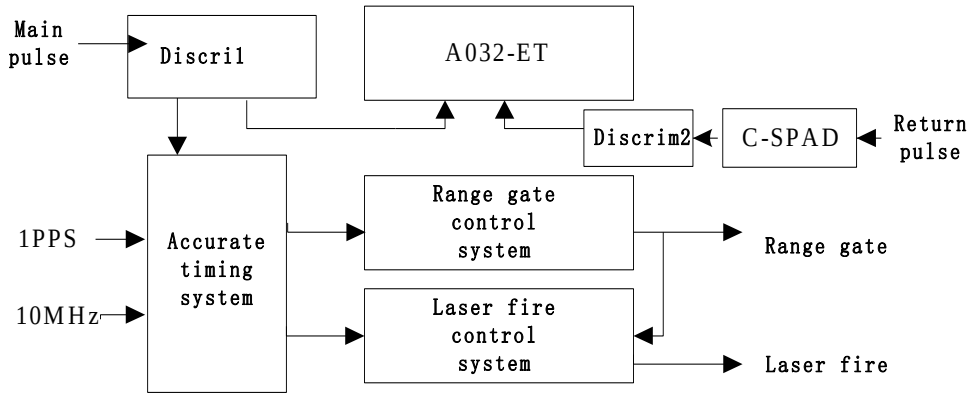

Figure 6. The block diagram of the hardware control system configuration

The hardware control system is mainly composed of three parts: accurate timing part, range gate control part and laser fire control part.

The detailed specifications of the ns kHz Laser system are summarized in the Table 2.

Table2. Specifications of the ns kHz Laser

Model	DS20-532
Wavelength	532 nm
Average Power @ 10 kHz	18 Watts
Nominal Pulse Width @ 10 kHz	40 ns
Pulse Energy @ 10 kHz	1.8 mJ
Beam Mode	TEM00 - M2 < 1.1
Polarization	100:1 Vertical
Beam Diameter	1.0 mm
Beam Divergence	1.6 mrad
Pulse-to-Pulse Instability	<3% rms
Long-Term Instability	+/- 3%
Pointing Stability	< 25 μrad
Pulse Repetition Rate	500 to 10kHz

4. Preparation of daylight tracking

As you know, the system hardware and software were ready for daylight tracking since the end of 2005. But because of some special projects, we did not carry out the tracking. And the research of the daylight tracking was continued. At 11 am of May 16th, 2008, we tried once daylight tracking. The system got the return pulses of satellite ERS-2, and following is the data process result on the screen. It also means that the breakthrough of daylight tracking was achieved in Changchun station.

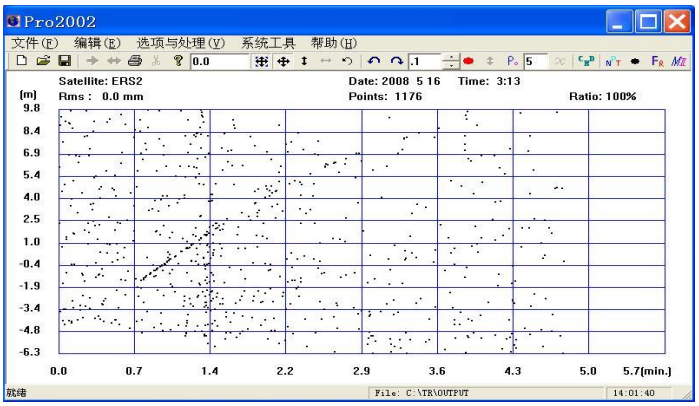

Figure 7. First result of Changchun station daylight tracking

From the experiment result, we find that we must solve the too much noise problems.
In the future we must improve our system:

- Using Variable receive iris with Φ0.5mm minimum aperture to get smaller Receiving field of view :30"
- Improve mount pointing performance and transmit/receive boresight

5. Data Analysis

From the beginning of 2008, Changchun Observatory has carried out routine short-arc (3-day) orbit determination and station residual analysis on LAGEOS SLR data. Meanwhile, we commence analysis in some aspects of related issues, such as the satellite precise orbit determination and its preliminary applications. The short-arc orbit determination accuracy is around 1.2cm with moderate difference. So now Changchun Observatory has the foundation in SLR POD work. Routine POD and residual analysis results on LAGEOS-1/2 have been put on the Changchun station website.

In the case of our study, the choice of gravity model has slight effect on precision of LAGEOS orbit determination. The influencing magnitude is on sub-mm level. The station coordinates can also be determined in POD process, and the proper value can do help to improve orbit determination precision. The cause of variability of station coordinates need to be further investigated. What we can do using POD results, how to apply them in relevant geodynamic and geophysical problems, how to combine them with our observational duty, need seriously consideration. We wish the POD work in Changchun will build a bridge to connect theoretical research and observational work.

References

1. Yang Fumin, Huang Peicheng, Ivan Prochazka, Zhang Zhongping, Chen Wanzhen, Zhang Haifeng, Wang Yuanming, Meng Wendong, Wang Jie, Liao Yin, Zou Guangnan, Wang Luyuan, Zhao You, Fan Cunbo, Han Xingwei. *The Preliminary Results of Laser Time Transfer (LTT) Experiment.* Proc. of 16th International Workshop on Laser Ranging, Poznan, Poland, 2008
2. ZHAO You, HAN Xingwei, FAN Cunbo, DAI Tongyu. *Fulfillment of SLR daylight tracking of Changchun station.* Proceedings of 15th International Laser Ranging Workshop, Canberra, Australia, Oct.15-21, 2006, pp587-592
3. FAN Cunbo, DONG Xue, ZHAO You, HAN Xingwei. *A032-ET Experimental Test on Changchun SLR*. Proceedings of 15th International Laser Ranging Workshop, Canberra, Australia, Oct.15-21, 2006, pp300-305
4. ZHAO You, FAN Cunbo, HAN Xingwei, LIU Chengzhi, SHI Jianyong, ZHANG Ziang. SHAO Baodong, ZHANG Haitong. etc. *System Improvement and GIOVE-A Observation of Changchun SLR.* Proceedings of 15th International Laser Ranging Workshop, Canberra, Australia, Oct.15-21, 2006, pp399-404

First SLR Operation in Korea using TROS, Chinese Transportable Ranging Observation System

H. Lim (1)**, T. Guo, P. Wang** (2)**, H. Jeon, Y. Seo, J. Park** (1)**, T. Zou** (2)

(1) Korea Astronomy and Space Science Institute
(2) Institute of Seismology, China Earthquake Administration

hclim@kasi.re.kr /Fax: +82-42-861-5610

Abstract

The memorandum of agreement (MoA) between Institute of Seismology, China Earthquake Administration (ISCEA) and Korea Astronomy and Space Science Institute (KASI) was concluded for a productive collaboration in the field of space geodesy in June 2008, which specially includes a collaborative operation of TROS in Korea. TROS was moved to Korea in August 2008 on the basis of MoA and it will be operated by July 2009 in KASI headquarter in Daejeon. The all-electronic part of TROS is integrated in one FPGA board, including event timer, GPS locked clock, range gate generator, servo system, software and so on. Additionally, it is capable of KHz ranging and ISCEA succeeded in obtaining laser ranging data using KHz laser system in the beginning of 2008. Now TROS is operated by using a laser system with several Hz repetition rate because the new KHz laser system is not decided. ISCEA brought a new KHz Laser system in January 2009, but it's not easy to move to Korea. KASI and ISCEA want to contribute to the international laser ranging societies by a collaborative operation of TROS.

TROS upgrade

The second Chinese mobile system, TROS was developed by ISCEA in 2000 and had been operated for several years. However, all electronic systems had not only been upgraded for the KHz laser ranging since 2005 but also the external feature was changed to be more stable and convenient for transportation. The all-electronic part of TROS was integrated in one FPGA board, including event timer, GPS locked clock, range gate generator, servo system, software and so on. A new KHz laser system provided by a University of China was installed in Beijing in the beginning of 2008. Even though there was stability problem in KHz laser system, TROS got some successful KHz results in Beijing experiment. TROS upgrades enhanced the signal return rate remarkably and improved the tracking precision and system reliability. Figure 1 shows external change between old and new TROS system. Tables 1 also show comparisons in laser, servo and electronic system. The schematic diagram of TROS FPGA board is represented for KHz laser ranging capability. Finally, Figure 3 shows KHz laser ranging result, which was done in March 2008 for Ajisai satellite.

Figure 1. Exterior change of TROS (left : old, right : new)

Table 1. TROS upgrade for laser, servo and electronic system

Component	Feature	Old	New
Laser System	Max. repetition rate	10Hz	1KHz
	Pulse width	25~35ps	10ps
	Energy per shot	30mJ	1~1.5mJ
Servo System	Resolution	1"	0.1"
	Max. arc speed	1500"/s	20000"/s
	Signal	Mix of analog and digital	All digital
	Index point	Manual	Automation
	Feedback	2 sensor (inductosyn and velocity meter)	Optical encoder
Electronic System	Stability of Frequency	$5X10^{-12}$	$2X10^{-12}$ (Atom frequency)
	Precision of PPS	<100ns	<20ns
	Precision of Gate	<200ns	<5ns
	Resolution of Gate	100ns	2ns
	Capability of Gate	300ns—800ms, max 20Hz	50ns—5s, max 10KHz
	Fire Control	1—10 times/second	1—2000 times/second
	Control Method	Cable	Laptop and Wireless
	Time Counter	Interval Time Counter	Event Counter

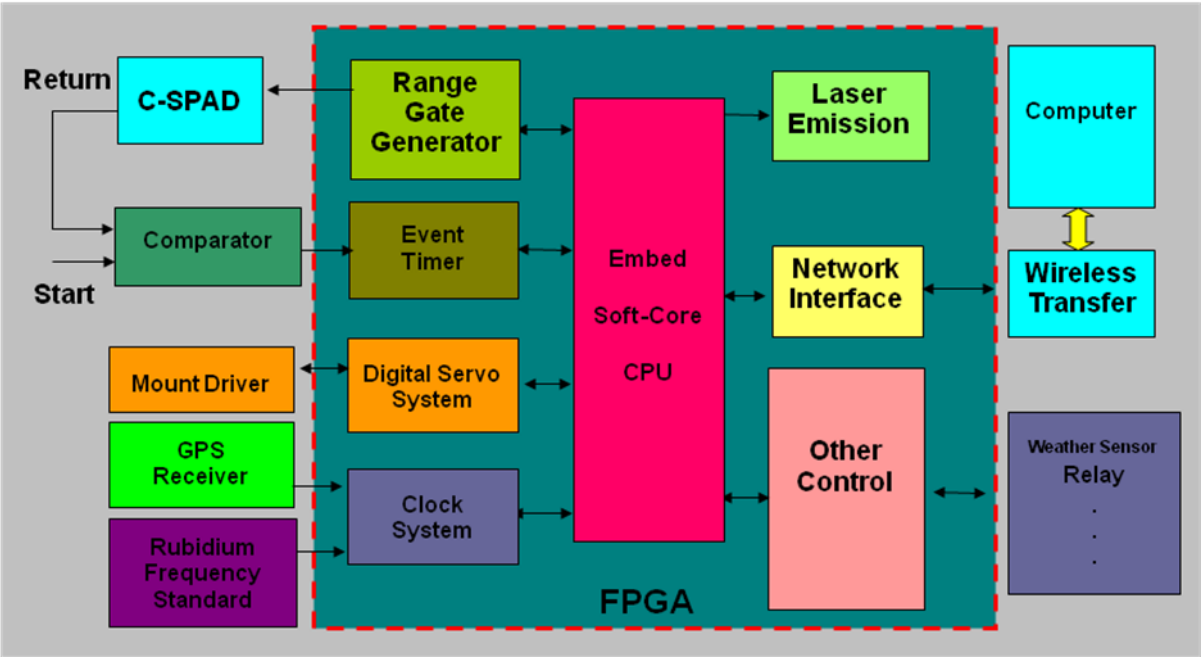

Figure 2. TROS FPGA board for KHz laser ranging

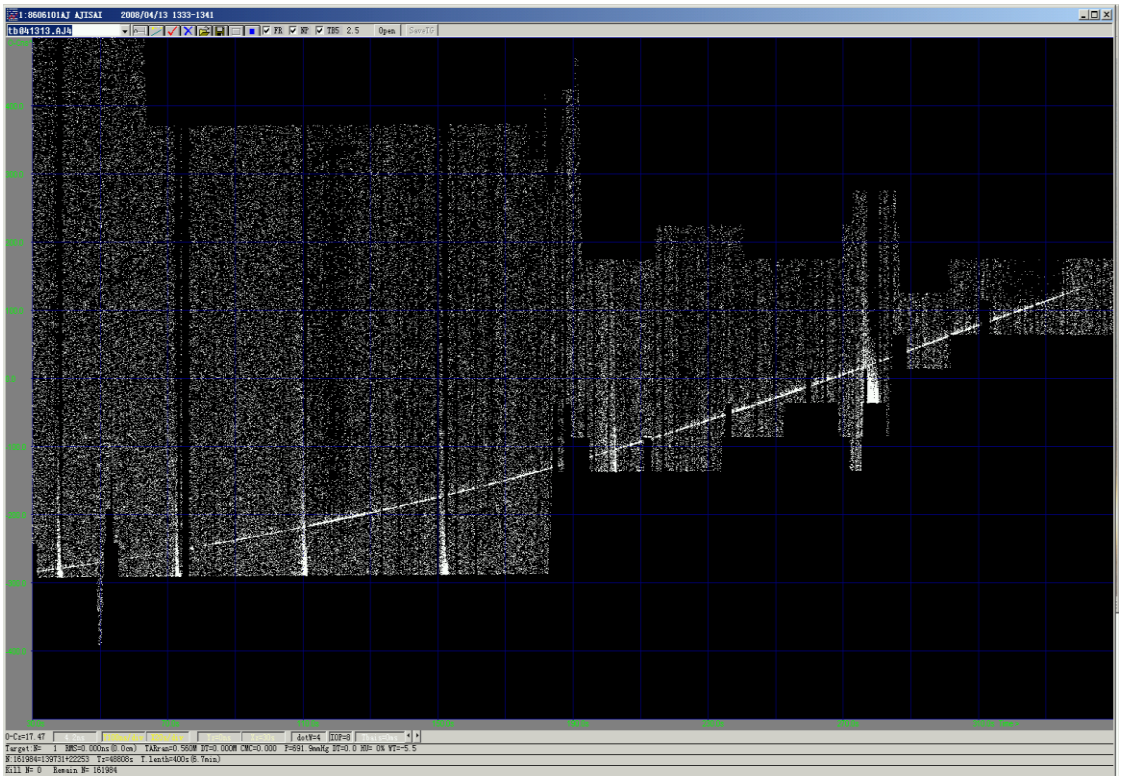

Figure 3. TROS result of KHz laser ranging (Ajisai satellite)

TROS operation in Korea

The MoA was made between ISCEA and KASI for a productive collaboration in the field of Space Geodesy in June 2008, expecially for TROS operatoin in Korea. TROS was moved to

Korea in August 2008 on the basis of MoA and it was scheduled to be operated for 12 months in KASI headquarter in Daejeon. TROS uses an old laser system with several Hz repetition rate because the new KHz laser system had not been decided before TROS was moved to Korea, ISCEA brought a new KHz Laser system in January 2009, but it's not easy to move to Korea. In the early days of TROS operation, there were some problems with the instrument, including some part damage when TROS was in the ship and some misalignment of laser, and some device are too old and inefficiency. In addition, it was very difficult to find the satellite using the ICCD camera due to high background light because the site is 5km away from Daejeon downtown.

After 4 days of TROS installation, we got the first pass of Ajisai satellite on Aug 26th, 2008. However, the normal operation was difficult because it was mostly cloudy and sometimes foggy. Even though we hoped to contribute to the international laser ranging societies by a collaborative operation of TROS in Korea, we could not transfer SLR measurements data to ILRS data center because TROS operation is temporary in Korea and the measurements are performed occasionally due to the bad weather. However, we hope China and Korea will keep good and close relationship in the field of SLR technology and its applications.

Now KHz SLR control system is tested in Wuhan(7231) and Beijing(7249) stations, and all ILRS correlative satellites results can be obtained, including LEO, Lageos1/2, high pass and geostationary orbit satellites.

References

Guo, T., Xia, Z. et al., CMONOC transportable SLR system, *Proceedings of 11th International Workshop on Laser Ranging*, Deggendorf, Germany, pp. 121–125, 1998.

Wang, P, Guo T, Liu H, Zou T., China Mobile SLR System Update, *The 4th China-Korea SLR workshop*, 2008.

Actuality and futurity of San Juan SLR Station

Liu Weidong[1], Han Yanben[1], Liu chengzhi[1], Zhao Limin[1], Yin Zhiqiang[1], R. Podesta[2], E Actis[2], E.Alonso[2], A.A. Gonzalez[2], A. M. Pacheco[2]

[1]National Astronomical Observatories of Chinese Academy of Sciences
[2]Observatorio Astronomico Felix Aguilar, National University of San Juan of Argentina

Abstract

San Juan 7406 SLR station is operated by National Astronomical Observatories of Chinese Academy of Sciences (NAOC) and Observatorio Astronomico Felix Aguilar (OAFA) of National University of San Juan of Argentina. The SLR station began to operate in the end of February of 2006. Due to the colleagues of the SLR team work hard and the lot of clear nights in San Juan region, San Juan SLR station obtained excellent results in the past two years and more. Our SLR team has established an upgrade plan on the SLR system. We hope that the SLR system can implement daylight tracking and kHz operating, also improve the precision of observations. According to the suggestion of ILRS, we will soon install a GPS receiver collocated with the SLR system.

Site

The San Juan 7406 SLR station is located in the Observatorio Astronomico Felix Aguilar of National University of San Juan of Argentina (OAFA), about 10km from San Juan city. The San Juan city is situated on the east side of Andes, 1300km northwest of Buenos Aires, the capital of Argentina. OAFA has approximately 300 nights for SLR observation a year. The geographic position of the site is 31° 30′ 31.050" S, 68° 37′ 23.377" W and 727.22m elevation.

Operations

The San Juan station began routine operations on February 23, 2006. Due to the excellent work of the observers from NAOC and OAFA, and a lot of clear nights in the region, the total passes kept continuously and exceeded by 7500 passes, especially for high satellites passes exceeded by 1200 passes, during 2007 to 2008. We are cooperating with Beijing SLR station to perform some experiments of daylight tracking, and our previous the AZ-EL inductosyns system will be replaced by a new optical angle encoder system in order to make preparations for daylight tracking.

Dual Readheads angle encoder

Laser

Due to the unstable laser, it is very difficult that the San Juan SLR system to keep and improve the single-shot accuracy for the LAGEOS and calibration, as well as the measure of short term bias stability. As a result of long-time operation, in order to keep the system to work properly, the maintenances of the laser become both very trouble and difficult. Therefore we need the laser which is very stable, more or less maintenance free.

Weather: Approximately 330 nights for SLR observation from Oct 2007 through Sep 2008

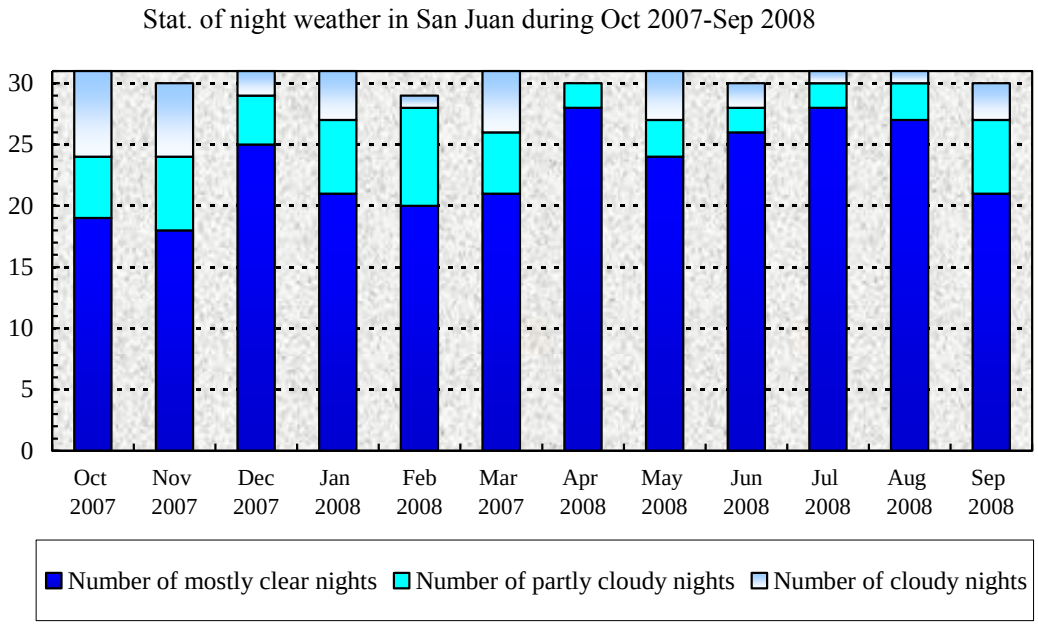

System calibration

When usually ranging to Lageos, the received energy is vary from single photon up to multi photons (about 10 photons, the levels obtainable from LAGEOS with San Juan SLR parameters), so that the received energy for ranging to the calibration target should be correspond to Lageos. We can refer to the Fig.1 (curves of C-SPAD characteristic both compensated and uncompensated), use the C-SPAD characteristic of time walk uncompensated output (relative to single-photon-level) that vary evidently with the increase of received photons. First, measure the time intervals (T1, RMS values, mean value of several times measurements) of calibration target of uncompensated output by single photon (Semi Train＜20% return quote), and then select a suitable reference value (e.g. time walk uncompensated is -25ps), adjust the received energy at SPAD by adjusting the filter or controlling laser energy, measure the time intervals (T2) of uncompensated output, and calculate the D-value of T1 and T2. Now we can know which the received energy is right or not, simultaneously measure the time intervals of the compensated output (single to multi photon), and compare the time intervals whether it meets the requirement. In this way we can know definitely the received energy for ranging to target. We think of selecting suitable photon number range for ranging to the calibration target that decrease the times of ranging to the target, reduce the error by the jitter, and improve the single-shot accuracy of calibration target.

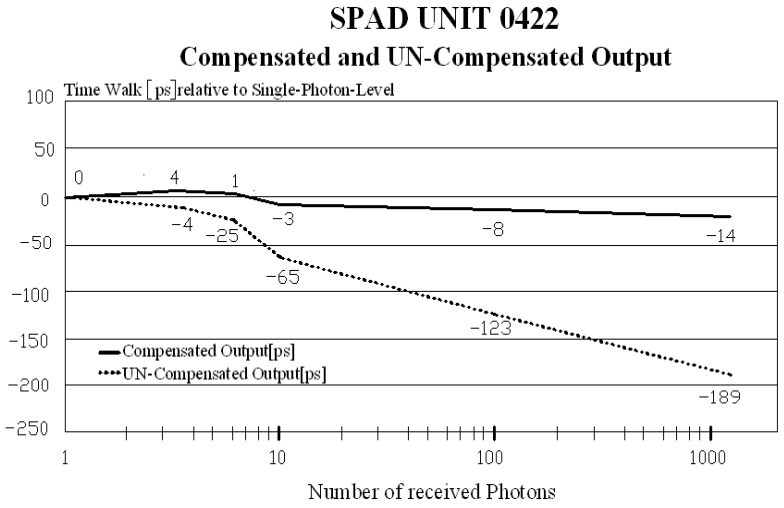

Figure 1. Mean values for each measurement of both curves

A Future Plan

The NAOC and OAFA will continue the cooperation in the San Juan SLR system. At the same time we will also enhance the related research. Our SLR team has established an upgrade plan on the SLR system. The first step will to change the laser system to a semiconductor pumped laser and thus bring the system to high repetition rate and daylight ranging capabilities. We hope that the SLR system can implement routine daylight tracking and high repetition rate operating, also improve the precision of observations in order to obtain more high-quality data for the ILRS. According to the suggestion of ILRS, we will soon install a GPS receiver collocated with the SLR system.

References

[1] Han Yanben et al., Successful operation of a cooperative SLR station of China and Argentina in San Juan, Chinese Science Bulletin, 53(16):2417-2420, 2008.

[2] Zhao You, Han Xingwei, Fan Cunbo, Dai Tongyu. Fulfillment of SLR daylight tracking of Changchun station[C]. Proc. of 15th Int.Workshop on Laser Ranging. Canberra, 10/2006; http://cddis.gsfc.nasa.gov/lw15/index.html.

[3] G. Kirchner, F. Koid. Graz KHz SLR System: Design, Experiences and Results[C]. Proc. of 14th Int.Workshop on Laser Ranging, San Fernando, Spain, 06/2004; http://cddis.gsfc.nasa.gov/lw14/index.html.

[4] Yu. Artyukh, E. Boole, V. Vedin.Instrumentation for Creating KHz SLR Timing Systems[C]. Proc. of 15th Int.Workshop on Laser Ranging. Canberra, 10/2006; http://cddis.gsfc.nasa.gov/lw15/index.html.

Contact

Liu Weidong Fax: 86-10-64860253
National Astronomical Observatories E-mail: wdliu@bao.ac.cn
Chinese Academy of Sciences, 20A Datun Road Chaoyang District, Beijing 100012, China

Field maintenance of the SLR telescope at TIGO

B.Sierk (1)**, S.Riepl** (1)**, C.Guaitiao** (2)**, M.Avendaño** (2)**, V.Mora** (2)**, A.Fernandez** (2)**, Roberto Castillo** (3)

(1) Federal Agency of Cartography and Geodesy, Germany
(2) Universidad de Concepción, Chile
(3) Paranal Observatory, European Southern Observatory (ESO)

bernd.sierk@bkg.bund.de /Fax: +56-41-2207031

Abstract

We report a major maintenance service of the laser telescope at the Transportable Integrated Geodetic Observatory (TIGO), in Concepción, Chile, which has been carried out under field conditions in August and September 2008. The purpose of this work was to improve the transmission properties of the 50 cm refracting telescope, whose optical path is folded by four Coudé prisms. The coatings of these critical components had degraded over several years of continuous operation. The implementation of the repair service, carried out on site in absence of service infrastructure and buildings, involved the replacement of these prisms and their mounts within the hermetically sealed optical Coudé train. Quasi clean-room conditions were established by constructing two tents around the site with air conditioning and filtering devices. The entire telescope structure had to be lifted to access and replace the critical components, requiring a complete re-alignment and survey of the instrument. This paper documents the practical implementation of the on-site maintenance, which significantly improved the transmission properties and overall performance of the SLR system.

Introduction

In March 2006, the TIGO SLR unit was upgraded by a passively (SESAM) mode-locked oscillator and diode pumped amplifiers. Since then, the modernized system operating at 100 Hz repetition rate has proved to operate significantly more stable than its forerunner. This enabled a strong increase of TIGO's SLR data productivity at its fundamental wavelength 847 nm. However, the two-color ranging capability of CONL, currently the only operative Ti:Saph system of the ILRS network, has continuously declined. Fig. 1 shows the number of observations per normal point at the second harmonic (423.5 nm) obtained in 2002 and 2003. The plot shows that return rates at the blue wavelength have continuously decreased since the installation of TIGO in Concepción. By the end of 2006 two-color ranging was stopped completely to yield the entire pulse energy to the fundamental (IR) wavelength. But even with this setup, the station's capability to track HEO missions at has been limited to night time.

The likely main reason for the declining transmission properties of the SLR system are damages of optical components along the transmit and detection path, which have deteriorated over six years of continuous operation. The mobile SLR unit of TIGO features a 50 cm refracting Coudé telescope, whose cross section is depicted in Fig. 2. The instrument is protected by a waterproof cart with a removable dome and is supported on the platform by three adjustable feet. The optical path is folded by four AR-coated prisms, indicated in Fig. 2. The outgoing beam from the Ti:Saph laser located inside the operation unit (container) is

coupled into the telescope through a hermetically sealed tunnel (indicated in the lower left part of Fig. 2). Slight overpressure and a constant flow of dry and clean air pumped through the tunnel prevents dust and humidity from entering the optical path. The outgoing beam is reflected into the azimuth axis by prism FP7, folded over 110° by FP4 and FP2 and reflected into the elevation axis by FP1. The beam is subsequently expanded by an adjustable triplet lens, and folded over two large flat mirrors before being recollimated by the front lens.

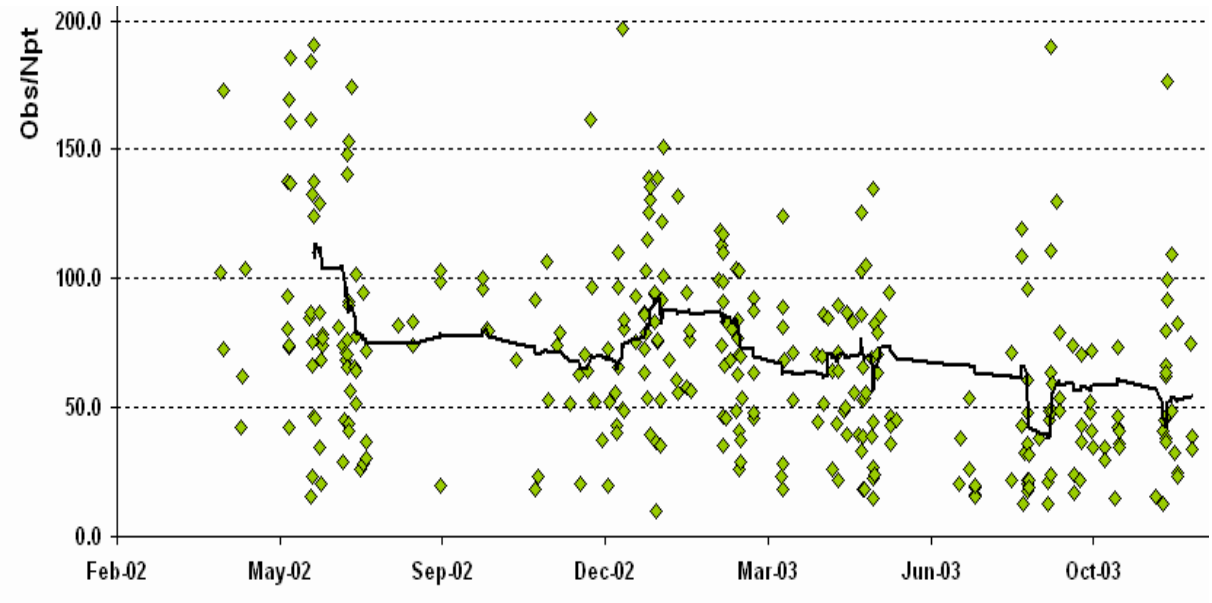

Figure 1. Number of observations per normal point at 423.5 nm during TIGO's first two years of operation. The return rate has fallen by approx. 50 % in less than two years, presumably due to the degradation of optical components.

After inspections confirmed significant damages on all four prisms in the Coudé path, it was decided to replace them in a single maintenance effort. As optical workshops were not available the delicate work had to be carried out under field conditions at the TIGO site, moreover during the rough rain season to minimize the loss of data, while at the same time maintaining a clean and dry environment to protect the optics. This paper briefly documents the implementation of the prism replacement and the re-alignment of the telescope.

Setting up an optical workshop in the field

Due to TIGO‘s design as a transportable geodetic observatory, its laser telescope is located on an open air platform, only protected by a cart structure with a small dome. It is connected to the laser system through a hermetically sealed tunnel. One challenge was to provide dry and clean conditions for installation and adjustment of delicate optical components in absence of a service building. Dust particles entering the Coudé path during several days of maintenance while the beam tunnel was to be opened were likely to remain in the optical path, settle on the new prisms' surfaces and subsequently cause new damages on the AR-coatings.

In order to prevent this, we set up a protective construction around the telescope module consisting of two tents, depicted in Fig. 3: First a large stable pavilion tent was erected, which was provided by a catering company. This external tent provided rain and wind

protection during the intensive rain season in Southern Chile on a 12x12 m area around the telescope. The smaller second tent was built inside the external one and enclosed the telescope cart in a 6x6 m area. Inside this internal tent, we installed an air filtering and conditioning system, hourly pumping 3400 m^3 of clean and dry air (> 99 % filer ting efficiency for 5 µm particle size and < 20% rel. humidity) from the pre-heated external into the internal structure. By injection through a tube system a constant dry air circulation and overpressure inside the internal tent were obtained, pushing dust particles outside the internal tent. With this setup, "quasi clean room conditions" were established, allowing for the replacement of the optical components in the field.

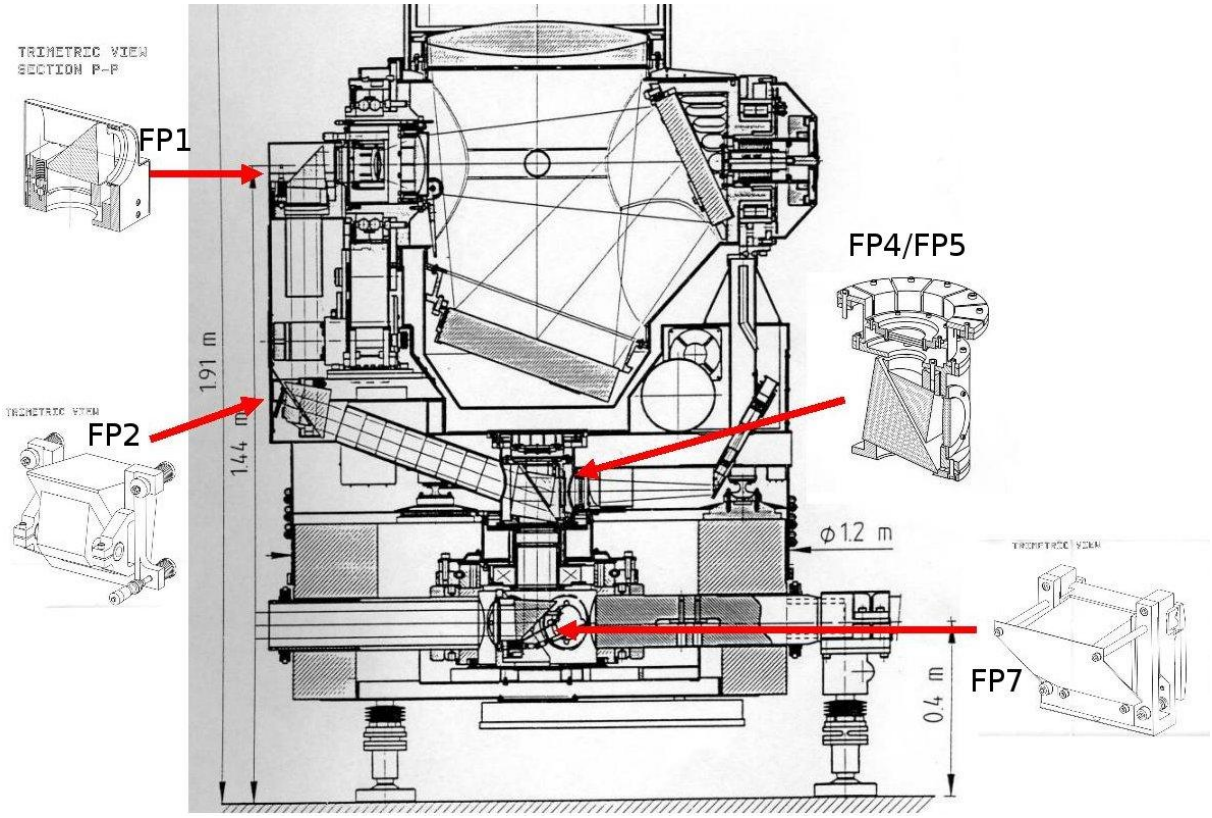

Figure 2. Cross section of the TIGO SLR telescope. The positions of the replaced prisms and their mounts are indicated.

Prism replacement

The moving part of the telescope, which rotates about the azimuth axis, is mounted on three flat air bearings floating on a monolithic granite bench, indicated by the shaded areas in Fig. 2. In order to access the lowest prism FP7 (reflecting the beam into the azimuth axis) the entire mechanical structure including the granite bench, with a total weight of about 2000 kg, had to be lifted by about 40 cm, which was done by a built-in manually operated mechanism. After disassembling various mechanical parts of the telescope FP7 and the other Coudé prisms were removed together with their mounts. The prisms of size 115 x 98 mm are cemented into their individual mounts by a high-performance flexible epoxy (3M Scotch-Weld 2216B/A). At it is difficult to remove the cemented optics from the mounts without damage, we decided to re-build the four complex and individually different mounts. This work, as well as the installation of the new prisms (manufactured by Laser Components,

Munich) was performed at an opto-mechanical workshop in Santiago de Chile, run by European Southern Observatory (ESO) staff. Due to differences in the dimension of the spare parts, slight modifications of the mechanical mounts had to be designed.

Figure 3. Construction of two interleaved tents to provide clean work conditions.

Re-installation and alignment

Three weeks after its disassembly the telescope was lifted again and the new prism mounts were installed. Due to the modifications of mechanical and optical components a complete re-alignment of the telescope optics had to be done. Several new alignment procedures were applied to ensure that the transmitted beam was exactly centered and aligned with respect to both the azimuth and vertical axis. After replacing FP7 a flat mirror was positioned in place of the FP4/FP5 combination and precisely levelled in order to reflect the beam back into the spatial beam splitter (perforated mirror for separation of transmission and reception beam) inside the SLR container. For this adjustment over a distance of about 8 meters through the beam tunnel the second harmonic (423.5 nm) of the attenuated pulsed laser beam was used, and precisely centered in the azimuth axis. Similar techniques, using calibration mirrors and a HeNe auxiliary laser (620 nm) were used for the re-alignment of the parallel axis (between FP2 and FP1) as well as the elevation axis. Some mechanical modifications to the prism mounts allowed for a more accurate adjustment of the parallelism between the transmission, reception and pointing reference (cross-line) axes. For example the surfaces of prisms FP4 and FP5, the latter projecting the reference cross-line into the field of view (see Fig. 2), had to be positioned highly parallel w.r.t. each other. In absence of the required optical alignment tools (goniometer bench) this could be achieved by making FP5 adjustable and using an MCP camera inside the container unit to manually align the cross-hair reference with the transmission beam.

Since the telescope and with it the system invariant point had been moved several times as the cart structure was lifted and re-installed during the maintenance process, the eccentricity w.r.t. the reference point had to be redetermined. Table 1 shows the results of the post-maintenance survey as well as the previous coordinates relative to SRP.

Figure 4. Access to the prisms required working underneath the mechanical structure supporting the telescope. Great care was taken to prevent dust from entering the open Coudé path.

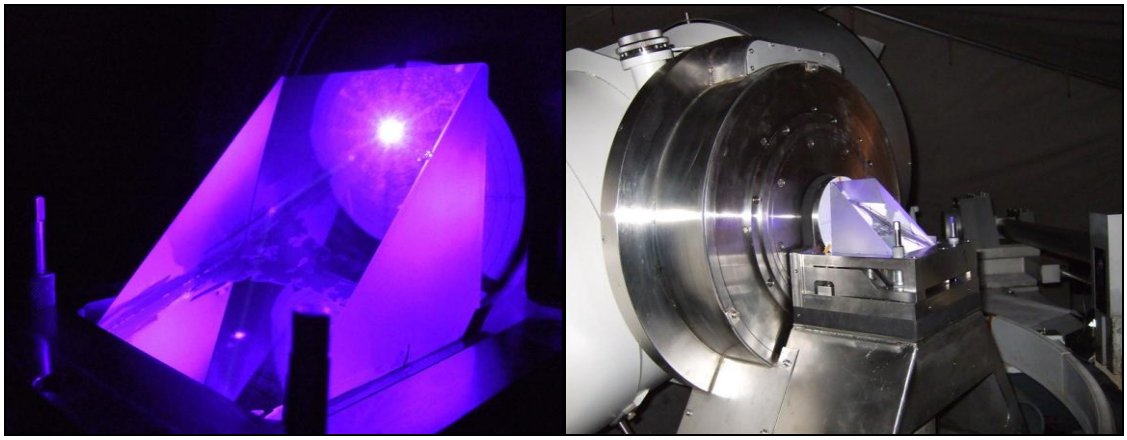

Figure 5. The blue (423.5 nm) second harmonic of the transmitted beam was used to re-align the optics, utilizing various improvised alignment tools.

Table 1. Changes of eccentricity vector from system invariant point to SRP

Component	Old ecc. Values [m]	New ecc. Values [m]
	valid UNTIL 08-10-2008	valid SINCE 08-10-2008
North	0.1956±0.0007	0.1996±0.0007
East	0.0008±0.0007	0.0085±0.0007
Up	1.4667±0.0006	1.4627±0.0006

Summary

We have carried out an optical maintenance service under field conditions for a complex mobile telescope system. Quasi clean room conditions were established around the telescope at the SLR site and the critical optical components folding the Coudé path were removed. The new prisms were cemented into improved mounts and a complete re-alignment was performed using dedicated alignment strategies. As a result of the prism replacement TIGO-SLR (CONL) is now fully capable of daylight tracking GNSS satellites (GPS, GIOVE, GLONASS and COMPASS), which had been difficult before. The improved tracking

performance is also reflected in the station´s GNSS observation statistics, as can be seen in Fig. 6. The chart shows that TIGO's tracking performance for high targets has more than tripled since the successful telescope maintenance. After upgrading its detector system it is expected that CONL will resume two-color operation in April 2009.

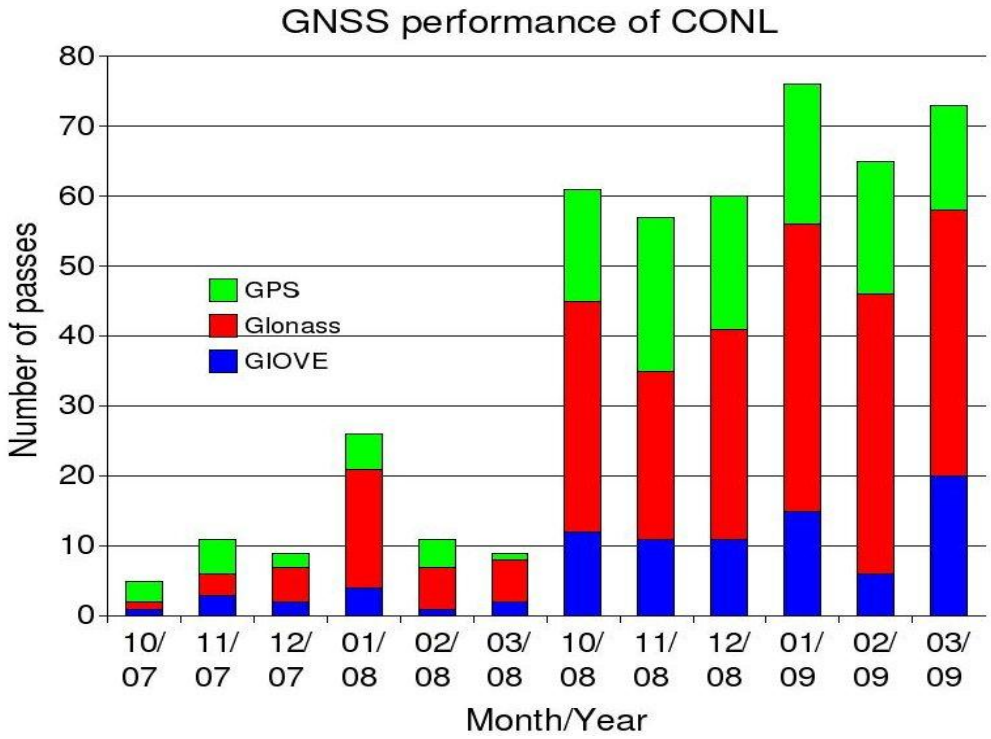

Figure 6. GNSS observation statistics for CONL: 6 month of data after the maintenance are plotted (Sept. 2008-March 2009) along with the corresponding period of the previous year. The strong increase of HEO passes per month is a result of the improved system transmission after the telescope upgrade.

State of the SLR in Russia

V.B. Burmistrov (1)**, V.D. Glotov** (2)**, N.N. Parkhomenko** (1)**, M.A. Sadovnikov** (1)**, V.D. Shargorodsky** (1)**, V.P. Vasiliev** (1)

(1) Science-Research Institute for Precision Instrument Engineering (IPIE), Moscow
natalia.n@g23.relcom.ru / Fax: +7(495)2349859

(2) Information-Analytical Centre (IAC), Korolev (Moscow region), Russia
vladimir.glotov@mcc.rsa.ru / Fax: +7(495) 5135075

Abstract

After lifting of some formal restrictions, the Russian SLR stations are now able to resume observation data delivery to the ILRS.
Examples are presented of LAGEOS observation data obtained at the upgraded Altay SLR station, as well as parameters and outlook of the station and its basic subsystems.

During a long period, the Russian SLR stations were unable to deliver measurement data to the ILRS. Currently, in accordance with a recent decision of the State Administration, it is permitted to deliver measurement data from two Russian stations (Altay and Baikonur) to the ILRS, as well as to resume data delivery from the Komsomolsk station.

The Altay SLR station has been recently upgraded: a new laser has been installed with a pulse repetition rate of 300 Hz (instead of 5 Hz), and a higher average output power (0.75 W instead of 0.25 W).

The basic functions of the Data Collection and Analysis Center are:

- Provision of ephemeris data for the SLR stations
- Collection and storage of measurement data from all stations
- Monitoring of measurement data accuracy, completeness, and correctness of data delivery
- Calculation of normal point data and their delivery to the ILRS Data Centers (during the first phase of operation)
- «Feedback» to SLR stations and ILRS concerning measurement data quality and completeness

In Tables 1 and 2, correction data for the Altay and Komsomolsk SLR station coordinates are presented.

Table 1. Correction of Altay Station Coordinates

Date	UTC	Dur	Inc	%	Ele	ME	RMS	ORMS	SCNAME
02:01:08	14:51	11	7	100	32:39	0.069	0.009	0.070	Lageos-1
05:01:08	14:17	7	5	100	39:45	0.045	0.011	0.046	Lageos-1
05:03:08	22:21	7	5	100	33:43	0.018	0.010	0.021	Lageos-1
13:03:08	22:01	9	6	100	31:43	0.015	0.004	0.015	Lageos-1
26:03:08	21:47	13	8	100	44:54	0.009	0.011	0.014	Lageos-1
19:04:08	20:46	8	5	100	52:54	0.019	0.015	0.024	Lageos-1
14:07:08	19:51	18	10	100	47:75	0.013	0.005	0.014	Lageos-1
24:07:08	16:49	9	6	100	50:56	-0.035	0.008	0.036	Lageos-1
13:08:08	21:21	13	7	88	30:51	0.012	0.008	0.014	Lageos-1
18:08:08	17:59	23	11	100	31:78	-0.007	0.012	0.014	Lageos-1
28:08:08	22:03	11	7	100	29:49	-0.022	0.006	0.023	Lageos-1
13:09:08	21:15	17	10	100	32:53	-0.023	0.008	0.025	Lageos-1
09:10:08	13:47	37	7	100	30:39	0.020	0.015	0.025	Lageos-1
28:01:08	00:07	5	4	100	51:55	-0.023	0.008	0.024	Lageos-2
16:02:08	22:13	9	6	100	40:57	0.031	0.010	0.033	Lageos-2
01:03:08	20:01	3	3	100	48:48	0.013	0.012	0.017	Lageos-2
08:03:08	18:45	14	8	100	38:42	0.005	0.012	0.013	Lageos-2
13:03:08	17:23	7	5	100	30:31	-0.016	0.006	0.017	Lageos-2
13:03:08	21:15	9	6	100	68:80	0.006	0.005	0.008	Lageos-2
13:04:08	18:54	8	5	100	55:78	0.013	0.008	0.015	Lageos-2
21:04:08	15:43	15	9	100	42:64	0.009	0.010	0.013	Lageos-2
24:04:08	17:45	17	10	100	36:80	0.017	0.009	0.020	Lageos-2
09:10:08	22:35	45	6	100	30:38	0.002	0.032	0.032	Lageos-2

Coordinates: X=543.406156; Y=3955.302241; Z=4957.821063

Table 2. Correction of Komsomolsk Station Coordinates

Date	UTC	Dur	Inc	%	Ele	ME	RMS	ORMS	SCNAME
02:01:08	11:03	16	9	90	31:40	-0.002	0.016	0.016	Lageos-1
11:01:08	09:23	6	5	100	55:63	0.009	0.012	0.015	Lageos-1
14:01:08	09:13	3	3	100	28:34	-0.035	0.024	0.043	Lageos-1
18:02:08	19:17	7	5	100	31:40	-0.002	0.008	0.008	Lageos-1
22:08:08	15:47	20	10	91	41:62	-0.001	0.017	0.017	Lageos-1
01:10:08	17:45	5	3	75	41:47	0.042	0.024	0.049	Lageos-1
03:02:08	19:11	11	4	67	44:49	0.024	0.014	0.028	Lageos-2
05:02:08	19:16	3	3	100	37:43	-0.015	0.039	0.042	Lageos-2
17:02:08	20:33	10	7	100	39:66	-0.014	0.011	0.018	Lageos-2
20:02:08	18:53	22	12	100	37:71	-0.015	0.011	0.019	Lageos-2
22:02:08	19:14	20	7	64	56:76	-0.016	0.016	0.023	Lageos-2
23:02:08	17:35	9	5	83	40:53	0.005	0.005	0.007	Lageos-2
25:02:08	17:39	14	9	100	50:60	-0.008	0.011	0.014	Lageos-2
27:02:08	17:59	11	7	100	47:65	-0.027	0.013	0.030	Lageos-2
06:03:08	18:41	9	6	100	56:81	0.010	0.006	0.012	Lageos-2
10:03:08	18:59	11	7	100	33:59	0.012	0.012	0.017	Lageos-2
05:04:08	14:03	17	9	90	58:70	-0.006	0.014	0.016	Lageos-2
15:04:08	11:19	11	7	100	41:46	-0.045	0.056	0.072	Lageos-2
01:10:08	18:03	26	11	85	38:63	0.050	0.016	0.052	Lageos-2

Coordinates: X=-2948.545480; Y=2774.313007; Z=4912.302412

Figure 1 shows an example of normal point data deviation from the smoothed LAGEOS-2 orbit obtained by the Altay SLR station.

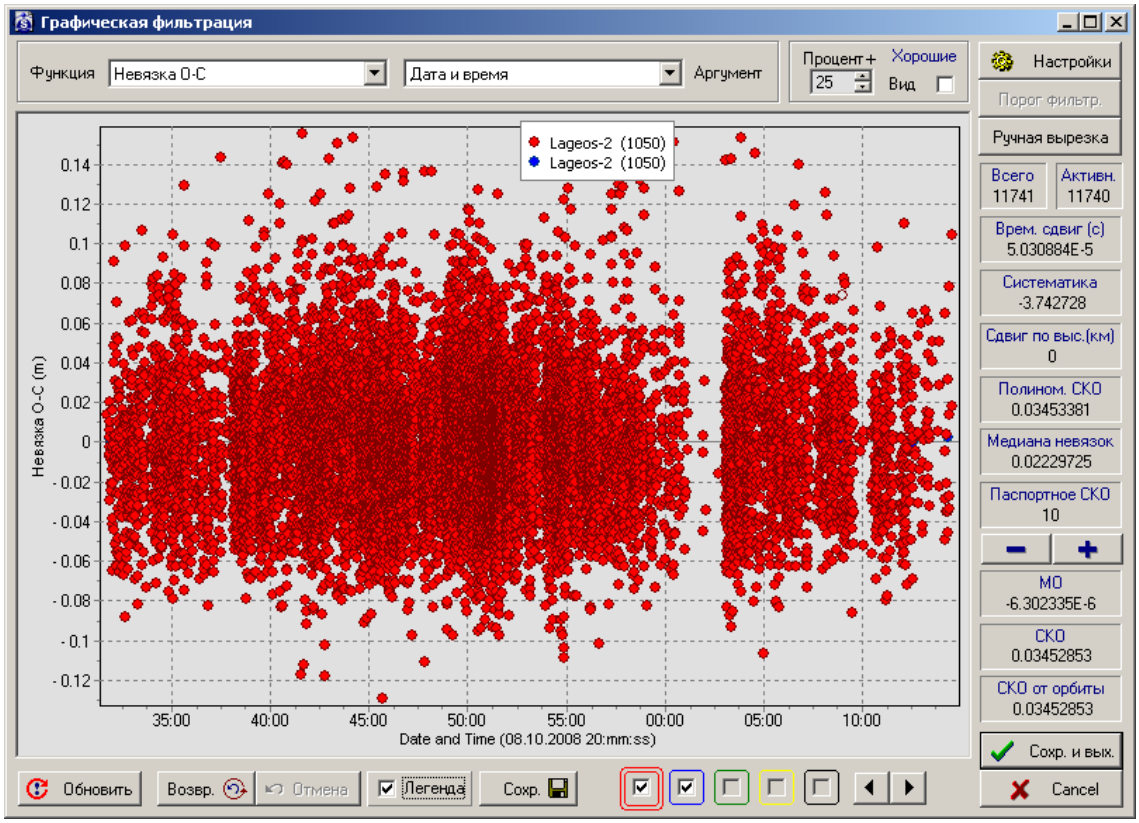

Figure 1. Normal point data deviations from the smoothed orbit (Altay SLR station, LAGEOS-2, 08.10.2008)

The overall view of the Altay station is presented in Figure 2, while Figure 3 shows the station telescope, and in the accompanying table the basic parameters of the station are shown for SLR, angle measurements, and photometry.

Figure 2. Current view of the Altay SLR station

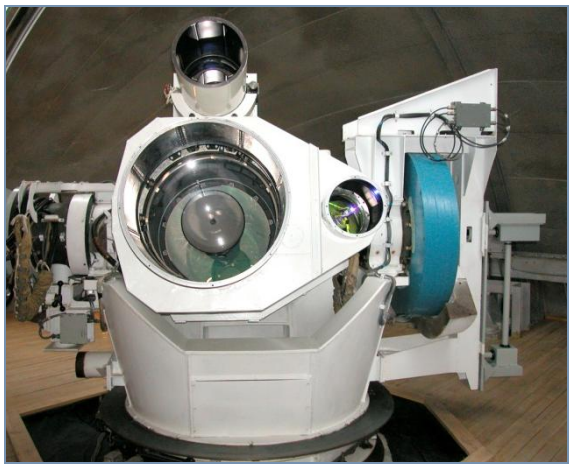

BASIC PARAMETERS

- Receive aperture 60 cm
- Transmit aperture 20cm
- Tracking camera: ICCD, FOV 10'x12'
- Laser 2,5 mJ 150 ps 300 Hz
- Photometry: up to 15^m
- Angle measurements ±2″

Figure 3. Altay station telescope

On top of the main telescope, as seen in Figure 3, another instrument is based: a wide-FOV telescope WFT-35 (35 cm in diameter) used for sky observation, primarily in the GEO belt. In Figure 4, its outlook is presented together with a table of basic parameters and an example of sky fragment view, while the three bright points in the lower right corner are three GEO spacecraft.

BASIC PARAMETERS

- Aperture – 0,35 m
- CCD format: 4096x4096
- Angular FOV: 6.25 sq.deg
- Exposition time: up to 2.5 sec
- Minimum brightness for HEO SC: 16^m
- SC position measurement accuracy: ≤ 0.4 arcsec
- GEO area scanning rate 600 sq. deg/h

Purpose:

GEO SC search and angle measurement

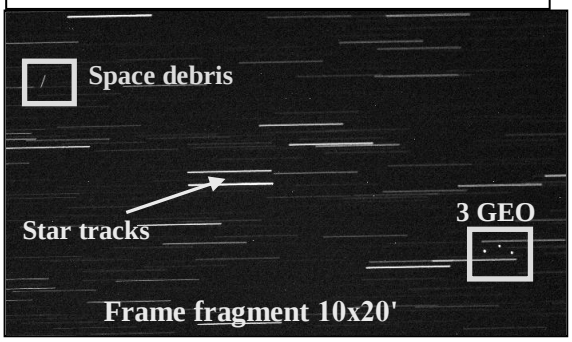

Figure 4. Wide field telescope

The Altay station main telescope is provided with an adaptive optical system used to improve the resolution of distant object images. As an example, four images of the International Space Station (ISS) are shown in Figure 5.

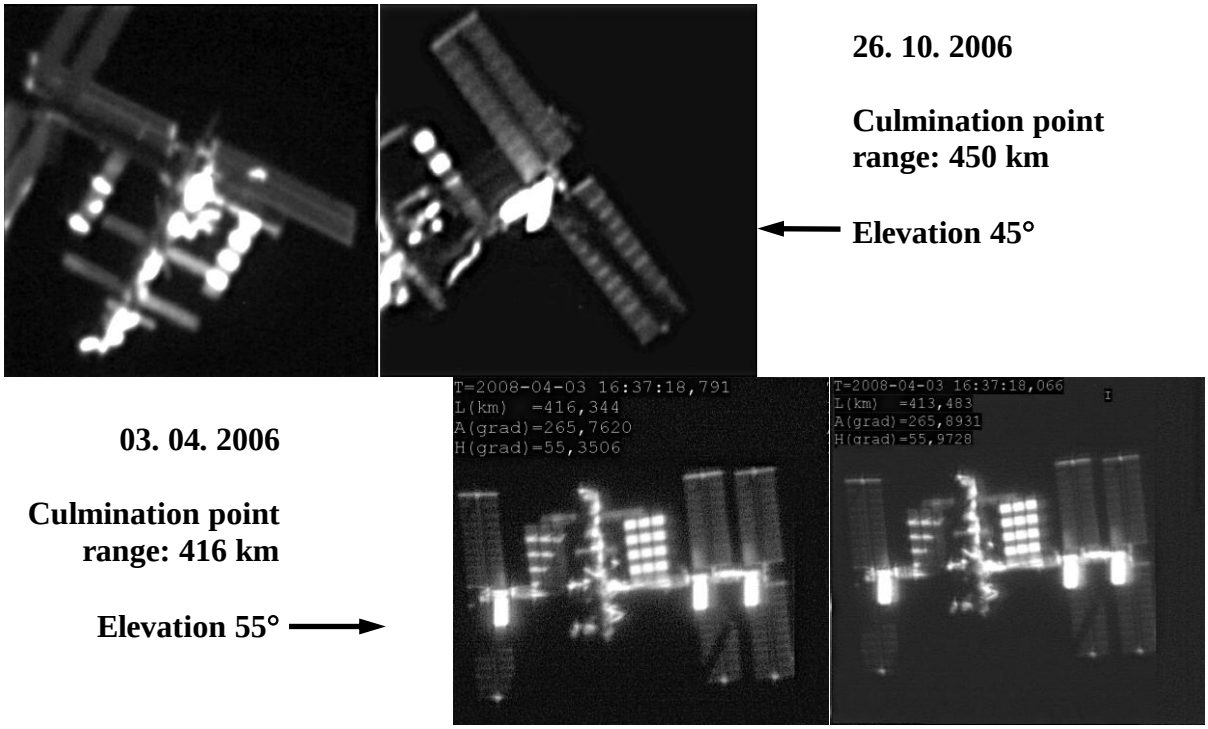

Figure 5. ISS images (with the adaptive optic system activated)

The Baikonur and Komsomolsk SLR station parameters and basic features have been described in earlier presentations (Workshop 14 and 15 accordingly).
In Figure 6, a map is presented with positions of current and future SLR stations which are and will be provided by the Institute for Precision Instrument Engineering (IPIE) for the Russian Academy of Sciences (RAS) and other services during the next few years.

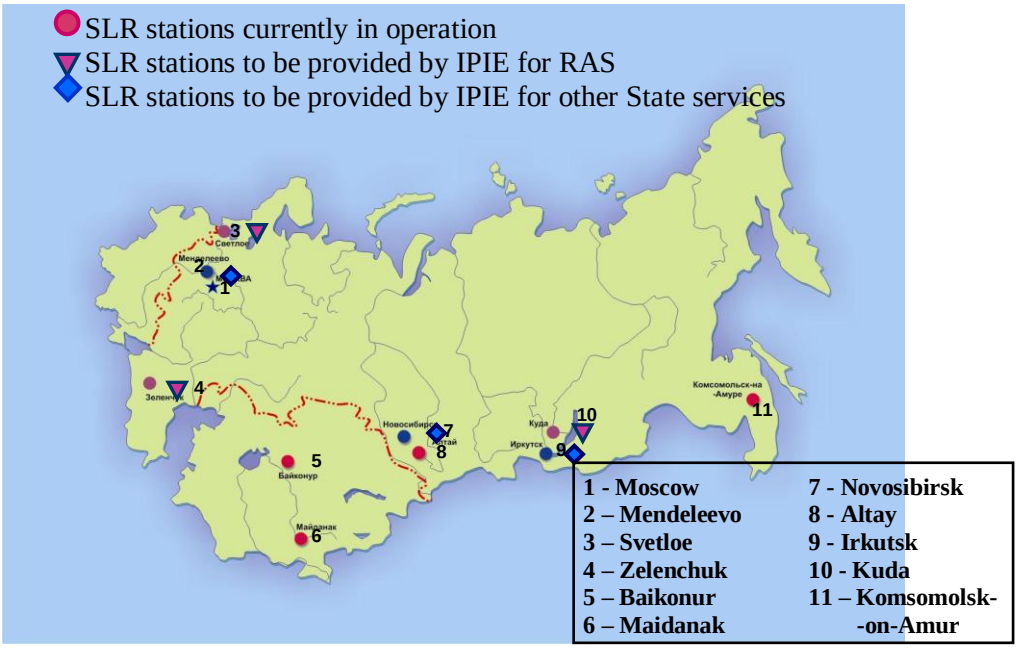

Figure 6. Russian SLR network

Operational Issues and New Missions

Chairs: Mike Pearlman and Ben Greene

Session Summary

The session started off with a short overview of ESA's Earth Observation Program -The Living Planet. An array of current and planned missions extending out through the next decade support applications including: gravity field and ocean circulation, polar ice monitoring, soil moisture, global wind profiles, Earth magnetic field, and clouds and aerosols. Aside from a three year extension of ERS-2 and Envisat, the program includes several new Earth Explorer Missions: GOCE (2009), Cryosat-2 (2009), SMOS, ADM/Aeolus, Swarm (2011), and GAMES to initiate long term monitoring services. Satellites such as PROBA-2 (2009), are also planned for launch to support related technology development. Several of these missions including GOCE, SWARM, Cryosat-2, and PROBA-2 will require SLR tracking. The Galileo complex will also be populated over the next 5 years.

Two missions from JAXA are being prepared. SOHLA-1, a demonstration of small, low cost technical payloads, will be launched in early 2009. The spacecraft will be spinning, which will limit access to the retroreflector array to only a few seconds in every few minute revolution period. Astro-G, a space-borne VLBI antenna, is planned for launch by JAXA in 2012. It will be in a highly elliptical orbit and will have an antenna with a bi-modal, switching configuration, which will limit normal points to very short intervals and require some special data handling procedures.

The Precision Expandable Radar Calibration Satellite (PERCS), being proposed by NRL for calibrating radars and studying drag and electromagnetic conditions in orbit, will carry over 1000 retroreflectors distributed inside and outside of a spherical deployable frame.

Consideration for an optical link for the ACES Mission was presented along with concepts for resolving the range biases in one-way ranging experiments and a novel application of SPADs using no optics. An IR camera and aircraft radio detection beacon using a patched antenna array was also presented, offering promise of new aircraft detection safety systems for laser ranging.

The status of the implementation of the SLR Consolidated Laser Ranging Data Format was reviewed; full implementation is scheduled for early 2010. MOBLAS-8 returned to operation and is doing well.

Posters included some historical SLR information, a status on recent updates to the ILRS website, and the upcoming ANDE mission scheduled for launch in May 2009.

An overview of ESA's upcoming missions equipped with SLR

M. Otten, T.A. Springer, Daniel Navarro-Reyes, Pierre Femenias, Pierrik Vuilleumier, Rune Floberhagen, Mark Drinkwater, Roger Haagmans, Berthyl Duesmann, J. Dow
ESA/ESOC, Germany
michiel.otten@esa.int

Abstract

In this presentation we will give an overview of ESA's upcoming missions equipped with Satellite Laser Ranging reflectors. This overview will include the ESA Earth Observation missions: GOCE (2008), Proba-2 (2009), CryoSat-2 (2009), Swarm (2010), Sentenil-3A (2012), Proba-V (2012) and Sentenil-3B (2014). Besides these Earth Observation missions ESA's Galileo spacecrafts will be equipped with a satellite laser reflector. We will also give a short status on the future of Envisat and ERS-2.
In each of the overviews we will specifically focus on the mission characteristics that are important to the Satellite Laser Ranging community.

Applications of the Precision Expandable Radar Calibration Target (PERCS) to Laser Imaging and Tracking Systems

Paul A. Bernhardt, Plasma Physics Division
Andy Nicholas
Space Science Division

Linda Thomas, Mark Davis, Ray Burris
NCST
Naval Research Laboratory
Washington, DC 20375
bern@ppd.nrl.navy.mil

Chuck Hoberman, Matt Davis
Hoberman Associates, Inc.
New York, NY 10013

Abstract

A large (10 m) diameter sphere, with conducting edges composed of open-faced polygons, is being planed for launch in low earth orbit. The primary purpose of the Precision Expandable Radar Calibration Target (PERCS) is calibration of high frequency (3 to 30 MHz) backscatter radars used for geophysical studies of the upper atmosphere. The PERCS sphere with 180 vertices and 360 edges provides about 200 square-meters radar cross section at HF frequencies [Bernhardt et al., 2008]. Measurements of radar backscatter from a sphere with known radar cross section will calibrate ground-based HF radars to permit absolute measurements of the strength of meteor trail echoes and scatter from auroral disturbances in the ionosphere. The addition of corner cube retro-reflectors at the 180 vertices enhances the use of PERCS by permitting (1) high accuracy measurements of the target position, (2) determination of its orientation, and (3) estimation of the PERCS rotation rate. With these measurements using laser backscatter from the retro-reflectors permits studies of the electrodynamic drag of the conducting wire-frame sphere moving in low-earth-orbit (LEO) across magnetic field lines. Currents induced in the conducting struts of PERCS will interact with Earth's geomagnetic field yielding forces that affect both the orbit and the rotation of the sphere. A mechanical model for deployment of the 10 meter diameter sphere from a 1-meter stowed configuration has been developed at NRL and Hoberman Associates. The model also includes corner reflectors at vertices of polyhedral wire frame with design considerations of the diffraction pattern of the reflected laser signals as well as the effects of the velocity aberration from the orbiting sphere. Some vertices will be vacant of reflectors at selected wavelengths so that the unique orientation of the PERCS can be determined from ground laser observations. The PERCS sphere is being considered for launch in the 2011 to 2012 time period.

Introduction

The Naval Research Laboratory in conjunction with Hoberman Associates of New York has developed a new concept for deployment of large satellites in space. The Precision Expandable Radar Calibration Sphere (PERCS) was first designed to provide an HF radar

calibration target using spherical wire frame. The primary purpose of the PERCS sphere in orbit is to calibrate the antenna patterns and system sensitivity for space weather radars. For this objective, extensive numerical simulation of radar cross section (RCS) in the 3 to 30 MHz frequency band was performed a reported in a paper by Bernhardt et al. [2008]. Future activities for PERCS will be to construct (1) a scale mode for RCS testing, (2) a mechanical section for structural testing and (3) the spaceflight version for launch into orbit. The final PERCS satellite will 10.2 meters in diameter with an orbit altitude of 600 to 800 km in a high inclination (> 80 degrees) orbit.

Once the large wire frame structure was conceived, it became immediately obvious that corner-cube retroreflectors could be added to the structure to provide calibration for laser satellite tracking. Currently the PERCS satellite has 180 vertices and each vertex will have a holder for 3 retro-reflectors both on the inside and outside of the satellite frame. These corner cube reflectors can provide precision data on both the position and orientation of the orbiting sphere.

The next step in the PERCS concept was that the retro-reflectors could provide precise measurements of the electrodynamic drag of the satellite. As the conducting wire frame passes though the ionosphere crossing magnetic field lines, currents will be induced in the edges. The Lorentz (J cross B) force from the satellite motion will affect the satellite position and rotation rate. The optical tracking of the satellite orientation and position is essential to determine the effects of these forces. The orbit of the satellite will also be determined by the solar illumination. In darkness, the wire frame sphere will polarize to about 2 Volts across the 10-meter diameter structure. In sunlight, electrons will be removed from the conducting edges so that the satellite will charge positive. The deflection forces of this charged object crossing magnetic field lines will perturb the orbit. The least important force for the PERCS satellite could be the collisional drag. The 10-meter diameter sphere will have a drag cross section of less than 2 square meters because of its wire frame structure. Each edge on the sphere is less than 2 cm in diameter.

Status on the PERCS Design.

For the PERCS project, Hoberman Designs the creator and manufacturer of the famous Hoberman Sphere has been contracted to design the expandable satellite. Figure 1 illustrates the current design for the PERCS sphere. The stowed configure for the sphere starts out at 1.25 meters diameter. Torsion springs in each of the three scissors that comprise an edge cause the sphere to open with a distributed force.

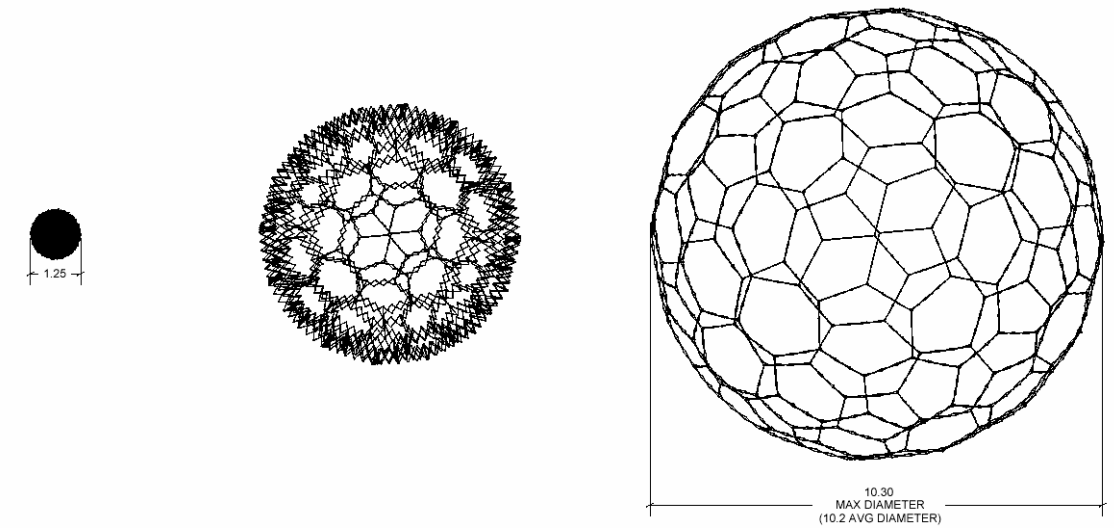

Figure 1. Expandable structure for the PERCS satellite with 180 vertices.

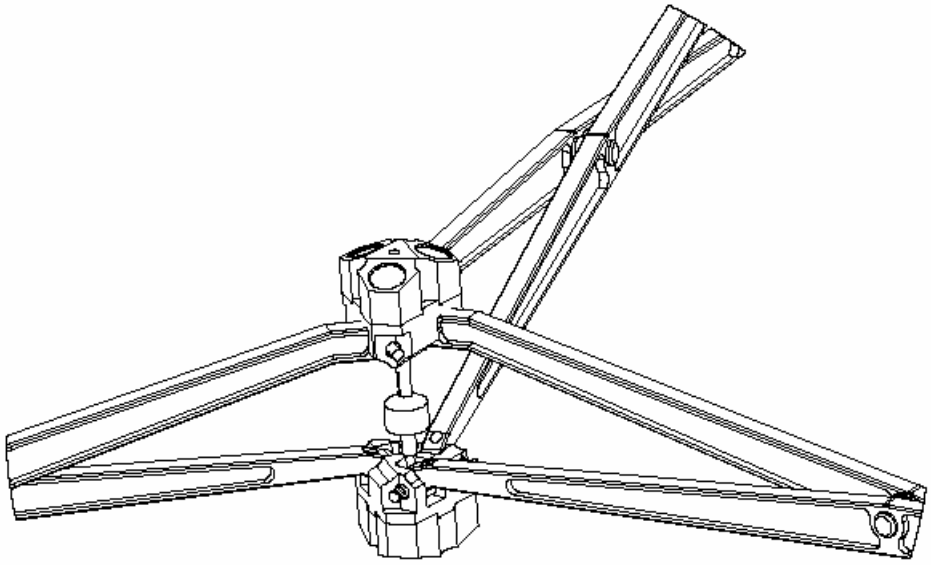

Figure 2. Retro-reflector holders for 1-cm corner-cubes on each PERCS vertex.

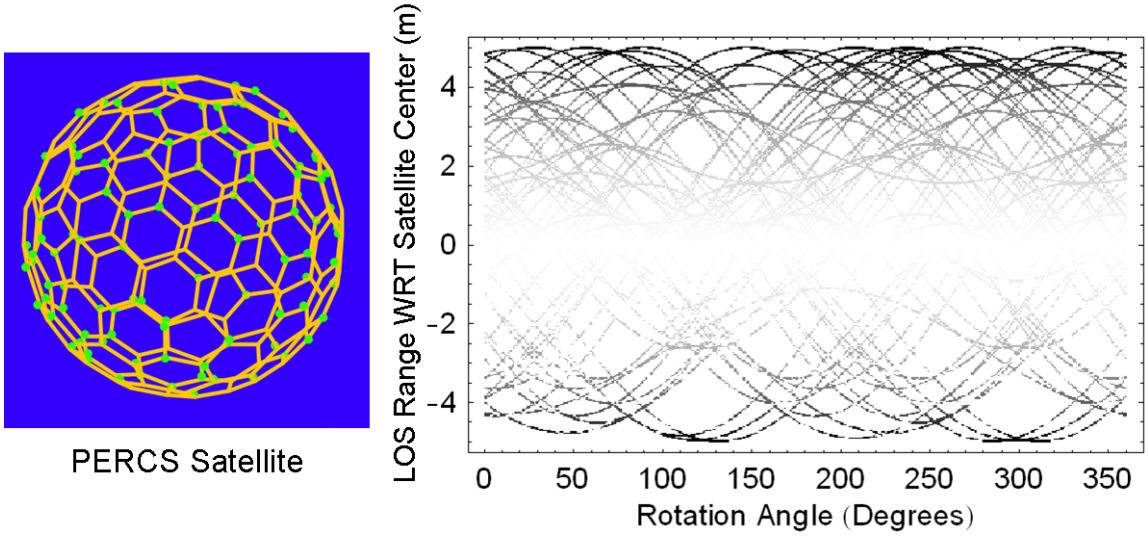

Figure 3. Coding of the PERCS retro-reflector locations to yield the orientation of the sphere in sphere. The line-of-sight (LOS) returns for a ground laser pulse provide unique time sequence depending on which side of the sphere is facing the viewer.

Each vertex of the deployed sphere has retro-reflector holders that are illustrated in Figure 2. The PERCS structure opens up into a locked configuration that has a precise distance between each vertex as well as a precise distance across a sphere diameter. The retro-reflector holders are populated with a fixed pattern that does not fill every position on a vertex. This allows measurement of the orientation of the sphere with a coded laser pulse response. Figure 3 shows a simulated pulse return from PERCS using a fixed coding of the retro-reflector locations. The sphere reflects laser pulses from both the inside and outside of the sphere. The line-of-sight (LOS) pulse return plot uses the zero as the reference distance at the center of the satellite in Figure 6, left frame. The strongest echoes are either from the front closest to the observer (negative distance offset) or from the inside back of the satellite at the farthest (positive distance) from the observer.

The PERCS satellite is currently in the design phase and funding has been allocated for construction of one pentagon section (Figure 4). It is hoped that that the fully constructed satellite is finished by 2011 and that PERCS will be in orbit by 2012. Investigators interested in joining the PERCS science team could contact the authors at the e-mail address given above.

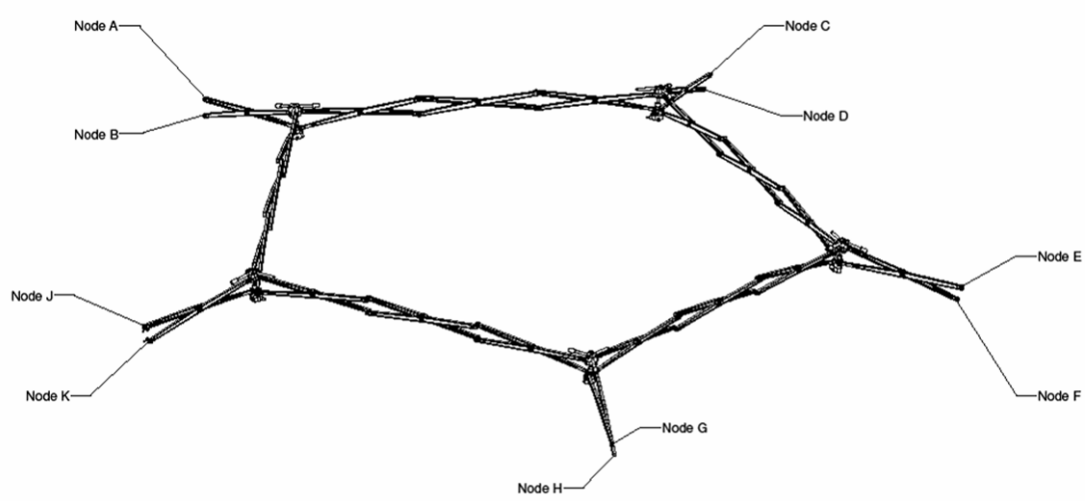

Figure 4. Pentagon section of the PRERCS satellite under construction by Hoberman Associates.

References

Paul A. Bernhardt, Carl L. Siefring, Joe F. Thomason, Serafin P. Rodriquez, Andrew C. Nicholas, Steven M. Koss, Mike Nurnberger, Chuck Hoberman, Matthew Davis, David L. Hysell, Michael C. Kelley, The Design and Applications of a Versatile HF Radar Calibration Target in Low Earth Orbit, *Radio Science, 43*, RS1010, doi:10.1029/2007RS003692, 2008

SLR Return Analysis for SOHLA-1

Takahiro Inoue, Shinichi Nakamura, Ryo Nakamura, Keisuke Yoshihara (1), **Hiroo Kunimori** (2), **Toshimichi Otsubo** (3)

(1) Japan Aerospace Exploration Agency
(2) National Institute of Information and Communications Technology
(3) Hitotsubashi University

inoue.takahiro@jaxa.jp / Fax: +81-29-868-2990

Abstract

SOHLA-1, which is planned to be launched in 2009, is a 50kg-class spin stabilized satellite. One of the missions of SOHLA-1 is the tech-demo of the low-cost, micro-GPS receiver developed by JAXA(Japan Aerospace Exploration Agency) based on COTS automobile technology. SLR is needed for the calibration of GPS based satellite positioning. The SLR data are intermittently observed because of the satellite's spin. To evaluate the impact of spin on return availability, the patterns of observation data are simulated.

Introduction

SOHLA-1 is a 50kg-class spin stabilized satellite based on JAXA's Micro-LabSat which was launched in 2002 by a Japanese H-IIA launch vehicle as a piggyback payload[Kato05]. Table.1 lists the main characteristics of SOHLA-1. The mission of SOHLA-1 is the engineering demonstration by a 50kg-class micro satellite for validation of technique to identify a location of discharge of thunder on the Earth. The goal also includes a short period of development time and at low cost. A characteristic feature of SOHLA-1 is that some components of the satellite are manufactured by universities and middle and small-sized enterprises joining in an organization called SOHLA(Space Oriented Higashiosaka Leading Association) established to embark on space business. Since SOHLA had no experience to be engaged in the space project, JAXA has given them wide range of technical support covered from design phase to assembly integration and test phase. In JAXA, the project is defined as the first attempt of the technical transfer in the field of small satellite technology to industry.

SOHLA-1 carries newly developed miniature GPS receiver and the Laser Reflector Array(LRA). One of the missions of SOHLA-1 is to evaluate the GPS receiver's performance. Then, SLR data are needed in order to calibrate the GPS receiver's data.

Since SOHLA-1 is a spin-stabilized satellite, and LRA is mounted only one side, SLR data are expected to be obtained intermittently. To evaluate the impact of spin on return availability, the patterns of observation data are simulated.

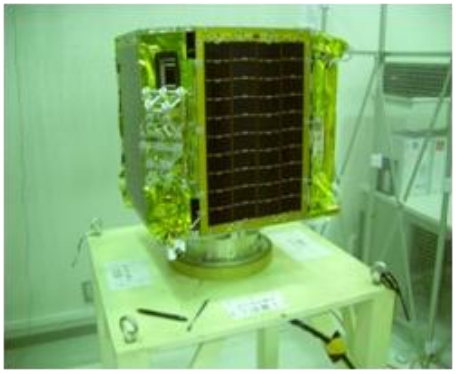

Figure 1. SOHLA-1

Table 1. Main Characteristics of SOHLA-1

Configuration	Shape of octagonal prism dimensioned by 500×500×500mm
Mass	56.9 kg
Attitude	Spin stabilized
Power	30-40W
Mission Duration	1 year
Orbit	Sun-synchronous Altitude:666km Inclination: 98.06deg Cycled period: about 1.6 hours

Condition for SLR

Figures.2~4 show the Laser Reflector Array mounted on SOHLA-1. LR consists of 12 corner cube retro-reflectors(CCR), and the shape of each CCR is the same as that of AJISAI (size of 42mm in each side of rectangular shaped aperture). Its material is BK7, and the viewing angle coverage of the LR is about 60 degree along the spin axis, and is about 30 deg in the direction of perpendicular to spin axis. This LRA is mounted at only one side of the spinning satellite. Therefore, LRA spins along with satellite.

Figure.5 shows the direction of spin axis in equatorial coordinate system. The spin axis lies in the plane containing the solar direction and the normal to the orbital plane. The angle of spin axis and the solar direction is 45 degrees. This indicates that direction of spin axis depends on the solar direction, and spin axis changes slowly in one year cycle.
The spin rate of SOHLA-1 is set nominally 3rpm and is controllable within a range of +/- 1rpm.

From these conditions, we expect that SLR return pulse is intermittently observed. Whether SLR return is available or not depends on spin axis direction, spin rate and relative position with respect to the SLR stations. If return availability is too low to gather SLR data under the specific condition, JAXA should inform SLR colleagues of the information whether each pass can be tracked or not. The return availability is simulated in the following section.

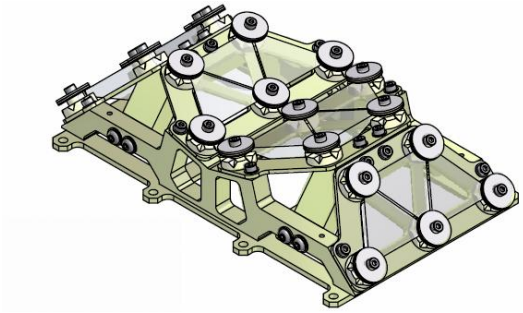

Figure 2. Overview of LRA

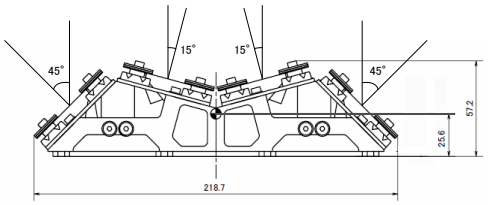

Figure 3. Coverage of LRA

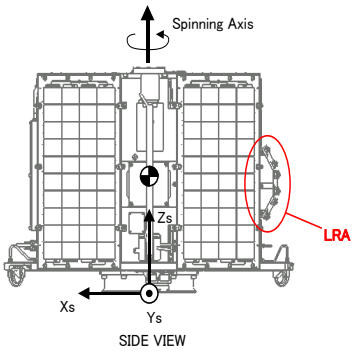

Figure 4. Mounted Position of LRA

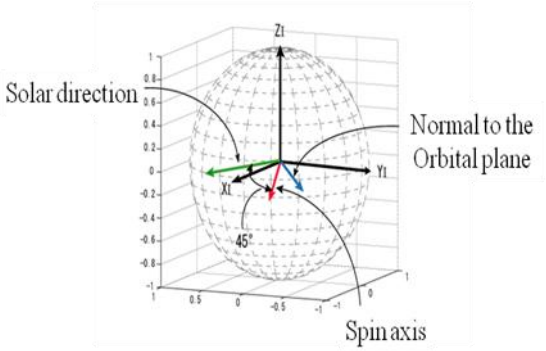

Figure 5. Direction of Spin Axis

Simulations of return availability

At first, we simulate the return intermittency. We study two typical cases return variation like Figure.6 and 7. In Fig.6, SLR station "sees" LR all the time at each spin during the pass, and in Fig7, it does not always because spin axis direction is oriented so that LR is not responding to SLR station during the part of the pass. Each case shows the time series of distance variation between SLR station and LRA on SOHLA-1. The number of zero in vertical axis in the figures means the O-C distance between the SLR station and the CoM of SOHLA-1.

Each case shows that the distance variation changes cyclically because of the spin. Its period of time depends on the spin rate. The thick red points at the bottom of the curve are return available points. So, we can get the return laser pulse only while appropriate incident angle, its period is about 3~4 seconds in every spin, which period is 15~30 seconds. Smaller bin size in comparable to 3-4 seconds for QLNP is desirable. In practical we see that QLNP with 5 seconds bin size can be acceptable.

If we can get the return through the pass like Figure.6, nominal return availability is about 0.15 and the amount of return data will be acceptable to generate the QLNP. However, the amount of return data will not be enough if the pass like Figure.7 is dominant.

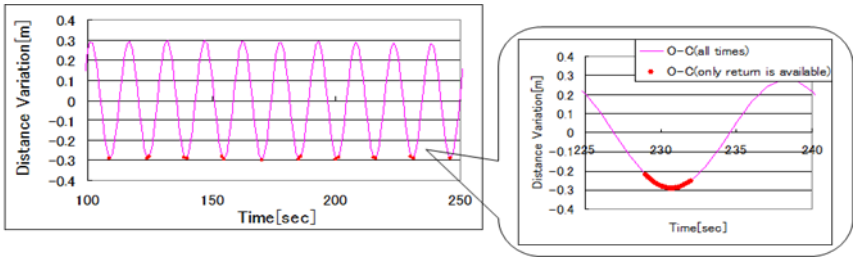

Figure 6. Return Intermittency ~case1~

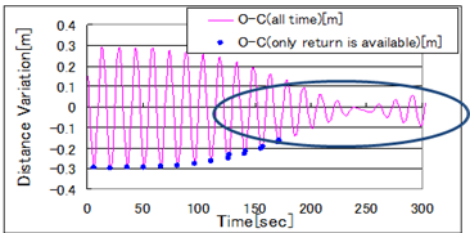

Figure 7. Return Intermittency ~case2~

Then, we have analysed the availability of return data which depends on three major parameters, which are relative position, spin axis direction, and spin rate.

Figures.8~10 show the results of the simulations and Tables.2~4 show the corresponding condition, respectively. In the Figures, the return availability means the proportions of the return available time in one pass. The value of y-axis shows the probability distribution of passes. From the results, there are two peaks in all cases. We can find that strong peak at 10% of return availability is the case that intermittent return is available through the pass like Fig.6. And we also find that weaker peak at between 5~10% of return availability is the case like Figure.7. Therefore, the case of Figure.6 is dominant, and we can get enough return data in all the cases.

Table 2. Condition of Return Analysis ~Dependency on Spin Axis Direction~

Period of time	Num. of passes	Spin rate [rpm]	Station
2009/ 03/15~05/01	~100	3	GMSL
2009/ 07/01~08/01	60~70		
2009/ 11/01~12/01	60~70		

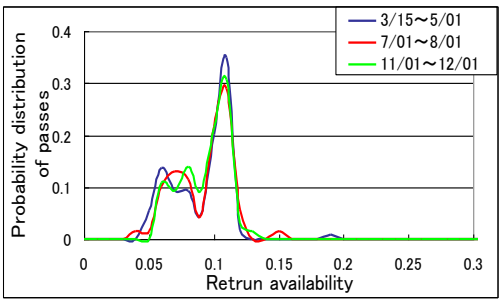

Figure 8. Result of Return Analysis ~Dependency on Spin Axis Direction~

Table 3. Condition of Return Analysis
~Dependency on Spin Rate~

Period of time	Num. of passes	Spin rate [rpm]	Station
2009/ 03/15~05/01	~100	2	GMSL
		3	
		4	

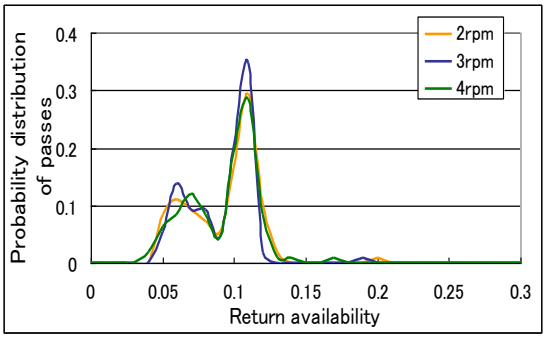

Figure 9. Result of Return Analysis
~Dependency on Spin Rate~

Table 4. Condition of Return Analysis
~Dependency on Relative Position~

Period of time	Num. of passes	Spin rate [rpm]	Station
2009/ 03/15~05/01	~100	3	MLRO
			GMSL
			HA4T
			YARL

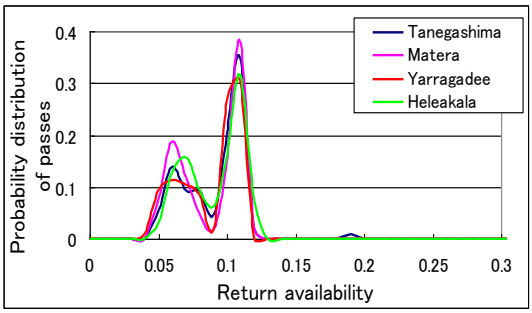

Figure 10. Result of Return Analysis
~Dependency on Relative Position

Summary and future plan

The return availability of SOHLA-1 is simulated. From the simulations, we find that the SLR return is intermittently observed, and its nominal cycle is 20 seconds. In a 20 seconds cycle, the duration of continuous return is less than 5 seconds. Then QLNP with 5 seconds bin size can be practically accepted. We also find that the laser pulse return is not available in case of inappropriate incident angle, but this case is uncommon. So, we can get enough return at all the passes as long as stations know the characteristics of intermittency of returns and adapt to observe it.

SOHLA-1 has been launched successfully in January 23 and ILRS tracking campaign is scheduled on March 9th to 22nd. JAXA is ready to generate prediction and to track SOHLA-1 by JAXA/SLR. We expect to obtain SLR data enough to succeed in SOHLA-1's mission.

Reference

Kato, M. et al., *Road map of small satellite in JAXA*, IAC-05.B5.6.B.01, 2005
Nakamura, Y. et al., *SOHLA-1 – Low Cost Satellite Development with Technology Transfer Program of JAXA*, IAC-05-B5.6.B.08, 2005
Nakamura, R., *SOHLA-1 SLR Tracking Standards*, http://god.tksc.jaxa.jp/, 2007

SLR return analysis for ASTRO-G

Ryo Nakamura (1)**, Takahiro Inoue** (1)**, Shinichi Nakamura** (1)**, Keisuke Yoshihara** (1)**, Hiroshi Takeuchi** (1)**, Hiroo Kunimori** (2) **, Toshimichi Otsubo** (3)

(1) Japan Aerospace Exploration Agency
(2) National Institute of Information and Communications Technology
(3) Hitotsubashi University

nakamura.ryoh@jaxa.jp / Fax: +81-29-868-2990

Abstract

The next-generation space radio telescope, Astro-G, which is planned to be launched in 2012 and injected into a highly elliptical orbit with an apogee height of 25000km and a perigee height of 1000 km, has a requirement of orbit determination accuracy higher than 10cm using GPS and SLR. The SLR role is a precise orbit determination (POD) especially near the apogee. The SLR data are expected to have considerably time variation not only because of a laser retro reflector array (LRRA) on a moving gimbal, but also because of an observation mode called phase referencing observations. The expected returns from Astro-G are simulated and proper bin sizes and editing methods for making QLNPs are studied.

Introduction

ASTRO-G is a next-generation space radio telescope designed to reveal phenomena such as the relativistic phenomena in the space around super-massive black holes at the centers of galaxies [Tsuboi08]. The satellite will be launched by H2A rocket from Tanegashima Space Center in 2012 and injected into an elliptical orbit with an apogee height of 25000km and a perigee height of 1000 km. The observation project is known as VSOP-2, which is extending the successes of VSOP/HALCA project (1997-2005). HALCA demonstrated successfully the technologies required for the space very-long-baseline interferometry (VLBI). In the VSOP-2 project, observation bands will be shifted to higher (up to 43GHz) frequencies compared to the VSOP. The project features direct imaging observation of astronomical phenomena with a level of high-spatial resolution (40 micro arc sec. at its best) never achieved before. In order to successfully conduct a phase referencing observation, one of the observation modes in which the antenna points to a target radio source and a calibration source in a switching manner, a precise orbit determination (POD) is required [Asaki08][Otsubo06]. The accuracy requirement is at least 10 cm. In order to achieve the orbit determination accuracy, the satellite will carry a GPS receiver and a laser retro-reflector array (LRRA) for SLR.

Satellite Overview

Astro-G satellite image is shown in Figure 1. The satellite will be equipped with a 9.6-metre large deployable antenna and 8, 22, 43 GHz band receivers. Astro-G will be injected to an elliptical orbit parameters of which are listed in Table. 1. The apogee height is 25000km, higher than the altitude of GPS satellites. The higher frequency observation and high altitude of the satellite's apogee enable an observation with higher resolution. The angular resolution will be 0.040 milliarcsec. at 43GHz, 10 times better than the VSOP's 0.4 milli arc sec. at 5GHz. For the POD, Astro-G will carry a multi-frequency GPS receiver. Because of its apogee altitude (25000km) higher than that of GPS satellites, however, only1-2 GPS satellites

can be used for the orbit determination at the apogee (See Figure 2), which results in degradation of the orbit determination accuracy. Therefore, Astro-G will also carry a LRRA for SLR, mounted next to a Ka-band link antenna that is steerable independent of the satellite body.

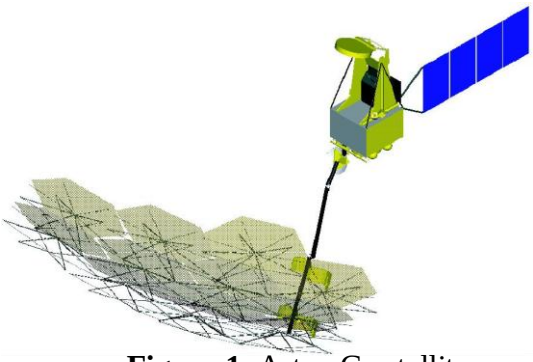

Figure 1. Astro-G satellite

Table 1. Orbital Parameters of Astro-G

Apogee altitude	25000km
Perigee altitude	1000km
Inclination	31deg
Eccentricity	0.62
Precession of AOP	+258deg/year
Precession of LAN	-167deg/year
Orbital period	7.45hour

Figure 2. Number of visible GPS satellites

Laser Retro-Reflector Array

Figure 3 shows a preliminary design of a LRRA for Astro-G. The LRRA consists of two parts. One is a center area, which has a pyramid shape for supporting wide range of laser incident angle at low altitudes. Another part is a surrounding area composed of flat corner cubes for increasing effective aperture area at high altitude. The corner cubes of center area are 28mm in diameter, coated on the back faces and 30deg-slanted. The corner cubes of surrounding area are 28mm (inner ring) or 38mm (outer ring) in diameter, uncoated on back faces and not slanted. As shown in Figure 4, the LRRA is mounted next to Ka-band link antenna, because no specific plane of Astro-G always directs to the Earth. Therefore, the LRRA position and attitude (pointing direction) is synchronized with those of the Ka-band link antenna. Phase referencing observation, one of the observation modes of Astro-G, causes a attitude oscillation, which results in a fluctuation of position and attitude of Ka-band link antenna. Therefore, the LRRA position and pointing direction is varied because of Phase

referencing observations, and the SLR observations (residuals or O-C) is time-varying as a result.

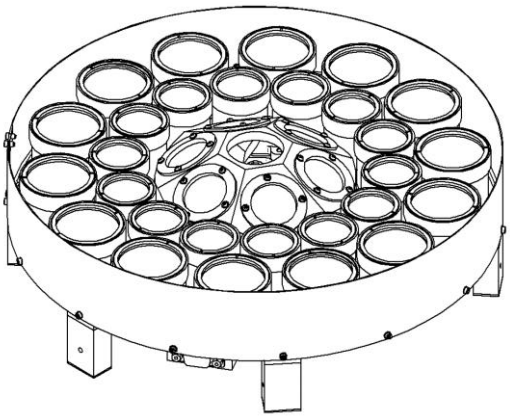

Figure 3. Preliminary design of LRRA for Astro-G

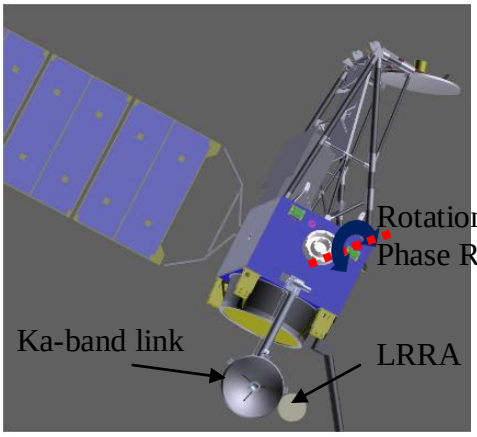

Figure 4. Position of LRRA and Ka-band link antenna

Phase Referencing Observations

In the VSOP-2 project, phase referencing observations are proposed for mitigating the phase fluctuation due to the Earth's atmosphere, because observations are made not only by Astro-G, a space telescope, but also by terrestrial telescopes. As shown in Figure 5, in phase referencing observations, telescopes are alternately pointed toward a target source and a calibrator. One cycle of the typical phase referencing observations consists of 58 cycles of small (about 3-deg) switching and one cycle of large (about 10-deg) switching. One cycle is represented as steps 1-7 as shown in Table 2.

Table 2. One cycle of a typical phase referencing observation

Step	Operation
1	Observation of a target (15sec)
2	Attitude change to a calibrator (15sec,3deg)
3	Observation of the calibrator (15sec)
4	Attitude change to the target (15sec,3deg)
Steps 1-4 are repeated 58 times.	
5	Attitude change to a calibrator (45sec,10deg)
6	Observation of the calibrator (45sec)
7	Attitude change to the target (45sec,10deg)

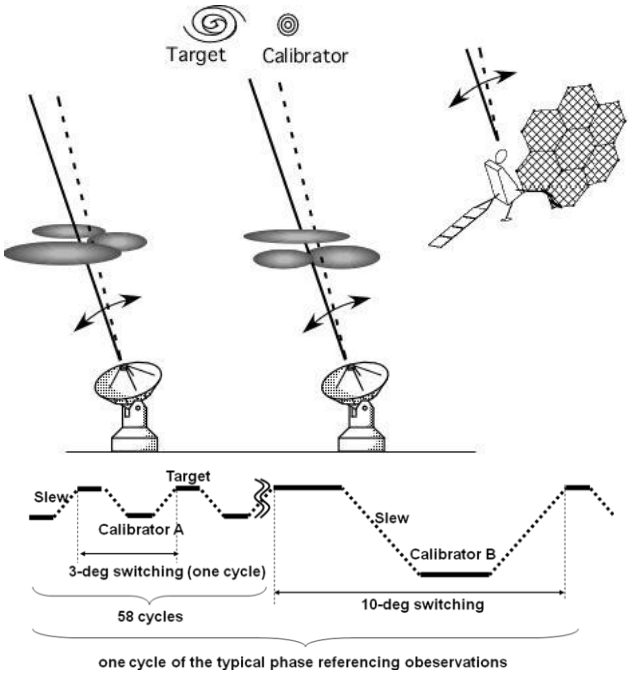

Figure 5. Schematic representation of phase referencing observation in VSOP-2 project

Simulated Return Pattern

As mentioned in section 3, the SLR observations (residuals or O-C) is time-varying due to the phase referencing observations. We simulated SLR return (residuals or O-C) patterns expected to be received at GMSL and YARL. The simulations were done for four cases (two for altitudes change and two for rotation axis (see Figure 4) direction change). Ka-band link antenna is assumed to be directed to the center of the Earth. Figure 6 shows the simulated return pattern for 3-deg switching. Figure 7 shows the simulated return for 3-deg and 10-deg switching.

Atitude	Rtation axis direction	GMSL	YARL
1000km	Stellite's radial direction	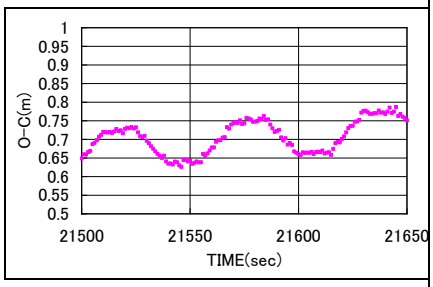	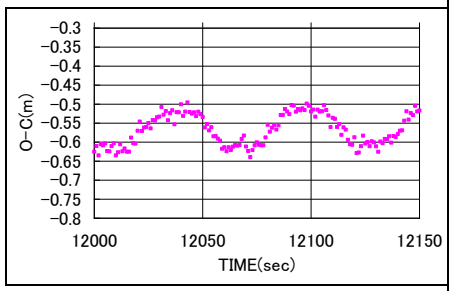
	Stellite's along track direction	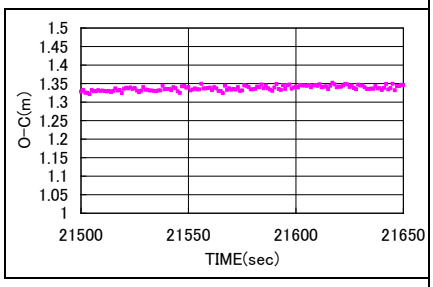	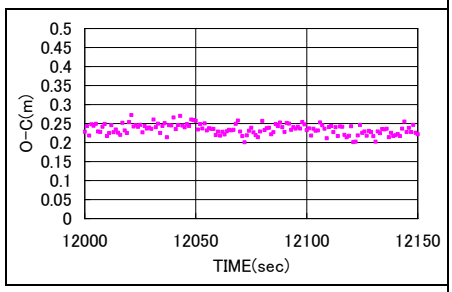
Apogee (25000km)	Stellite's radial direction	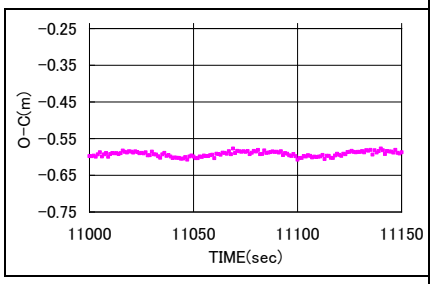	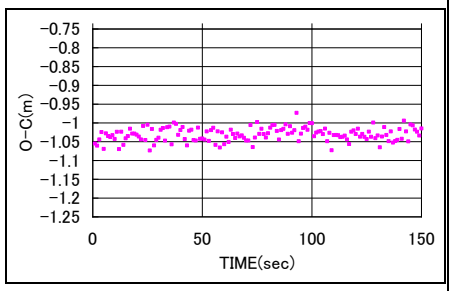
	Stellite's along track direction	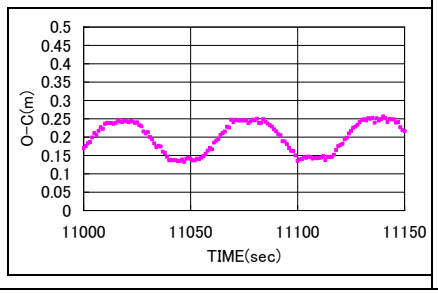	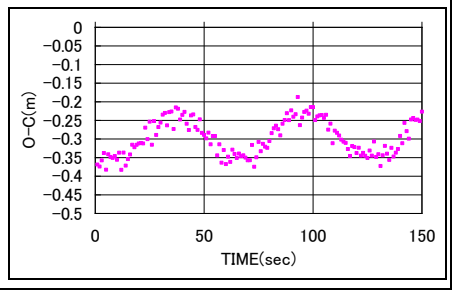

Figure 6. Simulated return pattern for 3-deg switching

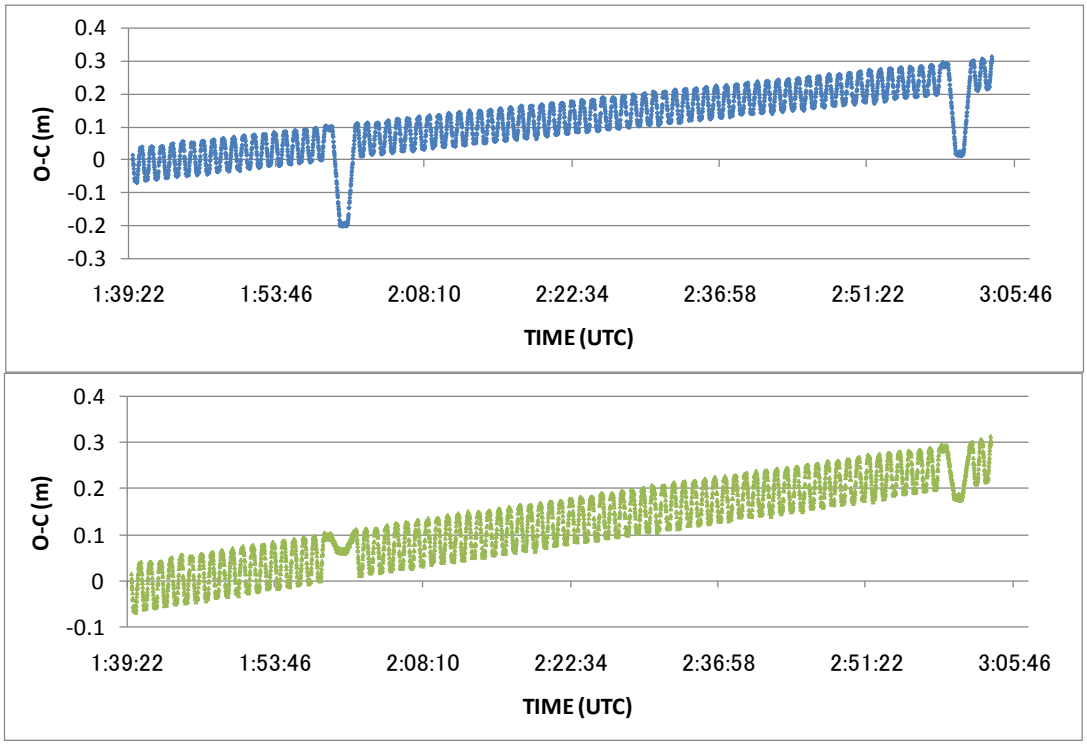

Figure 7. Simulated return pattern for 3-deg and 10-deg switching
(10-deg switching sometimes causes a spike (above) and sometimes not (below).)

Required Data Handling

As is obvious from the simulation result, the observation data from Astro-G requires careful handling. There are two concerns about the data handling. The first one is regarding a bin size of a QLNP. If a large bin size (for example, 15sec) is used, the fluctuation of the LRRA position caused by the phase referencing observation cannot be observed. This works against the POD. Smaller bin size is preferable, so that we can identify the data variation due to the phase referencing operation. In practice, we can choose a 5-sec bin size for Astro-G's QLNP. Another option is to send full rate data. In that case, however, large volumes of data such as data from kHz ranging stations will be another issue. The second concern is regarding a data screening criteria. If tight rejection criteria are applied to the data like shown in the Figure 6 (above), QLNP may have some bias as a result. Figure 8 shows a result of an iterative 2.5-sigma rejection. Triangular plots represent the rejected data after four iteration. At the upper parts of the fluctuation, the data at the above edge are rejected, which results in a downward bias of the QLNP. Similarly, at the lower parts of the fluctuation, the data at the below edge are rejected, which results in an upward bias of the QLNP. These biases also lead to degradation of the orbit determination. In order to avoid the normal point biases caused by data rejection, loose data screening criteria or manual data rejection is mandatory. Even if we are going to take an option of full rate data transmission, since noise reduction should be done on each site, the loose data screening criteria or manual data reduction with these characteristics in mind are of high importance.

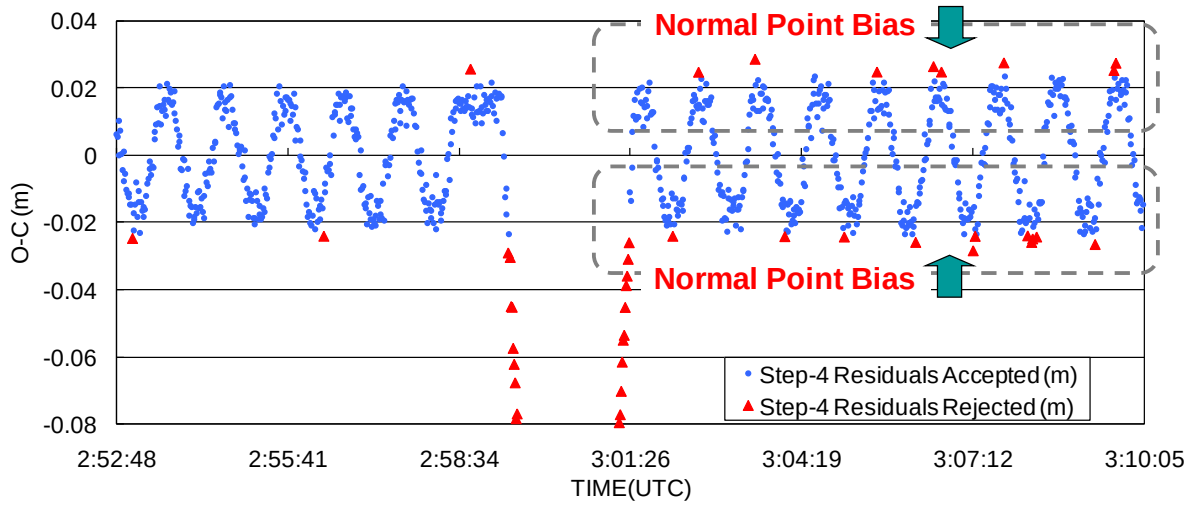

Figure 8. Result of Data Screening (After Iterative 2.5-sigma rejection)

Summary

A POD (10cm accuracy) is required for mission success of Astro-G, which is a space radio telescope and a successor of HALCA. One of the advanced observation modes of Astro-G is a phase referencing observations. SLR observations (O-C) are time-varying, because the position and pointing direction of LRRA (mounted next to Ka antenna) are varied due to the phase referencing observations. QLNP with 5 sec bin size is required for observing fluctuation of the LRRA position and pointing direction. Transmission of full rate data is another consideration. In order to avoid the normal point bias caused by data rejection, a loose data screening criteria or a manual data rejection is mandatory.

References

Asaki, Y., Takeuchi, H., and Yoshikawa, M., *Next Space-VLBI Mission, VSOP-2, and the Precise Orbit Determination*, Proc. of ION GNSS 2008

Otsubo, T., Kubo-oka, T., Saito, H., Hirabayashi, H., Kato, T., Yoshikawa, M., Asaki, Y., and Nakamura, S., *Possibility of laser ranging support for the next-generation space VLBI mission, ASTRO-G*, Proc. of 15th International Laser Ranging Workshop, 2006

Tsuboi, M., *VSOP2/ASTRO-G project*, Journal of Physics: Conference Series 131, 2008

Satellite Laser Ranging Tracking through the Years

C. Noll
NASA Goddard Space Flight Center, Code 690, Greenbelt, MD 20771, USA.
Carey.Noll@nasa.gov/Fax: 301-614-6015

Abstract

Satellites equipped with retroreflectors have been tracked by laser systems since 1964. Satellite laser ranging supports a variety of geodetic, earth sensing, navigation, and space science applications. This poster will show the history of satellite laser ranging from the late 1960's through the present and will include retro-equipped satellites on the horizon.

Satellite Tracking History

Initial laser ranges to a satellite in Earth orbit took place in 1964 with the launch of Beacon Explorer-B (BE-B), the first satellite equipped with laser retroreflectors. Since that time, the global network of laser ranging sites has tracked over eighty satellites including arrays placed on the Moon. Satellite and Lunar laser ranging continue to make important contributions to scientific investigations into solid Earth, atmosphere, and ocean processes. SLR also provides Precise Orbit Determination (POD) for several Earth sensing missions (e.g., altimetry, etc.), leading to more accurate measurements of ocean surface, land, and ice topography. Several of these missions have relied on SLR when other radiometric tracking systems have failed (e.g., GPS and DORIS on TOPEX/Poseidon, PRARE on ERS-1, GPS on METEOR-3M and GFO-1) making SLR the only method for providing the POD required for instrument data products. A list of satellites equipped with retroreflectors (past, current, and future) and tracked by SLR is shown in Table 1. The table summarizes the data yield (approximate through fall 2008) and includes a list of any co-located instrumentation (e.g., GNSS, DORIS, or PRARE). Figure 1 shows this rich history in graphical format, as well as future plans, from mid-1960 through 2015. The satellite missions supported by laser ranging are shown in four categories: geodetic, Earth sensing, navigation, and space science or engineering applications.

The data generated by the laser ranging stations tracking these satellites, as well as products derived from these data, are available from the Crustal Dynamics Data Information System (CDDIS, *http://cddis.nasa.gov*). The CDDIS is NASA's active archive and information service of space geodesy data and products and currently serves as a key global data center for the ILRS. For over 25 years, the CDDIS has provided continuous, long term, public access to the data and product sets required for many interdisciplinary studies of the global Earth Science community,

Table 1. ILRS Satellite Tracking Information

Satellite	Start Date	End Date	Number of Years	Number of Passes	Co-Located Instrument?
Current and Past Satellites					
ADEOS-1	Oct-1996	Aug-1997	2	750	
ADEOS-2	Dec-2002	Jan-2003	2	180	
Ajisai	Aug-1986	---	23	152,260	
ALOS	Aug-2006	Aug-2006	1	90	
ANDERR-Active	Jan-2007	Dec-2007	1	430	
ANDERR-Passive	Jan-2007	May-2008	2	650	
BE-C	Jan-1976	---	21	66,790	
CHAMP	Jul-2000	---	9	13,650	GNSS
DIADEM-1C	Apr-1997	Nov-1997	1	2,350	
DIADEM-1D	Apr-1997	Nov-1997	1	2,590	
Envisat	Apr-2002	---	7	34,820	DORIS
ERS-1	Jul-1991	Mar-2000	9	26,080	PRARE*
ERS-2	Apr-1995	---	14	66,620	GNSS
Etalon-1	Jan-1989	---	20	15,890	
Etalon-2	Jul-1989	---	20	15,720	
ETS-8	Mar-2007	---	2	390	
FIZEAU	Jun-1995	Oct-1998	4	4,790	
GEOS-3	Oct-1998	May-1999	2	2,130	
GFO-1	Apr-1998	Aug-2008	11	43,070	GNSS*
GFZ-1	Apr-1995	Jun-1999	5	5,140	
GIOVE-A	May-2006	---	3	1,590	GNSS
GIOVE-B	May-2008	---	1	140	GNSS
GLONASS (31 sats.)	Oct-1994	---	15	47,980	GNSS
GP-B	Jul-2004	Jun-2006	3	2,910	GNSS
GPS-35	Oct-1993	---	16	7,440	GNSS
GPS-36	Apr-1994	---	15	6,500	GNSS
GRACE-A	Mar-2002	---	7	12,550	GNSS
GRACE-B	Mar-2002	---	7	11,860	GNSS
ICESat	Mar-2003	---	6	5,320	GNSS
Jason-1	Dec-2001	---	8	48,110	GNSS, DORIS
Jason-2	Jun-2008	---	1	990	GNSS, DORIS
LAGEOS-1	May-1976	---	33	152,350	
LAGEOS-2	Oct-1992	---	17	88,750	
LARETS	Nov-2003	Aug-2008	6	19,740	
LRE	Dec-2001	Mar-2002	2	40	
METEOR-3	Jan-1994	Nov-1995	2	6,280	PRARE*
METEOR-3M	Dec-2001	Mar-2006	6	1,800	GNSS*
MOON	Jun-1996	---	13	1,210	
MSTI-2	Jun-1994	Oct-1994	1	60	
OICETS	Apr-2006	---	1	120	
Reflector	Dec-2001	Aug-2004	4	3,620	
RESURS	Dec-1995	Oct-1998	4	2,020	
Starlette	Jan-1976	---	33	123,160	
STARSHINE-3	Oct-2001	Jun-2003	3	50	
Stella	Sep-1993	---	16	62,990	
SUNSAT	May-1999	May-2001	3	1,800	
TerraSAR-X	Jun-2007	---	2	3,070	GNSS
TiPS	Jun-1996	Oct-1997	2	1,680	
TOPEX	Jan-1992	Dec-2005	14	105,060	GNSS*, DORIS*
WESTPAC	Jul-1998	Jan-2002	5	5,480	
ZEIA	Mar-1997	Jul-1997	1	150	

Table 1. ILRS Satellite Tracking Information (continued)

Future Satellites		
Satellite	**Launch Date**	**Co-Located Instrument**
COMPASS-M1	2008	GNSS
GOCE	2009	GNSS
SOHLA-1	2009	GNSS
LRO-LR	2009	
PROBA-2	2009	GNSS
GIOVE-A2	---	GNSS
QZS-1	2009	
TanDEM-X	2009	GNSS
Galileo	2009	GNSS
NPOESS	2012	GNSS

Note: * indicates co-located instrument failure

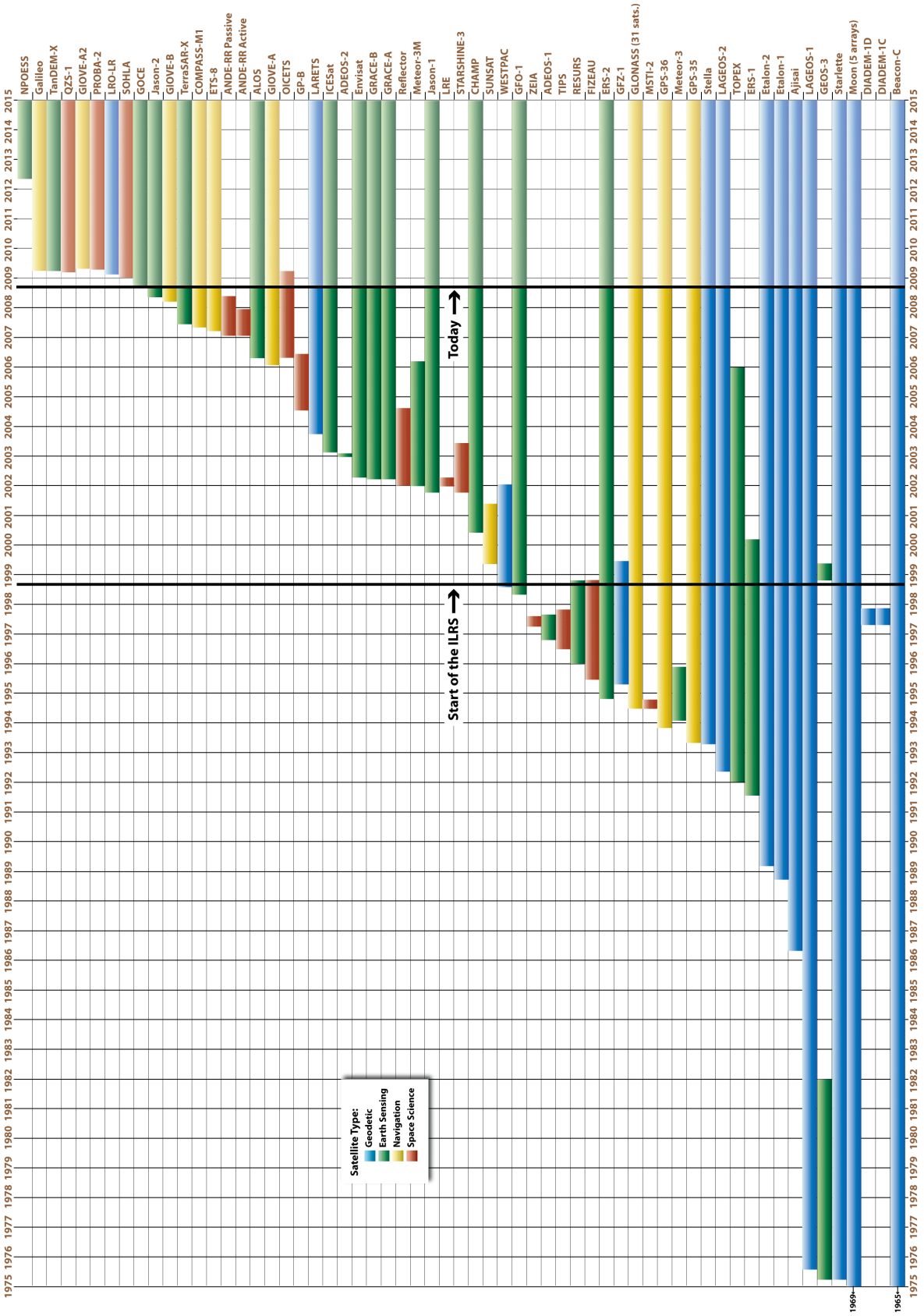

Figure 1. Satellite and Lunar Laser Ranging Tracking History

ILRS Web Site Update: Using the ILRS Web Site to Monitor Performance

C. Noll (1)**, M. Torrence** (2)

(1) NASA Goddard Space Flight Center, Code 690, Greenbelt, MD 20771, USA
Carey.Noll@nasa.gov/Fax: 301-614-6015

(2) SGT, Inc., 7701 Greenbelt Road, Suite 400, Greenbelt, MD 20770, USA
mark.h.torrence.1@gsfc.nasa.gov

Abstract

The ILRS Web site, http://ilrs.gsfc.nasa.gov, is the central source of information for all aspects of the service. The Web site provides information on the organization and operation of ILRS and descriptions of ILRS components, data, and products. Furthermore, the Web site and provides an entry point to the archive of these data and products available through the data centers. Links are provided to extensive information on the ILRS network stations including performance assessments and data quality evaluations. Descriptions of supported satellite missions (current, future, and past) are provided to aid in station acquisition and data analysis. This poster will detail recent improvements made in several areas of the ILRS Web site including specific examples of key sections and webpages.

Station Performance Report Cards

The ILRS performance "report cards" are issued quarterly by the ILRS Central Bureau (CB). These reports tabulate the previous 12 months of data quality, quantity, and operational compliance by station. The statistics are presented in two tables (one for artificial satellites and a second for lunar reflectors) by station and sorted by total passes in descending order. Plots of data volume (passes, normal points, minutes of data) and RMS (LAGEOS, Starlette, calibration) are created from this information and available on the report card Web site. An excerpt from Table 1 of the 2008 second quarter report card (01-Jul-2007 through 30-Jun-2008), is shown in Figure 1; the full report card can be found on the ILRS Web site at: *http://ilrs.gsfc.nasa.gov/stations/site_info/global_report_cards/perf_2008q2_wLLR.html*.

Site Information		Data Volume									Data Quality		
Column 1	2	3	4	5	6	7	8	9	10	11	12	13	14
Location	Station Number	LEO pass Tot	LAGEOS pass Tot	High pass Tot	Total passes	LEO NP Total	LAGEOS NP Total	High NP Total	Total NP	Minutes of Data	Cal. RMS	Star RMS	LAG RMS
Baseline		1000	400	100	1500								
Yarragadee	7090	9638	1988	1373	12999	204021	25377	12731	242129	166320	4.7	8.9	9.4
San_Juan	7406	5255	1082	1303	7640	84520	13173	8659	106352	92649	13.1	13.9	15.2
Mount_Stromlo_2	7825	5297	1274	484	7055	70033	12860	3586	86479	66201	3.1	4.2	5.8
Graz	7839	4651	740	519	5910	92498	8291	4272	105061	61353	1.9	3.4	5.2
Wettzell	8834	4094	1033	411	5538	43417	7905	1727	53049	38825	4.6	12.1	19.1
Herstmoncex	7840	3881	888	374	5143	61069	10396	1582	73047	44178	7.3	12.1	15.4
Changchun	7237	3954	593	570	5117	44205	4953	2970	52128	37099	13.0	13.8	16.7

Figure 1. Table 1 of the ILRS Report Card for the second quarter of 2008.

Summary plots for the values in columns 3-14 of Table 1 of each report card are also linked and available. Examples of selected plots are shown in Figure 2.

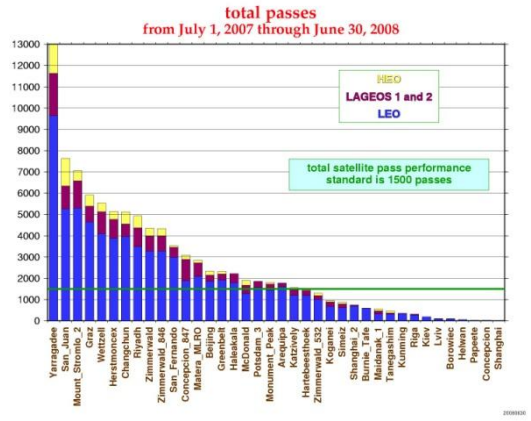

Figure 2a. Total passes for the second quarter of 2008.

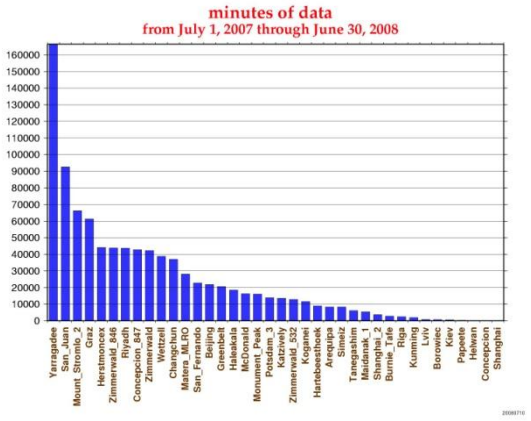

Figure 2b. Total minutes of data for the second quarter of 2008.

A third table in each ILRS report card summarizes the orbital analysis of the data as performed by five AC/AACs (DGFI, Hitotsubashi University, JCET, MCC, and the Shanghai Astronomical Observatory). An example of this table (Table 2) is shown in Figure 3; Figure 4 shows an example weekly report from Hitotsubashi University used in the computation of this summary table.

Site Information		DGFI Orbital Analysis				Hitotsubashi Univ. Orbital Analysis				JCET Orbital Analysis				MCC Orbital Analysis				SHAO Orbital Analysis			
Station Location	Station Number	LAG NP RMS (mm)	short term (mm)	long term (mm)	% good LAG. NP	LAG NP RMS (mm)	short term (mm)	long term (mm)	% good LAG. NP	LAG NP RMS (mm)	short term (mm)	long term (mm)	% good LAG. NP	LAG NP RMS (mm)	short term (mm)	long term (mm)	% good LAG. NP	LAG NP RMS (mm)	short term (mm)	long term (mm)	% good LAG. NP
Baseline		10.0	20.0	20.0	95	10.0	20.0	20.0	95	10.0	20.0	20.0	95	10.0	20.0	20.0	95	10.0	20.0	20.0	95
Yarragadee	7090	2.8	23.8	3.6	100.0	1.7	8.4	2.1	100.0	3.1	18.1	3.6	99.8	2.1	10.7	1.8	98.6	2.1	12.7	1.5	95.6
San_Juan	7406	6.3	34.3	5.5	99.4	4.6	22.7	10.4	99.2	5.4	18.5		94.3	6.3	19.3	10.9	96.5	5.1	26.2	3.4	94.2
Mount_Stromlo_2	7825	2.9	20.2	5.5	99.2	2.8	8.8	5.6	99.7	3.6	16.6	3.0	99.3	3.2	14.7	4.5	96.0	2.5	13.0	2.7	96.0
Graz	7839	1.7	13.4	4.1	100.0	1.1	6.8	2.3	100.0	2.1	15.1	4.0	99.5	2.2	6.5	3.2	98.9	1.2	11.5	2.5	96.1
Wettzell	8834	3.2	24.2	16.0	99.9	3.1	13.4	8.8	99.8	3.6	17.4	4.4	97.5	3.1	13.2	1.9	97.0	2.4	21.5	4.7	95.6
Herstmoncex	7840	2.9	22.2	7.3	100.0	2.1	8.4	2.5	100.0	3.1	15.3	4.4	99.4	2.8	8.4	1.7	98.1	2.0	13.9	1.8	94.6
Changchun	7237	7.2	28.5	9.6	100.0	7.0	22.2	17.3	100.0	6.4	22.2	6.0	97.6	7.6	22.0	6.4	94.0	5.9	28.1	9.6	98.4

Figure 3. Table 3 of the ILRS Report Card for the second quarter of 2008.

The report card is used to assess the performance of the stations in the ILRS network. The CB maintains lists of the operational and associate stations, classified according to the results posted in the ILRS report cards. Performance guidelines, defined on the ILRS Web site, cover yearly data quantity (number of passes), data quality (normal point precision and short and long term bias stability) and operational compliance factors (timely data delivery, correct data formatting, required station documentation). Current operational vs. associate status can be viewed on the ILRS Web site at: *http://ilrs.gsfc.nasa.gov/stations/*.

```
# @createdAt    2008/08/13 00:31:48
#
# each line contains:
#   sat            = 4-char satellite name
#   site           = 4-char site name (CDP ID)
#   date/time      = pass starting time
#   dur            = pass duration (min)
#   rb             = estimated range bias (mm) with 1-sigma error
#   tb             = estimated time bias (microsec) with 1-sigma error
#   prec           = post-fit scattering rms (mm)
#   bad/total      = number of bad/total normal-points
#   rms            = single-shot rms (mm)
#   pres/temp/humi = pressure (hPa), temperature (K) and humidity (%)
#   sdelay         = applied system delay (mm)
#   shft           = system delay shift (mm)
#   rms            = calibration single-shot rms (mm)
#   cfg            = system configuration flag; SCH and SCI
#   r              = data release flag
#   wlen           = laser wavelength (nm)
#
#  1824 = KIEV
# sat site       date  time dur   rb mm   error        tb us    error    prec bad total  rms   pres  temp hum  sdelay shft  rms cfg r wlen
 ENVI 1824 2008/07/29 18:38   5    -141 (    65 )      -56.2 (   15.8 )    28   0 /  16   41  998.6 289.1  59   16638   19   39 0 2 0  532
 ERS2 1824 2008/07/29 19:09   4    -101 (    71 )      -60.3 (   19.5 )    28   0 /  19   42  998.6 288.5  61   16637   14   39 0 2 0  532
 ENVI 1824 2008/07/29 20:19   4      21 (   148 )      -54.9 (   72.5 )   111   1 /   8   45  999.3 288.3  60   16637   14   39 0 2 0  532
 ERS2 1824 2008/07/29 20:51   1      -9 ( ----- )  --------.- ( ----.- )     0   1 /   2   39  999.3 288.0  61   16644    0   42 0 2 0  532
 STEL 1824 2008/07/30 00:04   3     -98 (    46 )      -33.5 (   19.3 )    14   0 /   9   42  999.3 286.2  71   16637   22   43 0 2 0  532
 LAG1 1824 2008/07/30 00:41   2     -36 (    79 )  --------.- ( ----.- )    62   0 /   3   53  999.9 286.0  71   16638   20   43 0 2 0  532
 ENVI 1824 2008/07/30 18:08   4     -25 (    23 )      -43.2 (    7.0 )     5   1 /   8   42  996.6 291.4  51   16554    0   25 0 2 0  532
 LAG2 1824 2008/07/30 18:37  14     223 (    52 )      -22.4 (   85.6 )    14   0 /   9   69  996.7 291.3  51   16554    0   25 0 2 0  532
 LAG1 1824 2008/07/30 19:09  20     178 (    60 )      -38.1 (   53.6 )    32   0 /  12   58  996.8 291.3  52   16554    0   25 0 2 0  532
 ENVI 1824 2008/07/30 19:46   5    -100 (    35 )      -51.3 (    8.8 )    17   0 /  24   44  997.0 291.2  53   16554    0   25 0 2 0  532
 ERS2 1824 2008/07/30 20:21   1    -317 (   118 )  --------.- ( ----.- )    31   0 /   6   54  997.3 290.1  53   16554    0   25 0 2 0  532
 LAG1 1824 2008/07/30 22:45  22      15 (    67 )      -74.5 (   41.1 )    18   1 /  11   55  997.0 288.5  59   16631    0   29 0 2 0  532
 ENVI 1824 2008/07/31 19:20   1    -450 (    14 )  --------.- ( ----.- )     4   0 /   7   35 1002.6 290.6  58   16384    0   36 0 2 0  532
 ERS2 1824 2008/07/31 19:45   5    -130 (    22 )      -54.4 (    4.3 )     9   0 /  15   39 1002.6 290.5  59   16377   15   30 0 2 0  532
 STEL 1824 2008/08/01 00:50   6     -89 (    44 )      -29.3 (    8.8 )    25   0 /  14   31 1002.6 287.9  68   16364   10   28 0 2 0  532
 STRL 1824 2008/08/01 01:18   3     -65 (    50 )      -43.1 (   21.9 )    13   0 /   8   30 1002.6 287.7  68   16364   10   28 0 2 0  532
 ENVI 1824 2008/08/01 18:45   2     -73 (     6 )  --------.- ( ----.- )     2   0 /  10   38  998.3 292.3  47   16395    0   29 0 2 0  532
 :
 :
```

Figure 4. Example of weekly station bias report from Hitotsubashi University.

Real-Time Daily Station Status Reports

Station status information is available on a daily and near-real time basis through the EUROSTAT utility. These reports allow the ILRS community to quickly view the status of the stations in the tracking network. ILRS stations can automatically upload status information to EUROSTAT (maintained by the Astronomical Institute of the University of Berne, AIUB) that is then used to generate an overview of the current activities of the tracking stations. The real-time report (Figure 5) shows actual station operations at that point in time. The daily report (Figure 6) provides a one-line entry per day showing if stations are currently staffed, operational, off-shift, off-line because of system problems, etc. The ILRS would like to encourage all stations in the network to participate in the daily and, if possible, real-time exchange of status information.

Station-Specific Performance Charts

To further aid analysis by station operators and users, the ILRS Central Bureau generates data plots summarizing station performance and environmental parameters. These plots, created for each active station in the network, are accessible through the Stations section of the ILRS Web site. After selecting a station, the user is presented with several tabs. The “LAGEOS Performance” tab will yield several plots created to summarize station performance on LAGEOS: RMS, calibration RMS, system delay, observations per normal point, and full-rate observations per pass. For each parameter, two plots are generated, one covering the last year and a second showing the information from 2000 to the present. Examples of these plots for selected stations in the network are shown in Figure 7.

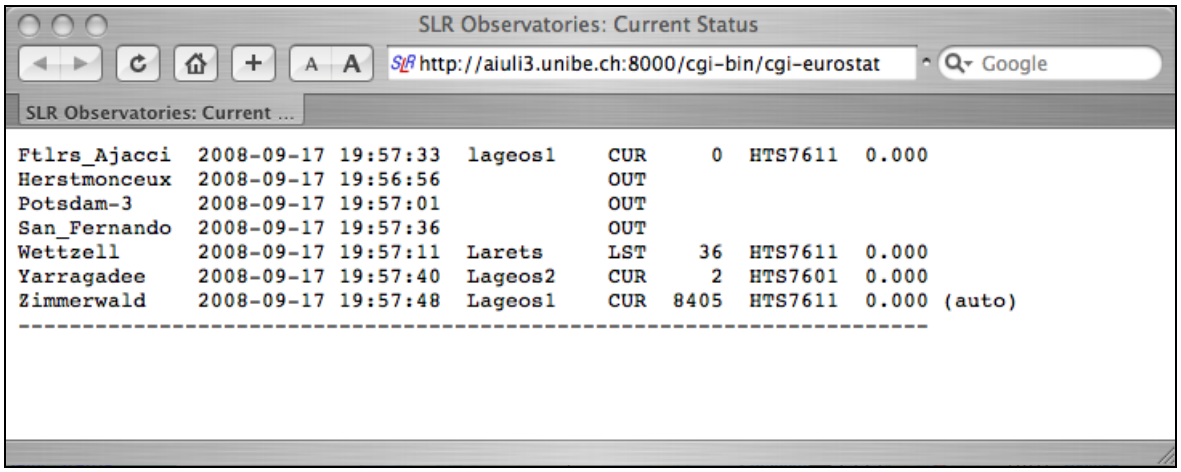

Figure 5. EUROSTAT real-time station status report.

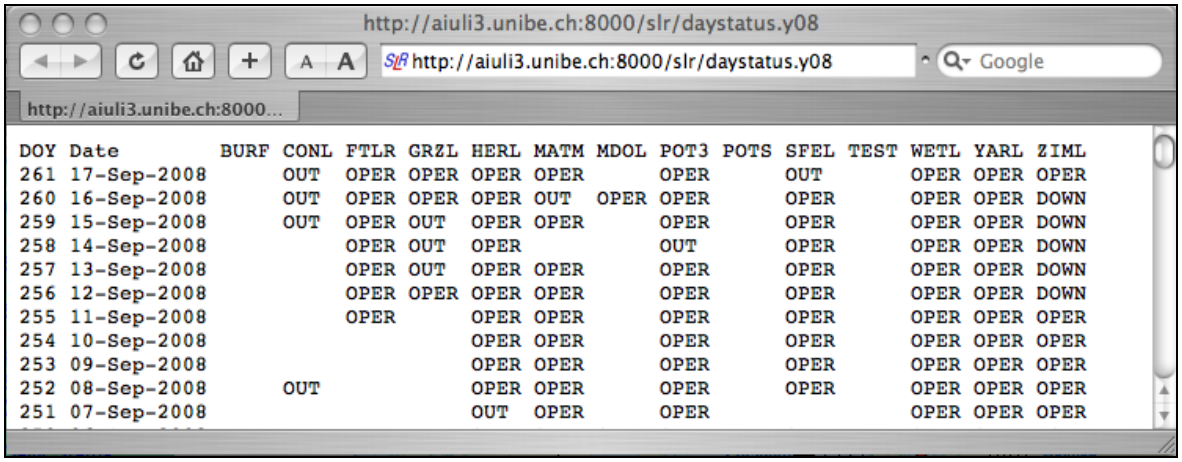

Figure 6. Daily station status report (for Sept. 17, 2008).

The "Satellite Data Info" tab shows a table of plots providing statistics on all currently tracked satellites as a function of time; full-rate observations per normal point and normal point rms are also computed as a function of range and time. Examples of these satellite plots for a selected station in the network are shown in Figure 8. These plots are also accessible through the Satellite Missions section of the ILRS Web site (organized by mission, matrix of all stations tracking mission).

The "Meteorological Data" tab presents plots of environmental parameters: temperature, humidity, and pressure; plots spanning the last year and since 2000 are also created for this category. Examples of these met data plots are shown in Figure 9.

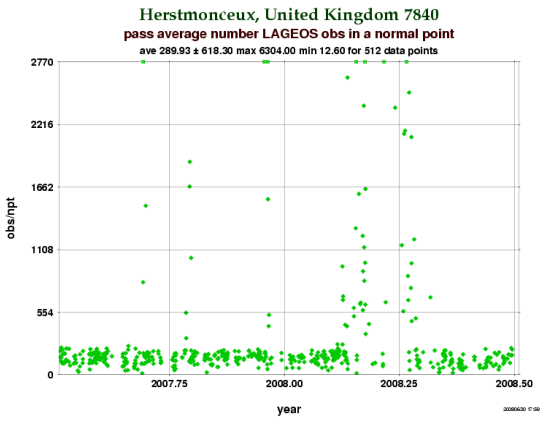

Figure 7a. Average number of LAGEOS observations per normal point at Herstmonceux for the past year.

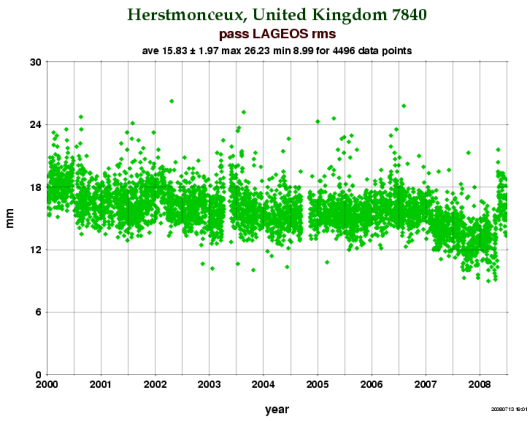

Figure 7b. Average LAGEOS pass RMS at Herstmonceux for the past ten years.

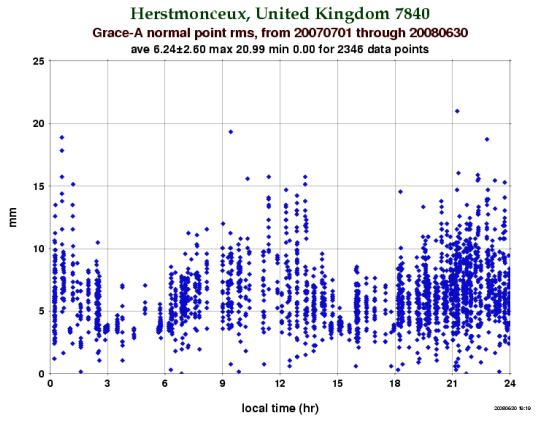

Figure 8a. GRACE-A normal point RMS at Herstmonceux (as a function of local time) for the past year.

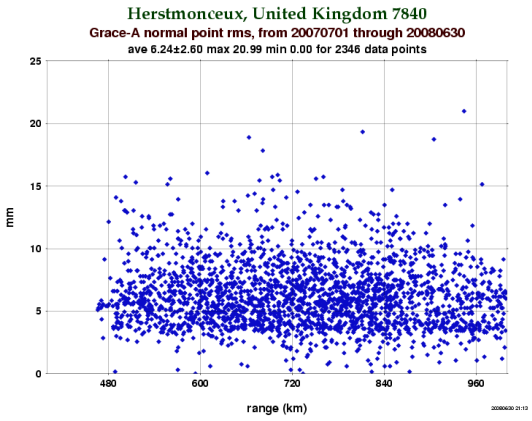

Figure 8b. GRACE-A normal point RMS at Herstmonceux (as a function of range) for the past year.

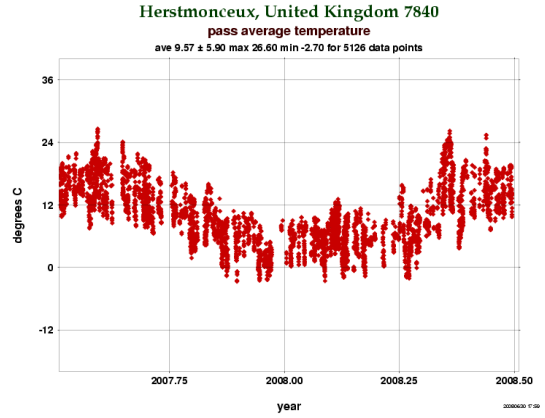

Figure 9a. Average temperature at Herstmonceux for the past year.

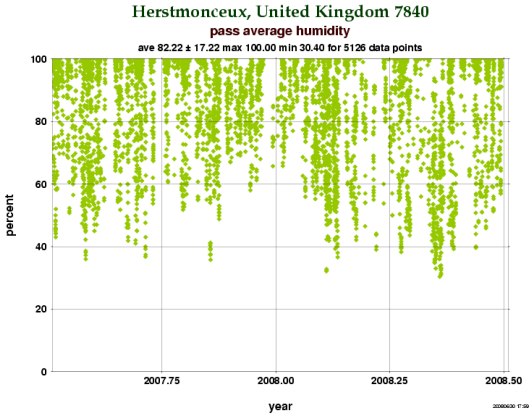

Figure 9b. Average humidity at Herstmonceux for the past year.

The Atmospheric Neutral Density Experiment (ANDE)

A. Nicholas[1], T. Finne[1], I. Galysh[2], M. Davis[2], L. Thomas[2],and L. Healy[3]
[1]Space Science Division
[2]Space Systems Development
[3]Spacecraft Engineering
US Naval Research Laboratory, 4555 Overlook Ave, SW, Washington, DC 20375

Introduction

The Naval Research Laboratory has developed a satellite suite, the Atmospheric Neutral Density Experiment[1] (ANDE), to improve precision orbit determination and prediction by monitoring total atmospheric density between 300 and 400 km. The ANDE risk reduction (ANDERR) flight was deployed into orbit by the Space Shuttle Discovery on December 21, 2006 (Figure 1). The primary ANDERR mission objective, a test of the Shuttle deployment mechanism for the follow-on ANDE flight (scheduled for mid-2009), was successful. The primary ANDE mission objectives are to measure the variability of atmospheric density driven by solar and geomagnetic forcings for improved orbit determination and to provide a test object for the US space surveillance network (SSN). A joint effort between the Space Science Division and the Naval Center for Space Technology to routinely process and analyze the ANDE data has led to improved orbit determination and prediction using an atmospheric model correction method. The ANDE data provide a valuable tool for correcting deficiencies in atmospheric models and have led to advancements in miniature sensor technology. These advancements are pivotal for multi-point in-situ space weather sensing.

Mission Objectives

The ANDE satellite suite consists of a series of four nearly perfect spherical micro-satellites with instrumentation to perform two interrelated mission objectives. The first objective is to monitor the total neutral density along the orbit for improved orbit determination of resident space objects. The second is to provide a test object for both radar and optical SSN sensors. The DoD Space Test Program will provide launch services for two missions (ANDERR and ANDE), with each mission flying a pair of ANDE spacecraft.

The major source of error in determining the orbit of objects in Low Earth Orbit (LEO), i.e. altitudes less than 1000 km, is the computation of acceleration due to atmospheric drag. This acceleration is governed by equation (1),

$$a_d = -\frac{1}{2} B \rho v^2 \quad (1) \qquad\qquad B = \frac{C_D A}{m} \quad (2)$$

where a_d is the acceleration, ρ is the atmospheric density and v is the orbital velocity relative to the medium (including cross-track and radial velocities). Equation 2 defines the ballistic coefficient, B, with C_D being the coefficient of drag, A the projected frontal area and m the mass of the object. The constant and well-determined cross section and surface properties of the ANDE spherical spacecraft provide an ideal set of objects for monitoring atmospheric drag and the calibration of SSN assets.

ANDE Data Flow

The 20th Space Control Squadron, USAF in Dahlgren, VA, processes the SSN radar observation data of the ANDERR spacecraft. The product is a set of orbital state vectors and corresponding radar observations, which is provided to NRL up to three times a day. These state vectors are processed at NRL using Special-K orbit determination software to produce a set of ephemeredes. These ephemeris files are reformatted into the consolidated prediction format used by the International Laser Ranging Service tracking stations. A set of predictions is also computed once per day using the NRL Orbit Covariance Estimation and Analysis (OCEAN) orbit determination code. The radar observation data are merged with the SLR observation data and processed by OCEAN to generate a 2-day satellite laser ranging augmented set of predictions that includes the atmospheric correction. Figure 2 depicts the two data flow processes.

Data Processing and Analysis

A comparison between the values of C_D for the two spacecraft from the OCEAN run, using an atmospheric model (NRLMSISE-00) and a priori area and mass information, yields excellent agreement between the two objects even as the altitude separation between the two spacecraft increases due to differential drag. The retrieved values of C_D for the two spacecraft are presented as a function of time in Figure 3a. These results are non-physical as the value of C_D is well below the theoretical limit of 2; the atmospheric model is over-estimating the density and the OCEAN code is correcting for this by scaling the B term down to fit the observations. The ANDERR data provide a global climate monitoring metric, which showed a consistent over-estimation[2] of total density by climatology models by an average of 26.6%.

The primary drivers of the atmosphere are solar radiation heating and geomagnetic heating. The solar driver is input into the atmospheric model in the form of the F10.7 cm radio flux, an easy to measure ground-based proxy for the solar ultraviolet flux that heats the atmosphere. The A_p index is a measure of geomagnetic activity at the Earth and is used by atmospheric models to drive the geomagnetic heating in the atmosphere. A wavelet analysis was performed on the C_D density corrections; $F_{10.7}$, A_p and the solar wind velocity (V_{sw}) time series to further investigate the causes of periodicities observed during 2007. The wavelet power spectra are presented in Figure 3b as a function of day of year for 2007. The plots have been formatted to a range of 2 to 20 days with white contours representing the 95% significance level. The short-term oscillations (5,7,9 days) were much more prevalent and stronger in both the A_p and V_{sw} data in the first half of 2007 than in the second half of the year. This is also evident in the 9-day period in the C_D atmospheric corrections derived from the ANDERR spacecraft orbits. The strong 18-day periods observed in the $F_{10.7}$ data are also observed in the C_D corrections although there is a significant time lag and atmospheric recovery period associated with this data. The analysis technique applied to the ANDERR data set separates geomagnetic forcing of the atmosphere from solar irradiance forcing of the atmosphere.

Sensor Miniaturization

On the second flight of the ANDE program (scheduled for mid-2009), one spacecraft will carry miniaturized sensors to measure the density and composition of the atmosphere. NRL has collaborated with NASA Goddard Space Flight Center to develop a small wind and

temperature spectrometer (Figure 4). The technology push to reduce the size, weight and power of such sensors is pivotal for multi point in-situ space weather sensing.
[Sponsored by NRL and ONR]

References

[1]Nicholas A.C., Thonnard S.E., Galysh I., Kalmanson P., Bruninga B., Kelly H., Ritterhouse S., Englehardt J., Doherty K., McGuire J., Niemi D., Heidt H., Hallada M., Dayton D., Ulibarri L., Hill R., Gaddis M., Cockreham B., "An Overview Of The ANDE Risk Reduction Flight", Proceedings of the AMOS Technical Conference, Maui, HI., Sept. 2002.

[2]Nicholas A.C., J. M. Picone. J. Emmert. J. DeYoung, L. Healy, L. Wasiczko. M. Davis, C. Cox, "Preliminary Results from the Atmospheric Neutral Density Experiment Risk Reduction Mission", Proc. of the AAS/AIAA Astrodynamics Specialist Conference, paper #AAS 07-265, Mackinac Island, MI, Aug 20-24, 2007.

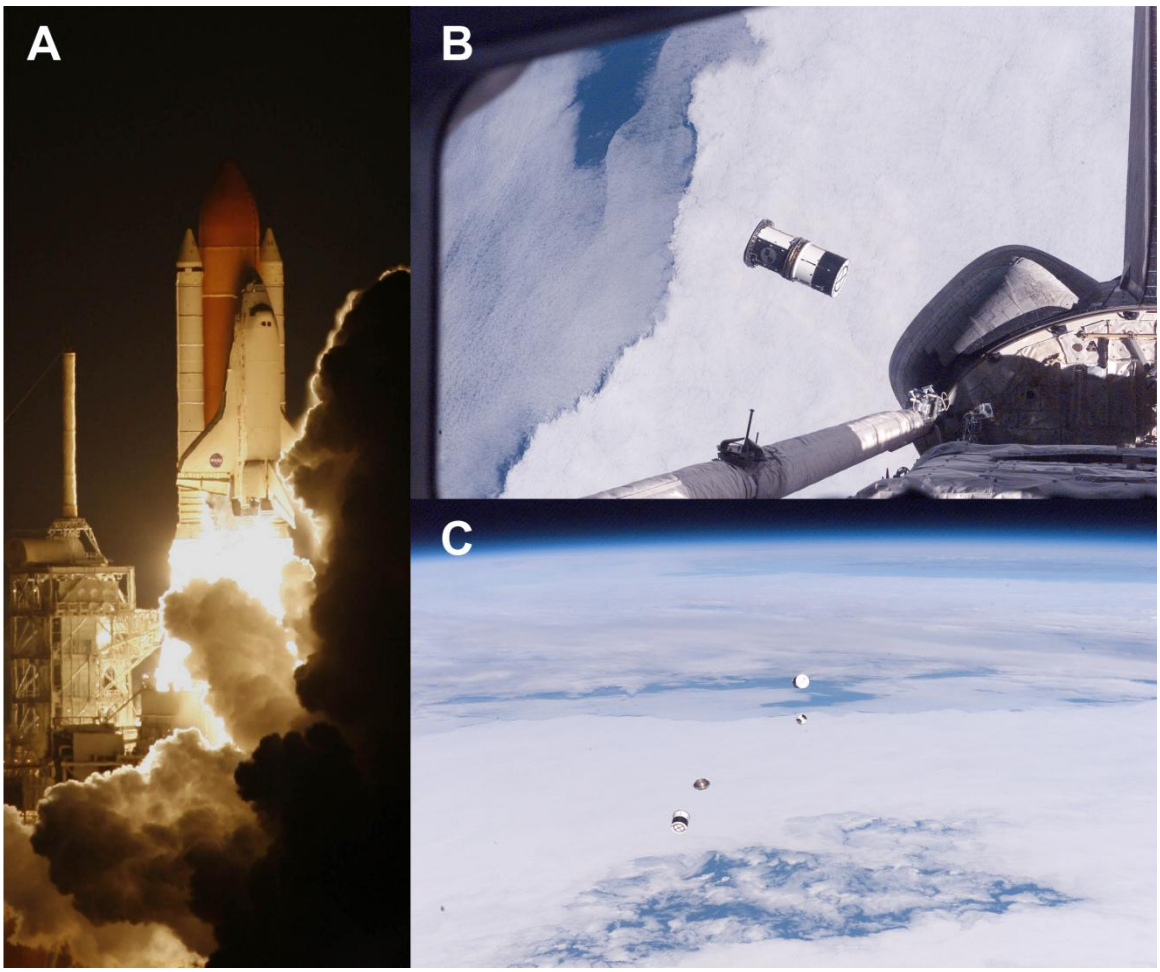

Figure 1. Depicts the launch (a) and deployment (b,c) of the Atmospheric Neutral Density Experiment Risk Reduction (ANDERR) spacecraft from the space shuttle Discovery on December 21, 2006 during the STS-116 mission. (Photos courtesy of NASA)

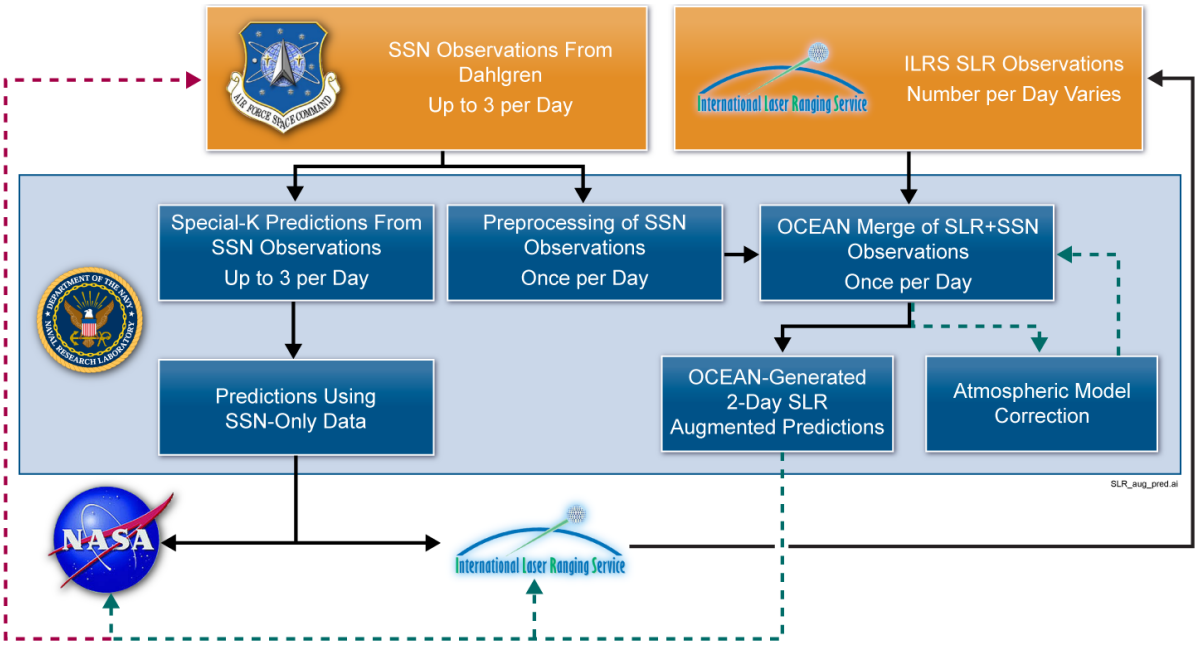

Figure 2. A schematic of the data flow and processing of ANDE observations, green dashed lines represent functions demonstrated during the ANDERR mission. The red dashed line is expected to be complete after the final ANDE flight.

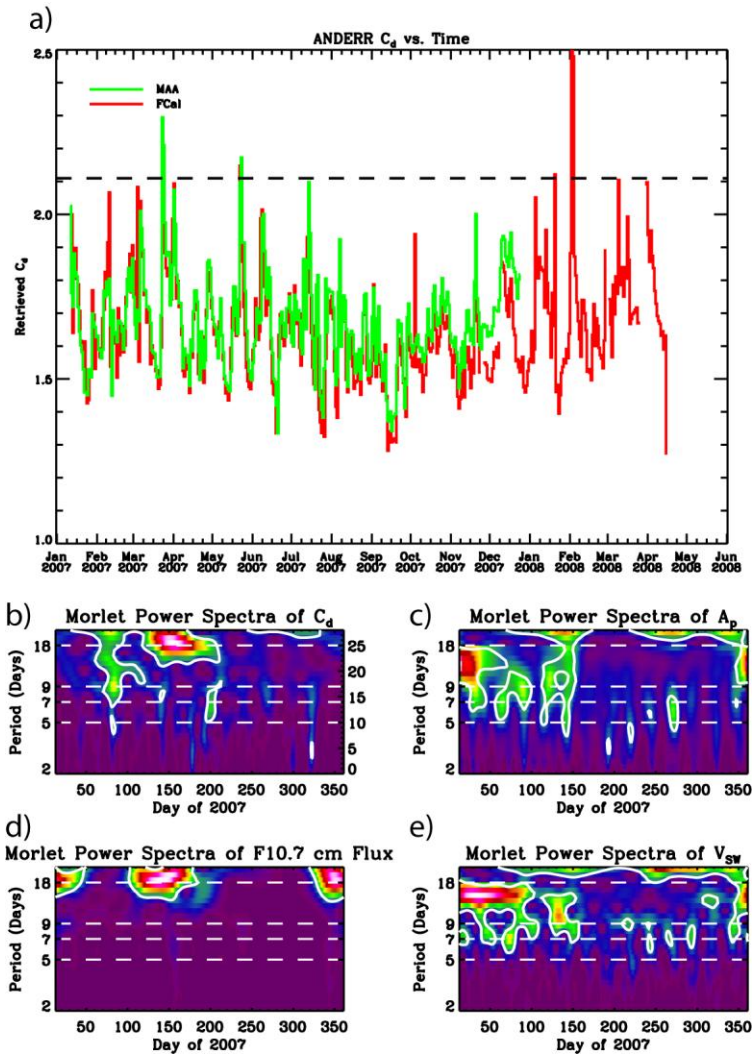

Figure 3. (a) OCEAN fitted C_D values, using NRLMSISE-00 for the ANDERR spacecraft. (b-e) Morlet power spectra for the C_D, A_p, F10.7 and V_{sw} respectively. The white contour is the 95% significance level.

Figure 4. The ANDE Wind and Temperature Spectrometer.

Considerations for an optical link for the ACES mission

Ulrich Schreiber[1], **Ivan Procházka**[2]

[1]Technische Universität München,
FESG – Geodätisches Observatorium Wettzell, 93444 Bad Kötzting, Germany
[2]Czech Electrotechnical University, Brehova 7, 11519 Prague 1, Czech Republic

Abstract

The design of an atomic clock ensemble to be operated on the International Space Station (ISS) is currently under development in Europe. This experiment constitutes a high precision timescale in space and offers the great opportunity to study the behavior of "state of the art" atomic clocks in a micro-gravity environment. A key element for this project is a microwave link between one or several ground stations and the ISS clock ensemble. Due to systematic delays on the propagation path of the microwave link (insufficient knowledge of the dielectric number as a function of time in the troposphere and ionosphere and phase center variations) there remains an uncertainty in the time comparison (ie. the time difference of a specific epoch on the ground and in space) of up to several nanoseconds. Optical technologies, based on time of flight measurements of ultra short laser pulses, offer the prospect to reduce this uncertainty in time comparison to approximately 25 ps one way. The successful LTT (Laser Time Transfer) project on the Chinese Compass M1 satellite is based an earlier version of the proposed experiment below. Furthermore we note, that a similar system, T2L2 (Time Transfer by Laser Link) was initially part of the ESA selection in 1997 for ACES, but shifted to the Jason 2 satellite mission following a re-arrangement of the project in 2000.

Scientific Objectives

Timescale comparisons by GPS and TWSTFT (microwave) techniques are in routine operation for many time laboratories around the world. The comparison of timescales by means of cw optical frequency transfer is the most advanced technique in this respect and has been used to compare optical clocks over distances of several kilometers [1,2]. While this approach essentially works on a narrow bandwidth transmission line, it fails to provide a direct link to an exact epoch (point in time) for the two timescales under investigation with an accuracy of better than several ns. In order to compare the epochs of two widely separated timescales at high precision, one has to apply a broadband technique such as the time of flight measurement of ultra-short laser pulses. Such an approach is characterized by several critical aspects, which are:

- Geometrically well defined start point of optical range measurement
- A well defined propagation path with clearly modeled path delays (given in the visible)
- Geometrically well defined end point of optical range measurement
- 2- way ranging to establish a precise distance and to derive the epoch of arrival at the ISS
- Low jitter conversion of laser pulse to time (epoch)

The ACES mission provides a unique opportunity for the evaluation of the limits in precise clock comparison investigation. The existing microwave link serves as a reference against

which the optical technique can be compared. Apart from improving the atmospheric propagation models by comparing the refractive index to the microwave propagation delay (including phase center stability of the microwave antenna), SLR will provide independent precise optically derived orbits of the ISS as well as a link between a timescale on the ground and the ACES timescale with an accuracy of about 100 ps.

Method

Satellite laser ranging (SLR) provides a viable technique to achieve these objectives. However some detailed considerations are required to utilize the full potential. When the time of arrival of a laser pulse is determined, the corresponding epoch is not obtained instantaneously. The conversion process of an optical pulse to an electrical signal causes a delay and the mapping of this electrical pulse on the timescale of a clock is subject to further delays. These delays are usually not constant and among other effects they vary as a function of operating temperature and signal strength. In order to minimize these influences, SLR adopts frequent system calibration procedures, where the time of flight of laser pulses over an a priori known distance are used to establish the currently valid value of this unavoidable system delay. In order to do a time comparison between a precise clock on the ground and the atomic clock ensemble in space SLR operations to a corner cube on the satellite are an essential ingredient. From SLR ranges one can precisely compute the time of arrival of the laser pulse at the location of the corner cube of the satellite with respect to the timescale of the SLR system on the ground, in turn can be used to relate the timescale on the ground to the timescale of the atomic clock ensemble. The corresponding epoch t_{rec} of the time of arrival of the laser pulse at the spacecraft with respect to the timescale established by the atomic clock ensemble is

$$t_{rec} = t_{start} + \frac{r}{c} + \tau_{sat} + \tau_{off} ,$$

where t_{start} is the epoch when the laser pulse passes the reference point of the SLR system on the ground. τ_{sat} is the internal timing delay on board of the satellite and τ_{off} is the offset between the timescale on the satellite and the timescale on the ground. It is important to note that the quantity *r/c* can be determined very well with SLR and that this is the particular strength of the ranging technique. (For simplicity this discussion does not look at relativistic effects or clock drifts.) In order to determine the best available value for τ_{off} as the prime quantity of interest, τ_{sat} must be both established well and be kept as constant as possible. This is where the ultimate challenge of the clock comparison sits. Apart from electronic delays the conversion of light into an electrical signal represent the most critical components in the ranging link. The delay associated with the generation of photo-electrons from an incidence light pulse (photoelectric effect) depends very much on the input signal strength, which in turn is hard to control because of the speckle nature of the SLR pulse as a result of passing through the turbulent atmosphere. Figure 1 shows the modeled delay for the generation of an electrical output pulse from 3 different levels of optical input intensity for a silicon solid state detector [3] with thick absorption layer.

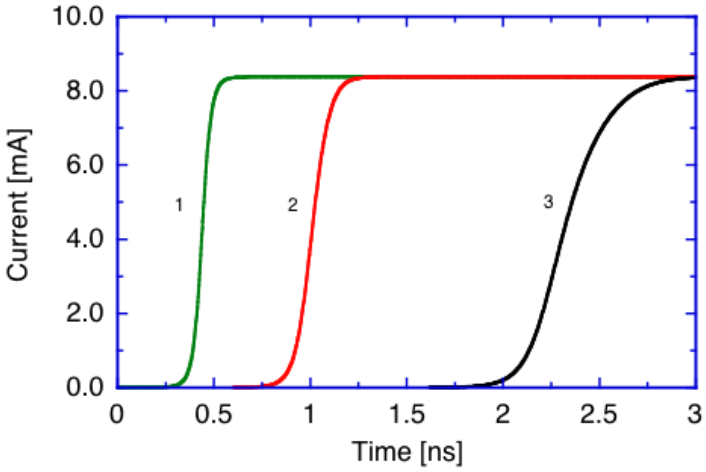

Figure 1. Output signal response to an input light pulse at t = 0, for a strong signal of 100 photo-electrons (1), a moderate signal of 10 photo-electrons (2) and a single photo-electron (3).

For the model 3 different levels of signal strength have been investigated ie. 100 photo-electrons (1), 10 photo-electrons (2) and 1 photo-electron. As one can see from fig. 1, one obtains the shortest delay for the strongest input signal. This reduction in response time comes from a shortcut of the electron multiplication process in the avalanche region of the semiconductor. Intensity variations therefore lead to a varying delay and are extremely hard to quantify. However, if the input light level is reduced so much, that the detector strictly operates in the single photo-electron regime, the corresponding timing-jitter is minimized. Thin layer photo-detectors, such as the K14-SPAD [4] reduce the unavoidable jitter approximately by a factor of 5. This comes at the expense of sensor sensitivity, but for the ranging to the ISS this drawback is not an issue.

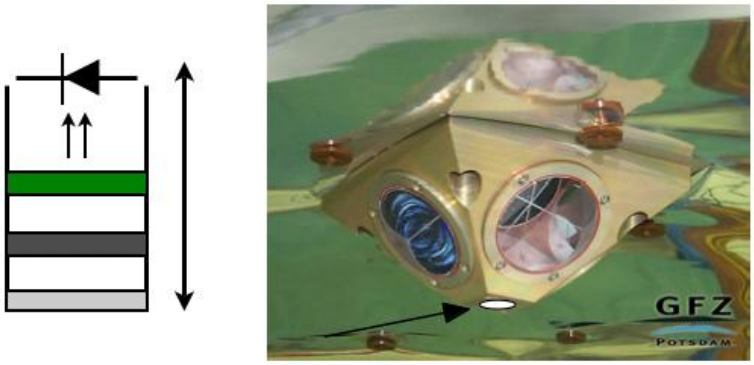

Figure 2. Retro-reflector as used on the Satellite Champ. Only one corner cube contributes to the echo at each incoming laser pulse. The arrow marks the location, where the wide-angle detector should be located. The left side illustrates the detection scheme (see text for details).

Figure 2 shows the proposed reflector element for the ACES project. It mainly uses the GFZ design, which has been successfully applied to the Champ satellite. At the location indicated on the lower part of the photo in Fig. 2 the wide acceptance angle photo-detector arrangement is located. The basic principle of the detector arrangement is sketched on the left

side of fig. 2. The light enters at the lower part of the sketch. An optional diffusor plate sits at the beginning of a small 1 – 2 cm long duct in order to scatter the incoming light evenly around the duct. This is followed by a spectral filter (bandwidth 0.3 to 10 nm, the exact value to be yet determined) around the frequency doubled Nd:YAG laser line (532 nm). A K14-SPAD is located at the bottom of the duct. This avalanche diode is operated in the Geiger mode with a gate pulse derived at equidistant time intervals from the onboard timing system. As a consequence of this, the ranging procedure requires all participating laser stations to fire laser pulses such that the arrival time at the satellite is pre-determined to within $\sim < 1$ μs. This procedure has been successfully tested on the Chinese Compass-M1 satellite [5]. The detected laser pulses are timed on the satellite with respect to the local timescale. The length of the receiver duct along with the diffuser and the input aperture determines the total attenuation of the incoming laser beam in order to operate the photodiode in the single photo-electron regime for low jitter detection.

Principle of Operation

The principle of operation is based on low light flux time coherent detection of laser pulses and aims at synchronizing transmitter and receiver such, that the laser pulse arrives at the receiver shortly after the activation of the gate-pulse required for Geiger mode operation [6,7]. Since only the first photo-electron after gate-on can be detected and timed, the signal of interest has to arrive earlier than a statistically probable noise event. If the laser pulse arrives at the detector on the satellite within the first 100 ns, the probability of obtaining a valid datation on board of the satellite is very high. For the ACES mission the following cases of illumination and a constant flux-rate of the sun as parameterized below have been used:

Solar induced average photon flux is: 0.2 watts/m^2/0.1 nm (wavelength window). This corresponds to 10^{18} photons/s/m^2/0.1 nm. The Earth albedo is assumed to be 10%. The field of view of the detector on the satellite is approx. 1 radian at about 400 km altitude.

Case 1 – Detector illuminated by direct sunlight: > 10^{10} photons per second

photon-counting impossible, however there is no damage on the photodiode and the recovery of the photodiode takes place within a few seconds after the full illumination.

Case 2 – Daylight operation, the entire footprint on the Earth illuminated by sunlight

$3*10^{12}$ photons/s/10 nm on detector active area diameter of 1 mm
$1*10^{11}$ photons/s/10 nm on detector active area diameter of 200 μm
$2*10^{9}$ photons/s/10 nm on detector active area diameter of 25 μm

Case 3 – Night time on entire footprint with a reduction on photon flux of a factor of 1000, which is a pessimistic estimate.

$3*10^{9}$ photons/s/10 nm on detector active area diameter of 1 mm
$1*10^{8}$ photons/s/10 nm on detector active area diameter of 200 μm
$2*10^{6}$ photonos/s/10 nm on detector active area diameter of 25 μm

The above listed values correspond to a worst case scenario estimates. The back–ground photon flux depends, among others, on the optical receiver filter bandwidth. A 10 nm

bandwidth is used for the calculations above. With a narrower filter bandwidth the background photon flux is decreased linearly, e.g. 30 times less for 0.3 nm filter. However this must be balanced against the desired operational robustness of the receiver unit, which improves with wider filters.

System Requirements

There are essentially 3 relevant subsystems to consider. These are a) the retro-reflector assembly, b) the optical receiver and c) the event timing unit. All of these subsystems are discussed individually below:

a) Retro-reflector Assembly: As indicated in figure 2, a modified version of the Champ or Grace reflector array design is proposed. The metal part of the assembly is with 10 cm length on a side slightly larger than for the mission Champ and Grace, since it will also house the active optical receiver element. Approximately 1 cm increase in length and width of the baseplate is required for that purpose. The corner cubes have already demonstrated their suitability for a low Earth orbiter application. There are no ambiguities for SLR applications since only one corner cube is contributing to the signal at any laser shot from any direction and with a theoretical cross section of ca. 1 million square meter it is an easy SLR target. At the same time the optical receiver can be reached from any directions with the exception of low elevation angles of the satellite relative to the observing SLR station. The eccentricity between the CCR-Array and the geometric point of reference of the atomic clock ensemble has to be determined with millimeter accuracy prior to the launch of the payload. The weight of the CCR-Array is below 0.5 kg.

b) Optical Receiver: The basic design of the optical receiver contains 3 parts. These are the detector optics, the photo-detector itself and the necessary electronic circuits. The latter in particular consists of a gating circuit, a break-down quenching circuit, the detector chip temperature control, the gate voltage biasing circuit and the power supply, which generates all required voltages out of the +/- 5 Volt supply voltage from the general supply line. Depending on the general design of the ACES package, it has to be determined whether the electronic circuit will be located inside the CCR-Assembly or inside the ACES package. The power requirement for the entire detector package is typically below 3 watts at maximum. The detector optics, consisting of the diffusor plate, the spectral filter, something between blocking glass with 10 nm of bandwidth or an interference filter of 0.3 nm bandwidth and maybe an iris or baffle for the reduction of unwanted background light result in a unit with a volume of about 3 square centimeters, no requirement for power and about 25 grams of weight. This includes also the K-14 SPAD (photo-detector). In particular we propose:

200 μm detection chip K14 SPAD, vacuum housing, TE temperature stabilization
timing resolution: 30 ps (rms)
timing stability: ≈ 10 ps
power consumption: 3 Watts
weight: optics and detector electronics: ≈ 500g
temperature range: -30… +30 C
For stabilized temperature (+/- 2 K), higher timing stability (1ps) is obtained
Gate time before event: > 0.1 μs (fully illuminated FOV)
>20 μs (full darkness)

c) Timing Electronics: The epoch of the arrival of the laser pulse at the spacecraft has to be recorded on the onboard timing system. This function is obtained from the PRARE microwave system, which provides a synchronized timescale between a suitable microwave transmitter/receiver station on the ground and the ACES payload. The output of the optical detector package is a NIM-pulse with very sharp rise time, which is passed on to the PRARE system. Figure 3 shows the FPGA hardware dedicated for the timing of the optical signals as provided by TimeTech GmbH.

Figure 3. Prototype of the event timing hardware on the microwave link electronics.

The PRARE package determines the corresponding epoch of the leading edge of the pulse and also handles coarse filtering functions, the telemetry of the recorded events to the PRARE ground stations and generates the required Geiger mode gates for the K-14 SPAD. Appropriate repetition rates have to be defined by the science team. They may cover a range from 10 Hz up to 10 kHz. The limiting factor will be the allocated bandwidth of the telemetry down link rather than technical reasons on the detector package or at the PRARE control system. Figure 4 gives a block diagram of the general concept of the optical link with respect to the entire ACES payload.

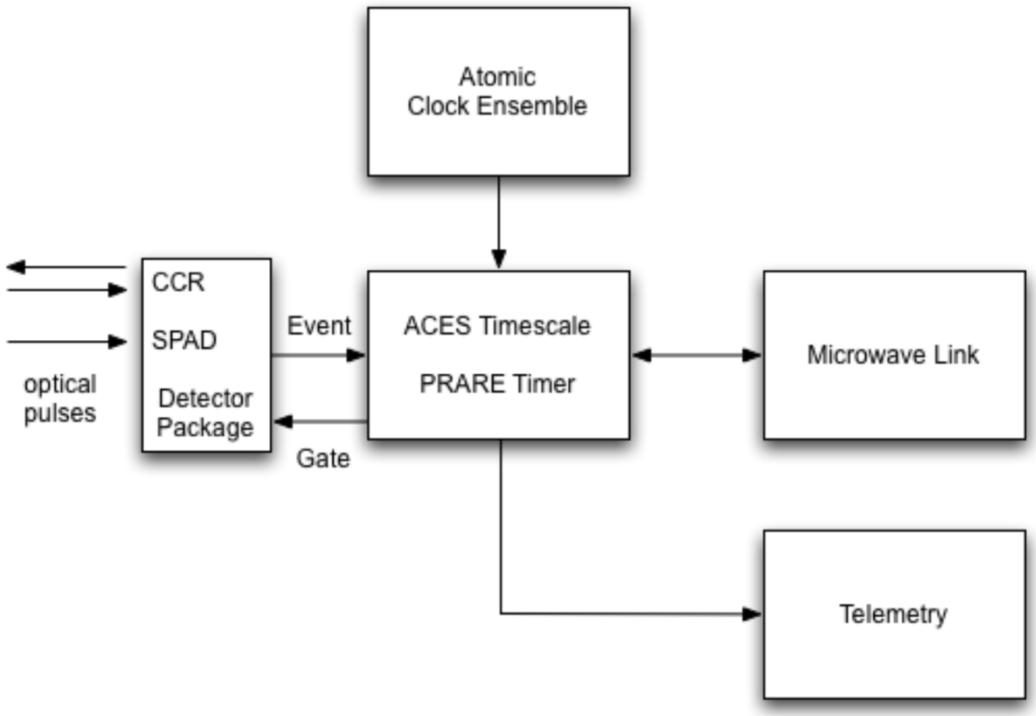

Figure 4. Simplified block diagram of the ACES payload and the interfacing to the optical timing package.

It can be seen, that the required modifications to the ACES payload are minimal. Furthermore, both weight and power consumption of the optical package are low.

d) Operating Modes: All participating SLR stations have to have the ability to fire the laser at a predefined epoch with a required accuracy of about 0.1 μs in order to contribute significantly to the data yield for a fully illuminated Earth in the field of view. This condition relaxes by 1 – 2 orders of magnitude for an entirely dark footprint of the detector on the ground. Furthermore they have to time the start epoch of laser fire preferably to much better than 100 ps of resolution. Finally the stations must be capable of generating fullrate SLR observation data, in order to allow the time comparison between the timescale on the ground and at the atomic clock ensemble in a post-processing analysis step independent from the ranging network. Therefore the impact of this mission on the tracking network in terms of hardware requirements is minimal. Furthermore the operation follows standard ILRS ranging procedures. In order to guarantee eye-safety at the ISS (if applicable) the ILRS has a number of established procedures such as elevation or time restricted tracking as well as laser output power control (both by increased beam divergence and reduction of transmit energy.

e) Laser Tracking Calibration: As shown in the range equation in the introductory part of this proposal, there are several extra delays to be dealt with. While τ_{off} is the offset between the timescale on the ground and the timescale of ACES and hence the quantity of interest, τ_{sat} describes the internal signal delay at the satellite. This delay is caused by cables, the transfer time of the signal in the detector unit and by varying signal levels at the photodiode. Cable, detector and electronic delays have to be calibrated preflight. They are constant over the mission, if the detector and subsequent electronics are temperature controlled and the optical signal level is kept at or below the single photo-electron level, corresponding to state 3 in fig. 1. Using a second channel for event timing would provide the possibility to also evaluate characteristics of the rise-time of the signal and classify them with respect to the optical signal strength. So signal levels corresponding to the states 2 and 3 can be identified, tagged and removed from the time comparison process. This mode of operation has to be implemented by preflight laboratory calibrations. Standard ILRS network calibration procedures are removing ground station biases from the round trip ranging to the ACES optical detector package. Laser ranging stations with a good timing system like the H maser timescale in the Wettzell observatory will provide the most significant input to the optical tracking to the ACES package.

Conclusion

The Chinese Compass M1 mission as well as T2L2 have demonstrated that time transfer via an optical laser link is a viable application for comparing the timescale between ground and satellite as well as between to remote locations on the ground (common view and non-common view). From that point of view it is a challenging task to extend the time transfer to a precise clock ensemble in a microgravity environment, which is tied to the ground with a two way microwave satellite time and frequency transfer unit, one of these components providing the necessary event timing capabilities. Apart from linking two distinctly different high precision time transfer techniques together, such an experiment will allow a study of residual refraction uncertainties between the optical and the microwave regime. We hope that this time transfer experiment can be eventually accommodated on the ACES space segment.

References

1. Martin M. Boyd, Andrew D. Ludlow, Sebastian Blatt, Seth M. Foreman, Tetsuya Ido, Tanya Zelevinsky, and Jun Ye, **Physical Review Letters** 98, 083002 (2007).
2. Seth M. Foreman, Andrew D. Ludlow, Marcio H. G. de Miranda, Jason E. Stalnaker, Scott A. Diddams, and Jun Ye, **Physical Review Letters** 99, 153601 (d2007)
3. U. Schreiber, A. Schlicht, K.H. Haufe; **Proceedings of the SPIE**, Vol. 3865, 64 – 73, (1999)
4. Ivan Prochazka, Karel Hamal, Lucas Král; **Journal of Modern Optics,** Vol. 54, No.2-3, p.151-162, (2007)
5. Ivan Prochazka, Yang Fumin; Photon counting module for laser time transfer via Earth orbiting satellite, accepted for **Journal of Modern Optics**, 2008
6. A.W. Lightstone, R.J. McIntyre; IEEE Trans. Electron Devices, **ED-28**, 1210, (1981)
7. U. Schreiber, K.H. Haufe, J-F Mangin, J-M Torre, C. Veillet; Proceedings of the SPIE, Vol. 2310, 25 – 32, (1994)

Aircraft Illumination Avoidance Using Infrared and Radio Detection

T. W. Murphy, Jr.[1], W. A. Coles[1], C. D. Hoyle[2], K. H. Kassabian[1], J. F. Melser[1], H. E. Swanson[3], J. K. Tu[1], A. A. White[1]

[1]University of California, San Diego, La Jolla, CA, USA
[2]Humboldt State University, Arcata, CA, USA
[3]University of Washington, Seattle, WA, USA

Abstract

We describe here a dual passive aircraft avoidance system involving both infrared and radio detection of aircraft in the vicinity of a transmitted laser beam. The infrared imager detects image motion of a thermally emissive source against the cold backdrop of space, while the radio receiver detects transmissions at 1090 MHz from the aircraft transponder. Together, these systems form a semi-redundant but complementary scheme for aircraft avoidance.

Introduction

The transmission through the atmosphere of a laser beam whose energy density exceeds the eye-safe threshold requires safety precautions. In the U.S., the Federal Aviation Administration (FAA) recognizes human spotters with laser kill-switches and eyes on the sky as appropriate hardware, but has typically not endorsed possibly more robust and sensitive technological solutions to the problem. We have developed a scheme that may satisfy FAA requirements and transform the way laser-transmitting observatories currently operate. Rather than relying on active radar—which must send powerful pulses of radio frequency (RF) energy in order to cope with the $1/r^4$ signal loss, possibly disrupting electronic activities at the site—we use strictly passive systems that have no possibility of creating local problems. The first we describe is an infrared camera taking video-rate images and sensing motion of an infrared-detectable source within the field of view. The second, and more powerful method is the detection of RF pulse-trains from the transponders installed in virtually every airplane. We describe these systems in greater detail below.

Infrared Camera System

We purchased an infrared camera detection system from Image Labs in Bozeman, MT. The camera images a 5°×7° field of view at thermal infrared wavelengths. A source need not generate power on board to be visible. The thermal emission from the surface of an object at even –20°C (253 K) outshines the cold background sky, which may be well below 200 K within an atmospheric-transmission band. The camera takes 30 images per second, and looks for an object that is moving in three consecutive frames. Software makes a decision about whether the object is likely to be a real aircraft (rather than a bird, bat, or moth) based on trajectory and angular velocity.

The infrared system has a range limit for small airplanes of about 5–8 km, after which the object spans a smaller solid angle than an individual pixel and begins to be diluted. So the infrared system is optimal for nearby airplanes. A worst-case scenario might have a small plane traveling at 100 m/s at a distance of 200 m. The airplane will therefore have an angular velocity of 0.5 rad/s, crossing *half* the roughly 0.1 radian field of view in 0.1 seconds, which is

three frames at video rate. Thus the system is *just* capable of protecting against such an extreme (thus rare) event.

Transponder Detector Overview

In the U.S., all commercial airplanes, and all airplanes traveling above 10,000 feet (3048 m)—except within 2500 ft (762 m) of the surface—are required to carry an operating transponder. Periodic interrogations from ground radar stations and other airborne aircraft request a response from the transponder. Depending on the interrogation, the response may be Mode-A (temporary 12-bit aircraft identity), Mode-C (12-bit encoded altitude), or Mode-S (variable length data packets that can be permanent aircraft identification, present coordinates, etc.). In all cases, the transponder sends ~0.5 μs pulses of RF energy at 1090±3 MHz. For small planes, the peak power must be at least 70 W, while for commercial planes, the peak power must be at least 125 W. In no case is the peak power permitted to exceed 500 W. Commercial planes also send unsolicited Mode-S pulse streams once per second even in the absence of interrogations.

The strong signal levels make detection of the pulses straightforward even at distances well in excess of 100 km. In practice, airplanes over the relatively remote southern New Mexico skies transmit about 15–40 transponder pulses per second. But even if this were cut to a single transmission per second, a detection scheme capable of sensing that a source is within 15° of the laser transmission axis would conservatively protect the aircraft at angular rates up to 12° per second, or 0.2 rad/s. This is not as fast as the infrared camera, and it is in this respect that the systems are complementary: the infrared system handles nearby high-angular-rate airplanes, while the transponder system is suited for distant aircraft beyond the range of the infrared camera. However, the two systems have substantial overlap. An aircraft traveling at the speed of sound travels less than 0.2 rad/s at a distance of 2 km, which is well within the sensitivity range of the infrared camera. Because the transponder system is the main innovation in our detection scheme, we spend the rest of the paper discussing the details of its design and operation.

Transponder Detector Concept

In order to be effective, we need directional sensitivity to radio signals at 1090 MHz, independent of distance or power transmitted. We also would like narrow-band performance so that we may be less sensitive to RF activity away from 1090 MHz. We have therefore chosen to use patch antennas arranged in a phased array to accomplish these goals. Patch antennas are naturally narrow-band (roughly 1% bandpass if fabricated on standard circuit board material), and convenient for mounting on a plate in front of the telescope. We fabricated patches on low-loss circuit board material, with dimensions tuned to deliver 50 Ω impedance (maximizing power received) at exactly 1090 MHz. We studied a variety of array configurations, and selected a hexagonal symmetry employing a central patch surrounded by a ring of six patches. This choice gave the best compromise between beam width and sidelobe levels of the options we studied (also a six-element pattern with five-fold symmetry and a 9-element array on a square pattern).

By comparing the array signal, which has a narrow beam width, to that from a single patch antenna, which has a broad beam width, we may discern when the signal originates from the main beam—independent of signal level. This is possible because the array signal is only greater than the broad signal within the main beam: the array sidelobes are always lower than the broad antenna response. Figure 1 illustrates the antenna response as a function of angle.

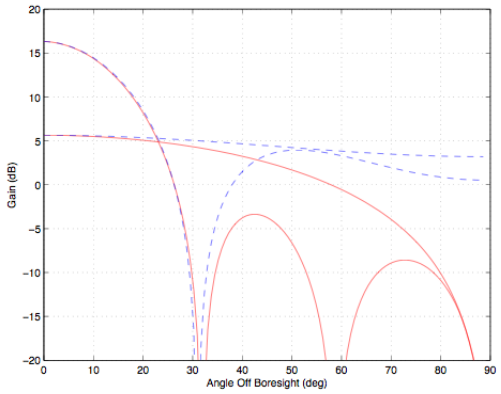

Figure 1. Gain of the broad-beam and narrow-beam antennas as a function of the angular separation of the transponder from the axis. The lines plotted in solid red are H-plane cuts through the gains of the antennas actually used and the lines plotted in dashed blue are E-plane cuts. If the antennas are pointed to zero elevation, the E plane is the vertical plane and the H plane is horizontal. The power received is proportional to the gain.

The ratio of the array signal to the broad signal is then 11 dB in the center of the beam, dropping to 0 dB (equal) at about 23°. The ratio of beams is shown in Figure 2.

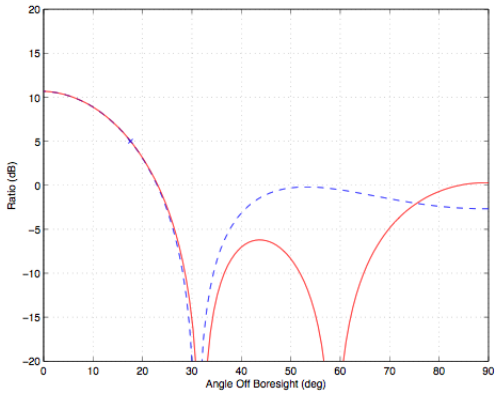

Figure 2. Cuts through the ratio at azimuths ϕ = 0° (red solid line) and 90° (blue dashed line), corresponding to the highest sidelobes. The "x" marks a robust detection threshold for concluding that aircraft is too close to the beam axis.

The advantage of the ratio measurement is that details of transmitter distance, power, polarization, etc. are all common-mode and do not impact the ratio. Thus requiring an array/beam ratio of 5.5 dB translates to a beam half-angle of about 17° in our design, which is appropriate for the task.

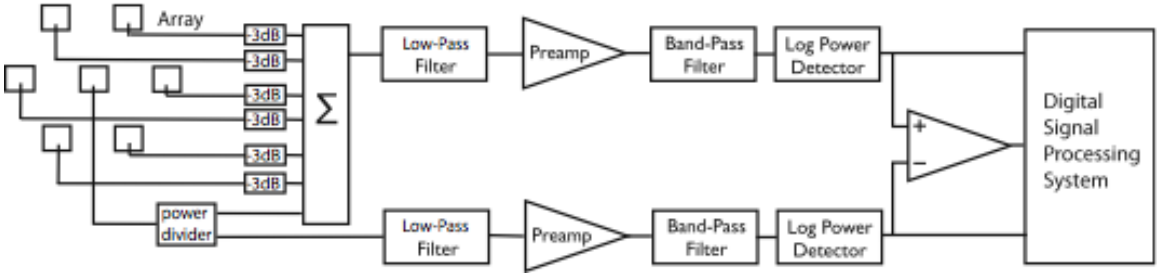

Figure 3. Block diagram of the analog signal flow. The patches are shown with the E-field vertical. The azimuthal angle is defined with respect to the horizontal. The array is drawn approximately to scale. The center patch is used both as an array element and as the broad beam element.

Figure 3 shows the electronic implementation of the transponder detector system. We use the central patch antenna both as an element of the array and as the single broad-beam antenna against which to compare the array signal for a ratio. To do this we split the power from the central element into two equal components, one for the array, and one for the broad-beam receiver. To compensate for this the other array elements must be attenuated by a factor of two (–3dB), so all seven elements are added with equal power levels to form the array output. For each chain, a filtered and amplified signal is presented to a logarithmic power detector. The difference in outputs of these two power detectors is therefore proportional to the ratio of the directional to broad signals. A signal processor then makes decisions about shuttering the laser based on the beam ratio and also absolute strengths of the input signals. For instance, if either of the signals is strong enough to saturate its power detector, the laser should be shuttered regardless of what the ratio comparison reports.

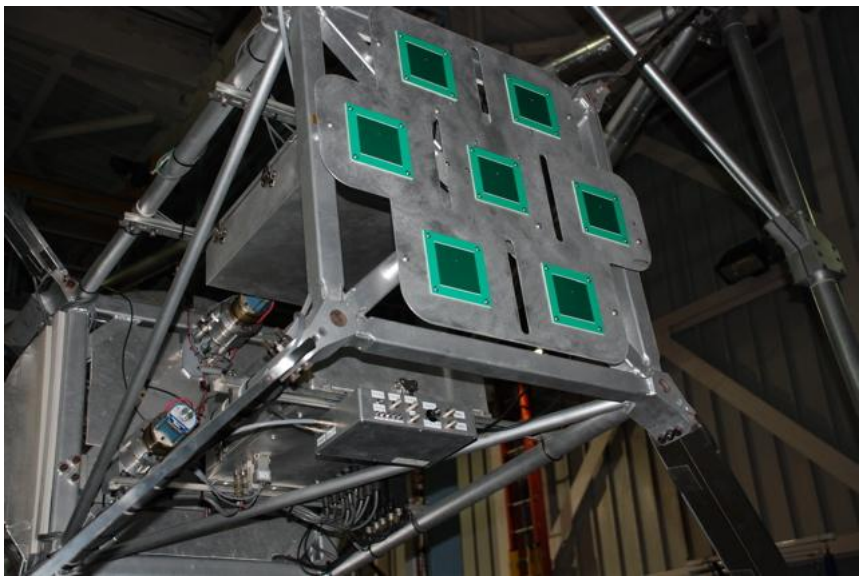

Figure 4. Patch array installed on the Apache Point Observatory 3.5 meter telescope, on the skyward end of the secondary mirror. The small box just below with white labels contains the RF processing electronics.

Figure 4 shows the array as deployed on the Apache Point 3.5 meter telescope in 2008 December. The electronics are split into two boxes—in part to keep the thermal emissions in front of the telescope to < 3 W. The box visible in Figure 4 contains the RF electronics,

difference amplifiers, and discriminators that decide when the signal levels merit laser shutter closure. In a separate location is a box containing the power supply and a microcontroller that is used to capture codes associated with received transmissions so that we may understand more about the airplane responsible for the trigger. In this way, we can recover the identification number and altitude of an airplane crossing the beam. Together with telescope pointing information, we may approximate the range to the aircraft.

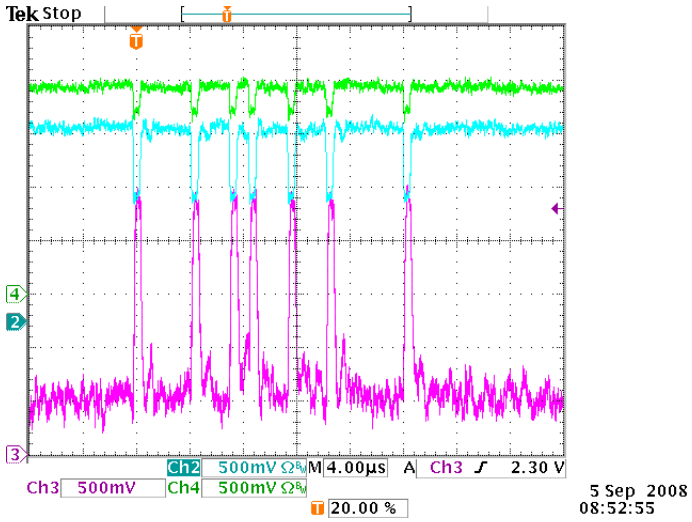

Figure 5. Example pulse train obtained in San Diego, showing both the broad antenna signal (green) and the directional signal (cyan), as well as the output of the difference amplifier (magenta) with a gain of four. The pulse pattern represents the code 4360, which could either be a Mode-A identity or a Mode-C altitude (corresponding to an altitude of 4600 feet). The broad and directional baselines are offset for clarity, and sit at about 2.0 V when no signal is present. In this case, the directional signal is far stronger than the broad signal, indicating that the source is within the primary beam of the array.

Figure 5 shows a representative pulse pattern captured for a plane at an altitude of 4600 feet. A simple threshold on the magenta signal provides an alert to an aircraft in the beam.

The antenna system was deployed on the Apache Point Observatory 3.5 m telescope on 19 December, 2008 (Figure 4). Setting the detection threshold to sense airplanes within 20 km at 70 W peak power, or 52 km at 500 W, we typically record about 12 airplanes per night through the slit of the telescope enclosure, when open. This is based on the first ten full nights of open-dome operation. Note that the solid angle of visible sky is restricted by the dome to a range of 1.9–2.7 steradians depending on telescope elevation angle, averaging only 36% of the sky. Of the ~12 detected planes per night, about three cross the threshold to qualify as an "in-beam" detection, resulting in an average of 100 s of shuttered time per night, out of about 44,000 s of open time (~0.2% closure). As yet, there have been no false closures not associated with aircraft. Typical detection rates are about 15 events per second during a pass, about 40% of which are associated with Mode-C altitude codes, 25% associated with Mode-A identity codes, 30% with distance measuring equipment (DME: also at 1090 MHz) pulses, and 5% identified as Mode-S information packets. We decode and record the Mode-A and Mode-C information, but cannot decode the Mode-S information with the present microcontroller. Figure 6 demonstrates the behavior of a typical beam-crossing detection. The metal dome shields the antenna from line-of-sight detection at large angles, which results in a relatively tight

truncation of the sequence. The central beam crossing is robustly detected in 408 events, roughly centered in the crossing of the open dome slit.

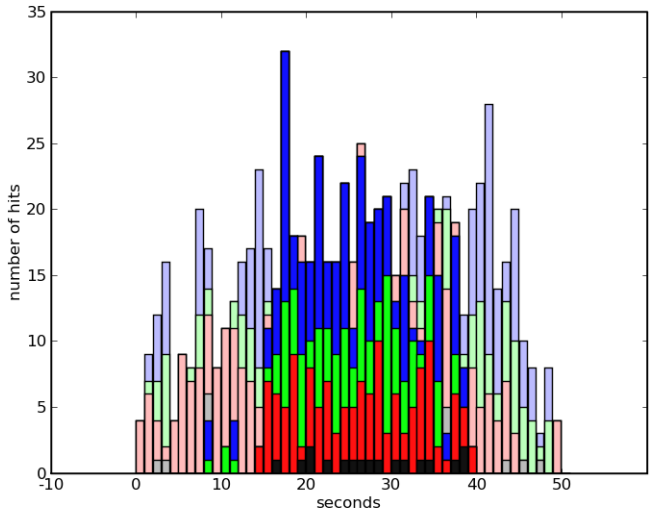

Figure 6. Event rate in 1 s bins for a pass acquired on 31 December 2008, for an airplane squawking identity code 6755 at an altitude of 39,000 ft, while the telescope was at an elevation angle of 54°. Event types are coded as blue for identity (Mode-A), green for altitude (Mode-C), red for DME, and black for Mode-S. Saturated shades represent those detections deemed to be in the central beam by the ratio criterion.

More details on the design and construction of the transponder antenna array will soon be published in Coles et al. (2009).

References

W. A. Coles, T. W. Murphy Jr., J. F. Melser, J. K. Tu, A. A. White and K. H. Kassabian, *Publications of the Astronomical Society of the Pacific*, in preparation, (2009)

Implementing the Consolidated laser Ranging Data (CRD) Format throughout the ILRS Network

R. L. Ricklefs[1], C. Noll[2], J. Horvath[3], O. Brogdon[3], E. C. Pavlis[4]

[1]The University of Texas at Austin, Center for Space Research
[2]NASA Goddard Space Flight Center
[3]HTSI
[4]University of Maryland, Baltimore County, Joint Center for Earth Systems Technology

ricklefs@csr.utexas.edu

Abstract

Technological changes in recent years and new missions such as LRO and T2L2 with novel use of laser signals mandated the revision and consolidation of the various ILRS data formats. The new laser data format is required to accommodate higher precision laser data and include additional data fields with ancillary information. After several years of development, the Consolidated laser Ranging Data (CRD) format, which accommodates full-rate, sampled engineering, and normal point data in a unified, expanded, flexible format, is ready to be implemented throughout the ILRS network. The first step in implementation requires the Operations Centers (OCs) and Data Centers (DCs) to be able to accept and distribute data in the CRD format. Next, a number of analysis centers (ACs) must be able to ingest data in the new format for testing and validating each station's transition from old to new format. Finally, the stations need to produce the CRD format. Owing to the changes in precision and total restructuring of the data format, it has been decided to require validation step for each station's normal points in the new format prior to their being made generally available. The timetable, details, and status of implementation of this plan are presented here.

Introduction

The CRD format [1] was the result of a multi-year effort to create a flexible, expandable format to support current needs and those of future generations of ranging activities. Technology changes such as kHz ranging and multi-channel detectors required rethinking the data format structure and required new data fields. New missions carrying one-way transponders, such as LRO and T2L2, require higher precision timing and additional data fields not present in the old format. Lunar laser ranging (LLR), especially the APOLLO system, also benefits from having a full rate and normal point data format capable of including all the fields needed by analysts.

Current Status

Version 1.00 of the CRD documentation and sample code was released on the ILRS website (http://ilrs.gsfc.nasa.gov/products_formats_procedures/crd.html) on 30 June 2008. Sometime later an "errata page" was published on this website to keep track of minor changes or errors found between releases. An announcement from the ILRS Central Bureau with a call for implementation of the CRD format by stations, analysts, and operations and data centers was emailed on 13 August 2008.

MLRS CRD data, which has been available in various earlier versions, began to be deposited in v1.00 on 7 July, and is currently being validated. Several other stations have recently begun to produce CRD-formatted data. Operations Centers (OCs), Date Centers (DCs), and several Analysis Centers (ACs) are either ready to accept CRD data or will be by the end of 2008. The main thrusts at this time are finalizing the production data flow and procedures for data validation at the OCs and ACs, as well as encouraging the stations and analysts to implement the new format.

Official Timetable

The official timetable included in the ILRS CB announcement contained the following elements. These are already dated as explained below.

1. BY NOW – Stations and ACs should begin conversion to the CRD format.
2. October 15 – NASA OC, operated by HTSI, is ready to accept data in CRD format, to QC old/new format and to perform Validation "Step 2".
3. Dec 1 – Analysis Centers (ACs) will be able to compare data in the old and new formats.
4. April 15, 2009 – All stations must submit data in the CRD format.
5. Dec 31, 2009 – Only CRD data will be accepted and archived.

Normal Point Validation

The CRD format represents a major change in format with increased flexibility and expandability. Due to changes in precision and sequence of records, the addition of new fields, and the variety of ways in which the format can be implemented, CRD normal point content can differ from the old. This means that having different results between old and new format data does not necessarily mean wrong results - see figures 1 and 2. In fact one should expect to see differences when using the CRD format for the same tracking data. Therefore, a formal and thorough validation process is required before CRD-formatted data submission is accepted from a station as the final data product. A flowchart of the validation process is shown in figure 3.

Although full rate and sampled engineering data will also be written in the CRD format, the ILRS will not have a formal procedure to validate these data products. Validating these data types is left as a cooperative project between the stations and the users of those products.

Validation Process Step 1 - Stations

Stations need to implement the CRD format, producing at least normal points in the new format. CRD full rate files are needed for LRO, T2L2 and other investigations. The initial validation will naturally be at the stations. The ILRS CRD sample code will help the stations get started with this task. First, the CRD files must be tested for compliance with the format, which can be accomplished with the ***crd_chk*** program. Next the content of the old and new format files must be compared. Normal points and sampled engineering data can be compared with ***crd_cstg_np_cmp***, while full rate files can be compared with ***crd_merit_fr_cmp***.

When the station is satisfied with its validation results, it may proceed to Step 2

Validation Process Step 2 – Stations contact their OC

At this point the station contacts its OC (HTSI or EDC) with the starting date of CRD-formatted file delivery. The stations are expected to continue sending CRD and old format files in parallel until notified by their OC. As usual, the OC will immediately distribute data in the old format. Meanwhile, CRD normal points will undergo 3 phases of testing before they become publicly available.

Validation Process Step 3 – OCs and ACs

OCs will begin receiving CRD normal points (and possibly full rate and sampled engineering data) from the station. Phase 1 of the validation plan requires the responsible OC, EDC or HTSI, to confirm format compliance and content agreement for the station's normal points using version 1.0 of the CRD sample code. In addition, the OC will flow the normal points through its quality assessment algorithms to insure the validity of meteorological and other data, as described on the ILRS web page. As mentioned above, the content checks may show differences which are not significant to end results of data analysis. This fact prompted the establishment of the next phases of testing.

Phase 2 follows, in which HTSI passes the CRD normal point files through its daily automated prediction generation software package for short-arc comparisons. The short-arc analysis uses NASA Goddard's Geodyn, a well known orbital analysis and modeling package. This step compares the normal points at a higher level, insuring that differences due to precision and filtering do not significantly affect the outcome. Figures 1 and 2 show a pass that fails the content check while passing the more important short-arc analysis.
Once HTSI is satisfied with 2 weeks of CRD deposits from the station, the data is transferred to a hidden directory on the CDDIS ftp site, and the Analysis Working Group (AWG) and designated ACs are notified for the validation process.

A number of the ACs have agreed to test the CRD data by comparing long arcs from the old and new format normal points. Each of the ACs uses a different software suite, so that when all analysts agree that the station has passed its tests, the result will be robust. When the data has passed these tests, the responsible OC is notified.

During this validation process the OC and ACs may find problems with the data, which will be communicated to the station. The station may have to answer questions, resubmit corrected data, and insure that the corrections are in all subsequent data.

The goal is for the OCs to pass the data to the AC after at least 2 weeks of data has passed the validation tests. The ACs should finish their tests in another 2 weeks, limiting the validation period for a station to about 30 days. In reality, this time span will be longer, especially for the first few stations.

Post-validation

Once the responsible OC is notified by the analysts that the data has passed their tests, the OC officially notifies the station with the good news, and the station ceases sending data in the old format. The OC then notifies the DCs, and the DCs store CRD data from the validation period and thereafter in the ILRS archives in CRD-specific directories. Until

January 31, 2010 the OCs will convert CRD normal points for validated stations into the old format and store them in the ILRS archives. This will allow analysis centers to use data from validated stations before they are able to accept CRD files.

A web page showing station validation status and progress is maintained on the ILRS website at http://ilrs.gsfc.nasa.gov/products_formats_procedures/crd_station_status.html. See Figure 4 for an example.

Conclusion

The ILRS community will immediately begin converting its processes to produce and use laser ranging data in the CRD format. To minimize the chance that converting to a more complex and demanding format will adversely affects analysis results, a formal data validation procedure has been put into place. With an ambitious plan to complete conversion **by early 2010, starting this process early is essential.**

Acknowledgments

The authors would like to acknowledge their colleagues around the world that have contributed to the design and implementation of the CRD format. Christopher Moore of EOS deserves special recognition for his work in redesigning the initial CRD format and pushing it in a more productive direction. We would also like to acknowledge the moral support from ILRS and funding support from NASA.

References

[1] Ricklefs, R. L., and Moore, C. J. , "Consolidated Laser Ranging Data Format (CRD) Version 1.00", http://ilrs.gsfc.nasa.gov/docs/crd_v1.00.pdf.

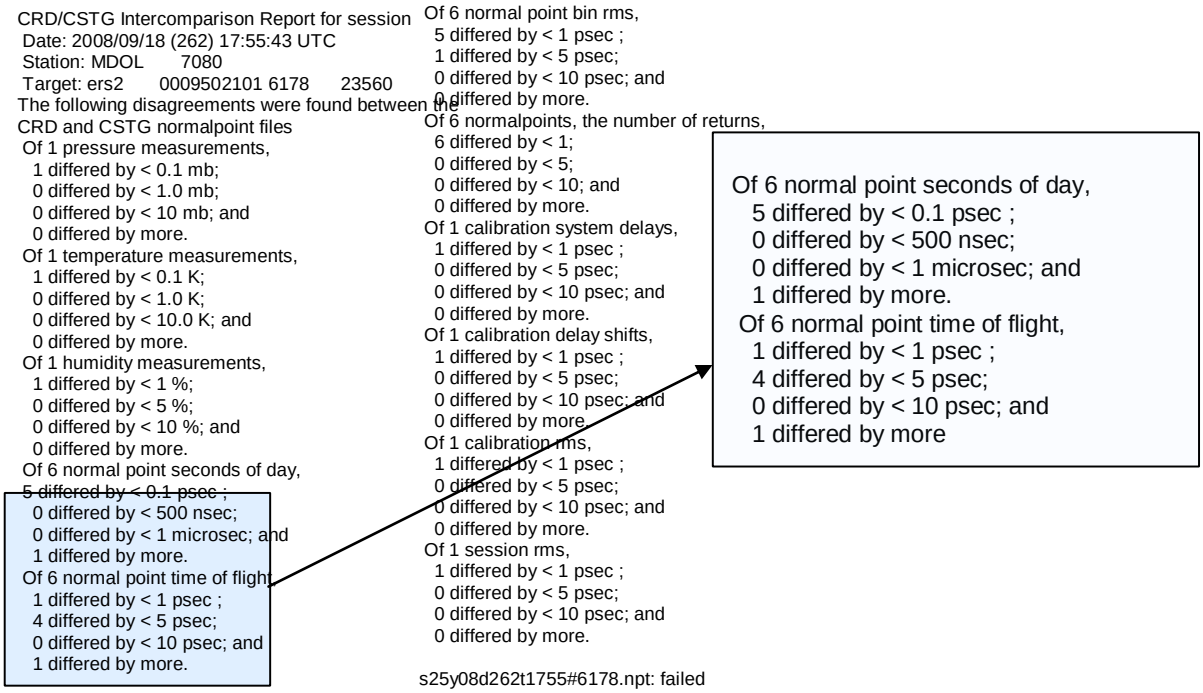

Figure 1. Pass fails content test

RESIDUAL SUMMARY BY STATION

NUMBER	MEAN	RMS	NO.-WTD	WTD-MEAN	WTD-RMS	TYPE	CONFIGURATION	
6	-0.9333	1.0324	6	**-0.9333**	**1.0324**	2W RANGE	MLRS1CRD	9502101
6	-0.9412	1.0403	6	**-0.9412**	**1.0403**	2W RANGE	MLRS1 NP	9502101

Figure 2. Same pass successfully passes short arc test

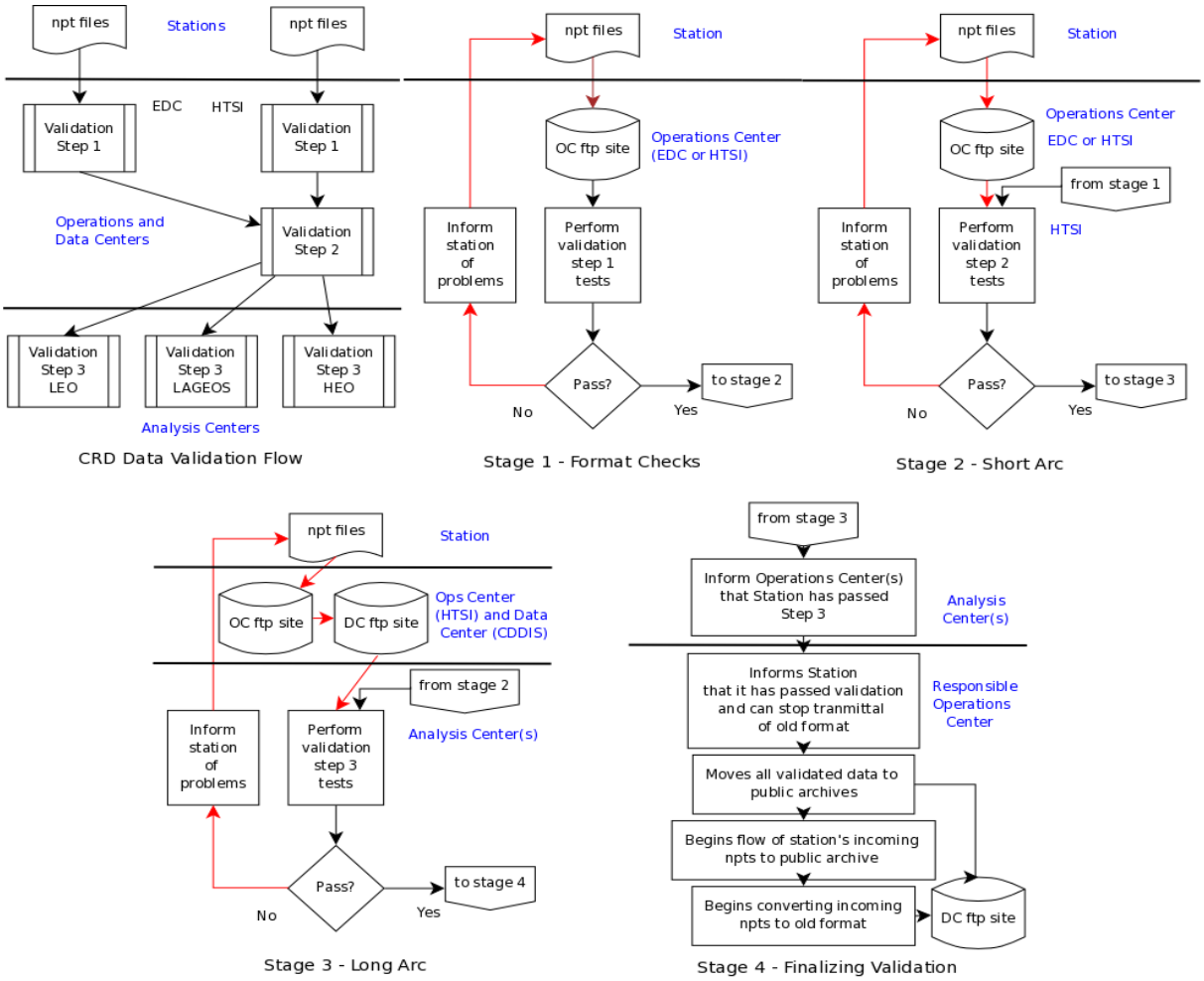

Figure 3. Validation Process Flowchart

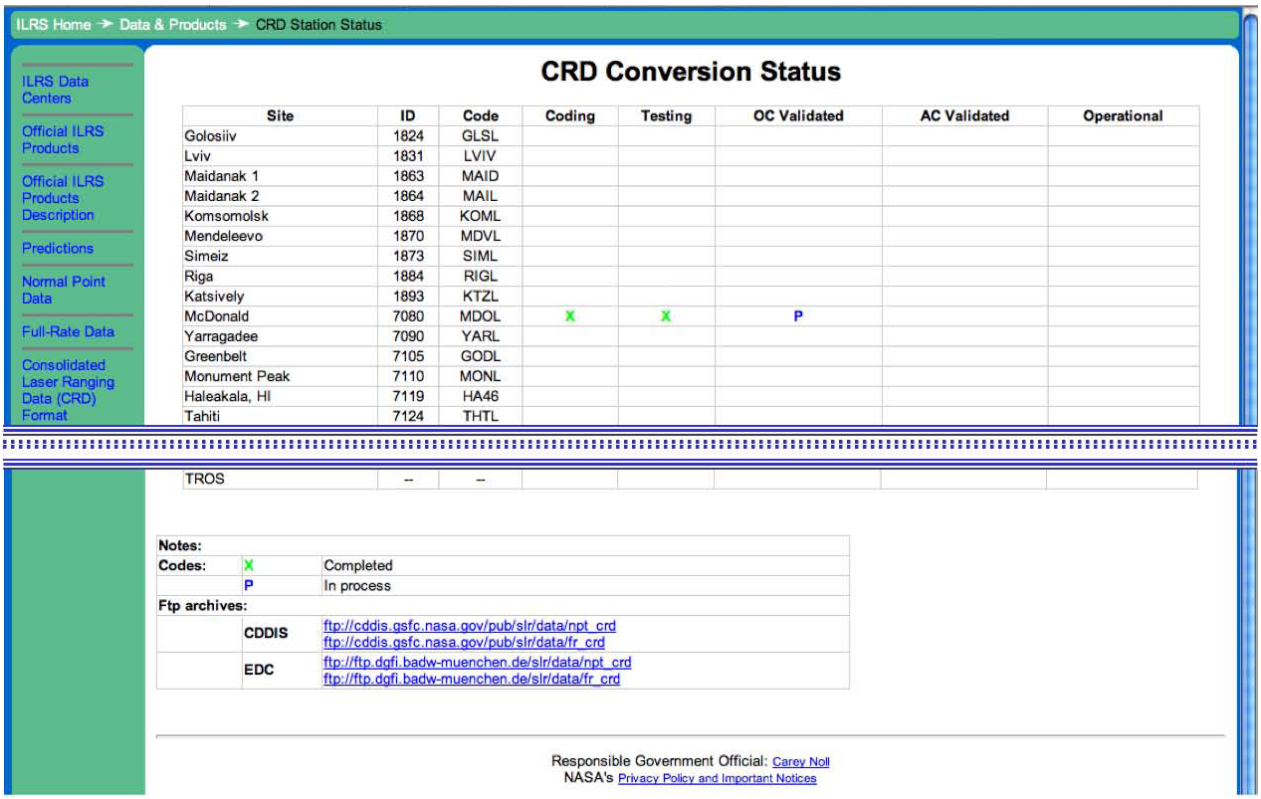

ILRS Home → Data & Products → CRD Station Status

ILRS Data Centers
Official ILRS Products
Official ILRS Products Description
Predictions
Normal Point Data
Full-Rate Data
Consolidated Laser Ranging Data (CRD) Format

CRD Conversion Status

Site	ID	Code	Coding	Testing	OC Validated	AC Validated	Operational
Golosiiv	1824	GLSL					
Lviv	1831	LVIV					
Maidanak 1	1863	MAID					
Maidanak 2	1864	MAIL					
Komsomolsk	1868	KOML					
Mendeleevo	1870	MDVL					
Simeiz	1873	SIML					
Riga	1884	RIGL					
Katsively	1893	KTZL					
McDonald	7080	MDOL	X	X	P		
Yarragadee	7090	YARL					
Greenbelt	7105	GODL					
Monument Peak	7110	MONL					
Haleakala, HI	7119	HA46					
Tahiti	7124	THTL					
TROS	--	--					

Notes:		
Codes:	X	Completed
	P	In process
Ftp archives:		
	CDDIS	ftp://cddis.gsfc.nasa.gov/pub/slr/data/npt_crd ftp://cddis.gsfc.nasa.gov/pub/slr/data/fr_crd
	EDC	ftp://ftp.dgfi.badw-muenchen.de/slr/data/npt_crd ftp://ftp.dgfi.badw-muenchen.de/slr/data/fr_crd

Responsible Government Official: Carey Noll
NASA's Privacy Policy and Important Notices

Figure 4. ILRS website CRD Conversion Status

Moblas 8 Return to Operations

Scott Wetzel, Howard Donovan, Julie Horvath, Dennis McCollums, Thomas Oldham, Alice Nelson, Don Patterson, Mike Henick
NASA SLR / HTSI, USA
scott.wetzel@honeywell.com

Abstract

The MOBLAS 8 station located on the island of Tahiti has been operational at that location since 1997. Recently, in 2007, the station suffered from multiple failures of components and subsystems. Due to the changeover of station personnel and the removal of HTSI from the island to help with the operations and maintenance in 2004, the multiple failures of the system caused the MOBLAS 8 system to be inoperable in March 2007. Working closely with NASA, CNES, and UFP, HTSI developed a training plan for the station manager from the Moblas 8 site as well as the TLRS-3 station manager from Arequipa, Peru. Following the training back at NASA's Goddard Space Flight Center (GSFC) in Greenbelt, Maryland, the MOBLAS 8 Station Manager worked with HTSI personnel to repair subsystems and components at GSFC. Later, two HTSI engineers traveled to the MOBLAS 8 station to work with the Station Manager and the UFP and CNES crew to complete the system and site repairs, resulting in the restart of operations at this critical site in the South Pacific. This paper chronicles the work that was planned and executed along with the benefits to the NASA, UFP, CNES and the ILRS with the repairs and efforts to return the station to operations.

Targets, Signatures and Biases

Chairs: Graham Appleby and Toshimichi Otsubo

Session Summary

Five oral papers were presented during the session, mainly covering retro-reflector array design and optical response functions. The continuing development of new missions that will require laser tracking support is evident, as is the ongoing and welcome dialogue between mission engineers and the laser community in developing the best array solutions to maximise the effectiveness of the tracking. The contents of the individual papers are outlined below.

Signal Strength Measurements and Retro-reflector Array Design. David Arnold presented some very interesting work on retro array design and chamber-testing, with particular emphasis on concepts for the next generation GPS satellites. He also described proposals for a campaign of ranging experiments that will enable the determination of relative signal strengths between the existing GNSS missions.

Effects of Ranging in Circular Polarization. John Luck described his and Chris Moore's Mt Stromlo experiments to determine pulse energy levels leaving the telescope as a function of its attitude and initial pulse polarisation. Statistically significant results were obtained suggesting that polarisation effects are present both in return signal strength variations and in range correction.

Laser Retro-reflector Arrays on the Compass Satellites. Yang Fumin and colleagues described the laser arrays on the GEO and MEO elements of the emerging Chinese COMPASS GNSS. The arrays are expected to give a strong link budget for the ground stations, and in-flight results will test the response of their novel and unique-for-GNSS uncoated corner cubes.

Laser Retro-reflector Array Development for STSAT-2. Sang-Hyun Lee and colleagues described an in-depth analysis of the retro-array on the HEO (perigee 300km, apogee 1500km) two-satellite STSAT-2 technology mission. The LRAs are 'standard' compact 9-cube arrays, but placed on the side of the rotating satellites will result in bursts of returns during each pass. This work was also presented as a poster.

Optical Response Simulation for ASTRO-G Laser Reflector Array. Toshi Otsubo and colleagues described an optical response simulation for the proposed HEO VLBI mission ASTRO-G, which very interestingly may see the ILRS supporting an astrophysics mission. Novel shading systems are under consideration to reduce the apparent 'depth' of the array in order to maximise the accuracy with which the range centre-of-mass correction may be determined.

Signal strength

David Arnold
94 Pierce Rd, Watertown, MA 02472-3035
Phone: 617-924-3811, Email: david-arnold@earthlink.net
Skype: david-arnold.earthlink.net

Abstract

Very high cross section is requried for retroreflector arrays on high altitude satellites. Uncoated solid cubes and hollow retroreflectors are being considered for future satellites. It would be helpful to measure the in-orbit cross section of existing high altitude arrays. Measuring the energy received at the satellite using the sensors on the T2L2 satellite would be helpful in understanding discrepancies between measured and calculated signal strength.

Measuring Signal Strength

- Measure relative cross section of existing GNSS retroreflector arrays
- Measure transmitted beam pattern in absolute units using the sensor on the T2L2 satellite
- Measure cross section of retroreflector arrays in the laboratory before launch

Why measure signal strength?

- High altitude GNSS satellites require very high cross section. Present arrays give weak signals
- Uncoated cubes appear to give higher cross section than coated cubes.
- ETS-8 uses uncoated cubes but can only be observed from Asian stations. COMPASS uses uncoated cubes and gives global visibility
- Quantitative signal strength measurements would be helpful for designing future GNSS arrays.

Relative signal strength

- It is not possible to measure absolute signal strength because of various uncertainties.
- Relative signal strength can be measured relatively accurately
- The variation of signal strength with range can be accurately computed
- Uncertainties in atmospheric models cancel if observations are made at the same zenith angle.

Method of analysis

- Correct observations to a standard range such as 20 megameters
- Do a semi-log plot of signal strength for each satellite and station vs zenith angle
- There should be a constant difference (ratio) between the plots for different satellites.

Experiment plan

- Range to COMPASS, GLONASS, GPS, Giove-A, Giove-B using same system set up
- Range as often as possible for a few minutes per satellite at a variety of zenith angle
- Make estimates of relative return rates if possible
- Deposit full-rate and NP data

T2L2 experiment

- Calculated and measured signal strengths can differ by an order of magnitude
- The sensor on T2L2 can measure the signal received at the satellite
- Measuring the signal strength at the satellite can help determine whether the discrepancies between measured and calculated signal strength are on the uplink or the downlink

Beam pattern

- Scanning the transmitted beam across the T2L2 satellite can be used to map the transmitted beam pattern
- The central part of the beam pattern may not contain the total energy due to large angle scattering.
- Measuring the absolute signal received at the satellite can determine the signal lost to atmospheric absorption or large angle scattering.

Variations in transmitted beam

- Measurements of the beam pattern received at the T2L2 satellite can be used to study the received energy and beam divergence as a function of:
- Atmospheric conditions
- Zenith angle
- Station parameters
- Beam divergence is limited by seeing conditions. Variations in seeing conditions can change the beam divergence and signal strength. Narrow beams may be most sensitive to seeing conditions.

Positive and negative dihedral angle offsets in uncoated cubes

- A dihedral angle offset in an uncoated cube produces an asymmetrical diffraction pattern when linear polarization is used.
- An equal mixture of positive and negative offsets eliminates the polarization

asymmetry.

- A thermal study suggests that an equal mixture of positive and negative offsets is more stable.
- Specification of 0.0 +/- .5 arcsec gives angles from -.5 to +.5 arcsec. Specification of .75 +/- .5 arcsec gives angles from .25 to 1.25 arcsec.

Diffraction patterns

A mixture of positive and negative dihedral angle offsets produces a pattern that has the same shape as a cube with no dihedral angle offset. The diffraction patterns are from -50 to +50 μrad in each direction. The units are relative to the Airy peak. Reflection factor in a coated cube is 93%.

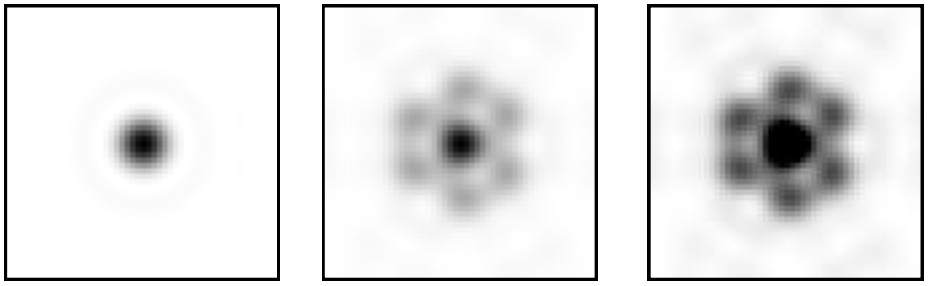

(a) (b) (c)

(a) Coated 1.5 inch, no dihedral offset, .93 maximum. (Airy pattern)
(b) No dihedral angle offset, .24 maximum, uncoated, circular polarization
(c) Same as (b) with .12 maximum

All plots below are .12 max

+.75 arcsec dihedral offset

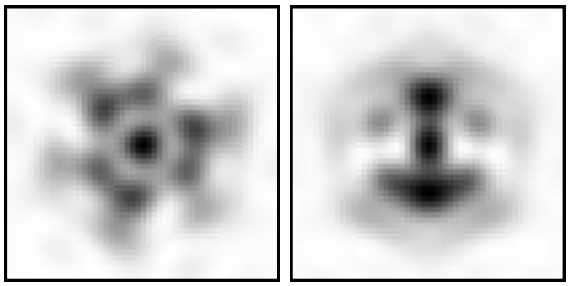

Circular Linear

-.75 arcsec offset

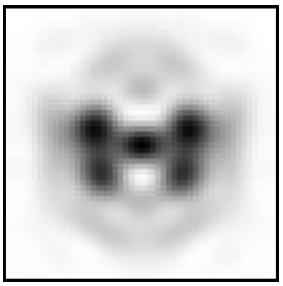

Linear

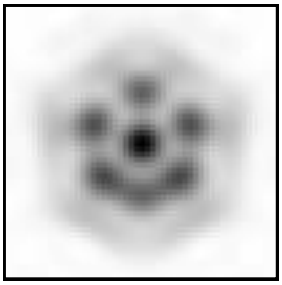

Average of +.75 and -.75
Linear

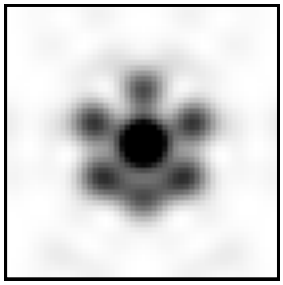

No offset
Linear

Analysis and testing of uncoated cube corners

- During the APOLLO program analytical calculations and laboratory tests were done.
- Analytical programs were developed at SAO in 1971 for the LAGEOS mission.
- LNF in Italy has thermal vacuum laboratory facilities, thermal modeling program, and optical ray tracing program using CodeV.
- Reinhart Neubert measured an uncoated cube.
- Optical ray tracing program recently developed by Toshimichi Otsubo.

LNF Space Climactic Facility, Simone Dell'Agnello

- Spare GPS array (flight qualified)
- Section of LAGEOS cubes
- LARES cubes and whole array
- Russian prototype cube corners
- Proposed LUNAR cube
- NASA hollow cube
- Maintain facility for testing future arrays?

Effects Of Ranging In Circular Polarization

J. McK. Luck, C.J. Moore
EOS Space Systems Pty. Limited, Canberra, Australia
john-luck@bigpond.com

Abstract

As reported at the 2007 Grasse Technical Workshop, Stromlo SLR can alternate between linear and circular polarization transmitted beams by the insertion and removal of a quarter-wave plate (QWP). Control of insertion and removal allows coincidence with Normal Point bin boundaries. This paper presents an analysis of data obtained using ETS-8 during a very clear night in September 2008, in addition to a re-analysis of the 4 Lageos passes described in the Grasse (2007) workshop. By careful use of classical statistics, the results show significant differences between the two polarization states in range measurements and return rates, in the senses predicted by Dave Arnold. Correlations depending upon the angle between the transmitted (linear) polarization vector and the velocity aberration vector are also examined. The targets used are suitable for this experiment because their retroreflectors are uncoated.

Introduction

It has been predicted by Arnold (2002) that, when ranging to spherical targets having uncoated retroreflectors, the use of circular polarization will result in:

- Shorter ranges, by about 4 mm in the Lageos cases,
- Greater return rates,
- Reduced scatter.

In particular, he states:

> "If linear polarization is used, the transfer function with uncoated cubes has a "dumbbell" shape which can introduce a systematic error if no correction is applied. The problem can be corrected by applying a correction for the asymmetry. The asymmetry can be eliminated by using circular polarization."

and

> "The Lageos 2 retroreflector array was tested in the laboratory before launch . . . the testing showed a difference in the range correction for Lageos between linear and circular polarization".

Arnold also predicts that, in linear polarization, they will be affected by the angle between the satellite's velocity aberration vector and the direction of the polarization vector as it reaches the target, which here will be called the "Arnold angle". This is a candidate explanation for the anecdotal observation by several observers at different stations that the satellite "seems to disappear in certain parts of the sky", although another possible explanation is that the turning mirrors in the telescope's Coude transmit path have unequal p- and s-reflectances, due perhaps to coating degradation.

Lageos-1 and -2 were the prime targets in this study. ETS-8 was also chosen because, although its cube-corner array is planar, it carries uncoated cubes. Being in geostationary orbit, the array geometry as seen by a ground station is nominally constant.

During these studies, anomalies showed up in the calculations of velocities from the CPF predictions of satellite position.

Ranging Differences Between Circular And Linear Polarization

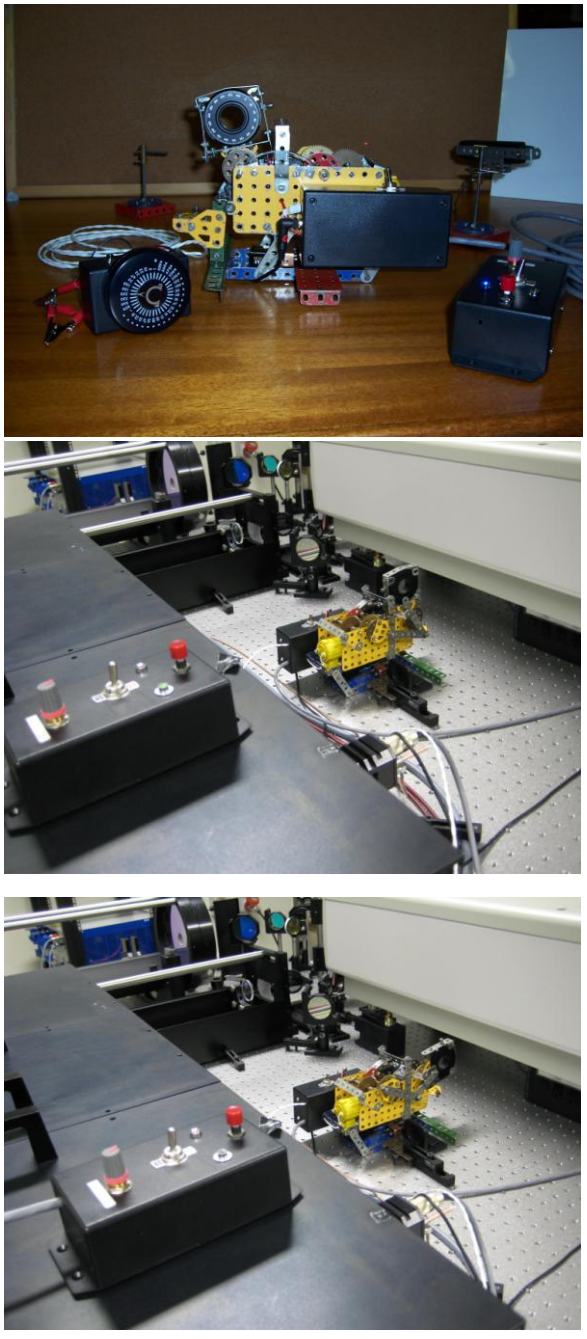

Figure 1. Quarter Wave-Plate Inserter.
(Top) In fabrication workshop.
(Middle) On laser table, QWP OUT of path.
(Lower) On laser table, QWP IN laser path.

Experimental Setup and Processing Strategy

A quarter wave plate (QWP) was mounted in an Inserter to convert the outgoing laser from linear to circular polarization. The Inserter (Figure 1) was fabricated from a mechanical engineering prototype system, and placed on the laser table between the frequency doubler and the Transmit/ Receive mirror, so it did not affect the return path. Alternate insertion and withdrawal of the QWP into the laser beam was performed by remote control. The laser was disabled for a few seconds during these changes of state, which generally occurred on Normal Point bin boundaries. Thus, alternate Normal Points were in either the IN (circular) or OUT (linear) state, so minimizing variations due to atmospherics, the Arnold angle, poor trend-curve fitting during processing, and so on.

Full-rate data files from normal Stromlo post-processing were used. They contained only returns accepted by the final filter. CPF predictions from HTSI (JAXA for ETS-8) were interpolated iteratively to “bounce” time at the satellite on ITRF X,Y,Z coordinates using an 8-point Lagrange interpolator, before calculating the topocentric ranges. Atmospheric refractions corrections were applied using the Mendes-Pavlis formula (ILRS RSG, 2002-4).

The predictions were completed by fitting polynomials of degree 1-9 through the residuals so formed, including both IN and OUT data together, and the lowest-degree adequate fit was chosen subjectively. (It was felt that fitting all returns together gave a better common baseline for comparing INs vs. OUTs rather than

fitting separate curves.) Evaluations of the selected polynomial at each return were added to the earlier predictions, and new residuals (here called "***departures***") were formed, from which Normal Points were calculated in accordance with ILRS instructions (Sinclair, 1997). The results of a Lageos-1 pass re-processed in this manner, shown in Figure 2, suggest that the trend curve adopted does indeed remove all systematic variations. It is noted that the Normal Points produced by this special processing are, in general, somewhat different from the regular Stromlo NPs, possibly due to different choices of trend functions; in this study, strenuous efforts were made to get the "departures" graph as flat and smooth as possible.

Observations

Passes observed with the QWP operation were:

Lageos-1, 2007 Sep 08 at 12:55 UTC (night)
Lageos-1, 2007 Sep 09 at 15:05 UTC (night)
Lageos-2, 2007 Sep 11 at 23:20 UTC (day)
Lageos-2, 2007 Sep 12 at 07:40 UTC (evening)
ETS-VIII, 2008 Sep 11 at 09:47 UTC (night) (the next year)

and, without QWP operation as a "contra" check on interpretation of the analyses:

Lageos-2, 2008 Sep 10 at 12:30 UTC (night).

Some exploratory results on the first four Lageos passes were presented at the Grasse ILRS Technical Workshop (Luck et al, 2007).

Statistical Analysis

For the comparisons between circular (C) and linear (L) polarizations, only returns lying in "Adjacent Pairs" of NPs were used, i.e. in bins having returns from the other state in at least one adjoining bin. This restriction sought to reduce further any observational bias between states, and was applied to both NP and FR comparisons.

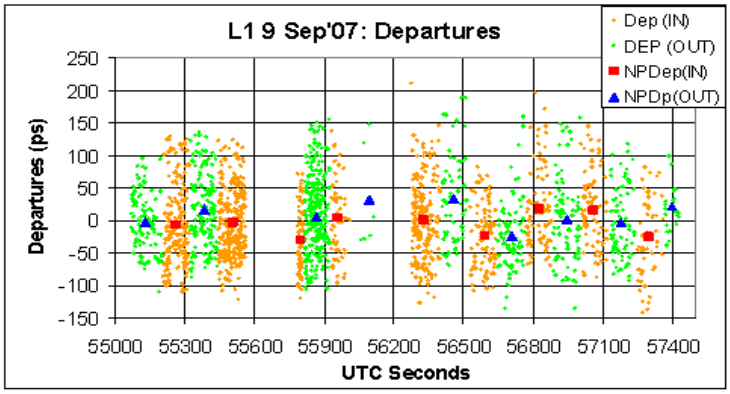

Figure 2. Residuals from final trend curve ("departures") for a Lageos-1 pass, showing also the Normal Points. The trend curve was a polynomial of degree 6 (order 7).

The tests performed, and reported in Table I, were based on elementary statistical hypothesis testing (see e.g. Hoel (1966)) and the statistical tables contained therein (and elsewhere). The tests are all one-tailed and assessed in terms of percentage confidence that the null hypothesis has been rejected correctly, i.e. using the *'p-value'*, e.g.:

Confidence = 100 [1 – Pr{ $z > \hat{z}$ | null hypothesis (H_0) is true }]

or equivalent statement for other tests, and $\hat{z}$ is the calculated test statistic appropriate to the test.

Difference between Means

We define Student's t statistic as,:

$\hat{t}$ = [(Mean of NP/ FR departures, C) – 3.1 ps – (Mean of NP/FR departures, L)]/ s

where the extra delay due to QWP presence in the transmit path is 3.1 ps (catalog data), except for the "contra" pass, and, for example $s = \sqrt{s_C^2 / n_C + s_L^2 / n_L}$ is the "pooled" sample

standard error of the difference. Here n_C, n_L and s_C^2, s_L^2 are the numbers of NPs (or FR points) and the variances of the NPs (or FR points) about their means in each state. There are $n_C + n_L - 2$ degrees of freedom (d.f.).

Ratio of Normal Point Variances

Fisher's F test statistic is given by $\hat{F} = s_L^2 / s_C^2$ with $n_L - 1, n_C - 1$ degrees of freedom. Note that, if Arnold's prediction is true that C-scatter is less than L-scatter then $\hat{F}$ is significantly greater than 1. But there is little statistical power in this test for FR data.

Return Rates

The 'population proportion' test was used: in each adjacent pair, the ratio of return rates was calculated, viz: $r_i = [returnrate / shot(C)] / [returnrate / shot(L)]$, from which the proportion $\hat{p} = [num.pairs \text{ with } r_i > 1] / [total\ num.pairs]$ was obtained. If return rates are equal, then $H0: p_0 = 0.5$ is expected, and tested against $H1: p > 0.5$, with the test statistic $\hat{z} = (\hat{p} - p_0) / \sqrt{p_0(1-p_0)/n}$ being distributed as Normal(0,1). For the passes in this experiment it was difficult to get the number of shots fired per bin, so the time interval between the first and last accepted returns in a bin was used instead.

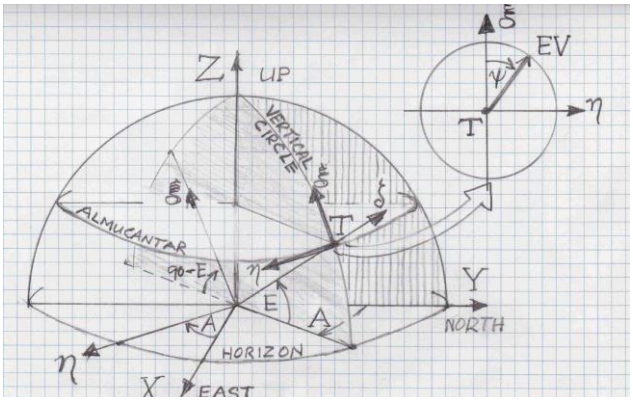

Figure 3. Position angle ψ in local ENU coordinates.

Discussion of Results

The results given in Table 1 come from a re-computation after the Poznan Workshop, and are less optimistic that ranging in circular polarization produces measurable improvements. Greater attention was paid to the boundaries between QWP 'IN' and 'OUT' states. Though the changes were generally small, they sometimes caused quite pronounced differences. We conclude that this statistical instability means that the data are not yet sufficiently precise to draw firm conclusions. Nevertheless, some of the results were suggestive:

- The return rate proportions (see row "Confidence: C rate>L rate") seem to suggest higher rates with circular polarization. However, the test used is not particularly sensitive so a better one is sought.
- With FR data, the mean difference in ranges was highly significant (see rows "Confidence: C mean<L mean"), except for one QWP pass and, of course, the check pass. However, with NP data, none of the passes yielded significant (>95%) differences in the means.
- Neither the FR nor the NP tests showed significant differences in variances (see rows "Confidence: C RMS<L RMS").

Table 1. Results of Statistical Tests

C = circular polarization ("IN"), L = linear polarization ("OUT"). Data from Adjacent Pairs only.

Target	LAG-1	LAG-1	LAG-2	LAG-2	ETS-8	LAG-2 *
Date observed	8 Sep'07	9 Sep'07	11Sep'07	12Sep'07	11Sep'08	10Sep'08
FULL RATE DATA						
Num.returns (C)	1813	1040	1397	1958	1372	672
Num.returns (L)	1292	813	1107	2092	1064	646
Mean departure (ps) (C)	0.6	-2.4	-1.6	-1.0	-2.0	3.0
Mean departure (ps) (L)	-0.7	5.6	2.6	-0.3	0.4	-3.0
Mean(C)– 3.1 –Mean(L) (ps)	-1.8	-11.1	-7.3	-3.8	-5.5	* 6.0
SS RMS (ps) (C)	66.4	57.9	53.0	47.6	47.4	43.1
SS RMS (ps) (L)	70.7	58.0	50.8	48.3	48.0	40.5
Pooled RMS (ps)	2.5	2.7	2.1	1.5	2.0	2.3
Student's 't' of Diff.of Means	-0.718	-4.113	-3.513	-2.549	-2.819	2.608
Confidence: C mean<L mean	**76.4%**	**100.0%**	**100.0%**	**99.5%**	**99.8%**	**< 50 %**
Fisher's 'F' of Variance Ratio	1.13	1.00	0.92	1.03	1.03	0.88
Confidence: C RMS < L RMS	**99.2%**	**50.7%**	**6.7%**	**73.2%**	**67.3%**	**5.1%**
NORMAL POINTS						
Num.Normal Pts, =(C) = (L)	9	8	11	12	13	8
Mean NP departure (ps) (C)	0.1	-2.5	-4.4	-1.9	-1.6	1.7
Mean NP departure (ps) (L)	0.2	6.8	2.8	-1.2	1.4	-3.2
Mean(C)- 3.1- Mean(L) (ps)	-3.2	-12.4	-10.3	-3.8	-6.1	* 4.9
RMS of NPs (ps) (C)	12.6	15.8	11.1	14.3	13.7	12.2
RMS of NPs (ps) (L)	22.2	17.5	16.5	17.5	11.6	11.0
Pooled NP RMS (ps)	8.5	8.3	6.0	6.5	5.0	5.8
Students't' of Diff of NP Means	-0.373	-1.489	-1.716	-0.575	-1.229	0.841
Confidence: C-mean<L-mean	**64.3%**	**92.1%**	**94.9%**	**71.4%**	**88.5%**	**< 50%**
Fisher's 'F' of Variance Ratio	3.11	1.24	2.21	1.50	0.71	0.82
Confidence: C RMS < L RMS	**93.5%**	**60.7%**	**88.6%**	**74.4%**	**28.1%**	**39.8%**
RETURN RATE PROPORTION						
Num. Adjacent Pairs	9	8	11	12	13	8
Num.APs with C rate > L rate	9	7	9	8	5	6
Normal 'z'	3.00	2.12	2.11	1.16	-0.83	1.41
Confidence: C rate > L rate	**99.9%**	**98.3%**	**98.3%**	**87.6%**	**20.3%**	**92.1%**

Effects In Linear Polarization

Electric Vector Orientation

Depending on the type of coatings on the mirrors in the transmit optical path and their condition, there may be changes in the direction and intensity of the electric vector (EV) if transmitting in linear polarization. These changes are due to inequalities of the p- (parallel to plane of incidence) and s- (perpendicular) components of the reflectances. They produce variations as the Coudé mirrors rotate in azimuth and elevation because the planes of incidence change even though the angles of incidence remain constant at 45^{o}. If the p- and s-reflectances are substantially unequal, this phenomenon could be a candidate as the cause of disappearing returns in certain sections of otherwise crystal-clear skies.

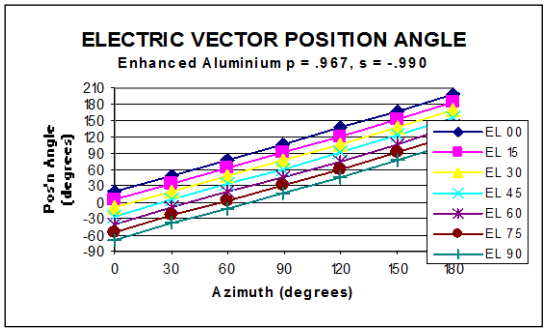

Figure 4. Difference in EV position angle between enhanced aluminium and perfect coatings, as telescope rotates.

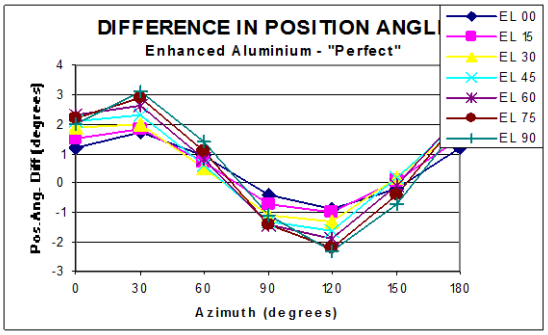

Figure 5. General behaviour of EV position angle as telescope rotates in azimuth and elevation.

For Figures 4-6, the EV was mapped through the Stromlo SLR as if all the 45° turning mirrors after the laser table were coated with enhanced aluminium, p = 0.967, s = 0.990. In effect, four surfaces were experiencing 'plane-of-incidence' changes. Curved surfaces were ignored. The initial EV is vertical, while the final EV is given in terms of its "position angle" with respect to the vertical circle (see Figure.3). Comparisons were made against "perfect" coatings (p = s = 1.00). Figure 4 shows the overall variation of the EV position angle as the telescope rotates in azimuth and elevation. Figure 5, at much larger scale, demonstrates the variations amounting to about 4° due to unequal reflectances, compared with perfect coatings. Figure 6 reveals a 14% variation in final transmitted energy (square of EV amplitude), which is quite appreciable even for reflectances relatively close to 1.

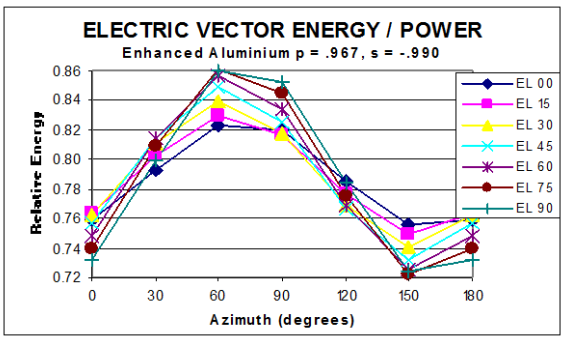

Figure 6: Electric vector energy as telescope rotates, with enhanced aluminium coatings.

An initial experiment to measure transmitted energy at Herstmonceux SLR in 2007 showed somewhat similar variations (8%) as their telescope rotated in azimuth only, possibly indicating coatings degradation (Smith and Appleby, 2007).

Arnold Angle

Given the EV position angle algorithm, it was relatively easy to calculate the "Arnold Angle", i.e. the angle, at the target, between the incident polarization vector and the velocity aberration vector which is the relative inertial velocity of the satellite w.r.t. the station (Arnold, 2007). This angle is virtually constant at 122.8° for ETS-8 tracked from Stromlo, as expected, since ETS-8 is in geostationary orbit. The result for one of the Lageos test passes is shown in Figure7. However, it is not thought feasible at present to detect this effect in view of all

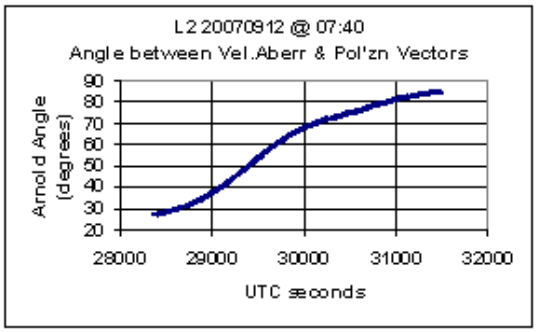

Figure 7. Angle between polarization vector and velocity aberration vector, for a Lageos pass tracked from Stromlo.

the other factors affecting return rates, especially as Stromlo does not have a return signal strength monitor.

Trend Function

In studies of this sort it is crucial that the trend function from which departures are formed be able to remove all known and unknown systematic errors in the data. For this, fitting simple models such as range- and time-bias ($residual_i = rangebias + rdot_i*timebias$) (which have physical meaning) prior to empirical polynomial fitting gave inconsistent results, as did fitting a set of osculating Kepler elements. These depend on the $rdot_i$ which were obtained by numerical differentiation of CPF position predictions using an 8-point Lagrange differentiator rigorously tested against known functions and Werner Gurtner's HERMITE subroutine.

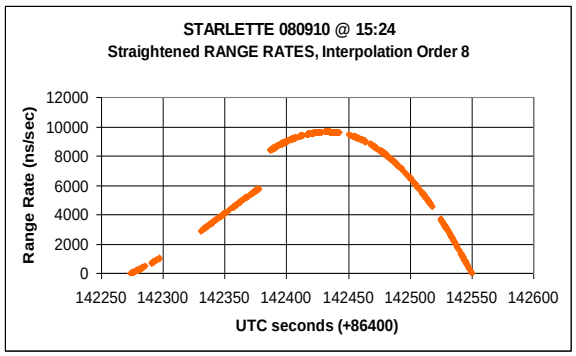

Figure 8. Range rates obtained by numerical differentiation of CPF positions. A trend line has been removed to highlight discontinuities.

Upon investigation, discontinuities were found in the rates so calculated (Fig.8). A study is continuing to ascertain whether the problem lies with my software (inconceivable!) or with the CPF files. This might also explain a quite-often-observed difficulty obtaining nice flat "departures" in regular Stromlo processing.

Summary and Conclusions

From judicious elementary statistical analysis of the limited data collected on satellites carrying uncoated cube corners, there is tantalizing evidence suggesting that:

- Range measurements are shorter in circular polarization than in linear, when comparing Full-Rate data though not when comparing Normal Points. This applies to the planar-array ETS-8 as well as to the spherical-array Lageos;
- Return rates are perhaps greater in circular polarization than in linear, but only for the spherical-array Lageos targets;
- There is no evidence of differences in RMS scatter between polarizations;
- The Lageos "check" pass showed no statistically significant differences, as expected since there were none.

However, these effects are considered to be merely on the verge of detectability under the conditions obtaining at the time of the Stromlo experiments, so at this stage we make no firm recommendation on the desirability of ranging in circular polarization.

When ranging in linear polarization, there will theoretically be appreciable variations in transmitted electric vector orientation and especially energy as the telescope rotates in azimuth and elevations, if the p- and s-reflectances of the Coudé mirrors are unequal. There is perhaps some supporting observational evidence from Herstmonceux. An algorithm has been developed for interpreting effects of the "Arnold angle" if ever they become detectable. Worrying discontinuities in CPF predictions are suspected.

Acknowledgements

Vicki Smith took the Herstmonceux energy measurements. Bart Clarke (HTSI) has provided CPF files with velocity data for further investigation of CPF anomalies.

References

Arnold, D.A., *Retroreflector Array Transfer Functions*. Proc. 13th International Workshop on Laser Ranging, Annapolis, MD, October 2002, in session "Target Design, Signatures and Biases".

Arnold, D.A., Private Communication, 15 September 2007.

Hoel,P.G. (1966): *Introduction to Mathematical Statistics*, 3rd ed., John Wiley & Sons, Inc.

ILRS RSG (2002-4): *Refraction Study Group Activities*. Includes subroutine links. http://ilrs.gsfc.nasa.gov/working_groups/refraction_study_group/rswg_activities_meetings/index.html.

Luck, J., V.Smith and C.J.Moore, *Circular Polarization Experiment*, Presentation to ILRS Fall Technical Workshop, Grasse, France, October 2007. http://www.oca.eu/Gemini/ecoles_colloq/colloques/ilrs2007/PresentationsPdf/10_Session.pdf/10.9_CircularPolarization.pdf.

Sinclair,A.T., 1997, *Data Screening and Normal Point Formation*. http://ilrs.gsfc.nasa.gov/products_formats_procedures/normal_point/np_algo.html.

Smith,V. and G.Appleby, *Herstmonceux Energy Tests*, Presentation to ILRS Fall Technical Workshop, Grasse, France, October, 2007. http://www.oca.eu/Gemini/ecoles_colloq/colloques/ilrs2007/PresentationsPdf/10_Session.pdf/10.8_Appleby_HerstmonceuxEnergyTests.pdf.

Laser Retro-reflector Arrays on the Compass Satellites

Yang Fumin, Chen Wanzhen, Wang Yuanming, Li Pu
Shanghai Astronomical Observatory, Chinese Academy of Sciences, China
yangfm@shao.ac.cn / Fax: +86-21-64696290

Abstract

"COMPASS" is the regional satellite navigation system in China, and the constellation will consist of 12 satellites, of which 5 GEO, 3 IGSO and 4 MEO. The effective reflective areas of LRAs for these satellites are 770cm^2 for GEO and IGSO, 360cm^2 for MEO respectively. The diameter of the corner cubes is 33mm. Each corner cube is uncoated both on front and back faces. The paper presents the characteristics of the LRAs of the COMPASS satellites.

Introduction

The COMPASS, the Chinese name is Beidou , is the regional satellite navigation system in China, which will cover the most areas of the East Asia region, and expect to be operational by 2011.The COMPASS constellation will consist of 12 satellites with different orbital altitudes. There will be 5 GEO, 3 IGSO and 4 MEO. The orbital altitudes for GEO and IGSO are 36000 km, while 21500 km for MEO. All of those satellites will be equipped with the laser retro-reflector array (LRA) for precise orbit determination.

The experimental COMPASS satellite M1 with a MEO orbit was launched on April 13, 2007 (UTC). The LRA onboard COMPASS-M1 has been successfully tracked by the ILRS stations since December 2008. Fig. 1 is the drawing of COMPASS-M1.

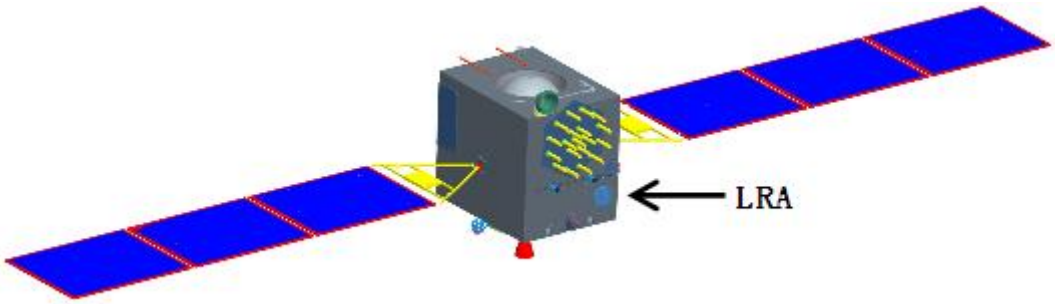

Figure 1. Drawing of COMPASS-M1 Navigation Satellite

Design and Performance of the LRA

The orbital altitude of the COMPASS-M1 is 21500 km, so the velocity aberration for the COMPASS-M1 is about 5.2 arc seconds. We choose the diameter of the corner cubes for the COMPASS-M1 and COMPASS satellites follow-on is 33 mm, equals to 1.3 inches. For compensation of the velocity aberration, the 0.6 arc seconds (±0.3″) dihedral offsets were adopted for the COMPASS-M1's corner cubes. All the surfaces of the corner cubes are without coating. The fused silica material for the corner cubes was made by the Shanghai LengGuang Co. in China. Fig. 2 and Table 1 show the photos and parameters of the

COMPASS-M1 (MEO) and the COMPASS GEO/IGSO respectively. We choose the hexagon array for the GEO/IGSO in order to reduce the returned pulse spread and to achieve better ranging precision.

Figure 2. The LRAs on MEO and GEO/IGSO

Table 1. Parameters of COMPASS-M1 (MEO) and COMPASS GEO/IGSO

	M1(MEO)	GEO/IGSO
Size	31.6×28 cm	49×43cm
Diameter of corner cube	33mm	33mm
Number	42	90
Reflective area	360cm^2	770cm^2
Dihedral offset	0.6″	0.5″
Weight	2.45 kg	5.0 kg

The optical performance of each corner cube must be carefully measured by the ZYGO interferometer in our laboratory. Fig. 3 shows the ZYGO and one of the measurements. The LRA must pass all the space environmental simulation testing. Fig. 4 shows one of the testing.

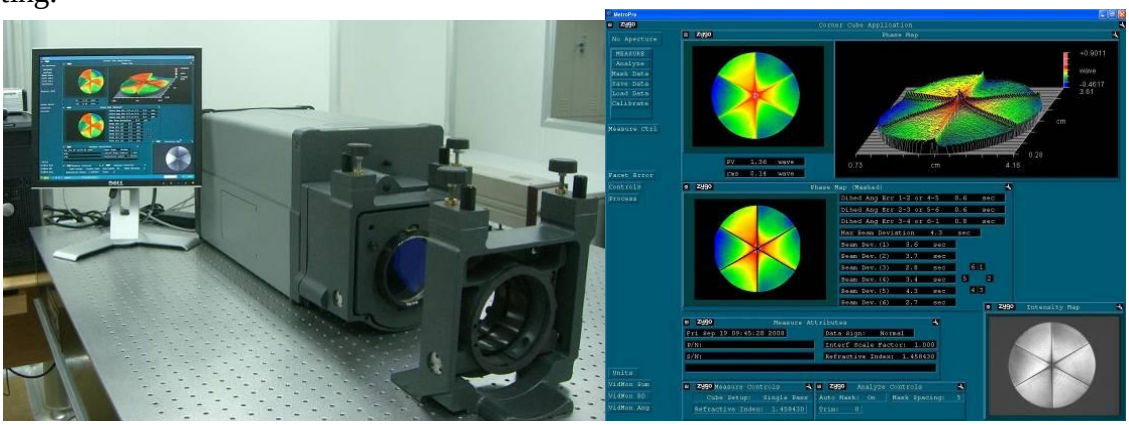

Figure 3. Testing of LRA's optical performance with ZYGO interferometer

Figure 4. Environmental testing of LRA

Table 2 and 3 list the cross section, range and signal strength and the parameters of the LRA on different satellites respectively from Dr. David Arnold (private communication).

Table 2. Cross section, range and signal for different satellites (by David Arnold)

Sat.	Cross section	Range (0 deg.)	Range^4	Signal strength	Range (45 deg.)	Range^4	Signal strength
Lageos	15	5.8	1	1.000	6.8	1	1.000
Etalon	55	19.0	115	.032	20.5	82	.044
GPS	19	20.0	141	.009	21.5	100	.012
GIOVE-A	45	23.9	288	.010	25.4	195	.015
Glonass	80	19.0	115	.046	20.5	82	.065
Compass-M1	80	21.0	189	.028	23.0	131	.041
ETS-8	140	36.0	1484	.0063	37.6	935	.010

Table 3. Parameters of LRA on different satellites (by David Arnold)

Satellite	Cube Number	Diameter (inch)	Coating	Dihedral Offset	Vendor
Lageos1	422	1.5	uncoat	1.25	Perkin-Elmer
Lageos2	422	1.5	uncoat	1.25	Zygo
Etalon	2140	1.06	coat	-	IPIE
GPS	32	1.06	coat	-	IPIE
GIOVE-A	76	1.06	coat	-	IPIE
Glonass	132	1.06	coat	-	IPIE
Compass-M1	42	1.3	uncoat	0.6	SHAO
ETS-8	36	1.6	uncoat	0.5	ITE
Perkin-Elmer Headquarters-- Waltham, MA, USA ZYGO Zygo Corp., Middlefield, CT, USA IPIE Institute for Precision Instrument Engineering, Russia SHAO Shanghai Astronomical Observatory, China. ITE ITE, Inc., Laurel, MD, USA					

The Observations of the COMPASS-M1 at the Changchun Station

The Changchun SLR station was chosen for the experiment of the COMPASS-M1 LRA ranging and the laser time transfer (LTT) in the beginning of 2007. Some upgrading was done before the launch. A new powerful mode-locked Nd:YAG laser with 100-150 mJ in 532 nm, 250 ps, 20 Hz was borrowed from the North China Research Institute of Electro-Optic (NCRIEO) in Beijing (Fig. 5). A 210mm diameter transmitter was installed to replace the old 150 mm transmitter for smaller beam divergence, and the new Coude mirrors were used (Fig.6).

Figure 5. Active-active mode-locked Nd:YAG laser

Figure 6. Changchun SLR Telescope

The laser ranging experiment to the COMPASS-M1 has been successful from the beginning. Fig. 7 shows the real-time display of the COMPASS-M1 tracking on May 1, 2007. Fig. 8 shows the range residuals of the COMPASS-M1 on September 5, 2007.

Fig. 9 shows the range residuals after fitting, and about 18550 returns with the range precision of 24 mm were obtained during 2 hours.

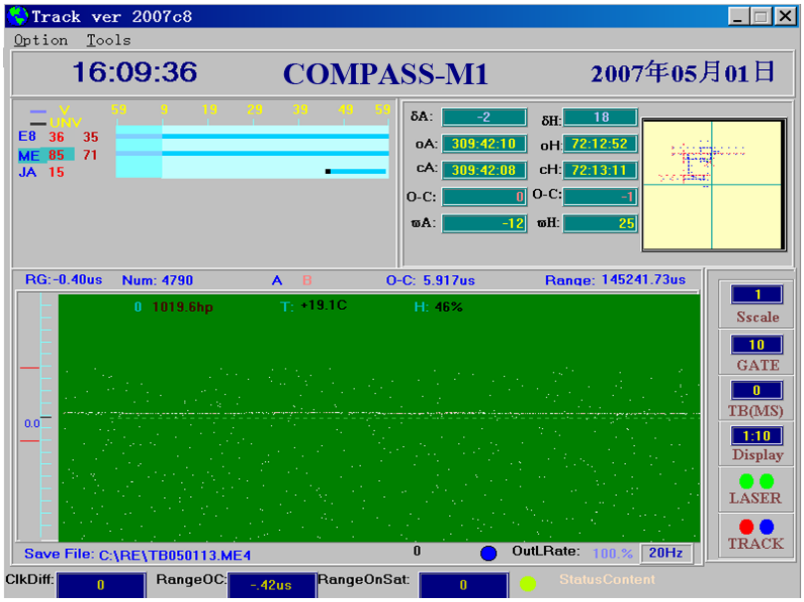

Figure 7. Real-time display for Compass-M1 tracking on May 1, 2007

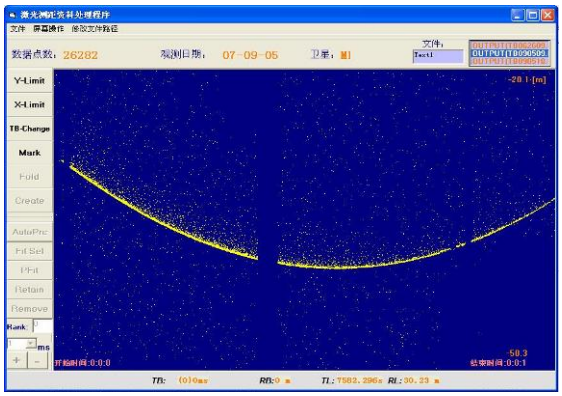

Figure 8. Range residuals of Compass-M1 on Sept. 5, 2007

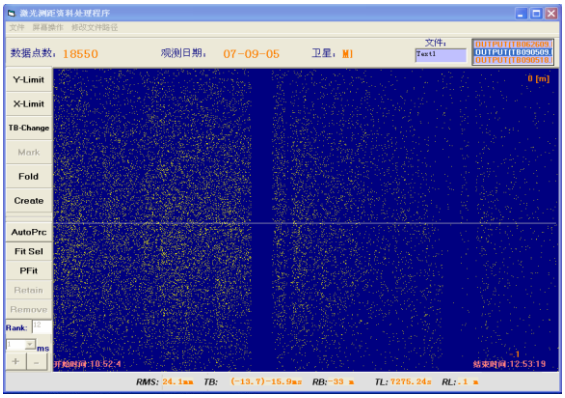

Figure 9. Range residuals after data fitting

The comparison of the return signal strength among the GNSS satellites had been done during several nights. The return signal strengths from COMPASS-M1 were much stronger than those signals from GPS-35/36 and GLOVE-A when these satellites were at the same elevations. More careful comparison of the signal strengths among the GNSS satellites have been carried out by some of the ILRS stations since December 2008.

Summary

The shape and parameters of 12 sets of the LRAs of the COMPASS satellites are introduced in this paper.

（1） It is shown from the ranging data of the COMPASS-M1 at the Changchun station that the performance of the LRA of the COMPASS-M1 is excellent, and the return signal strength from the COMPASS-M1 is much stronger than those from GPS-35/36 and GIOVE-A.

（2） The uncoated corner cubes are fine for the high orbit satellites, such as GNSS and GEO satellites.

SLR Coverage Analysis for STSAT-2

KyungHee Kim (1)**, Sang-Hyun Lee** (1)**, Jun Ho Lee** (2)**, Jonghan Jin** (3)**, Noh Hoon Myung** (1)

(1) Satellite Technology Research Center (SaTReC), Korea Advanced Institute of Science and Technology (KAIST),
(2) Department of optical engineering, Kongju National University
(3) BUPE Group, KAIST

khkim@satrec.kaist.ac.kr /Fax: +82-42-861-0064

Abstract

The STSAT-2 (Science and Technology of Satellite – 2) is a low earth orbit micro satellite for the space technology research and space science. This satellite is the first Korean satellite which will be launched by the KSLV-1 (Korea Space Launch Vehicle – 1) in 2009 in Korea. It has three missions: the DREAM mission, the SLR mission and the space core technology verification mission. Among other things, the SLR mission is to measure the precise distance between the STSAT-2 and a SLR ground station and then to determine the precise orbit of it. In this paper, as one of the SLR mission analysis, the SLR coverage is analyzed during the SLR mission according to the attitude status of the operation concept. Finally, the result is provided.

Introduction

This satellite is the first Korean satellite which will be launched by the KSLV-1 (Korea Space Launch Vehicle – 1) in 2009 in Korea. Table 1 shows the summery of the STSAT-2. As showed in table 1, this orbit of the STSAT-2 is not a sun synchronous orbit. The figure 1 shows the eclipse period of the STSAT-2 for 1 year. This eclipse period changes from the minimum 0 minute to the maximum 37minutes.

The STSAT-2 has 3 major missions: Dual channel Radiometer for Earth and Atmosphere Monitoring (DREAM), Satellite Laser Ranging (SLR), Satellite Bus Technology Verification (SaTReC KAIST, 2005).

Table 1. Summary of the STSAT-2 specifications

Property	Value
Orbit	Inclination : 80^{o}, Apogee : 1500 km, Perigee : 300 km
Lifetime	2years
Instrument	DREAM : 10.66kg, 16W
	SLR : 0.82kg
Weight	100kg
Power	160W @EOL

Attitude Control	3-axis attitude stabilized control
	Pointing Accuracy : < 0.14^{o} (2σ)
	Attitude Knowledge : < 0.066^{o} (2σ)
RF link margin	S-band : 3dB @ 10deg
	X-band : 3dB @10deg
Data Rate	S-band Uplink : 1.2kbps, 9.6kbps
	S-band Downlink : 9.6kbps, 38.4kbps
	X-band Downlink : 10Mbps
Launch	July 31, 2009 by KSLV-1 (STSAT-2A) January 31, 2010 (STSAT-2B)

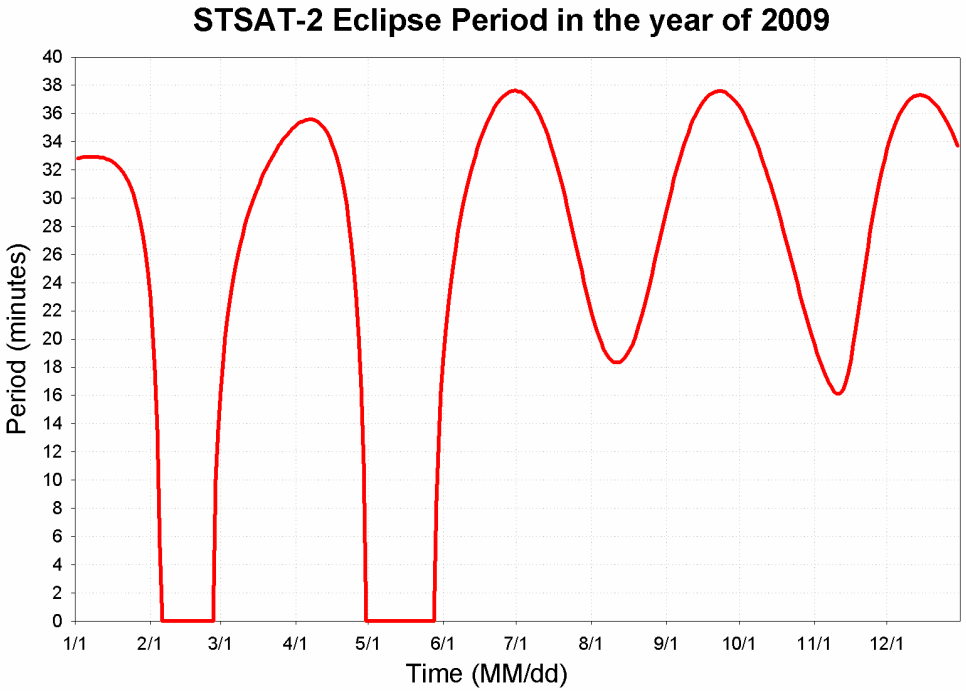

Figure 1. The eclipse period of the STSAT-2

SLR mission requirements

The SLR mission, the second mission, is to measure the distance between the STSAT-2 and SLR ground stations to determine a precise orbit. The LRA for the SLR mission is equipped with +Z axis of the STSAT-2. The operation concept of STSAT-2 has 3 attitude control modes.

1) Sun pointing mode of -Z axis
2) Earth pointing mode of +Z axis
3) KAIST ground station pointing mode of +Z axis

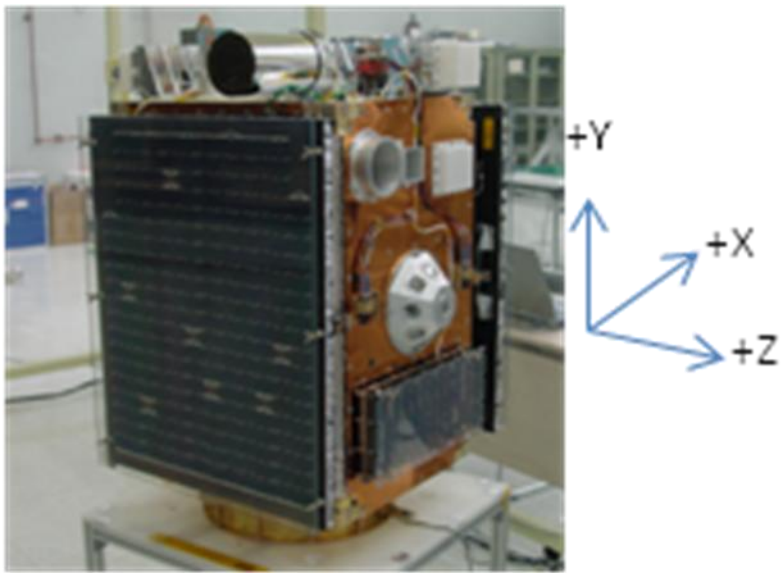

Figure 2. STSAT-2 Configuration

But there is no specified attitude control mode for the SLR mission. That means; the SLR mission should be operated in all of 3 attitude modes during the pass time at the SLR stations.

To carry out properly the SLR mission in these various attitude modes, the SLR mission needs the mission requirements. There are 4 requirements for the SLR mission.

1) The elevation angle of the SLR ground stations for the SLR mission should be more than 30 degrees.
2) The contact time during the pass time should be more than 1 minute to obtain the useful data at the SLR ground stations.
3) The observation time should be in the night time at China SLR stations.
4) The field of view of the SLR equipped with the STSAT-2 should be within ± 60° during the contact time for the measurement.

The analysis of the mission requirements

The requirements for the SLR mission should be examined whether they are possible to apply for the SLR mission. To verify the requirements analyzes the coverage of STSAT-2. The coverage means to examine which range of these requirements is able to apply for the SLR mission. At first, the contact time is analyzed for the coverage at the Shanghai station and the Herstmonceux station. The table 2 shows the position in the geocentric map of these stations (ILRS homepage).

Table 2. The position of the Shanghai station and the Herstmonceux station

No.	Station	Latitude (degree)	Longitude (degree)	Altitude (m)
1	Shanghai	31.0975	121.1917	27.832
2	Herstmonceux	50.86738	0.336122	75.404

The contact time is obtained from the orbit dynamics (Wiley *et al*., 1992). As a analysis result of the requirement 1 to 3, the Shanghai station can measure the SLR for the average 3minutes of 1 pass time per 2 days in the night time and the Herstmonceux station can measure the SLR for the average 12minutes of 2 pass time per 1 day in the day and night time (Jun Ho Lee *et al*. 2005).

Secondly, to verify the requirement 4, the field of view between the LRA of the STSAT-2 and the SLR station during the pass time about 3 attitude modes is examined using the Satellite Tool Kit 6.0. The Shanghai station can experience all of 3 attitude modes during the pass time: 1) The sun pointing mode, 2) the earth pointing mode, 3) the KAIST ground station pointing mode. As the analysis result, the contact duration within the $\pm 60^{o}$ of the field of view during the sun pointing mode is about 22% of the pass time, the contact duration within the $\pm 60^{o}$ of the field of view during the earth pointing mode is about 11% of the pass time, and the contact duration within the $\pm 60^{o}$ of the field of view during the KAIST ground station pointing mode is about 83% of the pass time in the Shanghai station. The Herstmonceux station can experience 2 attitude modes of 3 attitude modes during the pass time: 1) The sun pointing mode, 2) the earth pointing mode. As the result of the analysis, the contact duration within the $\pm 60^{o}$ of the field of view during the sun pointing mode is about 28% of the pass time, and the contact duration within the $\pm 60^{o}$ of the field of view during the earth pointing mode is about 11% of the pass time in the Herstmonceux station. The field of view is distributed between the minimum 11% and the maximum 83%. Assuming one pass time is about 14minutes, 11% of the field of view means 1.54minutes

Conclusion

In this paper, the requirements of the SLR mission, the second mission of the STSAT-2, were examined relating to the orbit property and the attitude modes. To verify the mission requirements, Two SLR stations were chosen because these stations may be possible to observe the STSAT-2: 1) the Shanghai station, 2) the Herstmonceux station. The coverage analysis firstly was performed to verify the requirement 1 to 3. The result shows to satisfy the requirement 1 to 3. The analysis of the field of view also was performed using the orbit calculation and the attitude mode control. The result shows that the field of view between the SLR of the STSAT-2 and these stations is able to be within $\pm 60^{o}$ during the pass time of these stations. As a result, four requirements for the SLR mission are valid. Thus, the precise orbit data obtained from the SLR mission will be able to use for the DREAM mission data processing and the satellite operation.

References

SaTReC KAIST, *STSAT-2 SDR Data Packag*, SDRreview meeting, pp PMD-D_3, Taejon, 2005.

Satellite Tool Kit Ver 6.0, Analytical Graphics, Inc., 2003.

Jun Ho Lee, Seung Bum Kim, KyungHee Kim, Sang Hyung Lee, Yong Jo Lm, Yang Fumin, Chen Wanshen, *Korea's first satellite for satellite laser ranging*, Acta Astroautica, 56, pp 547~553, 2005.

Wiley J. Larson, James R. Wertz, *Space Mission Analysis and Design*, 2th ed., Microcosm, inc., Torrance, 1992.
http://ilrs.gsfc.nasa.gov/sations/index.html.

Optical Response Simulation for ASTRO-G Laser Reflector Array

Toshimichi Otsubo (1), **Mihoko Kobayashi** (1), **Hiroo Kunimori** (2), **Shinichi Nakamura** (3)**, Hiroshi Takeuchi** (4)

(1) Hitotsubashi University, Japan,
2-1 Naka, Kunitachi, Tokyo 186-8601 Japan
(2) National Institute of Information and Communications Technology, Japan,
4-2-1 Nukui-kika, Koganei, Tokyo 184-8795 Japan
(3) Institute of Space and Astronautical Science,
Japan Aerospace Exploration Agency,
2-1-1 Sengen, Tsukuba, Ibaraki 305-8505 Japan
(4) Consolidated Space Tracking and Data Acquisition Dept.,
Japan Aerospace Exploration Agency,
3-1-1 Yoshinodai, Sagamihara, Kanagawa 229-8510 Japan

t.otsubo@srv.cc.hit-u.ac.jp

Abstract

Optical response of retroreflectors is studied for the precise laser range measurement to ASTRO-G, to be launched in 2012. Geometric variation on incidence angle and velocity aberration is modeled assuming the orbit and attitude of this satellite. Due to its highly elliptic orbit unfamiliar to the satellite laser ranging community, the reflector configuration has to be designed with a number of new concepts. Optical response of each retroreflector is then precisely simulated as a four-dimensional function, which is to be used for simulating the response from its whole reflector array.

1. Introduction: highly elliptic orbit of ASTRO-G

A next-generation satellite mission ASTRO-G (Fig. 1) is being developed at Japanese Aerospace Exploration Agency (JAXA). This satellite is for radio astronomical studies utilising the space VLBI technique, and is scheduled to be launched in the fiscal year of 2012.

This ASTRO-G satellite, with a 9.6-metre mesh antenna, will receive high frequency radio signals up to 43 GHz and enhance the resolution of images by approximately 10 times than the former Japanese mission known as HALCA. It is expected to provide high-resolution imaging of active galactic nuclei, motion in galactic star forming regions, observations of extragalactic water masers, etc.

Figure 1. ASTRO-G satellite.

This satellite requires centimeter-level precision of orbit to obtain precise images of these radio-astronomical targets. Laser ranging retroreflctor array is onboard as well as a GNSS receiver. The orbit determination simulation is ongoing for this satellite (Otsubo, et al., 2006).

It adopts a highly elliptic orbit.
With an eccentricity of 0.62, its altitude varies from 1000 km (perigee) to 25000 km (apogee). The orbital period is about 7.5 hours and the inclination is set to 31 degrees. Unlike existing SLR targets orbiting almost circularly around the Earth, the station-to-satellite distance varies nearly 30 times through the orbit, which means its SLR link budget changes by as much as 30^4 (~ 10^6) between the perigee and the apogee.

The angle of incidence toward the reflector array varies up to nearly 60 degrees at low altitude (Fig. 2) due to this type of orbit. In this calculation, the reflector array is modeled to point one of three Ka-band antennas or the geocentre. Ten existing SLR stations are assumed to track it every minute. The result is far different from 20000-km. GNSS satellites in which the angle of incidence does not exceed 14 degrees.

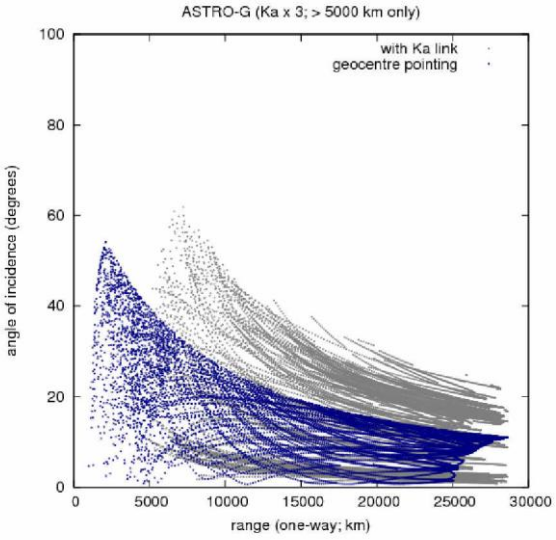

Figure 2. Angle of incidence toward ASTRO-G retroreflector array.

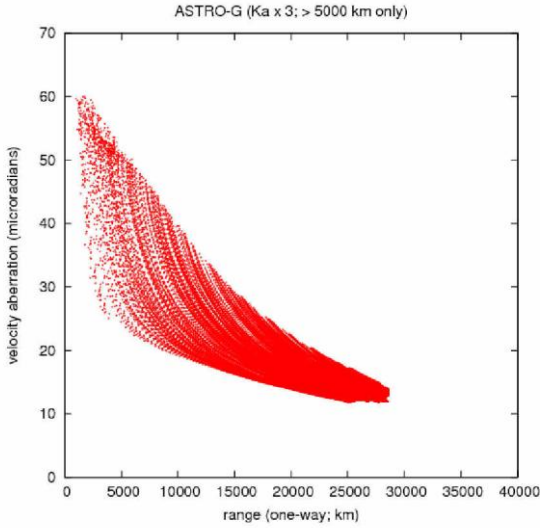

Figure 3. Velocity aberration of ASTRO-G seen from existing SLR stations.

This type of orbit also brings a new challenge in terms of velocity aberration. In the case of circular-orbit satellites, the velocity aberration stays in a certain small range throughout the orbit. However, as indicated in Fig. 3, the velocity aberration of ASTRO-G varies from 12 microseconds around the apogee to 60 microseconds around the perigee. None of existing or past satellites have experienced such a huge variation of velocity aberration.

We have to tackle these unprecedented problems when designing its reflector array.
This paper deals with a preliminary part of optimisation studies of a reflector array to be carried on the ASTRO-G satellite.

2. Basic concept of ASTRO-G reflector array

A planar array is common for GNSS satellites around 20000 km of altitude, and a compact pyramid-style array is common for low-earth remote sensing satellites at or below 1500 km

of altitude. In order to cope with the wide range of angles of incidence shown in Fig. 2, we have devised a basic concept of a reflector array for ASTRO-G as seen in Fig. 4. It is basically the combination of the GNSS-type array in the surrounding area and the low-earth-orbiter-type array in the central area.

Three types of circular-faced reflectors are currently assumed. The central six reflectors are 28 mm in diameter, all slanted by 30 degrees, and coated on backfaces. The surrounding 14 reflectors (called 'inner ring') are also 28 mm in diameter, not slanted, and uncoated on backfaces. Finally, the outer 14 reflectors ('outer ring') are the same as the inner ring except for its size of 38-mm diameter.

The slanted and coated six reflectors are placed at the centre, so that the centre-of-mass correction changes smoothly with respect to the angle of incidence and also so that most of the area on the array panel can be spent for the non-slanted reflectors whose amount is the key to succeed long-distance laser ranging.

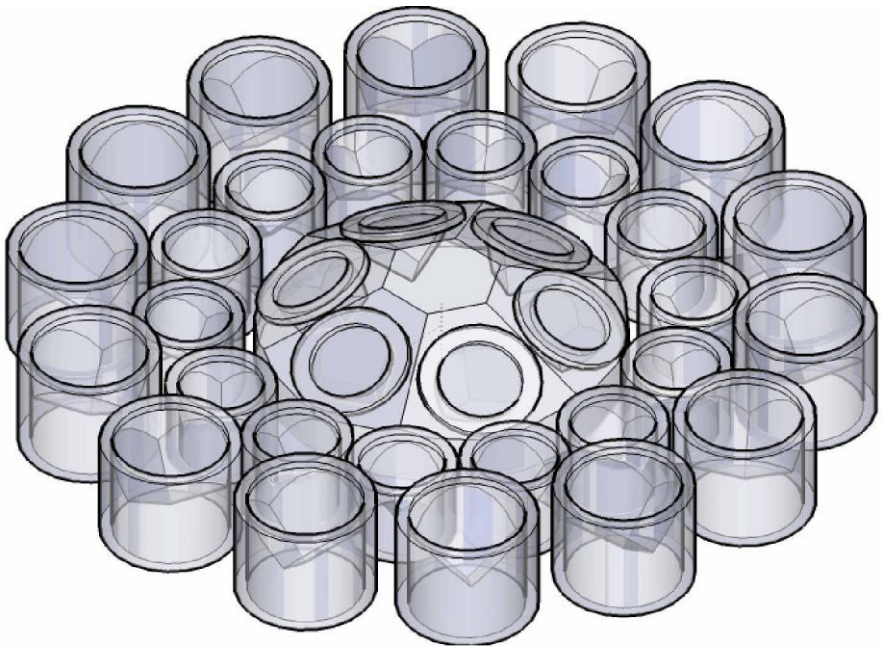

Figure 4. Basic design of ASTRO-G retroreflector array.

3. Numerical simulation of four-dimensional reflector response

It is necessary to numerically simulate the precise response pattern of each reflector in order to find the optimised combination of the components. Hitotsubashi University has embarked software development required for this study as we had only constructed two dimensional models (Otsubo and Appleby, 2003). The new program is written in C#.

The optical response is described as a four-dimensional function, i.e., two dimensions for angle of incidence including azimuthal angle, and two dimensions for velocity aberration that is a two-dimentional relative velocity vector perpendicular to the line of sight.

The software firstly set every parameter of a retroreflector, such as optical index, shape of front face, backface coating, dihedral angle. It then calculates the actual path length inside the reflector taking a small (0.2 mm) grid size of ray tracing, for a given angle of incidence. It finally generates a far-field diffraction pattern of 2 microradians' mesh size based on the phase difference of outgoing rays. This sequence is repeated for every angle of incidence separated by 2 degrees.

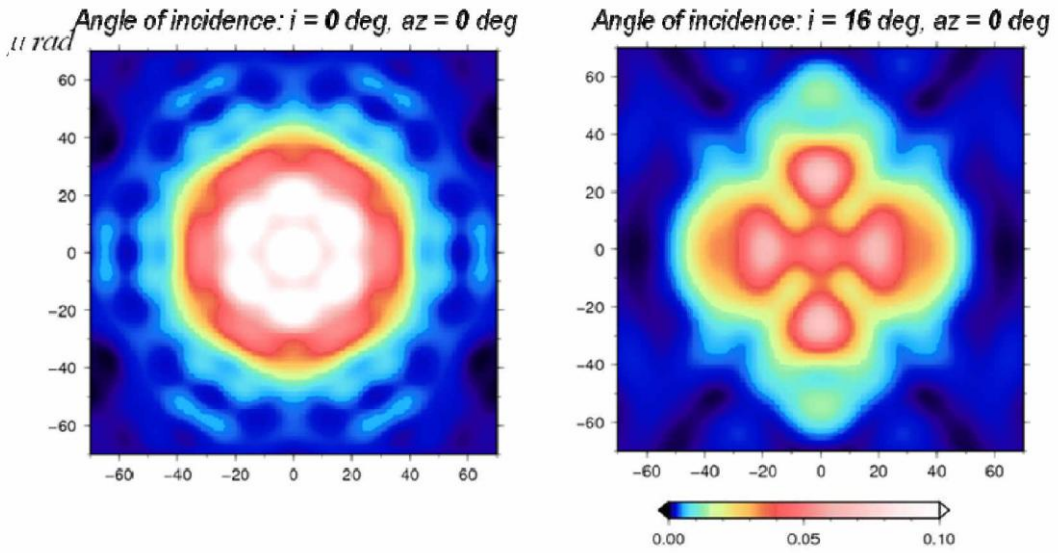

Figure 5. Far-field diffraction patterns of a 38-mm-diameter circular-face reflector with backface uncoated and 0.75-arcsecond dihedral angle.
Left: angle of incidence = 0, right: angle of incidence = 16 degrees.

Two examples of far-field diffraction patterns are shown in Fig. 5 for the outer ring reflector. Dihedral angle is set to 0.75 arcseconds. The left graph is the zero angle of incidence and it shows a diffraction pattern with azimuthal symmetry every 60 degrees. In the right graph, the angle of incidence is set to 16 degrees upward with respect to the plane of this paper, and the diffraction pattern is broadened along the up-down axis since the effective aperture is horizontally long. These patterns are calculated every two degrees of two-dimensional angle of incidence.
It should be noted that this software is still being developed and these are still preliminary results.

4. Link budget estimation for ASTRO-G reflector array

Based upon simulated orbits of ASTRO-G and the existing laser ranging stations, the link budget of laser ranging observations is estimated. This work is very important for the feasibility analysis of the laser reflector array.

As the Asian and Australian stations have recently succeeded in laser ranging to the geostationary satellite ETS-VIII (Uchimura, et al., 2004), simulated observations to ETS-VIII assuming JAXA Tanegashima station (30.5-deg N) are used as a baseline in the following analysis. Although the optimisation of dihedral angle should be made, we set the dihedral angles at 0.75 arcseconds for central reflectors, and 2.0 arcseconds for inner and

outer ring reflectors. The other parameters are the same as given in Section 2.

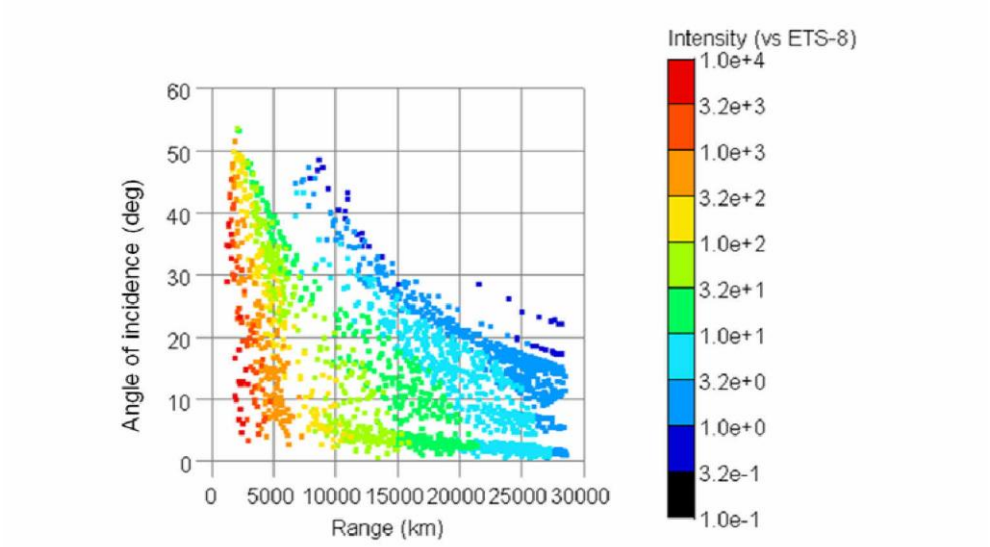

Figure 6. Intensity of estimated returns from ASTRO-G satellite, in comparison with ETS-VIII.

The result is shown in Fig. 6. The intensity is estimated to be stronger than ETS-VIII in almost 98% of the time. The remaining 2% is plotted as dark blue dots that are scattered both in [1] > 25000 km range with ~20 degrees of angle of incidence and in [2] 7000-15000 km range with ~40 degrees of angle of incidence. The intensity is expected to be just 1 to 10 times stronger than ETS-VIII for 76 % of the time (light blue and medium blue dots) as the satellite flies slowly around the apogee. Nevertheless, it is clear that ASTRO-G will be observable as long as a station can track ETS-VIII.

5. Conclusions and future studies

Laser ranging to highly elliptic orbits is challenging. A basic design of ASTRO-G laser reflector array is almost finished. It is a combined structure of a GNSS-type array and a low-earth-orbiter-type array. Using newly developed software for four-dimensional optical response, the link budget to ASTRO-G is estimated. This satellite will give stronger returns than ETS- VIII for most of the time.

There are still remaining studies for optimising the details of reflector configuration, such as dihedral angles, slant angle of central reflectors, and target signature effects. We plan to continue further numerical simulations to find the best combination of a number of configuration parameters.

References

1. T. Otsubo, T. Kubo-oka, H. Saito, H. Hirabayashi, T. Kato, M. Yoshikawa, Y. Murata, Y. Asaki and S. Nakamura, Possibility of laser ranging support for the next-generation space VLBI mission, ASTRO-G, Proceedings of 15th International

Workshop on Laser Ranging, 2006.
2. T. Otsubo, G. M. Appleby, System-dependent centre-of-mass correction for spherical geodetic satellites, Journal of Geophysical Research, 109, B4, 9-1-9-10, 2003.
3. T. Uchimura, M. Sawabe, A. Suzuki, H. Noda, Laser retroreflector array of geostationary satellite, ETS- VIII, Proceedings of 14th International Workshop on Laser Ranging, 2004.

Laser Retroreflector Array Development for STSAT-2

Sang-Hyun Lee, Kyunghee Kim (1)**, Jun Ho Lee** (2)**, Jonghan Jin** (3)**, Noh Hoon Myung** (1)

(1) Satellite Technology Research Center (SaTReC), KAIST.
(2) Department of Optical Engineering, Kongju National University.
(3) BUPE Group, KAIST

shlee@satrec.kaist.ac.kr /Fax: +82-42-8610064

Abstract

STSAT-2(Science and Technology Satellite-2) is a microsatellite to experiment advanced satellite technology and research space science and now has been completed the flight model development. STSAT-2 will be launched by KSLV-1 at Naro space center of Korea in 2009 and injected an elliptical orbit having 300km at the perigee and 1500km at the apogee. It has three missions: as the first mission is to predict total precipitable water using microwave radiometer (DREAM); the secondary mission is to measure precise distance between STSAT-2 and SLR ground station for precision orbit determination of STSAT-2; the last mission is to verify the space core technologies of bus. STSAT-2 is equipped with a laser retroreflector array having hemispherical configuration with one-nadir-looking corner cube in the center and surrounded by an angled ring of eight corner cubes like Shunzhou-IV, ERS-1&2, and Envisat. This paper introduces STSAT-2 mission and describes the development result of LRA.

Introduction

STSAT-2 is the first Korean satellite, which is equipped with laser retroreflector array for SLR. The objectives of STSAT-2 consist of three missions, which are the domestic development of a low earth orbit 100kg satellite which will be launched by KSLV-1(Korea Space Launch Vehicle-1) from the domestic space center (Naro Space Center), the development of advanced technology for small spacecraft, and the development and operation of world-class space science payloads (Jun Ho Lee, 2005).

STSAT-2 has an elliptical orbit having 300km at the perigee and 1500km at the apogee. Some period among one year has partially sunlight period without eclipse. The minimum eclipse time has 0% and the maximum eclipse time about 35% (Kyunghee Kim, 2007).

STSAT-2 has two payloads: the main payload, microwave radiometer (DREAM, Dual-channel Radiometer for Earth and Atmosphere Monitoring) and the secondary payload, laser retroreflector array. The DREAM mission objectives are to acquire brightness temperature of the liquid water from Earth atmosphere and surface and to predict the total precipitable water after post-processing. The mission objective of spacecraft technologies is to develop a thermally, mechanically, electrically stable and radial resistant spacecraft system having high precision attitude determination and control capability in a high eccentric ellipsoidal orbit. For spacecraft technology experiments, STSAT-2 has the following instrumentations onboard:

(1) Pulsed Plasma Thruster (PPT)

(2) Dual-Head Star Tracker (DHST)
(3) Fine Digital Sun Sensor (FDSS)
(4) Compact on-board computer
(5) High-speed data transmission (10Mbps)

Figure 1 shows the STSAT-2 configuration and table 1 summarizes the specifications of STSAT-2 (SaTReC, 2005).

Figure 1. STSAT-2 configuration

Table 1. STSAT-2 specifications

Items	Values	Items	Values
Orbit	300×1500km, Circular orbit Inclination : 80°	Expected Life	2 years
Launch Date	July 31, 2009 (STSAT-2A) January 31, 2010 (STSAT-2B)	Payloads	DREAM : 10.66kg LRA : 0.82kg
RF Link Margin	S-band : 3dB @ 10deg X-band : 3 dB @ 10deg	Attitude Control	3-axis stabilization
Power	200W @ BOL	Weight	100kg
Eccentricity	0.082435	Period	102.998min

Satellite Laser Ranging Mission

The SLR mission objectives are to determine the more precise orbit of STSAT-2 than possible with S-band tracking data alone, to calibrate the main payload DREAM, and finally to support the science research such as earth science and geodynamics. Additionally, the precise orbit determination of STSAT-2 can be used to evaluate the performance of the first Korean launcher (KSLV-1). SLR data of STSAT-2 will provide the unique opportunity to investigate the variations of an ellipsoidal orbit.

Laser Retroreflector Array

LRA consists of nine corner cubes and symmetrically mounted on a hemispherical surface with one nadir-looking corner cube in the center and surrounded by an angled ring of eight

corner cubes like Shunzhou-IV, ERS-1&2, Envisat, ALOS, GFO-1 and Jason-1. LRA configuration is shown in Figure 2.

The diameter of corner cube is 31.5mm and the height 22.3mm. Corner cubes were made of fused silica. Corner cube assembly consists of corner cube housing, corner cube, PTFE ring, flexture, corner supporter, and cover. PTFE ring is a kind of Teflon and was inserted to absorb vibration and shock and isolate thermal conduction between corner cube and flexture.

LRA is equipped on the satellite's earth panel and allows laser ranging in the field of view angles of 360 degree in azimuth and 60 degree elevation. The dimensions of laser retroreflector array have 200mm in diameter and 65mm in height. The beam divergence is fourteen arcsec in STSAT-2A and twelve arcsec in STSAT-2B. Table 1 summarizes the specifications of laser retroreflector array (SaTReC, 2005).

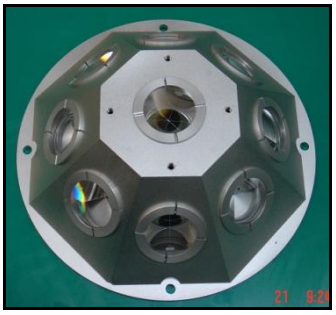

Figure 2. Laser retroreflector array configuration of STSAT-2

Table 2. Specifications of laser retroreflector array

Items	Values	Items	Values
Corner Cube Diameter	31.5mm	Corner Cube Height	22.3mm
LRA Size	ϕ200×65(Height)mm	Field of View	±60°
Dihedral Angle Offset	1.5″ (STSAT-2A) 1.2″ (STSAT-2B)	Weight	815g
Divergence	14±2arcsec (STSAT-2A) 12±2arcsec (STSAT-2B)	Material	Fused Silica
Surface Flatness	λ/10	Coating	No Coating

Phase Center of Laser Retroreflector Array

Figure 3 shows the center of gravity of satellite and the phase center of laser retroreflector array. O is satellite-based origin and CG the satellite center of gravity. The vector C is from satellite-based origin to the center of gravity of satellite, C=(-7.6, 381.4, 1.9)mm in the STSAT-2A and (-0.18, 412.16, 0.03)mm in the STSAT-2B. The distances between the center of gravity of satellite and the optical center of LRA are 267mm in the STSAT-2A and 271.2mm in the STSAT-2B. Here, PC is the phase center. The vector L is from the satellite-based origin to the LRA mass center, (-0.34, 381.92, 310.98)mm.

For the nadir-facing cube, the phase center is -h×n in the z direction from the plane of the front faces of that cube. For the STSAT-2 cubes, h=22.3mm and n=1.464. So the phase center for the nadir cube is -32.65mm in z direction. The z-component of array phase center for that cube is +2.87mm from the mass center of laser retroreflector array, but will vary at the level of a few mm depending upon which of the other cubes are visible from the tracking station. However, ignoring that effect here, and defining vector L′ as the vector from the satellite-based origin to the phase center of the retroreflector array, we have L′=(-0.34, 381.92, 313.85)mm. The plane of the front faces of the cubes is +35.52mm in the z direction from the LRA mass center. Finally, the vector PC from the satellite center of gravity to the phase center of the retroreflector array is PC=L′-C. So, PC=(7.26, 0.52, 311.95)mm in the STSAT-2A and (-0.16, -30.24, 313.82)mm in the satellite fixed frame. Figure 3 shows the phase center of laser retroreflecture array.

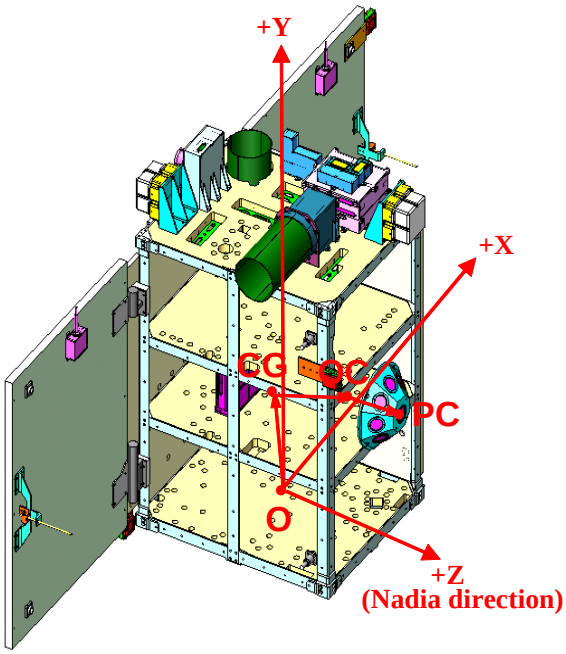

Figure 3. Phase center of laser retroreflector array

Beam Divergence Test Results

The beam divergence and dihedral angle offset test of corner cubes were performed by single pass method using Zygo interferometer with 632nm wavelength He-Ne laser. The dihedral angle offsets change between 1.08 arcsec and 2.03 arcsec in the STSAT-2A and 0.9 arcsec and 1.66 arcsec in the STSAT-2B. The average beam divergences of corner cubes have 14.5″ in the STSA-2A(Sang-Hyun Lee, 2007) and 10.4″ in the STSAT-2B (Sang-Hyun Lee, 2007).

Environmental Test Results

The vibration and thermal vacuum test of laser retroreflector array were performed. The test level is acceptance level. The vibration test levels are 9.5grms in random test and 2g for lateral and 3g for vertical in sine test. After vibration test, the visual inspections were without cracks appeared at the edge of corner cube in engineering model. This result is because the

anti-vibration material, PTFE ring , were inserted between corner cube and flexture to isolate vibration and shock.

The thermal vacuum test of laser retroreflector array was integrated on +z satellite's earth panel and performed by system level and acceptance level. In order to measure temperature difference between corner cube (Fused silica) and housing (Al 6061), two thermocouples were attached on the center of corner cube and housing. The test conditions are as follows:

- Number of cycle : 3
- Dwell time : 6 ~ 7 hours
- Shroud temperature : -120°C ~ 100°C

The minimum temperature of corner cube is -21.1°C and the maximum +62.8°C. The temperature difference between corner cube and housing is 2.7°C. As the temperature difference is small, the effect of the thermal expansion coefficient difference of two materials was not appeared in corner cubes. Therefore, the thermal vacuum test was successfully without damage and crack of corner cubes. Figure 4 shows the temperature profile of thermal vacuum test and test result and Figure 5 shows the environmental test pictures (Sang-Hyun Lee, 2007).

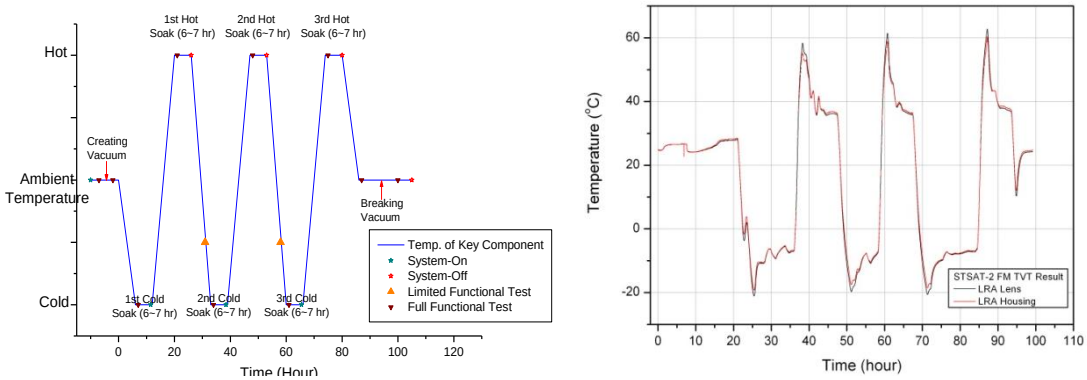

Figure 4. Temperature profile of thermal vacuum test and test result

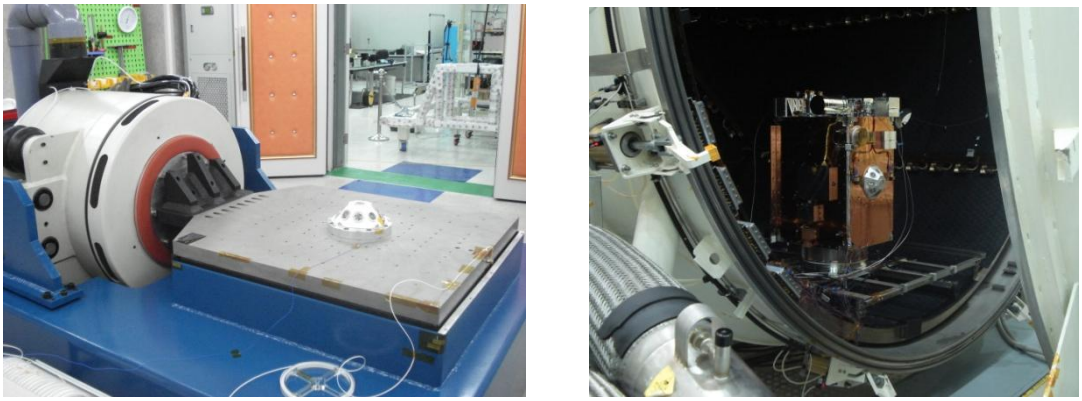

Figure 5. Environmental test pictures (vibration (left) and thermal vacuum (right))

Conclusion

The corner cubes and laser retroreflector arrays for STSAT-2 were manufactured and performed the various tests. The dihedral angle offset and beam divergence measurements were performed and have 14.5 arcsec in the STSAT-2A and 10.4 arcsec in the STSAT-2B. Also, the vibration and thermal vacuum test were performed successfully. After testing, we made sure the safety of laser retroreflector aray through visual inspections.

Acknowledgement

The authors would like to thank for their help of manufacturing laser retroreflector array of STSAT-2 to professor Yang Fumin, CHEN Wanzhen, and Zhang Jongping (Shanghai Astronomical Observatroy, CAS); professor Guo Tanyoung and Wang Peiyuan (Institute Seismology of China Earthquake Administrations).

References

Jun Ho Lee, Sung Bum Kim, Kyung Hee Kim, Sang Hyun Lee, Yong Jo Im, Yang Fumin, Chen Wanzhen, *Korea's first satellite for satellite laser ranging*, *Acta Astronotica*, pp.547—553, 2005.

Kyunghee Kim, Sang-Hyun Lee, Jun Ho Lee, Hyung-Myung Kim, "*Link Budget Analysis of SLR for STSAT-2*", 2007 Korean Space Science Society Spring Conference, 2007.

SaTReC, KAIST, *STSAT-2 CDR Data Package*,2005.

SaTReC, KAIST, *LRA CDR Data Package for STSAT-2*,2005.

Sang-Hyun Lee, Kyunghee Kim, Jun Ho Lee, Jonghan Jin, Hyung-Myung Kim, "*Protoflight Model Development of Laser Retroreflector Array for STSAT-2*", Journal of the Korean Society for Aeronautical and Space Sciences, Vol. 35, No. 12, 2007, pp.1135-1142.

Sang-Hyun Lee, Kyunghee Kim, Jun Ho Lee, Jonghan Jin, Seung-Woo Kim, "*Flight Model Development of Laser Retroreflector Array for STSAT-2*", 2007 Korean Space Science Society Spring Conference, 2007.

Advanced Systems and Techniques: Transponders, Altimeters, and Time Transfer

Chairs: John Degnan and Ulrich Schreiber

Session Summary

Altimeters

- Simulators for Planetary Exploration presented by I. Prochazka, U. Schreiber
- Present Airbourne Photonic 3D-Imagers and future Planetary Hardware presented by J. Degnan

Transponders

- Field Simulation of balanced transponders using artificial Satellites demonstrating feasibility of Mars links presented by U. Schreiber
- Preliminary Design of Mars Transponder Mission presented by T. Murphy

Time Transfer

- First Data of T2L2 presented by E. Samain
- Preliminary Results from LTT presented by F.Yang

Miscellaneous

- One-Way System Calibration Techniques presented by T. Shoobridge
- Ranging to uncooperative Targets by F.Yang
- Engineering Activities at Riga SLR by J. Balodis

Transponders and One-Way ranging applications can be considered as an emerging technology. Inherently they make the ranging application more complex, because the precise calibration of the internal system delays at both ranging terminals is not a trivial task. However on the other side it generates the ability to cover much larger distances, since the signal intensity falls off with $1/r^2$ rather than as $1/r^4$ as it does in the usual two-way ranging approach. Another important aspect is the fact that common mode errors are not canceling for the one-way ranging setup. The growing number of satellite missions and proposals for planetary exploration have prompted efforts to better understand and visualize the method of optical altimetry in recent years. In order to outline the progress made since the last workshop, several aspects were covered in this session. Two types of simulators were shown, which allow to simulate altimetry measurements over an arbitrary topography, which among other sources can be taken from public archives. In one case it is also possible to investigate the requirements on the knowledge of the satellite orbit during the simulated mission. Another presentation impressively demonstrated optical imaging with additional time of flight information. Spacebourne Transponder applications are difficult to investigate in testbed operations, because they require an active space segment. By folding the respective ranging path back to Earth one has the opportunity to fully test active transponder setups in a convenient environment. Results from such efforts were shown as well as a new design for a Mars Transponder was introduced. Apart from extending the maximum range for a time of flight measurement, Transponder applications are useful to perform high precision time transfer. The first two very successful missions T2L2 and LTT are in space and first results were shown. The last section of the session was dealing with engineering aspects of Transponder applications, such as One-way ranging system calibration.

Engineering process of SLR for LEO orbiters

M.Abele (1)**, J.Balodis** (1)**, M.Caunite** (1)**, I.Janpaule** (1)**, Rubans** (1)**, G.Silabriedis** (2)**, A.Zarinsjh** (1)

(1) Institute of Geodesy and Geoinformation, University of Latvia
(2) Rigas GeoMetrs SIA

janis.balodis@lu.lv /Fax: +371-67034436

Abstract

A ground based satellite laser ranging system has been developed at the Institute of Geodesy and Geoinformation (GGI), University of Latvia in cooperation with a Riga municipality surveying company, Rigas GeoMetrs SIA The original small size telescope mount is based on the 70 cm broad firewall of the 150 year old University building. The first satellite ranging test results of the completed SLR system were unsuccessful. The modification was completed in early 2009 The transmitting and receiving paths were separated. Optical efficiency of both was improved. Additionally, the GNSS 5 base station network is developed in an area covering Riga city. The central base station and analysis center are located close to the SLR site.

Introduction

The experience gained in Riga and Australia by the personnel of the University of Latvia (Abele et.al., 1994, Abele et.al., 1996) has been applied to design a new satellite laser ranging system (SLR). Initially it was designed for ranging to Low Earth Orbiters (LEO), particularly the European Space Agency's (ESA) mission GOCE. However, we understand now that observations of LAGEOS are required as well. The first satellite laser attempts were not successful. Although tracking was good, there were no ranging results. In late 2008, the optical system was simplified. By the end of February 2009, the modification process seems to be finished.

Figure 1. SLR before (left) and after optics modification (right)

SLR technical characteristics

The SLR hardware and software is designed in GGI by integrating advanced industrially produced components. The transmitter is an EKSPLA diode-pumped, 17 mJ laser with a repetition rate of 50Hz and a 35 psec pulse width. The range receiver uses an A032-ET event timer, and epoch time is provided by a GPS-steered Quartzlock (UK) timing unit. The detector is a Hamamatsu PMT. The SLR system is located on the roof of a 150 year old, 5 story University building, as illustrated in Figure 1.

The reasons for the poor observation test results were examined with the conclusion that the optical channels were too complicated and redundant (see Figure 2). A simplification was agreed to (Figure 3), and a modification of the station was performed.

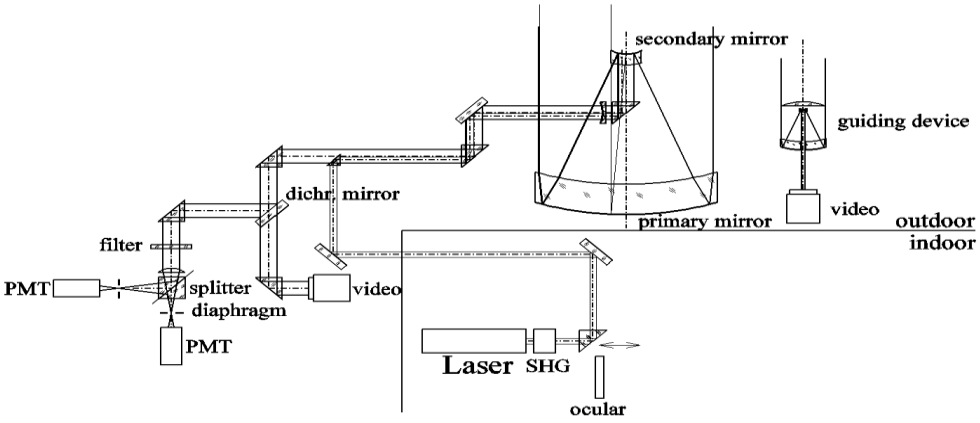

Figure 2. Initial optical scheme

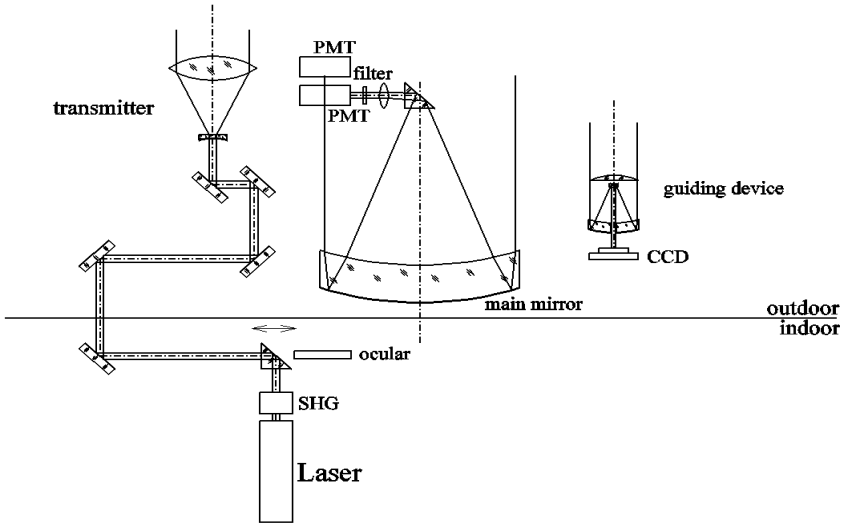

Figure 3. The modified optical scheme

The transmitter channel was separated from the receiver channel in the modified version. The number of reflecting surfaces in the receive channel was decreased significantly. The guiding telescope, supplied with a CCD camera, seems promising and aids the visual tracking and

pointing quality. Currently, both the SLR reconstruction and modification are completed. Good weather conditions are needed now to validate the success of the modification. Unfortunately, in recent years, the sky in Latvia is cloudy most of the time.

EUPOS®-RIGA augmentation system

The joint system of both the GNSS network and SLR will be used for LEO satellite positioning. The system consists of a *EUPOS® -RIGA* GNSS RTK five reference station network and a satellite laser ranging system developed by both GGI and Rigas GeoMetrs SIA. The *EUPOS® -RIGA* is a small subnet of the *EUPOS®* network, which consists of 470 base stations covering a wide area in Eastern Europe, including the Ukraine and part of Russian Federation (Rosenthal, 2008). The *EUPOS® -RIGA* base stations are equipped with JAVAD sensors, capable of utilizing both GPS and GLONASS signals. The JAVAD GNSS chock ring antennas were calibrated in Garbsen, Germany. The coordinates of the SLR and *EUPOS® -RIGA* base station antennas are determined in different coordinate systems – ITRF2005, ETRS89, LKS92. Furthermore, the elevation is determined in the Baltic height system using geometric leveling methods. The analysis center's server is connected to the GGI and the GNSS receivers via optical cables. The signal from each receiver is received at GGI with a latency of 1-2 msec. The Geo++ network solution software GNSMART is used for analysis. *EUPOS®-RIGA* has been operational for over one year, and its RTCM correction data is widely used by land surveyors in Riga city. The central base station is located about 20 m from the SLR site. The analysis of multipath effect for *EUPOS®-RIGA* network antennas has been performed, and the results were reported at the International Symposium on Global Navigation Satellite Systems (Silabriedis, 2009). The Bernese 5.0 academic version software has been obtained from GGI and will be used for the further research work.

References

Abele, M., Balodis, J., Kalnins, A., Rubans, A., Vjaters, J., West, O., Zarinjsh, A., *Portable Satellite Laser Ranging System.* In: Ninth International Workshop on Laser Ranging Instrumentation. Australian Government Publishing Service, 1996., p.160-166., Canberra, 1994.

Abele, M., Balodis, J.,Brodie-Hall, L.,Decker, W., Rao, U., K.,, Rubans, A., Vjaters,J., West, O., Zarinjsh, A., *Field tests of GPS Steered Portable Satellite Laser Ranging System.* International Association of Geodesy. Section I - Positioning. Commission X - Global and Regional Geodetic Networks. Subcommission for Europe (EUREF). Publication No. 5. Report on the Symposium of the IAG Subcommission for the European Reference Frame (EUREF) held in Ankara, Turkey, May 22-25, 1996. pp. 319-324., Munchen 1996.

Rosenthal, G., *European Position Determination System Status and Activities*. Third Meeting of the International Committee on Global Navigation Satellite Systems. Pasadena, U.S.A. 8-12 December 2008. http://www.unoosa.org/pdf/icg/2008/icg3/14.pdf

Silabriedis, G., Balodis, J., Baņuka, D.. *Analyses of the Positioning System EUPOS-RIGA Multipath.* Proceedings of the International Symposium on Global Navigation Satellite Systems, Space-based and Ground-based Augmentation Systems and Applications. Berlin, Germany, 11 - 14 November 2008. (Poster). P.125.

BepiColombo Laser Altimeter Simulator

K.U. Schreiber[a], M. Hiener[a], H. Michaelis[b]

[a]Forschungseinrichtung Satellitengeodaesie,
Technische Universitaet Muenchen
Geodaetisches Observatorium Wettzell, 93444 Bad Koetzting, Germany
[b]DLR e.V. Institute of Planetary Research
Rutherfordstr. 2, 12489 Berlin, Germany

schreiber@fs.wettzell.de

Abstract

One of the payload instruments for the BepiColombo Mercury Orbiter Mission is a laser altimeter, designed for a precise mapping of the terrain of the planet Mercury. BepicColombo is projected for an elliptical polar orbit with an apogee of about 1500 km and a perigee of about 400 km. While the proximity to the sun places substantial demands on the actual laser altimeter hardware design, the elliptical orbit and the unsufficient knowledge of the gravity field of Mercury provide similar challenges for the acutal measurement process. Therefore we have designed and created a numerical simulation tool, which allows us to develop and study suitable procedures for the actual measurement process of the laser altimeter. Different scenarios depending on the quality of the assumed satellite orbit and the presence of a terrain of unknown topography can be studied in detail. This paper describes the software concept and the basic functions of the altimeter simulation tool.

Key words: Laser Altimetry, Orbit Simulation, Laser Link Budget
PAGS: 06.30.Gv, 42.79.Qx, 95.55.-n, 42.50.Ar

1. Introduction

Laser altimetry for solar system bodies, although a well established technology, contains several severe challenges. Since it constitutes a range measurement based on the travel time of short optical laser pulses [1], this range measurement is related to the center of mass of the spacecraft and hence the satellite orbit defining the origin of the measured range. The reflection from the footprint of the laser on the probed celestial body marks the end of the distance of interest, from which the topography then can be derived. A simplified form of the ranging equation therefore is

$$r = ½\, c\Delta\tau\,, \tag{1}$$

with r the distance between the position of the satellite and the laser footprint on the ground, c the actual propagation velocity of light and $\Delta\tau$ the time between the laser pulse departure and return. The factor of 1/2 accounts for the two way passage of laser pulse.

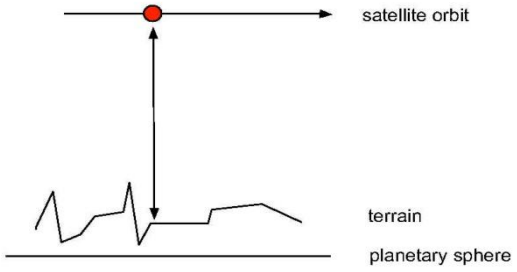

Figure 1. Pulse laser and detector are located on the satellite in orbit. Measuring the time of flight determines the contour of the terrain along the ground track of the satellite.

Figure 1 illustrates this concept. From a sequence of such range measurements one can eventually derive the topography of the probed celestial body along the ground track of the spacecraft. There are several ways in which such an altimeter can be operated. In accordance with the BepiColombo laser altimeter [5] we restrict ourselves to a fixed nadir pointing instrument, but the whole concept could also be extended to a sideways pointing or swath scanning sensor. When a suitable orbit is chosen a high percentage of the entire planetary surface can be mapped throughout the satellite mission. While orbit uncertainties may generate errors for the topographic mapping, they also cause difficulties during the measurement process in particular when a high background light level is present and techniques like receiver gating are required. The BepiColombo mission to Mercury is such an example [5].

In this paper we want to introduce and discuss a simulation program, which allows the investigation of the impact of orbit errors, unknown terrain variations and general system parameters on the shot by shot altimetry measurement [6]. Depending on a predefined orbit, the altimeter hardware layout and an arbitrary user supplied planetary topography the simulation program evaluates the signal link budget for each laser shot. So it is possible to test various hardware and flight configurations as well as a variety of ground return recovery strategies and to explore their limitations.

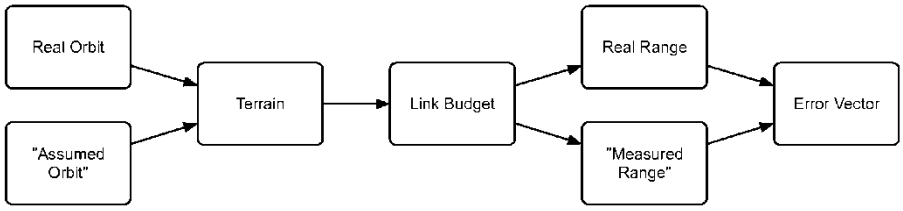

Figure 2. Flow chart of the simulation program.

2. Simulator Concept

The simulator is constructed from several subsystems. Figure 2 outlines the flow chart of the entire program. In order to study the influence of orbit uncertainties with respect to the data recovery strategy, the system generates two different orbits during the initialization of the

program. One of the orbits is the actual orbit used during the simulation run for the echo signal computation, while the other orbit corresponds to the one 'assumed' by the onboard range prediction and measurement processor. Both orbits are specified by the user at startup time. When they differ from each other, one can study the level of robustness of the echo identification and data acquistion procedure. The specific functions of the simulator are discussed below.

2.1. Satellite Orbit and Groundtrack

In order to simulate altimeter function the program first computes an unperturbed Keplerian orbit according to user supplied orbital parameters. Once the orbit is computed, the radius of the celestial body is used to establish the distance between the orbiter and the spherical body. In the next step a topographic structure is added to the object. This elevation model is also user provided and can be scaled in horizontal and vertical direction in order to test different scenarios. As a default configuration we have inserted a topographic map of central Europe into the program, because the alpine region provides substantial changes in the terrain profile. In order to study a more realistic scenario, textures of other solar system bodies may also be supplied by specifying a data-file where the topographic information is contained in a tabular form. Apart from using the entire terrain, the user is free to select a portion of interest. Figure 3 shows the default terrain as an example. While the figure displays the entire currently available surface structure, the highlighted area shows a subset with larger variations in topographic height. Sections like this can be selected from the simulation program during the setup phase to facilitate specific studies.

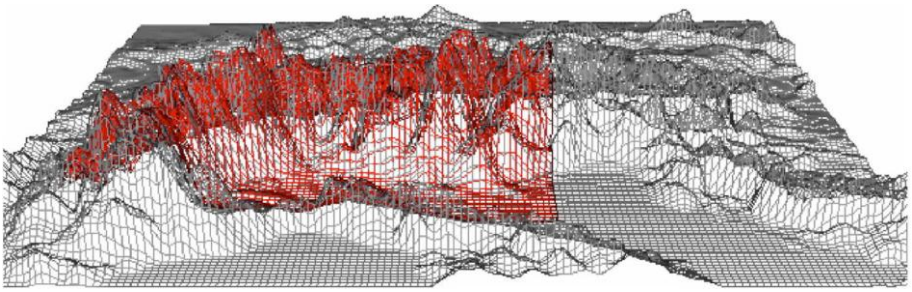

Figure 3. Central Europe as an example for a terrain profile used in the simulation process.

2.2. Laser Altimeter Parameters

The link budget for an orbiting altimeter can be calculated from a number of essential hardware and geometrical parameters [2]. Apart from the actual transmitter and receiver design, the range, terrain albedo and roughness, background optical radiation and attenuation along the path of signal propagation are important.

Table 1 summarizes the currently available transmitter parameters on the left side and quantifies the settings used for the examples in this paper. In a similar way one can define the system characteristics for the receiver part of the laser altimeter. They are shown on the right hand side of the table. Variable mission related parameters like the shot by shot range are obtained from the orbit calculation, while other mission related constant settings are also adjustable in the parameter panel. Table 2 shows the available items. The solar background radiation in tab. 2 can be switched on and off altogether in order to investigate the differences between a measurement in daylight or at nighttime. Since the parameter settings panel can be

viewed and altered at any time throughout the entire simulation run, it displays the instantaneous range and the angle of incidence of the laser beam on the planet surface as a result of the chosen topographic features.

Table 1. Available transmitter and receiver parameters for the simulator and their respective settings used throughout this paper

Transmitter		Receiver	
Wavelength:	1.064 μm	Detection Sampling Freq.:	200 MHz
Pulse Energy:	10000 μJ	Noise equivalent Power:	$3 \times 10^{-14} \frac{W}{\sqrt{Hz}}$
Pulse Width (FWHM):	6 ns	Detector Quant. Eff.:	0.4
Beam Div. (full angle):	00 μrad	Spectral Filter Bandw.:	0.2 nm
Telescope Diameter:	0.25 m	Receive Optics Transm.:	0.7
Pulse Repetition Freq.:	0.02 kHz	Field of View (full angle):	200 μrad
		Detection Gatewidth:	20 μs

Table 2. Mission related adjustable parameters

Mission Parameters
Surface Albedo: 0.26
Surface Roughness: 1 m (rms)
Solar Background radiation: 432.3 W/m^2srμm

2.3. Link Budget Calculation

Once the orbits are calculated and the altimeter and mission parameters are set up, the simulator loops either through an entire revolution of the satellite around the planet or through a user selected shorter segment of interest on a shot by shot basis. Depending on the repetition rate of the laser, the satellite is advanced along the 'true' orbit and the distance between the actual position and the planet surface including the terrain structure is computed. The intensity and temporal dispersion of the return signal is then calculated based on the hardware settings of the parameter panel. The program computes the return signal level for a nadir pointing instrument according to the general altimeter equation [3]

$$n_{pe} = \eta_q \eta_t \left(\frac{E_t}{h\nu} \right) \eta_r \left(\frac{A_r}{\pi r^2} \right) \frac{\beta}{\Omega_g} , \qquad (2)$$

where n_{pe} is the number of detected photo-electrons, η_q the detector quantum efficiency, η_t the transmit path transmission, $E_t / h\nu$ the number of generated photons at the laser output, η_r is the receive path transmission, A_r the effective receive telescope area, r the distance between altimeter and ground, β the surface albedo and Ω_g the scattering angle of the surface (π steradian). For simplicity we assume a nadir pointing instrument ($\theta = 0$) and that there is no atmosphere for the light to pass through. Otherwise β has a $\cos(\theta)$ dependence (assuming a surface with Lambertian scattering) and we would have to include additional signal attenuation to account for atmospheric absorption and scatter. In order to compute the signal

response as seen by the photo detector the signal broading due to the surface roughness across the laser footprint and the width of the laser pulse has to be incorporated. We assume a Gaussian distribution for the signal spread in time for both signal broadening processes.

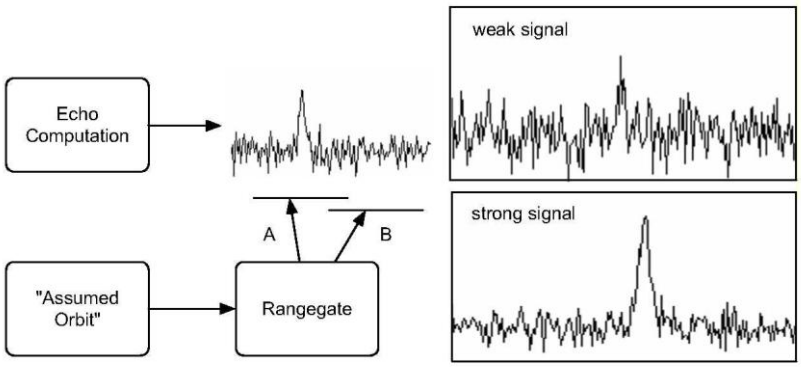

Figure 4. Example of the signal representation of the simulation program for a correctly and an incorrectly placed detector gate. Typical return signals with good and poor signal to noise ratio are also shown.

This part of the simulation program corresponds to true physical modeling section of the measurement process. From the 'assumed' orbit, which in this simulation corresponds to the best a priori knowledge of the true orbit and the epoch of the laser fire event a range-gate window of predefined length is computed. This time interval is filled with the appropriate level of background noise, which a real photodetector would have seen under these experimental conditions. In the next step the temporal structure of the computed return signal is inserted into the synthetic detector signal in the time domain. When the 'assumed' and the 'real' orbit are close enough and the range-gate is not too short, the simulated ground echo actually fits into the signal representation of the range-gate. This corresponds to case A in fig. 4. If the generated signal and the range-gate are too far apart in time, case B in fig. 4 applies and there is no echo signal contained in the synthetic range-gate. Since the altimeter and orbital parameters may vary substantially, the signal strength and shape of the ground response can also change over a wide dynamic range. Figure 4 (right side) gives two such examples to illustrate this variability, which outlines the importance of a suitable echo identification procedure.

2.4. Range-gate Generation

In the current version the simulation program uses the assumed orbit reduced by a 'best guess' predefined value to account for the expected terrain profile when it calculates the roundtrip time of the laser pulse. When the laser pulse is fired it opens the range-gate by a user specified offset time (typically around 20 μs) prior to the calculated return epoch and closes the range-gate after a similar delay past the expected echo event. After the range-gate is closed the entire measurement window is scanned for a valid return event. When a ground echo is identified within the gate, the offset from the center is determined and used as an additional correction for the prediction of the next laser shot. In this way it is possible to track the variation of the terrain with the receiver range-gate. After three consecutive successful datations, the gate module narrows the range-gate down to 500 m ≈ 1.5 μs in order to guard the detector from over loading due to the strong background radiation flux typical for Mercury. When the ground return is accidentally lost in the range window, the simulator

widens the window up again and the identification process restarts. Figure 5 shows the simulated ground echo for a low signal to noise ratio (SNR). One can see the full preset gatewidth corresponding to the initial operating situation in fig. 5a. The gatewidth reduces from 40 μs to less than 2 μs after 3 consecutive consistent signal detections in the wide gate as shown in fig. 5b. A short measurement gate speeds the echo detection process significantly up, reduces the probability of false alarms and lost datations and protects the photo-detector from excess signal loads. For the case of good SNR the respective signals are shown in fig. 6a and b. Comparing the two different observation cases, one can see that the altimeter controlling program needs to optimize operations for two operational parameters, namely low SNR and a proper range-gate tracking. Furthermore it is important to note how far the actual echo may be offset from the initially calculated distance in the large detection gates, when the assumed orbits and the terrain assumptions differ from the actual situation. This offset is adjusted shot by shot when the simulator switches over to the shorter gates.

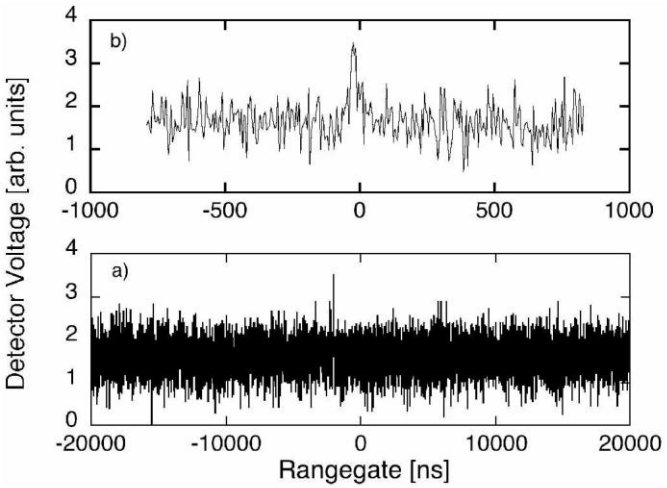

Figure 5. Simulated ground echo at a low signal to noise ratio for a large range-gate a) and the reduced gatewidth b).

2.5. Echo Signal Evaluation

The evaluation of the computed photo electric current as a function of time across the entire length of the range-gate is carried out in the next step of the simulation loop. This serves several purposes, which are

- identification of the ground return and timing the moment of detection
- finding the location of the return with respect to the opening time of the range-gate and readjusting the range-gate opening time for the return to be in the center of the next gate
- adjustment of the length of the range-gate for smallest reasonable size and high probability of an echo detection on the next shot

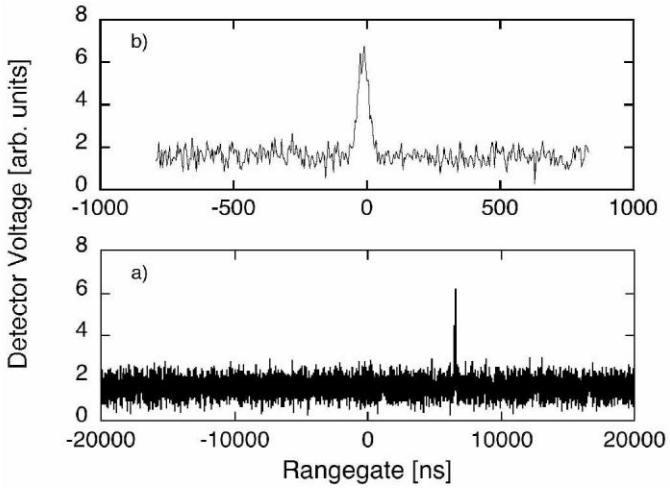

Figure 6. Simulated ground echo at a high signal to noise ratio for a large range-gate a) and the reduced gatewidth b).

So far, two different detection criteria have been implemented. The most common one is the threshold detection, which accepts the tallest signal peak within the range-gate as a return signal, provided the amplitude exceeds a predefined threshold. This method requires a reasonable SNR of two or more in order to be reliable. The other mechanism evaluates the width of the recorded echo. While noise contributions are usually transient events with rapid variations in amplitude (high bandwidth), ground echoes exhibit a much wider dispersion. If the laser pulse width (FWHM) is 6 ns and the rms surface roughness does not exceed a depth of 1 m, one may expect a detector pulse width of the order 4.5 ns, which is usually well discernable from noise only events even at a marginal SNR (fig. 5). The design of the simulation program is open to implement and investigate the applicability of any other signal recovery method such as Bayesian methods for example [4], in order to improve the detection probability. For the future we intend to add a combination of the threshold and the pulsewidth detection scheme as well as a correlation approach for low signal levels where the range-gate signal is correlated against a synthetic ground echo. The simulation program in general is designed to open the possibility to evaluate and compare entirely different data acquistion schemes for future missions such like the application of pulse trains in combination with the above mentioned correlation technique. New data evaluation methods can be added with little effort as user selectable subroutines in the echo detection parser loop.

2.6. Terrain Recovery

As the simulation program starts, it integrates the assumed satellite orbit or a selected section of it in order to obtain the satellite position for the next laser shot. Then it performs the link budget calculation and generates the respective detector signal, which in turn is analysed by the laser echo recovery procedure. This obtained range value is then subtracted from the 'actual' range value, which is computed from the 'real' orbit and the planet's surface contour. The resultant residual is interpreted as the range error value of the particular laser shot and the minimum of this value is the figure of merit of the range simulation in progress. The following properties of a laser altimeter can be studied in this way:

- Altimeter hardware design and properties
- Orbit precision requirements

- Signal recovery strategies
- Terrain slope recovery
- Laser link margins (e.g. for elliptical orbits)
- Background radiation (differences between night and day)

While the current orbit model is too simple to account for the effect of small perturbations and the current terrain is rather a one dimensional pattern, which repeats on a neighoring track when the available terrain spread is exceeded, there is no fundamental limitation that would prevent future model refinements to include spatial variations of the gravity field and eventually would allow the complete simulation of an altimeter mission including the full analysis with the aid of repeat cycles and crossover point alignments. Figure 7 shows an example of a simulated ground track. The parameter settings of the satellite passage over a rather variable terrain are listed in tab. 1. The simulations were carried out at an orbital height of around 800 km. There are 300 seconds worth of data plotted, taken at a simulated measurement rate of 10 Hz. This accumulates to a total of 3000 data points at a signal to noise ratio of about 4, similar to a return signal as shown in fig. 6.

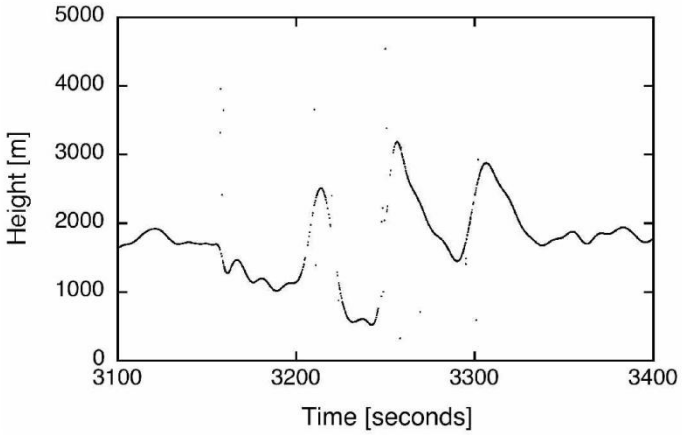

Figure 7. A simulated ground track for given parameterset (tab. 1) of the altimeter hardware. The track corresponds to a satellite height of 800 km.

Where the signal was reflected off from a steeply slopped terrain the experienced pulse broadening caused a reduction in signal amplitude, such that several data points were lost because the detected echo did not exceed the detection threshold value. The nevertheless seemingly rather smooth terrain variations are because of an interpolation between terrain grid points at 7 km separation. Since this gridspacing can be scaled during the initialization of the simulation program a much more rapid variation of the terrain could be examined if needed. Apart from some rare drop-outs where the rate of change exceeded the width of the small gate ($\Delta r \geq 1$ km/s) the topography could also be recovered without problem. However the recovery rate reduces substantially when the SNR drops to values below 2. Figure 8 shows such an example. As the altitude of the satellite increases from 530 km to 740 km, more and more false readings appear in the data file. However one can still recover the ground track without problems since the percentage of false readings is still well below the 10% level.

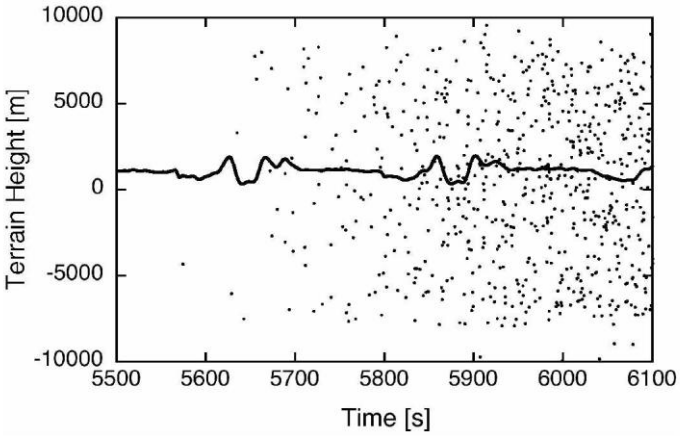

Figure 8. A simulated ground track for a signal to noise ratio below two. The corresponding orbital height went from 530 to 740 km.

3. Error Vector

For a laser repetition rate below 20 Hz and reasonable signal levels the simulation program runs roughly in real time on a standard office computer and Labview[1] version 8.2. However for a low return signal level requiring frequent switching between a large and a narrow range gate, the necessary time to complete a loop of simulation may go up by an order of magnitude. On the front panel of the simulation program there are a number of different diagrams available, which allow the investigation of the laser altimeter behavior and settings of the simulation in progress. At any time throughout the computation the user has full access to the altimeter parameter settings list and all values can be adjusted without the interruption of the program. All changes take effect from one shot to the next. While the shot by shot display of the range-gate content is the most educational diagram during the simulation run, other parameters like orbit distance, terrain contour recovery rate, the shot by shot deviation between the 'observed' and 'true' range (error vector) and the actually obtained pulse width are also summarized in individual charts. At the end of the simulation a data file containing the shot by shot record of the epoch of the measurement, the residual of 'true' range minus 'detected' range as well as the 'assumed' range minus the 'detected' range, the 'detected' range, the evaluated pulse width, the slope of the terrain in degrees and the slope induced dispersion of the laser pulse is written. The epoch relates to the initial point of the orbit integration and is arbitrarily chosen in the simulator. Figure 9 shows a small section of the time series of the residuals from the difference of the 'recovered' range and the 'true' range from the detector signal evaluation process. Since there was a reasonable SNR, the simulated measurement could reproduce the actually used range to within the boundaries of the specified sensor properties (pulse width, terrain roughness). The apparently blurry patches in the middle of the diagram are caused by steep terrain slopes, which increases the laser pulse spreading. As a result of this signal broadening the SNR reduces substantially and the measurement noise goes up accordingly.

[1]Manufacturer: National Instruments Inc.

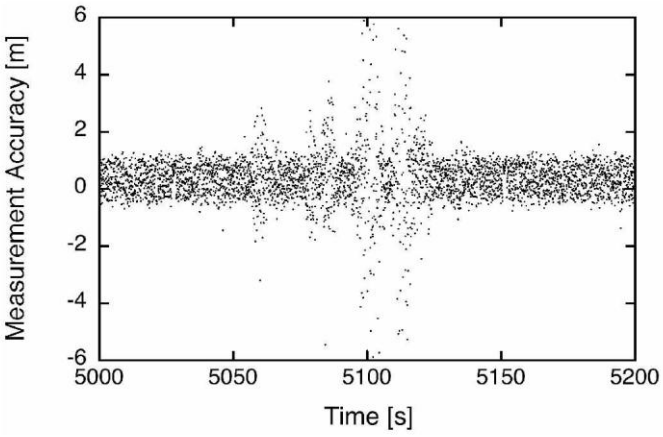

Figure 9. Time series of the error value of the 'recovered' range minus the 'true' range from the detector signal evaluation process. One can clearly see how steep slopes in the terrain reduce the measurement resolution by broadening the received signal pulse and reducing the SNR.

Figure 10 demonstrates this effect more clearly. For the same data section as shown in fig. 9 we have visualized the model terrain profile superimposed on the estimated return signal pulse width. While the terrain profile is shown in gray and slightly offset for better visibility, the laser pulse width was estimated by fitting a Gaussian to the 'detected' time domain voltage of the return signal. The result is displayed shot by shot in black dots. As expected the pulse width shows a minimum when the terrain slope approaches zero. This can be observed for mountain tops, valley bottoms and featureless areas. For a laser pulse width of 6 ns and a surface roughness of 1 m (rms), we obtain the expected minimum values which slightly exceeds 4 ns.[2] As one can see even very small contours in the ground profile reflect themselves in the laser pulse width. For extreme situations like the approximately 2500 m high mountain peak one can see that the pulse width estimates become very noise. This is because of a substantial reduction in the signal to noise ratio, which is a consequence of the spreading of the laser pulse in the time domain. Therefore these areas coincide with areas of reduced measurement accuracy as shown in fig. 9.

4. Impact of Orbit Errors

In order to evaluate the robustness of the range recovery algorithm a test run was performed, where both the assumed and the real orbit were equal, however with a bias for the time of 2 seconds between them. As a result one obtains a rapidly changing range offset of several hundred meter, accumulating to nearly 1 km over a section of 1000 seconds around the perigee of the elliptical orbit. Although the model errors for the radial distance variations are substantial, the resulting 1 m/s range offsets can be accomodated and tracked by the adaptive range-gate routine of the simulator without problem.

[2]The actual value is divided by 2 because of the two-way passage of the simulated laser beam

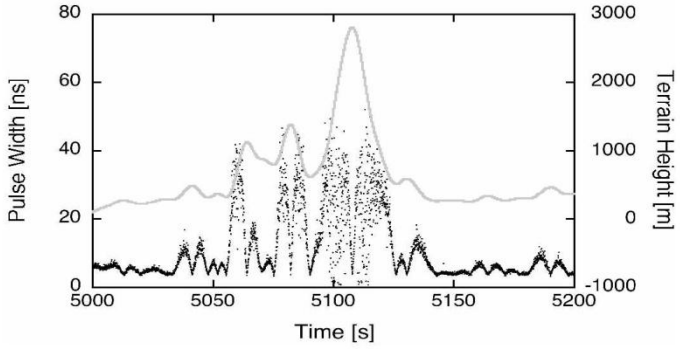

Figure 10. Time series of the estimated shot by shot pulse width of the return signal beam (black dots) superimposed on the corresponding terrain profile (gray line) for the same data section as fig. 9. One can see that the pulse width is a very sensitive measurement quantity for the terrain slope. Even small changes in terrain reflect themselves strongly in the pulse width.

Figure 11 shows a graphical representation for this example. However the resultant cumulative orbit error will place high demands on to the initial ground echo acquisition process, because the difference between the predicted (assumed) and the actually existent (real) range may differ by more than a kilometer. For a case of good SNR one will obtain ground echos within a few shots, but for weak signals in particular for a situation with a high variation of the topography the initial ground echo identification process may be much more difficult. It has been one of the major goals of this simulator project to provide a tool, where suitable data acquisition approaches can be developed and verified over a wide range of anticipated operational conditions.

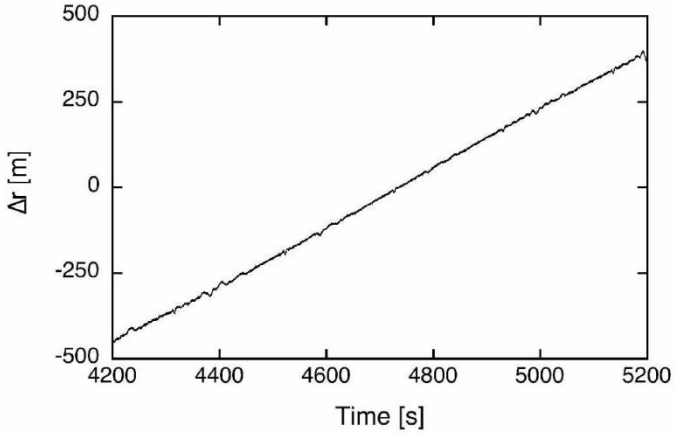

Figure 11. Time series of the error value of the 'true' range and the 'recovered' range from the detector signal evaluation process. The apparently discrete nature of this value is a result of the limited bandwidth of the sampling rate.

5. Conclusion

We have developed a flexible simulation program for spaceborne laser altimeter applications. The laser link budget and the structure of a ground echo in the time domain for a pulsed laser

with a Gaussian profile is calculated over a terrain of user specified roughness and topography on a shot by shot basis. A special feature of the simulation program is a clear separation between the physical model of the laser echo at the instantaneous satellite position and the echo recovery procedure, which works on a different set of orbital parameters. In this way one can not only test the signal response and echo recovery of the modeled altimeter design, but also test and optimize the control program algorithms and the influence of orbit uncertainties on the data recovery and signal identification. So far we have included basic test functions like an unperturbed Keplarian orbit around a spherical celestial body, a user defined terrain structure and two methods of ground echo recovery (threshold and pulsewidth detection). Parameters like current range, recovered terrain profile, pulse spreading of the ground echo and the difference value between the distance defined by the physical model and the distance obtained by the 'measurement' are continuously available for inspection throughout the simulation run. A datafile with a time series of the simulation results is generated at the end of a program run. It is intended to further develop this simulation program by adding more modules for echo reconstruction techniques, which will allow a higher and more robust echo identification rate at lower return signal levels. At the moment we can only analyse the terrain profile along the satellite ground track. If required, future versions of this simulator may be extend to also allow the reconstruction of a complete surface topography.

Acknowledgement

The work presented in this paper is based on the study LAPE-DLR-BG-3000-012 (Laser Altimeter for Planetary Exploration) carried out by DLR and partners in 2003. The authors acknowledge discussions and contributions of I.Leike and J.Oberst. KUS and MH acknowledge the support through an internal DLR grant.

References

[1] Degnan, J. J.; *"Millimeter Accuracy Satellite Laser Ranging: A Review"*; Contributions of space geodesy to geodynamics: technology, (AGU Publication Vol. 25), DE Smith and DL Turcotte editors, ISBN: 0-87590-526-9, 133 - 181, (1993)

[2] ESA study report; *"BepiColombo: An Interdisciplinary Cornerstone Mission to the Planet Mercury"*; ESA-SCI(2000)1, (2000)

[3] Gardner C.S.; *"Ranqinq Performance of satellite laser altimeters"*; Proc. IEEE **30,** (5), 1061 - 1072, (1992)

[4] Luthcke, S.B., Rowlands, D.D., McCarthy, J.J., Pavlis, D.E., Stoneking, E.; *"Spaceborne laser-altimeter-pointing bias calibration from range residual analysis"*; J. Spacecraft Rockets **37,** (3), 374 - 384, (2000)

[5] Thomas, N., Spohn, T., Barriot, J.-P., Benz, W., Beutler, G., Christensen, U., Dehant, V., Fallnich, C., Giardini, D., Groussin, O., Gunderson, K., Hauber, E., Hilchenbach, M., Iess, L., Lamy, P., Lara, L.-M. Lognonne, P., Lopez-Moreno, J.J., Michaelis, H., Oberst, J., Resendes, D., Reynaud, J.-L., Rodrigo, R, Sasaki, S., Seiferlein, K., Wieczorek, M., Whitby, J.; *"The BepiColombo Laser Altimeter (BELA): Concept and baseline design"*; Planetary and Space Science **55,** 1398 - 1413, (2007)

[6] Zuber, M.T., Smith, D.E., Solomon, S.C., Abshire, J.B., AFZAL, RS., Aharonson, O., Fishbaugh, K., Ford, P.J., Frey, F.V., Garvin, J.B., Head, J.W., Ivanov, A.B., Johnson, C.L., Muhleman, D.O., Neumann, G.A., Pettengill, G.H., Phillips, RJ., Sun, X.,

Zwally, H.J., Banerdt, W.B., Duxbury, T.C.; *"Observations of the North Polar Region of Mars from the Mars Orbiter Laser Altimeter"*; Science, **282,** 2053 - 2060, (1998)

Globally Contiguous, High Resolution Topographic Mapping of Planets and Moons via Photon-Counting

John J. Degnan
Sigma Space Corporation, Lanham, MD USA 20706
John.Degnan@sigmaspace.com

Abstract

High resolution topographic mapping of planets and moons from orbit can best be accomplished using mJ-class, multi-kHz laser transmitters and photon-counting detector arrays followed by multichannel timing receivers. An airborne 100-channel, scanning 3D imaging lidar has been successfully flight-tested, and the scaling of the technology to spacecraft altitudes is discussed. The specific requirements for two spaceborne lidars are briefly described: 1) A 16-beam pushbroom lidar for NASA's ICESat-II mission; and 2) a 100-beam scanning lidar for NASA's Jupiter Icy Moons Orbiter (JIMO) mission.

Advantages of Photon-Counting

Photon-counting lidar altimeters and imagers are the most efficient possible since each range measurement requires only one detected photon as opposed to hundreds or thousands in conventional laser pulse time of flight (TOF) altimeters [Degnan, 2001]. The GLAS altimeter on ICESat-I, for example, has a minimum detectable signal corresponding to roughly 100 photoelectrons but can produce in excess of 10,000 detected photoelectrons per pulse from high reflectance surfaces under extremely clear atmospheric conditions. Thus, single photon sensitivity translates to up to four orders of magnitude more imaging capability. Furthermore, single photon sensitivity combined with multistop timing capability enables the lidar to penetrate semi- porous obscurations such as vegetation, ground fog or haze, thin clouds, water columns, etc. and makes contiguous, high resolution topographic mapping on a single overflight possible with modest laser powers and telescope apertures – even from orbital altitudes.

Globally Mapping Planets and Moons

The feasibility of using photon-counting lidars in daylight was first demonstrated experimentally by NASA's "Microaltimeter" system. [Degnan et al, 2001]. The feasibility of spaceborne laser altimetry using mJ-class, multi-kHz lasers and photon-counting receivers was established theoretically through link analyses and modeling of the solar noise background [Degnan, 2002a]. The specific case of a Mars orbiter at a typical altitude of 300 km was analyzed. Correlation Range Receivers (CRR's) with carefully chosen "range bins" and "frame intervals" were proposed as the "optimum" approach for extracting the surface signal from the solar background under low "contrast" (SNR) conditions. Although wide swath multi-beam "pushbroom lidars" are one approach to large scale mapping, truly contiguous topographic mapping on a global scale with several meter horizontal resolution is best accomplished using a large array detector and an optical scanner [Degnan, 2000b].

Flight Testing of Second Generation 3D Imaging Lidar

Sigma has developed and flight-tested a highly successful airborne 3D Imaging and Polarimetric Lidar prototype, which demonstrates the latter approach [Degnan et al, 2007]. In this system, shown mounted on a camera tripod in Figure 1, a microchip laser transmitter produces 380 mW of infrared power at 1064 nm and a KTP Type II doubling crystal generates about 140 mW of green power (6 μJ @ 22 kHz). The green power at 532 nm is used for 3D imaging of the terrain while the residual 240 mW of 1064 nm power is dedicated to measuring the depolarization produced by the surface.

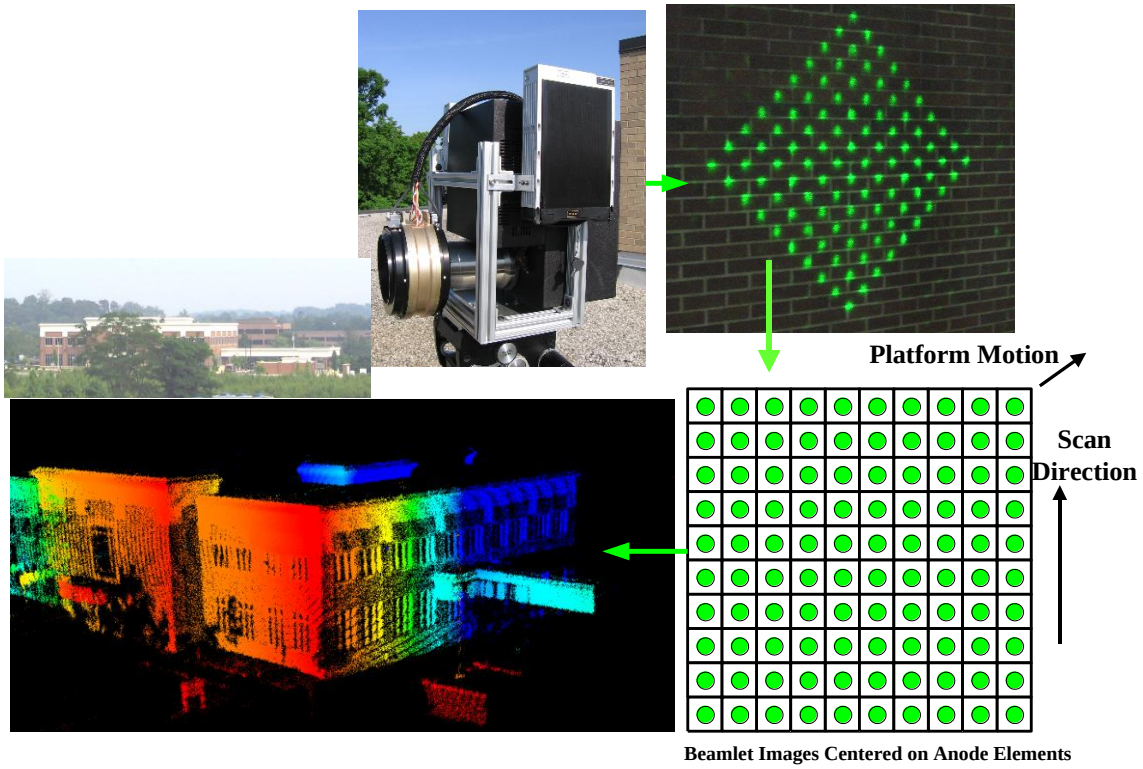

Figure 1. Clockwise from top left: Sigma 3D Imaging and Polarimetric Lidar during rooftop testing to local bank (photo inset); 10x10 beamlet array on bank wall; imaging of beamlets onto individual anodes of MCP/PMT; scanned 3D lidar image of bank.

After the two wavelengths are split by a dichroic beamsplitter, a Diffractive Optical Element (DOE) splits the 532nm beam into a 10x10 array of beamlets which are then recombined with the NIR polarimeter beam via a second dichroic. Both wavelengths are then transmitted through the central portion of a 3 inch diameter transmit/receive telescope and steered by an external dual rotating optical wedge scanner synchronized to the laser pulse. The telescope and scanner are aperture-shared by the two transmit wavelengths and their corresponding receivers .

Since the DOE is about 80% efficient, each 532 nm beamlet contains a little over 1 mW of green power (~50 nJ @ 22 kHz). The 100 individual ground beamlets are imaged onto the Microchannel Plate Photomultiplier (MCP/PMT) photocathode, and the microchannels guide the photons received from one beamlet to one anode of a matching 10x10 anode. array. Each anode is then input to one channel of a 100 channel timing receiver, which has a $\pm$ 93 psec timing resolution and a 1.6 nsec deadtime. Thus, each laser pulse produces a 10x10

pixel 3D image of a 1.5 m x 1.5 m square surface from the nominal design altitude of 1 km. A wide swath contiguous image of the terrain is generated by mosaicing these individual pulse images via the aircraft motion and the optical scanner. Sample flight images are shown in Figure 2.

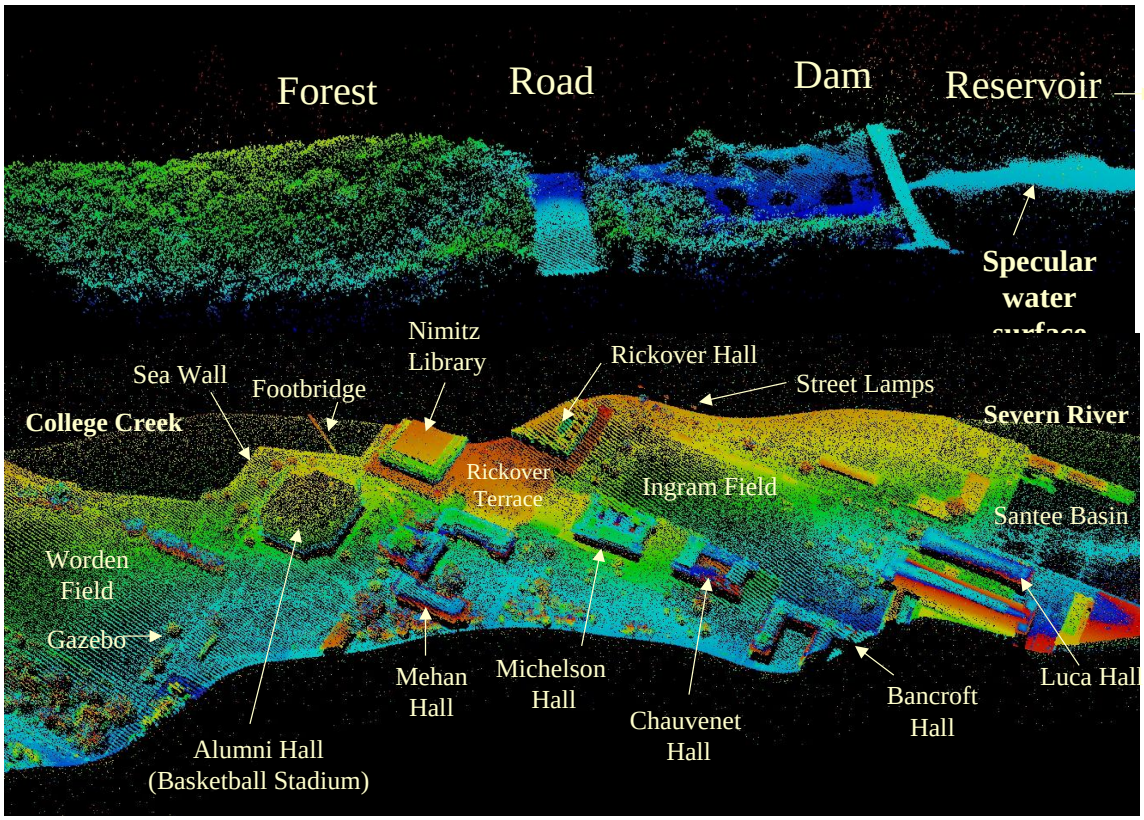

Figure 2. Sample inflight images taken with the 2nd Generation 3D Imaging Lidar: (a) Triadelphia Reservoir; (b) US Naval Academy Campus in Annapolis, MD.

Requirements for Contiguous Mapping

The Sigma 2nd generation 3D Imaging Lidar design is essentially an airborne prototype of a prior spaceborne 3D imaging lidar concept [Degnan, 2002b]. In order to map contiguously from an aircraft or spacecraft, the lidar instrument must satisfy three conditions on scan speed, laser repetition rate, and power-aperture product. For contiguous along-track imaging the scan frequency must satisfy the condition

$$f_{scan} \geq \frac{v_g}{\sqrt{2}(N\delta)} \qquad (1)$$

where v_g is the ground velocity of the aircraft/spacecraft, N^2 is the number of pixels in the NxN detector array, and δ is the desired horizontal ground resolution. For contiguous crosstrack imaging across a swath width S, the laser repetition rate must satisfy the condition

$$f_{qs} \geq \frac{2v_g S}{(N\delta)^2} \qquad (2)$$

Finally, we need a certain Transmitted Energy-Receive Aperture (E_tA_r) product to satisfy the altimeter link equation for all channels, and this requirement can be expressed as [Degnan, 2002a]

$$E_t A_r > \frac{n_p \pi h\nu N^2 R^2}{\eta_c \eta_r \rho \cos\sigma T_0^2} \tag{3}$$

where, from Poisson statistics, n_p =3 is the received photoelectrons per ranging channel per pulse required to achieve a per channel detection probability per pulse of 95% in photon-counting mode, R is the range to the surface, η_c is detector counting efficiency, η_r is the optical throughput efficiency of the receiver optics, $h\nu$ is the laser photon energy, ρ is the surface reflectance, σ is the surface slope, and T_0 is the one-way atmospheric transmission at zenith. Combining (2) and (3) gives a minimum Power-Aperture product, i.e.

$$P_t A_r = f_{qs} E_t A_r > \frac{n_p \pi h\nu}{\eta_c \eta_r \rho T_0^2} \frac{2v_g S R^2}{\delta^2} = \frac{2v_g S R^2}{C_a \delta^2} \tag{4}$$

where we have defined the "altimeter constant" C_a and used the fact that, for the vast majority of surfaces, cosσ ~1.

NASA's Jupiter Icy Moons Orbiter (JIMO) Mission

In late 2006, Sigma completed a preliminary study for NASA Headquarters on a scanning lidar for the JIMO mission. The science goal was to globally map the surfaces of three primary moons of Jupiter – Ganymede, Callisto, and Europa - from a 100 km orbit about each moon. The resolution goals were 10 m horizontal and sub-meter vertical. A major technical challenge was to map Europa in one month before Jupiter's intense radiation field damaged onboard electronics. However, later studies published by researchers JPL suggested that the Europa portion of the mission might be extended up to 3 or 4 months with proper shielding. Nevertheless, our study considered a 30 day requirement at Europa which led to a minimum swath width of 14.4 km which applied to all three Jovian moons because of the fixed orbital altitude. The results of our JIMO study are summarized in Table 1 assuming N^2 = 100 and a nominal surface reflectance for soil (ρ = 0.15 @ 532 nm).

Because of their larger diameter, Callisto and Ganymede require a minimum 56 and 60 days respectively to complete one global map. Since the ground velocity is highest at Ganymede, this moon drives the requirements on scan frequency, laser repetition rate, and power-aperture product as predicted by equations (1) through (4). The JIMO scan and repetition rate requirements actually fall below the capabilities of our current airborne lidar, i.e. f_{scan} = 25 Hz and f_{qs} = 22 kHz. The required Power-Aperture product of 1.12W-m^2 is well within the laser state of the art for modest telescope apertures, e.g., 3 W and 50 cm. To reduce instrument mass, volume, and prime power, the optical scanner would be placed internal to the telescope.

Table 1. Summary of JIMO lidar requirements, assuming a 30 day mission at Europa and an orbital altitude of 100 km at all three Jovian moons. The moon driving a particular lidar specification is indicated by **boldface** type.

Jovian Moon	Europa	Callisto	Ganymede
Lunar Mass, M_i (kg)	4.80×10^{22}	1.08×10^{23}	1.48×10^{23}
Mean Volumetric Radius, R_i, km	1569	2400	2634
Orbital period about Jupiter, Days	3.551	16.7	7.15
Surface Area, km^2	3.094×10^7	7.238×10^7	8.718×10^7
Satellite Altitude, r_i (km)	**100**	**100**	**100**
Ground Velocity, v_q (km/sec)	1.30	1.63	**1.83**
Satellite Orbital Period, min	126	154	151
Mission Duration, D_i (Days)	**30**	56	60
3D Imager Resolution, δ (m)	**10**	**10**	**10**
Polarimeter/Hyperspectral Resolution, $N\delta$ (m)	**100**	**100**	**100**
Swath Width, s_i (km)	**14.4**	14.4	14.4
Scanner FOV Half Angle, (deg)	**5.72**	5.72	5.72
Scan Frequency, Hz	9.2	11.5	**12.9**
Lidar PA-Product, W-m^2	0.797	0.998	**1.12**
Min. Laser Fire Rate, f_{qs} (kHz)	3.74	4.68	**5.26**

Cross Track Channel (CTC) Lidar on ICESat II

Sigma has proposed a visible 16-beam "pushbroom lidar" [Degnan, 2002b] to fly alongside the conventional 1064 nm lidar on NASA's ICESat-II mission. As presently envisioned , a DOE would generate 16 separate groundtracks from a single 4W frequency-doubled Nd-based transmitter (400 μJ @ 10 kHz @ 532 nm) or 0.25 W (25 μJ @ 10 kHz) per ranging channel. The 16 beams would be arranged such that periodic spacecraft yaw rotations of 90^o designed to follow the Sun would reproduce the same groundtrack pattern. The groundtracks would be separated by roughly 140 m on the ground for a total swath of 2.1 km. Besides providing greater spatial coverage, the photon-counting CTC lidar would provide improved alongtrack and crosstrack slope information, important to ice science.

Summary

Photon-counting lidars can detect single photon surface returns and thereby increase the spatial coverage and resolution by orders of magnitude relative to conventional multi-photon lidars for a given Power-Aperture Product. Rooftop and airborne tests of 1st and 2nd generation 3D imaging lidars have demonstrated the feasibility and accuracies of photon-counting lidars operating in daylight and their scalability to space platforms. Photon-counting lidars are ideal for planetary and lunar mapping missions where instrument mass, size, and prime power are heavily constrained. They are especially attractive for mapping the outer planets and their Moons where the solar background count rates are relatively low compared to Earth (e.g. 25 times less at Jupiter). The proposed Cross Track Channel (CTC) lidar on NASA's ICESat-II mission, if approved, will space qualify and lifetest all of the key components needed for future interplanetary pushbroom lidars, including the transmitter, detector, and timing electronics. Ruggedized lasers already meet or exceed the functional requirements of the JIMO and CTC missions. Optical scanners for globally contiguous

mappers will require further independent development and testing to demonstrate long term reliability.

References

Degnan, J. J., "Photon Counting Microlaser Rangers, Transponders, and Altimeters", Surveys in Geophysics, Vol 22, Nos. 5-6, pp. 431-447, 2001 .

Degnan, J., McGarry, J., Zagwodzki, T., Dabney, P., Geiger, J. , Chabot, R. , Steggerda, C. , Marzouk, J. and Chu, A. , "Design and performance of an airborne multikilohertz, photon-counting microlaser altimeterInt. Archives of Photogrammetry and Remote Sensing, Vol. XXXIV-3/W4, pp. 9-16, Annapolis, MD, 22-14 Oct. 2001.

Degnan, J.J., "Photon-Counting Multikilohertz Microlaser Altimeters for Airborne and Spaceborne Topographic Measurements", Journal of Geodynamics, 34, pp. 503-549, November, 2002a,.

Degnan, J.J., "A Conceptual Design for a Spaceborne 3D Imaging Lidar", J. e&i Electrotechnik und Informationstechnik, Vol.4, pp. 99-106, April, 2002b.

Degnan, J., Wells, D., Machan, R., Leventhal, E., "Second Generation 3D Imaging Lidars Based on Photon-Counting", SPIE Optics East , Boston, MA, September 9-12, 2007.

Altimetry and Transponder Ground Simulation Experiment

K.U. Schreiber[a], M. Hiener[a], B. Holzapfel[a], H. Michaelis[b], N. Brandl[c], K.-H. Haufe[c]

[a]Forschungseinrichtung Satellitengeodaesie, Technische Universitaet Muenchen
Geodaetisches Observatorium Wettzell, 93444 Bad Koetzting, Germany
[b]DLR e.V. Institute of Planetary Research, Rutherfordstr. 2, 12489 Berlin, Germany
[c]Bundesamt fuer Kartographie und Geodaesie
Geodaetisches Observatorium Wettzell, 93444 Bad Koetzting, Germany

schreiber©fs.wettzell.de

Abstract

We have designed and built a compact demonstrator unit for the investigation of altimetry and transponder applications. A small light-weight breadboard carries a compact frequency doubled Nd:YAG pulse laser, afocal beam expansion optics, a small receiver telescope with spectral and spatial filter arrangements and a photosensitive detection device (SPCM, PMT or SPAD). The output laser energy can be as high as 45 mJ with a pulse-width of 3 ns and the telescope aperture is 12 cm. Simulations [1] suggested that the link margin for low Earth orbiting satellites (LEO) is comfortable and that it may be possible to obtain echoes from a dual-station experiment in several different configurations. This paper outlines details of the experiment and presents the obtained results.

Key words: Satellite Laser Ranging, Optical Transponder, Laser Altimetry, Interplanetary Ranging
PACS: 06.30.Gv, 42.79.Qx, 95.55.-n, 42.50.Ar

1. Introduction

Laser ranging at interplanetary distances has become a viable option in recent times. The advances made in optical communications as a result of the need of higher transmission bandwidth for the recent generation of imaging satellites provides the necessary infrastructure namely pointing and spaceborne telescope design.

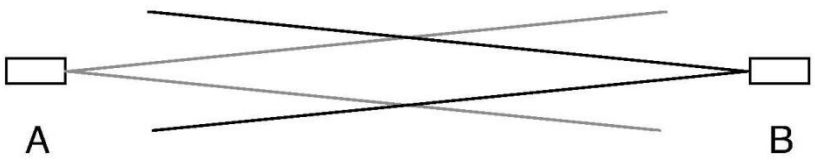

Figure 1. A transponder for optical ranging consists of a laser transmitter and a photo-sensitive receiver on both ends of the distance of interest.

This suggests to include inter-satellite ranging and Earth to interplanetary satellite ranging as newly available means of precise orbit determination (POD). In other cases of dedicated space missions for fundamental physics, such as the proposed "Einstein Gravity Explorer" [2] laser ranging may provide the tools for high-precision clock comparisons. Therefore it is time to study the potential of interplanetary ranging in more detail. Since dedicated experiments in space are far to expensive and time consuming to be realized, there are only two other possibilities left. Either an existing pulse laser equipped mission can be "misused" to evaluate an interplanetary optical ranging link or a ground based experiment has to be set up such that all relevant parameters of an interplanetary optical link can be examined in great detail. Figure 1 shows the basic concept of an optical transponder. There are two transmitters and receivers located at the ranging terminals A and B. They are firing short laser pulses at each other asynchronously and from a large distance. While the epochs of the detected signals are timed on each local computer, the epochs of laser fire are exchanged via telemetry between both stations. From this one can compute the range and the rate of change (on the radial component) between both stations as well as the respective clock offset. In this way the dependence of the receive signal on the covered distance follows a $1/r^2$ relationship rather than $1/r^4$ like in the case of a two-way optical link from backreflections off corner cubes on artificial satellites and on the moon [3]. While the moon is at about the largest distance that can be practically tracked by using passive retro-reflectors, transponder have the potential to work within the entire solar system on a reasonable link margin. Until today there have been two feasibility studies, which were performed as experiments of opportunity making use of NASA spaceprobes in orbit around Mars and in transfer to Mercury [4], namely:

- One-way ranging to Mars Global Surveyor at a distance of 80 million km
- Two-way ranging during a MESSENGER fly-by at a distance of 24 million km

The Mars Orbiter Laser Altimeter (MOLA) was orientated pointing toward Earth in order to detect laser pulses transmitted from the 1.2 m telescope of the Goddard Space Flight Center in Greenbelt. Since the transmitter of MOLA is no longer working only one-way ranging could be demonstrated successfully based on a very small number of unambiguously identified datations. In a similar way an equipment test of the Mercury Laser Altimeter (MLA) during a fly-by of the MESSENGER spacecraft was used to determine the range and clock offset between the spacecraft and the ground station in Greenbelt by a complete ranging link in both directions. Consistent results were obtained despite the fact that the number of data points were sparse and the laser pulse width of the altimeter was not ideal for such a ranging application.

2. Transponder Simulation

In a very general way one can consider satellite laser ranging (SLR) as a special laser transponder application. Provided that there are two ranging stations located sufficiently close together (within the divergence angle of the reflected laser beam), it is possible to test parts or all functions of a transponder link in an entirely ground based experiment. According to [1] the equivalent transponder distance r_t relative to an SLR laser link of the same station is a function of the actual slant range r_s. For a satellite in near circular orbit at the height h above sea level r_s can be expressed as

$$r_s(h,\Theta) = -r_E cos\Theta + \sqrt{(r_E cos\Theta)^2 + h(h+2r_E)} \quad , \tag{1}$$

where Θ is the zenith distance and r_E = 6378 km the mean radius of the Earth. The equivalent transponder distance then becomes

$$r_t(h,\Theta,\sigma_s) = r_s^2(h,\Theta)\sqrt{\frac{4\pi}{\sigma_s}\frac{1}{T_A^{sec\Theta}}} \quad . \tag{2}$$

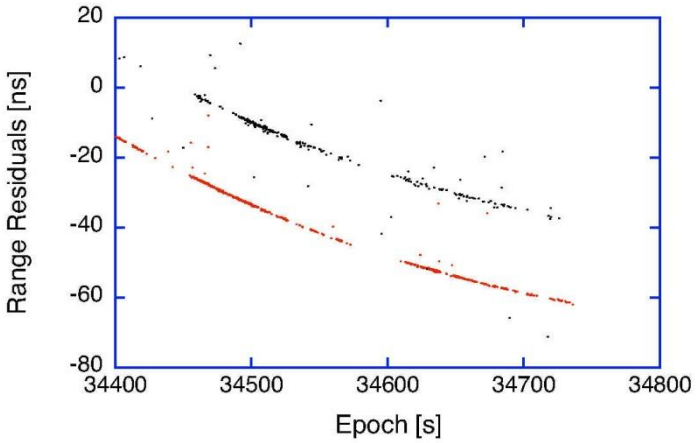

Figure 2. Example of a Topex pass observed by the WLRS on June 20, 2001 under cloudy conditions. The returns on the standard ranging configuration are shown on the lower trace, while the echoes on the small extra receive aperture are displayed on the upper trace.

One can see that it strongly depends on the slant range and on σ_s the laser cross-section of the target in square meters. In the following we are assuming an atmospheric transmission T_A of around 0.7**,** which is the maximum value for the given operational wavelength of the ranging systems of λ = 532 nm. It is difficult to establish a reliable value during the measurements. As pointed out in [1] "real world" tests of transponder functions for distances as far out as the outer planets of the solar system are possible. In a first test we have mounted a small telescope with an aperture of 12 cm to the Wettzell Laser Ranging System (WLRS), pointing along the optical axis of the main telescope in order to detect laser echos independently from the routine ranging hardware. Over a period of several month echoes from a number of satellites including Lageos and Etalon were recorded in parallel on the additional telescope. One example of a satellite pass from Topex on June, 20 in 2001 is shown in fig. 2. This was an intermediate step towards a transponder testbed installation, since it demonstrated a sufficient link margin for such a small receive signal aperture. At the same time this basic setup already resembles a simplified version of the basic layout of an asynchronous transponder concept as outlined in [1]. Figure 3 illustrates the entire operation principle. There are essentially two timescales involved, one for each terminal of the two stations separated by a large distance. Under typical conditions it can be assumed that there is an offset between the two timescales as well as there is a relative drift between them. In the case of an interplanetary transponder the range *r* between the two stations would be

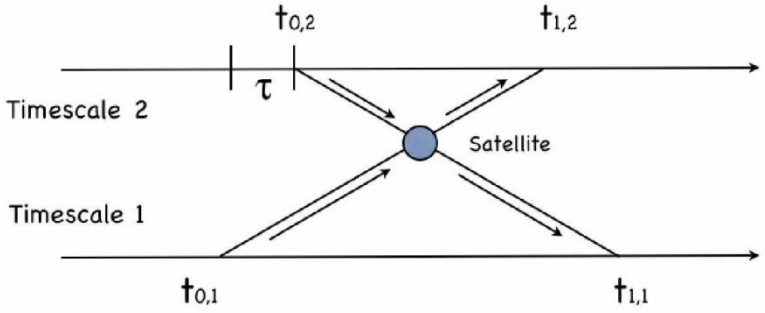

Figure 3. Functional diagram of the transponder simulation application. Time is progressing along the x-axis, while the distance is corresponds to the y-axis. For an interplanetary link laser pulses are transmitted directly between the two ranging terminals. In a ground based simulation experiment, geodetic satellites are used to backreflect the laser pulses, so that they can be detected by an independent ranging system on the ground near the transmitting station.

$$r = \frac{c}{2}[(t_{1,1} - t_{0,1})(t_{1,2} - t_{0,2})], \tag{3}$$

where c is the velocity of light and $t_{n,m}$ are the corresponding epoch registrations on each ranging terminals. During a typical transponder application many such pulses are transmitted from both sides and a priori range estimates have to be applied to work out the respective corresponding pairs of epoch registration used in eq. 3. However for a transponder simulation setup with a geodetic satellite reflector target employed there are essentially three scenarios available for studies. Case 1 is the usual satellite ranging operation for the station associated with timescale 1 alone. Case 2 is the additional laser ranging operation associated only with timescale 2. Transponder operations (case 3) can be realized by transmitting laser pulses asynchronously from one station, receiving it by the other station and vice versa. In the most simplified case both stations share the same telescope drive for pointing, while all other hardware components like timers, control system and lasers etc. are independent. More generally the two ranging terminals could be realized by two individual SLR stations in close proximity as proposed in a NASA concept [5].

3.Transponder Demonstrator Experiment

A balanced transponder link is characterized by a comparable number of recorded photo-electrons on both ends of the transmission path. For an optical satellite to satellite link this usually would mean the application of similar laser transmitters and telescope apertures on both terminals. However for a ground to satellite link it is desirable to have a large telescope and a powerful laser on the ground where it is readily accessible and only a low-power laser and small telescope in space. This reduces the demands on payload requirements substantially. Therefore we have followed a similar approach for our testbed experiment. The WLRS was used as Station A [6]. It operates a 0.75 m diameter telescope and a 180 mJ frequency doubled Nd:YAG laser. The pulse width is 80 ps. A Quantel Brio laser with 35 mJ (3 ns pulse width) with a transmit aperture of 3 cm was used for Station B. The corresponding transmitter divergence has a minimum of 24 arc seconds. The receive telescope is a 12 cm Maksutov type aperture with additional spatial and spectral filters in order to allow daylight operation. Several different photo-detectors may be attached.

Experiments were carried out with a PMT (12% quantum efficiency), the SPCM module of EG&G and a SPAD for single photo-electron detection.

Figure 4. Hardware layout of the transponder simulation module. On the left hand side one can see the laser (from the backside), the transmit and receive aperture. The top view on the right hand side also shows the filter arrangement behind the receive aperture and the photo detection device

Figure 4 shows the compact design of the transponder simulation module. A diaphragm in the receive path allows the adjustment of the receiver field of view in the range of 20 to 90 seconds of arc. Basic test operations of the transponder simulator were carried out by ranging to a local ground target, namely a diffuse reflecting concrete pillar 180 m away.

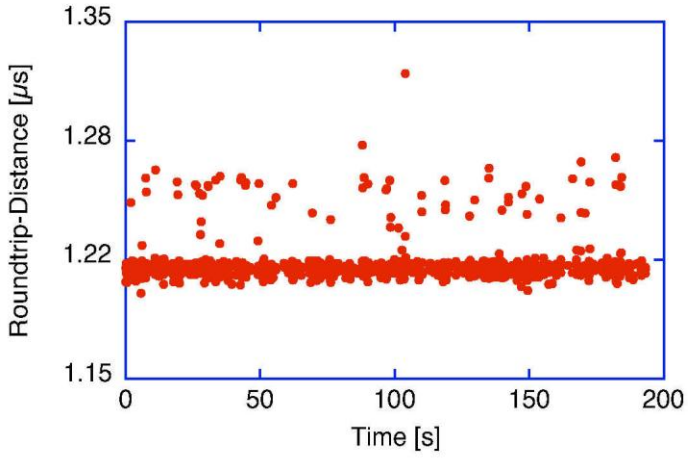

Figure 5. Example of a ground target range measurement sequence. The low energy laser pulse was reflected from a concrete pier at a distance of about 180 m.

Figure 5 shows a typical result of these ground tracks, detected with the photomultiplier as a receiver. In order to operate the full transponder experiment we have set up a completely independent ranging environment, including the event timer and control system software as outlined by the block diagram in fig. 6. For simplicity it is assumed that the computer control and data logging is part of the timer module. Each system needs a start and stop pulse to perform the range measurement function and in addition a gate signal to arm the detector for the reception of the return signal. Since both systems operate entirely asynchronous with a

repetition rate of 10 Hz in the case of the WLRS and 20 Hz for the transponder module, it is necessary to cross over both the detector signal cable and the rangegate generator signal between the two systems. Apart from this change both stations are treated like independent ranging environments. Following [1] link budget calculations show the expected return signal strength for a number of configurations summarized in table 1. For this calculation a zenith distance of 30° and an atmospheric transmission of 0.7 was used. This corresponds to reasonably good but not ideal conditions and assumes a collimated laser beam for both transmitters. In order to operate the simulation module on top of the laser telescope of the WLRS one has first to align the optical axis of the transmitter of the simulation module to be collinear with the corresponding optical axis of the receiver. This was done by imaging the ground target 180 m away from the simulator test location on the receive telescope of the simulation module. Once the laser beam was in the center of the field of view of the receiver telescope the alignment screws were tightened up. Then the entire base plate was lifted and mounted on a adjustable frame over the elevation axis of the WLRS telescope. Figure 7 shows the simulation module sitting on the much larger telescope of the WLRS. The alignment of the simulation module relative to the optical axis of the WLRS was achieved by pointing the two systems to a reference target approximately 5 km away from the ranging site. The entire simulator was adjusted with the mounting frame to also image the remote reference target in the eyepiece of the receiver telescope.

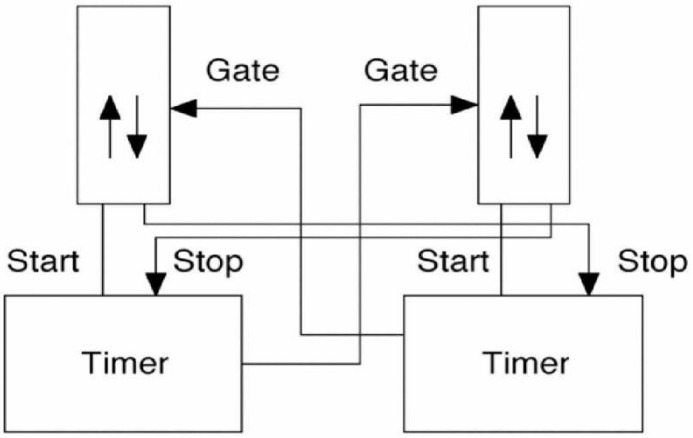

Figure 6. Block diagram illustrating the cable crossover required for the transponder simulation experiment.

Table 1. Expected link budget for ground based transponder simulation. The figures for the WLRS are computed for the Micro-Channel-Plate photomultiplier.

Configuration	n_{ph} Ajisai	n_{ph} Envisat	n_{ph} LAGEOS
WLRS - Transp.	4.5k	1.5k	10
Transp. - WLRS	10k	3.5k	24
WLRS - WLRS	240k	79k	547
Transp. - Transp.	817	272	1.8

Figure 7. Simulation module mounted on top of the WLRS telescope.

4.Experimental Results

4.1. Transponder Link

The transponder module remained on the WLRS telescope for one week and a total of 21 successful satellite passes were observed in different arrangements, covering all the different options of table 1. In this paper we only report results from the two most demanding configurations, namely the actual transponder setup and the case where a high Earth orbiting satellite (LAGEOS 1) has been observed with the transponder module in SLR configuration. Figure 8 shows the result for a daylight Beacon C path, asynchronously running in the transponder configuration (fig. 6). This satellite is in a near circular orbit approximately 1000 km above the ground. According to tab. 1 one would expect a stronger echo detection rate on the WLRS system, because of a link margin, which is by a factor of two higher and because of the much higher laser pulse rate. However the data recorded by the transponder hardware turned out to be much denser in the end. Although the reason for this behavior was not unambiguously identified, circumstances suggest that this happened because of a residual misalignment of the emitting laser beams between the two ranging systems. While the colinearity of the optical axis of both receivers has been verified repeatedly by observing a landmark several kilometers away, similar checks for the transmitting branches of the two system have not been possible. Therefore it is very likely that a small misalignment is responsible for the reduced link budget, because the divergence of the laser beam of the transponder had to be increased. In subsequent observations there were two regimes identified around 30 seconds of arc apart, where the return rate for each of the two systems is at a maximum [7]. After the noise and the trend was removed from the residuals of both data-sets by fitting a polynomial to the transponder data and applying the same parameters to the WLRS measurements, the plot of fig. 9 is obtained. The observed scatter of the WLRS data is much higher than for the simulation unit. This is caused by the much broader pulse width (3 ns) of the Brio laser. In comparison the WLRS laser provides a pulse width of 80 ps. There is more noise in the WLRS ranging window (fig. 8 bottom part) because of a repetition rate twice as high as for the WLRS laser. The effect appears to be smaller than it is in reality, since the WLRS operates under a much smaller field of view (50 µrad rather than 200 µrad) and also uses a cooled detector. The transponder system has not been calibrated to the reference point of the WLRS hence the observed offset of 10 ns between both systems.

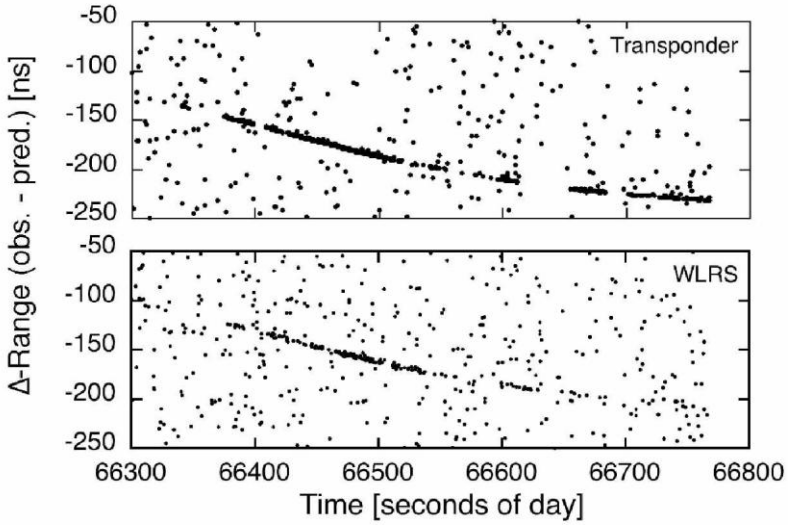

Figure 8. A simultaneous observation of a Beacon C satellite pass with both ranging systems in asynchronous transponder configuration. The pass was observed on August 16, 2008 in daylight.

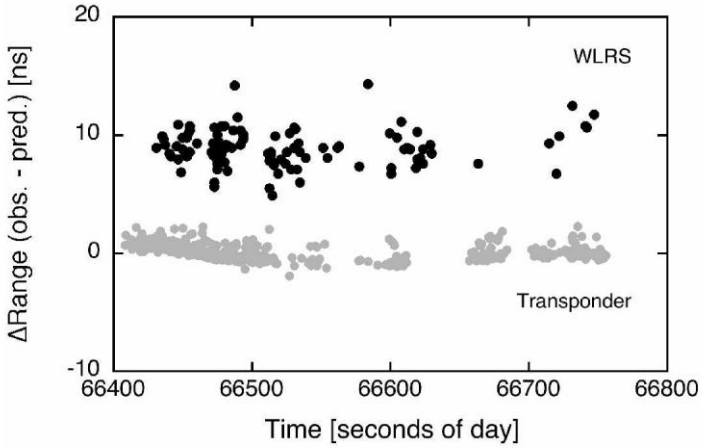

Figure 9. The filtered transponder echos from fig. 8. The data recorded on the WLRS exhibits a larger scatter caused by the 3 ns pulse width of the transponder transmitter. The offset between the two tracks is introduced for better visibility.

4.2. Biases from Receive Signal Intensity Variations

Apart from demonstrating the basic functions and the feasibility of this transponder link experiment, this setup is also useful to investigate systematic receive signal biases [8]. For this purpose only the WLRS laser fires and both telescopes receive the same return signal from the satellite. According to tab. 1 there is approximately a factor of 50 difference between the generated numbers of photo-electrons on each detector system. Some of this imbalance in receive power will usually be compensated by an adjustable gray wedge in the receiver path of the WLRS system, but there are no simple rules for the settings. However when the range residuals from a weak and a strong signal return level are plotted against each

other and intensity dependent detector delays appear, this will reflect as a systematic signature in the residual vs. residual plot.

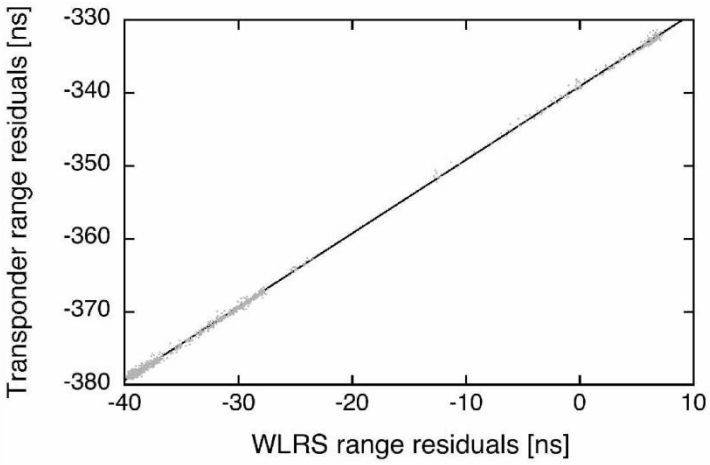

Figure 10. Range residual plot of a Beacon C pass taken on August 13, 2008. Simultaneous detections on both ranging systems are plotted against each other in this chart.

Figure 10 shows such an example for a observed Beacon C pass. A higher density of observations suggest higher intensity on the return signal. The linear regression of this data set yields a slope of 1.008, which is the first indication of a systematic difference between both signals. In the next step we have applied the linear regression to the data and then plotted these residuals versus time. This yields the scatter plot of fig. 11. The solid line superimposed on this data was derived by taking the average of all data points in 1 minute intervals. As expected, areas of high data density have a tendency towards shorter ranges. This is in accordance with both the behavior of avalanche photodiodes operated in the Geiger mode, where a higher return signal level by-passes several stages in the multiplication process, which leads to the breakdown of the bias voltage of the diode. Also photomultipliers employing a constant fraction discriminator for a signal voltage independent timing of the arrival of the laser pulse are expected to measure shorter ranges for higher signal levels, since the discriminator only works in a very limited signal voltage range.

4.3. Simulated Interplanetary Distance

Finally, we have also explored the weakest satellite link listed in tab. 1 and observed a LAGEOS satellite pass on the transponder module alone. The return echo rate was very weak as it is to be expected from a statistically obtained 2 photo-electrons from such a small system.

Figure 12 shows the measured range residuals. There were about 60 returns detected within 560 seconds. This means that 0.5% of all shots (repetition rate: 20 Hz) obtained a valid return signal. This is less than expected from tab. 1. A 2 photoelectron return signal level would usually result in a data rate of about 10%. We believe that this discrepancy can be attributed to both, a slightly larger beam divergence of the outgoing laser beam and an effective atmospheric transmission below the maximum value of T_A= 0.7. During the time, where valid satellite returns have been detected the slant range varied from 7500 km $\leq r_s \leq$ 6700 km with the marginally higher return rate at the longer distances at the beginning of the pass. With s_r = 7500 km, a radar cross section of the satellite LAGEOS of σ_s = 15 million square

meter and an assumed value of T_A = 0.6 the equivalent transponder distance for the here described transponder simulation module turns out to be r_t = 0.44 AU.

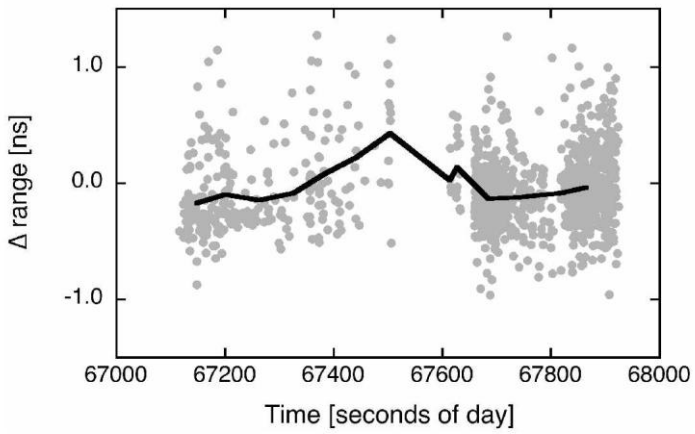

Figure 11. Range residual plot of a Beacon C pass taken on August 13, 2008. The residuals are obtained from a linear regression on simultaneous detections on both ranging systems. The black line was derived from this data set by averaging the data over 1 minute intervals.

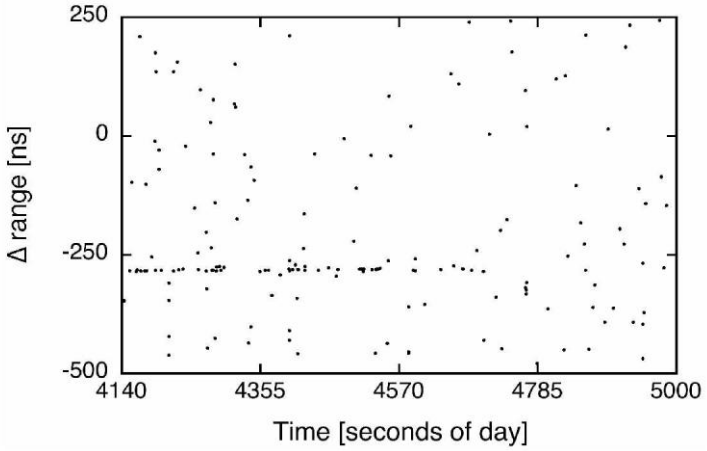

Figure 12. Range residual plot of a LAGEOS 1 pass taken on August 19, 2008 using the transponder module alone. The satellite track is very weak as expected from the low signal level calculated for this case (tab. 1).

If we apply the same calculation for the WLRS system, which routinely tracks GPS satellites and also obtained laser echoes from the Apollo 15 laser reflector, we find a convenient equivalent transponder distance of $r_t \approx 4$ AU and a maximum demonstrated marginal transponder distance of $r_t \approx 110$ AU. However this would require a balanced transponder link, with a space segment about 5 times more efficient than the module investigated in this paper.

5.Conclusion

In this paper we have simulated basic properties of optical interplanetary transponder links experimentally. A small transponder module comprising a pulse laser, a small telescope

including provisions for spectral and spatial filtering and an event timer unit was used together with the Wettzell Laser Ranging System for the simulation. During the experiment laser pulses from one system were transmitted to orbiting geodetic satellites. The back-reflections were recorded on the respective other system. The characteristics of the two independent ranging instruments were then used to compute the equivalent transponder deep space distance. While the transponder module showed sufficient sensitivity to cover distances of up to 0.44 AU, the WLRS has a comfortable l-way range margin of about 4 AU. However, since successful lunar echoes have been obtained from the WLRS in the past, it has demonstrated a very marginal equivalent transponder range to about 110 AU, but this cannot be called operational. While the laser link margin is certainly an important parameter, other needs like precise pointing and the alignment of the transmit and receive path are of similar concern for successful interplanetary transponder applications. This is also evident in our experiment, since the measured signal levels always lagged behind the link budget calculations. The great advantage of the transponder simulation is a complete end to end test of a transponder link under real conditions, including all of the involved hardware and the atmosphere, from an easily accessible ground based observatory. The only differences between this experiment and a real deep space transponder link are a double pass of the optical signal through the atmosphere and the alignment of the optical path between the observatory on the ground and an interplanetary spacecraft.

Acknowledgement

This project is supported by Bundesamt für Karographie and Geodäsie (BKG) and the Deutsches Zentrum für Luft- und Raumfahrt (DLR), Berlin. The authors would like to thank Wolfgang Schlüter from the Bundesamt für Kartographie und Geodäsie for their support of the project and Michael Wensauer for the assistance in preparing the necessary instrumentation.

References

[1] J. J. Degnan, *"Simulating Interplanetary Transponder and Laser Communications Experiments via Dual Station Ranging to SLR Satellites"*; Proceedings of the 15th International Workshop on Laser Ranging, Canberra, Australia

[2] S. Schiller, G.M. Tino, P. Gill, C. Salomon and 34 others; *Einstein Gravity Explorer - a medium-class fundamental physics mission*; Exp. Astron., DOI: 10.1007/s10686-008-9126-5, (2008)

[3] J. J. Degnan; *"Asynchronous laser transponders for precise interplanetary ranging and time transfer"*; J. Geodynamics **34**, 551 - 594, (2002)

[4] D. E. Smith, M. T. Zuber, X. Sun, G. A. Newman, J. F. Cavanaugh, J. F. McGarry, T. W. Zagwodzki; *"Two Way Laser Link over Interplanetary Distance"*; Science, **311**, 6. January 2006

[5] J. McGarry, T. Zagwodzki, P. Dabney, P. Dunn, J. Cheek; *"Laser Ranging at Planetary Distances from SLR2000"*; Proceedings of the 15th International Workshop on Laser Ranging, Canberra, Australia

[6] W. Schlüter, R. Dassing, P. Sperber, R. Kilger, U. Schreiber; *The Role of the Fundamental Station Illustrated by the Example Wettzell*; AGU Geodynamics Series Vol. 25, 125 - 132, (1993)

[7] B. Holzapfel, *"Transpondersimulationen für Anwendungen in den Geodätischen Raumverfahren*; Diploma Thesis; Universität der Bundeswehr, München, (2008)

[8] U. Schreiber, A. Schlicht, K.H. Haufe, *"Systematic Biases in Laser Range Measurements"*; Proceedings of the SPIE, **3865**, Laser Ranging and Atmospheric Lidar Techniques II, 64 - 73, (1999)

Testing Fundamental Gravity via Laser Ranging to Phobos

Thomas W. Murphy, Jr.[1], William Farr[2], William M. Folkner[2], André R. Girerd[2], Hamid Hemmati[2], Slava G. Turyshev[2], James G. Williams[2], and John J. Degnan[3]

[1]University of California, San Diego, 9500 Gilman Drive, La Jolla, CA 92093-0424, USA
[2]Jet Propulsion Laboratory, Caltech, 4800 Oak Grove Drive, Pasadena, CA 91109-0899, USA
[3]Sigma Space Corporation, 4801 Forbes Blvd., Lanham, MD 20706, USA

Abstract

Phobos Laser Ranging (PLR) is a concept for a space mission designed to advance tests of relativistic gravity in the solar system. PLR's primary objective is to measure the curvature of space around the Sun, represented by the PPN Eddington parameter γ, with an accuracy of two parts in 10^7. Other mission objectives include measurements of the time-rate-of-change of the gravitational constant, G and of the gravitational inverse square law at 1.5 AU distances—with up to two orders-of-magnitude improvement for each. A transponder on Phobos sending 0.25 mJ, 10 ps pulses at 1 kHz, and receiving asynchronous 1 kHz pulses from earth via a 12 cm aperture will permit worst-case links exceeding a photon per second. A total measurement precision of 50 ps demands a few hundred photons to average to 1 mm (3.3 ps) range precision. Existing SLR facilities—with appropriate augmentation—will be able to participate in PLR ranging. Since the Phobos orbit period is about 8 hours, each observatory is guaranteed visibility of the Phobos instrument every Earth day.

1. Introduction

Laser ranging from the Earth to passive targets on the lunar surface routinely operates at centimeter level accuracy (Williams et al., 2009). Millimeter-level accuracy lunar laser ranging (LLR) data has been achieved by the Apache-Point Observatory Lunar Laser-ranging Operation (APOLLO) (Murphy et al., 2008). Over the years, LLR has benefited from a number of improvements both in observing technology and data modeling. Today LLR is a primary technique to perform high-accuracy tests of relativistic gravity including tests of the Equivalence Principle (EP), of a time-variability in the gravitational constant, and of the inverse-square law of gravity.

The PLR mission described here would provide tests of relativistic gravity in the solar system to an unprecedented precision. It would test the weak-gravity-and-small-speed regime of the cosmologically motivated theories that explain the small acceleration rate of the Universe (a.k.a. dark energy) via modification of gravity at cosmological scales. PLR would search for a cosmologically-evolved scalar field that is predicted by modern theories of quantum gravity and cosmology, and also by superstring and brane-world models. The Eddington parameter, γ, whose value in general relativity is unity, is the most fundamental parameter in that ½(1−γ) is a measure, for example, of the fractional strength of the scalar gravity interaction in scalar-tensor theories of gravity (Turyshev, 2009). Specifically, the quantity ½(1−γ) defines corrections to the spacetime around massive bodies. To

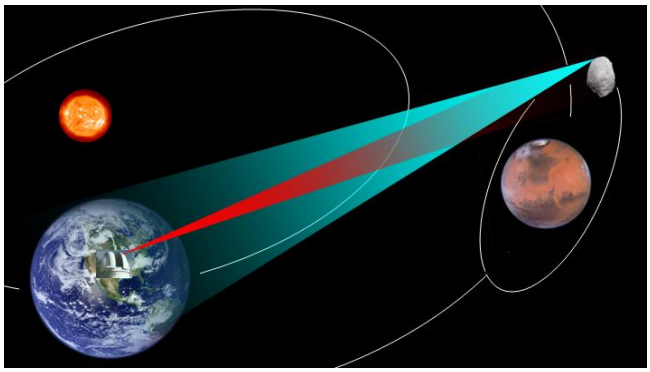

Figure 1. Concept of a laser transponder link between an observatory on Earth and a laser terminal on Phobos.

date, the most precise value for this parameter, $\gamma-1=(2.1\pm2.3)\times10^{-5}$, was obtained using microwave tracking to the Cassini spacecraft (Bertotti et al., 2003) during a solar conjunction experiment. This accuracy approaches the region where multiple tensor-scalar gravity models, consistent with recent cosmological observations (Spergel et al., 2007), predict a lower bound for the present value of this parameter at the level of $(1-\gamma) \sim 10^{-6}-10^{-7}$. Therefore, improving the measurement of γ would provide crucial information to separate modern scalar-tensor theories of gravity from general relativity, probe possible ways for gravity quantization, and test modern theories of cosmological evolution (Turyshev, 2009; Turyshev et al., 2009). With an accuracy of two parts in ten million anticipated from PLR measuring the Eddington parameter γ, this mission could discover a violation or extension of general relativity, and/or reveal the presence of any additional long range interaction.

The PLR experiment will build on the success of LLR, but will break the passive lunar paradigm (strong signal attenuation due to $1/r^4$ energy transfer) and extend the effectiveness of this technique to interplanetary scales (Fig. 1). At interplanetary distances, active techniques are required to achieve good signal strength (a benefit of $1/r^2$ energy transfer). The development of active laser techniques would extend the accuracies characteristic of passive laser ranging to interplanetary distances. Technology is available to conduct such measurements, achieving single-photon time resolution measured in tens of picoseconds (ps). One millimeter of range corresponds to 3.3 ps; millimeter range precision can be statistically achieved with a few hundred photons in both uplink/downlink directions. For comparison, several-meter accuracies have been achieved for radio tracking at Mars. Interplanetary laser ranging has been demonstrated with the MESSENGER spacecraft (Smith et al., 2006).

Building on our experience with APOLLO's design, construction and operations, LLR data analysis, and optical communications technology development, we propose a medium-class mission to Phobos that would be deployed on the surface of Mars' largest satellite and operate a pulsed laser transponder (time-of-flight) capable of achieving mm-class accuracies in ranging between Earth and Phobos. The resulting PLR experiment would initiate investigations in several science areas, focusing primarily on gravitational astrophysics over a nominal 3-year science mission.

2 Technical Overview of PLR Mission and Experiment

2.1 Mission Description

The Phobos Laser Ranging mission is based on deploying a laser ranging transponder instrument capable of supporting measurements of distances to Earth with 1 mm accuracy given daily hour-long tracking passes. Phobos was selected as the target body as being far enough from Earth to fully sample the solar system gravity field with relatively low cost of delivery while being free of an atmosphere which would induce variable refraction and scatter sunlight. Phobos rotates synchronously while orbiting about Mars with an 8 hour period. The anti-Mars point was selected as being easiest to land on, have full view of Earth three times per Earth day, and have good sunlight illumination for solar panels.

The PLR spacecraft configuration is fairly simple. The box-like main structure would have four legs rigidly attached for landing on Phobos (Fig. 2). The spacecraft easily fits within the fairing of an Atlas V-401 launch vehicle, the smallest Mars-capable vehicle under NASA contract for 2015 and beyond. After launch the four small solar panels, high-gain antenna, and laser ranging instrument will be deployed.

Following a 7-month cruise, when the spacecraft arrives at Mars, a propulsive maneuver will place it into a highly elliptical orbit about Mars. This will be followed by a maneuver at

apoapsis to raise the periapsis and match the plane of Phobos' orbit, and then a maneuver at peripasis to match the Phobos orbit period. Phobos will be observed from orbit for one month with a simple camera to improve the Phobos ephemeris and identify a specific landing location. Landing on Phobos will be done semi-autonomously using an altimeter and a feature detection camera similar to those used on the NEAR spacecraft.

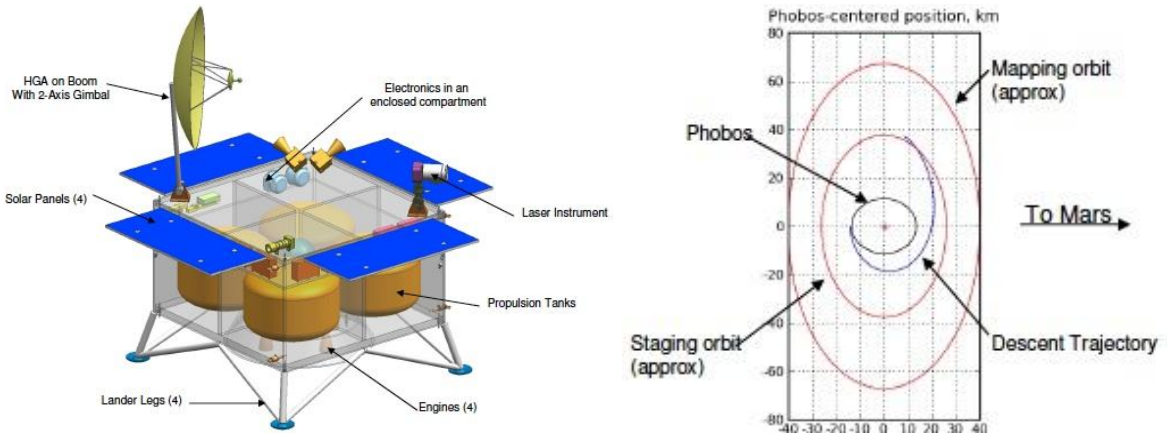

Figure 2. (a) PLR spacecraft in deployed configuration. (b) Phobos landing trajectory concept.

After landing, the spacecraft will have approximately three sun and Earth view periods of >3 hours, giving more than 5 hours with elevations >45˚ every Earth day. One of these view periods each day will be used for the hour-long laser ranging experiments. Once each week a second sunlit period will be used to send the instrument data to Earth via the high-gain antenna. Nominal science operations would continue for 3 years, covering two solar conjunctions. Since there are no expendables (e.g. propellant) during science operations, further observations could occur in an extended mission phase.

2.2 Measurement Description

The gravity parameter estimation is based on monitoring the light-time between Earth and Phobos. Unlike lunar laser ranging which measures the round-trip light-time from Earth to the Moon and back, PLR will use a combination of one-way light-times with asynchronous operation of the laser (Degnan, 2002). The advantages of the asynchronous scheme include: 1) noise immunity: the remote station does not transmit pulses in response to numerous background photon detections; 2) stable laser performance: steady pulse generation results in thermally stable conditions; 3) multiple Earth stations can range to the remote unit simultaneously without placing conflicting demands on the remote transmitter. The Earth stations will measure the times at which laser pulses are directed toward Phobos and the times of received photons. Similarly, the laser ranging instrument on Phobos will measure times of pulses transmitted towards Earth and the times of received photons from Earth. Scattered light will be rejected to first order by using a known laser pulse rate and filtering the measured times to find those separated by the signal rate. Timing will be done to an accuracy of 50 ps per photon, averaging down to < 3 ps for a typical observation. For the Earth station, the timing accuracy must be kept over the round-trip light time of ~3000 s. The laser ranging instrument accuracy need only be good over the few minutes it takes to collect enough photons to produce one-millimeter statistics. The timing scheme is indicated in Fig. 3a.

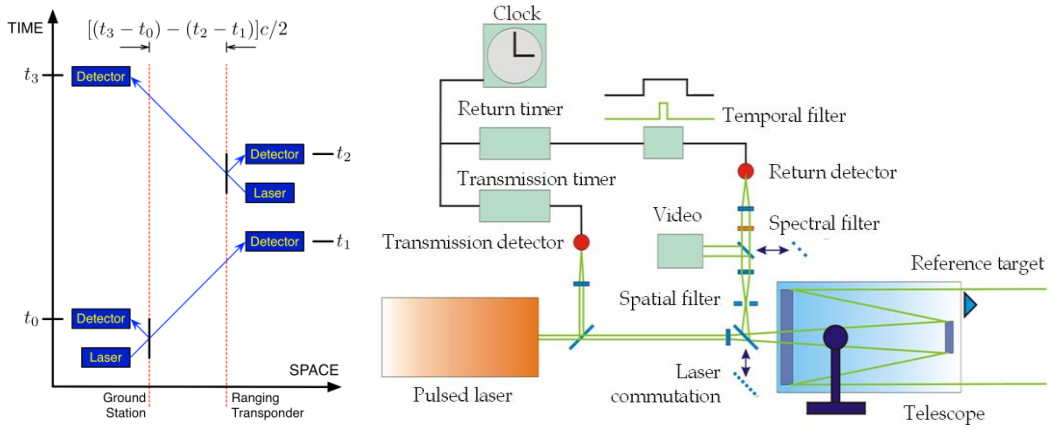

Figure 3. (a) Sequence of laser pulse time-tags used to derive Earth-Phobos round-trip light-time. (b) A block diagram of PLR and Earth instruments for timing transmitted & received pulse on common detector.

Both the Earth observatory and laser ranging instrument include a telescope and optics to have incoming light, and a small fraction of outgoing light, illuminate a photon sensitive detector array that records single photon arrivals (Fig. 3b). The power received by the telescope depends directly on the telescope's collecting area and inversely on the returning spot area. At the detector, both a pinhole restricting the field of view and a narrow-band-pass filter will be included to reduce background light.

If the combined timing uncertainty per photon is 50 ps (from laser pulse width, detector response, timing electronics, clock), then one needs $(50/3.3)^2 = 225$ photon events in order to establish the one-way distance to 1 mm (3.3 ps) precision. At the estimated worst-case rates, this is achieved in a few minutes of ranging. However, it is assumed that all other parameters (beam pointing, divergence) are satisfied, which will not be true all of the time, so hour-long tracking passes are used to ensure that enough valid measurements are obtained.

The laser ranging instrument on Phobos will transmit pulses at a wavelength of 1064-nm for greater power efficiency and lower atmospheric scattered light at the Earth receiver during near sun pointing operations. A laser pulse rate of 1 kHz will be used with 12 ps pulse-widths and

Table 1. Signal and noise estimated for laser ranging from Earth to Phobos and back.

Input Parameters	Earth to Phobos	Phobos to Earth
wavelength (nm)	532	1064
transmit power (w)	3	0.25
tx efficiency	0.5	0.5
tx beam divergence (μrad)	25	160
tx pointing loss (dB)	-2	-2
tx atmospheric loss	-3	-3
tx pulse frequency (kHz)	1	1
rx atmospheric loss (dB)	-4.3	-4.3
rx diameter (m)	0.1	1
rx efficiency	0.3	0.3
rx field of view (μrad)	240	20
rx detector efficiency	0.4	0.4
background (W/m/m/sr/μm)	32	32
scattered light radiance (W/m/m/sr	100	100
Earth sky radiance (W/m/m/sr/μm	0	1000
bandpass FWHM (nm)	0.2	0.2
range(AU)	2.6	2.6
Derived Parameters		
photon energy (aJ)	0.37	0.18
space loss (dB)	-166	-162
rx signal power (aW)	9.3	1.9
planet background power (pW)	0.05	2
scattered light power (W)	0.15	6.9
sky radiance power (pW)	0	69
timing window (μs)	1024	27
Summary Results		
incident signal power (aW)	2.8	5.70E-01
incident noise power (pW)	2.7	21.3
SNR (dB)	-60	-76
detected signal rate (Hz)	3	1.2
detected noise rate (MHz)	3	46
timing window (ns)	10	10
data volume (MB/day)	100	1570

power of 0.25 W. We selected a divergence of 160 μrad to cover the entire Earth at distances greater than 1 AU At closer ranges, the instrument must point to a specific area on the Earth. For a 1 m aperture on the Earth station at maximum Earth-Mars range, the average detection rate will be 1.2 photons per second.

Transmission from the Earth station will be at a wavelength of 532 nm and detected by the instrument on Phobos with an efficient, low noise silicon-based single photon detector. The beam transmitted from Earth will have an uplink divergence of 25 μrad to cover potential pointing and atmospheric seeing variations. Assuming a laser power of 3 W (3 mJ/pulse at 1 kHz repetition rate) and a 12 cm aperture on Phobos, the uplink will deliver 3 detected-photon/second at the maximum Earth-Mars range.

The background event rates—due to scattered sunlight, illuminated body in field-of-view, and the radiance of the Earth atmosphere—will be much greater than signal event rates. At Phobos the laser ranging instrument will search for pulses in a 1 kHz repeat pattern following the tracking passes, and select only pulses within a narrow window about the times of the expected pulses from Earth for transmission. At Earth, the photon timings will be matched against predicted pulse rate and Phobos-Earth range to select correct pulses. Table 1 summarizes the worst-case measurement signal and noise estimates (note, "tx" and "rx" in Table 1 stand for transmit and received).

2.3 Flight System

The PLR spacecraft includes all equipment necessary to deliver and support the laser ranging instrument on Phobos. The spacecraft structure is a simple box-like construction to accommodate the payload, spacecraft electronics, propulsion, attitude control, telecommunications, thermal, and power subsystems. The mass by subsystem is given by Table 2. There are several operating modes, a typical power by subsystem is also given in Table 2. With the Atlas V 401 as the launch vehicle, mass and volume capabilities are much greater than necessary, so subsystems have been optimized to minimize cost rather than mass. Selected redundancy has been included in subsystem design to reduce risk where cost effective.

The command and data handling subsystem is based on the architecture being developed for the Mars Science Laboratory (MSL). It includes RAD750 processors, interfaces to the attitude control, telecommunication, power, and payload subsystems, with sufficient memory storage to accumulate up to two weeks of instrument data.

The power subsystem includes 5.3 m^2 solar panels and batteries to operate in absence of sunlight. The battery size is dictated by the propulsion system operation during Mars orbit insertion.

Table 2. Flight System Mass and Power Estimates.

Subsystem	Mass (kg)	Power Peak (W)	Peak Power Mode
Laser Ranging Instrument	39.3	50	Science
Attitude Control	29.4	48	Landing
Command and Data	22.0	47	Science
Power	71.4	71	Orbit Insertion
Propulsion	170.6	217	Orbit Insertion
Structure/Mechanisms	203.6	0	
Launch Adaptor	14.8	0	
Cabling	40.4	0	
Telecom	21.0	64	Data Transmit
Thermal	38.4	165	Cruise
Spacecraft Total (dry)	650.9	619	Orbit Insertion
Contingency	280.1	266	
Spacecraft + Contingency	931.0	885	
Propellant	1216.2		
Spacecraft Total (wet)	2147.2		

Thermal control will be done using standard multi-layer insulation and heaters. Spacecraft and electronics will be located in a thermally isolated box that will be kept warm during dark

periods on Phobos. The propellant tanks will be kept warm until landing, and uncontrolled afterwards.

Telecommunications will utilize standard X-band transponders and traveling-wave tube amplifiers with a deployed pointable high-gain antenna 1.5-m diameter for sending instrument data to Earth, and two low-gain antennas used for contacts during cruise.

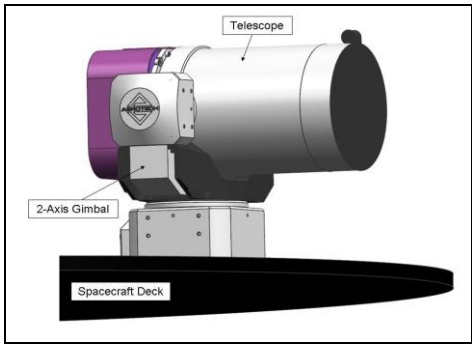

Figure 4. CAD model of laser ranging instrument telescope.

2.4 Payload

The instrument design is evolved from optical communications terminals under development for interplanetary missions. Prototypes of the communications terminals have been tested in airplanes. For the Phobos laser ranging science objectives, lower pulse rates are acceptable but higher timing resolution is required. The PLR instrument design is based on existing laboratory lasers and array photo-detectors which will be ruggedized to operate in space. The instrument is shown in Fig. 4 and a functional block diagram shown in Fig. 5.

The instrument consists of a gimbaled 12 cm telescope, a 250 mW Nd:YAG laser operating at 1064 nm, a silicon Geiger-mode (GM) avalanche photodiode detector (APD) array in 8x8 format, a multiplexed ASIC timing system to go with the detector, a clock, and an acquisition/pointing CCD camera with thermo-electric cooler. A small actuated mirror will impart a point-ahead angle to the beam with respect to the receiver direction of up to 330 μrad, which will be monitored via the centroid of a sample of the transmit beam imaged onto the CCD. A small fraction of the outgoing laser light will be reflected back from a reference mirror to the single-photon detector array for timing transmitted pulses. The laser will derive from a SESAM (Semiconductor Saturable Absorber Mirror) fiber seed laser, delivering 12 ps pulses at a 50 MHz repetition rate, followed by a pulse-picker that will accept only every 50,000th pulse to form a 1 kHz train. A laser diode-pumped regenerative amplifier will then deposit ~250 μJ of energy into each pulse for transmission to Earth.

The instrument electronics includes timing, pointing control, data storage, and a data post-processor. After acquiring photon times for the one hour tracking pass, the post-processor will look for the 1 kHz transmit pulse pattern from Earth and delete times outside a 10 ns window about that estimated rate, and format times into differences for reducing data volume. Edited times will be collected for transmission to Earth via radio, with a data volume of 5 MB per day.

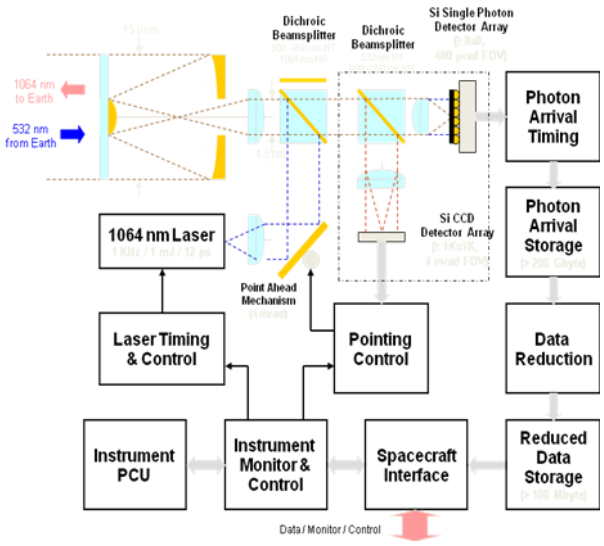

Figure 5. Instrument block diagram.

2.5 Ground Segment

One or more Earth observatories will be equipped similar to current lunar laser ranging stations and outfitted with membrane-type sunlight rejection filters for accurate measurements when Mars is near solar conjunction. The ground stations will use lasers very similar to those on Phobos, with the exception that the frequency will be doubled

and the pulse repetition rate will be continuously tunable so that the pulse arrival rate at Phobos is exactly 1 kHz. The detector used in the ground stations will be an InGaAsP hybrid photodiode with a thinned photocathode to reduce timing jitter to less than 40 ps. A solar rejection filter with passband at 532 and 1064 nm must cover the entire ~1 m aperture of the telescope, which is a demanding task but one that has been previously demonstrated.

2.6 Mission Operations

Science operations will be done for one-hour tracking passes each Earth day. The spacecraft will have three view periods each day to select for operations. The tracking pass time will be selected to accommodate a view of the selected ground observatory for that day. Times will be optimized to have the observatory view Phobos at a high elevation, and sample the Phobos orbit by varying the time to alternate between before and after maximum elevation at the spacecraft. Times will be selected one week in advance. Once per week the spacecraft will communicate with the NASA's Deep Space Network to download the previous week of science data and to upload the schedule of tracking times for the next week.

Acknowledgment

The work described in this report was performed at the Jet Propulsion Laboratory, California Institute of Technology, under a contract with the National Aeronautics and Space Administration.

References

Degnan, J.J., *J. Geodynamics* **34**, 551-594 (2002).

Bertotti, B., L. Iess, P. Tortora, *Nature* **425**, 374 (2003).

Murphy, T. W., Jr., and 12 colleagues, *Publ. Astron. Soc. Pacific* **120**(863), 20 (2008).

Turyshev, S.G., *Uspekhi Fizicheskikh Nauk* **179,** 3 (2009), arXiv:0809.3730 [gr-qc].

Smith, D.E., M.T. Zuber, X. Sun, G.A. Neumann, J.F. Cavanaugh, J.F.McGarry, and T.W. Zagwodzki, *Science* **311**(5757), 53 (2006).

Spergel, D.N., and 21 colleagues, *ApJS* **170**, 377 (2007), astro-ph/0603449.

Turyshev, S.G., and 14 colleagues, "Opportunities for Probing Fundamental Gravity with Solar System Experiments," A Science White Paper submitted to the Cosmology and Fundamental Physics Science Frontier Panel of the Astro2010, (2009), arXiv:0902.3004 [gr-qc].

Williams, J.G., S.G. Turyshev, D.H. Boggs, *Int. J. Mod. Phys. D*, (2009), gr-qc/0507083.

Time Transfer by Laser Link - T2L2 : First Data

E. Samain[1], Ph. Guillemot[2], P. Exertier[1], D. Albanese[1], P. Berio[1], O. Laurain[1], F. Para[1], J. Paris[1], J.-M. Torre[1], H. Viot[1], P. Vrancken[1], I. Petitbon[2], S. Leon[3]

[1]OCA – Observatoire de la Côte d'Azur, Caussol, France
[2]CNES –French Space Agency, Toulouse, France
[3]CNES –French Space Agency, Paris, France

etienne.samain@obs-azur.fr

Abstract

The T2L2 (Time Transfer by Laser Link) project, developed by CNES and OCA will permit the synchronization of remote ultra stable clocks and the determination of their performances over intercontinental distances. The principle is derived from laser telemetry technology with a dedicated space equipment deigned to record arrival time of laser pulses at the satellite. T2L2 was accepted in 2005 to be on board the Jason-2 altimetry satellite. It has been successfully launched from Vandenberg in 2008. T2L2 acquired the first laser pulses a few days after the launch.
First analysis permitted to validate some important characteristics of the instrument such as sensitivity, noise, dynamic, event timer precision and ground to space time stability. The instrumental model of the whole experiment that will permit to perform very precise time transfer at the pico-second level is currently under development.

1. Introduction

T2L2 [1],[2] is a two way time transfer technique based on the timing of optical pulses emitted by a laser station and detected by a dedicated space instrument. T2L2 was accepted as a passenger instrument on the Altimetry Jason-2 satellite [3] in 2005.

Basically, T2L2 realizes a space to ground time transfer between the ground clock linked to the laser station and space clock of the satellite. The ground to ground time transfer between several remote clocks at ground is obtained through these individual space to ground time transfers. It can be obtained in a common view mode, when the distance between the laser stations is smaller than roughly 5000 km, or in a non-common view mode when the distance is larger.

The ground segment of the experiment is a laser station able to time both the start and the return time with a resolution at the ps level (Fig. 1). The laser stations track the satellite as soon as the satellite is in the right field of view during the whole duration of the pass.

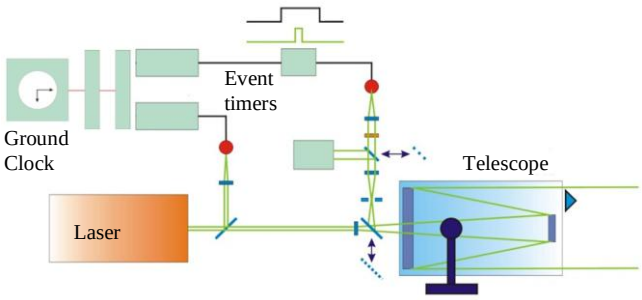

Figure 1. Laser station designed for T2L2

The space instrument is based on a photo detector and an event timer linked to the space clock. A laser ranging array (LRA) is also used to reflect the laser pulse toward the laser station. This LRA is provided by the JPL, basically for the orbit of the satellite through the laser ranging technique. The space clock is an ultra-stable oscillator (USO) coming from the Doris equipment.

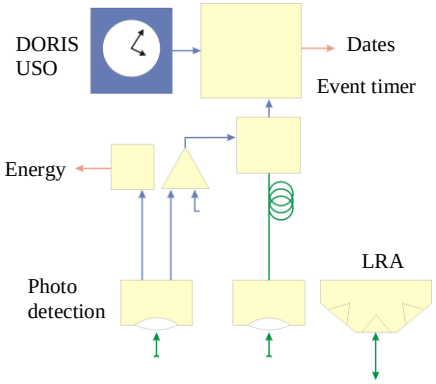

Figure 2. Synoptics of the T2L2 Space instrument

The mass of the T2L2 space equipment is 8 kg for the electronic module which is inside the satellite and 1.5 kg for the photo detection module located outside. Jason-2 is a French-American follow-on mission to Jason-1 and Topex/Poseidon. Conducted by NASA and CNES, its goal is to study the internal structure and dynamics of ocean currents. The satellite was placed in a 1,336 km orbit with 66◦ inclination by a Delta launcher. The time interval between two passes varies from 2 to 14 hours with a maximum duration of about 1000 s.

For a given laser pulse emitted by the laser station one get two dates at ground and one date at the satellite. From these 3 dates (which are called a triplet) we can extract the time delay between the ground clock and the space clock.

2. Exploitation

Since the launch, the exploitation phase started for at least 2 years and probably 5 years.
The objectives of the T2L2 experiment on Jason-2 include [4]:

- Validation of optical time transfer, including the validation of the experiment, its time stability and accuracy. It should further allow to demonstrate one-way laser ranging
- Scientific applications concerning time and frequency metrology allowing the calibration of radiofrequency time transfer (GPS and Two-Way), fundamental physics with the measurement of light speed anisotropy and alpha fine structure constant
- Characterization of the on-board Doris oscillator [5], especially above the South Atlantic Anomaly (SAA).

The T2L2 exploitation is driven by a T2L2 working group and implemented by an Instrumental Mission Center. The T2L2 working group is divided in 5 themes:
- Laser Station Network: communication between laser stations, schedule and priority, design of some dedicated instrumentation at ground
- Scientific Mission Center: data formats, definition of the data reduction algorithms, data distribution
- Microwave comparison and Time scale: T2L2-TwoWay-GPS comparisons with the permanent network, realization of some dedicated experiments with some mobile equipments
- T2L2 validation: collocation, common view, optimization of the instrumental model, Link budget

The Scientific Mission Center is responsible for developing the software for data reduction, for processing the ground and space data and for the dissemination of the products.

The Instrumental Mission Center objectives are threefold:
- Downloading data from the space segment, upload some remote controls to the instrument
- Processing a first level of data reduction
- Monitoring the results and the space instrument

3. Laser ranging requirements

T2L2 relies on the Laser Ranging network. The degree of participation will depend on the hardware used, but every laser station can contribute. The following table gives the scientific objectives achievable as a function of the equipment level for a given laser station.

Objectives	Interval meter	Event timer	Rubidium slaved on GPS	Cesium	H-Maser or atomic fountain	GPS or Two way time transfer	Laser pulse width < 100 ps	Laser pulse width > 100 ps	Start epoch Calibration
Time Transfer validation	o	x	✓	✓	✓	-	✓	~	✓
Time and frequency metrology	o	x	o	✓	✓	✓	✓	~	**x**
One-Way laser ranging	o	x	~	v	✓	-	✓	~	**x**
DORIS support	o	x	o	~	✓	-	✓	~	-
Link budget analysis	~	x	✓	✓		-	✓	✓	-
Fundamental physics	o	x	o	o	✓	-	✓	o	✓

x : required ; ✓ : ideal ; ~ : sufficient ; o : unsuitable ; - unnecessary

It is absolutely necessary to get the laser station data in the full-rate form with a time resolution in the pico-second range. The stations should measure the start events with an event timer connected to the clock that has to be synchronized. The new CRD format (full-rate version) is the nominal and official format for T2L2.

Some scientific objectives require the absolute start time of the transmitted laser pulses with accuracy in the 50 ps range. For that purpose, the T2L2 team will propose some calibration campaigns of the laser stations concerned. It will permit to measure (with a calibration station developed by OCA) the time delay between the laser pulses at the crossing axes of the telescope mount and the Pulse Per Second (PPS) signal of the reference clock (Fig. 3).

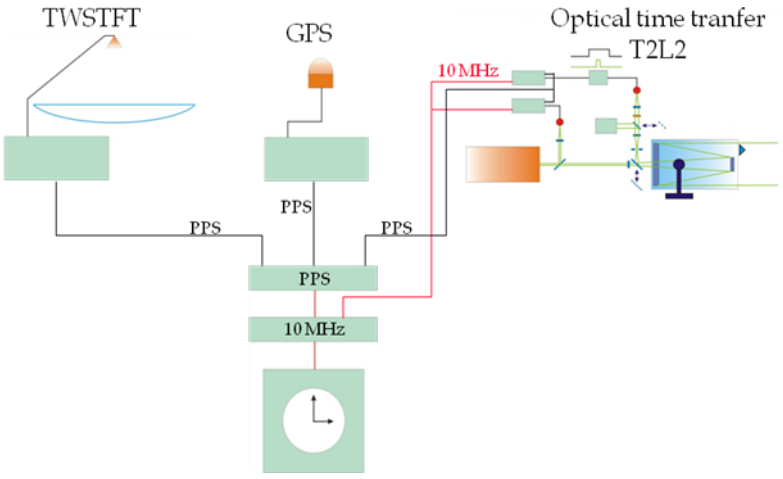

Figure 3. Delay determination between the optical pulse at the cross axe of the telescope and the electrical reference coming from the Time and frequency lab

T2L2 can detect some laser events even if the laser station does not obtain echoes. In order to exploit these events it is essential to record the entire laser start epochs even if there is no echo. T2L2 includes a self-asynchronous pre-triggered system so that laser stations can range normally without any synchronization constrain. Arrival times are recorded onboard and then downloaded to the Instrument Mission Center (CMI) every 2 hours. The laser events are identified after a post processing conducted by the Scientific Mission Center that allows reconstructing triplets (start time - return time and arrival time onboard), for every laser station. The T2L2 detection module includes a level compensation system to correct for varying amplitude during the pass over the station. It takes into account the distance evolution and the variation of the atmospheric transmission which both depend on the elevation angle. In order to obtain an energy level constant onboard, the laser energy of the station should remain constant during the whole pass. The return level should be adjusted at ground with some neutral density filter in front of the station return detector. Laser stations can operate in both a single pulse mode and a pulse train mode. In the pulse train mode, T2L2 will only detect the first pulse so that the other pulses will be ignored. Laser stations can work in a KHz mode (T2L2 dead time is roughly 200 µs) but the energy per pulse is usually low in that kHz regime. It is necessary to minimize the divergence of the laser beacon in order to reach the minimum threshold.

The following list are the important laser station characteristics in order to be compliant with the T2L2 project:

- Wavelength : 532.1 +/- .5 nm
- Event timer connected to the clock
- CRD Full Rate data : Upload to EDC
- No synchronization required
- Laser pulse Energy
- Min: 1 mJ sq = 10 µrad
- Max: 1 J sq = 5 µrad
- Pulse width 10 ps up to 500 ps (FWHM)
- Mono pulse or semi train
- Microwave link comparison: Time tag the start pulses with an accuracy of 50 ps (OCA calibration campaign)

4. First results

Among the whole laser ranging community, 16 stations provide the full rate data needed for the triplets extraction (start, return and arrival onboard). 8 of them use the right data format (CRD) that permits to extract the start epoch of the laser pulses at the ps level, and the others with a data format that only permits to get the epochs with a resolution of 100 ns.

Up to now, 5 to 15 passes coming from these 16 laser stations are extracted every day.
Figure 4 gives an overview of the laser pulse energy received and measured by T2L2 onboard Jason-2.

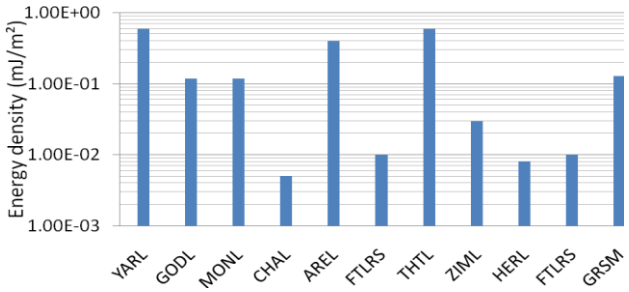

Figure 4. Energy received in the plane of the satellite of a few laser stations

A very preliminary link budget analysis has demonstrated a good agreement between the energy emitted by the stations and the energy received.

5. Ground space time transfer

5.1 Triplets extractions

The events recorded by the T2L2 space instrument don't contain any information of the source: the events of all the laser stations are blended together. The first step of the treatment consists in recognizing the laser events recorded by T2L2 with those emitted by the stations. The absolute frequency offset and the delay between space and ground are known with an accuracy that permits to directly recognize the events by their dates.

5.2 Instrumental corrections

The instrumentals corrections TCorr concern both the space and the ground segments.
At ground, the accuracy is obtained by an internal calibration. During the pass on the satellite (or just before or just after) some events are also acquired on a calibration target located at a known position. The final propagation delay is the difference between the data directly obtained on the satellite and those obtained on reference target.

At the satellite several considerations have to be taken into account [6]:
- Geometrical delay between the reference point of the T2L2 detection module and the reference point of the LRA. This is obtained with the attitude information given by the stellar sensors of Jason-2 and the knowledge of the geometry of the space optics.
- Time walk compensation of the photo detection module which is sensitive to the photon number received. This is done through the information given by the linear photo detector of the instrument that give, for each event detected, an energy received.
- Angular compensation of the photo detection. This is also computed from the attitude information.
- Event timer calibration based on some internal calibrations automatically generated.

5.3 Time of flight determination

The determination of the time of flight T_{Flight} between the ground and the space segment is of course fundamental for the time transfer computation. It permits to directly compare the start time T_{Start} at the station and the arrival time at the satellite of every laser events. This time of flight is based on the difference between the start time and the return time in the frame of the ground station divided by 2 and corrected by the distance between the LRA and the photo detection module T_{Proj}. At this stage the time of flight can be directly used echo by echo. If the precision of the measurements is optimal, this process is the best one: the uncertainty of the satellite position and the uncertainty introduced by the atmosphere are removed. It is also possible to compute a synthetic time of flight obtained over an integration duration of few tens of seconds. This method is pertinent in two cases:
- The return time at the laser station is more noisy than the noise introduce by the atmosphere [7]: this integration permits to decrease the noise by roughly $1/\sqrt{N}$, where N is the number of return integrated.
- The return photo-detector of the station is not “time-walk compensated”: mean photon number is set very low (typically 0.1). In this case, a lot of detections onboard the satellite don’t have a corresponding detection at ground and this synthetic time of flight permits to reconstruct a triplet with only one start time and one arrival time.
This synthetic time flight can be fitted on the time of flight measurement from a satellite orbit solution with a low order polynomial.

5.4 Ground to Space time transfer

The ground to space time transfer T_{GS} represents the time offset between the space and ground clocks. It is deduced from the difference between start time at ground and the arrival time at the satellite, which is compared with the time of flight T_{Flight} corrected by the Sagnac delay TSagnac .
We have:

$$T_{GS} = T_{Start} + T_{Flight} - T_{Sagnac} + T_{proj} + T_{corr}$$

Figure 5 is an illustrations of such a ground to space time transfer between the French mobile FTLRS station and the T2L2 space instrumentation. From the full rate data one can then compute a short term interpolation (typically 30 s) with a low order polynomial fit. This fit allows us to generate some interpolated data at some precise instant in the satellite time scale.

This is crucial in order to be able to compare ground to space time transfer coming from different laser stations at ground.

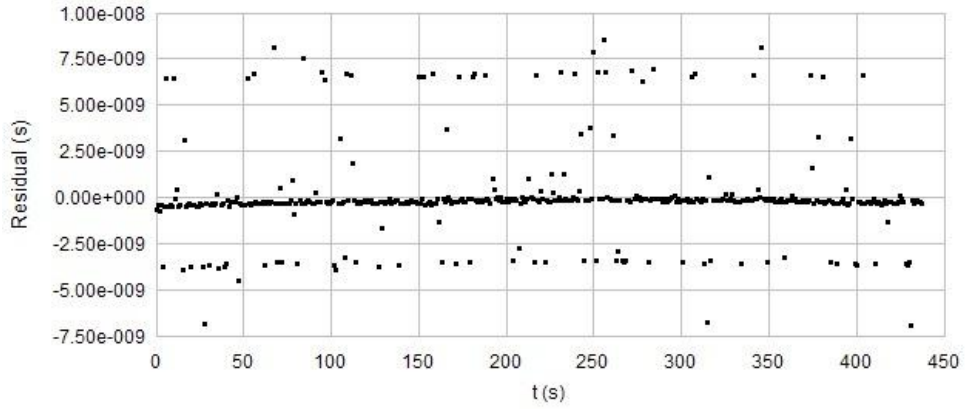

Figure 5. Ground to Space time transfer between the T2L2 DORIS oscillator and OCA's FTLRS.

6. Performances

Figure 6 represents the time stability measured by T2L2 of a pass acquired by the Wettzell station. It represents the time stability of the Wettzell's Hydrogen Maser compared to the T2L2's DORIS quartz oscillator. One obtain 40 ps @ 1 s and 7 ps @ 30 ps. For time integration greater than 30 s this measurement is limited by the DORIS time stability which is 5 ps @ 30 s and 10 ps @ 100 s.

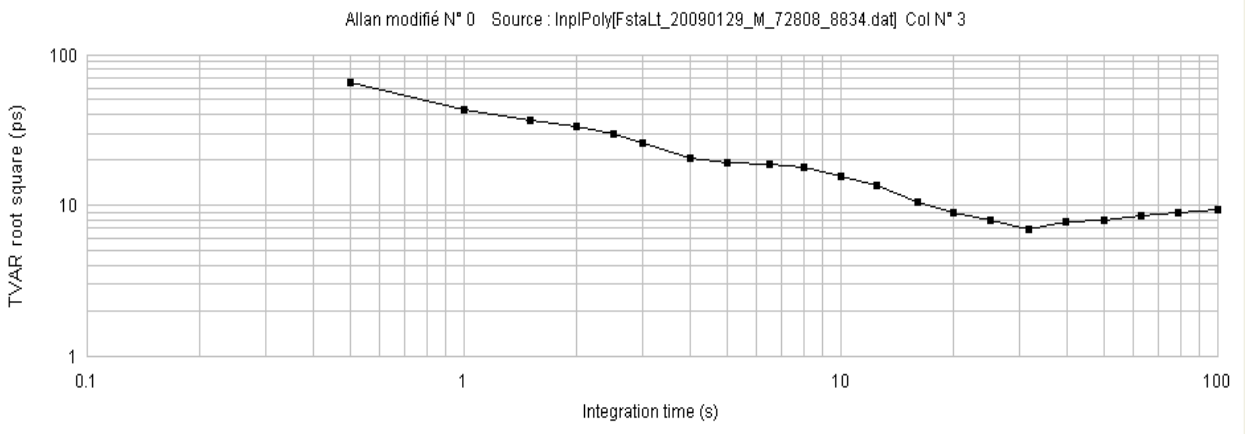

Figure 6. Time stability measured by T2L2 of the Wetzell's H-Maser compared to the T2L2's DORIS oscillator

7. Conclusions

T2L2 relies on the whole Laser Ranging network. Every laser station can contribute. Up to now 8 laser stations in the world have the right configuration for T2L2. Several other laser stations will participate but some data format and hardware upgrades are still needed.

The T2L2 time stability measured between space and ground is very promising: it has been possible to measured the phase between an Hydrogen Maser at ground and the T2L2's

DORIS oscillator with a stability of only 7 ps. This results represents the best time stability never obtained between a space clock and a ground clock.
A lot of works are still required to understand the physic and to improve the instrumental model of the hardware but the global performances seem to be in accordance with the specifications of the project.

A calibration campaign over several laser stations will permit to realize some absolute time transfer at ground with an accuracy better than 100 ps.

Acknowledgment

The authors would like to thanks all the laser ranging stations that have participate to the project. Many of them have adapted their hardware, upgraded their data format and spent a lot of time to understand the T2L2 requirements.

References

[1] P. Fridelance, E. Samain, C. Veillet, Experimental Astronomy, 191 (1996)
[2] P. Fridelance, C. Veillet, Metrologia, 32, 27 (1995)
[3] E. Samain et al, International Journal of Modern Physics D, Vol. 17, No. 7 1043–1054 (2008)
[4] Ph. Guillemot et al., Proceedings of the 20th EFTF (2006)
[5] Ph. Guillemot et al., Proceedings of the 23th EFTF / 63th IEEE-IFCS Joint Meeting (2009)
[6] P. Vrancken, Thèse de doctorat de Science de l'Univers de l'Université Nice – Sophia Antipolis (2008)
[7] Bender P.L., , no. 36 (edited by J.C. de Munck and T.A. Th. Spoelstra), Netherlands Geodetic Commission, 1992, 117-125.

Preliminary Results of the Laser Time Transfer (LTT) Project

Yang Fumin (1)**, Huang Peicheng** (1)**, Zhang Zhongping** (1)**, Chen Wanzhen** (1)**,**
Zhang Haifeng (1)**, Wang Yuanming** (1)**, Meng Wendong** (1)**,**
Wang Jie (2)**, Zou Guangnan** (2)**, Liao Ying** (2)**, Wang Luyuan** (2)**,**
Ivan Prochazka (3)**, Zhao You** (4)**, Fan Cunbo** (4)**, Han Xingwei** (4)

(1) Shanghai Astronomical Observatory, Chinese Academy of Sciences, China
(2) China Academy of Space Technology, Beijing, China
(3) Czech Technical University in Prague, Czech Republic
(4) National Astronomical Observatories / Changchun Observatory, CAS, China

yangfm@shao.ac.cn /Fax: +86-21-64696290

Abstract

The LTT payload onboard the Chinese experimental navigation satellite COMPASS-M1 with an orbital altitude of 21500 km was launched on April 13, 2007. The payload included dual-SPAD-detector, dual-timer based on TDC device, DSP, power supply and a LRA with the total mass of 7.05 kg (including LRA's 2.45 kg) and the power consumption of 18 W. The time transfer experiment at the Changchun SLR station has been performed since August 2007. The experiment has shown that the time and relative frequency differences between the ground hydrogen maser and the China-made space rubidium clocks have been obtained with the time precision of about 300ps for single measurement and the uncertainty of frequency difference measurement of about 3×10^{-14} in 2000 seconds. After 17 months orbital flight, the LTT payload has kept its good performance.

Introduction

The laser time transfer (LTT) project is a dedicated one for the COMPASS navigation system that uses for the time comparison between the space and the ground clocks with the laser ranging technique. The principle of LTT project and some ground testing of the flight module of the LTT payload were introduced in detail on the Laser Ranging Workshop in Canberra in 2006. [1]

The LTT payload onboard the Chinese experimental navigation satellite COMPASS-M1 was launched on April 13, 2007 (UTC). The time transfer experiment at the Changchun SLR station has been performed since August 2007. The time differences and the relative frequency differences between the onboard rubidium clocks and the ground hydrogen maser have been obtained.

Principle and Specification of LTT payload

The principle of LTT is shown in Fig. 1.

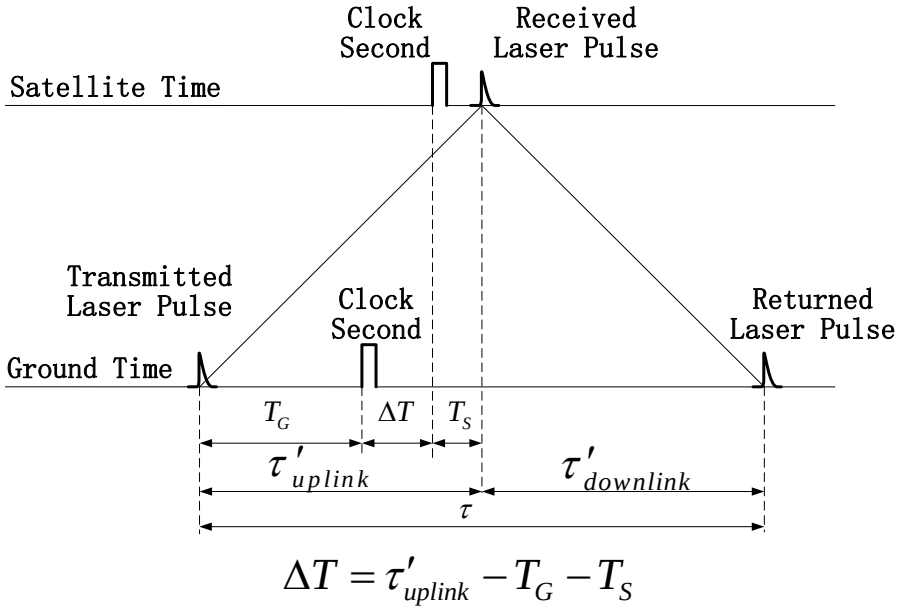

Figure 1. Principle of Laser Time Transfer (LTT)

The specifications of the 40 μm SPAD detector, the photos of LTT detector and timer can be seen on the Proceedings of Canberra Workshop in 2006 [1] [2]. The field of view of the detector is about 28°, and the bandwidth of the interference filter is about 8.8 nm.

Performance of the LTT ground station at Changchun

The Changchun SLR station was identified for the LTT experiment at the beginning of 2007. Some modifications were made, including a new powerful laser, a new transmitting telescope (210 mm aperture), two event timers (A032-ET), one set of hydrogen maser (made by Shanghai Observatory) and a LTT control package. The new laser borrowed from the North China Research Institute of Electro-Optics (NCRIEO) in Beijing is an active-active mode-locked Nd:YAG laser. The output is as follows: 100-150 mJ in 532 nm, 250 ps width, 20 Hz repetition. The laser firing at the Changchun SLR station was strictly controlled by the controller according to the range variation of the satellite. Therefore the laser pulses can arrive at the LTT detector in a short time interval behind the second pulses of the rubidium clock, in order to avoid the influence of the noises from the Earth's albedo. The laser firing jitter is about 10 ns.

Fig. 2 shows the LTT control room at Changchun. Fig. 3 shows the block diagram of the Changchun station for LTT experiment.

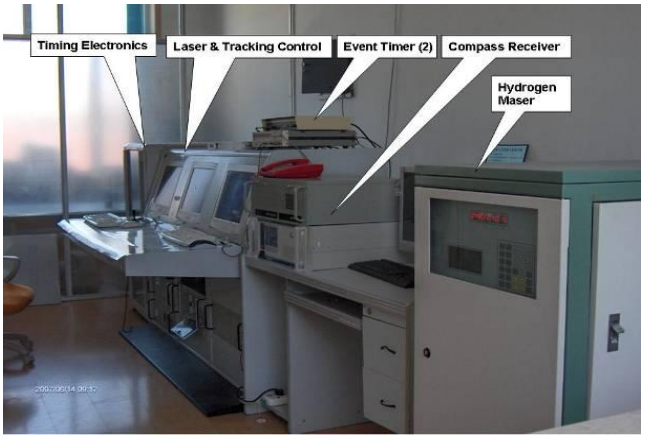

Figure 2. Changchun SLR & LTT Control Room

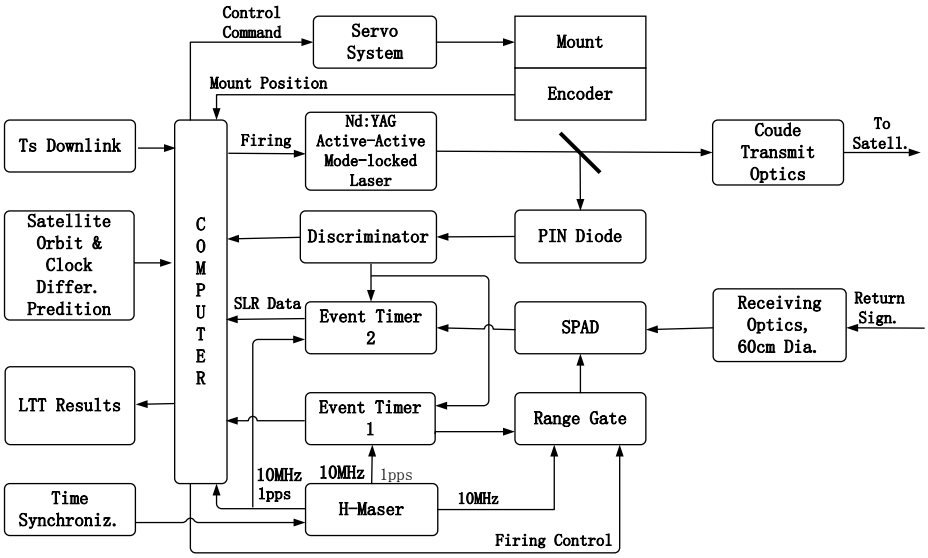

Figure 3. Block Diagram of Ground Station for LTT Experiment

Some results of the LTT experiment

The LTT experiment has been performed in August 2007. At the beginning, the experiment was suffered from the strong background noises due to the wide FOV.
Until December 2007, more LTT data had been obtained, but the experiment can be carried out in the nighttime only.

During the period of flight, the LTT detector had been directly exposed to the sun several times, but it has been rugged and safe. Some results of the LTT experiment are shown in the following figures (Fig. 4, and Fig. 7-10). Fig. 4 shows the 1552 clock differences were obtained during the pass of about 46 minutes when the satellite was in the Earth's shadow. Fig. 5 shows that sunlight can enter into the FOV of the detector when the satellite is nearby the Earth's shadows, because the FOV of the detector is about 28° which is bigger than the Earth's disk angle (26.4°) for the COMPASS-M1. Fig. 6 shows the whole process that the COMPASS-M1 was before, pass into and after the Earth's shadow on January 10, 2008. The passes B and D show the very strong noises caused by the direct sunlight.

Fig. 7, 8 and 9 shows the LTT results during the three time intervals respectively. We can see the detector recovered quickly and can keep the good timing performance after being exposed directly to the Sun (see Fig. 9). Fig. 10 shows the LTT payload was not in the Earth's shadow for 2 hours.

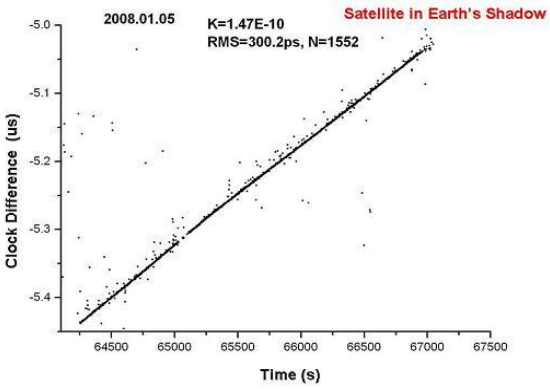

Figure 4. Clock differences from LTT on Jan 5, 2008

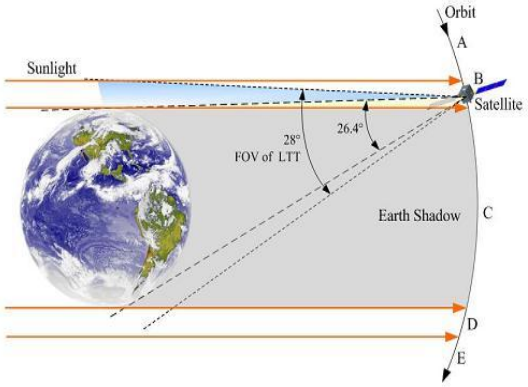

Figure 5. Sunlight can enter the FOV of detector nearby the Earth's shadow

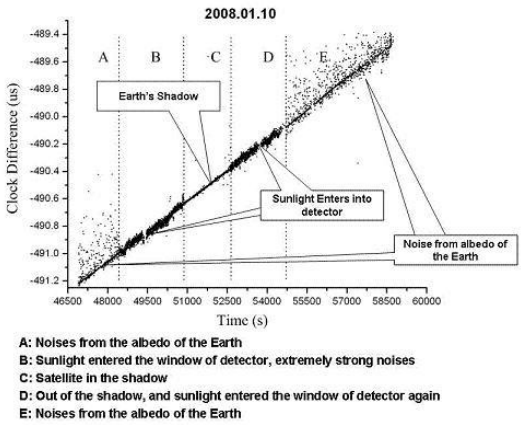

Figure 6. The whole process from LTT on Jan 10, 2008

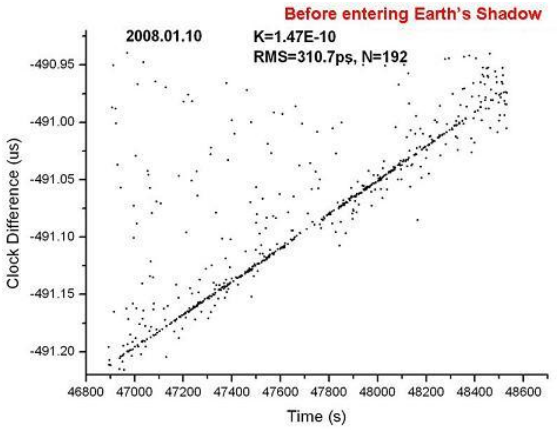

Figure 7. Clock differences before Earth's shadow on Jan 10, 2008

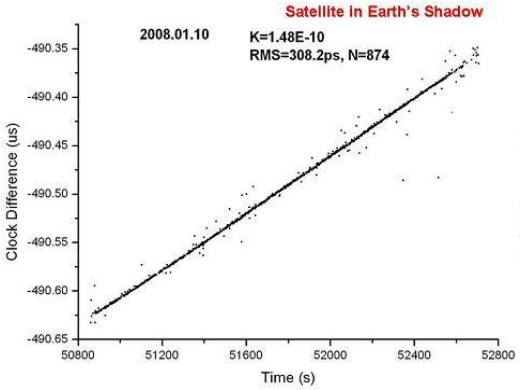

Figure 8. Clock differences in Earth's shadow on Jan 10, 2008

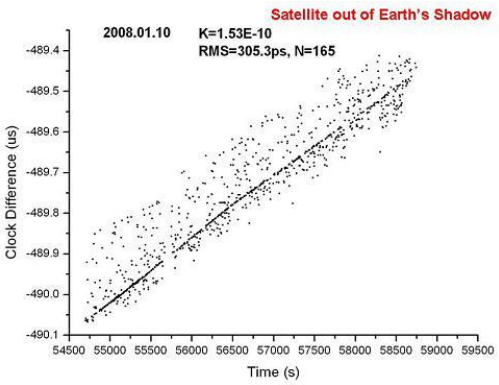

Figure 9. Clock differences after Earth's shadow on Jan 10, 2008

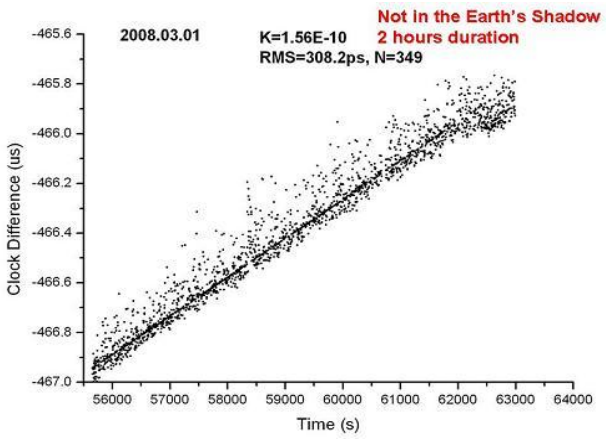

Figure 10. Clock differences on Mar 1, 2008 (no Earth's shadow)

During the LTT experiment, the time differences and the relative frequency differences between the China-made space-borne rubidium clocks and the ground hydrogen maser have been obtained successfully. The precision of the measurement for the time differences is about 300 ps (single measurement). The frequency drift of the China-made rubidium clocks is about 1.47E-10 and the stability of frequency is about E-13. The uncertainty of the measurement of the relative frequency differences is about 3E-14 in 2000 seconds.

Plans for Next Missions

2 new LTT payloads for the next Compass missions, IGSO orbit (24 hr period, with 55° inclination). One mission will be in orbit by mid-2009, another will be by the beginning of 2010.

Some upgrading of the new LTT payloads:

1) Add gating circuit in the payload for reducing the effect of the dead time of SPAD. It is of importance when the noises are strong.[3]
2) Reducing the FOV and adopting two FOV for two detectors respectively: one is bigger for nighttime experiment, another is smaller for daylight experiment.
3) 20 Hz onboard timing data will be downloaded in stead of 1 Hz before. During last mission(Compass-M1), only 1Hz timing data were downloaded in spite of 20Hz laser firing at the ground station, so a lot of useful data were lost.
4) Narrowing the bandwidth of the interferometric filter from 8.8nm to 4nm due to smaller FOV for IGSO orbit.

References

[1] Yang Fumin, Huang Peicheng, Chen Wanzhen, Zhang Zhongping, Wang Yuanming, Chen Juping, Guo Fang, Zou Guangnan, Liao Ying, Ivan Prochazka, Karel Hamal, Progress on Laser Time Transfer Project, Proceedings of the 15th International Workshop on Laser Ranging, Volume 2, p.406—413, Canberra, Australia , 2006.

[2] Karel Hamal, Ivan Prochazka, Lukas Kral, Yang Fumin, Photon Counting Module for Laser Time Transfer Space Mission, Proceedings of the 15th International Workshop on Laser Ranging, Volume 1, p.211—216, Canberra, Australia , 2006.

[3] Ivan Prochazka, Josef Blazej, Photon Counting Detectors for future Laser Time Transfer Missions, this Proceedings, Poznan, Poland, 2008.

Preliminary Results of Laser Ranging to Un-cooperative Targets at Shanghai SLR Station

Yang Fumin (1)**, Zhang Zhongping** (1)**, Chen Juping** (1)**,**
Chen Wanzhen (1)**, Wu Zhibo** (1)**, Zhang Haifeng** (1)**, Ivan Prochazka** (2)

(1) Shanghai Astronomical Observatory, Chinese Academy of Sciences, China
(2) Czech Technical University in Prague, Czech Republic

yangfm@shao.ac.cn /Fax: +86-21-64696290

Abstract

The laser returns from the un-cooperative targets have been obtained at the Shanghai SLR station in July 2008. These targets are the discarded Soviet and US rockets with the ID 1987-38B and 2007-006G respectively. The return signals from the targets with the range of 900 km were quite strong. The performance of the laser used for the experiment was introduced on the Canberra Workshop in 2006.

Introduction

The specification of the experimental laser ranging system for un-cooperative targets at the Shanghai station was introduced on the Laser Ranging Workshop in Canberra in 2006[1] . The major goal of the system is to develop the key techniques for laser ranging to un-cooperative targets. After some testing and upgrading, we have obtained some laser returns from the discarded Soviet and US rockets in July 2008 respectively. The preliminary results and analysis are given in the paper.

Performance of the laser ranging system

The high power laser used for the experiment was built by the North China Research Institute of Electro-Optics (NCRIEO) in Beijing. The output of the laser is as follows: 2J in 532 nm, 10ns pulse width, 0.6 mrad divergence, 20Hz repetition rate, 40W mean power in green. Fig. 1 shows the block diagram of the 40W Nd:YAG laser.

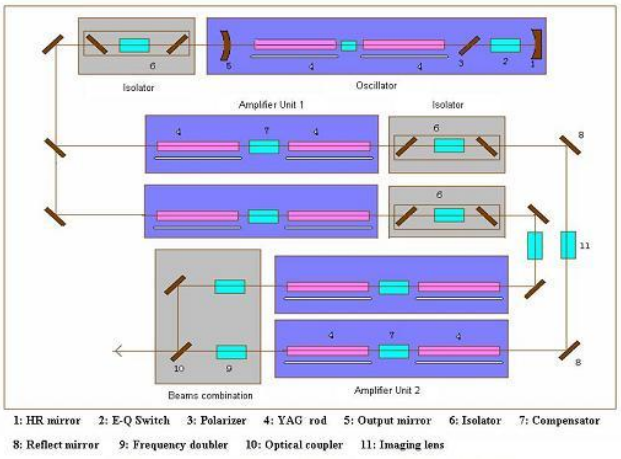

Figure 1. Diagram of the 40W laser (2J in 532nm, 20Hz)

There are 10 Nd:YAG rods in total in the laser system. The output of the oscillator which two rod are inside is divided into two beams, and then go to the amplifier unit 1 and the amplifier unit 2 in turn. The output from the amplifier unit 2 passes the frequency doublers, and then combine into on beam for ranging. Fig. 2 shows the photo of the laser. Fig. 3 shows the inner view of the laser. Fig. 4 shows the laser firing through the new 210mm aperture transmitter to the sky.

Figure 2. Photo of the laser

Figure 3. Inner view of the laser

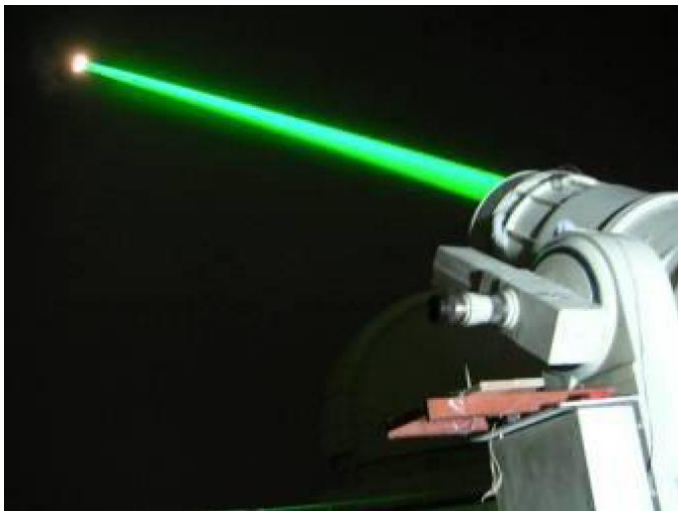

Figure 4. Laser firing

The C-SPAD detector and the Riga event timer were used for the experiment.
The returned signal strength expected from a 2-meter diameter target located 800 km away can be estimated by the following equation:

$$n_0 = \frac{\lambda \eta_q}{hc} \times \frac{E_t A_r \rho S \cos(\theta)}{\pi \theta_t^2 R^4} \times T^2 \times K_t \times K_r \times \alpha$$

Where

- n_0: Average number of photoelectrons received by detector
- λ: Wavelength of laser, 532nm
- η_q: Quantum efficiency of the detector, 0.2

h: Planck constant, 6.624×10^{-34} J·s
c: Light speed, 2.998×10^{8} m/s
E_t: Energy of laser pulse, 2J
Ar: Effective area of receive telescope, 0.245m^2
ρ: Reflectivity of the target's surface, 0.16
r: Equivalent radius of the target, 1m
cos(θ):Suppose the targets are spherical, cos(θ)=1
θ_t: Divergence of laser beam from telescope, 12 arcsec
R: Range of the targets, 800km
T: Atmospheric transmission, T^2=0.6
Kt: Eff. of transmitting optics, 0.60
Kr: Eff. of receiving optics, 0.60
α: Attenuation factor, 13dB

We have,

$$n_0 = 0.20 \text{ (Photoelectrons)}$$

The probability of detection by the C-SPAD detector with single photon sensitivity can be estimated by

$$P = 1 - e^{-n_0} = 1 - e^{-0.20} = 0.18$$

So we might get 18 returns in 5 seconds with the 20 Hz laser.

Preliminary Observational Results from the Un-cooperative Targets at Shanghai

After the installation of the new laser, we built the control and ranging interfaces and software for the experiment. Because the weather problem in Shanghai and some problems with the laser power supply, until July 2008, we have obtained some laser returns from the un-cooperative targets which are the discarded Soviet and US rockets with the ID 1987-38B (639×611 km) and 2007-006G (541×499 km) respectively. The residuals (O-C) for three passes are shown in Fig. 5-7, and the range variations for each pass are shown in Fig. 8-10. The maximum range obtained is 936 km.
Fig. 11 shows the statistics of the laser returns in 5 seconds bin from the ID 1987-38B on July 7, 2008. It is shown that 10-14 returns in 5 seconds were obtained when the telescope tracking were well, and it is roughly coincide with the estimation of the returned signal strength.

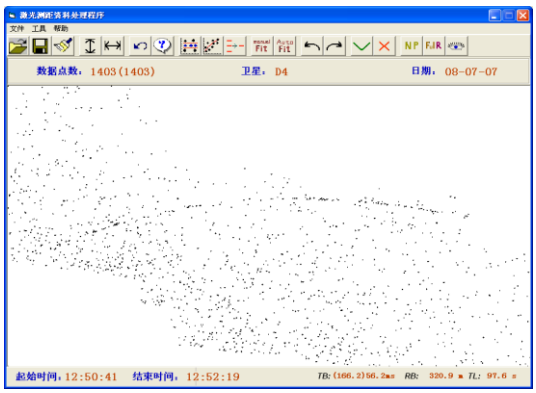

Figure 5. Returns from the discarded Soviet rocket (ID 1987-38B) on July 7, 2008

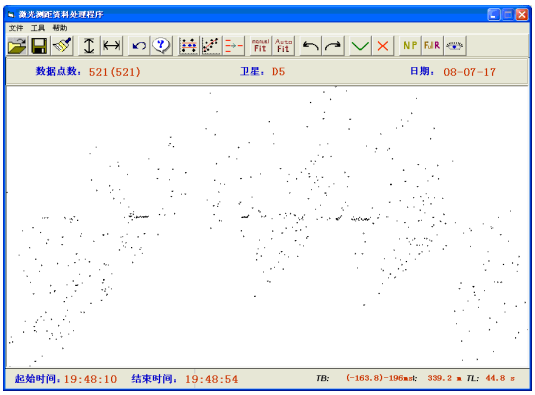

Figure 6. Returns from the discarded US rocket (ID 2007-006G) on July 17, 2008

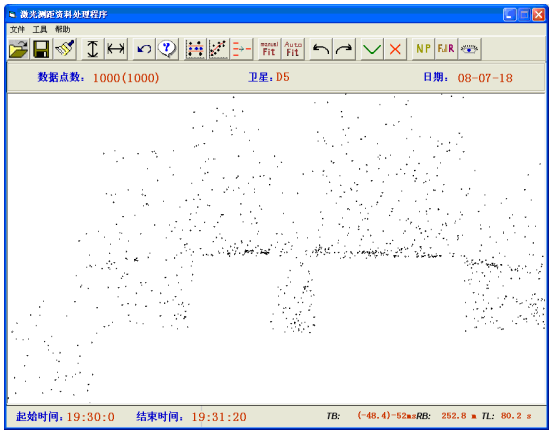

Figure 7. Returns from the discarded US rocket (ID 2007-006G) on July 18, 2008

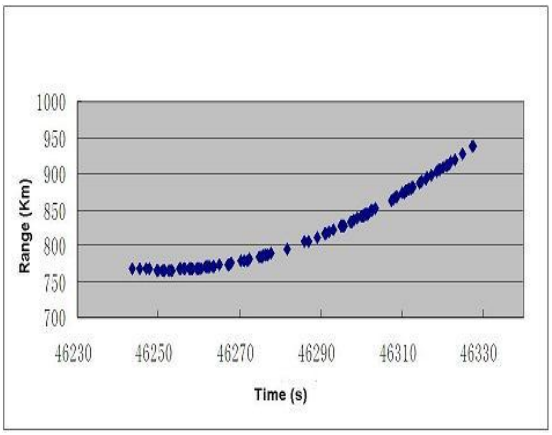

Figure 8. Ranging data of ID 1987-38B on July 7, 2008

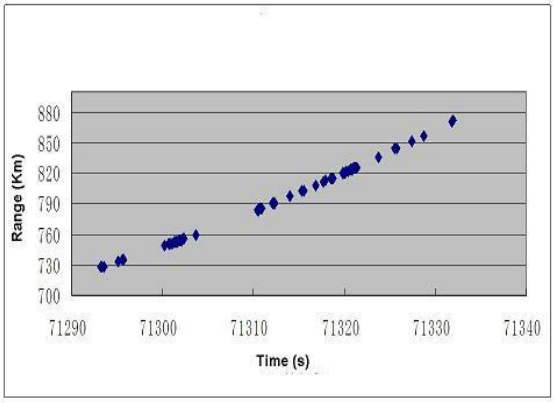

Figure 9. Ranging data of ID 2007-006G on July 17, 2008

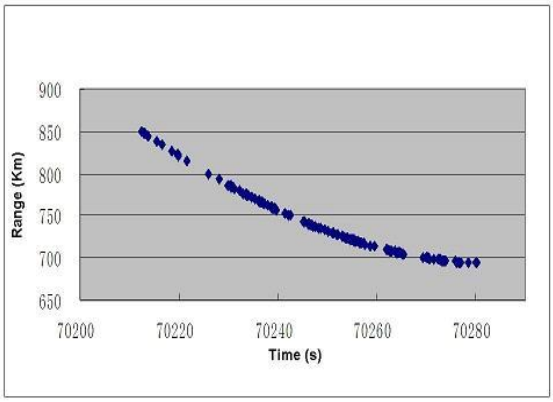

Figure 10. Ranging data of ID 2007-006G on July 18, 2008

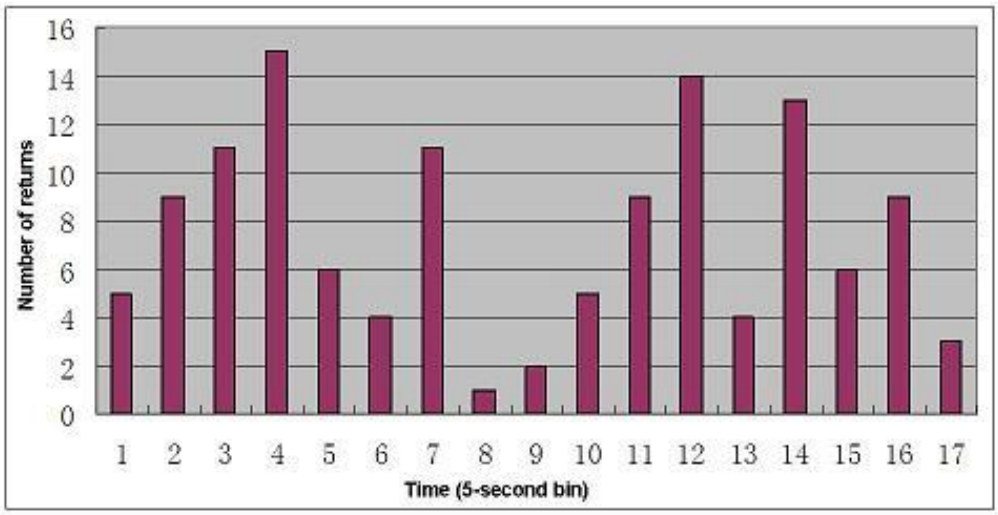

Figure 11. Statistics of returns (5-second bin) on July 7, 2008

Summary

The laser returns from the un-cooperative targets have been obtained at the Shanghai SLR station in July 2008. These targets are the discarded Soviet and US rockets with the ID 1987-38B and 2007-006G respectively. It is shown from the experiment that the return signals from the targets with the range of 900 km were quite strong. Further experiment for more distant and smaller targets is under way.

References

[1] Yang Fumin, Chen Wanzhen, Zhang Zhongping, Chen Juping, Wang Yuanming, K. Hamal, I. Prochazka, The Experimental Laser Ranging System for Space Debris at Shanghai, Proceedings of the 15th International Workshop on Laser Ranging, Volume 2, p.473—478, Canberra, Australia , 2006.

One Way System Calibration Techniques

Toby Shoobridge, David Benham
NERC Space Geodesy Facility
Herstmonceux, UK
Tooo@nerc.ac.uk

Abstract

It has always been necessary to make a two-way calibration to account for the delays in an SLR system. This is done by comparing the ranged measurement to a ground target of a known distance. With the current work in T2L2 and LRO it is now in addition necessary to provide as accurate an epoch as possible for the pulse as it passes the System Reference Point. Determining a one-way calibration for the transmit side delay proves difficult as the current two-way method cannot simply be divided so a new method is required. Our ongoing work to determine the transmit-side delay is presented. This includes measurements of the laser path from the start diode to the system reference point and the electronic delays in cables and equipment from the start diode to the epoch timer. The distance taken by the laser pulse path through the coudé path was measured using three techniques. The first used a laser rangefinder, more commonly used in building surveying. The second method was to make time-of-flight measurements of timed Hz laser pulses passing through the coudé and the third method used a combination of the telescope drawings and physical measurement. The laser rangefinder initially seems to have given the most repeatable and accurate result given that the manufacturers specify an accuracy of at worst 1.5mm over a 30m distance. The other independent methods will provide a good comparative check on this. The largest error contribution to the final result comes from the physical measurements made in the laser bed.

Aim and Necessity

The aim is to measure the delay in the various components of the SLR two-way calibration in order to understand the Transmit-side delay.

It has always been necessary to make a calibration to account for the two-way delays in an SLR system. Now the proposed work in T2L2 and LRO requires as accurate an epoch as possible for the laser pulse as it passes the system reference point. This report describes the technique and results that have been developed to estimate the components of the various delays necessary to achieve this epoch correction at the level of a few ns.

Current System Calibration Technique

The standard range calibration value is determined as the sum of the Transmit and Receive-side delays by ranging to a fixed ground target at a known distance. Unfortunately this result cannot simply be separated into the parts we are interested in.

Transmit-side Delay

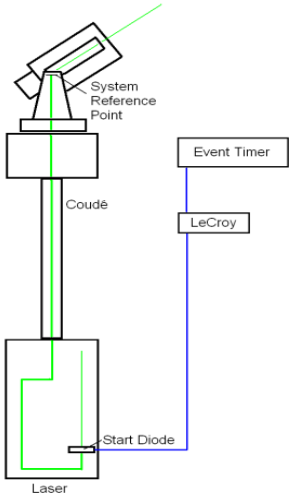

The Transmit-side delay is the sum of the times taken for the laser pulse to travel from the Start Diode to the System Reference Point and the propagation time for the Start Diode electronic pulse to travel through cables and electronic equipment to trigger the Event Timer. Described here are estimates of both these elements.

1. Measuring the Laser Path from the Start Diode to the System Reference Point

This was measured as two components, those being the optical delays in the laser bed (including the propagation effects of optics) and the Coudé path length.

a) Laser Bed

Physical Measurements were made with a rule along the Laser Path. The Effective increase in Path Length due to the Refractive Indices of Laser components was also calculated.

Addition to Effective Air Path for Various Refractive Indices											
Description	thick (mm)	er (mm)	ang (deg)	path (mm)	er path (mm)	ref index	er ref ind	lighttime (ps)	er time (ps)	eff airpath(mm)	er airp (mm)
45 deg Quarts Rotator Polarizer	4	0.05	0	4.000	0.050	1.5067	0.0001	20.089	0.252	6.027	0.076
Compensating Wedge x 4	4.4	0.1	56	5.269	0.120	1.5067	0.0001	26.465	0.603	7.939	0.181
Rod x 2	202.3	0.1	0	202.300	0.100	1.83	0.01	1234.030	7.353	370.209	2.206
Lens x 4	9.1	0.05	0	9.100	0.050	1.5067	0.0001	45.703	0.254	13.711	0.076
	0	0.05	0	0.000	0.150	1.7812	0.0001	0.000	0.891	0.000	0.267
Energy Monitor Splitter	1	0.05	45	1.132	0.057	1.5067	0.0002	5.688	0.285	1.706	0.086
Eyesafe (n/a)	0	0.05	0	0.000	0.050	1.5	0.03	0.000	0.250	0.000	0.075
KDP Doubler Crystal	20.4	0	0	20.400	0.000	1.49	0.03	101.320	2.040	30.396	0.612
Start Diode Splitter	1	0.05	45	1.132	0.057	1.5067	0.0001	5.688	0.285	1.706	0.085
Total Glass	242.2	0.5		243.334	0.633			1438.982	12.214	431.695	3.664
Amp Inclusive Length (mm)	2347.000	0.25									
Amp Air Path (mm)	2103.666	0.883									
Amp Effective Total Air Path (mm)	2535.360										
Time Amp Air Path(ps)	7012.219	5.887									
Time eff Airpath(ps)		24.4273005									
Amp Time(ps)	7012.219	ps									
error	30.314	ps									

Calculation of effective increase in laser path length due to propogation effects of various optics

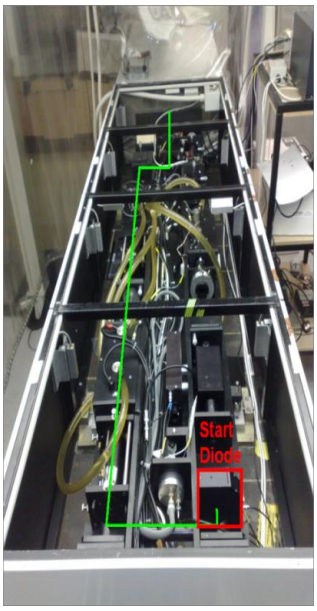

The 10 Hz Laser showing the laser path and position of Start Diode

b) Laser Path

Three methods were employed to measure the Coudé Path:

i) Physical Measurements and Technical Drawings

The original technical drawings of the telescope were used to calculate the Coude Path from the telescope base to the System Reference Point. The measurement from the telescope base to the Coude entrance was made using a tape measure and level. This simple method was used primarily as a useful comparison for the other methods.

ii) Reflected 10 Hz Laser Pulse

The Laser was fired through the coudé chain and reflected back via a mirror on the emitter as can be seen in these images.

Both the outgoing and returning laser pulses were used to trigger the same light-sensitive diode (circled in red) via the use of a beam splitter and a two-into-one fiber optic as shown below. The output from the diode was viewed via an oscilloscope. The time interval between the outgoing and returning pulse, estimated via the oscilloscope display, was used to calculate the laser path distance.

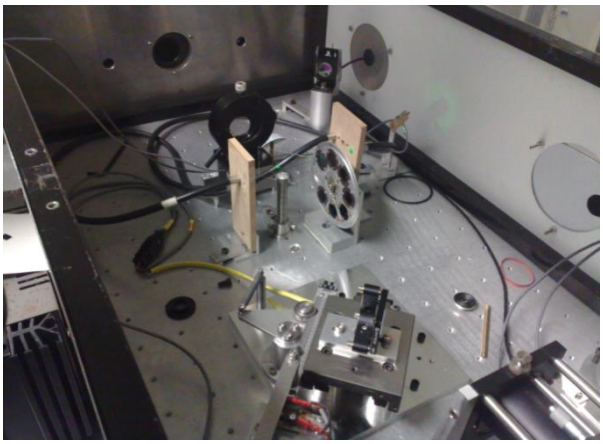

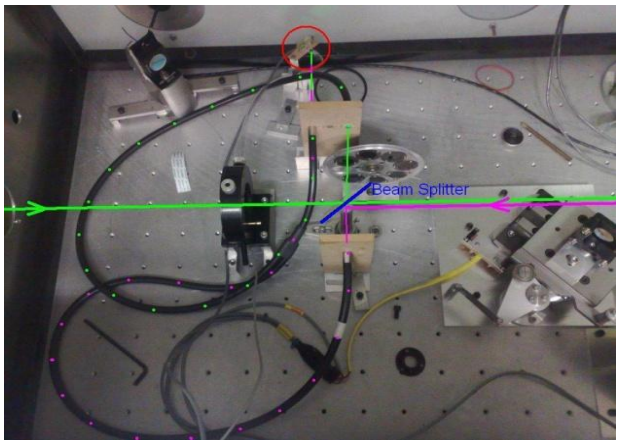

The two laser pulses and semi-trains can be seen clearly on the oscilloscope.

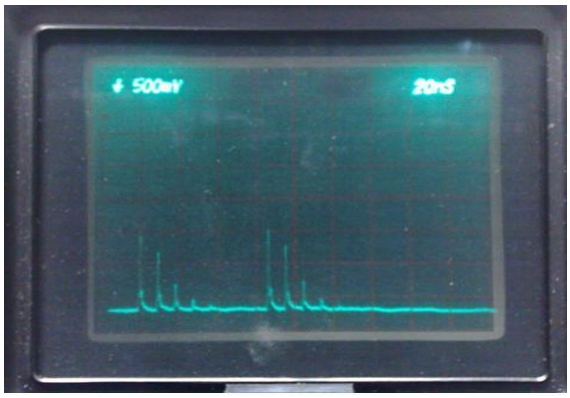

iii) Laser Rangefinder

A Bosch DLE 50 Laser Rangefinder, more commonly used as a building surveying tool, was used as a third method of measurement. The manufacturers state a typical accuracy of ±1.5mm over a 30m distance.

An adjustable mount was manufactured enabling the Rangefinder to be aligned to reflect correctly off all mirrors and measure directly the required coudé path length.

Having aligned the Rangefinder, the emitter was removed and replaced with a flat surface for the rangefinder to measure to. Measurements were taken with the telescope placed in varying azimuth positions to ensure no significant change in the measurement was present due to poor alignment for example. The process of alignment and measurement was repeated, and very good repeatability at the level of 1mm in the results was found.

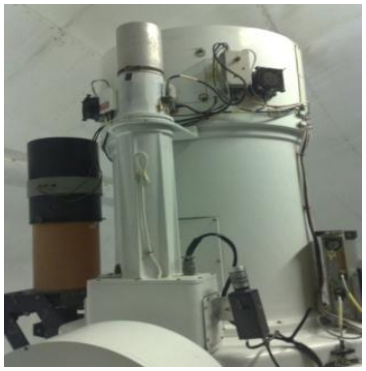

Telescope complete with emitter.

Emitter removed and replaced with flat surface.

Results

a) Physical Measurements and Technical Drawings

8.411 m Error ± 20 mm

- Difficulty in Physical Measurement of Coudé below Telescope

b) Reflected 10-Hz Laser

8.388 m Error ± 30 mm

- Limited by accuracy in interpreting the Oscilloscope display
- Research more accurate ways of measuring timing between outgoing and returning pulses

c) Bosch Laser Rangefinder

8.398 m Error ± 1.5 mm

- Most accurate and repeatable method

- All the results agree to within 25mm. The method we found to be best due to its accuracy and repeatability was that using the Bosch Laser Rangefinder; the result itself is also easily within the range of error of the other two methods.

2. Cables and Electronic Equipment

The delays in cables and electronic equipment comprise the Start Diode, LeCroy Discriminator, Event Timer and Cables.

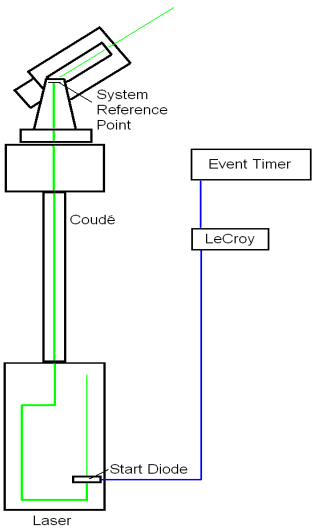

a) Start Diode

A Beam Splitter is used in the path of the laser to direct a small percentage of laser light to the Start Diode. The Diode is placed 25.5mm from the Beam Splitter, the time taken for the laser to pass through this space was included. There is also a delay in the Diode circuitry which is yet to be determined. This delay may prove difficult to determine due to the effects in the variation of the laser energy that reaches it and its temperature.

b) Cables and LeCroy Measurement

The pulse provided by the Start Diode passes through two cables, a LeCroy distribution device and some electronics before triggering the start in the Event Timer. The delay produced by these components was determined by making a series of calibrations with and without the various components in the chain. The resulting difference in the calibration values demonstrates the actual delay produced by each item. This method could not be employed for the electronics leading to the Event Timer, this delay is yet to be determined or may remain unknown.

c) Event timer

The delays inherent in the use of the event timer are as yet un-measured, but are estimated to be small and likely less than 1ns. Further work will address this issue.

Total Delay between Start Diode and Event Timer

Start Diode

- To be Determined
- Beam Splitter to Diode 0.027 m

Cables

- Diode to LeCroy: 13.350 m
- LeCroy to ET: 2.791 m

LeCroy

- LeCroy currently in use: 3.609 m

Event Timer

To be Determined

Total: 19.776 m

The results found using this method were compared to the calculated expected delay. The signal propagation through a cable can be expressed as a percentage of the speed of light. An approximate figure found for the coaxial cable in use is 66%. This would broadly agree with the results found for the cables tested. For example, the results for the cable between the Start Diode and the LeCroy discriminator are shown below.

Physical Length	8.868 m
Effective Length at 66% light speed	13.436 m
Effective Length using calibration method	13.349 m

Total Transmit-side Delay

The transmit-side delay can now be given as the difference between the time the laser passes through the System Reference Point and the time that ET is triggered.

Subtract Laser Path Delay from Cable and Electronic Equipment Delay

Transmit-side Delay = 19.77617 m - 13.49233 m
= 6.28383 m
= **20.946 ns** Error Estimate <1ns

So the Laser Pulse passes through the System Reference Point 21ns before the Event Timer is triggered. This result uses the electronic delays determined to date and the coudé path measurements made using the Bosch laser rangefinder.

Further Work

- More Tests on LeCroys and Cables
- Event Timer Delay
- Start Diode Delay
- Measure all Receive-side delays to close the loop and compare against our standard two-way calibration result
- Setup to enable measurement of Transmit-side delay as one measurement

Measuring the Transmit-side delay as one complete measurement.

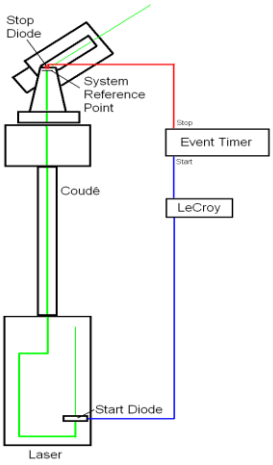

Another method to measure the transmit-side delay as a whole would be to place a diode in the laser path, on or near the system reference point. The pulse from this diode could then be fed to ET stop in place of the SPAD stop pulse. This replaces the outgoing beam (beyond the System Reference Point), returning beam and Receive-side delays with a cable and diode. This relies on having a good understanding of the delay produced by the diode and cable used. This method would be ideal if it could be a permanent fixture to the system that could be setup to calibrate for the Transmit-side Delay on a regular basis, perhaps immediately before and after any LRO or T2L2 observations. It would also allow for quick calibrations to account for any necessary changes that may be made to the system.

Conclusion

We are working towards providing an epoch for the time the laser pulse passes through the System Reference Point, as necessary for LRO and T2L2. The current measurement gives a 21ns correction to the currently-recorded observational epochs, with estimated precision better than 1ns. However, the electronic delays in the Start Diode and event timer are still to be included.

New achievements in the simulator of photon counting planetary altimeter

Josef Blazej, Ivan Prochazka
Czech Technical University in Prague, Brehova 7, 115 19 Prague, Czech Republic
blazej@fjfi.cvut.cz, http://blazej.cz

Abstract

We are presenting new achievements in single photon counting altimeter simulator. The existing planetary altimeter simulator has been extended. The new design is prepared for cooperating with map and surface relief system and results of the photon counting laser altimeter simulator are presented. The simulator is designed to be a theoretical and numerical complement for a Laser Altimeter Technology Demonstrator of the space borne laser altimeter for planetary studies built on our University.

Realizations of photon counting altimeter and lidar

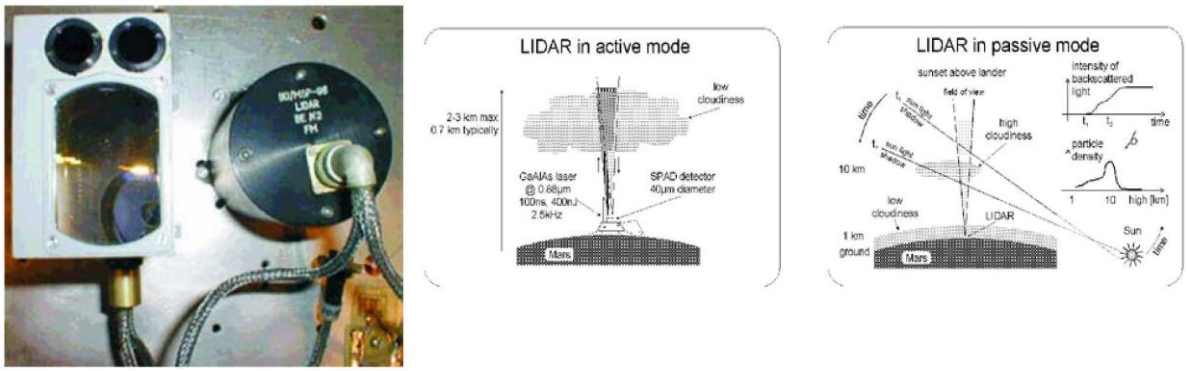

Photon counting altimeter on board of Soviet/Russian missions Mars 92 and 96 and Iidar on board NASA mission Mars Polar Lander 98. Photo of the flying modul (left) with big detector aperture and two smaller apertures of semiconductor lasers and operatinal scheme in active and passive mode.

The steady state photon counting simulator has been already developed by our group [4]. The presented results report the next step of development when a sequence of static simulations allow simulate a move of altimeter using existing terrain map. This work was initiated by the fact that the European Space Agency (ESA) has nominated [3] the photon counting altimeter as one of the attractive devices for planetary research. The requirements on the device are rather strict: total mass in the range of 5-8 kilograms, power consumption below 10 Watts. Additionally, the harsh radiation environment near some planets requires, among others, small optical aperture of the device. The photon counting concept of the altimeter together with its energy budget link and signal to noise ratio has been studied for ESA by U. Schreiber et al. [5]. This concept seems to be only one acceptable for these requirements. Together with Technology Demonstrator [2] of laser altimeter presented simulator is developing.

Modular structure of the simulator

Data describing surface height, slope, roughness, and albedo are extracted from map systems and together with calculated trajectory and background photon flux they are used for altimeter results simulation.

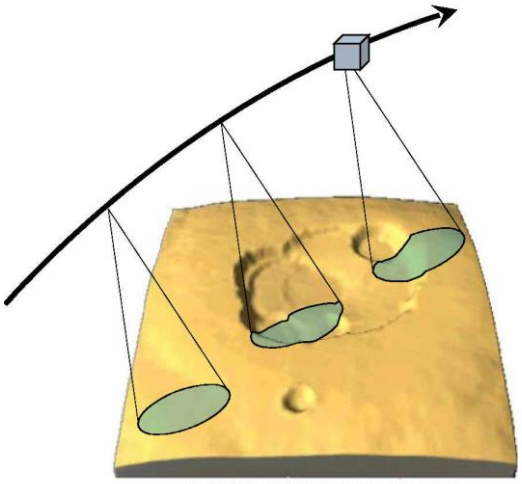

terrain: Alwyn Botha of www.the-planet-mars.com

The expected next step of our research is the integration of our simulator with some terrain map database. The physical model of simulator is based on classical time correlated photon counting scheme. The results of simulation are stored in text files and using internally called Gnuplot program are plotted in graphical report shown in the right poster frame.

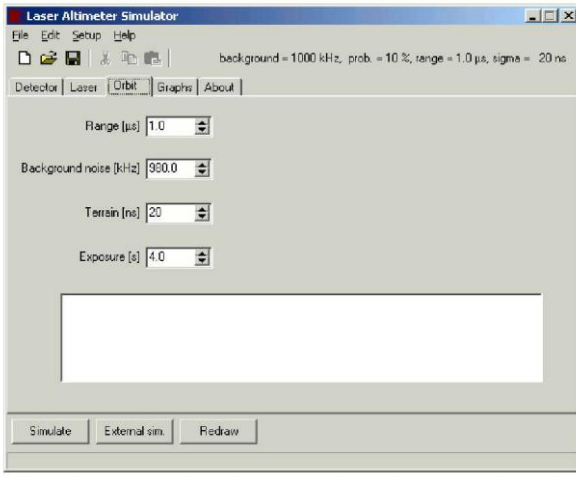

GUI (gray snapshot) allows set up of parameters of the laser (pulse width, repetition rate, wavelength), output optics (output divergence), detector (field of view, detection efficiency, dark noise, temporal resolution), orbit parameters (range, background noise, local terrain profile (on snapshot empty white rectangle), speed of altimeter), sequence of prepared orbit parameters and some parameters for control of graphical output.

Indoor photon counting signal processing tests

To realize altimeter or lidar ranging experiments in indoor conditions the Technology demonstrator - device with down-scale optical part - has been developed and constructed. The screenshot on right side is the measurement of time correlated photon counting acquired by multichannel analyzing card. Two signals (numbered 1 and 2) can be recognized.

The bottom figure represents the same data recalculated into detection probability in selected time window. Peeks of useful signals - echoes - can be recognized more easily.

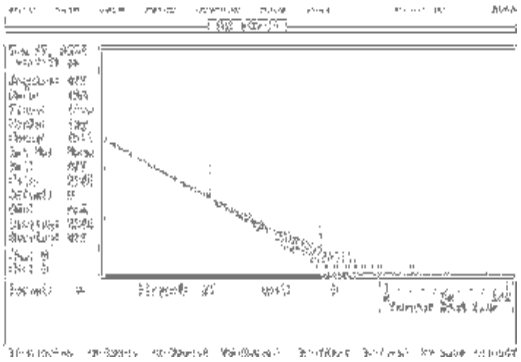

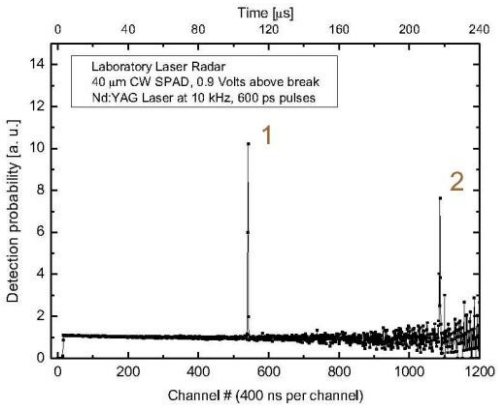

Compare both graphs of real experiment data with graphical output simulator report in right frame of this poster.

Surface relief reconstruction example

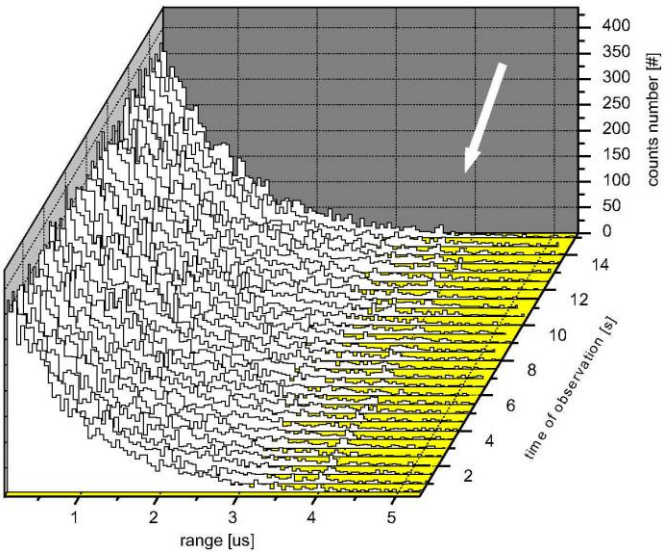

To demonstrate single photon counting altimeter operation the surface described in figure below left has been selected. It consists from 3 segments with different roughness and slope. The all other parameters (albedo, background photon flux, height, ...) are constant, the selected orbit segment is small in compare with its variations. Generally, the system of line segments is input format for any more complex modeled surface relief. The model is calculating with clean atmosphere without clouds.

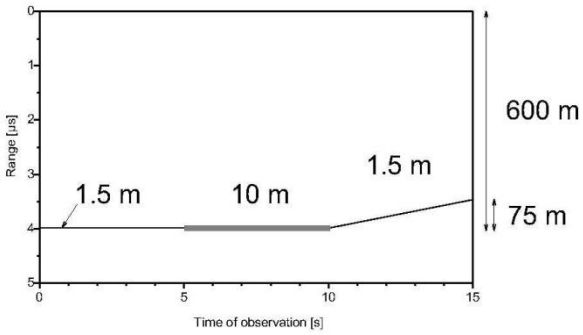

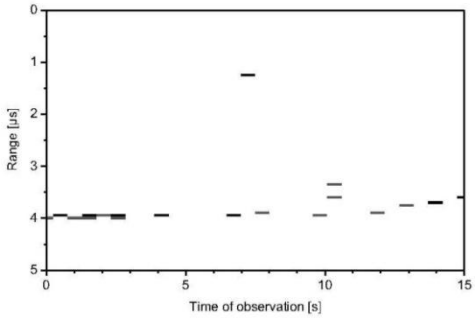

Altimeter operation parameters: 16 kHz rep. rate, 1 MHz overall background noise, 10 % efficiency incl. optics and albedo, sub-ns laser pulse and detector temporal resolution. Data have been separated into groups by 0.5 s (8000 echoes) Series of histograms are shown in the big top figure, the histogram cellwidth is 50 ns. The white arrow indicates the area, where the useful signal is observable. The reconstructed relies using application of 30 filtering criterion is in smaller right figure. The gray level corresponds to SNR.

The simulator user interface (GUI) is developed in Delphi environment. It allows set up of parameters of laser (pulse width, repetition rate, wavelength), output optics (output divergence), detector (FOV, DE, dark noise, temporal resolution), orbit parameters (range, background noise, local terrain profile, speed of altimeter), and some parameters for control of graphical output. From these the five parameters were calculated using radar equation - number of shots, range, noise, probability of detection, and the overall temporal resolution. These parameter inputs into simulator core based on a standard pseudo random number generator and the array of echoes is produced. Two histograms are calculated from this array and simulator produce the list of commands for plotting software to plot report as displayed in figure at next page. Optionally, the orbit parameters set is substituted by a external text file describing orbit and surface as a list of pre-calculated values.

Example of simulator graphical output report

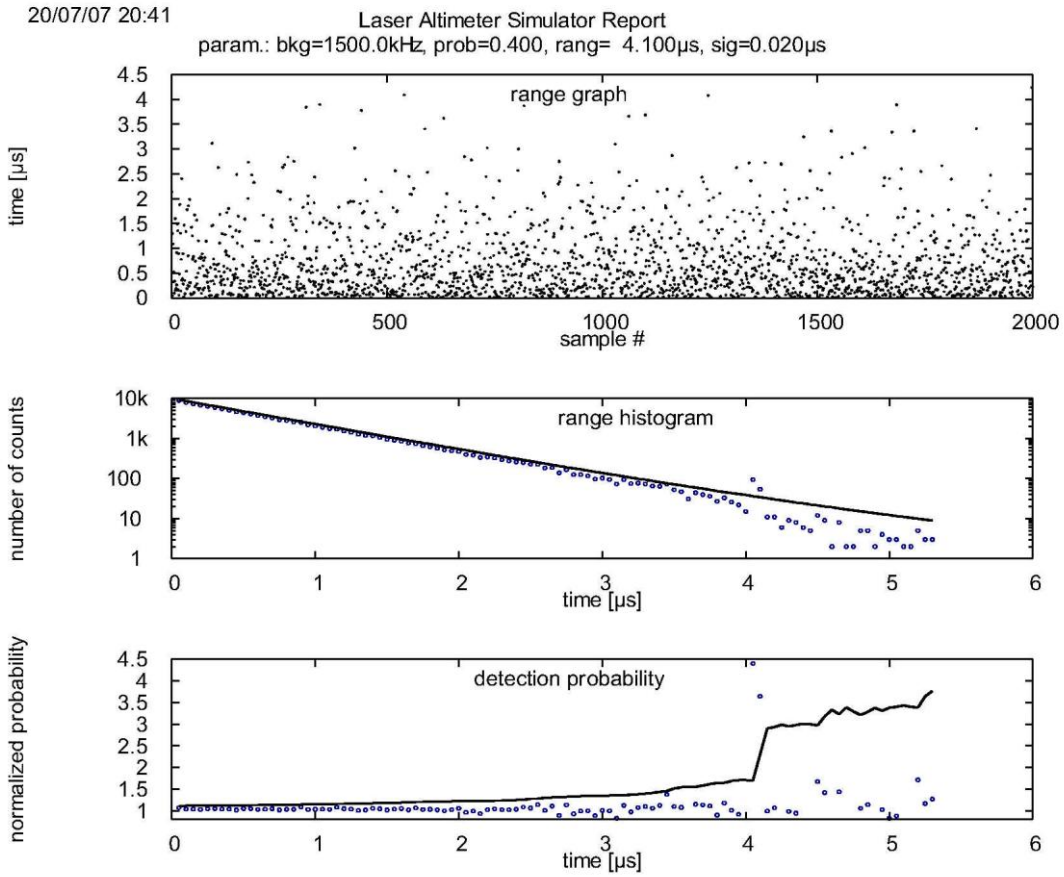

Automatically generated simulator output report. The black lines are distinguish levels of 30 criterion for counts number and detection probability respectively.

Acknowledgements

The financial support provided by the Research Framework MSM6840770015 and grant ME08065 of Ministry of Education of Czech Republic is greatly appreciated.

References

1. Bukharin, AV, Linkin, VM., Lipatov, AN., Lyash, AN., Makarov, VS., Pershin, S.M., Tiurin, AV, Russian compact Lidar for NASA "Mars Surveyor Program 98" in materials of 19th International Laser Radar Conference, Annapolis, Maryland, July, 1998, p. 241.
2. Blazej, J., Prochazka, I., Hamal, K., Fedyszynova, M., Yang, Fumin, et al., Photon counting laser altimeter for planetary exploration - the technology demonstrator. Journal of Optics A: Pure and Applied Optics. 2007, vol. 9, no. 6, p. S98.
3. Murphy, E., Rando, N., Falkner, P., Peacock, 1., Laser altimeter for planetary exploration, in Proc. SPIE 5240, edited by Ch. Werner 5240, USA, 2004, pp. 10-17.
4. Blazej, J., Photon counting space born altimeter simulator, In Laser Radar Techniques for Atmospheric Sensing, Proc. SPIE 5575, edited by U. Singh, USA, 2004, p.143

5. Schreiber, U. et al., Technical Concept for a European Laser Altimeter for Planetary Exploration, in Proceedings of the 14th International Laser Ranging Workshop and International Laser Ranging Service (ILRS) General Assembly, San Fernando, Cadiz, Spain, June7-11, 2004, published on line http://www.roa.es/14workshoplaser/papers/4. New%20Applications/4.Technical%20concept.pdf

WORKSHOP PARTICIPANTS

Altamimi Zuheir	Instytut Geographique National, ENSG/LAREG, France	altamimi@ensg.ign.fr
Appleby Graham	NERC SGF, United Kingdom	gapp@nerc.ac.uk
Arnold David	SAO, USA	david-arnold@earthlink.net
Arsov Kirco	Finnish Geodetic Institute, Finland	kirco.arsov@fgi.fi
Artyukh Yurijs	Institute of Electronics and Computer Science, Latvia	artyukh@edi.lv
Balodis Janis	University of Latvia, Latvia	janis.balodis@lu.lv
Bernhardt Paul	Naval Research Laboratory, USA	bern@ppd.nrl.navy.mil
Bespalko Vladimirs	Institute of Electronics and Computer Science, Latvia	bezpalko@edi.lv
Bianco Giuseppe	Agenzia Spaziale Italiana, Italy	giuseppe.bianco@asi.it
Biskupek Liliana	EGU, Germany	biskupek@mbox.ife.uni-hannover.de
Bobojć Andrzej	University of Warmia and Mazury, Poland	altair@uwm.edu.pl
Brzeziński Aleksander	Space Research Centre of the Polish Academy of Sciences, Poland	alek@cbk.waw.pl
Buls Jevgenijs	Institute of Electronics and Computer Science, Latvia	buls@edi.lv
Burmistrov Vladimir	Institute for Precision Instrument Engineering, Russia	niip@niipp-moskva.ru
Burris Harris	US Naval Research Observatory, USA	ray.burris@nrl.navy.mil
Carter David	NASA/GSFC, USA	David.L.Carter@nasa.gov
Chen Juping	Shanghai Astronomical Observatory, China	yangfm@shao.ac.cn
Chen Wanzhen	Shanghai Astronomical Observatory, China	cwz@shao.ac.cn
Cheng Minkang	University of Texas at Austin, USA	cheng@csr.utexas.edu
Ciufolini Ignazio	University of Salento, Italy	ignazio.ciufolini@unile.it
Clarke Christopher	NASA/Honeywell Technology Solutions, USA	christopher.clarke@honeywell.com
Combrinck Ludwig	Hartebeesthoek Radio Astronomy Observatory, South Africa	ludwig@hartrao.ac.za
Davis Mark	Honeywell, USA	mark.davis@nrl.navy.mil
Degnan John	Sigma Space Corporation, USA	John.Degnan@sigmaspace.com
Deleflie Florent	Observatoire de la Cote d'Azur, France	Florent.Deleflie@obs-azur.fr
Dell'Agnello Simone	INFN-LNF, Italy	Simone.dellagnello@lnf.infn.it
Ding Jian	Chinese Academy of Surveying and Mapping, China	qufeng@casm.ac.cn
Donovan Howard	NASA/Honeywell Technology Solutions, USA	Howard.Donovan@honeywell.com
Drożyner Andrzej	University of Warmia and Mazury, Poland	drozyner@uwm.edu.pl
Dube Maurice	SSAI, USA	Maury.Dube@nasa.gov
Dunn Peter	Raytheon, USA	Peter_j_dunn@raytheon.com
Exertier Pierre	OCA-GRGS, France	Pierre.Exertier@obs-azur.fr
Femenias Pierre	ESA - ESRIN, Italy	pierre.femenias@esa.int

Garate Jorge	San Fernando Naval Observatory, Spain	jgarate@roa.es
Gavrielides Tom	EOARD, United Kingdom	tom.gavrielides@london.af.mil
Glotov Vladimir	Mission Control Center, Russia	vladimir.glotov@mcc.rsa.ru
Greene Ben	EOS, Australia	bengreene@bengreene.net
Gross Richard	JPL/NASA, USA	Richard.Gross@jpl.nasa.gov
Grunwaldt Ludwig	GFZ, Germany	grun@gfz-potsdam.de
Hirsch Roman	Astronomical Observatory of A.Mickiewicz University, Poland	hirsch@amu.edu.pl
Horvath Julie	NASA/Honeywell Technology Solutions, USA	julie.horvath@honeywell.com
Huber Heinz	High Q Laser, German office, Germany	heinz.huber@highqlaser.at
Hurnik Hieronim	Astronomical Observatory of A. Mickiewicz University, Poland	hurnik@vesta.astro.amu.edu.pl
Inoue Takahiro	Japan Aerospace Exploration Agency, Japan	inoue.takahiro@jaxa.jp
Jackson Dale	Sandia National Laboratories, USA	dcjacks@sandia.gov
Kim Kyunghee	KAIST, Korea	khkim@satrec.kaist.ac.kr
Kirchner Georg	Austrian Academy of Sciences, Austria	Georg.Kirchner@oeaw.ac.at
Klosko Steven	NASA/GSFC/SGT, USA	sklosko@sgt-inc.com
Kodet Jan	Czech Technical University in Prague, Czech Republic	kodet@fjfi.cvut.cz
Koelbl Josef	EOS Optronics, Germany	sandra.weidmann@eos-optronics.com
Koidl Franz	Austrian Academy of Sciences, Austria	franz.koidl@oeaw.ac.at
Kopeikin Sergei	University of Missouri-Columbia, USA	kopeikins@missouri.edu
Kosek Wiesław	Space Research Centre of the Polish Academy of Sciences, Poland	kosek@cbk.waw.pl
Kucharski Daniel	Austrian Academy of Sciences, Austria	Daniel.Kucharski@oeaw.ac.at
Lauber Pierre	Technische Universitaet Muenchen, Germany	lauber@fs.wettzell.de
Lee Jun Ho	Kongju National University, Korea	jhlsat@kongju.ac.kr
Lee Sang-Hyun	KAIST, Korea	shlee@satrec.kaist.ac.kr
Lee Seng-Hum	KAIST, Korea	
Lejba Paweł	Space Research Centre of the Polish Academy of Sciences, Poland	plejba@cbk.poznan.pl
Li Rongwang	Yunnan Observatory, Chinese Academy of Sciences, China	billgacsli@163.com
Li Yuqiang	Yunnan Observatory, Chinese Academy of Sciences, China	lyq@ynao.ac.cn
Lim Hung-Chul	Korea Astronomy and Space Science Institute, Korea	hclim@kasi.re.kr
Lopez Fernandez Jose Antonio	IGN, Spain	ja.lopez@oan.es
Luceri Vincenza	e-GEOS, Italy	cinzia.luceri@telespazio.com
Luck John	EOS Space Systems, Australia	john-luck@bigpond.com
Łatka Jan K.	Space Research Centre of the Polish Academy of Sciences, Poland	jkl@cbk.waw.pl
Maberry Michael	University of Hawaii, USA	maberry@hawaii.edu
Makeyev Andriy	Crimean Laser Observatory, Ukraine	makeyev a.a@mail.ru

Mallama Anthony	Raytheon, USA	anthony.mallama@gmail.com
Mareyen Maria	Bundesamt fuer Kartografie und Geodaesie, Germany	maria.mareyen@bkg.bund.de
McGarry Jan	NASA/GSFC, USA	jan.mcgarry@nasa.gov
Medvedsky Mykhaylo	Main Astronomical Observatory of the National Academy of Science of Ukraine, Ukraine	medved@mao.kiev.ua
Michałek Piotr	Space Research Centre of the Polish Academy of Sciences, Poland	misiek@cbk.poznan.pl
Moore Christopher	EOS Space Systems, Australia	cmoore@eos-aus.com
Moshkov Vladislav	Science Research Institute for Precision Instrument Engineering, Russia	spb.niipp@rambler.ru
Mueller Horst	Deutsches Geodatisches Forschungsinstitut, Germany	mueller@dgfi.badw.de
Mueller Juergen	Leibniz Universitat Hannover, Germany	mueller@ife.uni-hannover.de
Murphy Tom	University of California, San Diego, USA	tmurphy@physics.ucsd.edu
Nararen Jyri	Finnish Geodetic Institute, Finland	naranen@iki.fi
Navarro Madrid Pedro Francisco	GMV, Aerospace and Demence, Spain	formacion@gmv.es
Nawrocki Jerzy	Space Research Centre of the Polish Academy of Sciences, Poland	nawrocki@cbk.poznan.pl
Neidhardt Alexander	TU Muenchen, Germany	neidhardt@fs.wettzell.de
Noyes Vince	Electro Optics Systems, Australia	vnoyes@midwest.com.au
Ohlert Johannes	University of Applied Sciences Giessen-Friedberg, Germany	jomo@monet.fh-friedberg.de
Otsubo Toshimichi	Hitotsubashi University, Japan	t.otsubo@srv.cc.hit-u.ac.jp
Otten Michiel	ESA/ESOC, Germany	michiel.otten@esa.int
Panafidina Natalia	GFZ, Germany	natasha@gfz-potsdam.de
Pap Viktor	Main Astronomical Observatory of the National Academy of Science of Ukraine, Ukraine	vic@mao.kiev.ua
Park Jong-Uk	Korea Astronomy and Space Science Institute, Korea	jupark@kasi.re.kr
Parkhomenko Nataliya	Institute for Precision Instrument Engineering, Russia	natalia.n@g23.relcom.ru
Pavlis Erricos	Joint Center for Earth Systems Technology, Univ. of Maryland, USA	epavlis@umbc.edu
Pearlman Michael	Harvard-Smithsonian Center for Astrophysics, USA	mpearlman@cfa.harvard.edu
Pierron Francis	Observatoire de la Cote d'Azur, France	Francis.Pierron@obs-azur.fr
Pierron Monique	Observatoire de la Cote d'Azur, France	Monique.Pierron@obs-azur.fr
Prochazka Ivan	Czech Technical University in Prague, Czech Republic	prochazk@fjfi.cvut.cz
Prokofjeva Arija	Institute of Electronics and Computer Science, Latvia	aria@edi.lv
Pudel Guido	University of Applied Sciences Giessen-Friedberg, Germany	Guido.Pudel@mnd.fh-friedberg.de
Qu Feng	Chinese Academy of Surveying and Mapping, China	qufeng@casm.ac.cn

Raja-Halli Arttu	Finnish Geodetic Institute, Finland	Arttu.raja-halli@fgi.fi
Ricklefs Randall	The University of Texas at Austin, USA	ricklefs@csr.utexas.edu
Ries John	The University of Texas at Austin, USA	ries@csr.utexas.edu
Rubans Augusts	University of Latvia, Latvia	inesej@inbox.lv
Rutkowska Milena	Space Research Centre of the Polish Academy of Sciences, Poland	milena@cbk.waw.pl
Sadovnikov Mikhail	Institute for Precision Instrument Engineering, Russia	niip@niipp-moskva.ru
Salminsh Kalvis	Institute of Astronomy University Latvia, Latvia	kalvis@lanet.lv
Samain Etienne	Observatoire de la Cote d'Azur, France	etienne.samain@obs-azur.fr
Schillak Stanisław	Space Research Centre of the Polish Academy of Sciences, Poland	sch@cbk.poznan.pl
Schmidt Michael	High Q Laser, Austria	michael.schmidt@highqlaser.at
Schreiber Ulrich	Technische Universitaet Muenchen, Germany	schreiber@fs.wettzell.de
Schutz Bob	University of Texas at Austin, USA	vlyons@csr.utexas.edu
Sciarretta Cecilia	Telespazio SpA, Italy	cecilia.sciarretta@telespazio.com
Seemueller Wolfgang	Deutsches Geodatisches Forschungsinstitut, Germany	seemueller@dgfi.badw.de
Seo Yoon-Kyung	Korea Astronomy and Space Science Institute, Korea	ykseo@kasi.re.kr
Shoobridge Toby	NERC SGF, United Kingdom	tooo@nerc.ac.uk
Sierk Bernd	BKG, Chile	sierk@tigo.cl
Smith David	NASA, USA	David.E.Smith@nasa.gov
Snopek Krzysztof	GFZ, Germany	snopek@gfz-potsdam.de
Springer Tim	ESA/ESOC, Germany	Tim.Springer@esa.int
Tercero Martinez Felix	Instituto Geografico Nacional, Spain	f.tercero@oan.es
Thaller Daniela	University of Bern, Switzerland	thaller@aiub.unibe.ch
Thomas Linda	US Navy, USA	linda.wasiczko@nrl.navy.mil
Torrence Mark	GSFC/SGT Inc, USA	Mark.H.Torrence@nasa.gov
Utzinger Johannes	University of Bern, Switzerland	johannes.utzinger@aiub.unibe.ch
Varghese Thomas	Cybioms Corporation, USA	tvarghes@cybioms.com
Vasiliev Vladimir	Institute for Precision Instrument Engineering, Russia	lavaser@kmail.ru
Vedins Vadims	Institute of Electronics and Computer Science, Latvia	vedinv@edi.lv
Vei Margarita	GFZ, Germany	vei@gfz-potsdam.de
Wei Zhibin	Chinese Academy of Surveying and Mapping, China	zhibinw@casm.ac.cn
Wetzel Scott	NASA/Honeywell Technology Solutions, USA	scott.wetzel@honeywell.com
Wiant Jerry	University of Texas, USA	jrwastro@yahoo.com
Wijaya Dudy Darmawan	Graz University of Technology, Austria	dudy.d.wijaya@student.tugraz.at
Wilkinson Matthew	NERC SGF, United Kingdom	matwi@nerc.ac.uk
Wnuk Edwin	Astronomical Observatory of A. Mickiewicz University, Poland	wnuk@amu.edu.pl

Wu Bin	Shanghai Astronomical Obserwatory, China	bwu@shao.ac.cn
Xiong Yaoheng	Yunnan Observatory, Chinese Academy of Sciences, China	xyh@ynao.ac.cn
Yang Fumin	Shanghai Astronomical Observatory, China	yangfm@shao.ac.cn
Yoshihara Keisuke	Japan Aerospace Exploration Agency, Japan	Yoshihara.keisuke@jaxa.jp
Zellar Ronald	NASA GSFC, USA	ron.zellar@nasa.gov
Zerhouni Wassila	Observatoire de Paris, France	wassila.zerhouni@obspm.fr
Zhang Zhongping	Shanghai Astronomical Observatory, China	zzp@shao.ac.cn
Zhao You	Changchun Observatory, China	youzhao@cho.ac.cn
Zhao Gang	Changchun Observatory, China	zhaog@cho.ac.cn
Zieliński Janusz	Space Research Centre of the Polish Academy of Sciences, Poland	jbz@cbk.waw.pl
Zuber Maria	MIT, USA	zuber@mit.edu